**Medical Radiology · Diagnostic Imaging**
*Series Editors:* H.-U. Kauczor · H. Hricak · M. Knauth

Hans-Ulrich Kauczor
Tobias Bäuerle *Editors*

# Imaging of Complications and Toxicity following Tumor Therapy

Springer

# Medical Radiology

## Diagnostic Imaging



For further volumes:
http://www.springer.com/series/4354

Medical Radiology—Diagnostic Imaging is a unique series that aims to document the most innovative technologies in all fields within diagnostic imaging and interventional radiology, thereby informing the physician in practice of the latest advances in diagnostic imaging and percutaneous image-guided minimally invasive procedures. The contents are intended to cover all organs, and all modern imaging techniques and image-guided treatment modalities, with special emphasis on applications in clinical practice. Each volume is a comprehensive reference book on a topical theme, and the editors are always experts of high international standing. Contributions are included from both clinicians and researchers, ensuring wide appeal. Medical Radiology —Radiation Oncology is a unique series that aims to document the most innovative technologies in all fields within radiology, thereby informing the physician in practice of the latest advances in diagnostic and treatment techniques. The contents range from contemporary statements relating to management for various disease sites to explanations of the newest techniques for tumor identification and of mechanisms for the enhancement of radiation effects, with the emphasis on maximizing cure and minimizing complications. Each volume is a comprehensive reference book on a topical theme, and the editors are always experts of high international standing. Contributions are included from both clinicians and researchers, ensuring wide appeal.

Hans-Ulrich Kauczor • Tobias Bäuerle
Editors

# Imaging of Complications and Toxicity following Tumor Therapy

Springer

*Editors*
Hans-Ulrich Kauczor
Dept. of Radiology
University Hospital Heidelberg
Heidelberg
Germany

Tobias Bäuerle
Institute of Radiology
University Hospital Erlangen
Erlangen
Germany

ISBN 978-3-319-12840-5 ISBN 978-3-319-12841-2 (eBook)
DOI 10.1007/978-3-319-12841-2

Library of Congress Control Number: 2015956140

Springer Cham Heidelberg New York Dordrecht London

Medical Radiology


Printed on acid-free paper

Springer International Publishing AG Switzerland is part of Springer Science+Business Media (www.springer.com)

# Contents

# Contributors

**Sharon Z. Adam** Department of Radiology, Tel Aviv Sourasky Medical Center, Tel Aviv, Israel

Department of Diagnostic Radiology, Northwestern University Feinberg School of Medicine, Chicago, IL, USA

**Maxim Avanesov** Department of Diagnostic and Interventional Radiology, Center for Radiology and Endoscopy, University Medical Center Hamburg-Eppendorf, Hamburg, Germany

**Edwin J.R. van Beek** Queen's Medical Research Institute, University of Edinburgh, Edinburgh, UK

**Arye Blachar** Computed Tomography and Magnetic Resonance Imaging Division, The Tel Aviv University Sackler School of Medicine, Tel Aviv, Israel

Department of Radiology, Tel Aviv Sourasky Medical Center, Tel Aviv, Israel

**Andreas Block** Department of Internal Medicine II and Clinic (Oncology Center), Center for Oncology, University Medical Center Hamburg-Eppendorf, Hamburg, Germany

**Hans Bloem** Department of Radiology, Leiden University Medical Center, Leiden, The Netherlands

**T. Bostel** Department of Radiooncology and Radiation Therapy, Heidelberg University Hospital, Heidelberg, Germany

**Mauricio Castillo** Division of Neuroradiology, University of North Carolina, Chapel Hill, NC, USA

**Teresa Margarida Cunha** Department of Radiology, Instituto Português de Oncologia de Lisboa Francisco Gentil, Lisbon, Portugal

**J.Y. Delattre** AP-HP, Groupe Hospitalier Pitié-Salpêtrière, Service de Neurologie 2-Mazarin, 47 Bd de l'hôpital, Paris, France

Centre OncoNeuroTox, Paris, France

Sorbonne Universités, Sorbonne Universités, UPMC Univ. Paris 06, Inserm, CNRS, UM 75, U 1127, UMR 7225, ICM, F-75013, Paris, France

**P. Hernáiz Driever** Department of Pediatric Oncology/Hematology, Charité-Universitätsmedizin Berlin, Berlin, Germany

**Marco Essig** Department of Radiology, University of Manitoba, Winnipeg, MB, Canada

**Rosemarie Forstner** Department of Radiology, Landeskliniken Salzburg, Paracelsus Medical University, Salzburg, Austria

**Ravit Geva** Department of Oncology, Tel Aviv Sourasky Medical Center, Tel Aviv, Israel

**Ulrich Hacker** University Cancer Center Leipzig (UCCL), University Hospital Leipzig, Leipzig, Germany

**Björn Jobke** Department of Radiology, Deutsches Krebsforschungszentrum (DKFZ), German Cancer Research Center, Heidelberg, Germany

**D-M. Koh** Department of Diagnostic Radiology, Royal Marsden Hospital, Sutton, Surrey, UK

**D. Leclercq** Centre OncoNeuroTox, Paris, France

Sorbonne Universités, Sorbonne Universités, UPMC Univ. Paris 06, Inserm, CNRS, UM 75, U 1127, UMR 7225, ICM, F-75013, Paris, France

Service de Neuroradiologie, Hôpital Salpêtrière, Paris, France

**Michael M. Lell** Department of Radiology, University Erlangen, Erlangen, Germany

**Florian Lordick** University Cancer Center Leipzig (UCCL), University Hospital Leipzig, Leipzig, Germany

**Gunnar K. Lund** Department of Diagnostic and Interventional Radiology, Center for Radiology and Endoscopy, University Medical Center Hamburg-Eppendorf, Hamburg, Germany

**Michal Mauda-Havakuk** Department of Radiology, Tel Aviv Sourasky Medical Center, Tel Aviv, Israel

**John T. Murchison** Department of Radiology, Royal Infirmary of Edinburgh, Edinburgh, UK

**Stefan M. Pfister** Division of Pediatric Neurooncology (B062), Deutsches Krebsforschungszentrum (DKFZ), Heidelberg, Germany

Department of Pediatric Hematology and Oncology, Heidelberg University Hospital, Heidelberg, Germany

**Dimitri Psimaras** AP-HP, Groupe Hospitalier Pitié-Salpêtrière, Service de Neurologie 2-Mazarin, 47 Bd de l'hôpital, Paris, France

Centre OncoNeuroTox, Paris, France

Sorbonne Universités, Sorbonne Universités, UPMC Univ. Paris 06, Inserm, CNRS, UM 75, U 1127, UMR 7225, ICM, F-75013, Paris, France

**Joana Ramalho** Division of Neuroradiology, University of North Carolina, Chapel Hill, NC, USA

**D. Ricard** Centre OncoNeuroTox, Paris, France

Sorbonne Universités, Sorbonne Universités, UPMC Univ. Paris 06, Inserm, CNRS, UM 75, U 1127, UMR 7225, ICM, F-75013, Paris, France

Service de Neurologie, Hôpital d'instruction des armées du Val-de-Grâce, Service de Santé des Armées, Paris, France

**Santiago Rossi** Centro de Diagnostico Dr Enrique Rossi, Buenos Aires, Argentina

**Cornelia Schaefer-Prokop** Department of Radiology, Meander Medical Center, Amersfoort, The Netherlands

Department of Radiology, Radboud University, Medical Center, Nijmegen, The Netherlands

**A. Shah** Department of Diagnostic Radiology, Royal Marsden Hospital, Sutton, Surrey, UK

**S.A. Sohaib** Department of Diagnostic Radiology, Royal Marsden Hospital, Sutton, Surrey, UK

Department of Diagnostic Radiology, Royal Marsden NHS Foundation Trust, Sutton, Surrey, England, UK

**F. Sterzing** Department of Radiooncology and Radiation Therapy, Heidelberg University Hospital, Heidelberg, Germany

**G. Tallen** Department of Pediatric Oncology/Hematology, Charité-Universitätsmedizin Berlin, Berlin, Germany

Department of Pediatrics, Faculty of Medicine, University of Calgary, Calgary, AL, Canada

**Chitra Viswanathan** Division of Diagnostic Imaging, Department of Diagnostic Radiology, University of Texas MD Anderson Cancer Center, Houston, TX, USA

**M. Warmuth-Metz** Department of Neuroradiology, Universität Würzburg, Würzburg, Germany

**Rianne Wittenberg** Department of Radiology, Meander Medical Center, Amersfoort, The Netherlands

# Part I

# Basics of Toxicity of Tumor Therapies

# Chemotherapy and Targeted Therapy

Florian Lordick and Ulrich Hacker

## Contents




**Abstract**

A precise knowledge of antineoplastic drugs is an indispensable basis for the care of patients with cancer. The mechanisms of action and resistance, cross-resistance patterns, pharmacodynamics and pharmacokinetics, pharmacological interaction, and last but not least potential adverse effects should be part of this knowledge. As contemporary cancer care requires interdisciplinary and multiprofessional structures, the radiologist is an important and integral part of the oncological treatment team. He has several key roles. Besides the determination of an accurate clinical staging which is the basis for all treatment recommendations, he evaluates the response to anticancer treatment and defines the remission status following treatment. Importantly, he assesses acute and long-term treatment toxicities, both having a tremendous impact on patients' safety and quality of life. This article summarizes the principles of medical anticancer treatment and outlines the major side effects associated with drug classes and specific antineoplastic compounds.


## Abbreviations

| | |
|---|---|
| 2-CDA | 2-Chlordeoxyadenosine |
| 5-FU | 5-Fluorouracil |
| 6-MP | 6-Mercaptopurine |
| 6-TG | 6-Thioguanine |


F. Lordick (✉) • U. Hacker
University Cancer Center Leipzig (UCCL),
University Hospital Leipzig,
Liebigstr. 20, Leipzig D- 04103, Germany
e-mail: direktion.uccl@medizin.uni-leipzig.de


Med Radiol Radiat Oncol (2014)
DOI: 10.1007/174_2014_1040, © Springer International Publishing Switzerland

| | |
|---|---|
| ACNU | Nimustine |
| ADL | Activity of daily living |
| AE | Adverse event |
| ALK | Anaplastic lymphoma kinase |
| AMSA | Amsacrine |
| AraC | Cytosine arabinoside |
| ARDS | Acute respiratory distress syndrome |
| BCNU | Carmustine |
| bcr/abl | Breakpoint cluster region protein/ Abelson murine leukemia viral oncogene homolog 1 |
| CCDP | Cisplatin |
| CCNU | Lomustine |
| CD | Cluster of differentiation |
| c-KIT | Hardy-Zuckerman 4 feline sarcoma viral oncogene homolog |
| CTC | Common Toxicity Criteria |
| CTCAE | Common Terminology Criteria for Adverse Events |
| CTLA-4 | Cytotoxic T-lymphocyte-associated protein 4 |
| DNA | Deoxyribonucleic acid |
| DTIC | Dacarbazine |
| EGFR | Epidermal growth factor receptor |
| EML4 | Echinoderm microtubule-associated protein-like 4 |
| HDAC | Histone deacetylase |
| HER2 | Human epidermal growth factor receptor 2 |
| ILD | Interstitial lung disease |
| mTOR | Mammalian target of rapamycin |
| MTX | Methotrexate |
| NCI | National Cancer Institute |
| NSCLC | Non-small cell lung cancer |
| PD-1 | Programmed cell death protein 1 |
| PDL-1 | Programmed cell death ligand 1 |
| PET | Positron emission tomography |
| PlGF | Placental growth factor |
| PRES | Progressive reversible encephalopathy syndrome |
| RAF | Rapidly accelerated fibrosarcoma |
| SOC | System Organ Class |
| TKI | Tyrosine kinase inhibitor |
| VEGF | Vascular endothelial growth factor |
| VEGFR2 | Vascular endothelial growth factor receptor 2 |
| VP-16 | Etoposide |
| WHO | World Health Organization |

## 1 Basic Principles of Medical Anticancer Therapy

Besides the locally active treatment modalities (surgery and radiation therapy), drug therapy is the third important column of anticancer treatment. Applied via the bloodstream, medical therapy can hit not only the primary tumor but also lymphatic and hematogenous disseminated tumor cells and metastases.

"Cytotoxic drug" denominates a compound that inhibits cell division and kills cells. By its effects on nucleic acid formation, DNA synthesis and repair, and protein synthesis and by the inhibition of particular protein functions that are associated with survival, proliferation, and migration, these drugs exert antiproliferative cytostatic effects or cytotoxic effects as programmed cell death (apoptosis), cell destruction (necrosis), and induction of senescence. Of note, all these effects do not only occur in neoplastic tumor cells but can alter also cells of the healthy tissue, depending on the susceptibility of particular organs to the cytotoxic drug effects. Therefore, cancer chemotherapy has transitioned from the use of cytotoxic drugs to the era of agents with an apparent selectivity for a cancer-specific target (Phelps and Sparreboom 2014). However, targets which are completely specific for cancer cells seem to be rare. And even if such characteristics exist, like the Philadelphia chromosome translocation in chronic myeloid leukemia coding for the cancer-specific bcr/abl tyrosine kinase (Heisterkamp et al. 1985), drugs hitting that target do not work absolutely target specific and do have an impact on functional structures of healthy tissue cells as well.

A classification of anticancer treatment into classical cytostatic or cytotoxic chemotherapy, antihormonal therapy, monoclonal antibody treatment, or treatment with tyrosine kinase inhibitors has historic reasons and appears arbitrary as the cell biological effects of those therapies are pleiotropic and have a great overlap. A certain relevance lies in the discrimination of the mostly non-cancer selective classical cytotoxic treatment ("chemotherapy") and the so-called selective targeted treatment forms like antihormonal therapy, therapeutic

antibodies, and kinase inhibitors. The therapeutic index of classical cytotoxic drugs like alkylating agents is often smaller than that of biologically targeted forms of therapy (Fig. 1).

Classical cytotoxic drugs have different mechanisms of action which are outlined in Fig. 2.

Hanahan and Weinberg described the hallmarks of cancer in a previous landmark article that was updated in 2011. These hallmarks include sustaining proliferative signaling, evading growth suppressors, resisting cell death, enabling replicative immortality, inducing angiogenesis, and activating invasion and metastasis. Conceptual progress in the last decade has added two emerging hallmarks of potential generality to this list – reprogramming of energy metabolism and evading immune destruction. The "tumor microenvironment" that consists of apparently normal cells adds to the complexity of current tumor characteristics which forms the basis for contemporary drug development and targeted treatment of cancer (Fig. 3) (Hanahan and Weinberg 2011).

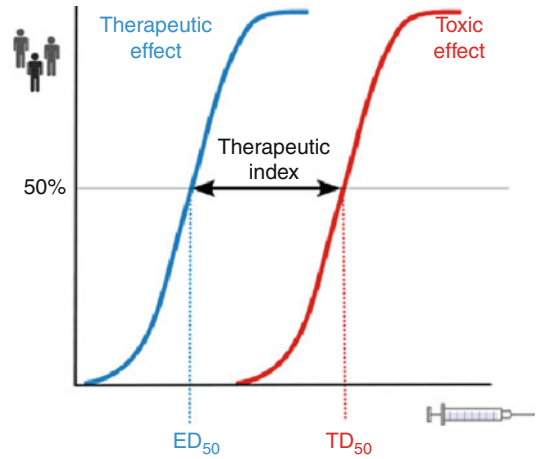


**Fig. 1** The concept of therapeutic index refers to the relationship between toxic and therapeutic doses. This pharmacodynamic parameter is relevant to clinical practice because it determines how safe or toxic a drug is. Both ED50 and TD50 are calculated from dose-response curves, which represent the frequency with which each dose of drug elicits the desired response or toxic effect in the population. The dose required to cause a therapeutic effect (positive response) in 50 % of a population is the ED50. The dose required to produce a toxic effect in 50 % of the studied population is the TD50 (Redrawn from Craig and Stitzel (2003))

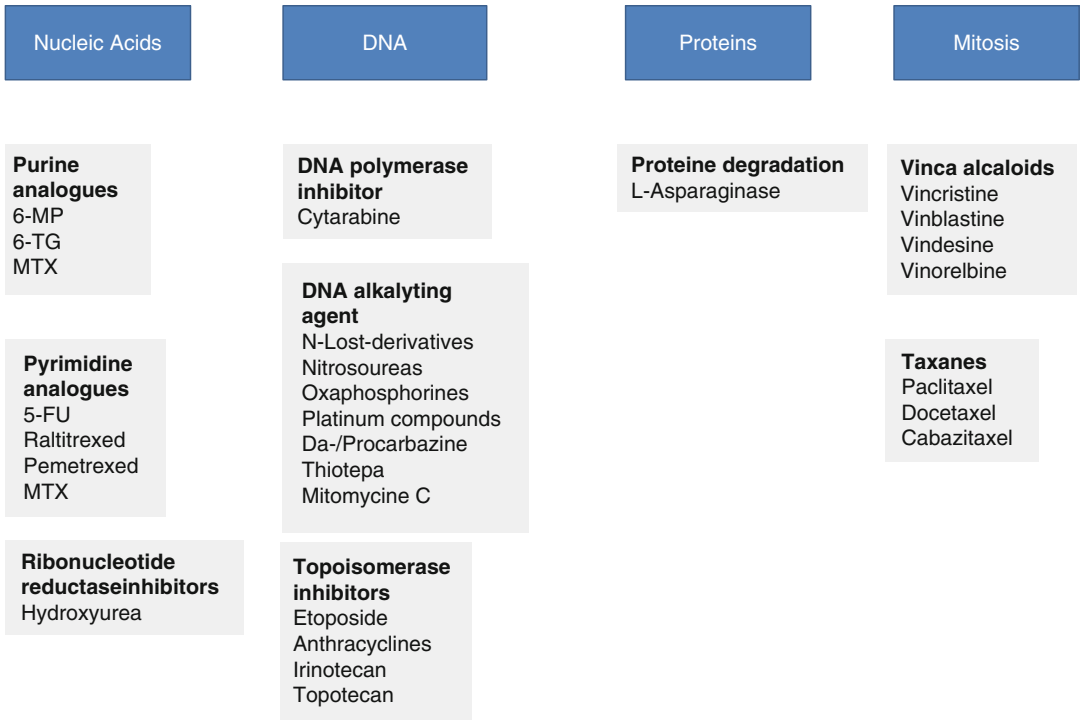


**Fig. 2** Target structures of classical cytotoxic drugs: *DNA* deoxyribonucleic acid, *MTX* methotrexate, *5-FU* 5-fluorouracil, *6-MP* 6-mercaptopurine, *6-TG* 6-thioguanine

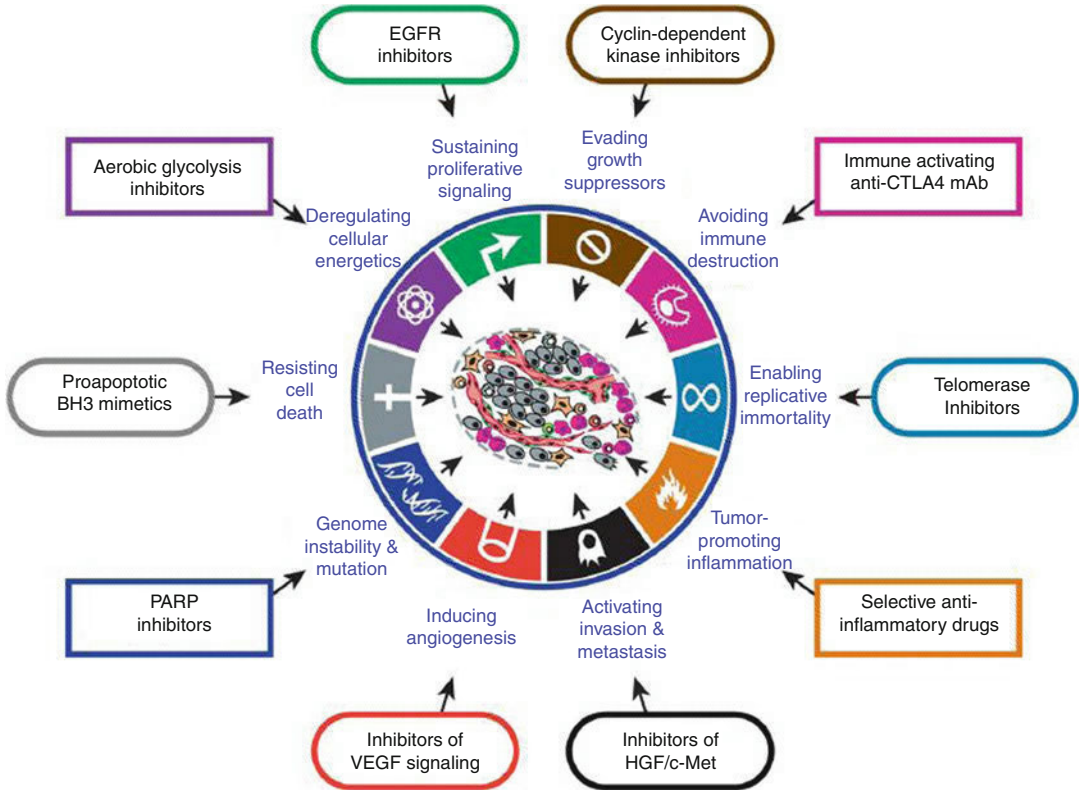


**Fig. 3** The hallmarks of cancer (Redrawn from Hanahan and Weinberg (2011)) are the basis for contemporary drug development and targeted anticancer treatment

## 2 Definitions of Anticancer Drug Therapy

### 2.1 Mono- Versus Combination Therapy

In principle, combination chemotherapy has advantages over monotherapy due to additive or multiplicative effects of tumor cell kill. Primary or secondary resistant tumor cell clones can be eradicated or suppressed by different mechanisms of action. Ideally, combinations have the following features:

- The combined agents are equally effective.
- Lack of cross-resistance.
- Different mechanisms of action.
- Additive or synergistic mechanisms of action.
- No overlapping toxicities.

For most combinations, this ideal situation does not exist. Especially with regard to side effects, some addition of toxicity must always be accepted when combinations are used.

### 2.2 Induction Chemotherapy

Induction chemotherapy is used when at the time of diagnosis no acceptable therapeutic alternative exists. Induction chemotherapy shall bring the cancer into a state of better therapeutic options. The goal is "the induction" of an optimal remission, which is at best a "complete remission." High treatment intensities are usually necessary for an optimal induction. Therefore, the probability of inducing adverse effects is usually high.

### 2.3 Consolidation Therapy

The consolidation therapy shall provide the eradication of clinically occult residual tumor. It shall improve the rate of true complete remissions. Thereby, consolidation shall increase the chances of cure or increase the duration of response.

## 2.4 Maintenance Therapy

Maintenance therapy, in its classical sense used in the treatment of hematological malignancies like acute leukemia, follows consolidation and shall eradicate or control further residual tumor cells, e.g., those that – due to kinetic resistance – were not yet eradicated by the previous treatment. Maintenance therapy can increase the chance of cure or prolong the time interval until further tumor progression. The latter goal is nowadays often chosen in the palliative treatment of solid tumors when a remission has been achieved by a more intensive treatment period preceding maintenance.

## 2.5 Perioperative (Neoadjuvant and/or Adjuvant) Chemotherapy

Neoadjuvant (also primary or preoperative) therapy is a treatment in patients with localized or locoregional tumor extension in which the application of local treatment alone (operation or radiation therapy) may lead to an unsatisfactory outcome. Neoadjuvant chemotherapy is applied to reduce the extent of surgery (e.g., in breast cancer, where size reduction of large tumors allows for more breast-conserving surgery following neoadjuvant chemotherapy) and to increase the chances of cure (like in gastric or muscle invasive bladder cancer). In some cancers (e.g., osteosarcoma and Ewing sarcoma), postoperative treatment is tailored on the basis of the achieved response during neoadjuvant therapy.

The goal of adjuvant chemotherapy is the eradication of subclinical metastases ("micrometastases") following primary local treatment (operation or radiation therapy). The clinical goal of treatment is to increase the cure rate.

Accepted indications for perioperative chemotherapy are shown in Table 1. As increased cure rates are the goal of neo-/adjuvant chemotherapy, optimal dose intensity is necessary and some toxicity must be accepted. On the other hand, treatment safety is of utmost importance as patients may survive with the operation alone. In addition, long-term side effects should be avoided as they may lead to a significant impairment of quality of life of cancer survivors; alter physical, cognitive, and social functioning; and may even induce secondary diseases (cancers, leukemia, organ dysfunctions, cardiovascular diseases, etc.) leading to a negative impact on life expectancy.

**Table 1** Examples for tumors with an established indication for perioperative (neoadjuvant or adjuvant) therapy

| |
|---|
| Breast cancer |
| Ovarian cancer |
| Esophageal cancer |
| Gastric cancer |
| Pancreatic cancer |
| Colon cancer |
| Rectal cancer |
| Lung cancer |
| Testicular cancer |
| Urothelial cancer |
| Ewing sarcoma |
| Osteosarcoma |
| Rhabdomyosarcoma |

## 2.6 Palliative Therapy

Palliative chemotherapy is a treatment intended to prolong life, to control symptoms, and to augment quality of life. In case of symptomatic disease, more intensive induction treatment regimens are often applied. For a further stabilization of the tumor, most often less intensive monotherapies are regarded as standard of care. Treatment-emergent side effects must be carefully weighed against potential treatment benefits.

# 3 Classification of Anticancer Drugs

The classification of anticancer drugs can follow different criteria. Traditionally, the World Health Organization (WHO) chose the mechanisms of action (e.g., alkylating agent) and the origin of compounds (e.g., antitumor antibiotics) as their leading criteria for classification. Table 2 groups the compounds predominantly according to their mechanisms of action.

## 4 Classification of Treatment Toxicity

Side effects of medical treatment have been classified according to uniform criteria as long as the drug is applied within a clinical study. Internationally, the so-called Common Toxicity Criteria (CTC) or the newer Common Terminology Criteria for Adverse Events (CTCAE) as developed and published by the National Cancer Institute (NCI, Bethesda, USA) are most commonly used. Meanwhile, these criteria have been well implemented into clinical practice and proved useful. Therefore, thorough oncologists and multidisciplinary teams use it outside of clinical studies in routine cancer care. The current version of CTCAE V4.03 can be downloaded from the Internet (http://evs.nci.nih.gov/ftp1/CTCAE/CTCAE_4.03_2010-06-14_QuickReference_8.5x11.pdf).

**Table 2** Classification of anticancer drugs according to their mechanisms of action and biochemical properties

| Drug class | Group | Compound |
|---|---|---|
| Alkylating agent | N-lost-derivatives | Bendamustine |
| | | Busulfan |
| | | Chlorambucil |
| | Nitrosourea derivatives | Nimustine (ACNU) |
| | | Carmustine (BCNU) |
| | | Lomustine (CCNU) |
| | Oxaphosphorines | Cyclophosphamide |
| | | Ifosfamide |
| | | Trofosfamide |
| | Platinum derivatives | Cisplatin (CDDP, DDP) |
| | | Carboplatin |
| | | Oxaliplatin |
| | Tetrazines | Dacarbazine (DTIC) |
| | | Temozolomide |
| | Aziridines | Thiotepa |
| | Others | Amsacrine (AMSA) |
| | | Estramustinphosphate |
| | | Procarbazine |
| | | Treosulfan |
| Antibiotics | Anthracyclines | Daunorubicin |
| | | Doxorubicin |
| | | Epirubicin |
| | | Idarubicin |
| | Anthracenedione | Mitoxantrone |
| | Others | Actinomycin-D |
| | | Bleomycin |
| | | Mitomycin C |
| Alkaloids | Podophyllotoxin derivative | Etoposide (VP-16) |
| | Vinca alkaloids | Vinblastine |
| | | Vincristine |
| | | Vindesine |
| | | Vinorelbine |
| | Taxanes | Cabazitaxel |
| | | Docetaxel |
| | | Paclitaxel |
| | Camptothecin derivatives | Irinotecan |
| | | Topotecan |

**Table 2** (continued)

| Drug class | Group | Compound |
|---|---|---|
| Antimetabolite | Antifolates | Methotrexate (MTX) |
| | | Pemetrexed |
| | Purine analogues | 6-Mercaptopurine (6-MP) |
| | | 6-Thioguanine (6-TG) |
| | | Fludarabine |
| | | 2-Chlordeoxyadenosine (2-CDA) |
| | Pyrimidine analogues | 5-Fluorouracil (5-FU) |
| | | Capecitabine |
| | | Clofarabine |
| | | Cytosine arabinoside (AraC) |
| | | Gemcitabine |
| | RNR inhibitor | Hydroxyurea |
| DNA demethylation | Demethylating agents | Azacytidine |
| | | Decitabine |
| Protein degradation | Enzyme | L-asparaginase |
| Aromatase inhibition | Nonsteroidal inhibitors | Anastrozole |
| | | Letrozole |
| | Steroidal inhibitor | Exemestane |
| Other hormonal therapies | Antiandrogens | Abiraterone |
| | | Bicalutamide |
| | | Flutamide |
| | | Nilutamide |
| | Antiestrogen | Fulvestrant |
| | Gestagens | Medroxyprogesterone acetate |
| | | Megestrol acetate |
| | Selective estrogen receptor modulators | Raloxifene |
| | | Tamoxifen |
| Immune modulators | Cytokines | Interferon alpha |
| | | Interleukin 2 |
| | IMIDs | Lenalidomide |
| | | Thalidomide |
| | | Pomalidomide |
| | Immune checkpoint inhibitors | Ipilimumab |
| | | Lambrolizumab |
| Monoclonal antibodies | CD20 antibodies | Rituximab |
| | | Ofatumumab |
| | CD30 antibody-toxin conjugate | Brentuximab vedotin |
| | CD33 antibody | Gemtuzumab ozogamicin |
| | CD52 antibody | Alemtuzumab |
| | EGFR antibodies | Cetuximab |
| | | Panitumumab |
| | HER2 antibodies | Trastuzumab |
| | | Pertuzumab |
| | HER2 antibody-toxin conjugate | Trastuzumab emtansine |
| | VEGF antibody | Bevacizumab |
| | VEGF recombinant fusion protein | Aflibercept |
| | VEGFR2 antibody | Ramucirumab |

(continued)

**Table 2** (continued)

| Drug class | Group | Compound |
|---|---|---|
| Tyrosine kinase inhibitors | Bcr/abl | Imatinib |
| | | Dasatinib |
| | | Nilotinib |
| | cKIT | Imatinib |
| | EGFR | Afatinib |
| | | Erlotinib |
| | | Gefitinib |
| | HER2 | Lapatinib |
| | Histone deacetylase (HDAC) | Romidepsin |
| | | Vorinostat |
| | mTOR | Temsirolimus |
| | | Everolimus |
| | Multiple kinases | Axitinib |
| | | Nintedanib |
| | | Pazopanib |
| | | Regorafenib |
| | | Sorafenib |
| | | Sunitinib |
| | Proteasome | Bortezomib |
| | | Carfilzomib |
| | RAF | Vemurafenib |
| | Smoothened receptor (hedgehog signaling) | Vismodegib |
| | Somatostatin receptors | Octreotide |
| | | Lanreotide |

Compounds are listed with their generic names. Where appropriate, commonly used abbreviations are listed in parentheses

The NCI Common Terminology Criteria for Adverse Events is a descriptive terminology which can be utilized for *adverse event (AE)* reporting. A grading (severity) scale is provided for each AE term. *System Organ Class (SOC)*, the highest level of the reporting hierarchy, is identified by anatomical or physiological system, etiology, or purpose (e.g., SOC Investigations for laboratory test results). Within each SOC, adverse events are listed and accompanied by descriptions of severity (grade).

An AE is any unfavorable and unintended sign (including an abnormal laboratory or imaging finding), symptom, or disease temporally associated with the use of a medical treatment or procedure that may or may not be considered related to the medical treatment or procedure. An AE is a term that is a unique representation of a specific event used for medical documentation and scientific analyses.

*Grade* refers to the severity of the AE. The CTCAE displays grades 1 through 5 with unique clinical descriptions of severity for each AE based on this general guideline (Table 3). Not all grades are appropriate for all AEs. Therefore, some AEs are listed with fewer than five options for grade selection.

## 5 Specific Toxicities Associated with Anticancer Treatment

All organ systems can be subject to treatment-emergent toxicities.

With classical cytotoxic treatment, myelosuppression (neutropenia, thrombocytopenia, and anemia) is a common side effect. Between 80 and 100 % of all patients undergoing chemotherapy have some grade of myelosuppression leading to

**Table 3** Toxicity grades according to the "Common Terminology Criteria for Adverse Events" (CTCAE) reporting system provided by the National Cancer Institute, Bethesda, USA

| Grade | Severity |
|---|---|
| Grade 1 | Mild; asymptomatic or mild symptoms; clinical or diagnostic observations only; intervention not indicated |
| Grade 2 | Moderate; minimal, local, or noninvasive intervention indicated; limiting age-appropriate instrumental activity of daily living (ADL)[a] |
| Grade 3 | Severe or medically significant but not immediately life-threatening; hospitalization or prolongation of hospitalization indicated; disabling; limiting self-care ADL[b] |
| Grade 4 | Life-threatening consequences; urgent intervention indicated |
| Grade 5 | Death related to an adverse event |

A semicolon indicates "or" within the description of the grade

[a]Instrumental ADL refer to preparing meals, shopping for groceries or clothes, using the telephone, managing money, etc.

[b]Self-care ADL refer to bathing, dressing and undressing, feeding self, using the toilet, taking medications, and not bedridden

alterations of the differential blood counts. Severity and duration depend of course on the applied cytotoxic drug and schedule as well as additional risk factors, like age and general health status. In case of neutropenia, patients are at particular risk of acquiring infections. Febrile neutropenia is an emergency situation during antineoplastic treatment. It requires immediate clarification and start of empiric antibiotic treatment. In most cases (except low-risk neutropenia in otherwise unimpaired and compliant patients), this should be done following hospitalization, and intravenous broad-spectrum antibiotics should be given (Klastersky and Paesmans 2013). In more than two thirds of patients, the focus of febrile neutropenia remains unknown, but pulmonary infections, bloodstream infections, urinary infections, infections of the skin and soft tissues, as well as infections of the upper aerodigestive tract should be excluded by appropriate clinical, paraclinical, and radiological diagnostics.

Apart from myelosuppression, non-hematological adverse events are common and need to be well known by the treatment team. Table 4 outlines a selection of substance- and group-specific non-hematological toxicities of anticancer drugs.

Our expectation was that with the introduction of new, more specific and biologically targeted drugs, the efficacy of anticancer treatment would increase, while the side effects would decrease. This hope was desperately disappointed (Niraula et al. 2012). International investigators analyzed all randomized controlled trials evaluating agents approved for the treatment of solid tumors by the US Food and Drug Administration between 2000 and 2010. Odds ratios were computed for three end points of safety and tolerability: treatment-related death, treatment discontinuation related to toxicity, and grade 3 or grade 4 adverse events (AEs). These were then pooled in a meta-analysis. Correlations between these end points and the hazard ratios for overall survival and progression-free survival were also assessed. The investigators came to the conclusion that new anticancer agents that lead to improvements in time-to-event end points also increase morbidity and treatment-related mortality. The balance between efficacy and toxicity may be less favorable in clinical practice because of selection of fewer patients with good performance status and limited comorbidities. Patients' baseline health characteristics should be considered when choosing therapy.

With the use of targeted therapies, novel side effects have emerged that are closely related to the specific mechanisms of action of the respective drug. Targeted therapies in general block certain signaling pathways that play important roles in promoting tumor cell survival and proliferation or interfere with stromal cells like vascular endothelial cells to inhibit tumor angiogenesis or with immune cells to modify antitumor immune responses. Monoclonal antibodies and tyrosine kinase inhibitors (TKI) represent the drug classes that are most commonly used for targeted cancer therapy. Furthermore, specific intracellular signaling checkpoints can be blocked by chemical compounds (i.e., mTOR inhibitors). Another group of drugs targets immune function to improve host anticancer immunity. CTLA-4 antibodies are used to enhance T-cell co-stimulation,

**Table 4** Selection of substance and group-specific non-hematological toxicities of anticancer drugs

| Substance/group | Typical adverse effect |
|---|---|
| Alemtuzumab | Opportunistic infection |
| Anthracyclines/mitoxantrone | Cardiomyopathy, cardiac arrhythmia |
| Aromatase inhibitors | Bone and joint pain, osteoporosis |
| Bevacizumab | Arterial hypertension, proteinuria, impaired wound healing, gut perforations, bleeding |
| Bleomycin | Pulmonary toxicity, lung fibrosis |
| Bortezomib | Neuropathy |
| Busulfan | Pulmonary toxicity, veno-occlusive disease |
| Cetuximab/panitumumab | Acneiform exanthema, allergic reactions |
| Chlorambucil | Pulmonary toxicity, lung fibrosis |
| Cytarabine | Central nervous toxicity (especially high-dose AraC leads to cerebellar alterations) |
| Docetaxel | Finger- and toenail alterations, edema, neuropathy, taste alterations |
| Erlotinib/gefitinib | Pneumonitis, acute respiratory distress syndrome (ARDS) |
| Fluoropyrimidines | Diarrhea, stomatitis, hand-foot syndrome, cardiotoxicity (arrhythmias, heart burn, myocardial infarction) |
| Imatinib | Edema, skin rash |
| Irinotecan | Diarrhea, cholinergic syndrome |
| Methotrexate | Central nervous toxicity, hepatic and pulmonary toxicity, nephrotoxicity in case of inadequate renal elimination |
| Mitomycin C | Hemolytic-uremic syndrome, pulmonary toxicity |
| Sunitinib/pazopanib/sorafenib/regorafenib | Arterial hypertension, hand-foot syndrome, thyroid disorders |
| mTOR inhibitors (everolimus, temsirolimus) | Arterial hypertension, pneumonitis, mucositis, erythema, hand-foot syndrome, hyperlipidemia |
| Nitrosoureas | Pulmonary toxicity, lung fibrosis, renal toxicity |
| Oxazaphosphorines (cyclophosphamide, ifosfamide) | Urothelial toxicity, renal toxicity, central nervous toxicity (reversible psychosyndrome with high-dose ifosfamide) |
| Paclitaxel/docetaxel | Neuropathy, allergic reactions, onycholysis |
| Platinum compounds | Renal impairment (cisplatin), ototoxicity (cisplatin), neuropathy (oxaliplatin > cisplatin >> carboplatin) |
| Tamoxifen | Thromboembolic events |
| Trastuzumab/pertuzumab/lapatinib | Cardiac toxicity |
| Vinca alkaloids | Neuropathy |

and drugs targeting the PD-1/PD-L1 pathway have been developed to block inhibitory immune checkpoints.

An overview of key side effects can be found in Table 2. Specific side effects resulting in pathological radiological findings are shortly summarized in the following section.

Agents Targeting the Epidermal Growth Factor Receptor (EGFR): The monoclonal antibodies (cetuximab, panitumumab) are used for the treatment of RAS wild-type metastatic colorectal cancer, while TKI (gefitinib, erlotinib, afatinib) represent a standard of care in the treatment of EGFR-mutated non-small cell lung cancer (NSCLC) patients. Skin toxicities occur with high frequency in both groups of drugs. In contrast, interstitial lung disease (ILD) represents a rare complication, and the mechanism is not fully understood. Disruption of the alveolar epithelial function however may play a role. Based on this, the frequency of ILD is higher in smokers and in patients with preexisting lung disease (Ando et al. 2006).

Agents Targeting Her-2: Chemotherapy combined with monoclonal antibodies (trastuzumab, pertuzumab) represents a treatment standard in

Her2-positive breast cancer and in Her2 gastric cancer (trastuzumab). The TKI lapatinib targeting EGFR and Her2neu is approved for the treatment of breast cancer. An important side effect of this class of drugs is cardiotoxicity that is related to the expression of Her2 on cardiomyocytes. Mechanistically, Her2 signaling results in sarcomere stability and initiates repair processes that are important to counteract toxic stress (Tocchetti et al. 2012).

Agents Targeting Tumor Angiogenesis: The monoclonal antibody bevacizumab binds vascular endothelial growth factor (VEGF), and the fusion construct aflibercept binds VEGF and placental growth factor (PlGF). Both drugs are used in combination with chemotherapy for the treatment of metastatic colorectal cancer. Additionally, a large number of TKI targeting VEGF receptors and other receptors are in clinical use for the treatment of a wide variety of cancer types (Table 2). Hypertension and proteinuria represent common side effects of VEGF-targeting therapy. Furthermore, the rate of thromboembolic complications is increased. Other side effects are related to impaired tissue repair capacity and comprise gastrointestinal pneumatosis perforations and the formation of fistulas (Shinagare et al. 2012). Overall, bleeding is a rare side effect. However, frequent bleeding complications have resulted in the exclusion of the use of bevacizumab in squamous cell carcinoma of the lung. Progressive reversible encephalopathy syndrome (PRES) is a very rare (≤0.1 %) but severe neurological complication that has been reported in patient treatment with bevacizumab or aflibercept (Seet and Rabinstein 2012). The disruption of cerebrovascular endothelial cell signaling is related to the disruption of cerebrovascular autoregulation preferentially in the posterior circulation of the brain. Finally, pancreatitis (sunitinib, sorafenib, pazopanib) and acalculous cholecystitis (sunitinib) have been reported in the literature on a casuistic basis.

Anaplastic Lymphoma Kinase (ALK) Inhibitors: ALK inhibitors are used for the treatment of NSCLC harboring specific genomic rearrangements (EML4-ALK). Pneumonitis has been reported with the use of the ALK inhibitor crizotinib and symptoms started within two months of treatment. The underlying mechanisms are not yet clarified.

RAF-Targeting Agents: RAF-targeting agents include the multi-TKI sorafenib for the treatment of renal cell and hepatocellular cancer as well as vemurafenib and dabrafenib, which are used for the treatment of melanoma harboring the B-Raf mutation V600E and other B-Raf mutations. An increase in the occurrence of cutaneous squamous cell carcinomas has been reported, and nodular panniculitis (Monfort et al. 2012) may result in increased radiotracer uptake during 18F-FDG positron emission tomography (PET).

Agents Targeting Mammalian Target of Rapamycin (mTOR) and Targeted Immune Modulators: These agents (everolimus, temsirolimus) are used for the treatment of breast and renal cancers and pancreatic neuroendocrine tumors. Mucositis and aphthous mucosal lesions are common side effects. Additionally, interstitial pneumonitis is an important side effect of this class of drugs with up to 36 % of patients showing any pulmonary abnormalities during treatment (Duran et al. 2014).

Ipilimumab is a novel targeted immune modulator that interacts with CLTA-4, thus fostering co-stimulatory function to improve host antitumor immune response. Due to immune function deregulation, autoimmune-related side effects like enterocolitis and hypophysitis may occur. Additionally, unspecific lymph node enlargement and soft tissue changes like myositis or fasciitis as well as retroperitoneal fat opacities due to lymphocyte infiltration may interfere with treatment response assessment (Bronstein et al. 2011).

As examples of "new toxicities" emerging from biologically selective targeted drugs, Fig. 4 displays a perforation at the rectosigmoid level that occurred during treatment of metastatic colorectal cancer with the anti-VEGF antibody bevacizumab. Another patient who was also treated for metastatic colorectal cancer received the monoclonal anti-EGFR antibody cetuximab plus chemotherapy and developed a grade 3 skin rash during weeks 4–6 of this combined treatment (Fig. 5).

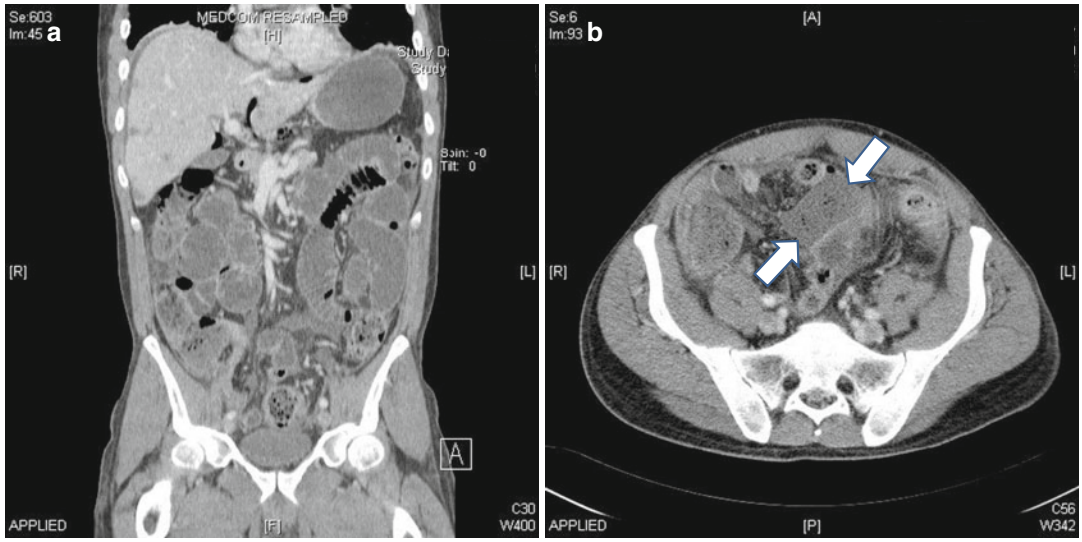


**Fig. 4** Gut perforation leading to an ileus and peritonitis, emerging from a pararectal abscess in a patient with colorectal cancer with simultaneous liver and lung metastases. (**a**) Is illustrating the coronary section through the abdomen; (**b**) is illustrating a transversal section through the pelvis. The two *white arrows* in **b** are highlighting the formation of a pararectal abscedation. This patient was treated with the anti-VEGF monoclonal antibody bevacizumab in combination with chemotherapy

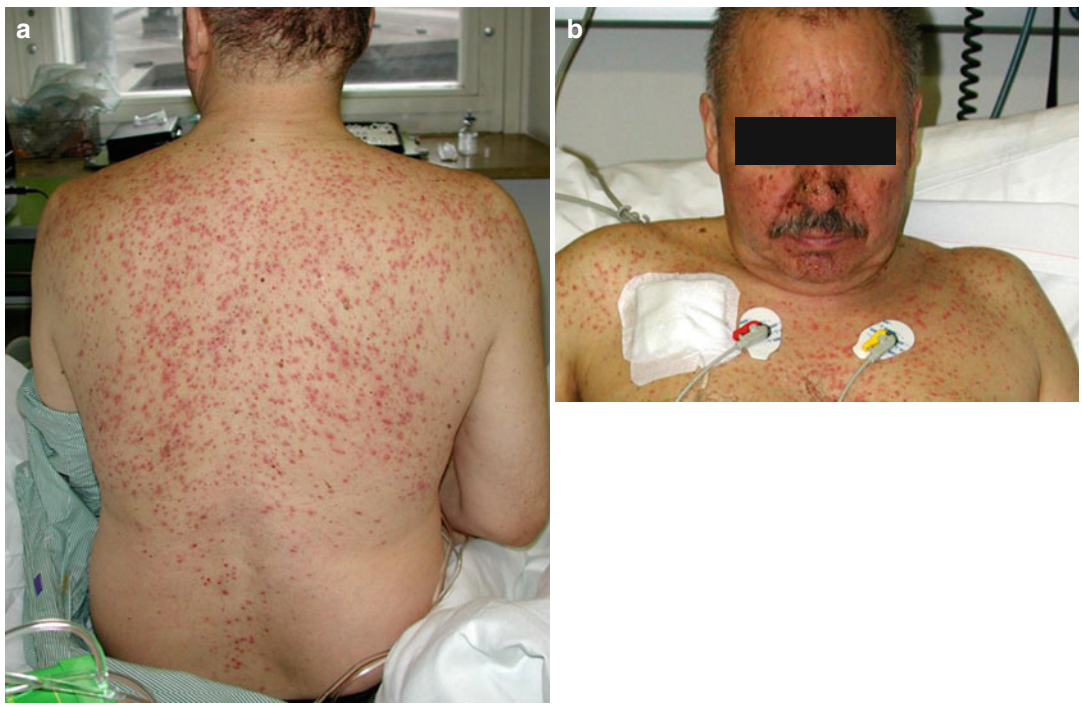


**Fig. 5** (**a**, **b**) Patient who developed severe (grade 3 according to CTCAE V4.03) skin rash during weeks 4–6 of chemotherapy combined with the anti-EGFR-directed monoclonal antibody cetuximab

**Conclusions**

For clinical practice, we have to state that medical anticancer treatment is more demanding than ever, as toxicities are very common, polymorphic and allotropic. They may lead to severe impairment of the patients' safety and quality of life. All members of the treatment team, including the radiologist, need to do their best to support patients during anticancer treatment. Treatment-emergent as well as tumor-related complications may not be missed, and the severity of events must be appropriately classified. In addition, for drug development it has been advocated to move "Toward Patient-Centered Drug Development in Oncology" (Basch 2013).

## References


Ando M, Okamoto I, Yamamoto N, Takeda K, Tamura K, Seto T, Ariyoshi Y, Fukuoka M (2006) Predictive factors for interstitial lung disease, antitumor response, and survival in non-small-cell lung cancer patients treated with gefitinib. J Clin Oncol 24(16):2549–2556. doi:10.1200/JCO2005.04.9866

Basch E (2013) Toward patient-centered drug development in oncology. N Engl J Med 369(5):397–400. doi:10.1056/NEJMp1114649

Bronstein Y, Ng CS, Hwu P, Hwu WJ (2011) Radiologic manifestations of immune-related adverse events in patients with metastatic melanoma undergoing anti-CTLA-4 antibody therapy. AJR Am J Roentgenol 197(6):W992–W1000. doi:10.2214/AJR.10.6198

Craig CR, Stitzel CR (2003) Modern pharmacology with clinical applications, 6th edn. Lippincott, Williams & Wilkins, Philadelphia

Duran I, Goebell PJ, Papazisis K, Ravaud A, Weichhart T, Rodriguez-Portal JA, Budde K (2014) Drug-induced pneumonitis in cancer patients treated with mTOR inhibitors: management and insights into possible mechanisms. Expert Opin Drug Saf 13(3):361–372. doi:10.1517/14740338.2014.888056

Hanahan D, Weinberg RA (2011) Hallmarks of cancer: the next generation. Cell 144(5):646–674. doi:10.1016/j.cell.2011.02.013

Heisterkamp N, Stam K, Groffen J, de Klein A, Grosveld G (1985) Structural organization of the bcr gene and its role in the Ph′ translocation. Nature 315(6022):758–761

Klastersky J, Paesmans M (2013) The Multinational Association for Supportive Care in Cancer (MASCC) risk index score: 10 years of use for identifying low-risk febrile neutropenic cancer patients. Support Care Cancer 21(5):1487–1495. doi:10.1007/s00520-013-1758-y

Monfort JB, Pages C, Schneider P, Neyns B, Comte C, Bagot M, Vignon-Pennamen MD, Viguier M, Lebbe C (2012) Vemurafenib-induced neutrophilic panniculitis. Melanoma Res 22(5):399–401. doi:10.1097/CMR.0b013e3283570792

Niraula S, Seruga B, Ocana A, Shao T, Goldstein R, Tannock IF, Amir E (2012) The price we pay for progress: a meta-analysis of harms of newly approved anticancer drugs. J Clin Oncol 30(24):3012–3019. doi:10.1200/JCO.2011.40.3824

Phelps MA, Sparreboom A (2014) A snapshot of challenges and solutions in cancer drug development and therapy. Clin Pharmacol Ther 95(4):341–346. doi:10.1038/clpt.2014.15

Seet RC, Rabinstein AA (2012) Clinical features and outcomes of posterior reversible encephalopathy syndrome following bevacizumab treatment. QJM 105(1):69–75. doi:10.1093/qjmed/hcr139

Shinagare AB, Howard SA, Krajewski KM, Zukotynski KA, Jagannathan JP, Ramaiya NH (2012) Pneumatosis intestinalis and bowel perforation associated with molecular targeted therapy: an emerging problem and the role of radiologists in its management. ARJ Am J Roentgenol 199(6):1259–1265. doi:10.2214/AJR.12.8782

Tocchetti CG, Ragone G, Coppola C, Rea D, Piscopo G, Scala S, De Lorenzo C, Iaffaioli RV, Arra C, Maurea N (2012) Detection, monitoring, and management of trastuzumab-induced left ventricular dysfunction: an actual challenge. Eur J Heart Fail 14(2):130–37. doi:10.1093/eurjhf/hfr165

# Radiotherapy

T. Bostel and F. Sterzing

## Contents




### Abstract

The focus of this chapter lies on the description of the general basics of early and late radiation effects and the translation of these pathogenetic processes into imaging; furthermore, a few short clinical examples including imaging patterns of those underlying pathogenetic normal tissue reactions are given to provide a better understanding. In addition, the margin concepts used in radiotherapy as well as the important radiation techniques are summarized, as it is very important for diagnostic radiologists to correlate post-therapeutic tissue and organ changes in follow-up examinations with dose characteristics of a certain treatment to achieve a higher degree of reliability in image interpretation. Furthermore, for



T. Bostel • F. Sterzing (✉)
Department of Radiooncology and Radiation Therapy,
Heidelberg University Hospital,
Im Neuenheimer Feld 400,
Heidelberg 69120, Germany
e-mail: bostel.tilmann@med.uni-heidelberg.de;
sterzing.florian@med.uni-heidelberg.de



DOI 10.1007/174_2014_1041, © Springer International Publishing Switzerland

a better understanding of the cellular basis of the various radiogenic tissue effects, a short refresher about the underlying radiobiological principles is given. The detailed description of specific radiation effects and imaging patterns of clinically relevant organs and tissues, however, follows in the specific organ chapters in order to avoid redundancy.

## Abbreviations

| | |
|---|---|
| CLE | Consequential late effects |
| COX-2 | Cyclooxygenase-2 |
| CT | Computed tomography |
| CTV | Clinical target volume |
| 3D | Three dimensional |
| 4D | Four dimensional |
| DNA | Deoxyribonucleic acid |
| EBRT | External-beam radiation therapy |
| e.g. | Exempli gratia |
| GTV | Gross tumor volume |
| Gy | Gray |
| i.e. | Id est |
| IL-1a | Interleukin-1 alpha |
| iNOS | Inducible nitric oxide synthase |
| IGRT | Image-guided radiotherapy |
| IMRT | Intensity-modulated radiation therapy |
| MRI | Magnetic resonance imaging |
| mRNA | Messenger ribonucleic acid |
| NTCP | Normal tissue complication probability |
| OAR | Organs at risk |
| PET | Positron emission tomography |
| PTV | Planning target volume |
| RBE | Relative biological effectiveness |
| RR | Relative risk |
| SBRT | Stereotactic body radiation therapy |
| TD | Tolerance dose |
| TGF-ß | Transforming growth factor-ß |
| TNF-a | Tumor necrosis factor alpha |
| VOD | Veno-occlusive disease |

## 1 Introduction

Radiotherapy plays a vital role in the oncological treatment concept besides surgical and systemic therapies. Moreover, it is an effective local cancer therapy like surgery, but beyond that it offers the chance for regional high-volume treatments of microscopic tumor deposits or lymphatic pathways as transition to systemic treatments. This pivotal role of radiotherapy is also supported by epidemiological data: More than half of all cancer patients can be cured nowadays, owing to improved efficacy of advanced and mostly multimodal cancer therapies, and around half of these patients receive either radiotherapy alone or radiotherapy in combination with other cancer treatments. Moreover, about two thirds of cancer patients gain valuable palliation by radiation to alleviate the symptoms and to improve the quality of life in the course of their advanced disease.

In recent years, substantial advances in radiological imaging as well as computer hardware and software along with improved design of medical linear accelerators have contributed significantly to the development in radiation therapy. Nowadays, existing modern radiation techniques enable the delivery of conformal dose distributions with steep dose gradients between the tumor and adjacent normal tissue structures. Thus, intensification of the radiation dose to the tumor and reduction of high-dose irradiation of sensitive organs and normal tissues are possible resulting in higher curing rates and lower rates of side effects (i.e., increased therapeutic ratio). However, despite these advances, modern radiotherapy still leaves significant proportions of healthy tissue structures exposed to relatively high doses. This is in part caused by the margin concepts used in radiotherapy. In general, the determination of the planning target volume (PTV) necessarily requires the inclusion of the visible or palpable extent of tumor (i.e., gross tumor volume, GTV) as well as an additional surrounding area without visible branches of the tumor in order to take microscopic disease into account (i.e., clinical target volume, CTV). Furthermore, a patient-specific safety margin is added, if necessary, to account for the range of target motion related to breathing, pulsations, or intestinal peristalsis (e.g., lung or liver lesions) that is often based on four-dimensional (4D) imaging information derived from the planning

CT. And finally, a margin to encompass variability in patient positioning (setup) and mechanical uncertainty is added to create the final PTV. This PTV concept accounts for all available radiation techniques, even though modern approaches such as stereotactic radiation therapy or intensity-modulated radiation therapy enable to adapt the dose distribution more precisely to the tumor boundaries than traditional radiation techniques, which in turn helps to spare the adjacent healthy organs and tissues. On the other hand, PTV can encompass extended areas of normal tissues, dependent on the tumor and disease stage, for example, irradiations of the whole body, whole brain, spinal column, or breast with or without the supraclavicular lymph nodes after breast-conserving surgical treatment.

In the follow-up care of cancer patients, however, it is very important that side effects after therapeutic irradiations are not in general regarded as an indicator for medical malpractice. Moreover, it is an indicator for the best-possible treatment and maximum cure probability when these radiogenic effects manifest with only a defined low incidence of sequelae of defined severity in cured patients (Dorr 2009) (Fig. 1). Regarding the evaluation of side effects, it has also to be mentioned that radiotherapy is increasingly combined with other local and systemic therapeutic approaches such as operation, chemotherapy, or molecular targeting which may lead not only to additive but also to synergistic effects for the tumor response and for organ-specific injuries (Dische et al. 1989; Pedersen et al. 1994). Furthermore, it has to be considered that a certain number of pathological conditions may be triggered by other reasons than specific tumor therapies, such as comorbidities, the tumor itself, or other non-oncological treatments, for example, obstipation due to analgesia with opioids.

As a consequence of increased numbers of cancer survivors and prolongation of survival times, late radiation sequelae as well as secondary cancers are more frequently seen than in the past. This subject has therefore gained more relevance in oncological studies as well as clinical follow-up examinations in recent years. Therefore, it is of utmost importance that radiologists are familiar

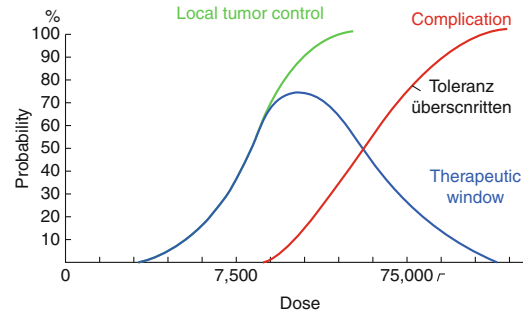


**Fig. 1** Dose dependency of tumor control (*green sigmoid curve*) and side effect (*red sigmoid curve*) probability (according to Holthusen): Due to the fact that both curves overlap, there is no chance for complete tumor destruction through radiotherapy without any risk of normal tissue complications – the third *blue curve* depicts the therapeutic window (Figure provided by courtesy of Dr. Dr. Thieke)

with the imaging patterns of these therapy-related tissue reactions as they may both mimic and obscure tumor relapses. Beyond interpretation of posttreatment imaging, diagnostic specialists can make further valuable contributions to increase the therapeutic ratio preceding the radiation treatment process (Terezakis et al. 2011). First of all, every cancer treatment, particularly radiotherapy, heavily relies on accurate staging of the cancerous disease in order to select an appropriate treatment regimen for each patient. It is obvious that misdiagnosis in staging may have fatal consequences for the patient with regard to therapy-associated complications and treatment outcome. For example, unrecognized local tumor extension in an early stage of the disease may result in an insufficient local therapy with persistence of residual tumor cells that trigger the further course of the disease, either with new local symptoms or with propagation of systemic spread of these cells. Similar devastating consequences may result from overtreatment, for example, through radiotherapy, with avoidable early and late therapy effects and worsening of the patient's general condition. This is especially important, since late sequelae of any oncological treatment are therapeutically difficult to influence and characterized by a progressive pattern in many cases (see below). Taken together, accurate staging is an essential precondition for a successful treatment

of cancer patients. Further input of diagnostic specialists may be provided during the routine radiation oncology workflow: Delineation of the macroscopic tumor (GTV) often requires additional advanced imaging modalities such as MRI or PET/CT and reaches beyond the normal anatomic information. As tumor imaging has been increasing in both the amount and the complexity of information, an in-depth knowledge of oncologic radiology has become more and more crucial in recent times. Furthermore, tumor tissue is often difficult to distinguish from normal tissue changes, for example, due to prior treatments or stromal reactions seen in infiltrating cancers, radiologic input may add to the precision in delineating the GTV. In summary, radiation therapy has become increasingly based on multimodal imaging, and oncologically trained diagnostic radiologists are increasingly important for the successful application of modern radiotherapy treatments (Terezakis et al. 2011).

## 2 Radiation Delivery Techniques

For radiologists it is important to consider not only the delivered overall dose for image interpretation of normal tissue changes but also the used treatment technique. This means that depending on the irradiation technique, a given specific overall dose may be distributed in normal tissues in completely different ways, and thus the organ exposure can vary significantly with consecutive different image presentations in the follow-up. Furthermore, it would be extremely helpful for radiologists if dose overlays from treatment planning software could be integrated into PACS workstations in the near future to achieve a higher degree of safety in image interpretation.

### 2.1 Traditional External-Beam Radiation Therapy (EBRT)

First, therapeutic applications of ionizing radiation started early after their discovery by Conrad Roentgen in 1895. For many decades, irradiation of cancerous tissues was performed with X-ray devices, which allowed only relatively low energy doses with peak doses near the entrance site of the beam. Thus, major drawbacks were dose-limiting radiation effects in skin and epidermis and the rapid decline of the depth-dose curve being unfavorable especially for the treatment of deep-seated local tumors.

It was only in the 1950s until high-energy linear accelerators were developed – a milestone for the specialty of radiation oncology. From the 1950s to the 1980s, radiation treatment was administered by the use of planar radiographs in two dimensions, which visualized osseous landmarks. These bony landmarks were used for delineation of radiation portals and localization of therapeutic targets. Depending on the tumor site, the number of beams used for radiotherapy ranged from two to six. However, treatment planning was limited by poor tumor visualization of mainly X-ray-based imaging methods and techniques available for radiation delivery (Purdy 2008; Bortfeld and Jeraj 2011).

### 2.2 Conformal Radiation Therapy

In the 1980s, cross-sectional imaging procedures (i.e., CT and MRI) entered clinical routine, which were essential for a more accurate delineation of cancerous tissues and risk structures. These advances in radiological imaging were fundamental for further progress in radiation oncology with development of computerized treatment planning and delivery systems that enabled an exquisite tailoring of 3D radiation dose distributions to the cancerous tissues (Bortfeld and Jeraj 2011). These 3D conformal dose applications were reached by the use of a larger number of lower-dose radiation beams aimed at the target volume from different directions (up to 10 beams) (Fig. 2). As a consequence, the low-dose exposition of healthy tissues was increased, but the amount of tissues receiving high doses was significantly decreased (Bortfeld and Jeraj 2011); thus, the dose in the tumor could be escalated, while the surrounding healthy tissues and organs at risk could be protected better than with traditional EBRT helping to increase the therapeutic ratio. Furthermore, dynamic multileaf collimators were developed and clinically established for more

precise shaping of radiation beams compared to the previously used lead blocks (Purdy 2008).

Modern conformal radiation therapy plans may also include intensity-modulated radiation therapy (i.e., IMRT) and stereotactic body radiation therapy (i.e., SBRT), which are described in the next two sections.

## 2.3 Intensity-Modulated Radiation Therapy (IMRT)

The mathematical basis of IMRT was developed in the early 1980s to address the problem of irradiation of complex-shaped tumors in close proximity to or within risk structures, for example, paraspinal tumors (Fig. 3). But it still took a while until theoretical knowledge was put into practice, with first IMRT treatments applied to patients in 1997. The concept of IMRT is based on two decisive pillars, which are inverse treatment planning and nonuniform photon intensities across each of several radiation beams – usually 5–9 in modern treatment plans (Brahme et al. 1982). In the pre-IMRT era, physical dose distribution was calculated by trial and error; this means by trying out different intensities and directions of radiation beams. IMRT, on the other hand, takes the abovementioned path of inverse treatment planning, that is, dose distribution is tailored exactly to the target volume at the beginning of the planning process. Subsequent modeling of the direction, contour, and intensity of each treatment beam follows this by computerized treatment planning systems. For this purpose, radiation beams are subdivided into many segments and subsegments (i.e., often more than 100), in which intensities can be specified independently of each other by the use of multiple overlapping field segments or moving collimator leaves. This enables reduction of the dose for a certain beam direction, if risk structures are included in the beam. However, this approach would result in underdosing of the target volume, if conventional radiation techniques were used (Fig. 4). In IMRT plans, the lack of dose in the target volume is compensated by additional dose through another beam (Sterzing et al. 2009; Paumier et al. 2011).

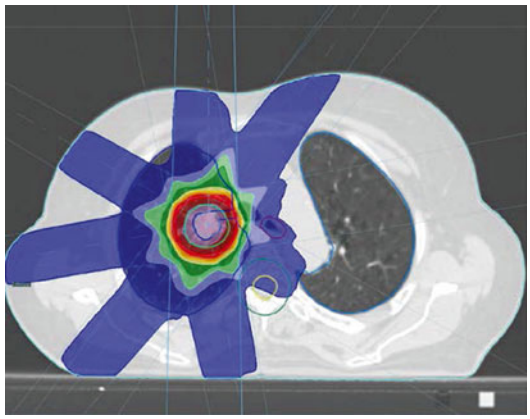

**Fig. 2** Dose distribution for primary irradiation of an NSCLC in the right upper lobe. The *purple-* and *red-colored* inner region represents the high-dose region. The *yellow*, *green*, and *blue* areas represent decreasing isodose lines towards the periphery

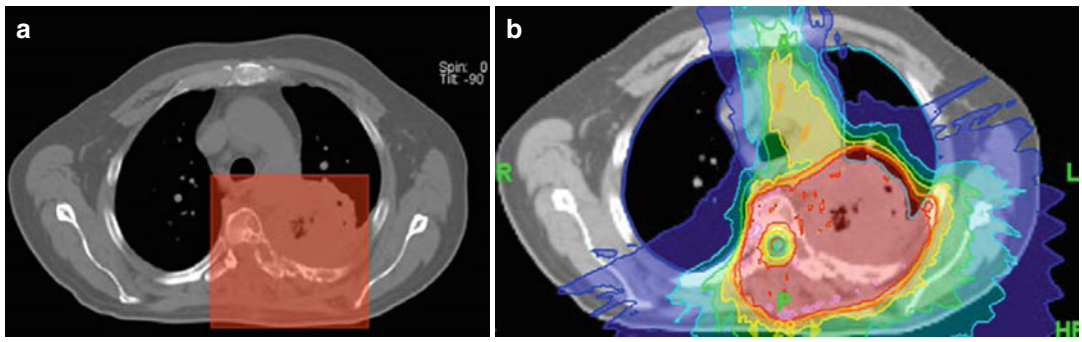


**Fig. 3** Presentation of a mass along the dorso-cranial thoracic wall left sided with infiltration of the paravertebral space, upper part of the thoracic spine and spinal canal in the planning CT (status post-laminectomy) (**a**). In IMRT plan (**b**) with depiction of steep dose gradients to the surrounding normal tissues and the **myelon** (*red* area represent high-dose area; *yellow*, *green*, and *blue* areas represent decreasing isodoses)

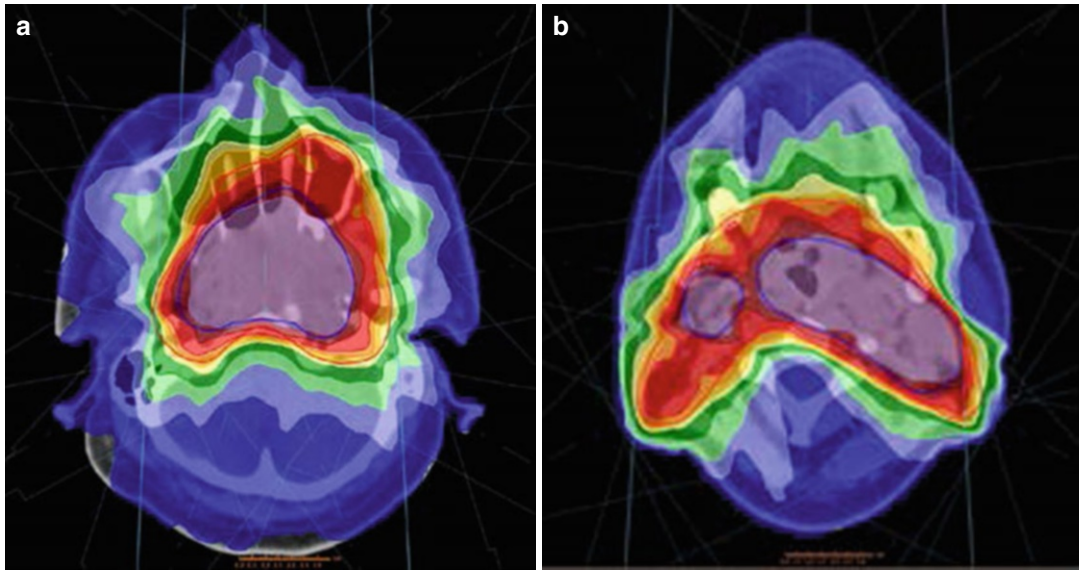


**Fig. 4** IMRT plan with 9 beams for irradiation of an advanced nasopharyngeal cancer with infiltration of the skull – note the *purple area* of dose distribution, which indicates the high-dose region encompassing the primary tumor and the steep dose gradients, which enables an excellent sparing of the adjacent brain stem (**a**). Same patient showing the integrated boost concept, that is, the primary tumor and lymph node metastases receive the boost (*purple-colored area*) and the cervical lymphatic pathways a slightly lower dose (*red-colored area*) to treat potential microscopic tumor deposits (**b**). The *yellow*, *green* and *blue* coloured areas indicate the decreasing isodoses towards the periphery

Taken together, accurate computation of an optimized dose distribution in IMRT makes it possible to apply a highly conformal radiation dose to tumors of complex shapes in the immediate vicinity of high-risk organs such as the optic nerve, the brain stem or spinal cord, the intestine, or the lungs without damaging healthy surrounding tissues. This implies that the high-dose region is smaller and the low-dose region is larger at IMRT than at 3D conformal radiation therapy (Purdy 2008; Paumier et al. 2011). However, the highly conformal nature of IMRT makes it more sensitive to geometric error, which was the rationale for development of image-guided radiation therapy (i.e., IGRT) techniques in order to ensure that radiation dose is delivered as planned (Perks et al. 2008; Boda-Heggemann et al. 2011; Sterzing et al. 2011).

## 2.4 Stereotactic Body Radiation Therapy (SBRT)

SBRT was pioneered in the 1980s and represents a special form of 3D conformal radiotherapy, which enables precise delivery of large single doses (in general, more than 3 Gy) in one or a just a few fractions to a confined area. Compared with other conformal radiation techniques, the advantage of SBRT lies mainly in maximization of tumor cell killing while minimizing the dose to the surrounding normal tissues (Kavanagh et al. 2011). Another advantage is shortening of the overall treatment time, which is more convenient for the patients.

However, safety and efficiency of this approach strongly depend on several factors such as adequate and very often multimodal treatment planning, accurate dose delivery, rigid immobilization, and/or regular image-guidance and dynamic-motion compensation methods.

The use of highly dose-intense or ablative treatment regimens imposes tough requirements on target delineation and definition of organs/structures at risk; thus, besides planning CT other imaging modalities like MRI or PET/CT are very often included into the planning process. Highly conformal dose distributions are achieved by the use of a large number of beams from various directions which are usually more narrowly

focused than those in 3D conformal and even IMRT plans for maximum protection of surrounding normal tissues and organs at risk (Debus et al. 1997; Terezakis et al. 2011) (Fig. 9b). Although this highly precise treatment approach can increase the therapeutic ratio, it also carries the risk of geometric miss either in treatment planning or during treatment due to positioning uncertainties or motion-related positioning changes (i.e., breathing, intestine peristalsis, vascular pulsation, or different fillings of adjacent hollow organs) with resulting insufficient dose coverage of the target lesion. As a consequence of this unfavorable case, there may be an increased risk for higher local recurrence rates and/or increased toxicities of adjacent normal tissues. Therefore, positioning uncertainties require localizing devices attached to either the patient or the treatment setup, dynamic-motion compensation methods, or immobilization devices as well as image guidance prior to treatment (Gademann et al. 1993; Boyd and Mehta 1999; Herfarth et al. 2004; Hof et al. 2007; Guckenberger et al. 2013).

## 2.5 Particle Therapy

Particle therapy is an emerging radiation technique that is available at an increasing but still small number of oncology centers. In general, protons and heavy ions such as carbon ions are used for their favorable physical and biological properties. The advantage of irradiation with charged particles compared to conventional radiotherapy with megavoltage X-rays (photons) is based on the completely different dose deposition in the penetrated tissues. While photons exhibit an exponential decrease of intensity with penetration depth, charged particles like protons or heavy ions deposit most of the energy with a pronounced sharp maximum at the end of their trajectory (the so-called Bragg peak) before a steep falloff in the dose deposition (Fig. 5). In this context, the initial energy level of these charged particles determines the penetration depth and the localization of the high-dose area (Bragg peak), respectively, and ensures a distinct distal margin with a narrow penumbra. Such "inverted" depth-dose profiles (Bragg curve) of charged particles represent a major advantage for the radiation therapy of deep-seated local tumors in comparison to conventional photon therapy (Fig. 6). The favorable dose profile is additionally enforced by an enhanced

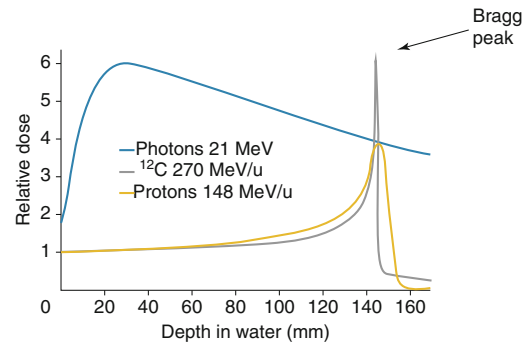


**Fig. 5** Depth-dose profiles of photons, protons, and carbon ions

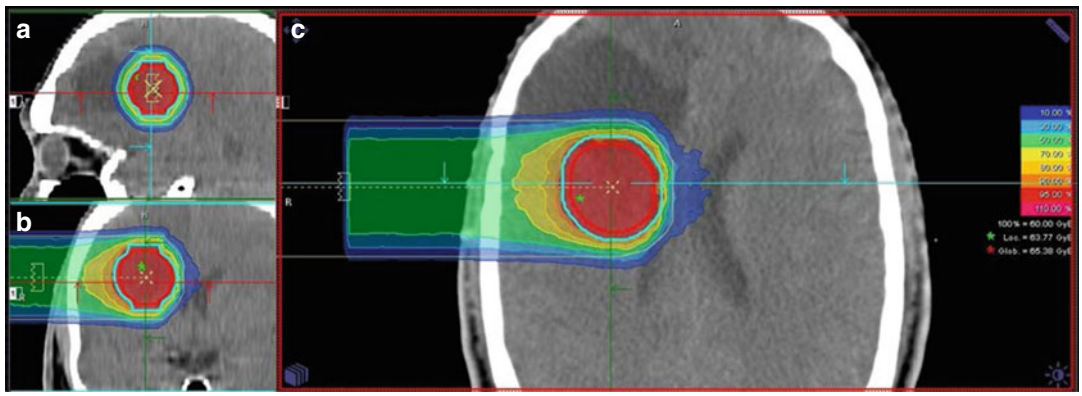


**Fig. 6** Sagittal (**a**), coronal (**b**) and transversal views (**c**) of the dose distribution for carbon ion therapy of a patient with recurrent glioblastoma in the right frontal lobe (Figure provided by courtesy of Dr. C. Vogt)

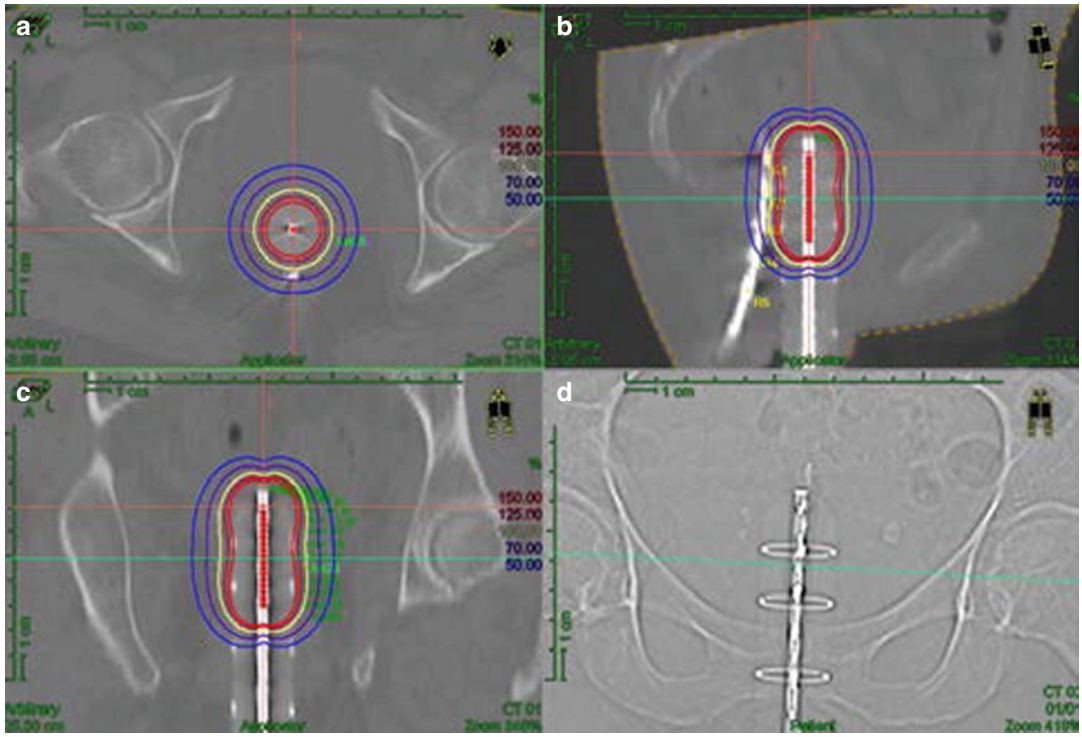


**Fig. 7** Planning CT in three dimensions (**a**–**c**) and an AP radiography (**d**) for brachytherapy of a cervical cancer with a regular positioned intravaginal applicator and narrowly confined dose distribution

relative biological effectiveness (RBE) of particles, likely due to the higher ionization density compared to photon irradiation.

Particle treatment is mostly used for tumors responding poorly to conventional photon treatment and tumors adjacent to critical radiosensitive anatomic structures (e.g., optic nerve, pituitary gland, eye, brain stem).

## 2.6 Brachytherapy

Brachytherapy describes internal irradiations of malignant lesions with a minimal distance between the radiation source and the cancerous tissue, which allows application of narrowly confined dose distributions. For this purpose, the radiation source has to be positioned within or nearby the tumor. The radioactive source releases high doses of radiation to local tissues over a known period of time, which is determined by the half-life of the used radionuclide. To guarantee the safety of the medical personnel, the irradiation is performed as afterloading therapy, that is, applicators in the form of metal or plastic needles or tubes are inserted as near as possible to the target lesion and secondary loaded with those small radioactive particles. In contact therapy, applicators are placed either directly on the skin or intracavital (Fig. 7). In contrast, interstitial treatments require an invasive implantation of the applicator(s) or radiation source carriers (i.e., studding the affected organ with tiny radioactive pins or permanent implants, the so-called seeds). Brachytherapy is commonly used in pelvic tumors (e.g., cervical and endometrial carcinoma and prostate cancer) but can be used for various other cancer sites. The main characteristic of brachytherapy is that radiation affects only a small confined area around the radiation source (Haie-Meder et al. 2011). Thus, radiation exposure of healthy tissues lying distant to the radiation source is minimized and much lower than in EBRT. This significantly reduces the normal tissue complication probability.

## 3 Radiation Biology: A Refresher

The effect of ionizing radiation on tissue is predominantly due to deoxyribonucleic acid (DNA) damage as a result of absorption of radiation energy, even though damage to other cellular structures such as membranes may also play an important role. This accounts for tumor tissue as well as the surrounding normal tissue. The toxicity of ionizing radiation on DNA is based either on direct deposition of radiation energy to the strands or by ionizing intracellular water molecules, which leads to the creation of hydroxyl radicals with consecutive damage of DNA and other cellular structures (Mahaney et al. 2009). This latter effect is enhanced in the presence of oxygen leading to production of more free radicals that promote genetic damage (the so-called oxygen effect) (Gray 1957).

DNA double-strand breaks are considered the main toxic lesion by which ionization radiation kills cell*s* (Goodhead 1994). As a consequence, repair pathways are initiated leading to rapid and accurate repair of such DNA lesions in most cases (Helleday et al. 2007, 2008). However, if such lesions remain unrepaired, they may lead to cell death and in the case of misrepair to mutations and genetic instability, potentially leading to carcinogenesis (Hall 2006). Additionally, repopulation of surviving cells may compensate for cell kills by ionizing radiation. Normal tissue is believed to be generally more resistant to ionizing radiation compared to most cancers.

Radiosensitivity strongly depends on tissue specifications, which is the cause for different reactions to irradiation. Nondividing and slowly proliferating tissues and cells are commonly able to tolerate higher radiation doses. If cellular damage exceeds repair capacities of affected cells, DNA mutations accumulate, and cells either stop dividing due to apoptosis or cellular senescence or become tumorigenic.

Generally, the balancing act between tumor cell destruction and normal tissue complications in radiotherapy is described by the term "therapeutic index," which defines the ratio of tumor control probability to normal tissue complication probability. To increase the therapeutic index, it is advantageous to divide the total dose into multiple small fractions when extended volumes of normal tissues are included in the PTV. In the daily routine, application of small single radiation doses (i.e., 1.8–2.0 Gy per day, five times per week) has proven to be practical, especially in curatively intended radiation treatments, allowing many of the critical tissue structures and organs (e.g., lungs, kidneys, heart, spinal cord) to recover relatively better than cancerous tissues (Thames et al. 1982). In the optimal case, the intervals between doses allow normal tissues to recover, while the tumor cells succumb to repeated insults. In contrast, organs and tissue types with rapid cell turnover including the hematopoietic system, mucosal tissue, or epithelia of the skin react much earlier to irradiation due to cell depletion (Rubin and Casarett 1968). To a certain degree, such radiation effects can be compensated by increased proliferation of surviving stem cells in the affected tissue complex (i.e., repopulation). This mechanism of repopulation is also found in most of malignant tumors. Since excessive fractionation results in prolongation of the treatment course, locoregional tumor control may be compromised due to tumor cell repopulation.

In general, cell killing with radiation has a nonlinear relationship with fraction size such that a course of radiation therapy given in a smaller number of large fractions is more damaging than the same total dose given in a larger number of smaller fractions (Terezakis et al. 2011). This is the rationale for hypofractionated radiotherapy, which uses higher radiation doses per fraction than conventional fractionated treatment regimes in a shortened overall treatment time (mostly more than 3 Gy in a few treatment sessions). In the clinical setting, the application of such hypofractionated radiations is suitable for palliative situations but also for stereotactic radiotherapy of single organ lesions. While treatment effect of conventional fractionated therapy regimes is based on difference of repair capabilities and damage recovery between normal and cancerous cells, the therapeutic effect of hypofractionated radiotherapy is dependent solely on high

precision. This implies that all cells included in the PTV have a much higher risk to be killed with the latter approach, irrespective of whether or not they are malignant. Thus, repopulation cannot take place anymore when hypofractionation is used as long as the administered radiation dose is high enough to guarantee complete destruction of all cancerous cell clones within the target volume. It is a fundamental requirement for this therapeutic approach using very sharp centrifugal dose gradients to ensure on the one hand induction of tumor necrosis, while on the other hand healthy tissues around the tumor remain largely unscathed.

Furthermore, depending on the irradiated tissue type, the severity of radiation-induced injury and nature of tissue response vary. It is a well-known fact that actively regenerating tissues are most sensitive to genetic damage after irradiation. In this context, the radiosensitivity of tissues depends both on inherent characteristics of cells, with the most important being the cell division rate and degree of differentiation, and on conditional factors including treatment parameters such as type of radiation, mode of delivery, total dose, and fractionation. Consequently, multipotent or pluripotent cells with a high mitotic rate and a long mitotic future are the most radiosensitive (Rubin and Casarett 1968).

The predominant radiation-induced late effects are characterized by the following:

- *Atrophy of epithelial tissues* including parenchymal and glandular organs
- *Fibrosis of stromal tissues*
- *Sclerosis of blood vessels* (Fajardo 2005)

These general parenchymal reactions will be described in detail in the following sections.

# 4 Basics of Radiation Effects of Normal Tissues

## 4.1 Classification of Radiation Effects

Depending on the time course of pathological changes, that is, the time of first diagnosis, *early (acute)* and *late (chronic) reactions* of normal tissues should be differentiated when radiotherapy is performed. Early effects occur typically during or shortly after therapeutic irradiation when an organ-specific threshold dose has been exceeded, while late effects manifest after a latent period that may last several months up to many years. By definition, early effects occur *within the first 90 days* after the start of radiation treatment; accordingly, all treatment-related tissue changes including related clinical symptoms as well as imaging, laboratory, and histologic findings afterward are classified as late side effects.

## 4.2 Radiobiological Characteristics of Early and Late Radiation Effects

Early reactions due to radiation treatments usually manifest in tissues with a rapid cell turnover such as the epidermis, mucosae of the upper and lower intestinal tract, or bone marrow, in which permanent cell loss is compensated by high proliferation activity of the germinal cell compartment. While under normal conditions there is a perfectly regulated equilibrium between permanent cell loss of the functional compartment and cell production in the germinal compartment, therapeutic irradiations lead to an imbalance concerning the cell numbers in those tissues through impairment of cell production in the face of ongoing physiological cell loss (Dorr 2009). As a consequence, progressive cell depletion finally causes loss of tissue integrity, which may be complicated by secondary infections. After completion of radiotherapy, acute tissue injury usually completely heals within a few weeks through proliferation of surviving stem cell clones within the irradiated volume or migration of stem cells into the radiation field from not irradiated tissues.

In contrast to that relative simple pathogenic reaction of rapid turnover tissues based on cell depletion as the leading mechanism, late reactions can occur in all organs and are much more variable and complex. The decisive pathological processes take place not only in the organ parenchyma but also in the connective tissue and the supplying blood vessels (Dorr et al. 2013). Usually, these underlying tissue changes are accompanied by affection of the immune system

(macrophages, mast cells). The relevance of these various tissue components for the development of chronic radiation reactions can be different for each organ system. Furthermore, late effects are not reversible and in most cases even progressive, with increasing severity occurring with longer follow-up times (Dorr 2009). In general, the risk for development of chronic radiation effects persists throughout the rest of patient's life and can be increased when re-irradiation is performed or other toxicants negatively affect the tissue in the following time (Jung et al. 2001).

## 4.3 Consequential Late Effects (CLE)

Early and late radiation reactions are independent from each other with regard to their pathogenesis. Thus, in general it is not possible to draw conclusions from the severity and duration of early radiogenic tissue damage on manifestation and extent of late toxicities in the same organ. However, as an exception to this rule, in some specific situations late effects can be strongly influenced by moderate or severe early effects within the same organ, resulting in the so-called consequential late effects (CLE) (Dorr and Hendry 2001). Typically, CLE arise when the early reaction is associated with collapse of integrity of epithelial tissues respectively protecting function against mechanical and/or chemical stress. This may result in an additional acute trauma of the underlying tissues (i.e., organ parenchyma, connective tissues, blood vessels) that further modulate the extent and course of late sequelae in the same organ. Therefore, CLE are mainly found in the draining urinary tract, intestinal system, lungs, oral and pharyngeal mucosa, and severely stressed areas of skin (Dorr and Hendry 2001; Dorr et al. 2005).

## 4.4 Cellular Basis of Radiation Effects

Regarding cancerous tissues, the sterilization of malignant cell clones is the main pathogenetic reaction that determines tumor response to irradiation. This means that malignant cell clones lose their ability to proliferate and finally die after a preset time. In rapid turnover tissues, the severity and duration of early radiation effects are mainly determined by the extent of cell depletion and associated complications such as secondary infections (see below).

In contrast, the mechanisms of late radiation sequelae have not yet been fully elucidated. The available studies indicate that radio-induced modifications of various cellular functions dominate toward antiproliferative effects of irradiation.

## 4.5 Tolerance Dose Concept

For many decades, the selection of radiation fields and doses depended only on empirical knowledge. When 3D-conformal RT was introduced into the clinical routine, there was a great need for guidelines taking the quantitative correlates of doses/volumes and clinical outcome into account. As a response to this issue, Emami et al. published in 1991 a landmark paper that introduced a mathematical model for partial organ tolerance doses (TDs), providing useful guidance for physicians in treatment planning (Emami et al. 1991). This TD concept proved to be crucial for radio-oncologists and physicists because it helped to predict or estimate the probability of severe treatment-related tissue complications within a defined period of time. In this context, the definitions "TD 5/5" and "TD 50/5" refer to a time interval of 5 years following irradiation and determine tolerance doses that lead to severe complications in 5 or 50 % of the patient population. Tolerance doses have been shown to be organ specific: TDs of the so-called "parallelly structured" organs, consisting of different independent functional units (e.g., the lung, liver, or salivary glands), are usually defined by the maximum dose of a defined sub-volume. In contrast, TDs of "serially structured" organs, where the function of one subsegment cannot compensate for that of others (e.g.,myelon or intestines), consider the maximum dose to any part.

In 2009, the Emami guidelines were updated and refined by the QUANTEC (Quantitative Analysis of Normal Tissue Effects in the Clinic)

data based on increasing numbers of studies dealing with 3D dosimetry, related side effects, and selection of appropriate statistical methods for a better prediction of the normal tissue complication probability (NTCP) (Bentzen et al. 2010; Marks et al. 2010).

## 4.6 Classification Systems

For evaluation of different oncological treatment concepts, the occurrence and degree of severity of side effects represent one of the most important criteria, which therefore has to be considered besides the known endpoints like tumor remission rate, survival, and quality of life. For complete and accurate reporting of side effects, all relevant systemic and organ-specific parameters have to be assessed prospectively and regularly, that is, before, during, and after treatment. Therefore, it is necessary to conduct a thorough anamnesis and an extensive physical examination besides regular laboratory tests and imaging procedures in certain time intervals (such as X-ray, CT, MRI, and nuclear medicine procedures). The time intervals for clinical examination depend on if early or late reactions are assessed. Early radiation effects may develop and deteriorate in a short period of time, which requires close clinical assessment. For example, radiation dermatitis can change from a slight erythema response to moist desquamation over just a few days. In addition, mechanical or chemical stress (e.g., tight clothing, excessive sweating in the skin folds) or superinfections may worsen those skin reactions. Thus, early reactions should be assessed at least weekly during and shortly after radiotherapy to initiate appropriate measures.

In contrast, late sequelae develop slowly over months up to years and are usually irreversible. Hence, clinical assessment with time intervals of several months after the end of radiotherapy is sufficient enough to document late effects. At a later time, the intervals may be extended to annual intervals. The fact that radiation effects (e.g., secondary tumor) may manifest even after several decades explains why follow-up examinations should be maintained for the rest of patient's life.

Up to now, several standardized classification systems have been established for reporting of normal tissue reactions due to oncological treatments (e.g., WHO, RTOG/EORTC, or CTCAE; see below). In this regard, it is important to consider which classification system and, if modified, which version has been utilized for assessment of normal tissue reactions to ensure comparability between institutions, studies, and investigators.

In general, complications are graded from 0 (no change) to 5 (death related to adverse effect), as described in the following:

- *Grade 1 reaction (mild)*: Reversible, healing spontaneously; no specific treatment or interruption of cancer therapy necessary
- *Grade 2 reaction (moderate)*: Require specific treatment on an outpatient basis; no dose reduction or interruption of cancer treatment necessary
- *Grade 3 reaction (severe)*: Require hospitalization and intense supportive care; if necessary, dose reduction or interruption of oncological treatment
- *Grade 4 reaction (life-threatening)*: Life-threatening condition, immediate hospitalization and intensive care required; discontinuation of therapy
- *Grade 5 reaction (death)*: Death related to side effect

The most widely used classification systems for documentation of normal tissue reactions are the following:

- *WHO* (World Health Organization) classification, which was established in 1979; initially only adapted to chemotherapy-related side effects.
- *RTOG/EORTC* classification, jointly developed by the Radiation Therapy Oncology Group and European Organisation for Research and Treatment of Cancer in the mid-1980s; specifically adapted to radiation treatment effects.
- *CTCAE* (Common Terminology Criteria for Adverse Events) classification, developed by the National Cancer Institute (NCI) and established in 2003 (originally derived from the CTC criteria) – the recent CTCAE version 4

**Table 1** Comparison of two frequently used classification systems for documentation of side effects, with an example for radiation pneumonitis

| Grade | General | CTCAE v4 | RTOG/EORTC |
|---|---|---|---|
| 0 | No change | No change | No change |
| 1 | Mild | Asymptomatic; clinical or diagnostic observations only; interventions not indicated | Mild symptoms of dry cough or dyspnea on exertion |
| 2 | Moderate | Symptomatic; medical intervention indicated; limiting instrumental activities of daily living (ADL) | Persistent cough requiring narcotic, antitussive agents/dyspnea with minimal effort but not at rest |
| 3 | Severe | Severe symptoms; limiting self-care ADL; oxygen indicated | Severe cough unresponsive to narcotic antitussive agent or dyspnea at rest/ clinical or radiologic evidence of acute pneumonitis/intermittent oxygen or steroids may be required |
| 4 | Life-threatening | Life-threatening respiratory compromise; urgent intervention indicated (e.g., tracheotomy or intubation) | Severe respiratory insufficiency/ continuous oxygen or assisted ventilation |
| 5 | Death related to side effect | Death | Death |

*CTCAE v4* the Common Terminology Criteria for Adverse Events, version 4, *RTOG/EORTC* Radiation Therapy Oncology Group and the European Organisation for Research and Treatment of Cancer

was published in 2009; all oncological treatments are considered.

- *LENT/SOMA* system (Late Effects of Normal Tissues/Subjective, Objective, Management and Analytic categories), developed by the NCI in the mid-1990s to assess specifically late sequelae of cancer treatments; therefore, sum scores that comprise subjective symptoms of the patient (S), objective clinical findings (O), therapeutic demands (M), and objective results of special examinations such as CT or MR scans, ECG, or lung function testing (A) are taken into account for an accurate assessment; all oncological treatments are considered.

In principle, all of these classification systems are largely comparable with each other; hence, translation of the scores from one system into the scores of another one is mostly possible without any loss of information (Table 1) but with exceptions (Dorr 2009). This translation cannot be recommended particularly for the LENT/SOMA scale, because the subjective component (symptoms) as part of the sum scores would be lost.

## 5 Early Radiation Effects

### 5.1 Pattern of Cell Divisions in Early-Reacting Tissues

Early radiation-related side effects may arise principally in every organ, but, as noted above, the majority of those reactions manifests in tissues with a rapid cell turnover (epithelia, oropharyngeal and gastrointestinal mucosa, hematopoietic system). It is a common characteristic of all of these early-reacting tissues (the so-called H-type tissues) that proliferation follows a hierarchic structure whereby stem cells and transit cells determine proliferation and highly differentiated, postmitotic cells maintain the normal function of those tissues. In this context, the generation of new cells takes place entirely in the germinative tissue layers, that is, the basal and suprabasal epithelial layers of oral mucosa, intestinal crypts, and bone marrow sinuses.

The balance between cell production in the germinal compartment and permanent cell loss from the functional compartment is based on the

pattern of the stem cell divisions. These cells divide usually asymmetrical into two different daughter cells, namely, one bigger stem cell and one smaller transit cell. The latter is also able to perform cell proliferation to a limited extent, which increases the number of cells per stem cell division (i.e., amplification). The resulting transit cells finally further differentiate and mature into postmitotic, functional cells in order to fulfill their specific tasks in the tissue complex before they die after a biologically predetermined period of time. In this context, it is assumed that cell renewal is regulated by the total number of functional cells in the meaning of a feedback loop mechanism (Dorr 2009). Furthermore, an influence of the stem cell counts seems to autoregulate the proliferation additionally (Paulus et al. 1992). The temporal course of acute radiation reactions is determined by the turnover time of irradiated tissues, that is, the time, in which all existing tissue cells at a certain point in time are completely replaced by new cells.

## 5.2 Pathogenesis of Early Radiation Reactions

In general, early radiation reactions of H-type tissues usually follow a fixed pattern of pathological changes, which can be differentiated in the following four components:

- Inflammatory and vascular reaction
- Cell depletion (main reaction)
- Secondary effects such as infections
- Healing period

The *initial phase* is determined by an inflammatoric reaction and vascular reaction disorder that both are initiated after only a few fractions in the setting of conventional fractionated radiotherapy. This reaction is mainly based on enhanced expression of pro-inflammatory proteins and cytokines (e.g., IL-1a, TNF-a, COX-2, etc.) in different cell populations (e.g., macrophages, endothelial and parenchyma cells) and functional disorders of vessel innervation. In addition, the activity of the inducible nitric oxide synthase (iNOS) can be stimulated with secondary cytotoxic effects (Rubin et al. 1995). The increased release of these cytokines acts locally either on surrounding other cells (paracrine) or on the releasing cells itself (autocrine) or systematically (endocrine), with further modulation of cytoplasmic, nuclear, and interstitial events. Provoked dysregulation of the cellular environment finally leads either to immediate cell death or alterations of cell receptor and gene expression with, for example, increased production of iNOS and various growth and inhibitory factors (Dittmann et al. 2005). However, the key signal cascades underlying these modulations of cellular tissue reactions have not yet been elucidated. Furthermore, it is still unclear which role these initial pathogenetic changes play for the following phases of acute radiation reactions and initiation of late sequelae. As a clinical correlate of these complex initial tissue changes, vessel dilatation and a more or less pronounced capillary leak syndrome (i.e., proteins or even cellular components leak from the vascular space to the interstitium) are seen, which, under unfavorable conditions, may result in deterioration of organ functions (e.g., brain, lungs, liver, kidneys). Consequently, erythema and edema develop in a variable extent of degree (Fig. 8). Furthermore, pain sensations in the irradiated volume may be triggered by the inflammatoric tissue changes.

The *second phase* is clinically the most important one and determined by cell depletion of tissue-specific stem cells. Lethal effects due to irradiation are mainly seen in the stem cell population, since the radiosensitivity of the other cell compartments decreases during the differentiation process. This fact is of utmost importance for the severity of early reactions, because stem cells form the basis for cell renewal as they represent the only cell population being able to reconstitute the integrity and correct function of the corresponding tissue structure after acute tissue damage (Dorr 2009). Thus, the stem cell population determines the tissue-specific radiation tolerance dose by its cell numbers and intrinsic radiation sensitivity. In parallel to irradiation-induced cell death in the compartments of stem cells and transit cells, differentiation process of transit cells to functional cells and loss of functional cells continues with the physiological rate regardless of

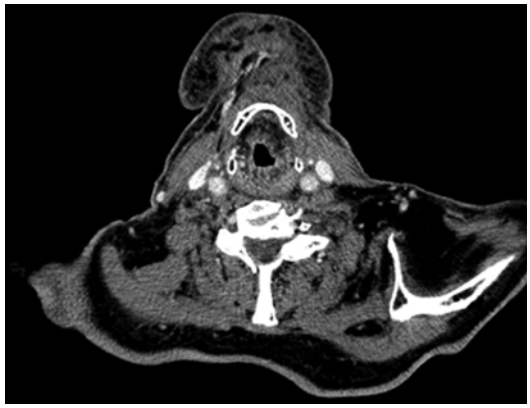

**Fig. 8** Typical edema of the hypopharyngeal mucosa and submental lymph edema 6 weeks after irradiation of an oropharyngeal cancer (Figure provided by courtesy of Dr. T. Welzel)

the irradiation. Finally, tissue hypoplasia develops with collapse of tissue integrity and associated clinical effects (e.g., moist desquamation, severe dysphagia, diarrhea), if a certain threshold is exceeded, whereby the severity of those effects depends on the applied doses. In the case of low radiation exposure, for example, the tissue hypoplasia can be only marginally impaired, so that no or just mild clinical effects are evident. However, the clinical consequences only manifest after a latency period, which is mainly determined by the turnover time of the corresponding tissues. Thus, the latency period until clinical manifestation of acute normal tissue reactions is not dose dependent, but rather tissue specific. However, there are major differences regarding the turnover time of tissues with a range between a few days like the epithelia of the gastrointestinal tract and several months like the urothelia in the bladder.

The *third phase* includes secondary effects due to collapse of normal epithelial structure (tissue hypoplasia), which normally constitutes a protective barrier function against mechanical and/or chemical stress. Clinically, this hypoplasia is seen as leukopenia or epidermal and mucosal epitheliolysis. This situation is often complicated by secondary infections, which either aggravate the local epithelial damage or lead to extensive infections that can even progress into septicemia with worsening of preexisting or additional clinical symptoms (e.g., pain, fever, dysphagia, dyspnea, etc.).

Furthermore, additional toxicants can significantly enhance these early reactions. This applies, particularly, for chemotherapy. Moreover, in epithelial tissues, mechanical exposure can influence early complications, such as epidermal irritation by clothing or in skin folds or oral mucosa trauma through dental prostheses or sharp-edged food components. Similarly, in oral mucosa, chemical stress such as alcohol, smoking, or spicy diet can enhance the tissue injury. In addition, secondary traumata can impact on the target structures of the late sequelae (blood vessels, connective tissue) that may aggravate the late radiation effects (the so-called consequential late effects, CLE; see above).

Finally, the *fourth phase* is determined by complete healing after radiotherapy within a few weeks, with the only exception for pronounced early reactions that result in defect situations such as ulcerations, local and systemic infections, extended scar formations, and other secondary complications. The healing process is provided by stem cells that either survived within the irradiated volume or migrated into the radiation field from the circulation (bone marrow cells) or from the margins (skin, oropharyngeal and gastrointestinal mucosa) to reconstruct the regular cell numbers and reconstitute the integrity and correct function of the tissue structure.

## 6 Chronic Radiation Effects

### 6.1 Concepts of Radiation Pathophysiology

Until today, classic concepts of radiation pathophysiology remain valid to describe late reactions in normal tissues (Michalowski 1981; Hendry and Thames 1986). More specifically, the traditional model for late effects differentiates two basic concepts that are based on either a cellular or functional approach to explain organ changes after irradiation. Both concepts require an appreciation of the relationship between the observed therapy-induced

clinical and subclinical adverse effects and the inherent structure of the organs at risk (Constine 2013). Therefore, the target cells in the organ (e.g., parenchymal, vascular), the structural organization of the functional subunits (parallel or in series), and the distribution of function (homogeneous or inhomogeneous) are highly relevant.

The *cellular concept* allocates chronic radiation sequelae generally to those tissues that are characterized by a flexible organization (the so-called F-type tissues), such as the kidney or liver. Thus, clinical manifestation of chronic side effects in F-type tissues is supposed to be dependent on a defined reduction of functional parenchyma cells below a certain threshold, exactly as in the case of H-type tissues (see above). Furthermore, these tissues do not allow clear distinction between proliferative and functional cells, in contrast to rapid turnover tissues. Rather, if required, functional cells are recruited into the proliferative cell compartment (or vice versa). The compensatory proliferation of the surviving, formerly functional cells finally results in mitotic cell death, which accelerates cell loss and consecutive impairment of the organ function. Until then, doomed but morphologically and physiologically intact cells are still capable of fulfilling their specific functions in the tissue. Hence, tissues with low division activities may also be sensitive to radiation, but in contrast to H-type tissues the organ injury manifests very late (after several months up to many years). This applies, for example, to the vascular endothelium, which provides a major contribution to the development of chronic sequelae of radiation (see below). Furthermore, the initial degree of cell depletion depends on the administered radiation dose and determines the characteristic (severity) of the following tissue effects. In other words, the higher the dose, the more clinical manifest tissue effects are seen after a certain latency period.

The *functional concept*, on the other hand, assumes that in late-responding tissues structures with stem cell-like characteristics, the so-called tissue-rescuing units (TRU), exist (Hendry and Thames 1986). Thus, an inactivation of these specific cells may lead to clinical manifestation of chronic radiation sequelae in the affected tissues and organs. This mechanism is also dose dependent, that is, both the severity of the tissue changes and the latency period until manifestation correlate with the radiation dose.

## 6.2 General Pathogenesis of Chronic Radiation Effects

The pathogenesis of late radiation sequelae is far more complex than the pathogenesis in early radiation effects. As already noted above, the following cell compartments trigger the underlying pathogenetic process:

- Epithelial tissues and organ parenchyma (e.g., pneumocytes of the lung, hepatocytes of the liver, neurons and glia cells of the central nervous system)
- Connective tissue (fibroblasts, increased collagen formation)
- Vascular system (mainly the capillary and small arterial vessels)
- Unspecific immune system

For different organs, the relevance of these different pathogenetic components may vary. In the liver, for example, parenchyma cells (hepatocytes) contribute only a minor part to the tissue changes after irradiation (i.e., veno-occlusive disease). In the lung, the vessels and connective (fibroblasts) and parenchymal tissues (particularly type II pneumocytes) seem to contribute similarly to development of treatment-related lung fibrosis. In contrast, late fibrotic changes in the bladder are secondary to the functional impairment, which is predominantly based on urothelial and endothelial changes and is not primarily radiation induced (Dorr 2009).

## 6.3 Dose Dependency of the Latency Period

The dose dependency of the latency period until manifestation of chronic radiation sequelae can be explained based on the underlying different organ and tissue reactions: On the one hand, higher doses cause more severe vascular damage with consecutive malnutrition of the downstream parenchyma (see below), and on the other hand,

more fibroblasts differentiate into postmitotic fibrocytes with increased synthesis and deposition of collagen in the irradiated tissues with consecutive impairment of the organ function (see below). Furthermore, these tissue and organ changes take place in a shorter period of time with increasing doses. Thus, induced parenchymal damage contributes to an organ-specific functional collapse, and in this context the latency period until clinical manifestation as well as the progression rate underlies a dose-dependent relationship. This means that with longer follow-up times more side effects are seen, even in patients with low radiation exposure (Dorr 2009).

## 6.4 Chronic Radiation Effects in the Vascular System

The most important radiation effect in the vascular system is the *progressive loss of small vessels* (particularly capillaries and arterioles), which often affects the organ function by decreased perfusion with insufficient supply of oxygen and nutrients (Fajardo 2005). In this regard, capillary endothelial cells seem to be of central importance for the vascular injury after irradiation with the consequence of disorders in the cellular function such as changes of the enzyme content that further triggers the depletion of small vessels. This vessel rarefication is generally regarded as an organ-unspecific, but pathognomonic reaction to irradiation. The cell cycle length of endothelial cells lasts about 1–3 months, which explains why capillary depletion manifests very late, typically as late effect. In arterioles, the main radiation effect is *progressive intimal fibrosis and sclerosis of the media layer*, which contributes (in addition to the capillary depletion) to the insufficient supply of the downstream parenchyma. As a consequence, deteriorated vascularization finally results in atrophy of the depending parenchyma. However, there are distinct differences regarding the morphological and functional consequences of such atrophy between the organs (Schultz-Hector 1992; Dorr 2009). Another sign of chronic sequelae of radiation is *telangiectasia* (i.e., pathologically dilated capillaries), which can be interpreted as regeneration of destroyed capillaries that typically occur in high-dose irradiated tissues and organs (Bentzen et al. 1990; Turesson 1990). In the skin, their occurrence may lead to cosmetic problems for the patients, while in other organs, such as the brain, retina, and mucous membranes of the gastrointestinal tract, small bleedings may complicate the further clinical course.

In general, radiation-induced vessel changes are predominantly confined to small- and medium-sized arteries and not equally distributed within a defined volume of irradiation, but rather focally despite radiation exposure of all small vessels in the same way. In contrast, large arteries and veins are less often affected by irradiation than the smaller vessels (Fajardo 2005).

In summary, the following radiation-induced main effects can be detected either based on histologic or clinical examinations in the arterial system:

- Initially, functional disorder of the vessel innervation and release of cytokines which lead to arterial vessel dilatation (*skin erythema*) – a typical early effect occurring during and shortly after irradiation (see Sect. 5.2).
- Additionally, it follows an increase of capillary permeability with exudation of plasma into the interstitium through impairment of the blood-tissue barrier (*edema*).
- In some cases, increased fragility of vessels with loss of cellular elements into the extracellular space (*hematoma, spontaneous bleedings*), occasionally occurring as life-threatening arterial perforation.
- Capillary depletion (*reduced perfusion*) with secondary ischemia and resulting impairment of the organ function, typically a late effect (see above) (Fig. 9).
- Telangiectasia (see above).
- Progressive intimal fibrosis and sclerosis of the tunica media that results in atherosclerotic remodeling of the vessel wall of predominantly small- and medium-sized arteries (*obliterating arteriopathy*) as well as occlusive thrombosis (*ischemia*).
- In rare cases, active arteritis within the radiation field with lymphocytic infiltrates localized generally in the tunica media and adventitia.

As noted above, veins are generally less often affected by irradiation than their arterial counterparts, whereas the radiation sensitivity seems to decrease with increasing size. Nevertheless, hyaline degeneration of the vessel wall may develop particularly in small veins after radiation exposure. Furthermore, the affected veins have an increased risk of vein thrombosis. The most widely known venous lesions occur as focal reactions after irradiation of the liver in terms of a veno-occlusive disease (VOD) – an imaging pattern often seen by radiologists in the follow-up, which has to be differentiated from recurrent tumor (Herfarth et al. 2003) (Fig. 10).

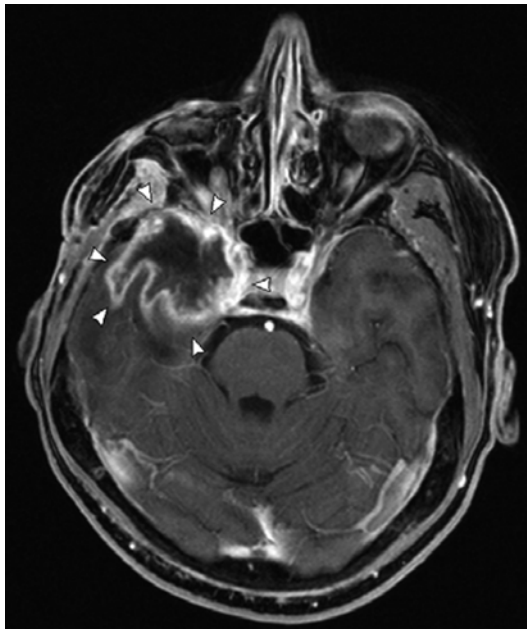

**Fig. 9** Extensive radiation necrosis (indicated by the *arrow heads*) in the right temporal lobe 6 months after re-irradiation of recurrent meningioma localized at the right wing of the sphenoid bone

## 6.5 Chronic Radiation Effects in the Mesenchymal Tissues

In modern radiotherapy, radiogenic changes of the connective tissues, particularly in the form of subcutaneous reactive fibroses, are the most common chronic side effect seen in follow-up examinations. In this regard, the term *reactive fibrosis* has to be differentiated from *reparative fibrosis or scarring*. The latter fibrotic type accompanies tissue defects, for example, radiation-induced skin ulcerations. The reactive fibrosis, in contrast, is a primarily radiation-induced tissue reaction, and moreover it is a dominating effect, which may occur practically in all tissues and organs (Fig. 11). The only organs and tissue structures where fibrosis is usually not seen are the central nervous system, the lenses, and the hemopoietic bone marrow unless a neoplasm or an inflammatory lesion had been present prior to irradiation. In addition, the supporting and connective tissues of

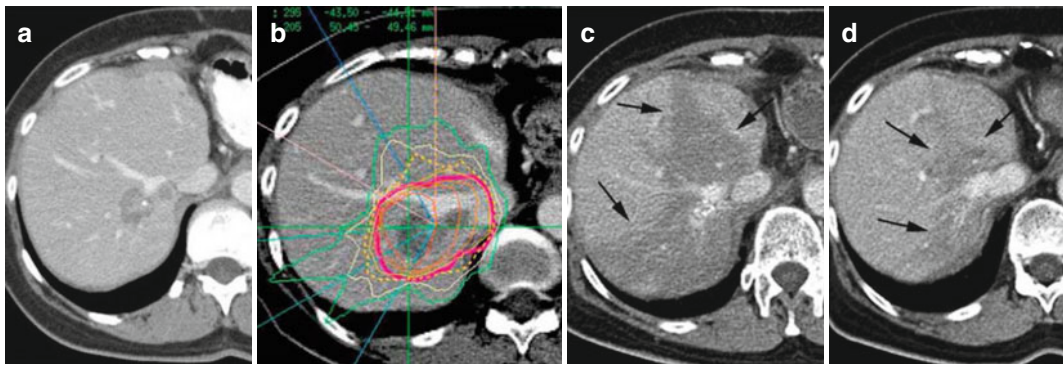


**Fig. 10** Colorectal cancer metastatic to liver with recurrence of a centrally located lesion after partial liver resection. The metastasis was stereotactically irradiated with 37.5 Gy in 3 fractions related to the 65 % isodose line (**a**), which is indicated with the *dotted line* in (**b**). In the follow-up after 2 months, the liver metastasis completely disappeared, and a focal reaction occurs instead (**c**; *arrows*). Recurrent radiation reaction after 6 months (**d**), no relapse of the irradiated metastasis (Figure provided by courtesy of Prof. Dr. K. Herfarth)

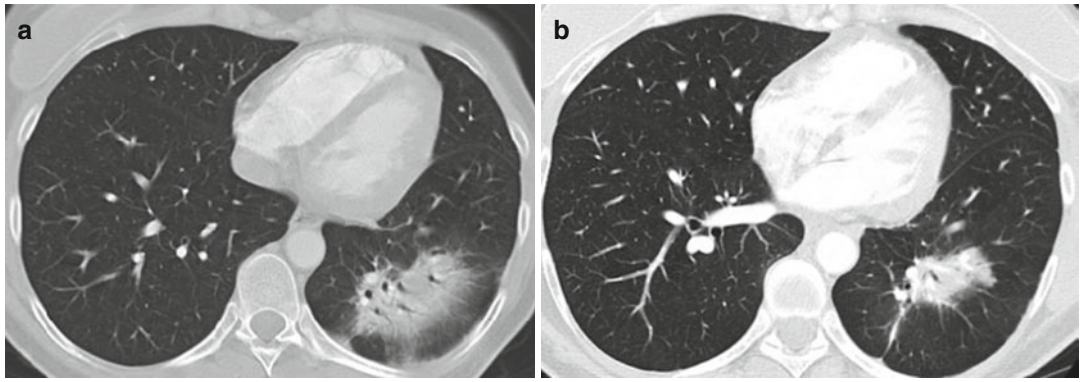


**Fig. 11** CT scan of the lung 4 (**a**) and 23 months (**b**) after stereotactic irradiation of a lung carcinoma in the left lower lobe. Demarcation of a diffuse opacification of the irradiated lung parts with a positive air bronchogram in terms of a typical radiation pneumonitis. The lung carcinoma cannot be differentiated anymore. In the further course, the extension of the tissue reaction decreases, and the bronchi and vessels in proximity are slightly distorted as imaging correlates for a transition of radiogenic pneumonitis into a scarring tissue reaction (Figure provided by courtesy of PD Dr. H. Hof)

children are much more sensitive to irradiation than in adults which may represent with growth disorders of the bone, cartilage, and soft tissues. In contrast, the supporting tissues of adults are relatively resistant to irradiation. The underlying pathophysiological mechanism of reactive fibrosis due to irradiation is based on stimulation of the differentiation of fibroblasts into fibrocytes, with the consequence of substantially increased collagen synthesis and deposition, which finally affects organ function (Rodemann and Bamberg 1995; Dorr 2009). These reactive fibrotic changes are characterized by a lack of cells and capillaries and formation of a tight collagenic fiber matrix. Moreover, the abovementioned vascular radiation damage maintains and stimulates this unfavorable process. Thus, radiation doses that cause vascular damage and reactive fibrosis are identical. Another factor, which stimulates the progression of such radiogenic fibroses, is the synthesis and release of transforming growth factor-ß (TGF-ß) from various cell populations that further triggers the differentiation from fibroblasts into fibrocytes (Hakenjos et al. 2000; Dorr 2009). Shortly after initiation of radiation treatments, increased expression of TGF-ß at the mRNA as well as protein level can be already observed that persists over a long period of time.

Since connective tissues exist ubiquitously in the human body, clinical consequences of such radiogenic scarring may differ depending on the location. Typical clinical presentations are the following:

- Generally, *diffuse pain sensations*.
- *Extensive fibrosis with shrinking inclination* – as a consequence, deforming skin retractions or esophageal, intestinal, or urinary tract strictures may present with obstruction or contraction signs such as dysphagia, ileus, contracted bladder, or pericardial restrictive disease.
- *Circumscribed collapse of the epithelium and the underlying connective tissues* resulting in a radiogenic skin ulceration or fistulation of hollow organs.
- Extended fibrotic changes with *decreased organ function* (e.g., myocardial failure, reduction in pulmonary function) *and tissue mobility* – as a consequence, joint contractures with serious movement constrictions and compression of the lymph vessels may occur with impaired lymph drainage in the upstream regions of the lymphatic system with consecutive lymphedema (Fig. 12).

## 6.6 General Chronic Radiation Effects in the Epithelia and Organ Parenchyma

In the organ parenchyma, therapeutic irradiations induce dose-depending depletion of stem cells.

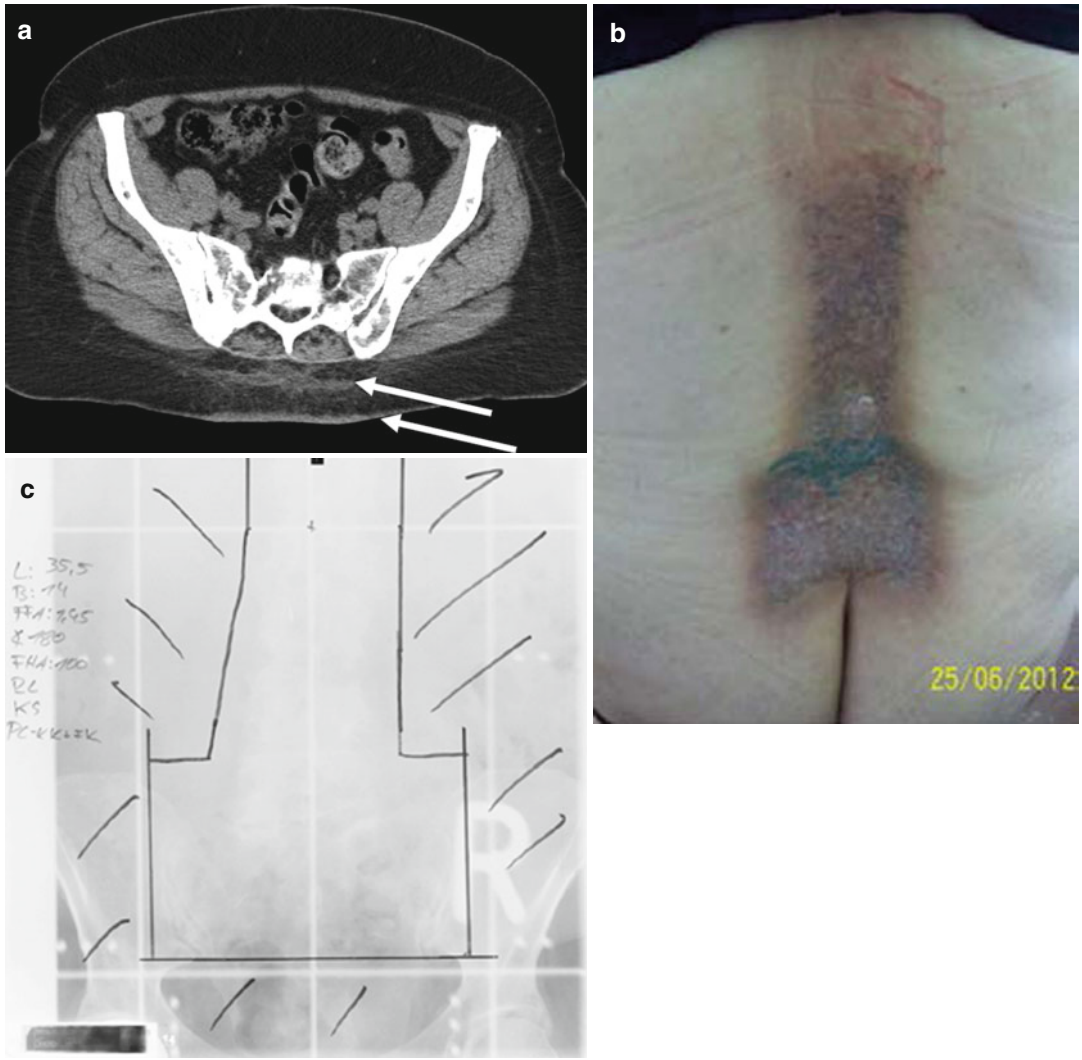


**Fig. 12** A 54-year-old woman with breast carcinoma and disseminated osseous metastases including the axial skeleton who was irradiated due to a painful metastasis of the vertebral body Th 11. Patient presented 3 months later with skin thickening and subcutaneous densification in the CT scan (**a**); clinically, massive fibrosis of the skin and the underlying tissues was seen (**c**) in correlation with the radiation field (**b**)

This takes place either by direct induction of cell death (i.e., apoptosis) with rapid and normally complete destruction and subsequent removal of severe damaged cells or by delayed cell death due to mitotic catastrophe. These radiation effects become still more enhanced, when resting or slowly proliferating parenchyma cells are recruited into an accelerated cell cycle to compensate the initial cell loss. However, all these regenerative attempts are also proving unsuccessful, with consecutive worsening of the organ function depending on the cell depletion. The fact that cell cycle in parenchyma cells often lasts several months explains why decreased organ function often manifests with long latency periods. But the latency period until onset of side effects is shortened with increasing doses, because, as noted above, cell depletion is dose dependent. Furthermore, chronic radiation effects are not reversible and often progressive whereby the progression rate depends on the administered radiation dose.

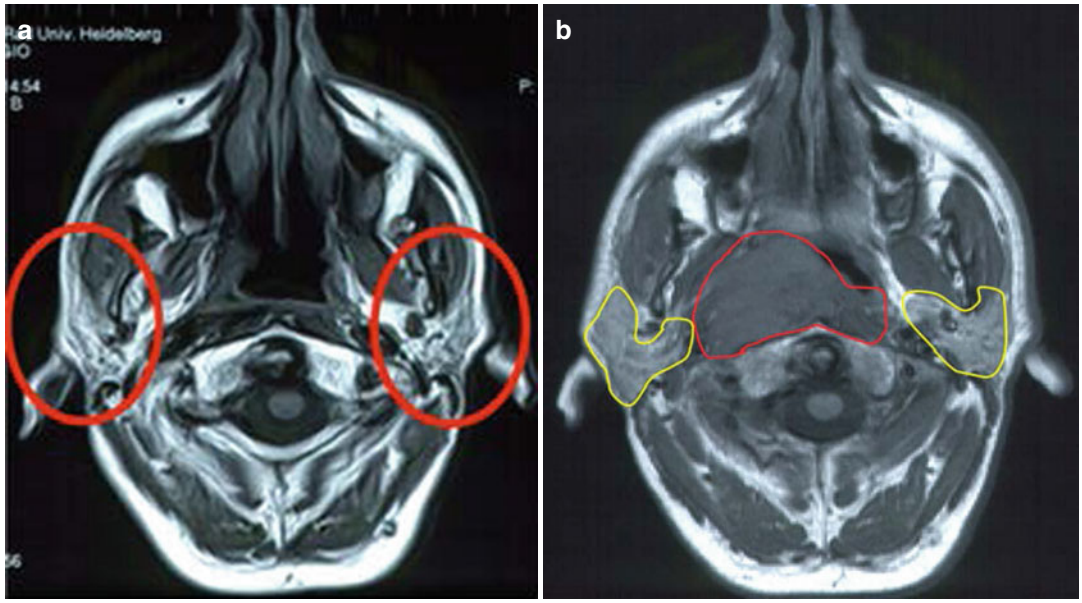


**Fig. 13** MRI of a 42-year-old man who was irradiated with conventional irradiation technique (opposed lateral fields) due to locally advanced nasopharyngeal cancer (surrounded by the *red line*) in proximity to the parotic glands (surrounded by the *yellow lines*) (**a**). Another MR scan 7 years later showed complete atrophy of the parotic glands in the same patient, in line with clinically evident severe xerostomia (**b**)

Therefore, the most common pathological delayed effect of therapeutic irradiations is *atrophy*, which may occur not only in parenchymatous tissues (e.g., kidney, lung) but also in all glands (salivary, mammary, cutaneous, etc.) and all lining epithelia (skin, alimentary, respiratory, and urinary tracts) (Fajardo 2005) (Fig. 13).

Typically, atrophic changes manifest focal and random in the irradiated tissues and organs. Another reaction pattern that is often seen by radiologists in imaging is *necrosis*, which rarely occurs in the acute phase during or shortly after radiation treatment as severe radiation injury of the skin and mucosae. More often, necrosis manifests delayed due to damage of the supplying vascular bed with consecutive ischemia (see above). The best-known site for delayed necrosis is the central nervous system, particularly the white matter of the cerebral hemispheres. Further epithelial/parenchymal lesions include *metaplasia, cellular atypia*, *dysplasia*, and *neoplasia* (Fajardo 2005).

In summary, for chronic radiation sequelae of normal tissues and organs, the following applies:

- The latency period of chronic radiation reactions is characterized by an inverse relationship to the dose.
- Regeneration mechanisms barely exist.
- Even after many years, radiogenic scarring and atrophy in tissues and organs can be enhanced through additional noxa such as mechanical stress or operative procedures; thus, operative measures in irradiated volumes have to be planned carefully and require close collaboration between surgeons and radio-oncologists

## 6.7 Modulation of the Immune System

The abovementioned delayed stromal tissue reactions are usually accompanied by a decrease of the normal inflammatory cell population such as granulocytes, macrophages, and lymphocytes (Fajardo 2005). Pathologically, the absence of cellular inflammatory response typically occurs in all tissues after irradiation with only a few exceptions such as fistulations, ulcerations, or

superimposed infections. These consistent histopathological findings are extremely useful for differential diagnosis of radiation pathology. In this context, radiologists should consider that terms such as enteritis or cystitis, which imply the presence of inflammation, are therefore generally not accurate when describing imaging features of radiogenic tissue changes.

## 7 Radiation-Induced Cancers

Nowadays, in about two thirds of cancer patients, survival times of more than 5 years can be reached through modern cancer therapy (Travis et al. 2008). However, cured cancer patients are at risk for development of second malignancies due to several reasons whereby the increased life expectancy is the most important factor. This risk is at least equal to that of comparable persons with no cancerous diseases in the history but can be even aggravated due to several reasons such as exposition with carcinogenic chemical substances or ionizing radiation for treatment of their primary tumor. As a consequence, potential induction of secondary cancers due to oncological treatments has increasingly moved to the fore in recent years. In summary, in the case of neoplastic secondary disease, the following underlying causes have to be considered:

- First, about 60 % of the so-called cancer survivors are older than 65 years, and therefore the risk for neoplastic secondary lesions is increased anyway *(risk factor age)*.
- Second, *genetic disposition* has to be taken into consideration in every patient with a cancerous disease (e.g., Fanconi anemia, hereditary colorectal cancer, mutations of the Rb or BRCA1 gene).
- Third, *exposure to common exogenous carcinogens* (smoking, abuse of alcohol, large consumption of red meat, etc.) that were causative in the first neoplasia may also trigger the development of a secondary malignant lesion.
- Fourth, *exposition with carcinogenic noxa as part of the cancer treatment* may account for development of a secondary tumor, if the latency period until manifestation is plausible and consistent with the experience of carcinogenesis

### 7.1 Secondary Cancer Rate

The most important condition for development of secondary cancers due to oncological treatments is the healing of the primary malignancy. Modern, mostly multimodal approaches in cancer therapy succeeded in raising the proportion of cured patients in a significant way, albeit to differing extents for various tumor entities. As a consequence of improved survival rates, secondary cancers increasingly became the focus of the oncological specialist disciplines. However, accurate statements on the relative risk of secondary cancers caused by a specific treatment require valid data based on either lifelong follow-up of cancer patients or, alternatively, reliable cancer registries.

### 7.2 Secondary Cancers in Adults

In the past, several large studies have been conducted to estimate the specific risk of induction of secondary tumors by radiation treatments of the first cancer in addition to age-related cancer risks. The study of Brenner et al. was a cohort study of the incidence of secondary cancers in more than 120,000 patients with prostate cancer that were either treated surgically or with radiotherapy (Brenner et al. 2000). Among the irradiated patients, the risk for development of solid secondary tumors was significantly increased by 6 % in average. The relative risk further increased in long-term survivors, with 15 and 34 % after more than 5 and 10 years, respectively. In absolute terms, prostate cancer patients developed a secondary malignancy due to irradiation in 1 of 290 treated patients, increasing to 1 in 70 for patients who survived more than 10 years after initial therapy. In this study, the most common contributors to radiation-specific risk elevation were cancers of the rectum, bladder, and lung, as well as sarcomas within the radiation field. Half of these tumors developed in the high-dose vol-

ume, whereas the other half (lung cancers) was believed to be associated to scatter irradiation.

In a large meta-analysis, about 25,000 patients with early breast cancer showed for irradiated women a significant excess incidence of contralateral breast cancer, (ipsilateral) lung cancer, and moreover a significant excess of non-cancer mortality mainly due to coronary heart disease (Clarke et al. 2005). For example, the risk for contralateral breast cancer was raised significantly from 7.5 to 9.3 % by postoperative radiotherapy after 15 years.

Aggravated risk for secondary tumors due to irradiation – mostly located within the prior high-dose volume – was also described for several other tumor entities such as cervical cancer (Kleinerman et al. 1995), testicular cancer (Travis et al. 1997), or Hodgkin's lymphoma (Swerdlow et al. 2000). In general, radiotherapy is more related to the induction of solid tumors than leukemia whereby the shortest latency periods between radiation exposure and emergence of secondary cancers range from 5 to 10 years. The vast majority of those radiation-induced tumors have longer latency with risk persisting mostly lifelong. However, despite potentially life-threatening late sequelae of radiotherapy, the direct benefit for adult cancer patients outweighs the risk due to avoidance of relapses. Furthermore, it has to be considered that incidence rates for secondary malignant lesions described in literature are generally related to older radiation techniques and that newer conformal radiation techniques may probably cause lower rates of second tumors. Lastly, even if the incidences of those radiation-induced malignancies were higher, the benefit would still exist as the relapses occur much earlier than the secondary malignancies, and thus treated patients profit through prolonged lifetime.

## 7.3 Secondary Cancers in Children

The development of treatment-related secondary cancers has moved to the fore very early in pediatric oncology, since the cumulative risk for second tumors steadily increases with increasing survival times. Hence, patients with cured childhood cancers are at much higher risk to develop a second or even third cancer than adult cancer patients whereby both radiotherapy and chemotherapy contribute to the increased lifetime risk. This was shown, for example, in a large investigation of more than 13,000 children who survived at least 5 years after initial treatment (Neglia et al. 2001). In this patient cohort, second malignancies were recorded in about 2.2 % after a mean latency period of 12 years. Among those tumors, leukemia was found in 8 % with a peak occurring after 5–9 years from primary treatment. The rest of those secondary cancers were solid (92 %) and significantly elevated during the whole observation period of up to 30 years. The most critical organs for second malignancies in this study population were the central nervous system, thyroid, and breast.

De Vathaire et al. evaluated the specific impact of radiotherapy for treatment of primary childhood cancers to development of second malignancies (de Vathaire et al. 1999). According to this study, the cumulative incidence for radiation-induced secondary cancers steadily increased with the follow-up times and was about 5 % after 25 years and 8 % after 30 years from initial treatment. The most radiosensitive organs for induction of second malignancies in pediatric radiotherapy are the central nervous system, thyroid, breast, bone, and soft tissues with more than 80 % of second solid cancers occurring in those tissues (de Vathaire et al. 1999). Furthermore, most of the recorded sarcomas and brain tumors developed within the prior high-dose volume, whereas carcinomas tended to develop more in volumes exposed to intermediate or low radiation doses.

The highest rates of excess malignancies were reported in long-term survivors of Hodgkin's lymphoma with an actuarial risk of 9.7 % for males and 16.8 % for females at 20 years after initial treatment, which was either performed as radiotherapy alone or as combination therapy comprising chemotherapy and radiotherapy (Wolden et al. 1998). Particularly remarkable in this respect is the much higher risk of females in this study population mainly due to second breast

cancers, which represented approximately one half of all recorded second malignancies. Moreover, 90 % of second solid cancers occurred in the radiation field or penumbra region, whereas most of these tumors were found in regions that received more than 30 Gy.

## 7.4 Development and Manifestation of Secondary Tumors

As noted above, irradiations may cause genetic instability, which either leads to cell death or in the case of misrepair to mutations with increased risk for carcinogenesis. However, further mutations are necessary to accumulate before cells become independent from external proliferation stimulants; thus, secondary cancers due to irradiation are relatively rare events. The dose dependency of cell kills explains why secondary cancers occur mainly at the penumbra and low-dose volume of the radiation field.

For second tumors arising in prior high-dose volumes, the underlying mechanism is assumed to be completely different to the mentioned molecular pathway. The main condition for that subpopulation of malignant neoplasms seems to be the induction of chronic radiation injury characterized by progressive microvascular damage, parenchymal atrophy, and chronic inflammation, being recognized as precancerous lesion (Trott 2009). Hence, optimized dose distributions that conform to the tumor treatment volume while avoiding adjacent normal tissues as best as possible could help to reduce the risk for these second tumors.

**Conclusion**

Nowadays, radiation therapy makes a major contribution to improve treatment outcome and patient's quality of life in cancerous diseases, not only in the curative but also in the palliative situation. In this regard, particularly gradual refinements of radiotherapy techniques and conceptions of basic biological principles had and still have major impact on improvement of treatment tolerance and response to therapy. Thus, radiation oncology is a highly dynamic specialty with an essential role in the oncological overall concept. In recent years, for example, high-precision irradiation techniques in combination with image guidance (IGRT) and, where appropriate, simultaneous or sequential application of systemic drugs (chemotherapy, molecular targeting) significantly contributed to exceed the therapeutic window, that is, tumor control rates were improved, while chronic radiation sequelae maintained at the same level or even decreased at the same time. However, despite all advances and efforts, therapy-related side effects cannot be completely avoided, so that these adverse normal tissue reactions still represent a dose-limiting factor. Moreover, modern cancer therapy strongly depends on imaging procedures (e.g., CT, MRI, PET/CT) for optimized treatment results. In radiotherapy, for example, modern imaging techniques play an increasingly important role not only before and after treatment (staging, treatment planning, follow-up examinations) but also during treatment by means of image-guided radiotherapy (IGRT) and replanning imaging studies, if required. In addition, as a result of advanced cancer treatments, the number of cancer survivors is steadily increasing; thus, more late sequelae of oncological treatments are seen nowadays. As a consequence, intense collaboration between radio-oncologists and radiologists is more important than ever. Therefore, diagnostic specialists with broad range of expertise in oncological imaging can significantly contribute to optimize the radiation oncology workflow at different steps, which, in the end, has the potential to further improve the care of cancer patients.

## References

Bentzen SM, Turesson I, Thames HD (1990) Fractionation sensitivity and latency of telangiectasia after postmastectomy radiotherapy: a graded-response analysis. Radiother Oncol 18:95–106

Bentzen SM, Constine LS, Deasy JO, Eisbruch A, Jackson A, Marks LB, Ten Haken RK, Yorke ED (2010) Quantitative Analyses of Normal Tissue Effects in the

Clinic (QUANTEC): an introduction to the scientific issues. Int J Radiat Oncol Biol Phys 76:S3–S9
Boda-Heggemann J, Lohr F, Wenz F, Flentje M, Guckenberger M (2011) kV cone-beam CT-based IGRT: a clinical review. Strahlenther Onkol 187:284–291
Bortfeld T, Jeraj R (2011) The physical basis and future of radiation therapy. Br J Radiol 84:485–498
Boyd TS, Mehta MP (1999) Stereotactic radiosurgery for brain metastases. Oncology 13:1397–1409; discussion, 1409–1410, 1413
Brahme A, Roos JE, Lax I (1982) Solution of an integral equation encountered in rotation therapy. Phys Med Biol 27:1221–1229
Brenner DJ, Curtis RE, Hall EJ, Ron E (2000) Second malignancies in prostate carcinoma patients after radiotherapy compared with surgery. Cancer 88:398–406
Clarke M, Collins R, Darby S, Davies C, Elphinstone P, Evans E, Godwin J, Gray R, Hicks C, James S, MacKinnon E, McGale P, McHugh T, Peto R, Taylor C, Wang Y, Early Breast Cancer Trialists' Collaborative G (2005) Effects of radiotherapy and of differences in the extent of surgery for early breast cancer on local recurrence and 15-year survival: an overview of the randomised trials. Lancet 366:2087–2106
Constine LS, Friedman D, Morris M, Williams JP, Rubin P, Okunieff P (2013) Chapter 12: Late effects of cancer treatment on normal tissues. In: Halperin EC, Wazer DE, Perez CA, Brady LW (eds) Perez & Brady's principles and practice of radiation oncology, 6th edn., pp 320–350
de Vathaire F, Hawkins M, Campbell S, Oberlin O, Raquin MA, Schlienger JY, Shamsaldin A, Diallo I, Bell J, Grimaud E, Hardiman C, Lagrange JL, Daly-Schveitzer N, Panis X, Zucker JM, Sancho-Garnier H, Eschwege F, Chavaudra J, Lemerle J (1999) Second malignant neoplasms after a first cancer in childhood: temporal pattern of risk according to type of treatment. Br J Cancer 79:1884–1893
Debus J, Engenhart-Cabillic R, Holz FG, Pastyr O, Rhein B, Bortfeld T, Wannenmacher M (1997) Stereotactic precision radiotherapy in the treatment of intraocular malignancies with a micro-multileaf collimator. Front Radiat Ther Oncol 30:39–46
Dische S, Warburton MF, Jones D, Lartigau E (1989) The recording of morbidity related to radiotherapy. Radiother Oncol 16:103–108
Dittmann K, Mayer C, Rodemann HP (2005) Inhibition of radiation-induced EGFR nuclear import by C225 (Cetuximab) suppresses DNA-PK activity. Radiother Oncol 76:157–161
Dorr W (2009) Chapter 13: Pathogenesis of normal-tissue side-effects. In: Joiner M, Van der Kogel A (eds) Basic clinical radiobiology, 4th edn. Hodder Arnold, London, pp 169–190
Dorr W, Hendry JH (2001) Consequential late effects in normal tissues. Radiother Oncol 61:223–231
Dorr W, Bertmann S, Herrmann T (2005) Radiation induced lung reactions in breast cancer therapy. Modulating factors and consequential effects. Strahlenther Onkol 181:567–573
Dorr W, Kallfels S, Herrmann T (2013) Late bone and soft tissue sequelae of childhood radiotherapy. Relevance of treatment age and radiation dose in 146 children treated between 1970 and 1997. Strahlenther Onkol 189:529–534
Emami B, Lyman J, Brown A, Coia L, Goitein M, Munzenrider JE, Shank B, Solin LJ, Wesson M (1991) Tolerance of normal tissue to therapeutic irradiation. Int J Radiat Oncol Biol Phys 21:109–122
Fajardo LF (2005) The pathology of ionizing radiation as defined by morphologic patterns. Acta Oncol 44:13–22
Gademann G, Schlegel W, Debus J, Schad L, Bortfeld T, Hover KH, Lorenz WJ, Wannenmacher M (1993) Fractionated stereotactically guided radiotherapy of head and neck tumors: a report on clinical use of a new system in 195 cases. Radiother Oncol 29:205–213
Goodhead DT (1994) Initial events in the cellular effects of ionizing radiations: clustered damage in DNA. Int J Radiat Biol 65:7–17
Gray LH (1957) Oxygenation in radiotherapy. I. Radiobiological considerations. Br J Radiol 30:403–406
Guckenberger M, Allgauer M, Appold S, Dieckmann K, Ernst I, Ganswindt U, Holy R, Nestle U, Nevinny-Stickel M, Semrau S, Sterzing F, Wittig A, Andratschke N (2013) Safety and efficacy of stereotactic body radiotherapy for stage 1 non-small-cell lung cancer in routine clinical practice: a patterns-of-care and outcome analysis. J Thorac Oncol 8:1050–1058
Haie-Meder C, Siebert FA, Potter R (2011) Image guided, adaptive, accelerated, high dose brachytherapy as model for advanced small volume radiotherapy. Radiother Oncol 100:333–343
Hakenjos L, Bamberg M, Rodemann HP (2000) TGF-beta1-mediated alterations of rat lung fibroblast differentiation resulting in the radiation-induced fibrotic phenotype. Int J Radiat Biol 76:503–509
Hall EJGA, Giaccia AJ (2006) Radiobiology for the radiologist, 6th edn. Lippincott Williams & Wilkins, Philadelphia
Helleday T, Lo J, van Gent DC, Engelward BP (2007) DNA double-strand break repair: from mechanistic understanding to cancer treatment. DNA Repair (Amst) 6:923–935
Helleday T, Petermann E, Lundin C, Hodgson B, Sharma RA (2008) DNA repair pathways as targets for cancer therapy. Nat Rev Cancer 8:193–204
Hendry JH, Thames HD (1986) The tissue-rescuing unit. Br J Radiol 59:628–630
Herfarth KK, Hof H, Bahner ML, Lohr F, Hoss A, van Kaick G, Wannenmacher M, Debus J (2003) Assessment of focal liver reaction by multiphasic CT after stereotactic single-dose radiotherapy of liver tumors. Int J Radiat Oncol Biol Phys 57:444–451
Herfarth KK, Debus J, Wannenmacher M (2004) Stereotactic radiation therapy of liver metastases: update of the initial phase-I/II trial. Front Radiat Ther Oncol 38:100–105
Hof H, Muenter M, Oetzel D, Hoess A, Debus J, Herfarth K (2007) Stereotactic single-dose radiotherapy (radiosurgery) of early stage nonsmall-cell lung cancer (NSCLC). Cancer 110:148–155

Jung H, Beck-Bornholdt HP, Svoboda V, Alberti W, Herrmann T (2001) Quantification of late complications after radiation therapy. Radiother Oncol 61:233–246

Kavanagh BD, Miften M, Rabinovitch RA (2011) Advances in treatment techniques: stereotactic body radiation therapy and the spread of hypofractionation. Cancer J 17:177–181

Kleinerman RA, Boice JD Jr, Storm HH, Sparen P, Andersen A, Pukkala E, Lynch CF, Hankey BF, Flannery JT (1995) Second primary cancer after treatment for cervical cancer. An international cancer registries study. Cancer 76:442–452

Mahaney BL, Meek K, Lees-Miller SP (2009) Repair of ionizing radiation-induced DNA double-strand breaks by non-homologous end-joining. Biochem J 417:639–650

Marks LB, Yorke ED, Jackson A, Ten Haken RK, Constine LS, Eisbruch A, Bentzen SM, Nam J, Deasy JO (2010) Use of normal tissue complication probability models in the clinic. Int J Radiat Oncol Biol Phys 76:S10–S19

Michalowski A (1981) Effects of radiation on normal tissues: hypothetical mechanisms and limitations of in situ assays of clonogenicity. Radiat Environ Biophys 19:157–172

Neglia JP, Friedman DL, Yasui Y, Mertens AC, Hammond S, Stovall M, Donaldson SS, Meadows AT, Robison LL (2001) Second malignant neoplasms in five-year survivors of childhood cancer: childhood cancer survivor study. J Natl Cancer Inst 93:618–629

Paulus U, Potten CS, Loeffler M (1992) A model of the control of cellular regeneration in the intestinal crypt after perturbation based solely on local stem cell regulation. Cell Prolif 25:559–578

Paumier A, Le Pechoux C, Beaudre A, Negretti L, Ferreira I, Roberti E, Brahim J, Lefkopoulos D, Daly-Schweitzer N, Bourhis J, Bonvalot S (2011) IMRT or conformal radiotherapy for adjuvant treatment of retroperitoneal sarcoma? Radiother Oncol 99:73–78

Pedersen D, Bentzen SM, Overgaard J (1994) Early and late radiotherapeutic morbidity in 442 consecutive patients with locally advanced carcinoma of the uterine cervix. Int J Radiat Oncol Biol Phys 29:941–952

Perks JR, Lehmann J, Chen AM, Yang CC, Stern RL, Purdy JA (2008) Comparison of peripheral dose from image-guided radiation therapy (IGRT) using kV cone beam CT to intensity-modulated radiation therapy (IMRT). Radiother Oncol 89:304–310

Purdy JA (2008) Dose to normal tissues outside the radiation therapy patient's treated volume: a review of different radiation therapy techniques. Health Phys 95:666–676

Rodemann HP, Bamberg M (1995) Cellular basis of radiation-induced fibrosis. Radiother Oncol 35:83–90

Rubin P, Casarett GW (1968) Clinical radiation pathology as applied to curative radiotherapy. Cancer 22:767–778

Rubin P, Johnston CJ, Williams JP, McDonald S, Finkelstein JN (1995) A perpetual cascade of cytokines postirradiation leads to pulmonary fibrosis. Int J Radiat Oncol Biol Phys 33:99–109

Schultz-Hector S (1992) Radiation-induced heart disease: review of experimental data on dose response and pathogenesis. Int J Radiat Biol 61:149–160

Sterzing F, Stoiber EM, Nill S, Bauer H, Huber P, Debus J, Munter MW (2009) Intensity modulated radiotherapy (IMRT) in the treatment of children and adolescents–a single institution's experience and a review of the literature. Radiat Oncol 4:37

Sterzing F, Engenhart-Cabillic R, Flentje M, Debus J (2011) Image-guided radiotherapy: a new dimension in radiation oncology. Dtsch Arztebl Int 108: 274–280

Swerdlow AJ, Barber JA, Hudson GV, Cunningham D, Gupta RK, Hancock BW, Horwich A, Lister TA, Linch DC (2000) Risk of second malignancy after Hodgkin's disease in a collaborative British cohort: the relation to age at treatment. J Clin Oncol 18:498–509

Terezakis SA, Heron DE, Lavigne RF, Diehn M, Loo BW Jr (2011) What the diagnostic radiologist needs to know about radiation oncology. Radiology 261:30–44

Thames HD Jr, Withers HR, Peters LJ, Fletcher GH (1982) Changes in early and late radiation responses with altered dose fractionation: implications for dose-survival relationships. Int J Radiat Oncol Biol Phys 8:219–226

Travis LB, Curtis RE, Storm H, Hall P, Holowaty E, Van Leeuwen FE, Kohler BA, Pukkala E, Lynch CF, Andersson M, Bergfeldt K, Clarke EA, Wiklund T, Stoter G, Gospodarowicz M, Sturgeon J, Fraumeni JF Jr, Boice JD Jr (1997) Risk of second malignant neoplasms among long-term survivors of testicular cancer. J Natl Cancer Inst 89:1429–1439

Travis LB, Allan IL, van Leewen FE (2008) Second cancers. In: de Vita VTJ, Lawrence TS, Rosenberg SA (eds) Cancer. Principles & practice of oncology, 8th edn. Kluwer/Lippincott William & Wilkins, Philadelphia, pp 2718–2743

Trott KR (2009) Chapter 25. Second cancers after radiotherapy. In: Joiner M, Van der Kogel A (eds) Basic clinical radiobiology, 4th edn. Hodder Arnold, London, pp 339–352

Turesson I (1990) Individual variation and dose dependency in the progression rate of skin telangiectasia. Int J Radiat Oncol Biol Phys 19: 1569–1574

Wolden SL, Lamborn KR, Cleary SF, Tate DJ, Donaldson SS (1998) Second cancers following pediatric Hodgkin's disease. J Clin Oncol 16:536–544

# Part II

# Brain

# Brain: Radiotherapy

Marco Essig

## Contents




**Abstract**

Radiation treatment to the brain is part of focal and systemic treatment concepts and can be applied in fractionated doses or a single dose. As there is always normal neuronal tissue affected, short- and long-term tissue changes are seen, including radiation necrosis, gliotic changes, and volume loss up to atrophy with a large variety of clinical symptomatology.

Some of the described changes are influenced by concomitant treatments like chemo- or immune-modulating therapies.

This chapter describes the typical imaging changes of normal and pathologic tissue after radiation treatment and how to differentiate treatment-related and disease-related changes based on functional imaging methods.


## Abbreviations

| | |
|---|---|
| ADC | Apparent diffusion coefficient |
| ASL | Arterial spin labeling |
| Cho | Choline |
| CR | Creatine-phosphocreatine |
| CSI | Chemical shift imaging/spectroscopic imaging |
| CT | Computed tomography |
| DCE | Dynamic contrast enhanced |
| DRN | Delayed radiation necrosis |
| DSC | Dynamic susceptibility contrast |
| DTI | Diffusion tensor imaging |
| DWI | Diffusion-weighted imaging |


M. Essig, MD, PhD, FRCPC
Department of Radiology, University of Manitoba, Winnipeg, MB, Canada
e-mail: messig@exchange.hsc.mb.ca



Med Radiol Radiat Oncol (2015)
DOI 10.1007/174_2015_1076, © Springer International Publishing Switzerland

| | |
|---|---|
| FA | Fractional anisotropy |
| FDG | Fludeoxyglucose |
| MRI | Magnetic resonance imaging |
| MRS | Magnetic resonance spectroscopy |
| NAA | N-acetylaspartate |
| nMSIVP | Normalized maximum slope of enhancement in initial vascular phase |
| PET | Positron emission tomography |
| PsP | Pseudoprogression |
| PSR | Pseudoresponse |
| RANO | Response Assessment in Neuro-Oncology |
| rCBV | Regional cerebral blood volume |

## 1 Introduction

Radiation treatment to the brain is done as primary, secondary, or combined treatment, both as part of a focal and/or a generalized treatment concept. Primary treatment can be applied as single- or multiple-dose radiation and may be followed by additional treatments. The secondary treatment concept can follow a primary surgical treatment or chemotherapy or a combination of different primary treatment concepts. Combined primary treatment is most often used in neuro-oncology of higher-grade primary intra-axial tumors and can be followed by different secondary treatments that may also include radiation, fractionated or single dose. Radiation can be applied as a focal treatment with either conformal fractionated doses or as a single high-dose radiation, commonly called radiosurgery.

In some instances radiation treatment can also be used as part of a generalized treatment concept including whole-brain radiation – primary or as a prophylactic or as part of a whole-body radiation like in leukemia.

With this variety of treatment options that include radiation, one can understand that the observed radiation-induced side effects can be quite complex. In general, we differentiate between direct and indirect complications after radiation treatment.

Direct complications are radiation-induced damages to the treated tissue, which may be permanent or reversible. The damage may result in malfunction that might be temporary or permanent.

The indirect complications or often called management-related changes are based on the delayed control of the disease process. An example is the increased risk of bleeding in radiosurgically treated arteriovenous malformations before their complete occlusion.

To understand the imaging effects of radiation, it is important to understand the concept of modern radiotherapy strategies, which are mainly based on different target volumes that are used for radiation treatment.

The gross tumor volume describes the amount of the lesion that is visible on clinical imaging and represents the core of the target volume. The clinical target volume, however, refers to an enlarged area, which includes subclinical or microscopic tumors spread around the gross tumor volume. The clinical target volume is most often an estimate and not visible on the imaging studies. Therefore, the planned target volume includes the clinical target volume and an additional safety margin that differs from lesion to lesion. With this concept, there are in nearly all cases normal cells affected that, if damaged, present with pathologic imaging characteristics even initially not been tumor infiltrated. The different target volumes often depend on the kind of radiation that is used: single high-dose/stereotactic radiation or conformal radiation over a longer period of time with lower individual daily dosages.

Direct radiation effects on the initial tumor volume also result in specific changes that can mimic the initial tumor and most often still contain more or less active tumor cells.

## 2 Effects of Radiation on the Brain

There are multiple effects of radiation on brain tissue including reversible and nonreversible ones. The nonreversible ones turn into permanent degeneration and atrophy of normal brain tissue.

Postradiation tumor treatment effects can be divided into pseudoprogression (PsP) and delayed radiation necrosis (DRN). PsP often appears several weeks up to multiple months after radiation. The main underlying pathophysiologic process that causes PsP is the transient interruption of myelin synthesis secondary to

radiation injury to the oligodendrocytes. PsP is a transient process with frequent spontaneous recovery without development of scar tissue (Brandsma et al. 2008; Clarke and Chang 2009; Brandes et al. 2008; Chaskis et al. 2009).

In contrast, DRN may appear months to several years after radiation therapy and causes permanent tissue changes. DRN presents pathophysiologically and radiologically as a degradation of the tissue with a space-occupying, partly necrotic lesion with tumor-mimicking mass effect, extending the initial tumor volume and resulting in permanent tissue dysfunction (Kumar et al. 2000; Mullins et al. 2005). Other delayed effects without development of focal lesions include cognitive decline and global brain atrophy (Kingsley and Kendall 1981).

The mechanisms of the tissue damage following radiotherapy are complex and not understood in detail. Tissue-specific components and individual radiosensitivity play an important role but are difficult to assess and not fully understood (Yu et al. 2012; Wiggenraad et al. 2011).

In the brain the pathways of tissue damage include small vessel injury with endothelial damage-inducing focal ischemic events with vasogenic and cytotoxic edema in the acute stage. Fibrosis, hyalinization, and gliosis are chronic changes that appear in the interval with additional vascular changes like telangiectasia, blood-brain barrier breakdown, and vascular malformations as common histologic findings after radiation.

There is also a direct effect of the brain cells as described above. Oligodendrocytes, for example, are sensitive to radiation and reduce in number significantly after radiation.

Both vascular and cellular damages, together with effects on the fibrinolytic enzyme system, lead to a brain volume loss after radiation.

## 3 Imaging Findings After Radiation of the Brain

Post-therapeutic imaging is challenging as there are multiple imaging findings that reflect post-therapeutic changes. Therefore, it is important to assess whether a tumor has grown or decreased in size, which can be very difficult if you have complex tumor geometry.

Another problem in modern radiotherapy strategies results from the fact that more aggressive first-line and additional second-line treatments like boost radiation are commonly used. Often radiation is further combined with other therapies like chemotherapy or even embolization. The combination of new concepts of chemotherapy like antiangiogenic treatment can significantly alter the imaging characteristics.

Distinguishing between recurrent tumor and radiation side effects is critical, however, because of their vastly different management strategies. Patients with recurrent tumor may undergo further surgery and chemo-/radiation therapy, while those with acute or delayed radiation changes may be managed conservatively with steroids.

To assess radiation-induced changes, all imaging modalities may play a role; however, MRI and PET are superior to CT to demonstrate acute and chronic changes. CT is mainly used in cases where the patient presents with acute symptoms or if there are contraindications for MRI

The imaging findings after radiation of the brain are multiplex and include white matter T2 hyperintensities, volume loss, and pathologic enhancement (Figs. 1 and 2). As these are similar findings in tumor recurrence and progression, the differentiation between tumor-related and treatment-related effects is a challenge for conventional imaging including CT and MRI (Fig. 3) (Reddy et al. 2013; Patel et al. 2011; Essig et al. 2011; Kickingereder et al. 2013). The timing for treatment-induced changes varies significantly in this respect, and even relative late-occurring changes can resolve completely.

In the post-therapeutic evaluation of gliomas, the two-dimensional area of contrast enhancement, known as the Macdonald criteria, is the most commonly used method to evaluate therapeutic response of high-grade gliomas (Macdonald et al. 1990). However, reliance on contrast enhancement is problematic because it is a nonspecific finding which reflects breakdown of the blood-brain barrier (Fig. 2). Contrast-enhancing lesions following therapy may be related to tumorous changes; however other processes such as PsP or DRN, postsurgical changes, postictal changes, and changes in steroid dosage present with similar morphologic characteristics (Clarke and Chang 2009; Kumar et al. 2000; Finn et al. 2007).

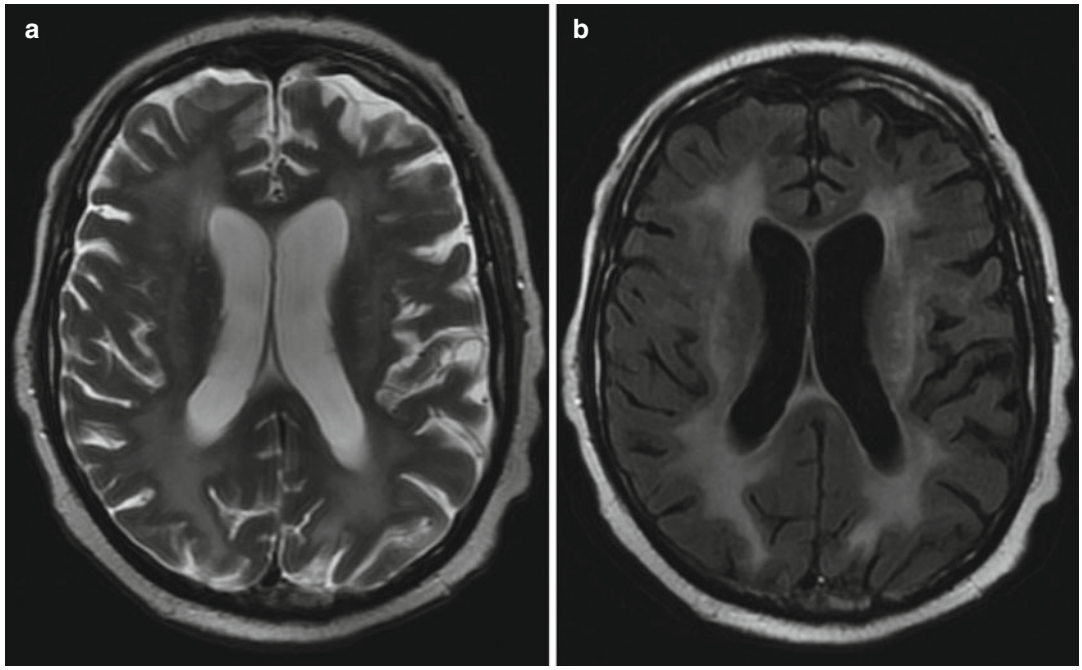


**Fig. 1** Radiation treatment-related changes include diffuse T2 hyperintensities reflecting leukoencephalopathic changes (**a**) and diffuse volume loss (**b**). Case of a 65-year-old patient after prophylactic whole-brain irradiation

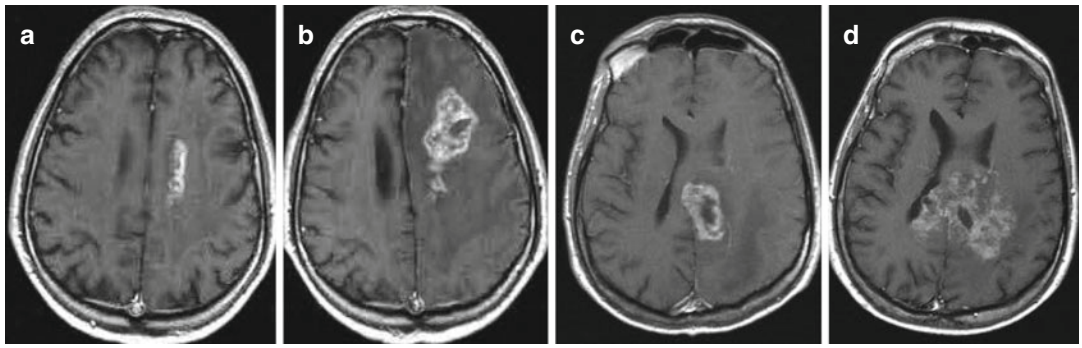


**Fig. 2** Pathologic enhancement in a patient with PsP after radiation treatment (**a**, **b**) and a patient with recurrent tumor (**c**, **d**). Both entities cannot be differentiated using conventional imaging sequences. Confirmation was obtained by follow-up examination at 8 months (**b**) and 5 months (**d**) respectively

These so-called pseudophenomena can occur in up to 40 % of patients who have been treated with combined radio- and chemotherapy and will explain the observed increased lesion size and enhancement during and after the end of treatment in up to 50 % of all cases as presented by Chamberlain in the publication in 2008 (Chamberlain 2008).

In the study by Reddy et al. (2013), T1 contrast enhancement patterns correlating with recurrent tumor included focal solid nodules and solid uniform enhancement with distinct margins. In their series, 85 % (17/20) of patients with ≥70 % recurrent tumor at reoperation demonstrated one of these patterns on the preoperative imaging studies. Contrary, the enhancement

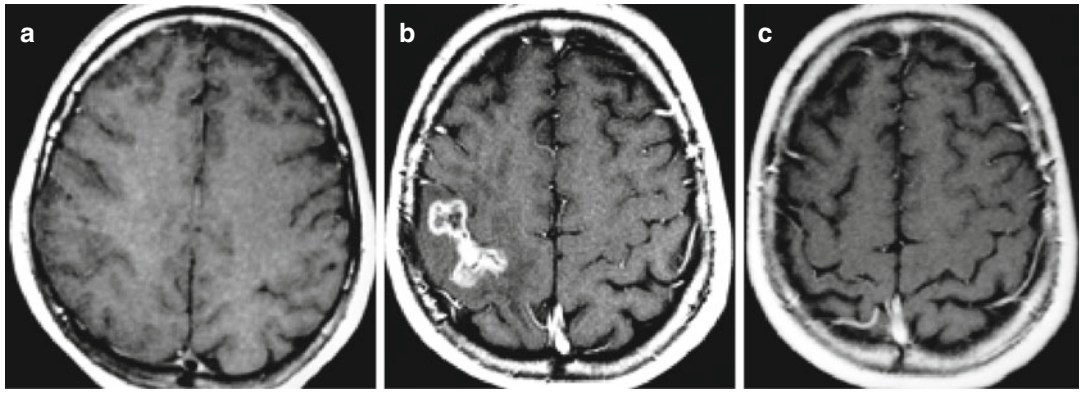


**Fig. 3** PsP in a patient with anaplastic astrocytoma. In an area without contrast enhancement in the pre-radiation workup (**a**) a tumor-like lesion developed on the 20-week follow-up (**b**) which completely resolved at the 33-week follow-up

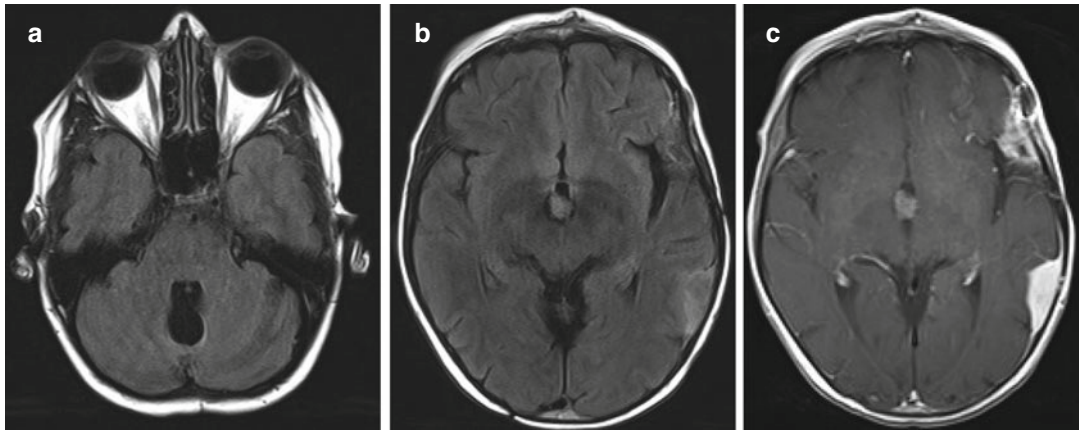


**Fig. 4** Radiation-induced secondary tumor (meningioma) in a patient treated with surgery and radiation in childhood for medulloblastoma. (**a**) Initial tumor bed on FLAIR without residual or recurrent tumor. (**b**) Extra-axial lesions on FLAIR that initiated 15 years after radiation. (**c**) Contrast-enhanced imaging confirms the classical appearance of meningiomas; the frontal lesion was histologically confirmed

patterns correlating with DRN included a hazy mesh-like diffuse enhancement and rim enhancement with feathery indistinct margins (Fig. 2). 94 % (17/18) of patients with ≥70 % treatment-related changes on histology demonstrated one of these two patterns. Thirteen cases had more mixed pathology (>30 % of tumor/necrosis) and demonstrated patterns associated with recurrence and/or necrosis.

The new Response Assessment in Neuro-Oncology (RANO) criteria (Van den Bent et al. 2011) tried to address some of the limitations of the McDonald criteria by including more information from FLAIR and T2-weighted imaging sequences and by adapting the baseline for assessment. The new baseline now addresses the early posttreatment changes like PsP.

Besides PsP and DRN, radiation-induced tumors are a rare side effect of radiation. Although rare, the most common induced tumors are meningiomas (Fig. 4) (Kunert et al. 2012; Mansouri et al. 2014; Madden et al. 2010). In the study of Kunert et al., 2 % of meningiomas were associated with previous radiation treatment

(Kunert et al. 2012). The average time after initial treatment was 24 years, and some of the patients developed multiple tumors which was described as a common feature by Mansouri et al. (2014) and is also found in our presented case.

Long-term effects after radiation include the volume loss of brain parenchyma, often correlated with cognitive decline and diffuse white matter changes (Green-Schloesser and Robbins 2012; Rane and Quaghebeur 2012; Szerlip et al. 2011; Lv et al. 2014), the latter often seen after whole-brain irradiation. In the study of Szerlip, patients accumulated white matter changes at an average rate of 0.07 % of total brain volume per month (Szerlip et al. 2011).

## 4 Advanced Imaging to Characterize Treatment-Related Changes

As the use of conventional contrast-enhanced MRI is not adequate to distinguish between PsP and true early progression and no other imaging technique has been validated to differentiate between the tumor progression/recurrence and DRN, intensive research has been done to evaluate the role of the so-called functional imaging (Young et al. 2011; Geer et al. 2012; Kong et al. 2011; Gahramanov et al. 2011; Hazle et al. 1997; Deviers et al. 2014).

Functional imaging techniques combine conventional imaging technology and conventional criteria with physiologic or pathophysiologic information derived from either the same imaging modality or hybrid systems like PET-CT or PET-MRI. Functional MRI techniques include MR perfusion imaging, diffusion-weighted imaging, and MR spectroscopy or spectroscopic imaging. The following will first describe the methods followed by examples that present how these modern imaging technologies can alter the decision process after radiation therapy.

### 4.1 MR Spectroscopy

Proton magnetic resonance spectroscopy (MRS) or chemical shift/spectroscopic imaging (CSI) is one of the first used functional imaging techniques that allowed to achieve detailed information about the integrity of brain tissue. The method has become a common clinical tool especially in the diagnostic workup of tumors and the differentiation from normal or physiologic neuronal tissue changes.

There are different elements that allow a spectroscopic characterization; however, due to the high concentration and their magnetic moment that allows the best signal to noise ratio, 1H protons are used most commonly in the clinical practice. The spectroscopic characterization of brain abnormalities relies mostly on the calculations of ratios between the main proton spectrum metabolites, notably *N*-acetylaspartate (NAA), a neuronal marker; choline-containing compounds (Cho), a marker of membrane turnover; and creatine-phosphocreatine (Cr), and on the presence of lipids and lactate (Alger et al. 1990; Negendank et al. 1996; Meyerand et al. 1999; Dowling et al. 2001; Demaerel et al. 1991; Vuori et al. 2004). Brain tumors typically exhibit a loss of NAA and an increase in the Cho content (Fig. 5). MRS has been also used to differentiate nontumor lesions like hamartomas from gliomas and to predict the outcome in patients with brain tumors (Wilson et al. 2013). In patients with seizures as a clinical sign for treatment- and tumor-related changes, it is important to identify tumor changes from scar tissue as this has a major impact on the further management of patients.

Follow-up assessment of cerebral tumors is a promising field for MRS (Deviers et al. 2014; Law 2004; Delorme and Weber 2006). Increase in size and contrast enhancement are typical findings in tumor progression but also reflect therapeutic-induced changes as outlined above. The method allows supplementary information about the possible extent and nature of changes on a routine MRI scan by analyzing the metabolite ratios. The ratio of choline to normal creatine level usually is significantly elevated in those areas consistent with tumor compared with those exhibiting predominantly treatment effect. In fact, the treatment effect is generally indicated by a marked depression of all the intracellular metabolite peaks from choline, creatine, and *N*-acetyl compounds (Fig. 6). However, MRS alone may not be helpful in instances where patients have

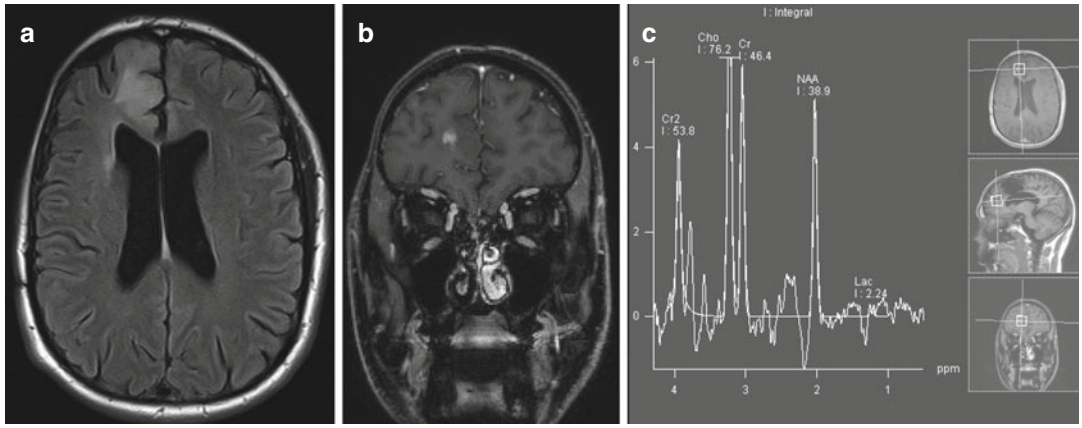


**Fig. 5** MRS in a histologically confirmed case of recurrent high-grade frontal lobe astrocytoma. Space-occupying right frontal lobe mass lesion superior of the initial tumor bed (**a**). Dot-like pathologic enhancement in the center (**b**). The MRS (**c**) presents reduced NAA, high elevated choline, and presence of lactate as an indicator of high membrane turnover and tumor necrosis

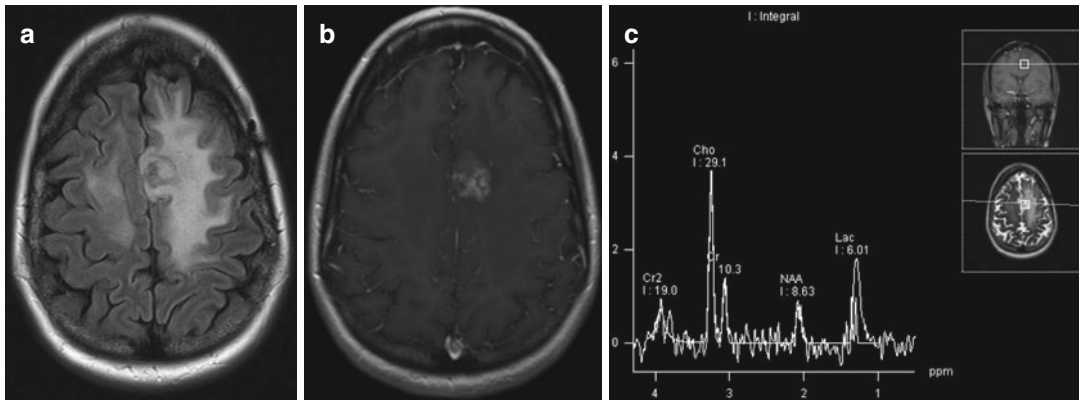


**Fig. 6** MR spectroscopy findings in a histologically confirmed treatment-related tissue change. The patient presented with a new area of contrast enhancement (**b**) with surrounding edema (**a**) and mass effect. MRS (**c**) presented a significant reduction of NAA and moderate reduction of creatine with a stable choline as compared to the normal contralateral side

mixed histologic findings comprised of necrosis and tumor. Because of this heterogeneity and as a result of low spatial resolution, MRS findings of choline and NAA resonances below the normal range may indicate variable histologic findings ranging from radiation necrosis, gliosis, and macrophage infiltration to mixed tissues that contain some regions of tumor. The careful choice of voxel placement and interpretation of results in concordance with other imaging and clinical findings is critical in distinguishing between tumor- and treatment-related changes. Furthermore, validation studies using image-guided acquisition of tissue need to be performed to correlate imaging with biology confidently as reflected in the recent study by Reddy et al. where the MRS performed in 10 patients out of their series did not provide additional information over the conventional enhancement patterns (Reddy et al. 2013).

## 4.2 Contrast-Enhanced Perfusion MRI

Perfusion can be assessed in several ways with MRI and has shown benefits not only for the differential

diagnosis, treatment decision, and/or biopsy planning but also for treatment monitoring. The most common way to assess perfusion in neuro-oncology is the contrast-enhanced first-pass dynamic susceptibility-weighted contrast-enhanced (DSC) MR echo-planar imaging approach using the model of the indicator dilution theory (Cha et al. 2002; Essig et al. 2013a). Newer perfusion imaging approaches like arterial spin labeling (ASL) do not need extrinsic contrast media application and use the blood as intrinsic contrast medium. As in brain neoplasms contrast media is given anyhow, the majority of centers do use DSC-MR perfusion, the method that is faster and more robust. Dynamic contrast-enhanced magnetic resonance imaging (DCE-MRI) is the second most common used method to assess perfusion by the acquisition of serial images before, during, and after the administration of extracellular low-molecular-weighted MR contrast media. The resulting signal intensity measurements of the tumor reflect a composite of tumor perfusion, vessel permeability, and the extravascular/extracellular space (Brix et al. 1991; Tofts and Kermode 1991).

### 4.2.1 DSC-MR Perfusion to Differentiate Treatment-Related Effects

rCBV appears to be elevated in patients with recurrent tumor compared to patients with radiation-related effects which likely is reflective of the increased vascular proliferation and leaky capillaries of recurrent tumor, while posttreatment tissue is composed of extensive fibrinoid necrosis, vascular dilation, and endothelial injury (Barajas et al. 2009; Hu et al. 2009; Lacerda and Law 2009; Essig et al. 2013b; Bisdas et al. 2011). Barajas et al. reported increased ph value and rCBV as well as lower relative PSR in recurrent glioblastoma compared to DRN (Barajas et al. 2009) (Fig. 7).

Many studies have documented the ability DSC perfusion MRI to predict tumor grade,

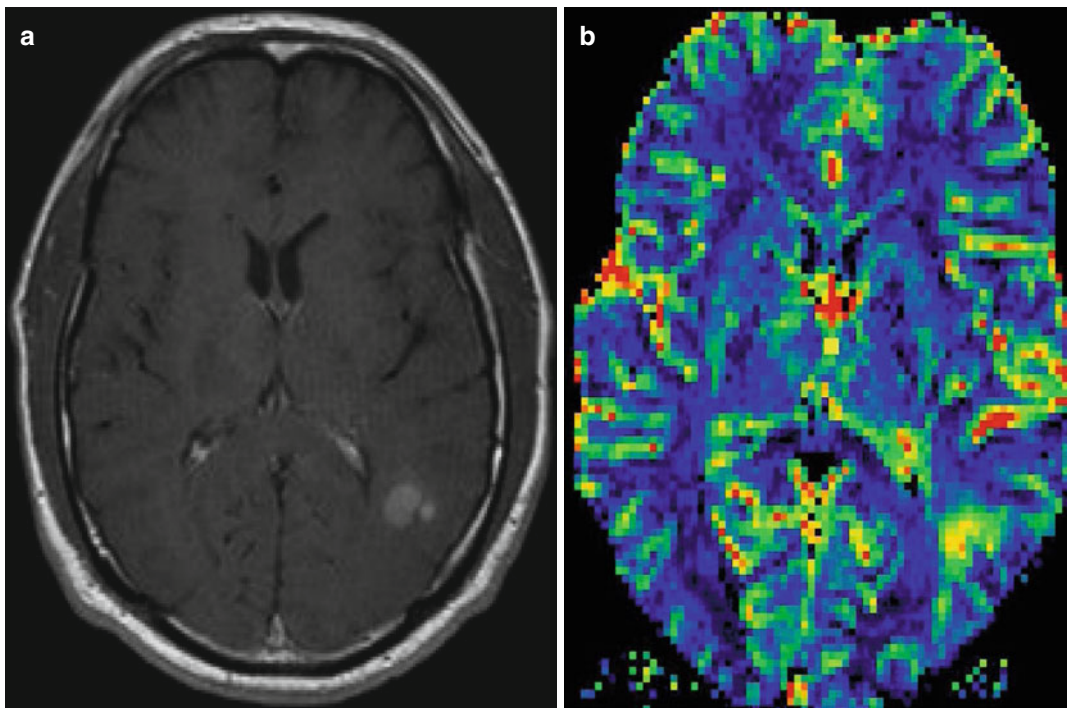


**Fig. 7** DSC perfusion MRI in a patient with recurrent high-grade glioma. The new contrast-enhanced nodule appeared at the superior border of the resection cavity. DSC-MRI reveals a high rCBV, which is suspicious of neovascularization

predict prognosis, and distinguish tumor recurrence from radiation necrosis (Barajas et al. 2009; Hu et al. 2009; Aronen et al. 1994; Knopp et al. 1999; Law et al. 2003, 2008; Caseiras et al. 2010).

Recently, a single-center prospective study of glioma patients was reported to address the lack of clinical long-term correlation (Matsusue et al. 2010). In this study, 59 consecutive patients with gliomas were evaluated by three neuroradiologists in consensus, first using conventional MRI sequences and afterwards with incorporation of qualitative analysis of perfusion imaging (which included both DSC and arterial spin-labeling perfusion MRI techniques). These imaging data were evaluated in conjunction with clinical data and were assessed in a multidisciplinary fashion with a clinical neuro-oncology team. Hypothetical treatment plans were created for each patient prospectively, first using conventional MRI and then using conventional MRI combined with perfusion MRI. Overall, it was concluded that the addition of perfusion imaging appeared to have a significant effect on neuroradiologists' and clinicians' confidence in tumor status as well as the course of clinical management. Larger multicenter confirmatory studies are needed.

rCBV appears to be elevated in patients with recurrent tumor compared with patients with DRN, likely reflective of the increased vascular proliferation and leaky capillaries of recurrent tumor, while DRN is composed of extensive fibrinoid necrosis, vascular dilation, and endothelial injury (Fig. 8) (Matsusue et al. 2010; Cha et al. 2007; Gahramanov et al. 2011; Mangla

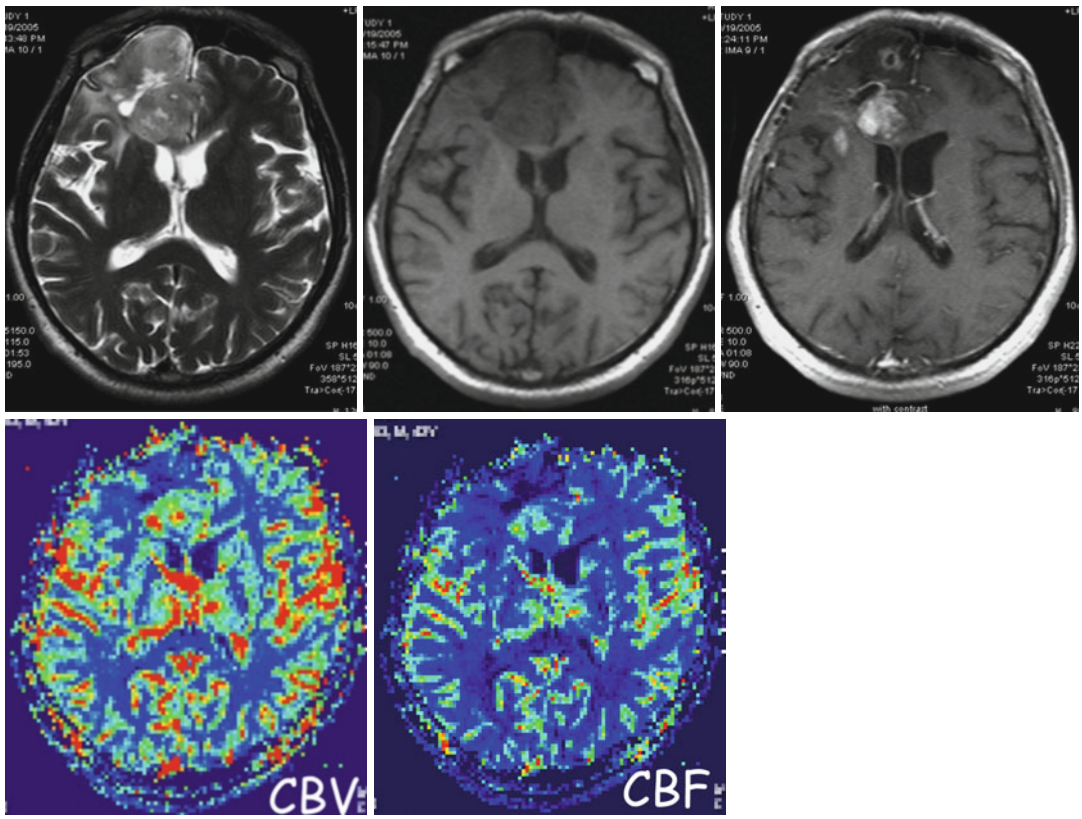


**Fig. 8** DSC perfusion MRI in a patient with right frontal malignant glioma (WHO grade IV) after combined radiochemotherapy. The tumor presented with growth and progressive mass effect with more pronounced contrast enhancement. Perfusion MRI presents high rCBV and rCBF values in the posterior aspect of the lesion with reduced perfusion in the anterior one

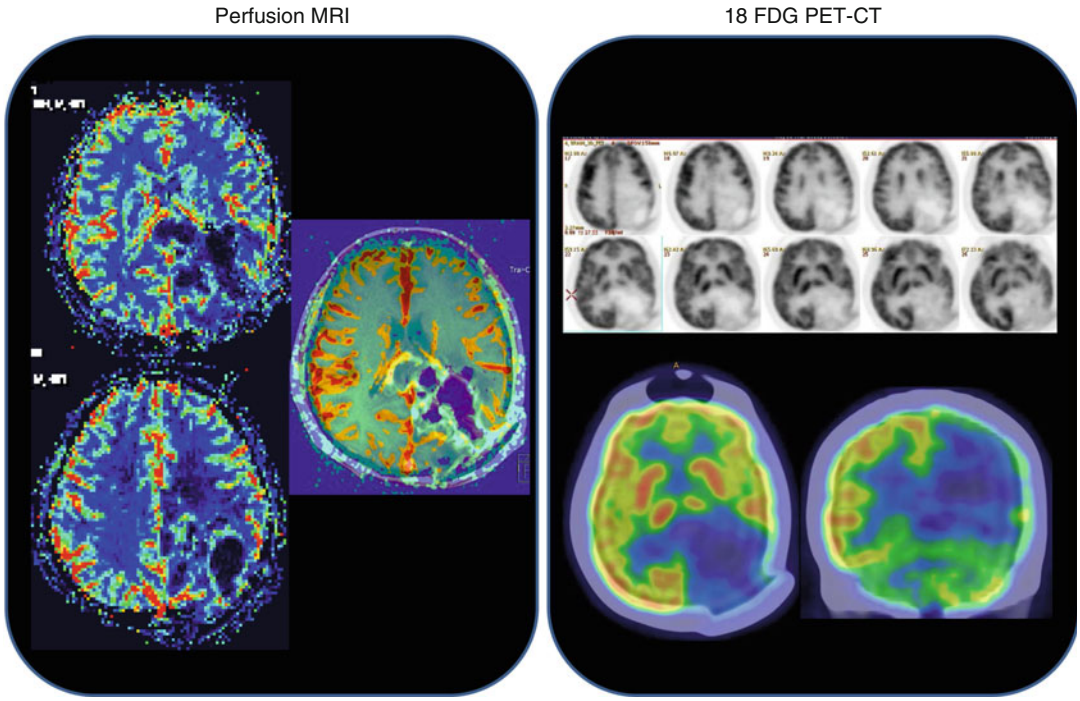


**Fig. 8** (continued)

et al. 2010; Geer et al. 2012). Barajas et al. recently reported increased ph value and rCBV as well as lower relative PSR in recurrent glioblastoma compared with DRN (Barajas et al. 2009).

### 4.2.2 DCE-MR Perfusion to Differentiate Treatment-Related Effects

DCE-MRI technique and pharmacokinetic analysis is more complex compared to DSC-MRI, and this is likely a major reason why this technique has not gained wider popularity. Non-pharmacokinetic model-based semiquantitative DCE techniques exist including evaluation of signal intensity time curves or "curve-ology." While semiquantitative metrics are less physiologically specific, they are relatively simple to derive and interpret. These techniques have been useful in tumors outside of the brain, such as prostate, cervical, and breast cancer (Alonzi et al. 2007; Mussurakis et al. 1998; Zelhof et al. 2009). Using analysis of signal intensity time curves, Narang et al. showed that the normalized maximum slope of enhancement in initial vascular phase (nMSIVP) allowed discrimination of recurrent tumor from treatment-induced necrosis. Their results indicated that the method is able to differentiate the two entities at a high sensitivity and specificity (Narang et al. 2011). The experience with DCE-MRI in the context of DRN is limited but also seems to indicate that there is lower permeability of DRN compared with recurrent tumor (Fig. 8).

A recent study of 18 high-grade glioma patients appeared to support this, where a $K^{trans}$ threshold of greater than 0.19 produced 100 % sensitivity and 83 % specificity for detecting recurrent glioma versus DRN. Based on these initial results, it is likely that both vascularity and permeability will be lower in PsP when compared with tumor recurrence.

Another situation where reliance on conventional contrast-enhanced MRI can be problematic is with the use of antiangiogenic agents such as bevacizumab in recurrent glioblastoma patients. These agents produce high response rates and 6-month progression-free survival; however,

their effects on overall survival appear rather modest (Batchelor et al. 2007). The term "pseudoresponse" refers to the rapid decrease in contrast enhancement without significant tumor reduction following treatment with antiangiogenic agents (Brandsma and van den Bent 2009). This phenomenon has been attributed to a decrease in vascular permeability due to "normalization" of the BBB induced by these agents (Gerstner et al. 2009). In addition, this vascular normalization has been shown to be reversible in patients who required a "drug holiday" (Batchelor et al. 2007). A "vascular normalization index" composed of changes in $K^{trans}$, rCBV, and circulating collagen IV appeared to be correlated with progression-free and overall survival as early as 1 day after treatment with cediranib (Sorensen et al. 2009). DCE perfusion can also be used for preoperative tumor grading (Nguyen et al. 2012).

## 4.3 Diffusion-Weighted Imaging and Diffusion Tensor Imaging

Diffusion-weighted imaging (DWI) is used routinely in the assessment of cerebral infarction and infectious diseases (Provenzale et al. 2006). Both, DWI and diffusion tensor imaging (DTI) play an important role in the diagnostic workup and monitoring of patients with cerebral tumors (Stadnik et al. 2003). The signal intensity of gliomas varies from hyper- over iso- to hypointense. The diffusion signal mainly depends on the cellularity of the lesion with some influence from the amount of necrosis, water content, and hemorrhage. The "normal" glioma appears hyperintense in DWI with a reduced apparent diffusion coefficient (ADC). ADC values cannot be used in individual cases to differentiate glioma types reliably (Stadnik et al. 2003; Kono et al. 2001; Sugahara et al. 1999; Gauvain et al. 2001; Lu et al. 2004; Stieltjes et al. 2006; Price et al. 2007). However, in the study of Kono et al. (2001), the combination of routine image interpretation and ADC values had the highest predictive value. In the study of Gauvain et al. (Gauvain et al. 2001), a clear distinction between the low-grade gliomas and the embryonal tumors was found. A differentiation between glioma and peritumoral edema based on ADC measurements was also not possible. In a recent study by Lu et al., peritumoral diffusion tensor metrics could not be used to distinguish intra-axial from extra-axial lesions or to determine the grade of gliomas preoperatively. However, peritumoral DTI values were reported to be helpful in distinguishing solitary intra-axial metastatic lesions from gliomas. In addition, the method enables one to distinguish presumed tumor-infiltrated edema from vasogenic edema composed purely of extracellular water. These capabilities of diffusion tensor MR imaging are helpful in current diagnostic scenarios and conceivably will be useful for broader applications in the future.

Stieltjes et al. used a model based on probabilistic voxel classification for a user-independent analysis of DTI-derived parameters (Stieltjes et al. 2006). The proposed quantification method proved to be highly reproducible both in healthy controls and patients. Fiber integrity in the corpus callosum was measured using this quantification method, and the profiles of fractional anisotropy (FA) provided additional information of the possible extent of infiltration of primary brain tumors when compared to conventional imaging (Fig. 9). This yielded additional information on the nature of ambiguous contralateral lesions in patients with primary brain tumors. The results show that DTI-derived parameters can be determined reproducibly and may have a strong impact on evaluation of contralateral extent of primary brain tumors. A recent study also proved that the method enables to predict the patterns of glioma recurrence (Fink et al. 2012).

## 4.4 Positron Emission Tomography (PET) and Single-Proton Emission Computed Tomography (SPECT)

PET using fluorodeoxyglucose (FDG) as tracer was found to be a promising methodology to differentiate tumor from treatment-related changes (Kim et al. 2010; Ozsunar et al. 2010) with a

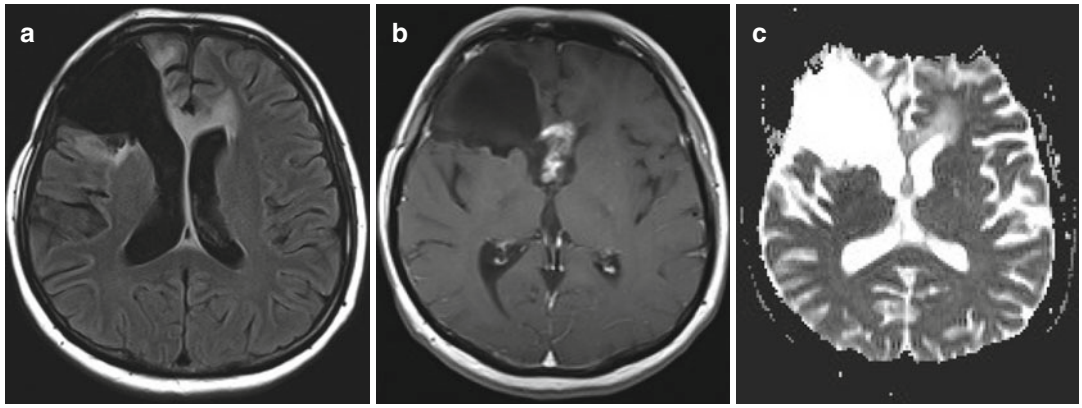


**Fig. 9** Diffusion-weighted imaging in a patient with recurrent anaplastic astrocytoma (**a**, **b**). The recurrent tumor is characterized by restricted diffusion (**c**). The higher the tumor cell density, the more diffusion restriction can be seen. In lesions with more treatment-related changes, this diffusion restriction is generally absent

sensitivity of up to 81 % and a specificity of up to more than 90 %. However, there have been reports that failed to confirm this based on the following problems. Firstly, the FDG uptake of normal gray matter is often as high as in tumors with often mixed uptakes, leading to non-conclusive results (Prat et al. 2010). Secondly, inflammatory cells also tend to accumulate FDG (Meler et al. 2007). These cells are often found in the border zone of both tumor and treatment changes. The accumulation has even been described in radiation necrosis. Newer tracers using amino acid analogs presented interesting results as they are more tumor specific and the uptake in normal tissue is rather low (Ceyssebs et al. 2006; Tsuyuguchi et al. 2004; Miyashita et al. 2008).

SPECT works similar as conventional nuclear medicine imaging but adds a three-dimensional information by including the CT technology which allows to see the uptake from multiple angles. Multiple SPECT tracers have been used to differentiate treatment-related changes and reported to be superior to structural imaging. Sensitivities range from 40 to 100 %, which shows the variability of the method. Another drawback is the fairly low spatial resolution and the high radiation doses applied. Approaches using higher-emitting tracers allowing for a higher resolution and lower dosage have the problem of substantial uptake in normal tissues, which lowers their sensitivity.

**Conclusion**

Radiation is commonly used in both neuro-oncologic and non-neuro-oncologic therapy concepts in the CNS. Because of the great variety in the use of radiation with a different degree of effect on pathologic and normal tissue, the imaging findings in radiation-induced tissue changes are complex. For the radiologist it is of importance to identify changes that are different from tumor-induced changes as it allows an early intervention or change in the treatment concept.

Standard morphologic imaging is often not sufficient to fulfill these requirements even if there are some typical findings that suggest treatment-induced changes. Advanced imaging tools like functional MR imaging and PET may enable a better differentiation.

## References

Alger JR, Frank JA, Bizzi A et al (1990) Metabolism of human gliomas: assessment with H-1 MR spectroscopy and F-18 fluorodeoxyglucose PET. Radiology 177:633–641

Alonzi R, Padhani AR, Allen C (2007) Dynamic contrast enhanced MRI in prostate cancer. Eur J Radiol 63:335–350

Aronen HJ, Gazit IE, Louis DN et al (1994) Cerebral blood volume maps of gliomas: comparison with tumor grade and histologic findings. Radiology 191: 41–51

Barajas RF, Chang JS, Sneed PK, Segal MR, McDermott MW, Cha S (2009) Distinguishing recurrent intra-axial metastatic tumor from radiation necrosis following gamma knife radiosurgery using dynamic susceptibility-weighted contrast-enhanced perfusion MR imaging. AJNR Am J Neuroradiol 30:367–372

Batchelor TT, Sorensen AG, di Tomaso E et al (2007) AZD2171, a pan-VEGF receptor tyrosine kinase inhibitor, normalizes tumor vasculature and alleviates edema in glioblastoma patients. Cancer Cell 11:83–95

Bisdas S, Naegele T, Ritz R et al (2011) Distinguishing recurrent high-grade gliomas from radiation injury: a pilot study using dynamic contrast-enhanced MR imaging. Acad Radiol 18:575–583

Brandes AA, Franceschi E, Tosoni A et al (2008) MGMT promoter methylation status can predict the incidence and outcome of pseudoprogression after concomitant radiochemotherapy in newly diagnosed glioblastoma patients. J Clin Oncol 26:2192–2197

Brandsma D, van den Bent MJ (2009) Pseudoprogression and pseudoresponse in the treatment of gliomas. Curr Opin Neurol 22:633–638

Brandsma D, Stalpers L, Taal W, Sminia P, van den Bent MJ (2008) Clinical features, mechanisms, and management of pseudoprogression in malignant gliomas. Lancet Oncol 9:453–461

Brix G, Semmler W, Port R et al (1991) Pharmacokinetic parameters in CNS Gd-DTPA enhanced MR imaging. J Comput Assist Tomogr 15(4):621–628

Caseiras GB, Chheang S, Babb J et al (2010) Relative cerebral blood volume measurements of low-grade gliomas predict patient outcome in a multi-institution setting. Eur J Radiol 73:215–220

Ceyssebs S, Van Laere K, de Groot T et al (2006) 11C-Methionine PET, histopathology, and survival in primary brain tumors and recurrence. AJNR Am J Neuroradiol 27:1432–1437

Cha S, Knopp EA, Johnson G et al (2002) Intracranial mass lesions: dynamic contrast-enhanced susceptibility-weighted echo-planar perfusion MR imaging. Radiology 223:11–29

Cha S, Lupo JM, Chen MH et al (2007) Differentiation of glioblastoma multiforme and single brain metastasis by peak height and percentage of signal intensity recovery derived from dynamic susceptibility-weighted contrast-enhanced perfusion MR imaging. AJNR Am J Neuroradiol 28:1078–1084

Chamberlain MC (2008) Pseudoprogression in Glioblastoma. J Clin Oncol 10:43–59

Chaskis C, Neyns B, Michotte A, De RM, Everaert H (2009) Pseudoprogression after radiotherapy with concurrent temozolomide for high-grade glioma: clinical observations and working recommendations. Surg Neurol 72:423–428

Clarke JL, Chang S (2009) Pseudoprogression and pseudoresponse: challenges in brain tumor imaging. Curr Neurol Neurosci Rep 9:241–246

Delorme S, Weber MA (2006) Applications of MRS in the evaluation of focal malignant brain lesions. Cancer Imaging 6:95–99

Demaerel P, Johannik K, van Hecke P et al (1991) Localized 1H NMR spectroscopy in fifty cases of newly diagnosed intracranial tumors. J Comput Assist Tomogr 15:67–76

Deviers A, Ken S, Fillerton T et al (2014) Evaluation of the lactate-n-acetyl aspartate ration defined with magnetic resonance spectroscopic imaging before radiation therapy as a new predictive marker of the site of relapse in patient with glioblastoma multiforme. Int J Radiat Oncol Biol Phys 90:385–393

Dowling C, Bollen AW, Noworolski SM et al (2001) Preoperative proton MR spectroscopic imaging of brain tumors: correlation with histopathologic analysis of resection specimens. AJNR Am J Neuroradiol 22:604–612

Essig M, Anzalone N, Combs SE et al (2011) MR imaging of neoplastic central nervous system lesions: review and recommendations for current practice. AJNR Am J Neuroradiol 33:803–817

Essig M, Shiroishi MS, Nguyen TB et al (2013a) Perfusion MRI: the five most frequently asked technical questions. Am J Roentgenol 200:24–34

Essig M, Nguyen TB, Shiroishi MS et al (2013b) Perfusion MRI: the five most asked clinical questions. Am J Roentgenol 201:495–510

Fink JR, Carr RB, Matsusue E et al (2012) Comparison of 3 T proton MR spectroscopy, MR perfusion and MR diffusion for distinguishing glioma recurrence from posttreatment effects. J Magn Reson Imaging 35: 56–63

Finn MA, Blumenthal DT, Salzman KL, Jensen RL (2007) Transient postictal MRI changes in patients with brain tumors may mimic disease progression. Surg Neurol 67:246–250

Gahramanov S, Raslan AM, Muldoon LL et al (2011) Potential for differentiation of pseudoprogression from true tumor progression with dynamic susceptibility-weighted contrast-enhanced magnetic resonance imaging using ferumoxytol vs. gadoteridol: a pilot study. Int J Radiat Oncol Biol Phys 79:514–523

Gauvain KM, McKinstry RC, Mukherjee P et al (2001) Evaluating pediatric brain tumor cellularity with diffusion-tensor imaging. AJR Am J Roentgenol 177:449–454

Geer CP, Simonds J, Anvery A et al (2012) Does MR perfusion imaging impact management decisions for patients with brain tumors? A prospective study. AJNR Am J Neuroradiol 33:556–562

Gerstner ER, Duda DG, di Tomaso E et al (2009) VEGF inhibitors in the treatment of cerebral edema in patients with brain cancer. Nat Rev Clin Oncol 6:229–236

Green-Schloesser D, Robbins ME (2012) Radiation induced cognitive impairment – from bench to bedside. Neurol Oncol 14:S37–S44

Hazle JD, Jackson EF, Schomer DF, Leeds NE (1997) Dynamic imaging of intracranial lesions using fast spin-echo imaging: differentiation of brain tumors and treatment effects. J Magn Reson Imaging 7:1084–1093

Hu LS, Baxter LC, Smith KA et al (2009) Relative cerebral blood volume values to differentiate high-grade

glioma recurrence from posttreatment radiation effect: direct correlation between image-guided tissue histopathology and localized dynamic susceptibility-weighted contrast-enhanced perfusion MR imaging measurements. AJNR Am J Neuroradiol 30:552–558

Kickingereder P, Dorn F, Blau T, Schmidt M, Kocher M, Galldiks N, Ruge MI (2013) Differentiation of local tumor recurrence from radiation induced changes after stereotactic radiosurgery of brain metastasis: case report and review of the literature. Radiat Oncol 8:52–59

Kim YH, Oh SW, Lim YJ et al (2010) Differentiating radiation necrosis from tumor recurrence in high grade gliomas: assessing the efficacy of 18F-FDG, 11C-methionie PET and perfusion MRI. Clin Neurol Neurosurg 112:758–765

Kingsley DP, Kendall BE (1981) CT of adverse effects of therapeutic radiation of the central nervous system. Am J Neuroradiol 2:453–460

Knopp EA, Cha S, Johnson G et al (1999) Glial neoplasms: dynamic contrast-enhanced T2*-weighted MR imaging. Radiology 211:791–798

Kong DS, Kim ST, Kim EH et al (2011) Diagnostic dilemma of pseudoprogression in the treatment of newly diagnosed glioblastomas: the role of assessing relative cerebralbloodflowvolumeandoxygen-6-methylguanine-DNA methyltransferase promoter methylation status. AJNR Am J Neuroradiol 32:382–387

Kono K, Inoue Y, Nakayama K et al (2001) The role of diffusion-weighted imaging in patients with brain tumors. AJNR Am J Neuroradiol 22:1081–1088

Kumar AJ, Leeds NE, Fuller GN et al (2000) Malignant gliomas: MR imaging spectrum of radiation therapy- and chemotherapy-induced necrosis of the brain after treatment. Radiology 217(2):377–384

Kunert P, Matzia E, Prokopienko M, Marchel A (2012) Radiation-induced tumours of meninges. Report on eight cases and review of the literature. Neurol Neurochir Pol 46:542–552

Lacerda S, Law M (2009) Magnetic resonance perfusion and permeability imaging in brain tumors. Neuroimag Clin N Am 19:527–557

Law M (2004) MR spectroscopy of brain tumors. Top Magn Reson Imaging 15:291–313

Law M, Yang S, Wang H et al (2003) Glioma grading: sensitivity, specificity, and predictive values of perfusion MR imaging and proton MR spectroscopic imaging compared with conventional MR imaging. AJNR Am J Neuroradiol 24:1989–1998

Law M, Young RJ, Babb JS et al (2008) Gliomas: predicting time to progression or survival with cerebral blood volume measurements at dynamic susceptibility-weighted contrast-enhanced perfusion MR imaging. Radiology 247:490–498

Lu S, Ahm D, Johnson G, Law M, Zagzag D, Grossman RI (2004) Diffusion-tensor MR imaging of intracranial neoplasia and associated peritumoral edema: introduction of the tumor infiltration index. Radiology 232(1):221–228

Lv XF, Zheng XL, Zhang WD, Liu LZ, Zhang YM, Chen MZ, Li L (2014) Radiation-induced changes in normal appearing gray matter in patients with nasopharyngeal carcinomas. A magnetic resonance imaging voxel-based morphometry study. Neuroradiology 56:423–430

Macdonald DR, Cascino TL, Schold SC Jr, Cairncross JG (1990) Response criteria for phase II studies of supratentorial malignant glioma. J Clin Oncol 8:1277–1280

Madden JR, Addo-Yobo SO, Donson AM et al (2010) Radiation induced glioblastoma multiforme in children treated for medulloblastoma with characteristics of both medulloblastoma and glioblastoma multiforme. J Pediatr Hematol Oncol 32:272–278

Mangla R, Singh G, Ziegelitz D et al (2010) Changes in relative cerebral blood volume 1 month after radiation-temozolomide therapy can help predict overall survival in patients with glioblastoma. Radiology 256:575–584

Mansouri, A, Badhiwala J, Mansouri S, Zadeh G (2014) The evolving role of radiosurgery in the management of radiation induced meningiomas: a review of current advances and future directions. Biomed Res Int. 2014:107526. doi: 10.1155/2014/107526

Matsusue E, Fink JR, Rockhill JK, Ogawa T, Maravilla KR (2010) Distinction between glioma progression and post-radiation change by combined physiologic MR imaging. Neuroradiology 52:297–306

Meler J, Sahlmann CO, Scheel AK (2007) 18F-FDG PET and PET-CT in fever of unknown origin. J Nucl Med 48:35–45

Meyerand ME, Pipes JM, Mamourian A, Tosteson TD, Dunn JF (1999) Classification of biopsy-confirmed brain tumors using single-voxel MR spectroscopy. AJNR Am J Neuroradiol 20:117–123

Miyashita M, Miyatake S, Imahori Y et al (2008) Evaluation of fluoride-labeled boronophenylalanine-PET imaging for the study of radiation effects in patients with glioblastomas. J Neurooncol 89:239–246

Mullins ME, Barest GD, Schaefer PW et al (2005) Radiation necrosis versus glioma recurrence: conventional MR imaging clues to diagnosis. AJNR Am J Neuroradiol 26(8):1967–1972

Mussurakis S, Gibbs P, Horsman A (1998) Primary breast abnormalities: selective pixel sampling on dynamic gadolinium-enhanced MR images. Radiology 206:465–473

Narang J, Jain R, Arbab AS et al (2011) Differentiating treatment-induced necrosis from recurrent/progressive brain tumor using nonmodel-based semiquantitative indices derived from dynamic contrast-enhanced T1-weighted MR perfusion. Neuro Oncol 13:1037–1046

Negendank WG, Sauter R, Brown TR et al (1996) Proton magnetic resonance spectroscopy in patients with glial tumors: a multicenter study. J Neurosurg 84:449–458

Nguyen TB, Cron GO, Mercier JF et al (2012) Diagnostic accuracy of dynamic contrast-enhanced MR imaging using a phase-derived vascular input function in the preoperative grading of gliomas. AJNR Am J Neuroradiol 33(8):1539–1545

Ozsunar Y, Mullins ME, Kwong K et al (2010) Glioma recurrence versus radiation necrosis? A pilot comparison of ASL, DSC MRI and FDG-PET. Acad Radiol 17:282–290

Patel TR, McHugh BJ, Bi WL, Minhja FJ, Knisely JP, Chiang VL (2011) A comprehensive review of MR

imaging changes following radiosurgery to 500 brain metastases. AJNR Am J Neuroradiol 32:1885–1892
Prat R, Galeano I, Lucas A et al (2010) Relative value of magnetic resonance spectroscopy, magnetic resonance perfusion and 2-18FDGfor detection of recurrence or grade increase in gliomas. J Clin Neurosci 17:50–53
Price SJ, Jena R, Burnet NG, Carpenter TA, Pickard JD, Gillard JH (2007) Predicting patterns of glioma recurrence using diffusion tensor imaging. Eur Radiol 17:1675–1684
Provenzale JM, Mukundan S, Barboriak DP (2006) Diffusion-weighted and perfusion MR imaging for brain tumor characterization and assessment of treatment response. Radiology 239(3):632–649
Rane N, Quaghebeur G (2012) CNS effects following the treatment of malignancy. Clin Radiol 67:61–68
Reddy K, Westerly D, Chen C (2013) MRI patterns of T1 enhancing radiation necrosis versus tumour recurrence in high grade gliomas. J Med Imaging Radiat Oncol 57:349–355
Sorensen AG, Batchelor TT, Zhang WT et al (2009) A "vascular normalization index" as potential mechanistic biomarker to predict survival after a single dose of cediranib in recurrent glioblastoma patients. Cancer Res 69:5296–5300
Stadnik TW, Demaerel P, Luypaert RR et al (2003) Imaging tutorial: differential diagnosis of bright lesion on diffusion-weighted MR images. Radiographics 23(1):e7
Stieltjes B, Schluter M, Didinger B, Weber MA, Hahn HK, Parzer P, Rexilius J, Konrad-Verse O, Peitgen HO, Essig M (2006) Diffusion tensor imaging in primary brain tumors: reproducible quantitative analysis of corpus callosum infiltration and contralateral involvement using a probabilistic mixture model. Neuroimage 31(2):531–542
Sugahara T, Korogi Y, Kochi M et al (1999) Usefulness of diffusion-weighted MRI with echo-planar technique in the evaluation of cellularity in gliomas. J Magn Reson Imaging 9:53–60
Szerlip N, Rutter C, Ram N et al (2011) Factors impacting volumetric white matter changes following whole brain radiation therapy. J Neurooncol 103:111–119
Tofts PS, Kermode AG (1991) Measurement of the blood–brain barrier permeability and leakage space using dynamic MR imaging. 1. Fundamental concepts. Magn Reson Med 17(2):357–367
Tsuyuguchi N, Takami T, Sunada I et al (2004) Methionine positron emission tomography for differentiation of recurrent brain tumor and radiation necrosis after stereotactic radiosurgery – in malignant glioma. Ann Nucl Med 18:291–296
Van den Bent MJ, Wefel JS, Schiff D et al (2011) Response assessment in neurooncology (a report of the RANO group): assessment of outcome in trial of diffuse low-grade gliomas. Lancet Oncol 12:583–593
Vuori K, Kankaanranta L, Hakkinen AM et al (2004) Low-grade gliomas and focal cortical developmental malformations: differentiation with proton MR spectroscopy. Radiology 230:703–708
Wiggenraad R, Verbeek-de Kanter A, Kal HB et al (2011) Dose effect relation in stereotactic radiotherapy for brain metastases. A systematic review. Radiother Oncol 98:292–297
Wilson M, Cummins CL, Macpherson L et al (2013) Magnetic resonance spectroscopy metabolite profiles predict survival in paediatric brain tumours. Eur J Cancer 13:457–464
Young RJ, Gupta A, Shah AD et al (2011) Potential utility of conventional MRI signs in diagnosing pseudoprogression in glioblastoma. Neurology 76:1918–1924
Yu JB, Schulder M, Knisely J (2012) Radiosurgical dose selection for brain metastases. Prog Neurol Surg 25:139–147
Zelhof B, Lowry M, Rodrigues G, Kraus S, Turnbull L (2009) Description of magnetic resonance imaging-derived enhancement variables in pathologically confirmed prostate cancer and normal peripheral zone regions. BJU Int 104:621–627

# Central Nervous System Complications in Patients Undergoing Chemotherapy

Dimitri Psimaras, D. Leclercq, D. Ricard, and J.Y. Delattre

## Contents



D. Psimaras (✉) • J.Y. Delattre
AP-HP, Groupe Hospitalier Pitié-Salpêtrière, Service de Neurologie 2-Mazarin, 47 Bd de l'hôpital, Paris 75013, France

Centre OncoNeuroTox, Paris, France

Sorbonne Universités, Sorbonne Universités, UPMC Univ. Paris 06, Inserm, CNRS, UM 75, U 1127, UMR 7225, ICM, F-75013, Paris, France
e-mail: dimitri.psimaras@psl.aphp.fr

D. Leclercq
Centre OncoNeuroTox, Paris, France

Sorbonne Universités, Sorbonne Universités, UPMC Univ. Paris 06, Inserm, CNRS, UM 75, U 1127, UMR 7225, ICM, F-75013, Paris, France

Service de Neuroradiologie, Hôpital Salpêtrière, Paris, France

D. Ricard
Centre OncoNeuroTox, Paris, France

Sorbonne Universités, Sorbonne Universités, UPMC Univ. Paris 06, Inserm, CNRS, UM 75, U 1127, UMR 7225, ICM, F-75013, Paris, France

Service de Neurologie, Hôpital d'instruction des armées du Val-de-Grâce, Service de Santé des Armées, Paris, France

**Abstract**

Anticancer treatments (cytotoxic chemotherapies, targeted therapies, and hormonotherapies) are known to induce early and delayed neurological toxicities, but it is often difficult to determine which drug is causing the symptoms in patients treated with multiple cytotoxic drugs. Acute encephalopathies and posterior reversible encephalopathies are the most characteristic syndromes. The main central nervous system (CNS) complications of commonly used agents are the subject of this chapter. As life expectancy increases in cancer patients and more complex regimens including innovative targeted therapies are developed, new toxicity profiles are emerging. To be able to provide early diagnosis, prevention, and treatment remains a difficult but important challenge since these complications may severely affect quality of life in patients who are cured of their cancer.

Med Radiol Diagn Imaging (2014),
DOI 10.1007/174_2014_1050, 

## Abbreviations

| | |
|---|---|
| AIDS | Acquired immunodeficiency syndrome |
| Ara-C | Cytarabine |
| CNS | Central nervous system |
| CSF | Cerebrospinal fluid |
| CVST | Cerebral venous sinus thrombosis |
| EEG | Electroencephalography |
| GVHD | Graft-versus-host disease |
| HSCT | Hematopoietic stem cell transplantation |
| IRIS | Immune reconstitution inflammatory syndrome |
| IT | Intrathecal |
| IV | Intravenous |
| MRI | Magnetic resonance imaging |
| MTX | Methotrexate |
| PML | Progressive multifocal leukoencephalopathy |
| PRES | Posterior reversible encephalopathy syndrome |

## 1 Introduction

Despite advances in the effectiveness of anticancer chemotherapy, from cytotoxic to biologic agents, neurotoxicity remains a common and limiting side effect. It can be difficult for the clinician to distinguish it from other neurological complications of cancer (e.g., metastatic, vascular, or infectious) and imaging is of great importance for differential diagnosis.

Chemotherapy-induced central nervous system (CNS) toxicity is much less frequent than peripheral nervous system toxicity. It can be delayed but is often acute, unpredictable, and reversible. Its incidence is not well established in the literature but risk seems to grow with age, exposure to high-dose regimens (or high concentrations due to impaired systemic clearance), and treatment combination (multiagent chemotherapy, intrathecal administration, concurrent or subsequent cerebral irradiation) (Shah 2005; Sul and DeAngelis 2006; Jansen et al. 2005; Keime-Guibert et al. 1998). The question of interindividual sensibility is also raised.

Neurotoxicity of chemotherapies used for brain tumors and extra-CNS tumors can vary. Brain tumors with already damaged cerebral parenchyma and altered blood-brain and blood-tumor barriers seem to be at higher risk for chemotherapy-induced CNS neurotoxicity. Moreover, a higher-dosage regimen is often necessary to target brain tumors; this is particularly the case for methotrexate (MTX) and aracytine as drugs that cross the blood-brain barrier only when used at high doses (Muldoon et al. 2007). Nevertheless, the correlation between chemotherapy and chemotherapy-induced toxicity cannot always be established since unrelated coincidental events may also occur (Fig. 1).

Cytotoxic agents are still the most frequent offenders (Table 1). Biologic agents may provoke encephalopathy (in particular posterior reversible encephalopathy syndrome) or vascular complications. Antineoplastic hormones can be responsible for cognitive alterations. Hematopoietic stem cell transplantation (HSCT) is also associated with drug-related neurological toxicity, particularly encephalopathy, but differentiating between this diagnosis and infections may be challenging. In this chapter, the main types of CNS syndromes as complications of antineoplastic chemotherapy/biologic agents will be reported first, followed by a description of the potential neurotoxicity of individual agents. The lack of reported toxicity will also be briefly noted as it may be of help for the clinician.

## 2 Main Types of Central Nervous System Complications

### 2.1 Acute and Subacute Complications

#### 2.1.1 Encephalopathy

Acute and subacute encephalopathy is a common problem in oncology patients. Symptoms vary from headaches, seizure, drowsiness, or confusion to coma. The diagnosis of drug-induced

encephalopathy is typically one of exclusion; a wide range of precipitating factors has to be examined (metabolic disorders, hypoxia, brain metastases, meningeal carcinomatosis, infection, paraneoplastic neurological syndromes, and other drugs). Two types of acute/subacute encephalopathies present a more characteristic clinical-radiological picture.

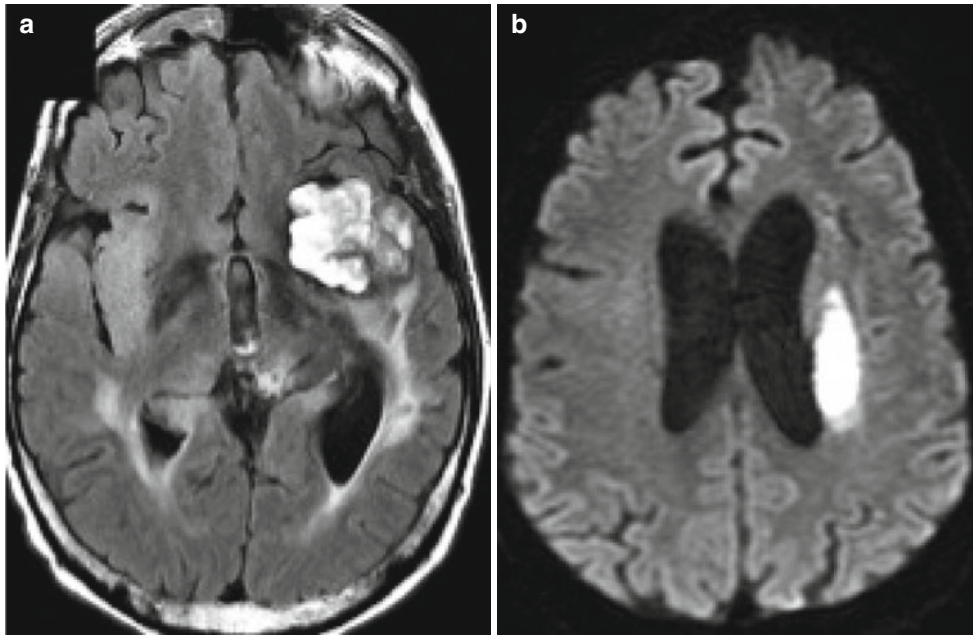


**Fig. 1** Parenchymal hematoma and secondary stroke in a patient with gliomatosis cerebri who received adjuvant temozolomide 3 days before. The possible link between temozolomide and stroke is unsettled; there are no vascular complications reported in the literature. (**a**) FLAIR images: left fronto-temporo-insular hemorrhagic lesion bulging in the sylvian fissure. Temporo-insular white matter hyperintensity and infiltrative hyperintensity in the right insular lobe and thalamus in relation to the gliomatosis cerebri. (**b**) Diffusion-weighted image: secondary acute deep middle cerebral ischemic stroke

**Table 1** Cytotoxic chemotherapies and neurotoxicity in central nervous system

| Delay/treatment | 0–4 weeks | 4 weeks to 6 months | >6 months |
|---|---|---|---|
| Aseptic meningitis | Methotrexate (IT)<br>Aracytine (IT)<br>Triphosphoramide (IT) | | |
| Cerebellar syndrome | Aracytine<br>Capecitabine<br>Carmustine<br>Ifosfamide<br>Vincristine | | |
| Cranial neuropathies | Carboplatin, Carmustine, Cisplatin, Ifosfamide, Methotrexate, Nelarabine, Oxaliplatin, Paclitaxel, Docetaxel, Vincristine, 5-FU Cytarabine, Etoposide | | |

(continued)

**Table 1** (continued)

| Delay/treatment | 0–4 weeks | 4 weeks to 6 months | >6 months |
|---|---|---|---|
| Encephalopathy | L-Asparaginase<br>Carmustine<br>Capecitabine<br>Carboplatin<br>Chlorambucil<br>Cisplatin<br>Cyclophosphamide<br>Cyclosporin<br>Cytarabine<br>Docetaxel<br>Etoposide<br>Fludarabine (high doses)<br>5-FU<br>Gemcitabine<br>Hexamethylamine<br>Ifosfamide<br>Mechlorethamine<br>Methotrexate<br>Nelarabine<br>Paclitaxel<br>Procarbazine<br>Taxanes<br>Thiotepa (high dose)<br>Vinca-alcaloides<br>Gemcitabine | Methotrexate | Carmustine<br>Cisplatin<br>Cytarabine<br>5-FU<br>Fludarabine (high doses)<br>Ifosfamide<br>Methotrexate<br>Vincristine |
| Headaches | Capecitabine, Clofarabine, Cisplatin, Dacarbazine, Estramustine, Fludarabine, Hexamethylamine, Mechlorethamine, Nelarabine, Procarbazine, Temozolomide, Thiotepa (IT), Topoisomerase I inhibitors | | |
| Myelopathy | Carmustine, Cisplatin, Cytarabine (IV or IT), Methotrexate (IV or IT), Nelarabine, Thiotepa, Vincristine | | |
| Seizures | Cisplatin<br>Busulfan<br>Cyclophosphamide<br>Ifosfamide<br>Mechlorethamine<br>Methotrexate<br>Nelarabine<br>Pentostatin<br>Taxanes<br>Temozolomide<br>Vincristine | 5-FU | |
| Stroke | L-Asparaginase, Carboplatin, Carmustine, Cisplatin, Cyclophosphamide, 5-FU, Gemcitabine, Methotrexate (IT), Paclitaxel | | |

*5-FU* 5-fluorouracil, *IV* intravenous, *IT* intrathecal

#### 2.1.1.1 Posterior Reversible Encephalopathy Syndrome (PRES)

Posterior reversible encephalopathy syndrome (PRES) is a well-described clinico-radiographic syndrome associated with headaches, seizures, altered level of consciousness, visual disturbances, and hyperintense lesions on magnetic resonance imaging. PRES was initially described in 1996 in patients with elevated blood pressure; it is typically associated with a number of clinical conditions: preeclampsia/eclampsia syndrome, autoimmune diseases, and immunosuppressive medications or antineoplastic therapy (Hinchey et al. 1996). Prior studies of PRES have included a minority of patients with chemotherapy as a presumed cause (Lee et al. 2008; Tlemsani et al. 2011; Liman et al. 2012). As time goes on, the causative agents list is getting longer (Table 2). MRI shows abnormalities within 72 h, on fluid-attenuated axial inversion recovery (FLAIR) sequences (Fig. 2). The lesions are bilateral and quite symmetrical, commonly in the white matter area and posterior regions. Contrast enhancement, gray matter (cortex or basal ganglia), or anterior involvements have also been described (Bartynski and Boardman 2007; Donmez et al. 2010). Clinical improvement is the rule after discontinuation of the responsible agent, generally in less than one week. MRI is normalized in 72 % of patients within 2 months (a median period of 41 days) (Helissey et al. 2012). Secondary vascular complications (ischemic or hemorrhage) are rare (Tlemsani et al. 2011). Reexposure to the putative responsible agent is safe if accompanied by vigilant clinical monitoring and blood pressure control. Relapse is possible (3–8 %) even many years later, still with a good outcome, except in rare cases (Roy et al. 2014).

**Table 2** Chemotherapies associated with posterior reversible encephalopathy syndrome (PRES)

| |
|---|
| Aflibercept |
| L-Asparaginase |
| Bevacizumab |
| Bortezomib |
| Carboplatin |
| Cediranib |
| Cisplatin |
| Cyclophosphamide |
| Cyclosporin |
| Cytarabine |
| 5-FU (5-fluorouracil) |
| Gemcitabine |
| Interferon alpha |
| Ipilimumab |
| Methotrexate |
| Oxaliplatin |
| Pazopanib |
| Rituximab |
| Sirolimus |
| Sorafenib |
| Sunitinib |
| Tacrolimus |
| Tamoxifen |
| Trastuzumab |
| Vincristine |
| Vinflunine |
| Vinorelbine |

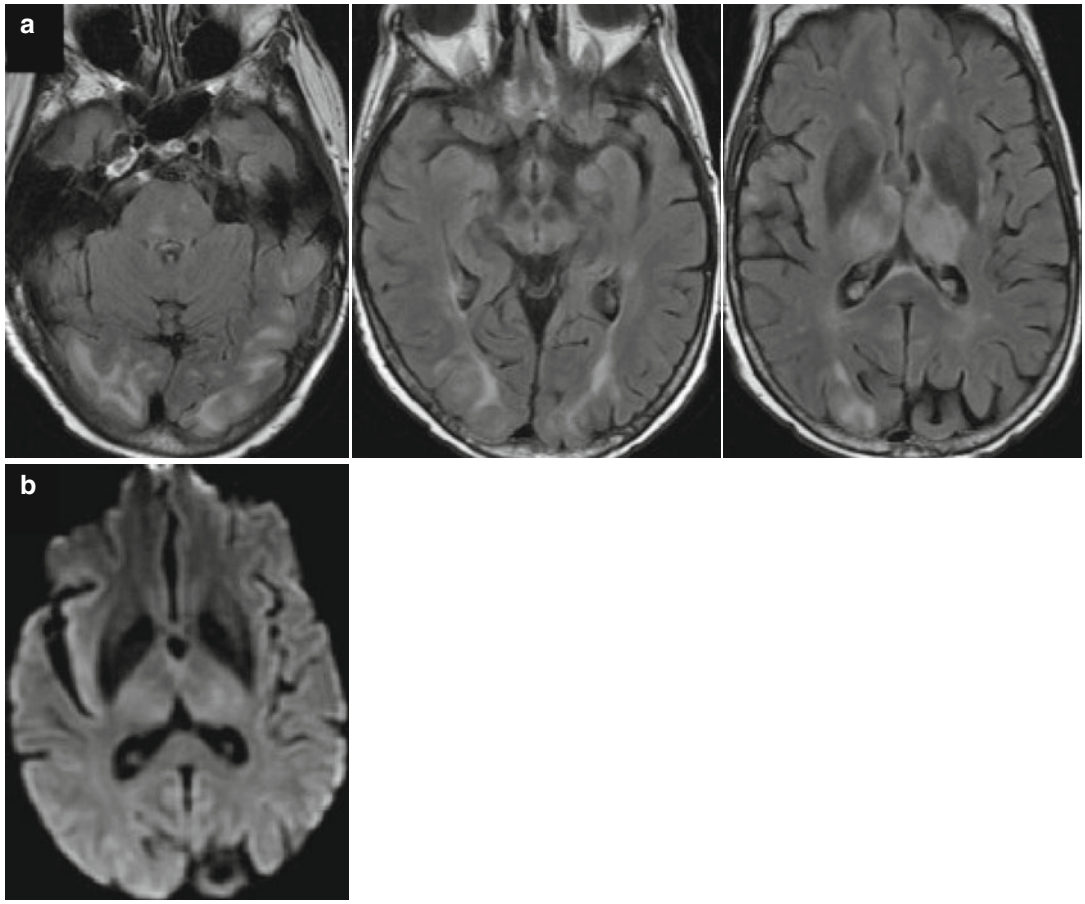


**Fig. 2** PRES in a 62-year-old patient treated with gemcitabine and cisplatin for pulmonary adenocarcinoma. One week after the last treatment, the patient presented with high blood pressure, headaches, prosopagnosia, alexia, and simultanagnosia. (**a**) MRI axial FLAIR images show bilateral symmetric hypersignal in the temporo-occipital subcortical white matter and in the thalami. (**b**) Diffusion-weighted images (DWI) are normal, without hypersignal, which is consistent with vasogenic edema. Clinical and radiological recovery was complete within one month after gemcitabine and cisplatin withdrawal

#### 2.1.1.2 Progressive Multifocal Leukoencephalopathy (PML)

Progressive multifocal leukoencephalopathy (PML) is a subacute demyelinating disorder caused by JC virus reactivation. It occurs more frequently in patients treated with chemotherapy (Table 3) or transplantation. Symptoms (cognitive deficiency, sensorimotor or visual disturbances) can occur many months to years after

**Table 3** Chemotherapies associated with progressive multifocal leukoencephalopathy

| |
|---|
| Alemtuzumab |
| Brentuximab |
| Cyclophosphamide |
| Efalizumab |
| Rituximab |
| Sirolimus |
| Tacrolimus |

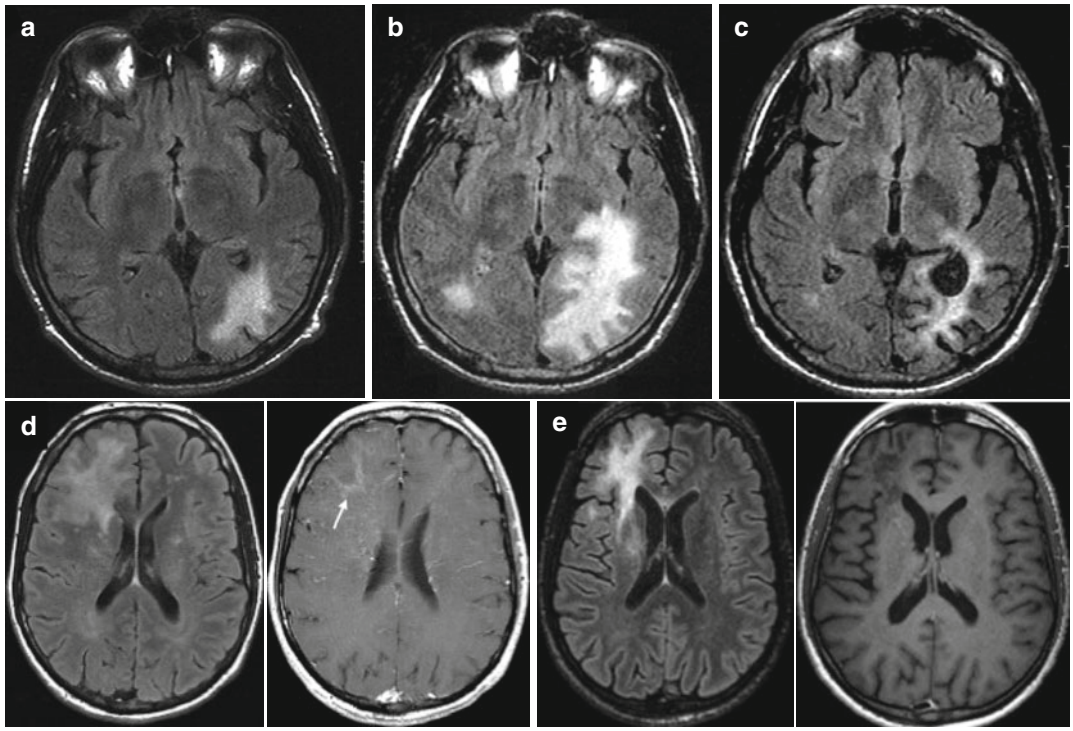


**Fig. 3** Progressive multifocal Leukoencephalopathy. PML in a HIV seronegative patient with B-cell lymphoma (Copyright). Evolution of FLAIR images before and during treatment. (**a**) Two months after the first neurological symptoms, axial FLAIR image shows a homogeneous hyperintensity in the left temporo-occipital white matter with respect to cortical gray matter and without mass effect. (**b**) One week after CHOP (cyclophosphamide, hydroxydaunorubicin, Oncovin, prednisone) polychemotherapy onset: progression of the temporo-occipital homogeneous white matter hyperintensity with bilateralization. (**c**) Three months after treatment onset: partial resolution. Hyperintense signal has diminished in both sides; apparition of a focal left temporo-occipital atrophy. PML IRIS in a HIV patient. (**d**) MRI performed 3 months after highly active antiretroviral therapy introduction: subcortical frontal FLAIR hyperintensity consistent with PML. Discrete local mass effect and contrast enhancement in perivascular spaces (*arrows*) suggestive of IRIS. The patient was treated with corticosteroid bolus injections. (**e**) Four-month follow-up: partial regression of the white matter hyperintensities, complete regression of the mass effect, and contrast enhancement

immunosuppression (or even at a time when immunosuppression is minimal). It occurs in the brain; the spinal cord and optic nerves are usually not involved. MRI is important for diagnosis. It shows subcortical white matter lesions, usually asymmetric and commonly non-enhancing. The incidence has grown with the immunodeficiency syndrome epidemic (85 % of PML cases) or in patients treated with various immunomodulating agents (after transplantation or for neurological or rheumatological immune diseases) (Major 2010). PML also occurs in cancer patients (Fig. 3), particularly patients treated for hematological malignancies such as lymphomas (Smolle et al. 2014; Auré et al. 2005) or glioma (Wu et al. 2011). Diagnosis is difficult and treatment is usually ineffective; early diagnosis can be of help for a favorable outcome after discontinuation of the immunosuppressive agent (Carson et al. 2009a). In this setting, patients with PML can develop immune reconstitution inflammatory syndrome (IRIS) when the cause of immunosuppression is

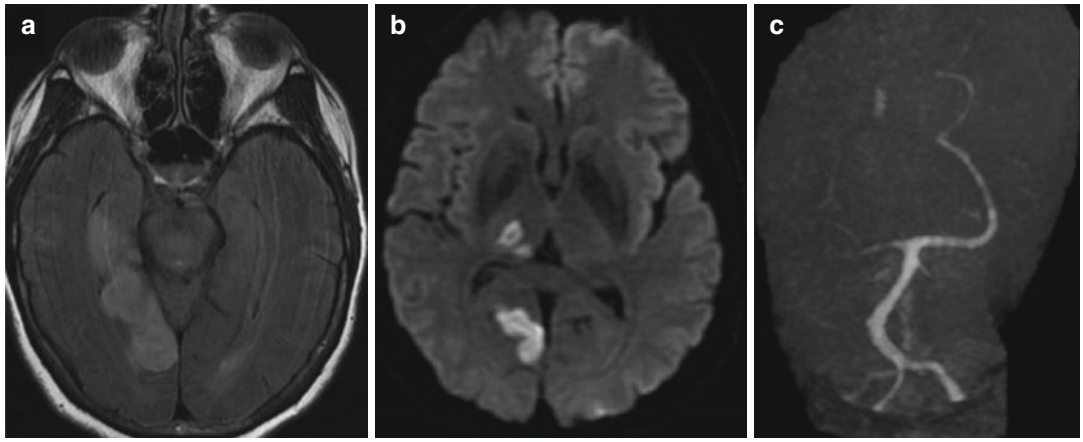


**Fig. 4** Ischemic stroke in a patient on hormonal therapy (anastrozole). The patient had been treated for breast cancer 3 years previously and was considered in remission. No other etiology or risk factor was found. MRI reveals a right cortico-subcortical temporo-occipital and thalamic hyperintensity on FLAIR (**a**) and diffusion-weighted images (**b**) and an occlusion of the right posterior cerebral artery on 3D TOF images (**c**)

removed e.g., in HIV patients, Fig. 3). A case of PML-IRIS has been described in a patient treated with brentuximab (von Geldern et al. 2012). The pathophysiology of IRIS is not yet understood. While reconstitution of the immune system is important for controlling the JC virus infection, CNS inflammation due to IRIS can result in death or permanent neurologic disability. Diagnosing PML-IRIS can be challenging, as currently there are no established diagnostic criteria; however, rapid clinical worsening and patchy contrast enhancement on MRI should raise the possibility of IRIS (Harrison et al. 2011).

### 2.1.2 Vascular Complications

CNS vascular disease is common in patients with cancer (Nguyen and DeAngelis 2006). Hemorrhagic and ischemic lesions are equally frequent. Chemotherapy is rarely found to be implicated.

#### 2.1.2.1 Ischemic Stroke

In a series of 10,963 cancer patients receiving chemotherapy, 16 ischemic strokes were registered (an incidence of 0.137 %) (Li et al. 2006); in almost all cases (15 out of 16 patients), the ischemic stroke occurred within 1 month after chemotherapy. Various cytotoxic chemotherapy agents have been reported to cause strokes (platinum compounds, 5-FU, docetaxel, paclitaxel, bleomycin, methotrexate, mitomycin C, gemcitabine, and cyclophosphamide). Hormonal chemotherapies (tamoxifen, raloxifene, estramustine phosphate, or danazol) also increase the risk of cardiovascular events and ischemic stroke (Fig. 4) (Mosca et al. 2009). More recently, a higher risk of stroke has been reported with antiangiogenic agents (bevacizumab), administered alone or in combination with other chemotherapies; the incidence was 1.7 % in patients treated with bevacizumab plus chemotherapy as compared to 0.5 % in patients treated with chemotherapy alone (Rieger et al. 2010; Gerstner et al. 2010).

#### 2.1.2.2 Hemorrhage

The incidence of cerebral hemorrhage (including intraparenchymal, subarachnoid, subdural, and epidural bleeding) is higher with the use of some targeted therapies. Antiangiogenic agents (bevacizumab, sorafenib, or sunitinib) or tyrosine kinase inhibitor via its action against platelet-derived growth factor receptor (dasatinib or imatinib) increase the incidence of intracranial hemorrhage in patients with cancer at a rate of around 2–4 % (Nghiemphu et al. 2008); the hemorrhage is however rarely symptomatic (Taillibert et al. 2009; Mitchell et al. 2010).

Cerebral venous sinus thrombosis: venous thromboembolism may also complicate the course of cancer patients treated with chemotherapy. In one series, 7 % of patients developed venous thromboembolism within 3 months of beginning chemotherapy (Otten et al. 2004). Cerebral venous sinus thrombosis is a classic complication of L-asparaginase therapy (Mitchell et al. 2010) and has also been reported with various agents (bevacizumab, cisplatin, danazol, methotrexate, tamoxifen, thalidomide, 5-FU). The outcome for these patients is often good (spontaneous resolution); sometimes, there is need for anticoagulation therapy even if hemorrhagic conversion is present.

### 2.1.3 Cerebellar Dysfunction

Cerebellar signs in an oncology patient are usually due to direct spread of cancer and rarely due to paraneoplastic syndromes or chemotherapy-induced disorders. Cytarabine and 5-fluorouracil (5-FU) are the cytoreductive agents most likely to cause acute or subacute cerebellar dysfunction including gait ataxia, dysmetria, dysarthria, and nystagmus. This dysfunction is usually reversible after discontinuation of the drug, but permanent dysfunction does occur (Sul and DeAngelis 2006; Lindner et al. 2008). Imaging findings are often normal. There is no proper treatment; plasmapheresis or hemodialysis may help (Lindner et al. 2008). Reintroduction of the drug is likely to reinduce cerebellar dysfunction.

### 2.1.4 Spinal Cord Toxicity and Intrathecal Chemotherapy

Intrathecal (IT) chemotherapy is an important component of the treatment and prophylaxis of malignancies in the central nervous system, especially in patients with acute lymphoblastic leukemia and aggressive lymphomas. Intrathecal chemotherapy is delivered through lumbar puncture or an intraventricular device placed under the scalp (e.g., Ommaya reservoir). A transverse myelopathy following lumbar IT therapy can be caused by MTX, cytarabine, thiotepa (rarely) or by combination of MTX, cytarabine, and steroids ("triple therapy"). There have been reports of other neurotoxicity attributed to the IT, including arachnoiditis and encephalopathy (Graber and Nolan 2010). Symptoms usually arise after multiple cycles of therapy. Paraplegia is the most frequent clinical manifestation followed by tetraplegia and cauda equina syndrome (Park et al. 2013; Jabbour et al. 2007). Most patients have shown poor recovery and are left with residual neurological deficits (Kwong et al. 2009) but may respond to steroids (Watterson et al. 1994). MRI may show an abnormal T2 signal within the cord, usually at the thoracic level; contrast enhancement varies (Counsel and Khangure 2007). Cerebrospinal fluid (CSF) is not specific; it usually shows elevated protein without cells (Graber and Nolan 2010). Intraventricular chemotherapy devices are associated with an overall complication rate of 11.4 % varying from misplacement to infections, or related to the toxicity of administered drugs (meningitis or encephalopathies) (Zairi et al. 2011).

## 2.2 Chronic Complications

The most emblematic chronic CNS complication in patients treated with chemotherapy *is an encephalopathy with cognitive dysfunction* (Soussain et al. 2009). Cognitive dysfunction encompasses a wide symptomatic range, from the mild "chemobrain" to severe dementia with leukoencephalopathy.

### 2.2.1 Mild Cognitive Dysfunction

In patients receiving chemotherapy for a tumor located outside the CNS (mainly breast cancers), the term "chemobrain" or "chemofog" has been coined to describe patients who develop post-chemotherapy mental changes associated with anxiety and fatigue but unrelated and independent from depression (Wefel et al. 2004). Patients report problems with memory retrieval, learning, and concentration that affect their quality of life and can result in diminished functional independence. On testing, global impairment of attention, memory, and executive functions has been reported in some studies but others could not demonstrate an objective decline (Wefel and Schagen 2012; Meyers 2008; Vardy et al. 2008). Cognitive

decline can persist after completion of treatment (Wefel and Schagen 2012; Meyers 2008) but often improves over a few months. Numerous factors contribute to cognitive dysfunction including disease burden, surgery, radiation, chemotherapy, seizure, and seizure therapy. The possible contributions of hormone therapy and of the cancer itself are also a subject of debate (Vardy et al. 2008). Methodological pitfalls such as heterogeneity of treatments, lack of standardized cognitive evaluations at baseline and during follow-up, and differences in the definition of impairment probably account for reported discrepancies. As a rule, standard brain imaging does not show significant changes in the follow-up of patients treated with standard chemotherapy alone (Yoshikawa et al. 2005). Functional neuroimaging studies showed greater recruitment of frontal cortical tissue or expanded spatial extent of brain activation during cognitive tasks in patients treated with conventional chemotherapy (Silverman et al. 2007) supporting the "chemobrain" hypothesis.

In CNS tumors, mainly represented by primary CNS non-Hodgkin's lymphomas treated with high-dose methotrexate, a mild/moderate form of cognitive dysfunction probably exists besides the severe form of cognitive dysfunction with leukoencephalopathy (see below) but its incidence is unknown, requiring prospective neuropsychologic testing with baseline evaluation to differentiate toxicity from disease-related cognitive involvement. On MRI, these patients may have some degree of periventricular white matter abnormalities, ventricular dilatation, and cortical atrophy.

#### 2.2.2 Severe Cognitive Dysfunction with Leukoencephalopathy

Delayed severe cognitive dysfunction with leukoencephalopathy is rare in the absence of associated cranial irradiation. It has, however, been reported after various combinations of high-dose chemotherapy administered in various forms (intravenous or intrathecal). It occurs several months or years after treatment mainly with methotrexate but also cytarabine, 5-FU, interferon-α, or high-dose fludarabine. Clinically, it is characterized by frontal-subcortical dementia associated with delayed processing, executive functions disorder, impaired memory, sleep disorders, and often gait abnormalities and incontinence. Older patients, those with preexisting vascular risk factors and those treated with multiple therapies, are at a higher risk. Structural imaging studies indicate white matter damage, ventricular dilatation, and brain atrophy (Inagaki et al. 2007). The degree of change of white matter seen on MRI is mostly correlated to neurocognitive impairment (Correa et al. 2012), but there are some patients with no correlation between severe MRI changes and clinical dysfunction (Fig. 5). No specific therapy can prevent the progressive decline, and overall the prognosis is poor. Fatal leukoencephalopathy has been reported in four adult patients who received a combination of drugs (BCNU, cyclophosphamide, cisplatin, melphalan, cytarabine, and etoposide) for non-CNS tumors (Moore-Maxwell et al. 2004). Patients initially presented focal neurological deficits or mental status changes that progressed to severe encephalopathy. A differential diagnosis to consider can be progressive multifocal leukoencephalopathy.

## 3 Specific Agents

### 3.1 Cytotoxic Agents

The toxicity of cytotoxic agents depends on the characteristics of the used agent (route of administration, cumulative dose) and on the patient's "degree of frailty" (e.g., other neurotoxic concomitant agents, predisposing illness, or renal failure). Neurotoxicity can vary from light and transient episodes to more severe and chronic ones and is sometimes idiosyncratic and unpredictable.

#### 3.1.1 Alkylating Agents

Alkylating agents are often used as single agents or in combination regimens with other conventional chemotherapy drugs or biologic agents. Alkylating agents cross the blood-brain barrier to various extents and may provoke many forms of toxicity in the CNS: encephalopathy, seizures, headache, cerebrovascular complications, and visual loss (Newton 2012a).

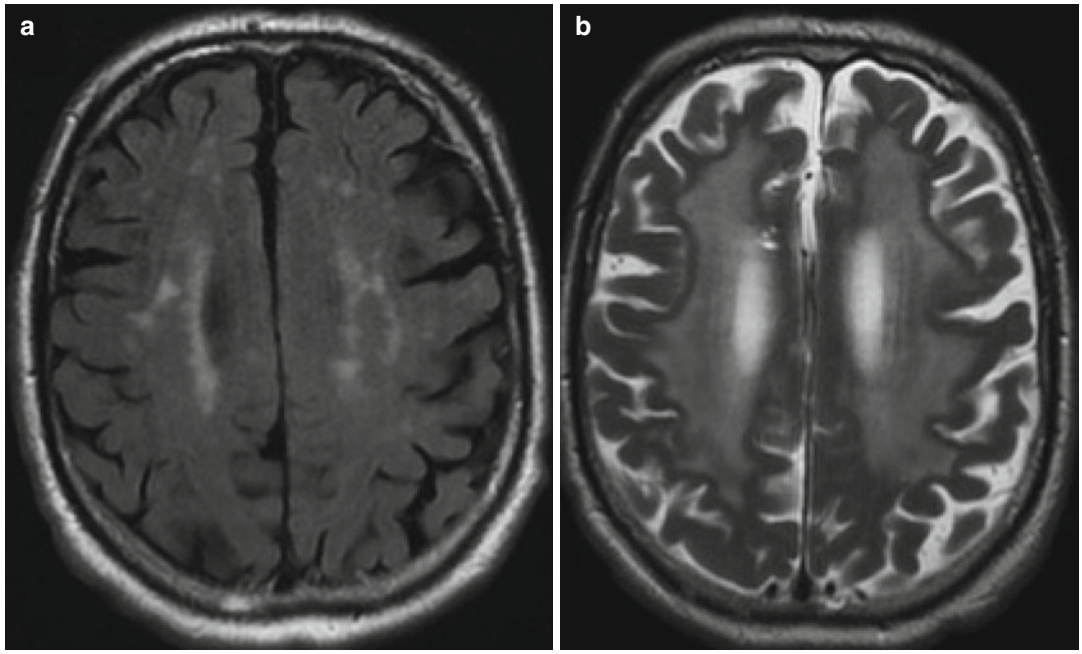


**Fig. 5** Delayed leukoencephalopathy in a diffuse large B lymphoma patient treated with intravenous and intrathecal methotrexate (aseptic meningitis within 1 month after intrathecal methotrexate). (**a**) FLAIR images before treatment: mild microvascular leukopathy. (**b**) T2 images 9 months after intrathecal methotrexate: symmetrical extensive supratentorial periventricular and subcortical white matter hyperintensity

#### 3.1.1.1 Bendamustine

Bendamustine is a nitrogen mustard used in the treatment of chronic lymphocytic leukemia and lymphomas. Central neurotoxicity has not been reported.

#### 3.1.1.2 Busulfan

Busulfan is an agent used essentially as a conditioning regimen for stem cell transplantation and rarely for chronic myeloid leukemia in adults. Busulfan is associated with a risk of seizures. The frequency of busulfan-related seizures is about 10 % in the literature in the absence of specific prophylaxis (Eberly et al. 2008). Seizures have been reported within 48 h of drug administration after oral or IV busulfan. This supports the use of anticonvulsant prophylaxis as a standard of treatment. The frequency is reduced to 1.3 % when anticonvulsants are used (Caselli et al. 2014).

#### 3.1.1.3 Chlorambucil

Chlorambucil is an oral drug, indicated for the treatment of leukemia, lymphomas, and Hodgkin's disease in multiagent chemotherapy regimens. Chlorambucil-induced neurotoxicity is extremely rare and restricted to a case report of an encephalopathy with myoclonus (Wyllie et al. 1997).

#### 3.1.1.4 Cyclophosphamide

Cyclophosphamide is often used in oncology but has little or no neurotoxicity. Exceptional cases of reversible encephalopathy or blurred vision are described with high doses of cyclophosphamide (Kende et al. 1979).

#### 3.1.1.5 Dacarbazine

Dacarbazine is approved for usage alone or with other drugs to treat Hodgkin's lymphoma or metastasized melanoma. There is no known neurotoxicity, except headache.

#### 3.1.1.6 Estramustine

Estramustine is mainly used for the treatment of refractory prostate cancer and is not associated with significant CNS toxicity except occasional headaches.

#### 3.1.1.7 Hexamethylamine

Hexamethylamine is mainly used for recurrent ovarian cancer. There are slight neurotoxic side effects, mainly mild and reversible encephalopathy and headaches.

#### 3.1.1.8 Ifosfamide

Ifosfamide is used for the treatment of many solid and hematopoietic tumors. It is estimated that 10–30 % of patients who receive high-dose IV ifosfamide develop an encephalopathy (Szabatura et al. 2014) usually reversible and characterized by confusion, often associated with hallucinations, cerebellar dysfunction, and seizures. Predisposing factors include previous cisplatin exposure, concomitant opioids, and CYP2B6 inhibitors (e.g., thiotepa) (Szabatura et al. 2014). Laboratory values that increased the risk of ifosfamide-induced encephalopathy included low serum albumin, increased serum creatinine, and increased hemoglobin (Szabatura et al. 2014). Electroencephalography (EEG) generally reveals diffuse, slow-wave activity, without epileptiform discharges. MRI is normal. The encephalopathy usually begins within 24 h of the drug's infusion but may be delayed for several days. The encephalopathy usually clears within 3–4 days, but persistent symptoms or even fatality may occur. Use of methylene blue, thiamine, and/or albumin as routine prophylaxis when administering ifosfamide is controversial (Richards et al. 2011).

#### 3.1.1.9 Mechlorethamine

Mechlorethamine is still used today in the treatment of Hodgkin's disease and other lymphomas. In high-dose IV regimens, such as in preparation for bone marrow transplantation, the drug has been reported to cause encephalopathy, headaches, or seizures; spontaneous recovery is the rule (Newton 2012b). MRI is normal.

#### 3.1.1.10 Nitrosoureas (Carmustine, Fotemustine, Lomustine, Nimustine, Semustine)

Nitrosoureas are used predominantly for the treatment of high-grade gliomas, melanoma and lymphoma and they have excellent penetration of the blood-brain barrier. Intra-arterial use can produce severe cerebral and ocular toxicity, but it is no longer administered. In conventional IV doses, the incidence of CNS toxicity is very low; encephalopathy is in rare cases described in patients with previous radiotherapy (Newton 2012a; Postma et al. 1998). The onset of symptoms is often delayed after drug administration. MRI is normal.

#### 3.1.1.11 Platinum Compounds (Cisplatin, Carboplatin, and Oxaliplatin)

Platinum compounds are used to treat various types of solid cancers (sarcomas, carcinomas, or testicular cancer), lymphomas, or germ cell tumors. Their main dose-limiting side effect is peripheral neuropathy, but a variety of CNS side effects are described and not so rarely: Lhermitte sign, encephalopathy with seizures (Steeghs et al. 2003), hyponatremia as a result of excessive hydration, or the syndrome of inappropriate antidiuretic hormone (SIADH) (Cheng et al. 2011). Cisplatin has been implicated in cerebral infarction (Li et al. 2006); this is a rare condition.

#### 3.1.1.12 Procarbazine

Procarbazine is used for Hodgkin's lymphoma and brain tumors. In patients with glioma, drowsiness is often reported (Postma et al. 1998).

#### 3.1.1.13 Temozolomide

Temozolomide is an oral chemotherapy drug used for brain tumor and melanoma. There are rare reports of headache (Yung et al. 2000).

#### 3.1.1.14 Thiotepa

Thiotepa is used to treat lymphoma and various cancers like breast, ovary, or bladder (IV administration) or patients with leptomeningeal metastases (IT administration). Neurotoxicity is more frequent when thiotepa is administrated IT (from aseptic meningitis to myelopathy). Encephalopathy can rarely occur in connection with high IV doses (Newton 2012a).

### 3.1.2 Antibiotics

#### 3.1.2.1 Bleomycin

Bleomycin is a drug used in the treatment of Hodgkin's lymphoma, germ cell tumors, and

head and neck cancer. Central neurotoxicity is very rare and attributed to coadministered agents (e.g., cisplatin).

#### 3.1.2.2 Mitomycine C

Mitomycine C is used in various solid cancers (upper gastrointestinal, anal, breast, or bladder cancers). Central neurotoxicity is extremely rare: cases of veno-occlusive disease or thrombotic microangiopathy have been reported (Pisoni et al. 2001).

### 3.1.3 Antimetabolites

#### 3.1.3.1 Capecitabine

Capecitabine is an oral analog of 5-FU, used in breast and gastrointestinal cancers. Like 5-FU, neurotoxicity is uncommon at standard doses. Rare cases of encephalopathy (Rajasekhar and Georges 2007) and cerebellar disorders (Renouf and Gill 2006) have been described.

#### 3.1.3.2 Clofarabine

Clofarabine is used for the treatment of relapsed or refractory acute lymphoblastic leukemia. It commonly causes mild headache, but in multiagent treatment it might predispose to central nervous system toxicity by increasing endothelial permeability (Tzachanis et al. 2014).

#### 3.1.3.3 Cytosine Arabinoside

Cytarabine (Ara-C) is commonly used in multiagent chemotherapy regimens for the treatment of leukemia, lymphoma, and neoplastic meningitis. It can be given systemically and intrathecally.

Intravenous (IV) cytarabine may cause several neurologic disorders. The most common central neurotoxicity is a subacute cerebellar syndrome (dysarthria, nystagmus, and appendicular and gait ataxia), usually noted in the context of high-dose IV therapy (>1 g/m$^2$), in up to 30 % of patients (Herzig et al. 1987). They may also develop confusion, lethargy, and drowsiness. The risk seems higher with renal failure (Smith et al. 1997), higher doses and association to other neurotoxic drugs, especially methotrexate. This syndrome can occur up to one month after Ara-C treatment and is usually reversible within 2 weeks after discontinuation; plasmapheresis or hemodialysis can help in severe cases (Lindner et al. 2008). MRI is usually normal, although cerebellar atrophy and reversible white matter abnormalities may be seen on T2-weighted or fluid-attenuated inversion recovery (FLAIR) sequences (Vaughn et al. 1993). The CSF is normal.

**Table 4** Chemotherapies associated with aseptic meningitis

| |
|---|
| Cetuximab |
| Cytarabine |
| Efalizumab |
| Immunoglobulines intraveineuses |
| Ipilimumab |
| Methotrexate |
| Muromonab-CD3 |

Intrathecal (IT) cytarabine can often be neurotoxic. Aseptic meningitis can be seen with IT administration of Ara-C, in up to 28 % of patients in some studies (Gállego Pérez-Larraya et al. 2011), commonly with the liposomal preparation (DepoCyt) of Ara-C. Cerebrospinal fluid analysis shows pleocytosis and elevated protein. Even if IT liposomal cytarabine is the most common offender in cases of aseptic meningitis, any other intrathecal agent and many targeted therapies can be associated with this syndrome (Table 4). Myelopathy can also be seen with IT Ara-C and presenting with back or radicular leg pain, ascending motor deficit, and bowel or bladder dysfunction usually occurring a few days following treatment (Dunton et al. 1986). Examination of the CSF usually reveals an elevated protein level and a modest pleocytosis. As to pathology, portions of the spinal cord reveal demyelination with associated white matter vacuolization, histologically indistinguishable from MTX-induced myelopathy (Hoffman et al. 1993). Encephalopathy (with or without seizures) and anosmia have rarely been described (Hoffman et al. 1993).

#### 3.1.3.4 Fludarabine

Fludarabine is used to treat chronic lymphocytic leukemia, indolent lymphomas, and macroglobulinemia. At low doses (less than 40 mg/m$^2$/day), the drug causes little neurotoxicity except for transient episodes of drowsiness and fatigue (Grever et al. 1988). T2-weighted MR images

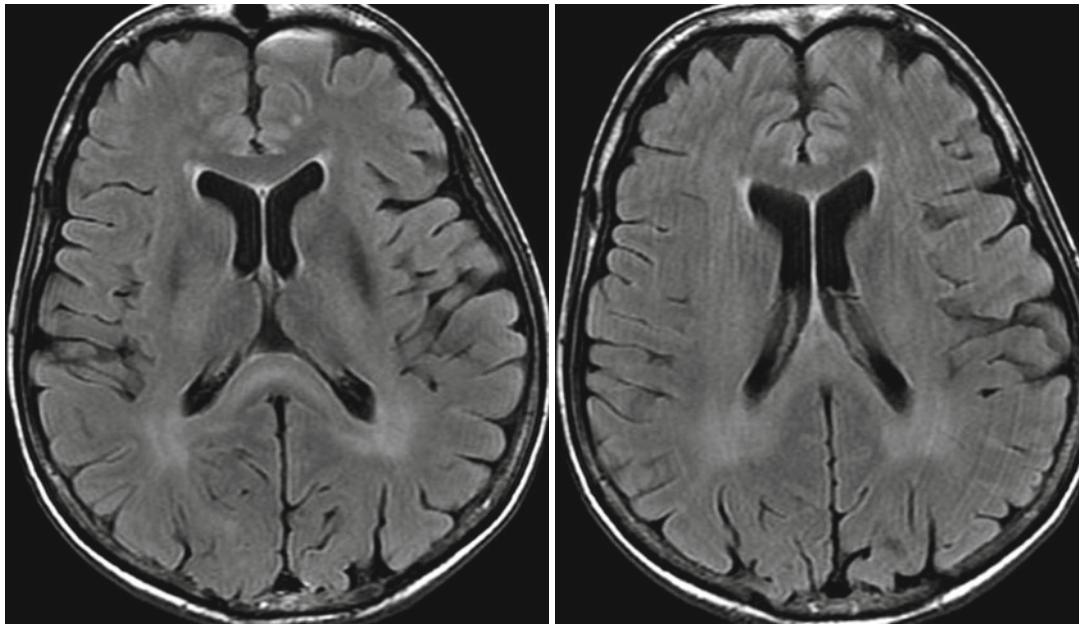

**Fig. 6** Leukopathy in a patient treated with 5-FU for ovarian cancer with peritoneal carcinosis. After the 3rd cycle of 5-FU, the patient became stuporous. MRI revealed a discrete white matter FLAIR hyperintensity in the splenium of the corpus callosum and the deep posterior white matter

may show foci of white matter hyperintensity (Cohen et al. 1993). At doses greater than 40 mg/m$^2$/day, a delayed progressive encephalopathy, characterized by cortical blindness, dementia, coma, and resulting in death can develop (Chun et al. 1986). The drug can also cause myelopathy.

#### 3.1.3.5 5-Fluorouracil

5-Fluorouracil (5-FU) has been used to treat a variety of cancers such as carcinoma of the breast, pancreas, colon, rectum, and stomach. Neurotoxicity is rare and usually occurs only in patients receiving high doses (>15 mg/kg/week) (Hammack and Cascino 1998) and can cause both acute and delayed neurotoxicity. Toxicity with low doses occurs in patients with dihydropyrimidine dehydrogenase deficiency, the initial rate-limiting enzyme in pyrimidine catabolism (Takimoto et al. 1996). Acute neurotoxicity is rare (up to 5 % of patients) and consists of cerebellar syndrome (acute onset of gait ataxia, dysmetria, dysarthria, and nystagmus) and encephalopathy (acute onset during chemotherapy treatment). Clinical signs usually reverse within a week after the drug is discontinued but may recur with reintroduction of 5-FU. Imaging is normal for cerebellar syndrome. In patients with encephalopathy, diffuse hyperintensity can be detected in bilateral cerebral white matter and corpus callosum on T2-weighted and FLAIR images. Diffusion-weighted MRI suggests restricted diffusion (Tha et al. 2002). Clinical and radiological symptoms improve with steroids and discontinuation of the drugs. Delayed encephalopathy is also described (Han et al. 2008) but is exceptional in our experience (Fig. 6). Cerebral infarcts and PRES can also been seen.

#### 3.1.3.6 Gemcitabine

Gemcitabine is a commonly used chemotherapeutic agent for a variety of tumors (pancreas, urothelial, and lung). Central nervous system toxicities have rarely been attributed to gemcitabine, except rare cases of encephalopathy and in particular PRES (Cioffi et al. 2012).

#### 3.1.3.7 Hydroxyurea

Hydroxyurea is used for the treatment of hematologic disorders, sickle cell disease, HIV infection, and inoperable meningiomas. Significant neurotoxicity has rarely been described.

#### 3.1.3.8 Methotrexate

MTX is given intravenously, intrathecally, and orally, against various cancer (leukemias, lymphomas, or solid tumors) and autoimmune disorders. Neurotoxicity is a well-recognized complication and risk factors include dose, route of administration, and other concurrent treatments (e.g., radiotherapy or Ara-C).

Intrathecal injection, either by intraventricular device or by lumbar puncture, is used for prophylaxis or treatment of leptomeningeal tumor. There are different complications with this route of administration. Aseptic meningitis is the most common form of acute MTX neurotoxicity with IT and it occurs in up to 10 % (Posner 2009); it is more frequent after lumbar than intraventricular injection. Symptoms (fever, headaches, back pain, vomiting) typically occur 2–4 h after drug infusion and may last for several days. The inflammatory reaction may cause arachnoiditis leading to cauda equina dysfunction (Bay et al. 2005). Encephalopathy is a rare condition with IT MTX alone (Boogerd et al. 1988) but can classically occur in combination with IV MTX in an acute (Fig. 7a), subacute (Fig. 7b), or chronic form. Intrathecal methotrexate-induced PRES in adults is exceedingly rare (Güler et al. 2014). Myelopathy (transverse myelopathy) has rarely been associated with IT MTX, usually occurring after several treatments; it can infrequently be severe (extensive transverse necrosis) (Shintaku et al. 2014).

Intravenous injection can in rare cases cause acute encephalopathy (within 24–48 h of the

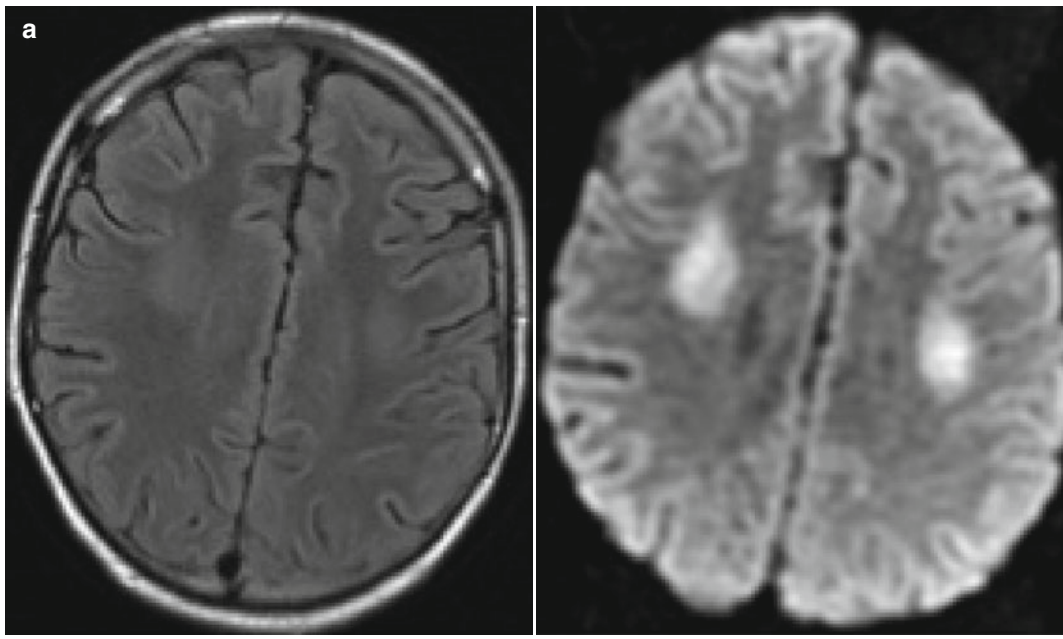


**Fig. 7** Methotrexate toxicity. (**a**) Acute methotrexate toxicity. A 17-year-old patient with diffuse large B lymphoma, presenting with headaches and confusion within 6 days intrathecal methotrexate treatment. Discrete bilateral FLAIR hyperintensity (*left*) in the corona radiata and intense well-delimited hypersignal on diffusion-weighted images (*right*). The patient fully recovered from this event. (**b**) Subacute post-methotrexate leukoencephalopathy in a patient treated 2 months previously with aracytin, dasatinib, and intrathecal methotrexate. FLAIR images immediately before treatment (*left*) show minimal microvascular leukopathy and discrete right subdural collection. FLAIR images 2 months after (*right*) show symmetrical extensive supratentorial periventricular and subcortical white matter hyperintensity. (**c**) Chronic methotrexate leukoencephalopathy. A patient with Waldenstrom's macroglobulinemia treated with cyclophosphamide, doxorubicine, vincristine, prednisone, intrathecal methotrexate, and autotransplantation. Three years after treatment, he developed cognitive disturbances with frontal lobe disorder, executive functions, and attention deficit. After 10 years, the symptoms are stable. MRI images show symmetric extensive supratentorial white matter FLAIR hyperintensity

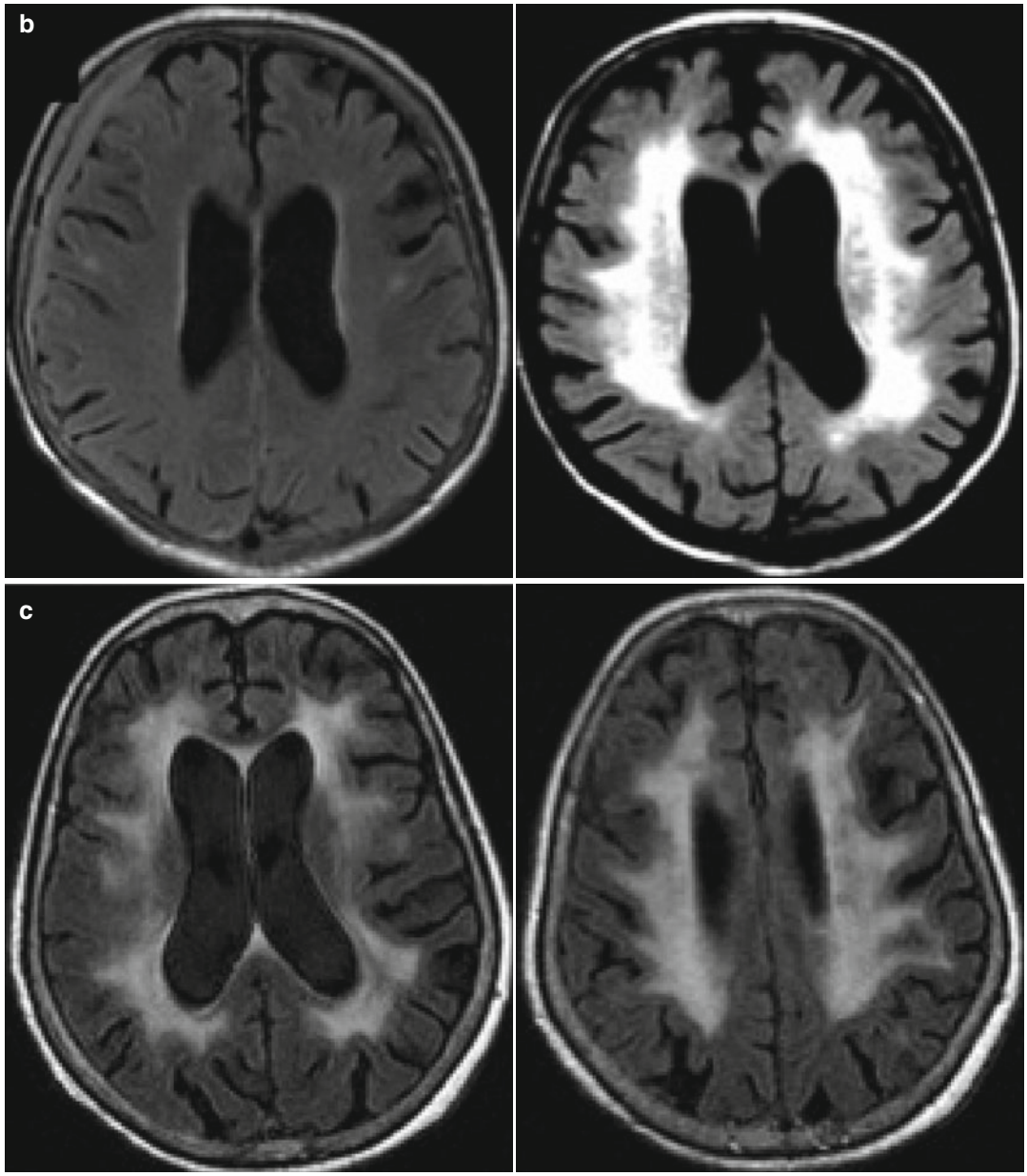


**Fig. 7** (continued)

treatment characterized by confusion, disorientation, drowsiness, and sometimes seizures). Another complication is stroke-like episodes characterized by transient focal neurologic deficits. This syndrome may occur in up to 15 % of patients, typically several days after high-dose IV MTX and last 12–72 h resolving spontaneously without sequelae (Hammack 2005). MRI is usually normal. PRES has also been described in patients receiving a combination of IV and IT MTX (Sánchez-Carpintero et al. 2001). Chronic leukoencephalopathy may develop several months or years after MTX administration (Fig. 7c). Patients present with progressive

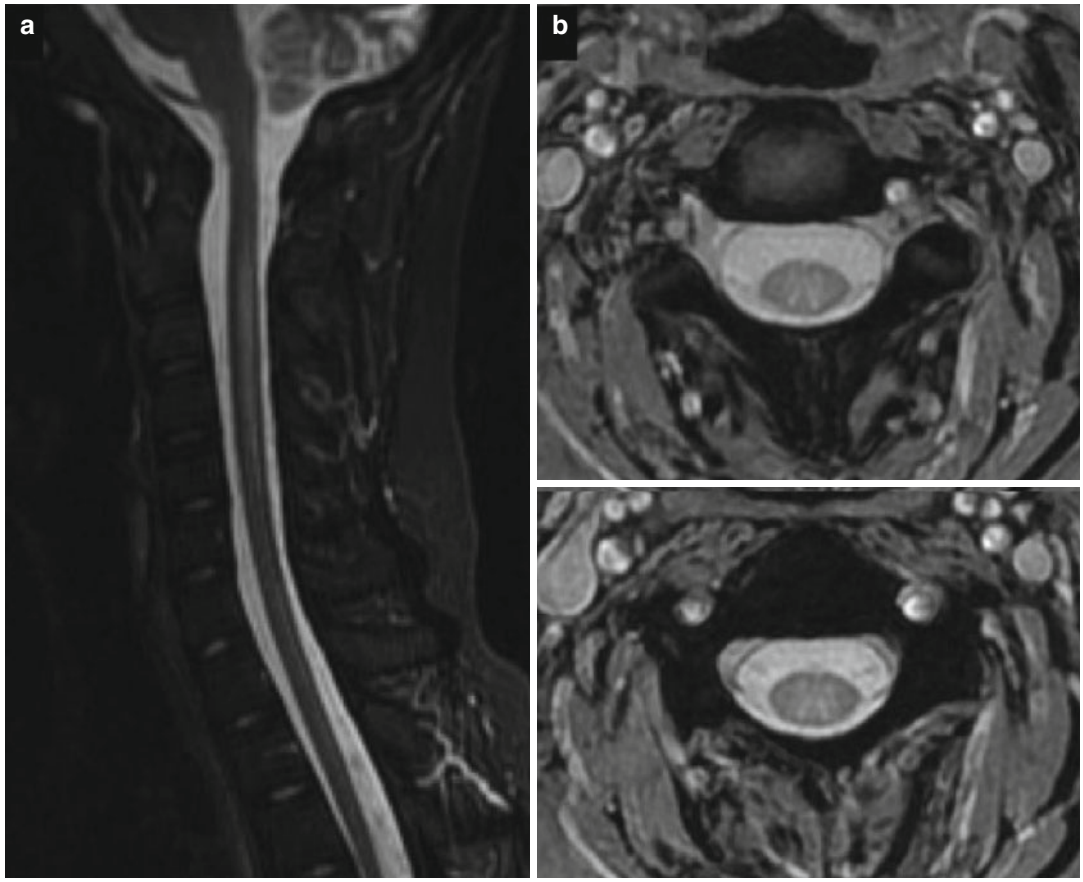


**Fig. 8** Myelitis in an acute lymphoblastic leukemia treated with nelarabine. Transient paresthesias in upper limbs appearing in the days following chemotherapy. After 3 months, paresthesias became permanent and associated with proprioceptive ataxia and cortico-spinal tract syndrome. Sagittal STIR (**a**) and axial T2 (**b**) images show a hyper T2 intensity in the posterior part of the cervical spinal cord

cognitive impairment, focal neurological deficits, gait abnormalities, and seizures. MRI reveals confluent bilateral subcortical and periventricular FLAIR/T2 hyperintensities, diffuse atrophy, ventricular dilation, cortical or basal ganglia calcifications. This syndrome occurs following repeated administration of high dose (and rarely standard dose) IV MTX; the frequency is higher in association with radiotherapy or IT MTX. The clinical course is variable: stabilization in some patients and progressive course leading to death in others.

MTX is finally a main agent in an oral form for the treatment of several systemic disorders (e.g., rheumatoid arthritis). Neurotoxicity is often mild, but PRES has been described (Hart et al. 2012) as severe encephalopathy (González-Suárez et al. 2014).

#### 3.1.3.9 Nelarabine

Nelarabine is indicated for refractory hematologic malignancies in adult and pediatric patients (T-cell acute lymphoblastic leukemia and T-cell lymphoblastic lymphoma). The most frequently reported central neurotoxicities (dose related) are drowsiness, seizures, and headaches with onset of symptomatology occurring most often within six to eight days following administration of nelarabine (Roecker et al. 2010). Severe and fatal neurological toxicities are exceptional but described (Hartz et al. 2013); they can be diffuse affecting all CNS or expressed only by myelopathy (Fig. 8).

#### 3.1.3.10 Pentostatin

Pentostatin is used in leukemia (hairy cell and chronic lymphocytic leukemia). Central nervous system toxicity is uncommon. At high doses, some patients manifest drowsiness or seizures. A case of PRES has been described in connection with concomitant deoxycoformycin and alemtuzumab (Cooksley and Haji-Michael 2011).

#### 3.1.3.11 Pemetrexed

Pemetrexed is an effective agent against mesothelioma and other solid tumors (e.g., non-small-cell lung cancer). Significant neurotoxicity has not been described.

### 3.1.4 Miscellaneous

#### 3.1.4.1 L-Asparaginase

L-asparaginase is indicated as a component of a multiagent chemotherapeutic regimen for the treatment of acute lymphoblastic leukemia. Cerebral venous sinus thrombosis (CVST) is a feature of asparaginase-related thrombosis (Fig. 9) and has been reported in 1–3 % of treated patients (Payne and Vora 2007). It typically involves the superior sagittal or transverse sinuses and may be associated with either ischemic or hemorrhagic venous infarction. CVST usually occurs during induction and rarely within 1–3 weeks following therapy (Corso et al. 1997). It reduces circulating levels of many hemostatic proteins including fibrinogen, plasminogen, and antithrombin-III. These anticoagulant deficiencies result in impaired inhibition of thrombin, which has been proposed as the main pathogenic mechanism for thrombosis. The clinical manifestation of CVST, depending on the site of thrombosis varies (seizures alone or in combination with headache and/or focal neurological deficits). Brain CT or MRI confirms the diagnosis. There have been several cases of PRES reported after L-asparaginase treatment in children with acute lymphoblastic leukemia, not always associated with hypertension (Hourani et al. 2008).

#### 3.1.4.2 Topoisomerase Inhibitors

Topoisomerase I inhibitors (camptothecin, irinotecan, topotecan) are used to treat lymphomas, leukemias, and refractory solid tumors. Significant CNS toxicity has not been described except rare cases of headache with topotecan and transient and reversible dysarthria during irinotecan infusion (Hamberg et al. 2008) with normal brain imaging.

Topoisomerase II inhibitors (daunorubicin, doxorubicin, epirubicin, etoposide, idarubicin, mitoxantrone, teniposide) are used in multiagent chemotherapeutic regimen for various solid tumors (non-seminomatous testicular cancer, small-cell lung cancer, breast cancer, cervical cancer, and germ cell tumors), sarcoma, and hematologic malignancies (Hodgkin's and non-Hodgkin's lymphoma and myeloid and non-myeloid leukemia). Significant neurotoxicity has not been described.

#### 3.1.4.3 Thalidomide

Thalidomide is used in the treatment of cutaneous disorders (e.g., erythema nodosum leprosum or discoid lupus) and various malignancies, especially multiple myeloma. Significant neurotoxicity has not been described.

### 3.1.5 Mitotic Spindle Inhibitors

Mitotic spindle inhibitors are often used in cancer treatment, but their CNS toxicity is rare (Newton 2012a).

#### 3.1.5.1 Taxanes (Paclitaxel, Docetaxel, Nab-paclitaxel)

Taxanes are used in frontline therapy for breast, ovarian, and lung cancer. CNS neurotoxicity (acute encephalopathy) has rarely been described (Muallaoğlu et al. 2012).

#### 3.1.5.2 Vinca-Alcaloides (Vinblastine, Vincristine, Vinflunine, Vinorelbine)

Vinca-alcaloides are part of multiple chemotherapy regimens used in the treatment of various cancers: hematological malignancies (acute lymphocytic leukemia, multiple myeloma, and Hodgkin's and non-Hodgkin's lymphoma), and solid tumors (breast, testicular, bladder, melanoma, lung, and brain cancer) or sarcoma. CNS neurotoxicity is rare. Acute encephalopathy is

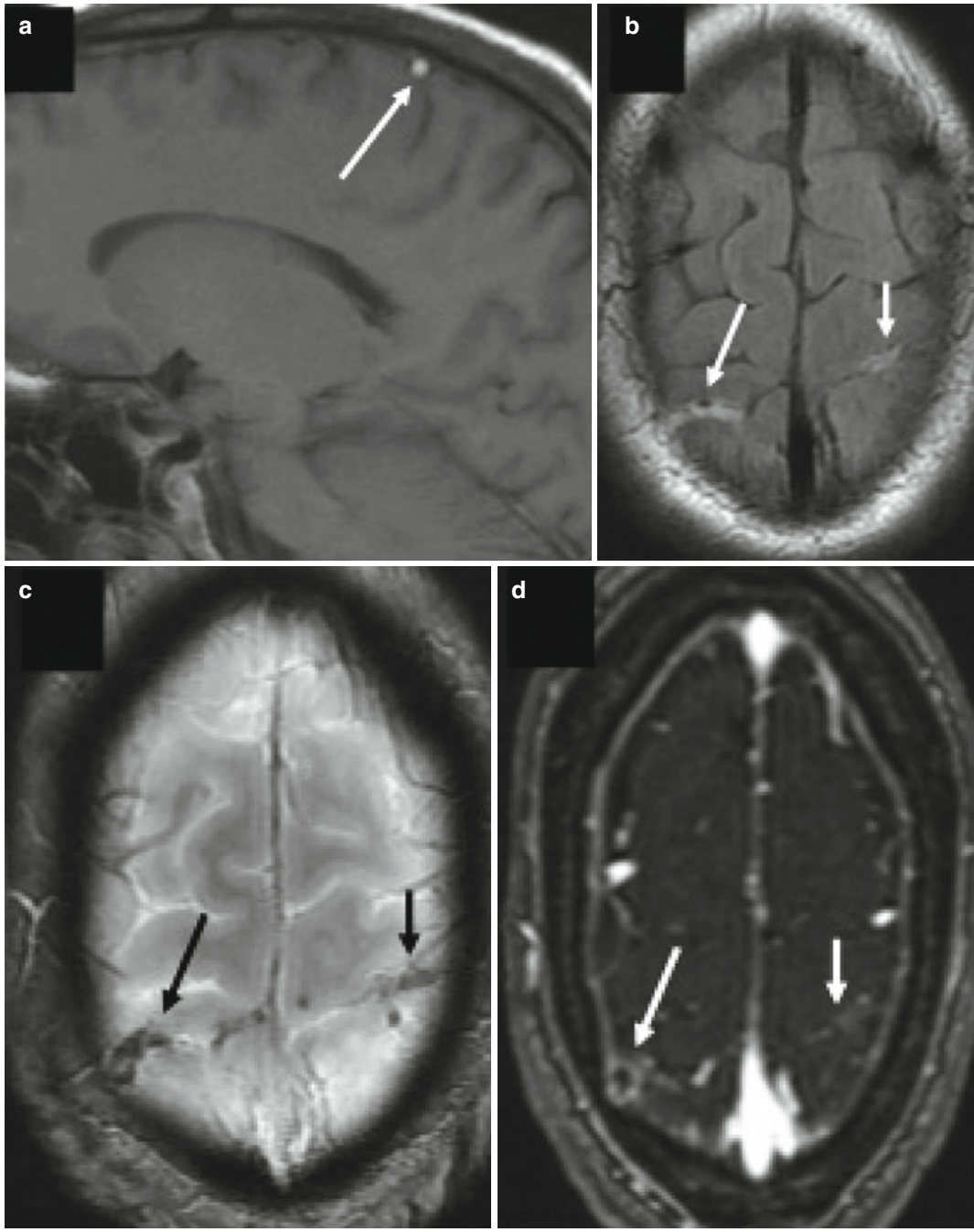


**Fig. 9** Cortical thrombosis in a patient treated with asparaginase for acute lymphoblastic leukemia. (**a**) Sagittal T1: hyper T1 thrombus in a cortical vein (*arrow*). (**b**) Axial FLAIR: hyperintense cortical veins (*arrows*) without associated parenchymal abnormality. (**c**) Axial T2*: The same veins (*arrows*) are hypointense, confirming the presence of a thrombus. (**d**) Post-contrast-images: lack of opacification of these two veins (*arrows*) while the other veins and the superior longitudinal sinus present a normal intense opacification

reported with vincristine. PRES has recently been described with vincristine (Hayase et al. 2014), vinflunine (Helissey et al. 2012), and vinorelbine (Chen and Huang 2012).

## 3.2 Biologic Agents

Several biologic approaches may be used to treat cancer including modulation of the immune system to destroy neoplastic cells, such as adaptive cellular therapy, vaccines, cytokines (interferons and interleukins), immune enhancers (levamisole), or colony-stimulating factors. Another developing field is targeted therapies (small molecule protein kinase inhibitors and monoclonal antibodies). The neurologic complications of targeted therapies (Table 5), antiangiogenic agents, cytokines, and colony-stimulating factors are considered below.

**Table 5** Targeted therapies and neurological complications

| | Frequent complications | Rare complications |
|---|---|---|
| Alemtuzumab | HHV6 encephalitis | Headaches, PML |
| Bevacizumab | Headaches | Stroke, ICH, PRES |
| Bortezomib | Headaches | PRES, ICH |
| Brentuximab | | PML |
| Cetuximab | Headaches | Aseptic meningitis |
| Dasatinib | Headaches | ICH |
| Efalizumab | | PML, aseptic meningitis |
| Gemtuzumab | | ICH |
| Imatinib | Headaches | Stroke, ICH |
| Ipilimumab | | PRES, aseptic meningitis |
| Lapatinib | Headaches | |
| Pazopanib | Headaches | PRES, stroke, ICH |
| Rituximab | Headaches, PML | PRES |
| Sirolimus | Headaches | PRES, PML |
| Sorafenib | Headaches | PRES, stroke, ICH |
| Sunitinib | Headaches | PRES, TIA |
| Trastuzumab | Headaches | PRES |
| Vorinostat | Headaches | |

*ICH* intracerebral hemorrhage, *PRES* posterior reversible encephalopathy syndrome, *TIA* transient ischemic attack, *PML* progressive multifocal leukoencephalopathy

### 3.2.1 Small Molecular Protein Kinase Inhibitors

#### 3.2.1.1 Receptor Tyrosine Kinase Inhibitors (R-TKI): Afatinib, Axitinib, Bosutinib, Cabozantinib, Crizotinib, Dasatinib, Imatinib, Erlotinib, Gefinitib, Lapatinib, Nilotinib, Plerixafor, Ponatinib, Tandutinib, Vandetanib

All these agents are used for the treatment of hemopathic malignancies (leukemia, lymphoma, myelodysplastic syndrome) and solid tumors (gastrointestinal, sarcoma, non-small-cell lung cancers, pancreatic adenocarcinoma, breast tumors, brain metastases, and thyroid cancer). Non-specific neurological symptoms like headache, dizziness, or insomnia are common symptoms; other neurological complications are uncommon. Rare cases of intracerebral hemorrhage in patients with brain tumors have been described with dasatinib and imatinib (Wen et al. 2009).

#### 3.2.1.2 Serine/Threonine Kinase Inhibitors: Everolimus, Sirolimus, Temsirolimus

Serine and threonine kinase inhibitors are used for solid tumors (melanomas, renal cell carcinoma, and astrocytoma in patients with tuberous sclerosis). No significant neurological complications have been described to date except a PRES with sirolimus (Moskowitz et al. 2007).

#### 3.2.1.3 Other Signal Transduction Inhibitors: Bortezomib, Romidepsin, Vorinostat

All these agents are used for the treatment of hemopathic malignancies (lymphoma and multiple myeloma). Central nervous system complications are uncommon except rare headaches. Rare cases of PRES have been described (Terwiel et al. 2010).

### 3.2.2 Monoclonal Antibodies

#### 3.2.2.1 Alemtuzumab

Alemtuzumab is used in chronic lymphocytic leukemia, peripheral and cutaneous T-cell lymphoma, and also proposed as treatment in various

autoimmune conditions and multiple sclerosis patients. Additionally, it is part of the anti-graft-versus-host disease-conditioning protocol for organ transplantations with high reported complications. The main complication of alemtuzumab is severe CNS infections related to profound immune suppression, particularly HHV6 encephalitis (Vu et al. 2007), PML, or other infectious encephalomyelopathies (Waggoner et al. 2009; Schmidt-Hieber et al. 2009).

#### 3.2.2.2 Brentuximab

Brentuximab is used in Hodgkin's lymphoma and systemic anaplastic large cell lymphoma. Rare association of this medication with PML and immune reconstitution inflammatory syndrome is reported (von Geldern et al. 2012).

#### 3.2.2.3 Cetuximab

Cetuximab is used for the treatment of metastatic colorectal cancer, metastatic non-small-cell lung cancer, and head and neck cancer. There are case reports of aseptic meningitis following the first cetuximab dose (Feinstein et al. 2009).

#### 3.2.2.4 Efalizumab

Efalizumab is a formerly available medication designed to treat autoimmune diseases, originally marketed to treat psoriasis. Known side effects include meningitis and PML (Carson et al. 2009a).

#### 3.2.2.5 Gemtuzumab

Gemtuzumab is used in acute myeloid leukemia. There have been several cases of intracranial hemorrhage in the phase II and III trials (Bross et al. 2001); prolonged thrombocytopenia increases the risk of intracranial hemorrhages.

#### 3.2.2.6 Ipilimumab

Ipilimumab is used for the treatment of metastatic melanoma. Aseptic meningitis (Eckert et al. 2009) and PRES (Maur et al. 2012) are rarely reported.

#### 3.2.2.7 Rituximab

Rituximab is used to treat lymphoid malignancies and peripheral neuropathy associated with monoclonal gammapathy, rheumatoid arthritis, and a variety of other immune-mediated disorders. Major and classical neurological complication is PML (Sikkema et al. 2013). In 2009, a case series of 57 HIV-negative PML patients (essentially B-cell malignancies) receiving rituximab has been reported (Carson et al. 2009b). Although PML rituximab-treated patient had received other immunosuppressive agents, there is a consensus that rituximab will increase the risk of PML. PRES is rarely described (Siddiqi 2011), as well as chronic meningoencephalitis from enteroviruses (Ganjoo et al. 2009). Intracerebral hemorrhage has been reported in a patient with intravascular lymphoma several hours after initial infusion of rituximab (Ganguly 2007).

#### 3.2.2.8 Other Monoclonal Antibodies (Ibritumomab, Muromomab, Ofatumumab, Panitunumab, Tositumomab)

Theses drugs are used in refractory chronic lymphocytic leukemia, relapsed or refractory non-Hodgkin's lymphoma, acute myelogenous leukemia, or metastatic colorectal cancer. No significant neurological complications have been described.

### 3.2.3 Antiangiogenic Agents

#### 3.2.3.1 Aflibercept

Aflibercept is used in macular degeneration and colorectal cancer. Cases of PRES have been observed (Chen et al. 2014).

#### 3.2.3.2 Bevacizumab

Bevacizumab is used to treat glioblastoma and various metastatic systemic cancers (colorectal, ovarian, breast, renal, and lung cancer). Central nervous system (CNS) hemorrhage is an uncommon but classical complication. In a retrospective review of the FDA MedWatch database of adverse events, 154 of 1,195 reports of bleeding associated with bevacizumab reported a CNS bleed (Letarte et al. 2013). They were the presumed cause of death in two-thirds of cases. Despite the overall increased risk of bleeding, brain metastases do not have an increased risk of

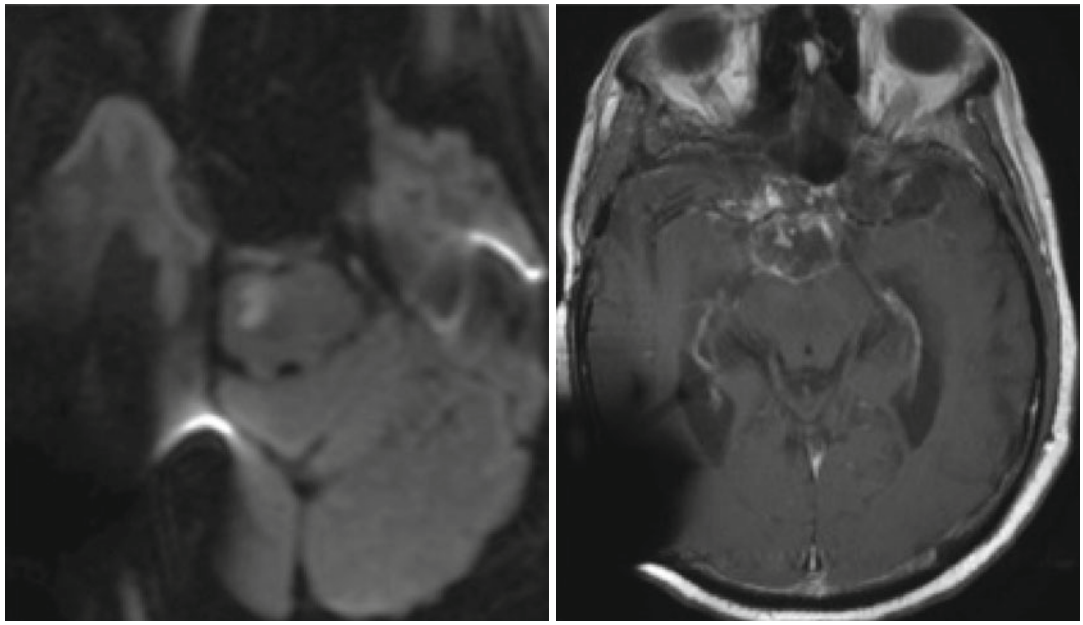

**Fig. 10** Ischemic stroke in a patient treated with bevacizumab. Anaplastic astrocytoma treated with surgery, temozolomide, radiotherapy, and bevacizumab. The patient presented with an acute neurologic deficit 4 days after bevacizumab introduction. MRI reveals a well-delimited left pontine diffusion hyperintensity (*left*). T1 post-gadolinium images (*right*) show a heterogeneous mass in the chiasmatic cistern corresponding to the glioma

hemorrhages over baseline when treated with bevacizumab (Besse et al. 2010) and rates of symptomatic hemorrhages are low in primary brain tumor (Cohen et al. 2009). Stroke (Fig. 10) seems more frequent than in the general population (Randall and Monk 2010). PRES is occasionally seen (Glusker et al. 2006).

#### 3.2.3.3 Cediranib

Although cediranib has shown promising results in several clinical trials, it is not yet approved for use. PRES is occasionally described (Kim et al. 2014).

#### 3.2.3.4 Sunitinib

Sunitinib is used for recurrent gastrointestinal tumor and advanced renal cell carcinoma. PRES is occasionally described (Costa et al. 2014).

#### 3.2.3.5 Sorafenib

Sorafenib is used for advanced renal cell carcinoma and hepatocellular carcinoma. PRES is occasionally described (Dogan et al. 2010). Transient ischemic attack has been reported in a patient with stenosis of the carotid and brachiocephalic arteries following long-term treatment with sorafenib for renal cell carcinoma (Maraiki and Aljubran 2014).

#### 3.2.3.6 Pazopanib

Pazopanib is used in metastatic renal cell carcinoma. PRES is occasionally described (Foerster et al. 2013).

### 3.2.4 Cytokines

#### 3.2.4.1 Interleukin-2

Interleukin-2 is currently used in the treatment of metastatic renal cell carcinoma and melanoma. Neurological complications (drowsiness, confusion) have been described in up to 30 % of patients but fortunately with rapid reversal after therapy was completed (Atkins et al. 1999).

#### 3.2.4.2 Interferon-α

Interferon-α is used in several non-oncologic conditions (hepatitis B and C, Behçet, condyloma) and oncologic conditions (melanoma,

chronic myelogenous leukemia, T-cell and non-Hodgkin's lymphoma, advanced renal cell cancer, and AIDS-related Kaposi sarcoma). Cognitive disorders, headaches, and dystonia are reported (Quarantini et al. 2007); they are mild and reversible with discontinuation of treatment. In a trivial number of cases, cognitive decline can persist for months after stopping treatment (Meyers et al. 1991). MRI is found normal.

#### 3.2.5 Colony-Stimulating Factors (Erythropoietins, Granulocyte Colony-Stimulating Factors, and Granulocyte-Macrophage Colony-Stimulating Factor)

Headache is a common complaint in patients treated with colony-stimulating factors (CSF). Central nervous system complications are rare. An encephalopathy has been rarely described (Delanty et al. 1997). A case of PRES is reported in a non-Hodgkin's lymphoma patient treated few days earlier with vincristine, ifosfamide, and etoposide (Leniger et al. 2000).

### 3.3 Antineoplastic Hormones

Agonists and antagonists hormones have selective antineoplastic activity and are used against breast and prostate carcinomas.

#### 3.3.1 Anti-estrogens

##### 3.3.1.1 Tamoxifen

Tamoxifen is used in women with estrogen receptor-positive breast cancer. Tamoxifen increases the risk for stroke (Bushnell and Goldstein 2004). Optic neuropathy has been reported (Zvorničanin et al. 2014).

##### 3.3.1.2 Toremifene

Adverse events (headaches and thromboembolic events) are similar to tamoxifen treatment but in a smaller proportion (Ye and Zhai 2014).

#### 3.3.2 Anti-aromatases

##### 3.3.2.1 Aminoglutethimide

It has been used to treat hormone-responsive breast and prostate cancer, adenocortical carcinoma, and ectopic Cushing disease. Dizziness, ataxia, and drowsiness have been rarely reported (Grem et al. 1988).

##### 3.3.2.2 Anastrozole

It has been used to treat hormone-responsive breast cancer in postmenopausal women. Apart from headaches, central nervous system complications are uncommon. In a large series of 656 patients, cerebral infarctions occurred in 0.3 % (2/656) of the patients (Sagara et al. 2010).

##### 3.3.2.3 Letrozole

Letrozole is used to treat breast cancer in postmenopausal women. Cerebrovascular events are reported in less than 2 % of patients and are usually thromboembolic (Simpson et al. 2004). Dizziness and memory impairment are also reported.

#### 3.3.3 Anti-androgens and Luteinizing Hormone-Releasing Hormone Analogs

##### 3.3.3.1 Goserelin

Goserelin is used as palliative therapy in advanced prostate and breast cancer. No significant neurological complications have been described.

##### 3.3.3.2 Leuprolide Acetate

Leuprolide is used for the treatment of advanced prostate cancer. Seizures are reported if there is brain damage prior to initiation of therapy with leuprolide (Akaboshi and Takeshita 2000).

#### 3.3.4 Other Antineoplastic Hormones

##### 3.3.4.1 Trastuzumab

Trastuzumab is used to treat certain types of breast cancer. No significant acute and chronic toxicities have been reported. PRES has been reported (Kaneda et al. 2012).

##### 3.3.4.2 Mitotane

Mitotane is used to treat inoperable adrenocortical carcinoma and Cushing disease. Central nervous system complications are a common adverse effect. These most commonly include drowsiness, confusion, dizziness, and headaches (Goto et al. 2008).

### 3.4 Hematopoietic Stem Cell Transplantation

Hematopoietic stem cell transplantation (HSCT) is generally performed in patients with several hematologic malignancies (in particular leukemia and lymphoma) and less often in those with nonmalignant disorders (Quant and Wen 2011). The frequency and type of neurological complications in patients undergoing HSCT depend on the type of HSCT (allogenic vs. autogenic) and the underlying disease. Allogenic HSCT is associated with higher neurological toxicity rates (up to 40 %) than autogenic HSCT (up to 10 %) (Rosenfeld and Pruitt 2006). The most frequently reported neurological complications are encephalopathy, infections, and cerebrovascular disorders. In a large retrospective study, the frequency and distribution of complications varied: subdural hematoma was more common in patients with acute myelogenous leukemia (AML) receiving autologous HSCT, whereas infections were more frequent in allogeneic HSCT (Saiz and Graus 2004).

Encephalopathy is the most common neurological complication in HSCT patients. Cerebral dysfunction is characterized by drowsiness, confusion, delirium, or seizures and has a poor prognosis (Woodard et al. 2004). When MRI is normal, encephalopathy can be secondary to systemic metabolic abnormalities or drug toxicity (e.g., antibiotic, amphotericin B). Abnormal MRI is often reported in chemotherapy-induced encephalopathy in HSCT, acute (with high-dose cytarabine for example), or delayed (e.g., purine analogs). PRES is also described in this setting either with cytotoxic agents (carboplatin, etoposide, fludarabine) or with immunosuppressants agents (cyclosporin, everolimus, sirolimus, tacrolimus) and is most common during the early post-transplant period (within one month after transplantation) (Fig. 11) (Pruitt et al. 2013). The immunosuppressant agents are often used for the prevention of graft-versus-host disease (GVHD) following allogeneic transplants.

Infections involving the CNS, classically occur more frequently in patients after allogenic than autogenic HSCT, particularly in the presence of severe GVHD. During the neutropenic period (early post-transplant period), infections may be due to bacteria, viruses, or fungi, and classic clinical clues may be absent due to the host's impaired inflammatory response. A CNS infection should always be suspected if the patient has new neurological signs, fever, or a systemic, particularly pulmonary, infection. *Aspergillus* species are the most common fungal CNS infections in HSCT patients (Quant and Wen 2011). MRI can show non-enhancing lesions of the basal ganglia, thalami, corpus callosum, or cerebral hemispheres representing infarctions (Fig. 12a) (DeLone et al. 1999). *Candida* (Fig. 12b), *Listeria monocytogenes*, and *Nocardia* can in rare cases cause brain infection in this condition. Within the 6 months following transplantation, patients with allogeneic HSCT are at increased risk of infections by virus and opportunistic organisms due to the immunosuppression necessary to prevent rejection of the graft and GVHD. *Toxoplasma gondii* is the most frequent parasitic CNS infection. MRI shows multiple mass lesions, which unlike those seen in acquired immunodeficiency syndrome may be non-contrast enhancing and rarely hemorrhagic (Maschke et al. 1999). The viruses more likely to cause neurologic complications are those of the herpes group. Routine prophylaxis with acyclovir has greatly reduced the incidence of encephalitis because of reactivation of CMV, HSV, or HHV6. Patients with HHV6 present with short-term memory loss, seizures, confusion, and behavioral changes. MRI is helpful (Fig. 12c), and CSF confirms the diagnosis. Patients can respond to ganciclovir or foscarnet. Other CNS infections are rare. After the sixth month, the risk of infections will persist in those patients who need elevated doses of immunosuppressive therapy.

Cerebrovascular disorders include ischemic strokes and intraparenchymal hemorrhages,

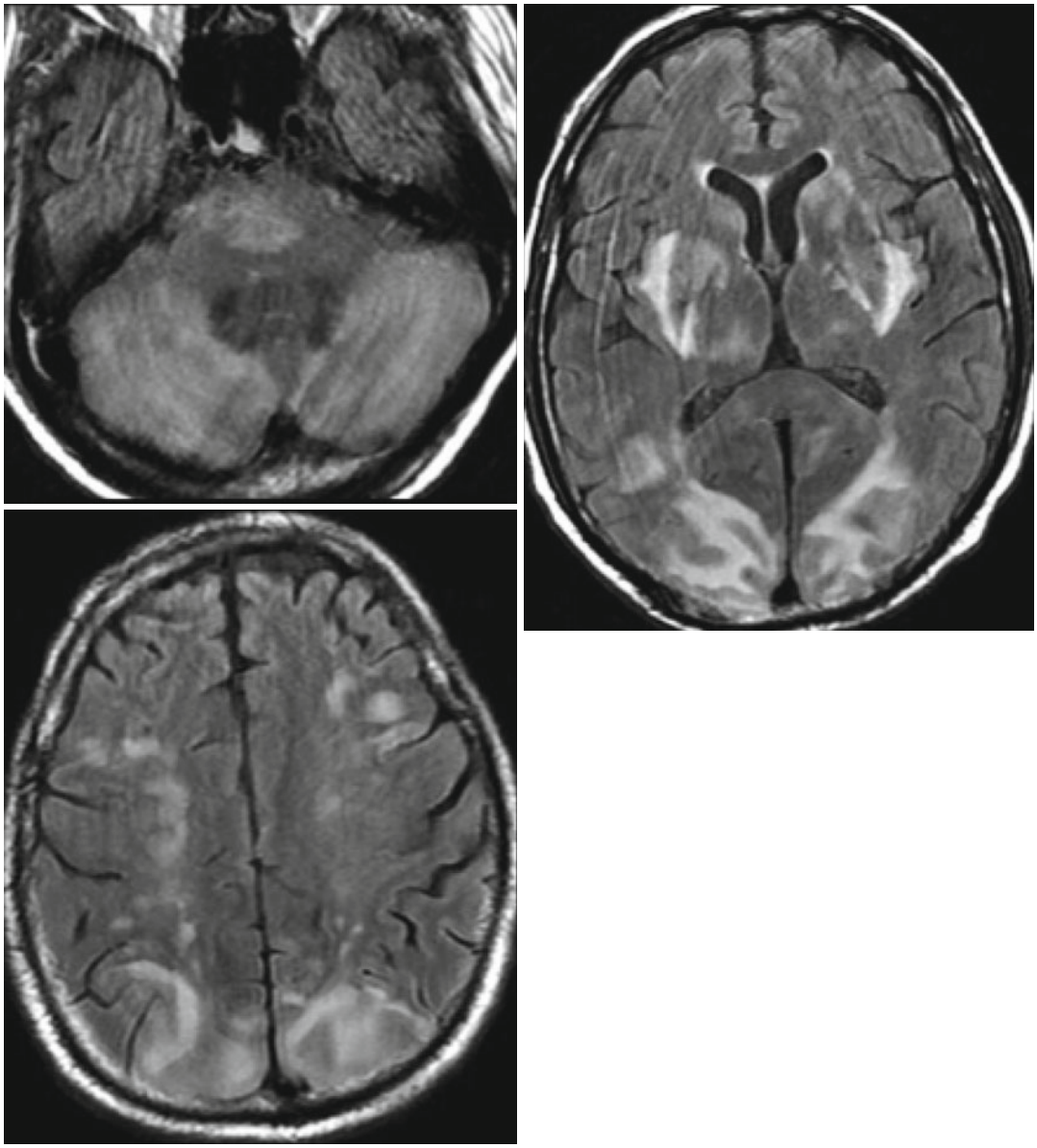

**Fig. 11** FLAIR images in a patient presenting cyclosporin-induced PRES. Symmetric and extensive vasogenic edema in the posterior fossa, temporo-occipito-parietal regions, frontal watershed zones, and basal ganglia

and subdural hemorrhages (SDHs) are rare. SDH is strongly associated with persistent low platelet counts and the development of post-lumbar puncture headache (Colosimo et al. 2000). Outcomes from cerebrovascular events are generally worse in the HSCT population compared to the general population (Coplin et al. 2001).

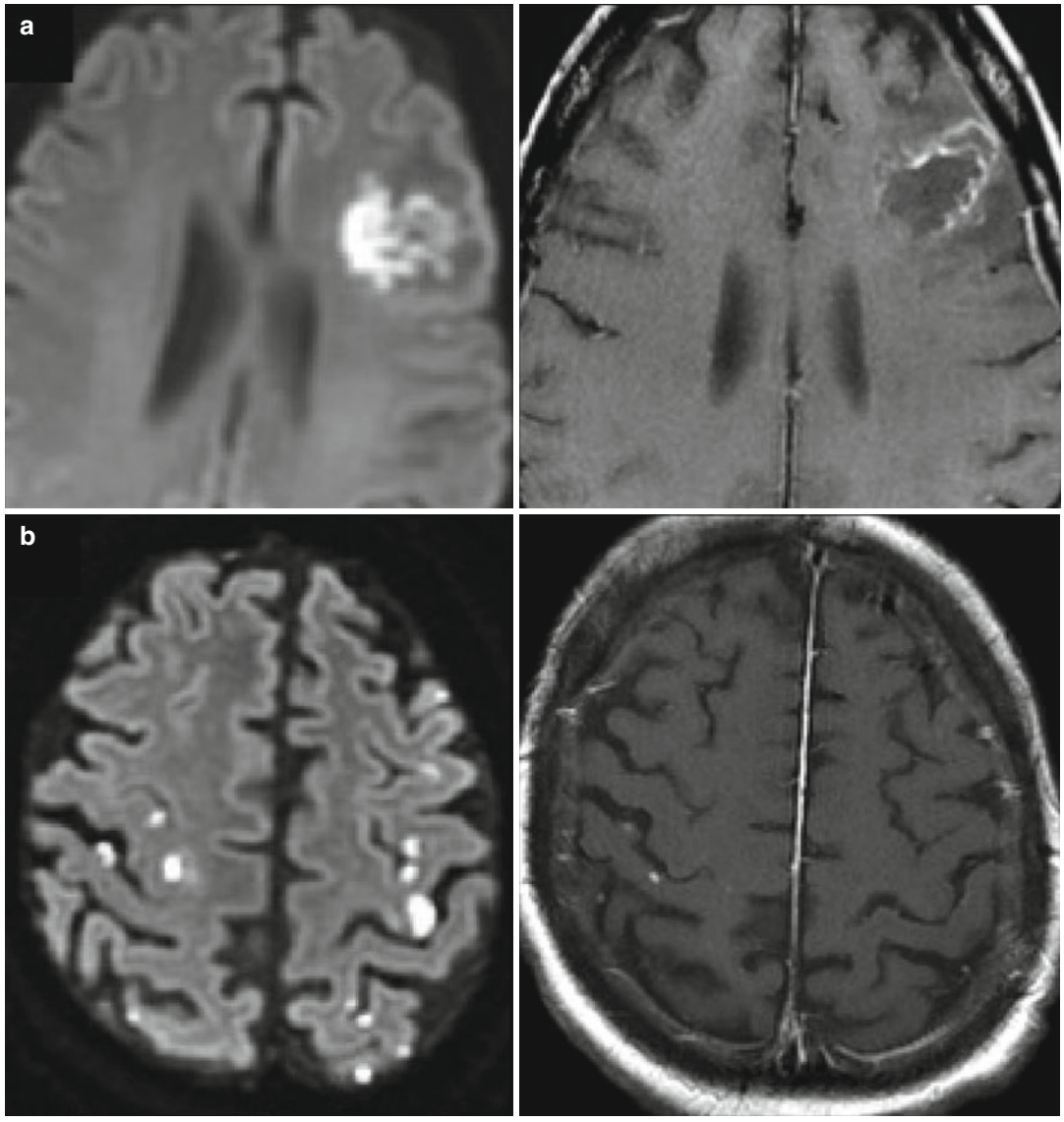


**Fig. 12** Chemotherapy-induced infectious disorders. (**a**) Cerebral aspergillosis. Hyperintense lesion with crenated borders on diffusion images (*left*) and minimal irregular incomplete peripheral enhancement on axial T1 post-gadolinium images (*right*). (**b**) Cerebral candidosis. Multiple small foci of emboli, hyperintense on diffusion (*left*) without associated contrast enhancement (*right*). (**c**) HHV6 encephalitis in a patient treated with bone marrow transplant. Coronal T2 images: both hippocampi (*arrows*) are hypertrophic and hyperintense in the acute phase (*left*). Two months after, both hippocampi (*arrows*) are atrophic (*right*)

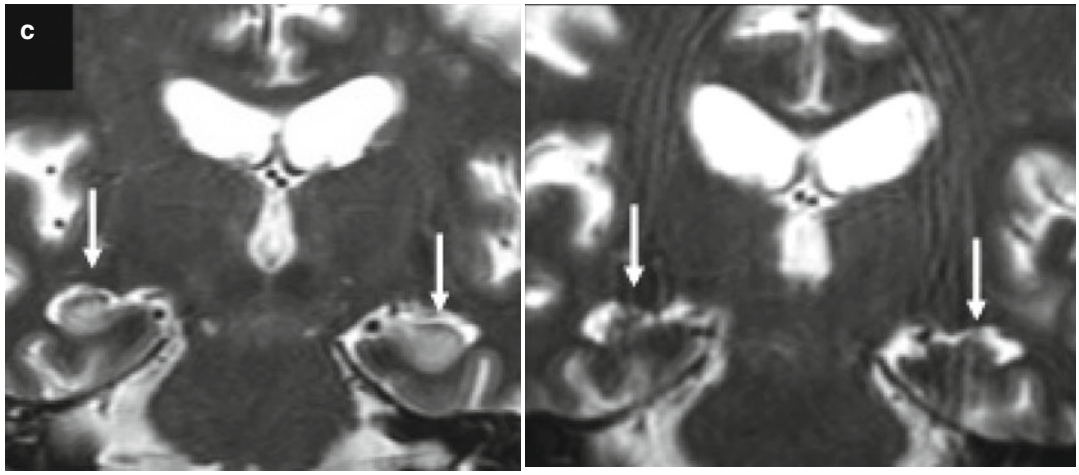


**Fig. 12** (continued)

## Conclusion

The nervous system is second only to the bone marrow as the most common site of chemotherapy toxicity. Neurotoxicity caused by chemotherapy is usually a diagnosis of exclusion requiring a thorough analysis of differential diagnosis. Also, the consequences of discontinuing a chemotherapeutic agent may have profound oncologic implications and the risk/benefit ratio should therefore be carefully weighted. Neurotoxicities from some drugs may be reversible (methotrexate) or do not necessarily recur if the agent is given again (ifosfamide). New agents and combinations may produce novel toxicities. With improved survival from cancer, at present unknown late toxicities may appear in the future.

## References

Akaboshi S, Takeshita K (2000) A case of atypical absence seizures induced by leuprolide acetate. Pediatr Neurol 23(3):266–268

Atkins MB, Lotze MT, Dutcher JP, Fisher RI, Weiss G, Margolin K, Abrams J, Sznol M, Parkinson D, Hawkins M, Paradise C, Kunkel L, Rosenberg SA (1999) High-dose recombinant interleukin 2 therapy for patients with metastatic melanoma: analysis of 270 patients treated between 1985 and 1993. J Clin Oncol 17(7):2105–2116

Auré K, Béhin A, Louillet F, Lafitte C, Sanson M, Vernant JP (2005) Dramatic improvement in non-AIDS related progressive multifocal leucoencephalopathy. J Neurol Neurosurg Psychiatry 76(9):1305–1306

Bartynski WS, Boardman JF (2007) Distinct imaging patterns and lesion distribution in posterior reversible encephalopathy syndrome. AJNR Am J Neuroradiol 28:1320–1327

Bay A, Oner AF, Etlik O et al (2005) Myelopathy due to intrathecal chemotherapy: report of six cases. J Pediatr Hematol Oncol 27:270–272

Besse B, Lasserre SF, Compton P, Huang J, Augustus S, Rohr UP (2010) Bevacizumab safety in patients with central nervous system metastases. Clin Cancer Res 16(1):269–278

Boogerd W, vd Sande JJ, Moffie D (1988) Acute fever and delayed leukoencephalopathy following low dose intraventricular methotrexate. J Neurol Neurosurg Psychiatry 51:1277–1283

Bross PF, Beitz J, Chen G, Chen XH, Duffy E, Kieffer L, Roy S, Sridhara R, Rahman A, Williams G, Pazdur R (2001) Approval summary: gemtuzumab ozogamicin in relapsed acute myeloid leukemia. Clin Cancer Res 7(6):1490–1496

Bushnell CD, Goldstein LB (2004) Risk of ischemic stroke with tamoxifen treatment for breast cancer: a metaanalysis. Neurology 63(7):1230–1233

Carson KR, Focosi D, Major EO et al (2009a) Monoclonal antibody-associated progressive multifocal leucoencephalopathy in patients treated with rituximab, natalizumab, and efalizumab: a Review from the Research on Adverse Drug Events and Reports (RADAR) Project. Lancet Oncol 10(8):816–824

Carson KR, Evens AM, Richey EA et al (2009b) Progressive multifocal leucoencephalopathy after rituximab therapy in HIV-negative patients: a report of 57 cases from the Research on Adverse Drug Events and Reports project. Blood 113: 4834–4840

Caselli D, Rosati A, Faraci M, Podda M, Ripaldi M, Longoni D, Cesaro S, Lo Nigro L, Paolicchi O, Maximova N, Menconi MC, Ziino O, Cicalese MP, Santarone S, Nesi F, Aricò M, Locatelli F, Prete A, Bone Marrow Transplantation Working Group of the Associazione Italiana Ematologia Oncologia Pediatrica (2014) Risk of seizures in children receiving busulphan-containing regimens for stem cell transplantation. Biol Blood Marrow Transplant 20(2): 282–285

Chen YH, Huang CH (2012) Reversible posterior leukoencephalopathy syndrome induced by vinorelbine. Clin Breast Cancer 12(3):222–225

Chen H, Modiano MR, Neal JW, Brahmer JR, Rigas JR, Jotte RM, Leighl NB, Riess JW, Kuo CJ, Liu L, Gao B, Dicioccio AT, Adjei AA, Wakelee HA (2014) A phase II multicentre study of ziv-aflibercept in combination with cisplatin and pemetrexed in patients with previously untreated advanced/metastatic non-squamous non-small cell lung cancer. Br J Cancer 110(3):602–608

Cheng CY, Lin YC, Chen JS, Chen CH, Deng ST (2011) Cisplatin-induced acute hyponatremia leading to a seizure and coma: a case report. Chang Gung Med J 34(6 Suppl):48–51

Chun HG, Leyland-Jones B, Caryk SM et al (1986) Central nervous system toxicity of fludarabine phosphate. Cancer Treat Rep 70:1225–1228

Cioffi P, Laudadio L, Nuzzo A, Belfiglio M, Petrelli F, Grappasonni I (2012) Gemcitabine-induced posterior reversible encephalopathy syndrome: a case report. J Oncol Pharm Pract 18(2):299–302

Cohen RB, Abdallah JM, Gray JR et al (1993) Reversible neurologic toxicity in patients treated with standard-dose fludarabine phosphate for mycosis fungoides and chronic lymphocytic leukemia. Ann Intern Med 118:114–116

Cohen MH, Shen YL, Keegan P, Pazdur R (2009) FDA drug approval summary: bevacizumab (Avastin) as treatment of recurrent glioblastoma multiforme. Oncologist 14(11):1131–1138

Colosimo M, McCarthy N, Jayasinghe R, Morton J, Taylor K, Durrant S (2000) Diagnosis and management of subdural haematoma complicating bone marrow transplantation. Bone Marrow Transplant 25(5):549–552

Cooksley T, Haji-Michael P (2011) Posterior reversible encephalopathy syndrome associated with deoxycoformycin and alemtuzumab. J R Coll Physicians Edinb 41(3):215–217

Coplin WM, Cochran MS, Levine SR, Crawford SW (2001) Stroke after bone marrow transplantation: frequency, aetiology and outcome. Brain 124(Pt 5):1043–1051

Correa DD, Shi W, Abrey LE, Deangelis LM, Omuro AM, Deutsch MB, Thaler HT (2012) Cognitive functions in primary CNS lymphoma after single or combined modality regimens. Neuro Oncol 14(1):101–108

Corso A, Castagnola C, Bernasconi C (1997) Thrombotic events are not exclusive to the remission induction period in patients with acute lymphoblastic leukemia: a report of two cases of cerebral sinus thrombosis. Ann Hematol 75(3):117–119

Costa R, Costa R, Costa R, Junior GM, Cartaxo HQ, de Barros AC. Reversible posterior encephalopathy syndrome secondary to sunitinib. Case Rep Oncol Med 2014 (Epub 2014 May 13)

Counsel P, Khangure M (2007) Myelopathy due to intrathecal chemotherapy: magnetic resonance imaging findings. Clin Radiol 62(2):172–176

Delanty N, Vaughan C, Frucht S et al (1997) Erythropoietin-associated hypertensive posterior leukoencephalopathy. Neurology 49:686–689

DeLone DR, Goldstein RA, Petermann G, Salamat MS, Miles JM, Knechtle SJ, Brown WD (1999) Disseminated aspergillosis involving the brain: distribution and imaging characteristics. AJNR Am J Neuroradiol 20(9):1597–1604

Dogan E, Aksoy S, Arslan C, Dede DS, Altundag K (2010) Probable sorafenib-induced reversible encephalopathy in a patient with hepatocellular carcinoma. Med Oncol 27(4):1436–1437

Donmez FY, Basaran C, Kayahan Ulu EM et al (2010) MRI features of posterior reversible encephalopathy syndrome in 33 patients. J Neuroimaging 20:22–28

Dunton SF, Nitschke R, Spruce WE, Bodensteiner J, Krous HF (1986) Progressive ascending paralysis following administration of intrathecal and intravenous cytosine arabinoside. A Pediatric Oncology Group study. Cancer 57(6):1083–1088

Eberly AL, Anderson GD, Bubalo JS, McCune JS (2008) Optimal prevention of seizures induced by high-dose busulfan. Pharmacotherapy 28:1502–1510

Eckert A, Schoeffler A, Dalle S et al (2009) Anti-CTLA4 monoclonal antibody induced sarcoidosis in a metastatic melanoma patient. Dermatology 218:69–70

Feinstein TM, Gibson MK, Argiris A (2009) Cetuximab-induced aseptic meningitis. Ann Oncol 20(9): 1609–1610

Foerster R, Welzel T, Debus J, Gruellich C, Jaeger D, Potthoff K (2013) Posterior reversible leukoencephalopathy syndrome associated with pazopanib. Case Rep Oncol 6(1):204–208

Gállego Pérez-Larraya J, Palma JA, Carmona-Iragui M et al (2011) Neurologic complications of intrathecal liposomal cytarabine administered prophylactically to patients with non-Hodgkin lymphoma. J Neurooncol 103(3):603–609

Ganguly S (2007) Acute intracerebral hemorrhage in intravascular lymphoma: a serious infusion related adverse event of rituximab. Am J Clin Oncol 30(2):211–212

Ganjoo KN, Raman R, Sobel RA et al (2009) Opportunistic enteroviral meningoencephalitis: an unusual treatable complication of rituximab therapy. Leuk Lymphoma 50(4):673–675

Gerstner ER, Frosch MP, Batchelor TT (2010) Diffusion magnetic resonance imaging detects pathologically confirmed, nonenhancing tumor progression in a patient with recurrent glioblastoma receiving bevacizumab. J Clin Oncol 28(6):e91–e93

Glusker P, Recht L, Lane B (2006) Reversible posterior leukoencephalopathy syndrome and bevacizumab. N Engl J Med 354(9):980–982

González-Suárez I, Aguilar-Amat MJ, Trigueros M, Borobia AM, Cruz A, Arpa J (2014) Leukoencephalopathy due to oral methotrexate. Cerebellum 13(1):178–183

Goto T, Miyako K, Kuromaru R, Ihara K, Torisu H, Sanefuji M, Nagamatsu R, Hara T (2008) Case report: adjuvant therapy with a high dose of mitotane for adrenocortical carcinoma in a 4-year-old boy. Clin Pediatr Endocrinol 17(3):71–74

Graber JJ, Nolan CP (2010) Myelopathies in patients with cancer. Arch Neurol 67(3):298–304

Grem JL, Falkson G, Love RR, Tormey DC (1988) A phase II evaluation of combination chemotherapy plus aminoglutethimide in women with metastatic or recurrent breast carcinoma. An Eastern Cooperative Oncology Group Pilot Study. Am J Clin Oncol 11(5):528–534

Grever MR, Kopecky KJ, Coltman CA et al (1988) Fludarabine monophosphate: a potentially useful agent in chronic lymphocytic leukemia. Nouv Rev Fr Hematol 30:457–459

Güler T, Cakmak OY, Toprak SK, Kibaroğlu S, Can U (2014) Intrathecal methotrexate-induced posterior reversible encephalopathy syndrome (PRES). Turk J Haematol 31(1):109–110

Hamberg P, De Jong FA, Brandsma D, Verweij J, Sleijfer S (2008) Irinotecan-induced central nervous system toxicity. Report on two cases and review of the literature. Acta Oncol 47(5):974–978

Hammack J (2005) Neurologic complications of chemotherapy and biologic therapies. In: Schiff D, O'Neill BP (eds) Principles of neuro-oncology. McGraw-Hill, New York, pp 679–710

Hammack JE, Cascino TL (1998) Chemotherapy and other common drug-induced toxicities of the central nervous system in patients with cancer. In: Vecht CJ (ed) Handbook of clinical neurology. Elsevier Science, Amsterdam, pp 481–514

Han R, Yang YM, Dietrich J, Luebke A, Mayer-Pröschel M, Noble M (2008) Systemic 5-fluorouracil treatment causes a syndrome of delayed myelin destruction in the central nervous system. J Biol 7(4):12

Harrison DM, Newsome SD, Skolasky RL, McArthur JC, Nath A (2011) Immune reconstitution is not a prognostic factor in progressive multifocal leukoencephalopathy. J Neuroimmunol 238:81–86

Hart C, Kinney MO, McCarron MO (2012) Posterior reversible encephalopathy syndrome and oral methotrexate. Clin Neurol Neurosurg 114(6):725–727

Hartz B, Löbel U, Hagel C, Escherich G (2013) Fatal neurological side-effects with necrosis of spinal cord following nelarabine treatment in a child with relapsed T-cell acute lymphoblastic leukemia. Am J Hematol 88(12):1096–1097

Hayase E, Sugita J, Fujimoto K, Ebata K, Yamakawa T, Yoshida M, Takemura R, Iwasaki J, Takahashi S, Shiratori S, Kondo T, Tanaka J, Teshima T (2014) Posterior reversible encephalopathy syndrome following paralytic ileus caused by vincristine in a patient with T cell lymphoblastic lymphoma. Rinsho Ketsueki 55(2):249–253

Helissey C, Chargari C, Lahutte M et al (2012) First case of posterior reversible encephalopathy syndrome associated with vinflunine. Invest New Drugs 30(5):2032–2034

Herzig RH, Hines JD, Herzig GP, Wolff SN, Cassileth PA, Lazarus HM, Adelstein DJ, Brown RA, Coccia PF, Strandjord S et al (1987) Cerebellar toxicity with high-dose cytosine arabinoside. J Clin Oncol 5(6):927–932

Hinchey J, Chaves C, Appignani B et al (1996) A reversible posterior leukoencephalopathy syndrome. N Engl J Med 334:494–500

Hoffman DL, Howard JR Jr, Sarma R, Riggs JE (1993) Encephalopathy, myelopathy, optic neuropathy, and anosmia associated with intravenous cytosine arabinoside. Clin Neuropharmacol 16(3):258–262

Hourani R, Abboud M, Hourani M, Khalifeh H, Muwakkit S (2008) L-asparaginase-induced posterior reversible encephalopathy syndrome during acute lymphoblastic leukemia treatment in children. Neuropediatrics 39(1):46–50

Inagaki M, Yoshikawa E, Matsuoka Y et al (2007) Smaller regional volumes of brain gray and white matter demonstrated in breast cancer survivors exposed to adjuvant chemotherapy. Cancer 109(1):146–156

Jabbour E, O'Brien S, Kantarjian H, Garcia-Manero G, Ferrajoli A, Ravandi F, Cabanillas M, Thomas DA (2007) Neurologic complications associated with intrathecal liposomal cytarabine given prophylactically in combination with high-dose methotrexate and cytarabine to patients with acute lymphocytic leukemia. Blood 109(8):3214–3218

Jansen C, Miakowski C, Dodd M et al (2005) Potential mechanisms for chemotherapy-induced impairments in cognitive function. Oncol Nurs Forum 32: 1151–1163

Kaneda H, Okamoto I, Satoh T, Nakagawa K (2012) Reversible posterior leukoencephalopathy syndrome and trastuzumab. Invest New Drugs 30(4):1766–1767

Keime-Guibert F, Napolitano M, Delattre JY (1998) Neurological com- plications of radiotherapy and chemotherapy. J Neurol 245:695–708

Kende G, Sirkin SR, Thomas PR et al (1979) Blurring of vision: a previously undescribed complication of cyclophosphamide therapy. Cancer 44:69–71

Kim CA, Price-Hiller J, Chu QS, Tankel K, Hennig R, Sawyer MB, Spratlin JL (2014) Atypical reversible posterior leukoencephalopathy syndrome (RPLS) induced by cediranib in a patient with metastatic rectal cancer. Invest New Drugs 23

Kwong YL, Yeung DY, Chan JC (2009) Intrathecal chemotherapy for hematologic malignancies: drugs and toxicities. Ann Hematol 88(3):193–201

Lee VH, Wijdicks EF, Manno EM et al (2008) Clinical spectrum of reversible posterior leukoencephalopathy syndrome. Arch Neurol 65:205–210

Leniger T, Kastrup O, Diener HC (2000) Reversible posterior leukencephalopathy syndrome induced by granulocyte stimulating factor filgrastim. J Neurol Neurosurg Psychiatry 69(2):280–281

Letarte N, Bressler LR, Villano JL (2013) Bevacizumab and central nervous system (CNS) hemorrhage. Cancer Chemother Pharmacol 71(6):1561–1565

Li SH, Chen WH, Tang Y, Rau KM, Chen YY, Huang TL, Liu JS, Huang CH (2006) Incidence of ischemic stroke post-chemotherapy: a retrospective review of 10,963 patients. Clin Neurol Neurosurg 108(2):150–156

Liman TG, Bohner G, Heuschmann PU et al (2012) The clinical and radiological spectrum of posterior reversible encephalopathy syndrome: the retrospective Berlin PRES study. J Neurol 259:155–164

Lindner LH, Ostermann H, Hiddemann W, Kiani A, Würfel M, Illmer T, Karsch C, Platzbecker U, Ehninger G, Schleyer E (2008) AraU accumulation in patients with renal insufficiency as a potential mechanism for cytarabine neurotoxicity. Int J Hematol 88(4):381–386

Major EO (2010) Progressive multifocal leukoencephalopathy in patients on immunomodulatory therapies. Annu Rev Med 61:35–47

Maraiki F, Aljubran A (2014) Carotid and brachiocephalic arteries stenosis with long term use of sorafenib. Hematol Oncol Stem Cell Ther 7(1):53–55

Maschke M, Dietrich U, Prumbaum M, Kastrup O, Turowski B, Schaefer UW, Diener HC (1999) Opportunistic CNS infection after bone marrow transplantation. Bone Marrow Transplant 23(11): 1167–1176

Maur M, Tomasello C, Frassoldati A, Dieci MV, Barbieri E, Conte P (2012) Posterior reversible encephalopathy syndrome during ipilimumab therapy for malignant melanoma. J Clin Oncol 30(6):e76–e78

Meyers CA (2008) How chemotherapy damages the central nervous system. J Biol 7:11

Meyers CA, Scheibel RS, Forman AD (1991) Persistent neurotoxicity of systemically administered interferon-alpha. Neurology 41(5):672–676

Mitchell L, Lambers M, Flege S, Kenet G, Li-Thiao-Te V, Holzhauer S, Bidlingmaier C, Frühwald MC, Heller C, Schmidt W, Pautard B, Nowak-Göttl U (2010) Validation of a predictive model for identifying an increased risk for thromboembolism in children with acute lymphoblastic leukemia: results of a multicenter cohort study. Blood 115(24):4999–5004

Moore-Maxwell CA, Datto MB, Hulette CM (2004) Chemotherapy-induced toxic leukoencephalopathy causes a wide range of symptoms: a series of four autopsies. Mod Pathol 17:241–247

Mosca L, Grady D, Barrett-Connor E, Collins P, Wenger N, Abramson BL, Paganini-Hill A, Geiger MJ, Dowsett SA, Amewou-Atisso M, Kornitzer M (2009) Effect of raloxifene on stroke and venous thromboembolism according to subgroups in postmenopausal women at increased risk of coronary heart disease. Stroke 40(1):147–155

Moskowitz A, Nolan C, Lis E, Castro-Malaspina H, Perales MA (2007) Posterior reversible encephalopathy syndrome due to sirolimus. Bone Marrow Transplant 39(10):653–654

Muallaoğlu S, Koçer M, Güler N (2012) Acute transient encephalopathy after weekly paclitaxel infusion. Med Oncol 29(2):1297–1299

Muldoon LL, Soussain C, Jahnke K, Johanson C et al (2007) Chemotherapy delivery issues in central nervous system malignancy: a reality check. J Clin Oncol 25:2295–2305

Newton HB (2012a) Neurological complications of chemotherapy to the central nervous system. Handb Clin Neurol 105:903–916

Newton HB (2012b) Neurological complications of alkylating agent chemotherapy. In: Wen P, Schiff D, Lee AQ (eds) Neurological complications of cancer therapy. Demos Medical, New York

Nghiemphu PL, Green RM, Pope WB, Lai A, Cloughesy TF (2008) Safety of anticoagulation use and bevacizumab in patients with glioma. Neuro Oncol 10(3):355–360

Nguyen T, DeAngelis LM (2006) Stroke in cancer patients. Curr Neurol Neurosci Rep 6:187–192

Otten HM, Mathijssen J, ten Cate H et al (2004) Symptomatic venous thromboembolism in cancer patients treated with chemotherapy—an underestimated phenomenon. Arch Intern Med 164: 190–194

Park S, Kang JI, Bang H, Kim BR, Lee J (2013) A case of the cauda equina syndrome associated with the intrathecal chemotherapy in a patient with primary central nervous system lymphoma. Ann Rehabil Med 37(3):420–425

Payne JH, Vora AJ (2007) Thrombosis and acute lymphoblastic leukaemia. Br J Haematol 138(4):430–445

Pisoni R, Ruggenenti P, Remuzzi G (2001) Drug-induced thrombotic microangiopathy: incidence, prevention and management. Drug Saf 24(7):491–501

Posner J (2009) Side effects of chemotherapy. In: Posner J (ed) Neurologic complications of cancer. University Press, Oxford, pp 447–487

Postma TJ, van Groeningen CJ, Witjes RJ, Weerts JG, Kralendonk JH, Heimans JJ (1998) Neurotoxicity of combination chemotherapy with procarbazine, CCNU and vincristine (PCV) for recurrent glioma. J Neurooncol 38(1):69–75

Pruitt AA, Graus F, Rosenfeld MR (2013) Neurological complications of transplantation: part I: hematopoietic cell transplantation. Neurohospitalist 3(1):24–38

Quant AL, Wen PY (2011) Common neurologic complications in hematopoietic stem cell transplant patients. In: Wen PY, Schiff D, Quant EL (eds) Neurologic complications of cancer therapy. Demos Medical, New York, pp 395–410

Quarantini LC, Miranda-Scippa A, Parana R, Sampaio AS, Bressan RA (2007) Acute dystonia after injection of pegylated interferon alpha-2b. Mov Disord 22(5):747–748

Rajasekhar A, Georges TJ (2007) Gemcitabine-induced reversible posterior leucoencephalopathy syndrome: a case report and review of the literature. Oncologist 12:1332–1335

Randall LM, Monk BJ (2010) Bevacizumab toxicities and their management in ovarian cancer. Gynecol Oncol 117(3):497–504

Renouf D, Gill S (2006) Capecitabine-induced cerebellar toxicity. Clin Colorectal Cancer 6:70–71

Richards A, Marshall H, McQuary A (2011) Evaluation of methylene blue, thiamine, and/or albumin in the prevention of ifosfamide-related neurotoxicity. J Oncol Pharm Pract 17(4):372–380

Rieger J, Bähr O, Müller K, Franz K, Steinbach J, Hattingen E (2010) Bevacizumab-induced diffusion-restricted lesions in malignant glioma patients. J Neurooncol 99(1):49–56

Roecker AM, Stockert A, Kisor DF (2010) Nelarabine in the treatment of refractory T-cell malignancies. Clin Med Insights Oncol 4:133–141

Rosenfeld MR, Pruitt A (2006) Neurologic complications of bone marrow, stem cell, and organ transplantation in patients with cancer. Semin Oncol 33(3): 352–361

Roy S, Gandhi AK, Jana M, Julka PK (2014) Recurrent posterior reversible encephalopathy syndrome after chemotherapy in hematologic malignancy-posterior reversible encephalopathy syndrome can strike twice!!! J Cancer Res Ther 10(2):393–396

Sagara Y, Kosha S, Baba S, Dokiya F, Tamada S, Sagara Y, Matsuyama Y, Ohi Y, Ando M, Rai Y, Sagara Y, Douchi T (2010) Adverse events and bone health during anastrozole therapy in postmenopausal Japanese breast cancer patients. Breast Cancer 17(3):212–217

Saiz A, Graus F (2004) Neurological complications of hematopoietic cell transplantation. Semin Neurol 24(4):427–434

Sánchez-Carpintero R, Narbona J, López de Mesa R, Arbizu J, Sierrasesúmaga L (2001) Transient posterior encephalopathy induced by chemotherapy in children. Pediatr Neurol 24(2):145–148

Schmidt-Hieber M, Zweigner J, Uharek L, Blau IW, Thiel E (2009) Central nervous system infections in immunocompromised patients: update on diagnostics and therapy. Leuk Lymphoma 50(1):24–36

Shah RR (2005) Mechanistic basis of adverse drug reactions: the perils of inappropriate dose schedules. Expert Opin Drug Saf 4:103–128

Shintaku M, Toyooka N, Koyama T, Teraoka S, Tsudo M (2014) Methotrexate myelopathy with extensive transverse necrosis: report of an autopsy case. Neuropathology 2

Siddiqi AI (2011) Rituximab as a possible cause of posterior reversible encephalopathy syndrome. Australas Med J 4(9):513–515

Sikkema T, Schuiling WJ, Hoogendoorn M (2013) Progressive multifocal leukoencephalopathy during treatment with rituximab and CHOP chemotherapy in a patient with a diffuse large B-cell lymphoma. BMJ Case Rep 25:2013

Silverman DHS, Dy CJ, Castellon SA, Lai J et al (2007) Altered frontocortical, cerebellar, and basal ganglia activity in adjuvant-treated breast cancer survivors 5–10 years after chemotherapy. Breast Cancer Res Treat 103:303–311

Simpson D, Curran MP, Perry CM (2004) Letrozole: a review of its use in postmenopausal women with breast cancer. Drugs 64(11):1213–1230

Smith GA, Damon LE, Rugo HS, Ries CA, Linker CA (1997) High-dose cytarabine dose modification reduces the incidence of neurotoxicity in patients with renal insufficiency. J Clin Oncol 15(2):833–839

Smolle E, Trojan A, Schuster SJ, Haybaeck J (2014) Progressive multifocal leukoencephalopathy- A case report and review of the literature. In Vivo 28(5):941–948

Soussain C, Ricard D, Fike JR, Mazeron JJ, Psimaras D, Delattre JY (2009) CNS complications of radiotherapy and chemotherapy. Lancet 374(9701): 1639–1651

Steeghs N, de Jongh FE, Sillevis Smitt PA et al (2003) Cisplatin-induced encephalopathy and seizures. Anticancer Drugs 14:443–446

Sul JK, DeAngelis LM (2006) Neurologic complications of cancer chemotherapy. Semin Oncol 33:324–332

Szabatura AH, Cirrone F, Harris C, McDonnell AM, Feng Y, Voit D, Neuberg D, Butrynski J, Fisher DC. An assessment of risk factors associated with ifosfamide-induced encephalopathy in a large academic cancer center. J Oncol Pharm Pract 2014

Taillibert S, Vincent LA, Granger B, Marie Y, Carpentier C, Guillevin R, Bellanger A, Mokhtari K, Rousseau A, Psimaras D, Dehais C, Sierra del Rio M, Meng Y, Laigle-Donadey F, Hoang-Xuan K, Sanson M, Delattre JY (2009) Bevacizumab and irinotecan for recurrent oligodendroglial tumors. Neurology 72(18):1601–1606

Takimoto CH, Lu ZH, Zhang R, Liang MD, Larson LV, Cantilena LR Jr, Grem JL, Allegra CJ, Diasio RB, Chu E (1996) Severe neurotoxicity following 5-fluorouracil-based chemotherapy in a patient with dihydropyrimidine dehydrogenase deficiency. Clin Cancer Res 2(3):477–481

Terwiel E, Hanrahan R, Lueck C, D'Rozario J (2010) Reversible posterior encephalopathy syndrome associated with bortezomib. Intern Med J 40(1):69–71

Tha KK, Terae S, Sugiura M et al (2002) Diffusion-weighted magnetic resonance imaging in early stage of 5-fluorouracil-induced leukoencephalopathy. Acta Neurol Scand 106:379–386

Tlemsani C, Mir O, Boudou-Rouquette P et al (2011) Posterior reversible encephalopathy syndrome induced by anti-VEGF agents. Target Oncol 6(4):253–258

Tzachanis D, Haider M, Papazisis G (2014) A case of subacute encephalopathy developing after treatment with clofarabine and methotrexate that resolved with corticosteroids. Am J Ther 1

Vardy J, Wefel J, Ahles T, Tannock I et al (2008) Cancer and cancer-therapy related cognitive dysfunction: an international perspective from the venice cognitive workshop. Ann Oncol 19:623–629

Vaughn DJ, Jarvik JG, Hackney D et al (1993) High-dose cytarabine neurotoxicity: MR findings during the acute phase. AJNR Am J Neuroradiol 14:1014–1016

von Geldern G, Pardo CA, Calabresi PA, Newsome SD (2012) PML-IRIS in a patient treated with brentuximab. Neurology 79(20):2075–2077

Vu T, Carrum G, Hutton G, Heslop HE, Brenner MK, Kamble R (2007) Human herpesvirus-6 encephalitis following allogeneic hematopoietic stem cell transplantation. Bone Marrow Transplant 39(11):705–709

Waggoner J, Martinu T, Palmer SM (2009) Progressive multifocal leukoencephalopathy following heightened immunosuppression after lung transplant. J Heart Lung Transplant 28(4):395–398

Watterson J, Toogood I, Nieder M et al (1994) Excessive spinal cord toxicity from in- tensive central nervous system-directed therapies. Cancer 74(11):3034–3041

Wefel JS, Schagen SB (2012) Chemotherapy-related cognitive dysfunction. Curr Neurol Neurosci Rep 12(3):267–275

Wefel JS, Lenzi R, Theriault R, Buzdar AU, Cruickshank S, Meyers CA (2004) 'Chemobrain' in breast carcinoma?: a prologue. Cancer 101(3):466–475

Wen PY, Yung WK, Lamborn KR, Norden AD, Cloughesy TF, Abrey LE, Fine HA, Chang SM, Robins HI, Fink K, Deangelis LM, Mehta M, Di Tomaso E, Drappatz J, Kesari S, Ligon KL, Aldape K, Jain RK, Stiles CD, Egorin MJ, Prados MD (2009) Phase II study of imatinib mesylate for recurrent meningiomas (North American Brain Tumor Consortium study 01–08). Neuro Oncol 11(6):853–860

Woodard P, Helton K, McDaniel H, Khan RB, Thompson S, Hale G, Benaim E, Kasow K, Leung W, Horwitz E, Srivastava DK, Tong X, Yusuf U, Cunningham JM, Handgretinger R (2004) Encephalopathy in pediatric patients after allogeneic hematopoietic stem cell transplantation is associated with a poor prognosis. Bone Marrow Transplant 33(11): 1151–1157

Wu J, Langford LA, Schellingerhout D, Guha-Thakurta N, Tummala S, Weinberg JS, Puduvalli VK (2011) Progressive multifocal leukoencephalopathy in a patient with glioblastoma. J Neurooncol 103(3): 791–796

Wyllie AR, Bayliff CD, Kovacs MJ (1997) Myoclonus due to chlorambucil in two adults with lymphoma. Ann Pharmacother 31(2):171–174

Ye QL, Zhai ZM (2014) Toremifene and tamoxifen have similar efficacy in the treatment of patients with breast cancer: a meta-analysis of randomized trials. Mol Biol Rep 41(2):751–756

Yoshikawa E, Matsuoka Y, Inagaki M, Nakano T et al (2005) No adverse effects of adjuvant chemotherapy on hippocampal volume in Japanese breast cancer survivors. Breast Cancer Res Treat 92:81–84

Yung WK, Albright RE, Olson J, Fredericks R, Fink K, Prados MD, Brada M, Spence A, Hohl RJ, Shapiro W, Glantz M, Greenberg H, Selker RG, Vick NA, Rampling R, Friedman H, Phillips P, Bruner J, Yue N, Osoba D, Zaknoen S, Levin VA (2000) A phase II study of temozolomide vs. procarbazine in patients with glioblastoma multiforme at first relapse. Br J Cancer 83(5):588–593

Zairi F, Le Rhun E, Tetard MC, Kotecki N, Assaker R (2011) Complications related to the placement of an intraventricular chemotherapy device. J Neurooncol 104(1):247–252

Zvorničanin J, Sinanović O, Zukić S, Jusufović V, Burina A. Tamoxifen associated bilateral optic neuropathy. Acta Neurol Belg 2014

# Part III

# Head and Neck

# Therapy-Induced Changes in Head and Neck

Michael M. Lell

## Contents




**Abstract**

Radiation with or without concomitant chemotherapy of the head and neck region is associated with acute and chronic toxicity and adverse effects on organ function. Therapy-induced dysphagia is a complex multifactorial disorder, constituting one of the most common and prominent problems affecting quality of life of the patients. Classical fluoroscopy is still the method of choice to search for morphologic (fistula, stricture, resection defect) and functional (impaired sensory or motor function of the pharyngoesophageal tube and larynx, xerostomia) deficits. Bone injury is another severe, although relatively rare, condition induced by radiation and specific drugs, especially bisphosphonates. While fatty replacement of the bone marrow within the radiation field is a deterministic effect without clinical significance for the patient, radiation-induced inflammation, fibrosis, disorganization of extracellular matrix, and tissue remodeling may lead to devitalized bone with mucosal ulceration, pathologic fracture, and fistula formation. Similar effects have been associated with osteoclast-inhibiting therapies, including bisphosphonates and denosumab.


## Abbreviations

| | |
|---|---|
| ADC | Apparent diffusion coefficient |
| ASBMR | American Society for Bone and Mineral Research |


M.M. Lell
Department of Radiology, University Erlangen, Erlangen, Germany
e-mail: michael.lell@uk-erlangen.de


Med Radiol Diagn Imaging (2015)
DOI 10.1007/174_2015_1077, © Springer International Publishing Switzerland

| | |
|---|---|
| BP | Bisphosphonate |
| CBCT | Cone beam computed tomography |
| CM | Contrast material |
| CTx | Chemotherapy |
| DARS | Dysphagia-aspiration-related structures |
| DWI | Diffusion-weighted imaging |
| FEES | Fiber-optic endoscopic evaluation of swallowing |
| MBS | Modified barium swallow |
| NPC | Nasopharyngeal cancer |
| ONJ | Osteonecrosis of the jaw |
| OPSE | Oropharyngeal swallow efficiency |
| ORES | Oral residue |
| ORN | Osteoradionecrosis |
| OTT | Oral transit time |
| PC | Pharyngeal constrictors |
| PRES | Pharyngeal residue |
| PTT | Pharyngeal transit time |
| RCTx | Radiochemotherapy |
| RTOG | Radiation Therapy Oncology Group |
| RTx | Radiation therapy |

## 1 Introduction

CT and MRI are well established in the pretherapeutic staging of head and neck tumors. Exact determination of infiltration depth and infiltration of critical structures like the cartilage, bone, nerves, or great vessels and demonstration of lymph node involvement are mandatory for therapy planning. The value of cross-sectional imaging in the tumor follow-up is at least as important, because early recurrence is often difficult to detect with clinical examination and endoscopy (Lell et al. 2000). For correct interpretation of posttherapeutic images, it is of great importance for the radiologist to be familiar with the type and time of therapy, be it surgery, chemotherapy (CTx), radiation therapy (RTx), or a combination. Each of the therapeutic approaches is associated with specific predictable effects on imaging. It is mandatory to differentiate those posttherapeutic changes from residual tumor and tumor recurrence to avoid unnecessary noninvasive or invasive procedures. While noninvasive procedures may burden the patient and the budget, invasive procedures may endanger the healing process, because due to altered perfusion and increased vulnerability of the mucosal surface, e.g., the risk of fistula formation and inflammation is increased if biopsy is performed following RTx.

MRI is the imaging modality of choice because it provides the highest soft tissue contrast and allows for additional diffusion-weighted and perfusion-weighted imaging, which adds functional information to morphology. Disadvantageous is the relatively long examination time of MRI as compared to CT, and many patients, especially those with breathing and swallowing impairment, may not be able to complete the examination without motion artifacts. CT has the advantage of high spatial resolution in all three dimensions (Lell et al. 2008) at a very short examination time (typically a few seconds).

In the follow-up after therapy, fluoroscopy has maintained its significance. While almost abandoned in the pretherapeutic staging in favor of endoscopy, the dynamic swallowing study precisely demonstrates mucosal dehiscence, fistula formation, anastomotic leak, disturbed coordination of muscle activity and aspiration in the early phase after therapy and stricture, deficient muscle coordination, inability to swallow, and (silent) aspiration in the later phase. The type of contrast material (CM) needs to be determined for each patient individually. Barium sulfate is the preferred CM providing the best contrast and mucosal coating, but must be avoided if mucosal dehiscence or leakage is suspected and should also be avoided in patients with aspiration. A swallow with tap water preceding each CM examination to screen for aspiration is helpful, although this test is not 100 % accurate. Nonionic iodinated CM should be used in those cases where barium is not indicated. Ionic iodinated CM should be completely avoided, because it has no advantages over nonionic CM and bears the risk of pulmonary edema in the case of aspiration. The "modified barium swallow" (MBS) is usually the first step in the evaluation of swallowing disorders and different consistencies of the barium bolus simulate typical eating behaviors. The entire swallowing channel including mouth, pharynx, and esophagus can be evaluated. MBS allows assessment of both the structure and function of the swallowing

mechanism. Because the flow of barium through the pharynx is very rapid, fluoroscopy with high frame rates (>15 frames per second) might be indicated in complex cases. Advantages of MBS are its noninvasive nature, the ability to evaluate the oral–pharyngeal and esophageal phase of swallowing, the visualization of cervical hardware after surgery or osteophytes, and the evaluation of the hyolaryngeal motion.

Parameters that can be derived from the MBS are: oral transit time (OTT), which is the time (usually < 1 s) measured from the first backward movement of the bolus (elevation of the tip of the tongue) until the head of the bolus enters the oropharynx (bolus passes the point where the ramus of the mandible crosses the tongue base); pharyngeal transit time (PTT), which is the time (usually < 1 s) from the entrance of the head of the bolus into the oropharynx until the tail of the bolus passes the cricopharyngeal muscle; pharyngeal delay, which is the time between the entrance of the head of the bolus into the oropharynx until the onset of laryngeal elevation; duration of cricopharyngeal opening; oral residue (ORES; percentage of oral bolus residue after first swallow); pharyngeal residue (PRES; percentage of pharyngeal bolus residue after first swallow); and percentage of aspirated bolus. The oropharyngeal swallow efficiency (OPSE) represents the percentage of the bolus swallowed divided by the bolus transit time, from the oral cavity through the cricopharyngeus: OPSE = [100-(PRES + ORES + ASP)]/(OTT+PTT) (Rademaker et al. 1994).

Fiber-optic endoscopic evaluation of swallowing (FEES) is an alternative method to diagnose swallow anomalies. The advantages of FEES are the direct view of anatomy (laryngeal and pharyngeal structures) and lesions, the procedure may be performed bedside, and real food and liquids can be used.

## 2 Swallowing and Swallowing Dysfunction After Therapy

### 2.1 Normal Swallowing

Swallowing occurs about once every minute in the awake adult due to saliva production (about 0.5 ml/min) and less frequently (about 6 times per hour) while asleep (Lear et al. 1965). Swallowing is a complex procedure involving about 30 pairs of muscles. Muscle activity is coordinated by nervous centers in the cortex and the medulla. Sensory fibers originate from the cranial nerves V, VII, IX, and X and motor fibers from the cranial nerves V, VII, IX–XII, and C1–C3 (Russi et al. 2012). The tongue is critical for speech, respiration, and swallowing and is composed of extrinsic (genioglossus, styloglossus, hyoglossus, palatoglossus) and intrinsic (superior and inferior longitudinal, transverse, and vertical) muscles. The tongue muscles are innervated by the hypoglossal (XII) nerve which consists of a lateral (l-XII) and a medial (m-XII) division; the overlying mucosa is innervated by the lingual and glossopharyngeal (CN XI) nerves (Mu and Sanders 2010). The muscles of pharynx may also be categorized as intrinsic (superior, middle, inferior pharyngeal constrictors, thyropharyngeus, cricopharyngeus) and extrinsic muscles. Extrinsic muscles can be further categorized into three subgroups: elevators and tensors of palate (levator veli palatini, tensor veli palatini, palatoglossus), superior and anterior displacers of the larynx (geniohyoid, mylohyoid, stylohyoid, thyrohyoid, digastric, stylopharyngeus, palatopharyngeus), and laryngeal inlet closers (aryepiglottic, thyroarytenoid, oblique arytenoids muscles) (Mittal 2011). These muscles are supplied by the branches of the trigeminal (CN V), facial (CN VII), glossopharyngeal (CN XI), vagus (CN X), ansa cervicalis, and hypoglossal (CN XII) nerves.

Three phases constitute the normal swallow, the oral phase, the oropharyngeal phase, and the esophageal phase. The oral phase includes the preparatory and early transport phase. The bolus is retained by closing the mouth, chopped, and mixed with saliva to get the appropriate consistency (intrinsic and extrinsic tongue muscles, suprahyoid muscles). Bolus entry into the oropharynx during mastication is prevented by contraction of the palatoglossus, styloglossus, and palatopharyngeus muscles and the base of the tongue. After mastication, the bolus is pushed back by the formation of a central groove in the tongue, the elevation of the tip of the tongue, and the contraction of the mylohyoid muscle.

The involuntary phase of swallow starts with the pharyngeal phase, which lasts about one second. The nasopharynx is closed by tension (m. tensor veli palatini) and upward movement of the soft palate (m. levator veli palatini). After the bolus enters the oropharynx, a ridgelike contraction (Passavant ridge) moves from the uppermost part of the posterior pharyngeal wall downwards. Simultaneously, the relaxed posterior pillars approximate one another, and the posterior tongue contracts against the palate to close off the oral cavity from the oropharynx. To close the airways, the vocal cords and arytenoids shut the laryngeal opening and the epiglottis swings down to cover the laryngeal vestibule. Laryngeal closure is highly important during swallowing. A three-tier system protects the airway from swallowed contents: (1) adduction of true vocal cords and arytenoids (glottic adductors: thyroarytenoid, lateral cricoarytenoid, transverse arytenoid muscles), (2) vertical approximation of closed arytenoids to the base of epiglottis (supraglottic adductors: oblique arytenoids and aryepiglottic muscles), and (3) descent of epiglottis to cover the closed glottis thereby closing the laryngeal vestibule. The hyoid bone and larynx move superiorly (2–3 cm) and anteriorly, positioning the larynx under the tongue base, outside of the bolus path (suprahyoid muscles: geniohyoid, mylohyoid, and digastric muscles). The pharynx widens and shortens, which is accompanied by an elevation of the upper esophageal sphincter by several centimeters (longitudinal group of muscles: palatopharyngeus, salpingopharyngeus, stylopharyngeus). These activities in conjunction with pharyngeal peristaltic contraction (circular group of muscles: superior, middle, inferior pharyngeal constrictor muscles) push the bolus through the open upper esophageal sphincter into the esophagus. A normal oropharyngeal phase consists of complete transfer of oral contents into the esophagus without any entry into the laryngeal inlet. Passage of the pharyngeal peristaltic contraction wave through the cricopharyngeus terminates upper esophageal sphincter relaxation and marks the transition between the pharyngeal and esophageal phases of swallowing.

The esophageal phase starts with the propagation of the bolus through the open upper esophageal sphincter, includes the bolus transport, and ends with the bolus passage through the lower esophageal sphincter. The travel time through the esophagus is 5–6 s. As the bolus passes the upper esophageal sphincter, the esophagus and lower esophageal sphincter relax to receive the bolus. A liquid bolus may move into the stomach by gravity alone, and the residual liquid is cleared by the peristaltic contraction wave. A solid bolus usually does not move down by gravity alone and peristaltic contraction for the transport is required. The esophagus is innervated by both parasympathetic and sympathetic nerves; the parasympathetics control peristalsis via the vagus nerve. Primary peristalsis is a reflex esophageal peristaltic contraction wave triggered by swallowing. It involves all phases of the swallowing reflex including the oral phase, pharyngeal peristalsis, upper esophageal sphincter relaxation, esophageal peristalsis, and lower esophageal sphincter relaxation. The peristaltic contractions are lumen-occluding contractions lasting 2–7 s that begin in the pharynx and move down the esophagus at a speed of about 4 cm/s in the esophagus, and it takes between 10 and 15 s to complete a primary peristaltic activity. Secondary peristalsis is triggered by distention and seen with retained bolus or distension associated with gastroesophageal reflux. Secondary peristalsis does not involve full swallowing reflex, and it is not accompanied by pharyngeal contraction or upper esophageal relaxation. The contraction wave starts above the bolus and proceeds distally to push the bolus into the stomach without involving the proximal esophagus above the bolus, pharynx, or oral cavity. Nonperistaltic or tertiary contractions of the esophagus are nonpropulsive irregular contraction or indentations of the distal esophagus.

## 2.2 Swallowing Dysfunction: Tumor and Surgery Related

Tumor infiltration as well as surgery, radiation, and chemotherapy interferes with the complex physiology of swallowing in multiple ways. Dysphagia can preexist with therapy and can be caused by obstructing, infiltrating, or ulcerating

tumors that disrupt the swallowing structures or cranial nerves (V, VII, IX–XII), damage of laryngeal sphincters (invading the suprahyoid muscles, preepiglottic space, prevertebral fascia), and pain. Pretreatment dysphagia with silent aspiration is present in 14–18 % of head and neck cancers (Russi et al. 2012). Surgical resection causes site-specific anatomic or neurologic damage resulting in different patterns of dysphagia and aspiration: resection of suprahyoid muscles increases the risk of aspiration, as these muscles elevate and drag the larynx anteriorly beneath the tongue base. Resection of the tongue base also increases the risk of aspiration, because the closure of both the oral and laryngeal valve is impaired (Zuydam et al. 2000; Pauloski et al. 2004). Borggreven et al. 2007 reported dysfunction in the oral or pharyngeal phase in >50 % of patients after resection of oral and oropharyngeal cancer. Six month after treatment penetration was detected in 38 % and aspiration in 34 % of the patients. 12 month after treatment, 41 % had penetration and 25 % aspiration. Based on scintigraphy, 66–69 % of the total liquid oral–pharyngeal bolus was swallowed. Preswallowing leakage either to the pharynx or into the esophagus occurred in 66 % (at 6 month) and 70 % (at 12 month) with aspiration in 10 % (at 6 month) and 21 % (at 12 month). The type of reconstruction can influence the postoperative swallowing function, and there is some controversy if primary closure (McConnel et al. 1998) or distal flap reconstruction (Borggreven et al. 2007) of the resection defect is preferential. Primary closure or healing by secondary intention showed good functional outcome, but this technique is suitable for smaller defects only; for larger defects especially if bone is exposed and the addition of radio(chemo)therapy is necessary, reconstructive techniques with different types of pedicle-based flaps (i.e., pectoralis, trapezius, latissimus dorsi flaps) or microvascular free flaps (i.e., radial, scapular, fibular, anterolateral thigh flaps) are required depending on the volume and type of tissue needed for reconstruction. In a prospective multicenter study (McConnel et al. 1998), the swallowing function of primary closure, distal myocutaneous flap, and microvascular free flap reconstruction was compared: patients who had primary closure were more efficient at swallowing liquids, had less pharyngeal residue, and had higher conversational intelligibility than those with a distal or free flap. No difference in speech and swallowing function was found between patients treated with distal or free flaps. A flap might act as an adynamic segment that impairs the driving force of the remaining tongue in its pistonlike function, thus reducing swallowing efficiency. In a single-center study, Khariwala et al. reported functional outcome of 191 cases with free flap reconstruction and concluded that besides poor outcomes after resection and reconstruction of tongue defects, the majority of the oral cavity resections (mandibular, floor of mouth, and buccal resections, regardless of size and extent) had little impact on swallowing outcome and good results after free flap reconstruction (Khariwala et al. 2007).

## 2.3 Swallowing Dysfunction: Radiotherapy/Chemotherapy Related

Radiotherapy (RTx) with or without concurrent chemotherapy (CTx) causes inflammation and edema in the mucosa as well as the underlying soft tissues (muscles and connective tissue). Both acute reactions result in dysphagia. Progressive thickening with accumulation of interstitial fluid is a typical finding of the irradiated mucosa as well as the retropharyngeal space (Fig. 1) within the first weeks. Fibrosis, stricture formation, tissue necrosis, and denervation occur as subacute or chronic reactions to RTx, leading to tissue shrinkage and signal reduction on T2-weighted MR images. The addition of CTx not only improves tumor response but also increases the rate of side effects contributing to functional impairment in swallowing function and thus dysphagia (Eisbruch et al. 2004; Nguyen et al. 2004). Noemayr et al. described the MRI characteristics and time course of RTx-induced changes in patients with head and neck cancer in detail (Nomayr et al. 2001).

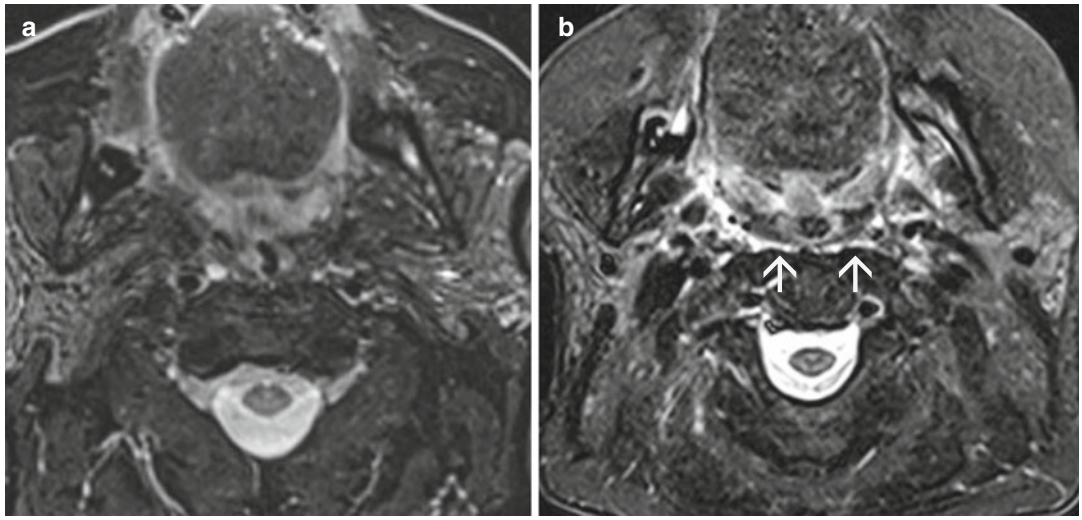


**Fig. 1** 61-year-old male with supraglottic cT1N2c G2 squamous cell carcinoma (not shown) before (**a**) and 4 weeks after combined radiochemotherapy (paclitaxel, cisplatin, 64 Gy target dose) (**b**). Marked hyperintensity of the mucosa and para- and retropharyngeal (*arrows*) spaces indicating inflammation and edema

### 2.3.1 Mucositis

RTx-induced dysphagia has a complex pathogenesis involving inflammation, edema, and fibrosis with consequent neurological and/or muscular damage. Oral mucositis remains one of the most common and troubling toxicities in the treatment of head and neck cancer, affecting virtually all patients in whom the oral mucosa receives >30 Gy. Severe mucositis is reported in patients being treated for cancer of the mouth and oropharynx (>90 %) and less frequently in patients with cancer of the hypopharynx and larynx (~65 %) (Sonis 2011). Erythema of the mucosa occurs after >10 Gy (end of first week in typical 2Gy/d regimes), after >20Gy first ulcerative changes, and after >30 Gy diffuse mucosal ulcerations follow. Lesions typically involve the mucosa of the cheeks, lips, ventral and lateral tongue, floor of the mouth, and soft palate and less frequently the mucosa of the dorsal tongue, gingiva, or the hard palate. Lesions of the latter sites are often of an infectious etiology (Sonis 2011). Ulcers related to severe mucositis are irregular and may be associated with peripheral erythema and covered by a pseudomembrane and persist for 2–4 weeks after the end of RTx before they finally resolve. Mucositis and edema cause obliteration of normal recessi (e.g., vallecula) and channels (e.g., pyriform sinus) interfering with bolus transport. Swallowing is painful; patients with severe mucositis cannot tolerate normal diet and rely on gastrostomy feeding. At imaging, mucositis, as all inflammatory processes, is characterized by submucosal edema (high signal intensity on T2-weighted/STIR images and decreased density in CT) and increased enhancement of the mucosal surface both on CT and T1-weighted MRI images following the administration of contrast material (Fig. 2). In later stages, fibrosis prevails over edema and fibrotic tissue accumulates diffusely below the skin, within the connective tissue layers, around muscles, and even between muscle fibers (Russi et al. 2012). Molecular markers (e.g., TGF-β) of radiation-related toxicity have been identified to promote fibrosis (Okunieff et al. 2008). The development of dysphagia is variable and depends on intensity of acute reactions as well as intrinsic radiosensitivity, based on genetics and comorbidities. Some patients experience an early onset of fibrosis after radiation therapy, others a delayed one, and there is a further group of patients in whom an additional trauma (e.g., surgery) is necessary (Liu and Gaston Pravia 2010). RTx-induced fibrosis may cause tongue atrophy with or without

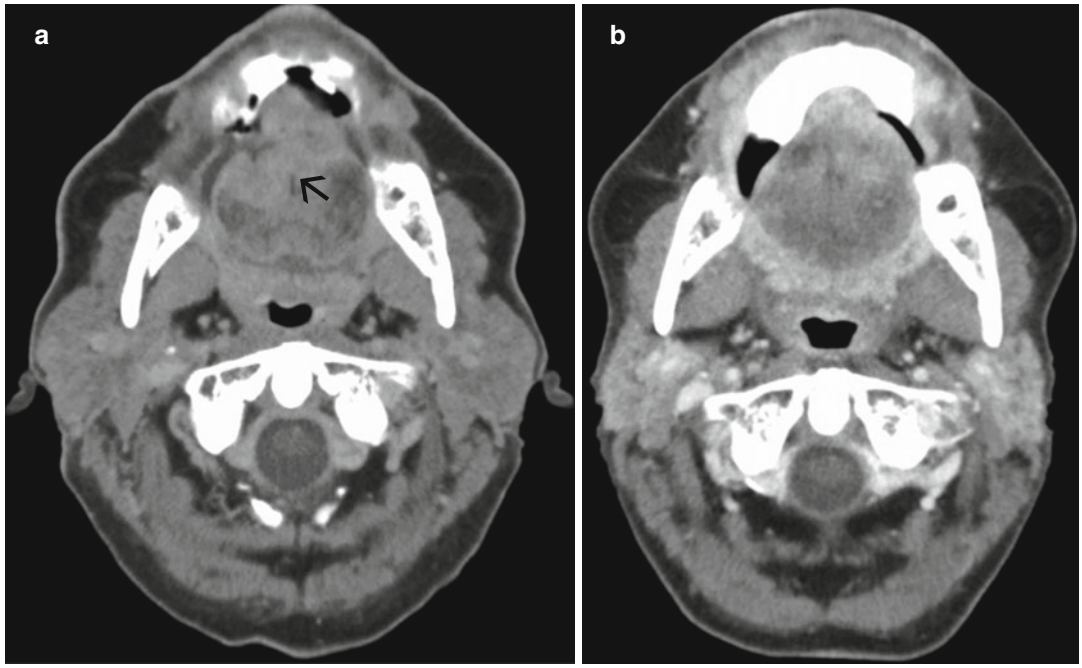


**Fig. 2** Mucositis in a 51-year-old patient prior to (**a**) and 4 months after (**b**) RCTx to treat tongue squamous cell carcinoma (*black arrow*). Diffuse contrast enhancement of the oral mucosa, lymphatic tissue, and salivary glands after RCTx. Oral inspection revealed extensive fibrosis and vulnerable mucosa with bleeding at contact

fasciculation, velopharyngeal incompetence with premature leakage, poor pharyngeal constriction, and vocal cord palsy. Delayed swallow-reflex triggering, reduced tongue-base contact to the posterior pharyngeal wall, laryngeal elevation, laryngeal and nasopharyngeal closure, prolonged OTT and PTT, and increased ORES and PRES promote swallow dysfunction and aspiration. In contrast to neurologic patients who usually aspirate before or during swallowing (pre- or intradeglutitive aspiration), patients after treatment of head and neck cancer predominantly experience postdeglutitive aspiration. Silent aspiration resulting from glottic and supraglottic laryngeal sensory loss after RCTx is an important risk factor of recurrent pneumonia (Fig. 3 and 4).

### 2.3.2 Myositis and Fibrosis

The muscles have different susceptibility to RTx-induced damage. Exposed to the same radiation dose, the sternocleidomastoid muscles demonstrate slight edema, fibrosis, and reduced thickness, while the pharyngeal constrictors (PC) demonstrate massive edema (T1 and T2 prolongation) and increased thickness (Popovtzer et al. 2009). Edema and inflammation within the PC might be secondary to acute mucositis – called the "bystander effect" (Denham et al. 2001) – which would explain the difference in those muscles attached to mucosa as compared to those in a remote location (sternocleidomastoid, pterygoids, masseter). The dysphagia-aspiration-related structures (DARS) have been identified as the PC muscles, the upper esophageal sphincter with the cricopharyngeal muscle and the esophagus inlet muscle, the tongue base, the larynx with vocal cords and arytenoids, velopharyngeal structures, and the posterior pharyngeal wall (Christianen et al. 2011). The rates of RTx- and RCTx-induced dysphagia vary: about 50 % of patients have chronic dysphagia associated with RCTx, 37 % progress to symptomatic stricture, and 7–37 % progress to develop complete stricture (Prisman et al. 2013). A complete stricture inhibits the

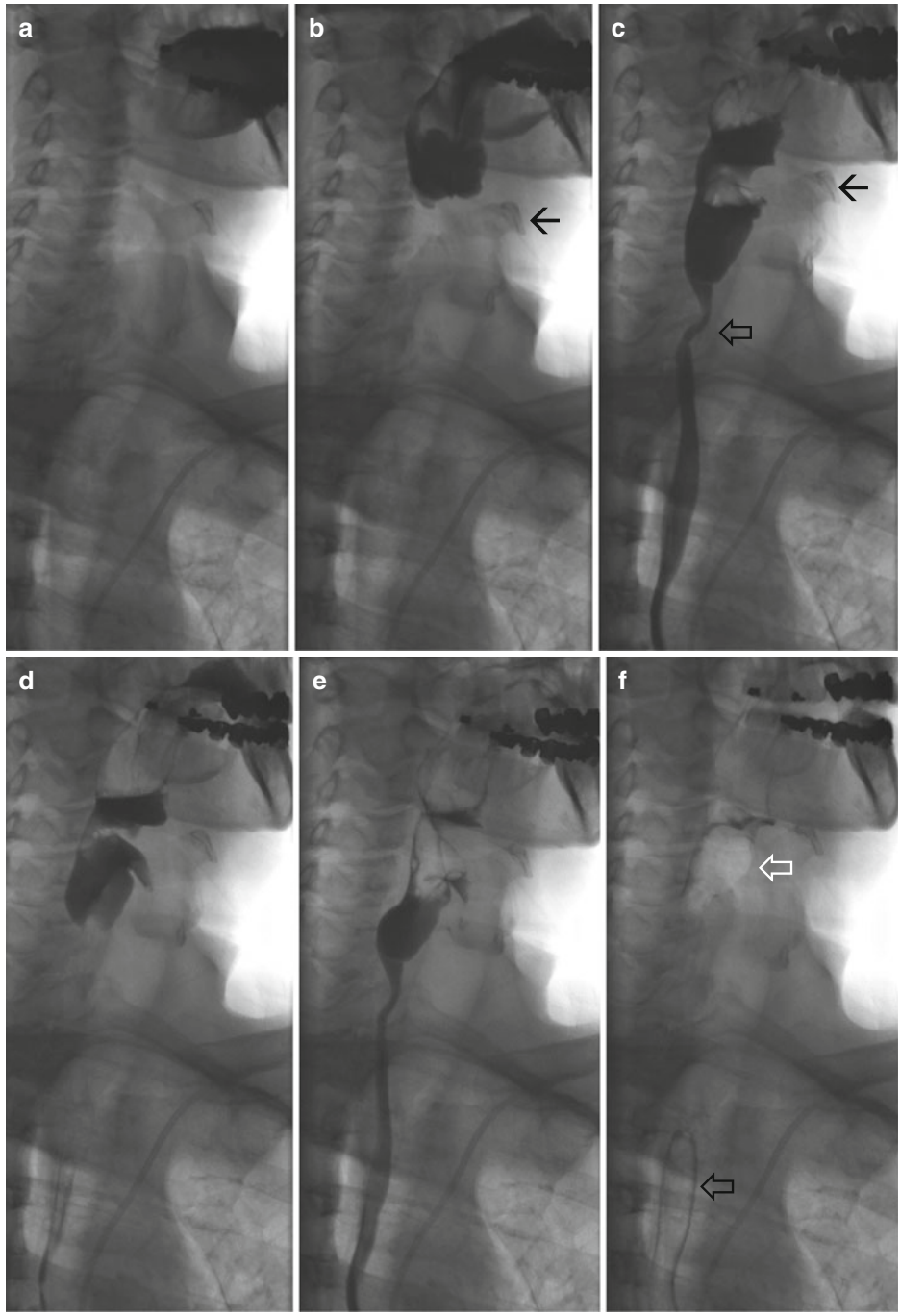


**Fig. 3** Barium swallow in a 53-year-old patient 14 months after RCTx (64 Gy target dose, 1.8Gy/fraction; 5-FU + cisplatin) of the bilateral neck and the pharynx to treat CUP syndrome. Oral phase is unremarkable with normal bolus control (**a**). Delayed triggering of the pharyngeal phase, epiglottic closure, and cranioventral movement of the hyolaryngeal complex (*black arrow* indicates hyoid) is initiated after bolus filled the valleculae (**b**). Timely but incomplete opening of the upper esophageal sphincter, long segment of narrow lumen in the proximal esophagus with smooth margins (*open black arrow*) indicating RTx-induced stenosis (**c**). Significant retention of the bolus within the piriform sinuses as well as the valleculae at the end of the first swallow (**d**), opening of the UES with stenosis of the proximal esophagus at the second swallow (**e**), and almost complete drain after five swallow attempts without aspiration (**f**). Note the air retention in the hypopharynx (*open white arrow*) after swallowing and regular distension of the more distal esophagus (*black arrow*)

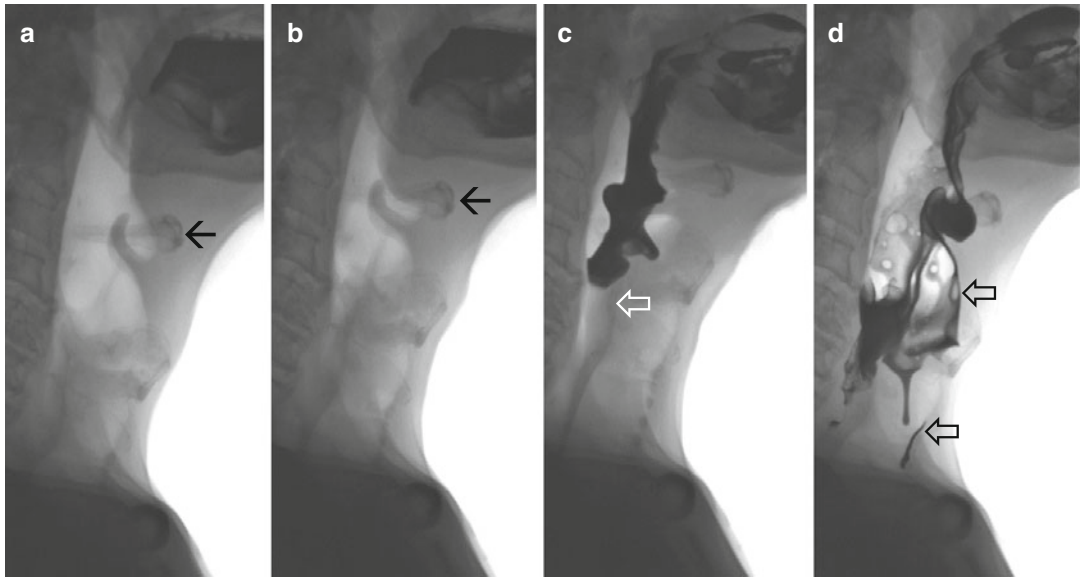


**Fig. 4** Barium swallow in a 78-year-old patient 8 years after RCTx (64 Gy target dose, 1.8 Gy/fraction; 5-FU + cisplatin) of the bilateral neck and the pharynx to treat CUP syndrome. Oral phase is unremarkable with normal bolus control (**a**). Timely triggering of the pharyngeal phase, epiglottic closure, and cranioventral movement of the hyolaryngeal complex (black arrow indicates hyoid) (**b**). Delayed and incomplete opening of the upper esophageal sphincter (*open white arrow*) (**c**) and early opening of the epiglottis and downward movement of the hyolaryngeal complex with massive intra- and postdeglutitive aspiration (*open black arrows*). Significant retention of the bolus within the piriform sinuses as well as the valleculae (**d**)

passage of food and liquids and permanent gastric tube or reconstructive surgery are required, whereas incomplete stricture allows the passage of liquids and certain food and may be treated with repetitive dilation. Mucosal strictures are typically short segments either proximal or distal to the tumor site and respond to dilation. Submucosal and muscular strictures tend to be longer and more difficult to manage. They are usually based on deep tissue injury at the site of the primary tumor as a result of tumor necrosis following therapy. A target dose higher than 50 Gy to the larynx or inferior PC significantly increases the risk of aspiration and stricture (Caglar et al. 2008); in a different study the highest correlation was found with target doses >60 Gy to the superior PC (Feng et al. 2007). In a retrospective review of 222 patients after definitive chemoradiotherapy, a 21 % overall rate of stricture was reported, hyperfractionation was a significant predictor of stricture, and female sex and hypopharyngeal tumor location were independent risk factors (Lee et al. 2007).

### 2.3.3 Xerostomia

Saliva is produced by acinar cells, drained to the excretory duct through ductal cells, and finally secreted into the oral cavity. It is predominantly composed of water (99.5 %) and the remaining 0.5 % includes amylase, inorganic salts, mucin, and bicarbonate. Xerostomia is probably the most common persistent oral sequela of RCTx. It causes oral discomfort and pain; increases the risk of caries, infection, difficulty in speaking, and dysphagia; and therefore dramatically affects quality of life. In patients with head and neck cancer whose major salivary glands were within the treated fields of RTx, the prevalence of xerostomia after therapy varies between 94 and 100 % (Sciubba and Goldenberg 2006). The risk depends largely on the dose and the field. A significant reduction or ebbing of salivary flow upon stimulation was reported for the parotid glands receiving radiation doses >26 Gy (Eisbruch et al. 1999). Blanco et al. (2005) also reported that 70 % of patients in whom both parotid glands were irradiated to mean doses >26 Gy had grade 4 xerostomia. In the PARSPORT trial,

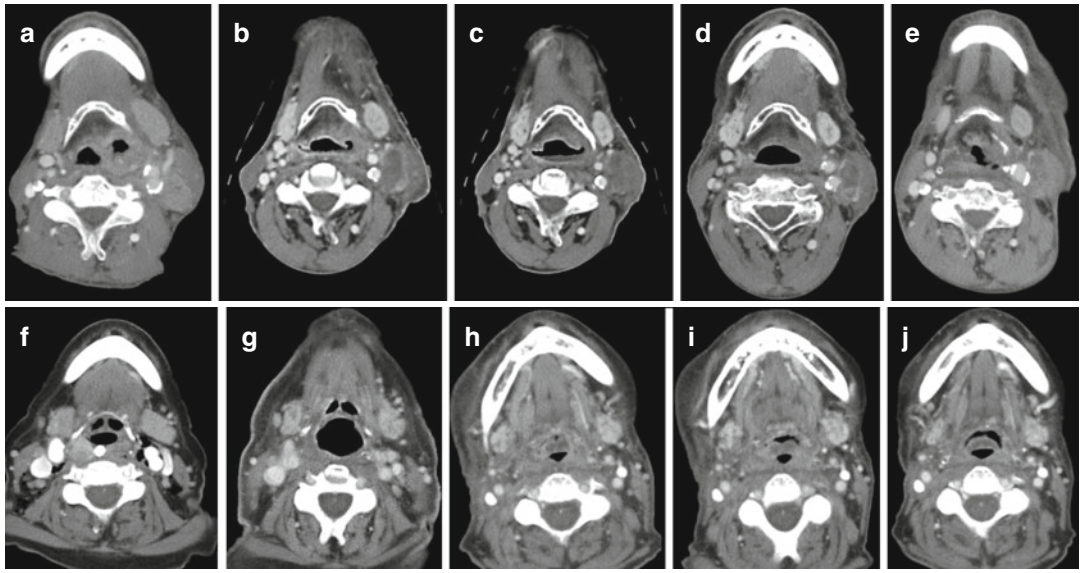


**Fig. 5** Soft tissue reactions in the short (**a**–**e**) and long (**f**–**j**) term after intensified radiochemotherapy (target dose 64 Gy; 1. cycle: 2 Gy/d; 2. cycle 2 × 1.4 Gy/d). Upper row: contrast-enhanced CT in a 63-year-old man treated with RCTx for hypopharyngeal cancer. Normal submandibular glands before therapy (**a**) and volume reduction and increased contrast enhancement after 48 Gy (**b**), after 56 Gy (**c**), 1 month after RCTx (**d**), and 3.5 months after RCTx (**e**). Gradual increase of edema in the pharyngeal mucosa, retropharyngeal space, and subcutaneous fat. Bottom row: contrast-enhanced CT in a 69-year-old woman treated with RCTx for hypopharyngeal cancer. Normal submandibular glands before therapy (**f**) and volume reduction and increased contrast enhancement 4 weeks after RTx (**g**), 11 months after RCTx (**h**), 14 months after RCTx (**i**), and 22 months after RCTx (**j**). Gradual increase of edema in the pharyngeal and epiglottic mucosa as well as in the subcutaneous fat. Subcutaneous edema decreases again in the 22-month control (**j**), whereas thickening of the epiglottis remains

parotid-sparing RTx resulted in a 25 % absolute reduction in Radiation Therapy Oncology Group (RTOG) grade 2+ xerostomia at 12 months (Nutting et al. 2011). A threshold of 39 Gy target dose was reported for the submandibular glands (Murdoch-Kinch et al. 2008). In a recent study sparing the contralateral submandibular gland in RTx resulted in a 35 % reduction in grade 2+ xerostomia at 12 months (Gensheimer et al. 2014). Noemayr et al. (2001) described an initial increase in signal intensity of the salivary glands on T2-weighted images and an average volume reduction of the parotid glands of 26 % after 30 Gy, 40 % after 70Gy, and 50 % 12 months after therapy. Similar changes can be detected on contrast-enhanced CT scans (Fig. 5). Both parotid and submandibular glands showed a similar increase in density after radiotherapy (Bronstein et al. 1987).

## 3 Therapy-Induced Bone Injury

### 3.1 Bone Marrow Conversion

Bone marrow is composed of red and yellow marrow. Red marrow consists of hematopoietic stem cells, whereas yellow marrow also contains abundant capillaries but is not directly involved in hematopoiesis. Red marrow is found in flat bones (i.e., pelvis, sternum, vertebrae) and yellow marrow in the medullary space of long bones. The stroma of the reticular network of yellow marrow is filled primarily with lipids. The higher fat content results in high signal intensity on T1-weighted MRI images (Fig. 6) and can be quantified with chemical shift imaging (Carmona et al. 2014; Kauczor et al. 1993). Both chemotherapy and radiation suppress the hematopoietic

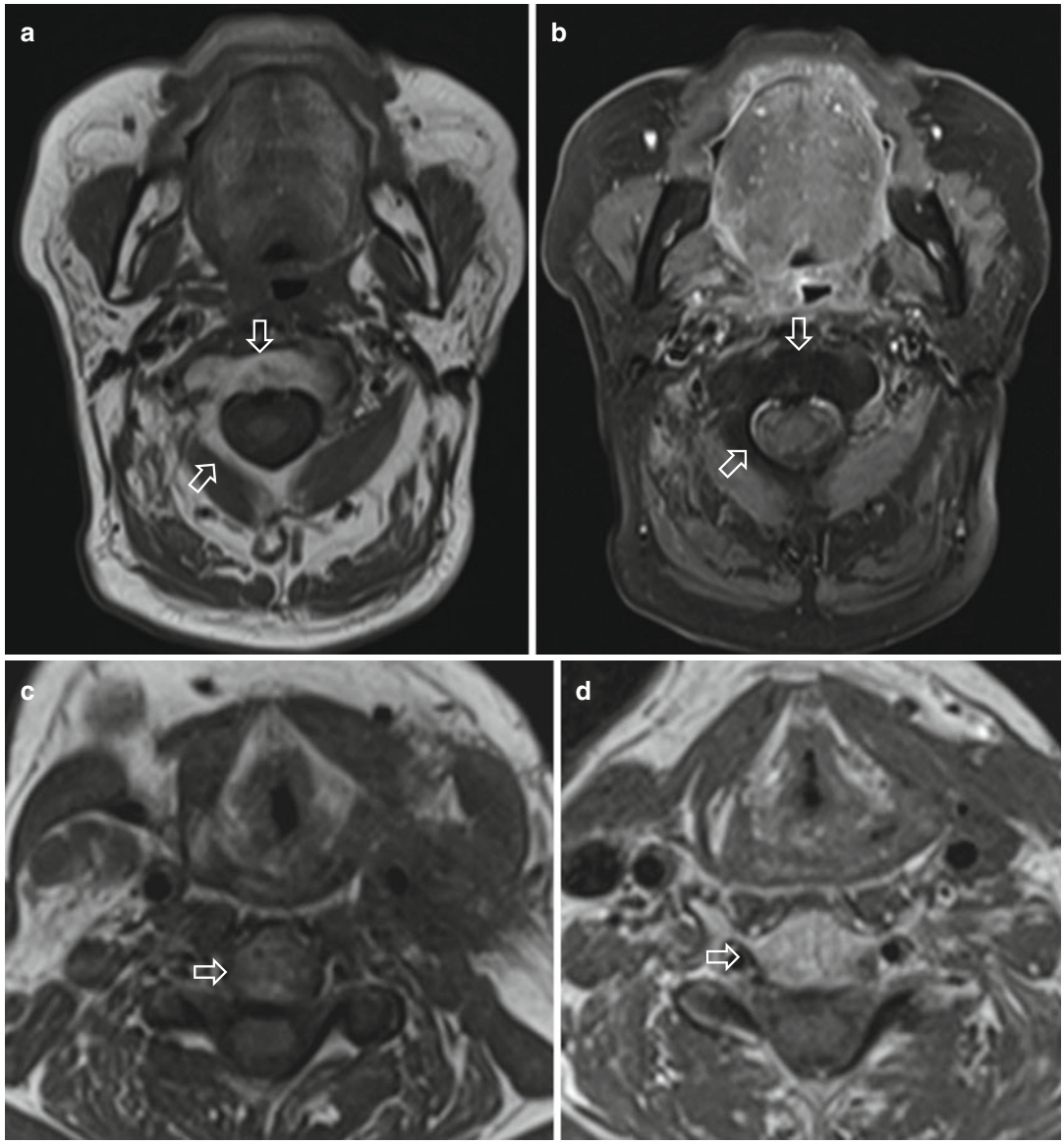


**Fig. 6** Fatty replacement of the bone marrow. MRI in a 73-year-old man treated with RCTx (64 Gy) for hypopharyngeal cancer ten years and additional RCTx (45Gy) for tumor recurrence 8 months ago. High signal intensity on T1-weighted image (**a**) indicating fatty replacement of the bone marrow with complete signal intensity loss after fat suppression (**b**). MRI in a 61-year-old man before (**c**) and after RCTx (64 Gy) (**d**) demonstrates bone marrow conversion (*arrow*)

system, inducing a shift from red to yellow marrow. The incidence of acute hematotoxicity depends on the type of chemotherapy received (Bazan et al. 2013). Irradiation with doses of >30 Gy results in fatty bone marrow replacement (Nomayr et al. 2001; Kauczor et al. 1993).

## 3.2 Osteoradionecrosis

Mandibular osteoradionecrosis (ORN) is a relatively rare but serious adverse effect in head and neck cancer patients. Its onset can be very variable with the majority of the ORN occurring

between 4 months and 3 years after RTx (Chrcanovic et al. 2010). There are different definitions of ORN; a widely used one is "irradiated bone that becomes devitalized and exposed through the overlying skin or mucosa without signs of healing for a period of more than three months, without recurrence of tumor" (Lyons and Ghazali 2008). Different classification systems exist, a recent one proposed by Karagozoglu (Karagozoglu et al. 2014): stage 0, exposure of mandibular bone < 1 month, negative radiographs; stage I, exposure of mandibular bone ≥1 month, negative radiographs, asymptomatic (I A) or symptomatic (pain, cutaneous fistulas (I B)); stage II, exposure of mandibular bone ≥1 month, lytic lesion on radiographs, not involving the lower border of the mandible (IIA, asymptomatic; IIB, symptomatic); and stage III, exposure of mandibular bone ≥1 month, lytic lesion on radiographs, involving the lower border of the mandible, irrespective of any other signs and symptoms.

There are different theories about the pathophysiology of ORN; a current concept is the radiation-induced fibroatrophic theory, where three distinct phases can be seen: the initial prefibrotic phase where endothelial cell damage (microvessel necrosis, vascular thrombosis) and cytokine-mediated acute inflammation predominate; the constitutive organized phase with abnormal fibroblastic activity and disorganization of extracellular matrix; and the fibroatrophic phase with tissue remodeling (failure of osteoblast repopulation, excessive proliferation of myofibroblasts) and incomplete healing, with increased risk of inflammation in the event of local injury (Lyons and Ghazali 2008).

The incidence and prevalence of ORN varies greatly in the literature, ranging from 1 to 37 %, with a decline in frequency within the last years (Sciubba and Goldenberg 2006), as indicated in a review of Wahl (2006) who reported an ORN rate of 3 %. ORN can occur spontaneously, due to periodontal and apical disease, and possibly after trauma induced by dentures or after surgery or tooth extraction. In a meta-analysis Nabil and Samman (2011) estimate that 7 % of patients undergoing postradiation tooth extraction will develop ORN, and the risk of developing post-extraction ORN is minimal in patients receiving RTx doses < 60 Gy. Pre-radiation dental screening in patients who will be subjected to radiotherapy to the head and neck region is aiming to locate and treat inflammatory foci, thus minimizing the risk of RTx-induced oral complications, especially ORN, but this approach is mainly based on clinical experience. Though radiation dose is related to the development of ORN, no consensus exists in the literature for a certain dose threshold. Thorn et al. observed RTx doses > 64 Gy in more than 90 % of the ORN cases; de Menezes et al. reported increasing rates of ORN with increasing doses (60 and 70 Gy).

The imaging features of ORN are similar to those of osteomyelitis and bisphosphonate-related osteonecrosis; therefore, the medical history is crucial for differentiation. CT or CBCT reveals a patchy radiopaque–radiolucent ill-defined lesion with cortical bone destruction and bone sequestration, but in contrast to osteomyelitis usually without periosteal reaction. Bone marrow edema (increased SI on T2-weighted images), bone marrow sclerosis (low SI on T2-weighted images), and contrast enhancement can be seen side by side (Fig. 7). MRI is more sensitive than CT in detecting the extent of bone marrow and soft tissue involvement and allows earlier diagnosis than CT, cone beam CT (CBCT), or radiography. Diffusion-weighted imaging (DWI) might help in differentiating recurrent tumor from ORN, as lower apparent diffusion coefficient (ADC) values have been reported in tumor than in necrosis (Avril et al. 2014), but DWI is often affected by susceptibility artifacts.

### 3.3 Drug-Induced Osteonecrosis

Osteonecrosis of the jaw (ONJ) was first reported by Marx et al. in 2003 (Marx 2003): 36 patients with painful bone exposure in the mandible, maxilla, or both that were unresponsive to surgical or medical treatments, all of them receiving intravenous pamidronate or zoledronate for the treatment of hypercalcemia related to bone metastases and multiple myeloma and one case for the treatment of osteoporosis. Bisphosphonate

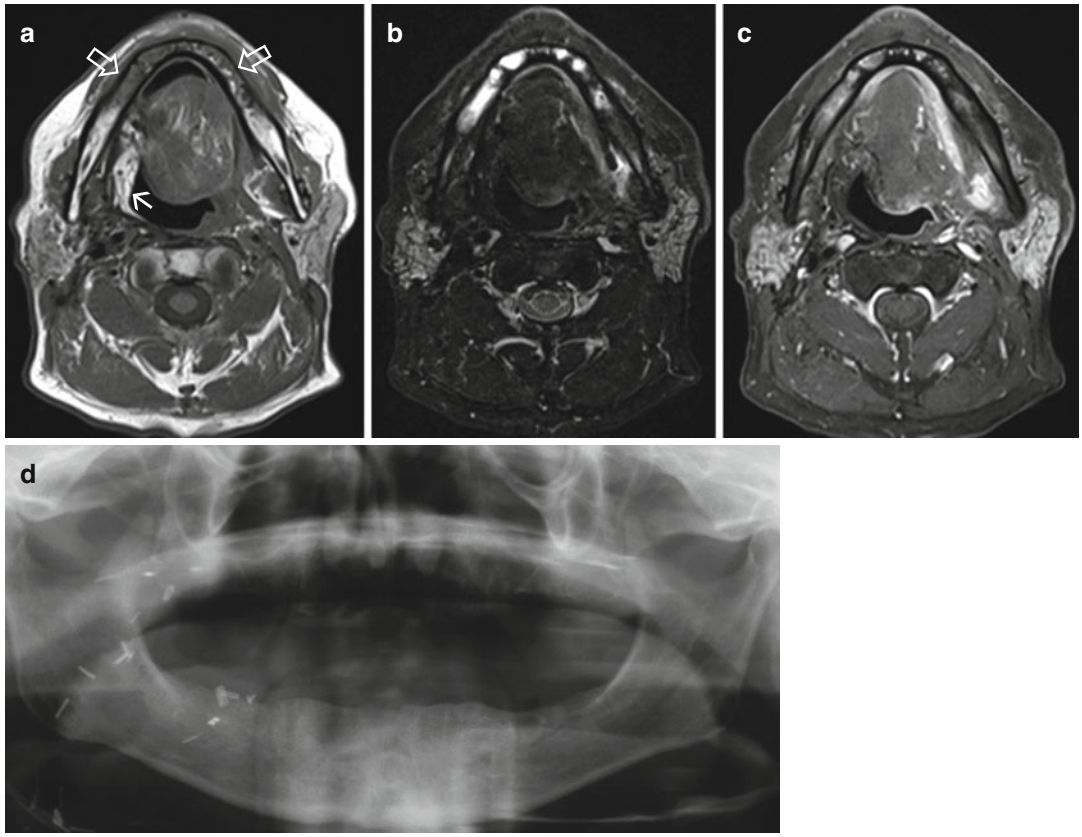


**Fig. 7** Osteoradionecrosis of the mandible after radiochemotherapy. MRI in a 62-year-old man treated with surgery and adjuvant RCTx for oropharyngeal cancer. Note free flap (*white arrow*) covering the resection defect in the right lateral oropharyngeal wall. Loss of fat signal in the bilateral ventral mandible (region 34–45) on T1w images (**a**) with markedly increased signal intensity on T2-weighted/STIR images (**b**) and diffuse contrast enhancement (**c**). Subtle lytic changes in panoramic radiograph (**d**) detectable without fracture or sequestration

(BP)-associated ONJ was defined by the American Society for Bone and Mineral Research (ASBMR) as an area of exposed bone in the maxillofacial region that does not heal within 8 weeks after identification by a health-care provider in a patient who was receiving or had been exposed to a BP and who has not received radiation therapy to the craniofacial region (Khosla et al. 2007). The definition has recently been modified: (I) exposed bone in the maxillofacial region that does not heal within 8 weeks after identification by a health-care provider, (II) exposure to an antiresorptive agent, and (III) no history of radiation therapy to the craniofacial region (Khan et al. 2015). ONJ occurs more frequently in patients receiving intravenously administered nitrogen-containing BPs, such as alendronate, ibandronate, pamidronate, risedronate, and zoledronic acid, for metastatic bone disease. The true incidence of ONJ is unknown; in the oncologic population it is considered 1–15 %, in the osteoporosis patient population 0.001–0.01 %, and in the general population less than 0.001 % (Khan et al. 2015). ONJ has been reported not only in patients with intravenous BP therapy but (rarely) also in patients receiving denosumab, bevacizumab, or sunitinib (Guarneri et al. 2010; Sivolella et al. 2013; Christodoulou et al. 2009; Brunello et al. 2009). Several potential mechanisms affecting the risk of ONJ have been proposed. ONJ is associated with inhibition of bone remodeling, especially of osteoclast activity, and thus, ONJ may occur with all osteoclast-inhibiting therapies, including BPs and denosumab. A more complete discussion can

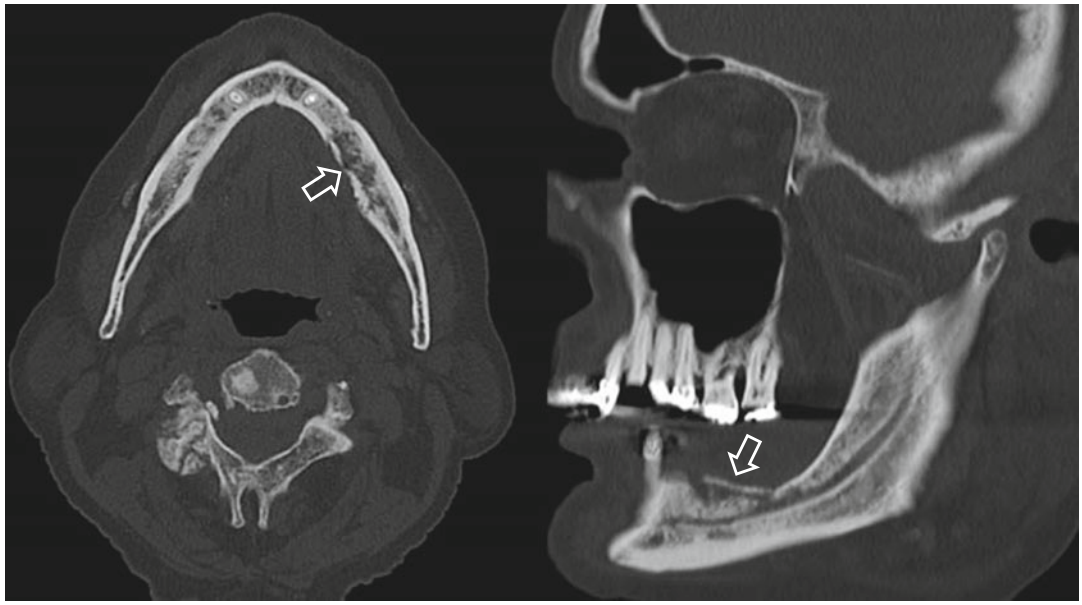

**Fig. 8** Bisphosphonate-induced osteonecrosis of the mandible. CT in a 74-year-old man with bone metastases of prostate cancer treated with bisphosphonates (zoledronate). Cortical disruption and sequestra formation (*arrow*), bilateral bone marrow sclerosis with focal areas of lysis, trabecular thickening, and prominence of the inferior alveolar nerve canal are demonstrated

be found in Sivolella et al. (2013). A long list of risk factors for the development on ONJ in the oncologic population has been reported, including i.v. BPs (dose and duration), dental disease, extraction, and concomitant chemotherapy.

ONJ is a clinical diagnosis based on history and physical exam. Radiographic features of ONJ remain relatively nonspecific. Radiographic findings of ONJ on intraoral and panoramic radiographs are increased trabecular density, incomplete healing of extraction sockets, sequestrum formation, thickening of the mandibular canal or sinus floor cortication, and periosteal bone formation (Khan et al. 2015).

CT or CBCT is considered the most useful diagnostic tool (Fig. 8). Structural alteration of trabecular bone is a consistent finding in patients with ONJ. Cortical disruption, focal bone marrow sclerosis, thickened sclerotic lamina dura, persisting alveolar socket, trabecular thickening, and sequestra formation are early signs, whereas diffuse osteosclerosis, oroantral fistula, osteolysis extending to sinus floor, osteosclerosis of adjacent bones, pathologic fracture, periosteal reaction, prominence of the inferior alveolar nerve canal, and chronic maxillary sinusitis secondary to osteonecrosis are late signs of ONJ. Typically, the size of the lesion on CT images is larger than the clinically exposed bone areas.

MRI appears to be superior in assessing bone marrow change at the early stage of ONJ, as well as the soft tissue reaction surrounding necrotic bone. One of the most consistent and earliest MRI findings is a decrease of bone marrow signal intensity on T1-weighted images that can be present prior to clinical features of ONJ. T2-weighted and short T1 inversion recovery (STIR) images usually demonstrate increased signal intensity. Areas of increased T2 signal intensity usually show irregular contrast enhancement on T1-weighted fat-saturated images. Sequestra have a low signal intensity on all sequences. The adjacent soft tissues may be thickened and edematous. Lymph node enlargement in level I and II can be observed. Because MRI is more sensitive in demonstrating bone marrow changes, the extent of ONJ appears to be larger than with CT (Stockmann et al. 2010).

## 4 Radiation-Induced Brain Injury

Both functional and anatomic deficits are summarized as RTx-induced brain injury. According to the time of onset after RTx, acute (days–weeks), delayed (1–6 months), and late injury (6 months–years) can be differentiated. While early and delayed brain injuries are potentially reversible, late brain injury, characterized by vascular damage, demyelination, and white matter necrosis, is irreversible and progressive. Nasopharyngeal cancer (NPC) is usually treated with RTx; in these patients the bilateral temporal lobes receive high doses of radiation because the superior retropharyngeal lymph nodes need to be included in the target field. These patients have a high chance of long-term survival and thus the potential for development of radiation-induced cognitive impairment, primarily due to damage to the temporal lobes. While RTx seemed to have adverse but insignificant effects on the cognitive functions in patients treated for NPC, those who developed temporal lobe necrosis after radiotherapy had significantly impaired memory, language, motor ability, and executive functions, although their general intelligence remained relatively intact (Cheung et al. 2000). 76.7 % of patients treated for NPC had significantly lower post-RTx cognitive functioning scores (i.e., short-term memory, language abilities, and list-generating fluency) compared with their pre-RTx scores, and the cognitive functioning scores also correlated with dose (target dose >36 Gy, percentage of the temporal lobe volume receiving >60 Gy (V60) greater than 10 %) (Hsiao et al. 2010).

Late radiation-induced brain injury can be divided into focal and diffuse injury. Focal necrosis presents as a mass lesion, with focal neurologic symptoms. The clinical course is unpredictable. Surgical removal of the necrotic mass is the treatment of choice and may be lifesaving. In focal necrosis a mass surrounding vasogenic edema is present. Contrast administration improves the delineation of the mass, which has irregular enhancement at the margins. Both CT and conventional MR imaging cannot reliably differentiate between RTx-induced necrosis and tumor recurrence. In both conditions, the increased tissue water content causes hypodensity in CT imaging and prolongation of T1 and T2 relaxation times in MRI (low SI on T1-weighted, high SI on T2-weighted images). The blood–brain barrier defect results in enhancement following the administration of contrast material in necrosis and recurrence, but an enhancing focus distant to the primary tumor, in the periventricular white matter, with "soap bubble"- or "Swiss cheese"-like appearance is suggestive for RTx-induced necrosis (Kumar et al. 2000). MR spectroscopy has been advocated to differentiate necrosis from tumor recurrence on the biochemical level. Tumor recurrence is characterized by high ratios of choline/creatine and choline/N-acetylaspartate, while radiation necrosis shows elevated lactate and lipid peaks. Diffusion-weighted and perfusion-weighted imaging can also help to differentiate both lesions. The rationale behind perfusion-weighted imaging is that recurrent tumors have a greater blood supply secondary to neo-angiogenesis compared to radiation necrosis. The rationale behind DWI was that tumors show restricted diffusion and lower ADC values due to hypercellularity; however, both DWI and ADC are heterogeneous due to variable cellularity and regions of mixed tumor and necrosis (Asao et al. 2005). In addition, radiation-induced inflammation may influence DWI and ADC.

Prominent clinical features of severe diffuse white matter injury include personality change, impairment of memory, confusion, learning difficulties (in children), and frank dementia, but most patients with periventricular MR abnormalities are asymptomatic. Diffuse RTx-induced brain injury is characterized by white matter hypodensity (CT) and spotted (around the horns of the ventricles) to confluent band-like periventricular high SI on T2-w/FLAIR images, MRI being more sensitive than CT. Necrotizing leukoencephalopathy, a term used to describe diffuse white matter injury following treatment with CTx, with or without additional RTx, shows similar changes on CT and MR (Valk and Dillon 1991).

**Conclusion**

Radiation and chemotherapy affect not only tumor tissue but also normal tissue in a

significant manner. Morphologic and functional deficits may occur in different frequency and severity. While tissue edema and subsequent fibrosis, bone marrow replacement, and function loss of the salivary glands occur frequently and predictably and can be affected by modifications of the radiation field, necrosis of the bone induced by radiation or drugs occurs relatively infrequently at usual doses and with a prolonged delay between exposure and incidence. Radiation-induced brain injury is a late adverse effect which can progress over time and might be difficult to differentiate from residual or recurrent tumor. Exact information about prior treatment and serial imaging is crucial for accurate diagnosis.

## References


Asao C, Korogi Y, Kitajima M et al (2005) Diffusion-weighted imaging of radiation-induced brain injury for differentiation from tumor recurrence. AJNR Am J Neuroradiol 26:1455–1460

Avril L, Lombardi T, Ailianou A et al (2014) Radiolucent lesions of the mandible: a pattern-based approach to diagnosis. Insights Imaging 5:85–101

Bazan JG, Luxton G, Kozak MM et al (2013) Impact of chemotherapy on normal tissue complication probability models of acute hematologic toxicity in patients receiving pelvic intensity modulated radiation therapy. Int J Radiat Oncol Biol Phys 87:983–991

Blanco AI, Chao KS, El Naqa I et al (2005) Dose-volume modeling of salivary function in patients with head-and-neck cancer receiving radiotherapy. Int J Radiat Oncol Biol Phys 62:1055–1069

Borggreven PA, Verdonck-de Leeuw I, Rinkel RN et al (2007) Swallowing after major surgery of the oral cavity or oropharynx: a prospective and longitudinal assessment of patients treated by microvascular soft tissue reconstruction. Head Neck 29:638–647

Bronstein AD, Nyberg DA, Schwartz AN et al (1987) Increased salivary gland density on contrast-enhanced CT after head and neck radiation. AJR Am J Roentgenol 149:1259–1263

Brunello A, Saia G, Bedogni A et al (2009) Worsening of osteonecrosis of the jaw during treatment with sunitinib in a patient with metastatic renal cell carcinoma. Bone 44:173–175

Caglar HB, Tishler RB, Othus M et al (2008) Dose to larynx predicts for swallowing complications after intensity-modulated radiotherapy. Int J Radiat Oncol Biol Phys 72:1110–1118

Carmona R, Pritz J, Bydder M et al (2014) Fat composition changes in bone marrow during chemotherapy and radiation therapy. Int J Radiat Oncol Biol Phys 90:155–163

Cheung M, Chan AS, Law SC et al (2000) Cognitive function of patients with nasopharyngeal carcinoma with and without temporal lobe radionecrosis. Arch Neurol 57:1347–1352

Chrcanovic BR, Reher P, Sousa AA et al (2010) Osteoradionecrosis of the jaws–a current overview–part 1: physiopathology and risk and predisposing factors. Oral Maxillofac Surg 14:3–16

Christianen ME, Langendijk JA, Westerlaan HE et al (2011) Delineation of organs at risk involved in swallowing for radiotherapy treatment planning. Radiother Oncol 101:394–402

Christodoulou C, Pervena A, Klouvas G et al (2009) Combination of bisphosphonates and antiangiogenic factors induces osteonecrosis of the jaw more frequently than bisphosphonates alone. Oncology (Williston Park) 76:209–211

Denham JW, Hauer-Jensen M, Peters LJ (2001) Is it time for a new formalism to categorize normal tissue radiation injury? Int J Radiat Oncol Biol Phys 50:1105–1106

Eisbruch A, Ten Haken RK, Kim HM et al (1999) Dose, volume, and function relationships in parotid salivary glands following conformal and intensity-modulated irradiation of head and neck cancer. Int J Radiat Oncol Biol Phys 45:577–587

Eisbruch A, Schwartz M, Rasch C et al (2004) Dysphagia and aspiration after chemoradiotherapy for head-and-neck cancer: which anatomic structures are affected and can they be spared by IMRT? Int J Radiat Oncol Biol Phys 60:1425–1439

Feng FY, Kim HM, Lyden TH et al (2007) Intensity-modulated radiotherapy of head and neck cancer aiming to reduce dysphagia: early dose-effect relationships for the swallowing structures. Int J Radiat Oncol Biol Phys 68:1289–1298

Gensheimer MF, Liao JJ, Garden AS et al (2014) Submandibular gland-sparing radiation therapy for locally advanced oropharyngeal squamous cell carcinoma: patterns of failure and xerostomia outcomes. Radiat Oncol 9:255

Guarneri V, Miles D, Robert N et al (2010) Bevacizumab and osteonecrosis of the jaw: incidence and association with bisphosphonate therapy in three large prospective trials in advanced breast cancer. Breast Cancer Res Treat 122:181–188

Hsiao KY, Yeh SA, Chang CC et al (2010) Cognitive function before and after intensity-modulated radiation therapy in patients with nasopharyngeal carcinoma: a prospective study. Int J Radiat Oncol Biol Phys 77: 722–726

Karagozoglu KH, Dekker HA, Rietveld D et al (2014) Proposal for a new staging system for osteoradionecrosis of the mandible. Med Oral Patol Oral Cir Bucal 19:e433–e437

Kauczor HU, Dieti B, Brix G et al (1993) Fatty replacement of bone marrow after radiation therapy for

Hodgkin disease: quantification with chemical shift imaging. J Magn Reson Imaging 3:575–580
Khan AA, Morrison A, Hanley DA et al (2015) Diagnosis and management of osteonecrosis of the jaw: a systematic review and international consensus. J Bone Miner Res 30:3–23
Khariwala SS, Vivek PP, Lorenz RR et al (2007) Swallowing outcomes after microvascular head and neck reconstruction: a prospective review of 191 cases. Laryngoscope 117:1359–1363
Khosla S, Burr D, Cauley J et al (2007) Bisphosphonate-associated osteonecrosis of the jaw: report of a task force of the American Society for Bone and Mineral Research. J Bone Miner Res 22:1479–1491
Kumar AJ, Leeds NE, Fuller GN et al (2000) Malignant gliomas: MR imaging spectrum of radiation therapy- and chemotherapy-induced necrosis of the brain after treatment. Radiology 217:377–384
Lear CS, Flanagan JB Jr, Moorrees CF (1965) The frequency of deglutition in man. Arch Oral Biol 10: 83–100
Lee NY, O'Meara W, Chan K et al (2007) Concurrent chemotherapy and intensity-modulated radiotherapy for locoregionally advanced laryngeal and hypopharyngeal cancers. Int J Radiat Oncol Biol Phys 69: 459–468
Lell M, Baum U, Greess H et al (2000) Head and neck tumors: imaging recurrent tumor and post-therapeutic changes with CT and MRI. Eur J Radiol 33:239–247
Lell MM, Gmelin C, Panknin C et al (2008) Thin-slice MDCT of the neck: impact on cancer staging. AJR Am J Roentgenol 190:785–789
Liu RM, Gaston Pravia KA (2010) Oxidative stress and glutathione in TGF-beta-mediated fibrogenesis. Free Radic Biol Med 48:1–15
Lyons A, Ghazali N (2008) Osteoradionecrosis of the jaws: current understanding of its pathophysiology and treatment. Br J Oral Maxillofac Surg 46:653–660
Marx RE (2003) Pamidronate (Aredia) and zoledronate (Zometa) induced avascular necrosis of the jaws: a growing epidemic. J Oral Maxillofac Surg 61:1115–1117
McConnel FM, Pauloski BR, Logemann JA et al (1998) Functional results of primary closure vs flaps in oropharyngeal reconstruction: a prospective study of speech and swallowing. Arch Otolaryngol Head Neck Surg 124:625–630
Mittal RK (2011) Motor function of the pharynx, esophagus, and its sphincters. Morgan & Claypool Life Sciences, San Rafael
Mu L, Sanders I (2010) Human tongue neuroanatomy: nerve supply and motor endplates. Clin Anat 23: 777–791
Murdoch-Kinch CA, Kim HM, Vineberg KA et al (2008) Dose-effect relationships for the submandibular salivary glands and implications for their sparing by intensity modulated radiotherapy. Int J Radiat Oncol Biol Phys 72:373–382
Nabil S, Samman N (2011) Incidence and prevention of osteoradionecrosis after dental extraction in irradiated patients: a systematic review. Int J Oral Maxillofac Surg 40:229–243
Nguyen NP, Moltz CC, Frank C et al (2004) Dysphagia following chemoradiation for locally advanced head and neck cancer. Ann Oncol 15:383–388
Nomayr A, Lell M, Sweeney R et al (2001) MRI appearance of radiation-induced changes of normal cervical tissues. Eur Radiol 11:1807–1817
Nutting CM, Morden JP, Harrington KJ et al (2011) Parotid-sparing intensity modulated versus conventional radiotherapy in head and neck cancer (PARSPORT): a phase 3 multicentre randomised controlled trial. Lancet Oncol 12:127–136
Okunieff P, Chen Y, Maguire DJ et al (2008) Molecular markers of radiation-related normal tissue toxicity. Cancer Metastasis Rev 27:363–374
Pauloski BR, Rademaker AW, Logemann JA et al (2004) Surgical variables affecting swallowing in patients treated for oral/oropharyngeal cancer. Head Neck 26:625–636
Popovtzer A, Cao Y, Feng FY et al (2009) Anatomical changes in the pharyngeal constrictors after chemo-irradiation of head and neck cancer and their dose-effect relationships: MRI-based study. Radiother Oncol 93:510–515
Prisman E, Miles BA, Genden EM (2013) Prevention and management of treatment-induced pharyngo-oesophageal stricture. Lancet Oncol 14:e380–e386
Rademaker AW, Pauloski BR, Logemann JA et al (1994) Oropharyngeal swallow efficiency as a representative measure of swallowing function. J Speech Hear Res 37:314–325
Russi EG, Corvo R, Merlotti A et al (2012) Swallowing dysfunction in head and neck cancer patients treated by radiotherapy: review and recommendations of the supportive task group of the Italian Association of Radiation Oncology. Cancer Treat Rev 38:1033–1049
Sciubba JJ, Goldenberg D (2006) Oral complications of radiotherapy. Lancet Oncol 7:175–183
Sivolella S, Lumachi F, Stellini E et al (2013) Denosumab and anti-angiogenetic drug-related osteonecrosis of the jaw: an uncommon but potentially severe disease. Anticancer Res 33:1793–1797
Sonis ST (2011) Oral mucositis. Anticancer Drugs 22: 607–612
Stockmann P, Hinkmann FM, Lell MM et al (2010) Panoramic radiograph, computed tomography or magnetic resonance imaging. Which imaging technique should be preferred in bisphosphonate-associated osteonecrosis of the jaw? A prospective clinical study. Clin Oral Investig 14:311–317
Valk PE, Dillon WP (1991) Radiation injury of the brain. AJNR Am J Neuroradiol 12:45–62
Wahl MJ (2006) Osteoradionecrosis prevention myths. Int J Radiat Oncol Biol Phys 64:661–669
Zuydam AC, Rogers SN, Brown JS et al (2000) Swallowing rehabilitation after oro-pharyngeal resection for squamous cell carcinoma. Br J Oral Maxillofac Surg 38:513–518

# Part IV

# Thorax/Lung/Breast

# Complications and Toxicity of Radiotherapy for the Breast, Lung and Heart

John T. Murchison and Edwin J.R. van Beek

## Contents



J.T. Murchison (✉)
Department of Radiology,
Royal Infirmary of Edinburgh,
Edinburgh, UK
e-mail: john.murchison@luht.scot.nhs.uk

E.J.R. van Beek
Queen's Medical Research Institute,
University of Edinburgh,
47 Little France Crescent,
Edinburgh EH16 4TJ, UK

**Abstract**

The side effects and toxicity of radiotherapy administered to the thorax can be separated into early and late types. The most important early effect is radiation pneumonitis which is dependent on various factors, the most important of which is dose. In the most severe cases, this can prove fatal, and the risk of developing severe radiation pneumonitis can limit therapeutic options. Early acute cardiac and cardiac side effects can also occur. The longer-term sequelae of thoracic irradiation include pulmonary radiation fibrosis, premature ischemic heart, cardiac valvular disease, radiation osteonecrosis, oesophageal strictures and the development of second cancers. These side effects are particularly relevant in the treatment of cancers of children and young adults especially in the treatment of lymphoma.

## 1 Introduction

Lung cancer and breast cancer are two of the most prevalent cancers worldwide. Radiotherapy is a commonly employed therapeutic approach in the treatment of these cancers. Patients with lung cancer with stage I and with stage II disease who are inoperable or who decline surgery will be treated with radiotherapy. For stage III lung cancer, the treatment of choice is radical radiotherapy often combined with chemotherapy.

Med Radiol Radiat Oncol (2015)
DOI 10.1007/174_2015_1083, © Springer International Publishing Switzerland

Radiotherapy is also the treatment of choice for the treatment of many breast cancer patients (either as part of breast-conserving therapy or for postmastectomy palliative treatment) as well as for other malignancies involving organs inside the chest, including lymphoma, oesophageal cancer, thyroid tumours, and occasionally thymic tumours (Park et al. 2000; Claude et al. 2004). In addition, radiotherapy has been used for various other non-cancer indications in the past, such as tuberculosis, and this still casts a historical shadow in the chest and is sometimes encountered on current imaging.

Thoracic complications of radiotherapy are directly related to the overall radiation dose as well as the fractionation of radiotherapy that has been employed (Nahum 2015). Furthermore, the radiation field has a direct impact on which portions of the chest are most affected. These complications can be divided into acute complications that relate to the immediate tissue reaction to radiation and chronic complications that are more related to the subsequent scarring and tissue destruction as well as to DNA damage to cells that survive the radiation.

## 2 Clinical Spectrum

The early signs of radiation-induced disease are mainly related to damage to the lungs. In most patients, symptoms are absent or minor, mainly resulting from the local toxic effects on lung tissue within the radiation portal. These are mild cough, occasionally some blood-streaked sputum, and fever. More severe symptoms tend to occur at 6–8 weeks after radiation, and these are usually the result from more significant radiation-induced pneumonitis (see below). Late symptoms are related to the development of pulmonary fibrosis and myocardial and coronary artery injury and the development of radiation-induced secondary cancers. The pulmonary fibrosis may be asymptomatic but if severe and extensive may be distressingly symptomatic with dyspnoea, cough, haemoptysis, orthopnoea and recurrent infections. Finger clubbing may also develop. The effects on the various tissues that may be damaged during radiotherapy can broadly be divided into effects on the lung, effects on the cardiovascular system and effects on other tissues within the radiation field with the risk of second malignancies.

## 3 Effects on the Lung

### 3.1 Radiation Pneumonitis

The exposure of lung tissue to ionising radiation during radiotherapy can lead to physiological changes within the lung tissue, leading on to radiation-induced lung injury. *Radiation pneumonitis* is a side effect of radiation of otherwise healthy lung tissues within the radiation field. The radiotherapy, which is intended to destroy the cancerous cells within that radiation field, results in damage to non-cancerous lung. Radiotherapy-related lung injury is divided into three sequential pathological phases: an acute exudative phase, a subacute organising or proliferative phase and a chronic fibrotic phase. The exudative phase may develop within a matter of weeks following the start of the radiotherapy regimen and in some cases is so severe that radiotherapy cannot be completed in the original schedule. The acute form of radiation pneumonitis can result in significant functional loss of the lung, and in patients with relatively impaired lung function at the onset of therapy, this may be life-threatening. The outcome of radiation pneumonitis is variable, ranging from complete resolution in milder cases to scarring of the lung with functional loss in more severe cases and in the most severe cases may result in death.

The incidence and severity of radiation pneumonitis remain difficult to evaluate. In addition, thresholds from 20 to 40 Gy, based on stratification according to the median of the percentage of irradiated lung volume, were also predictive factors above which radiation pneumonitis is more likely to occur. However, no absolute threshold exists with individual susceptibility variable and on the whole unpredictable. Several studies have extensively explored the risk factors for radiation pneumonitis, and dosimetric parameters seem to

be the most significant factors associated with lung toxicity (Claude et al. 2004; Billiet et al. 2014).

Radiation pneumonitis is a dose-limiting toxicity for patients undergoing radiotherapy and combined chemoradiotherapy for non-small cell lung cancer with elderly patients at greatest risk (Vogelius and Bentzen 2012). Previous or concomitant radiotherapy can also adversely affect the severity and timing of lung radiation side effects. Earlier and more severe radiation pneumonitis is seen after a second course of radiotherapy. Cytotoxic chemotherapeutic agents such as cyclophosphamide, vincristine, mitomycin and bleomycin can accentuate the pneumotoxic effects of the radiation. The pneumotoxic effect of the radiation can also be accentuated by drugs which of themselves do not cause lung damage such as adriamycin and actinomycin D (Lamoureux 1975). The inflammatory effects of radiation can be dampened by corticosteroids. The most severe cases can result in fatal pneumonitis which is related to dosimetric factors and tumour location (Palma et al. 2013).

Symptomatic radiation pneumonitis is a clinically important toxicity occurring in 15–40 % of patients receiving radiotherapy which may result in reduced respiratory function in affected patients. The risk of pneumonitis limits both the radiation therapy dose and the overall field/radiation volume that can safely be treated (Rodriques et al. 2007).

Newer methods of delivering radiotherapy, such as stereotactic body radiotherapy (SBRT) which is particularly used in localized early stage lung cancer where patients are not suitable for surgery, have shown a decrease in radiation pneumonitis. However patients managed with (SBRT) who have COPD and a heavy smoking history are still at increased risk of developing radiation pneumonitis (Inoue et al. 2015).

Patients with breast cancer who undergo mastectomy may receive additional radiotherapy to the chest wall to avoid local recurrence, and this treatment is directly related to chest wall and lung damage. Thus, pulmonary fibrosis in a subpleural (Fig. 1) distribution may develop due to focal radiation pneumonitis (Johansson et al. 2002).

Recently, it was shown that there is a threshold of radiation dose of 15 MeV to the chest wall, above which the risks to lung injury are increased (Omer et al. 2015).

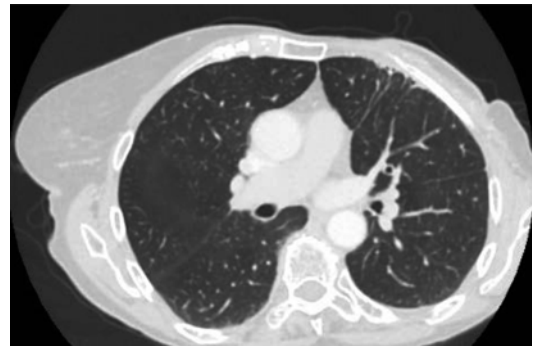

**Fig. 1** Subpleural fibrosis anteriorly just deep to the left chest wall due to previous radiotherapy for breast cancer. Note the previous left mastectomy

Pre-existing pulmonary fibrosis is a risk factor for developing acute radiation pneumonitis. The more severe the pre-existing fibrosis, the greater is the risk of developing radiation pneumonitis and the more likely it is that the resulting radiation pneumonitis will be severe and lead to death. However not all patients with pre-existing pulmonary fibrosis will develop radiation pneumonitis after thoracic radiotherapy. Early studies suggest that it may be possible to predict the future occurrence of radiation-induced pneumonitis by texture analysis of pretreatment CT images of lung cancer patients (Montgomery et al. 2013).

Radiation pneumonitis, when present, usually first becomes visible around 6–8 weeks after commencement of the radiotherapy (Figs. 2, 3, and 4), and is most evident around 3–4 months (Fig. 5) after the start of treatment. Radiation pneumonitis is due to an inflammatory response and so appears in the acute stages as airspace opacification. The most striking feature is the geometric distribution which correlates with the radiation portals. The line of demarcation between involved areas is usually roughly linear. In consolidation due to other causes such as infection, the margins are not linear unless they abut a fissural border. With radiation pneumonitis, such fissural borders are not observed and portions of adjacent different lobes will be involved if included in the radiation field. These

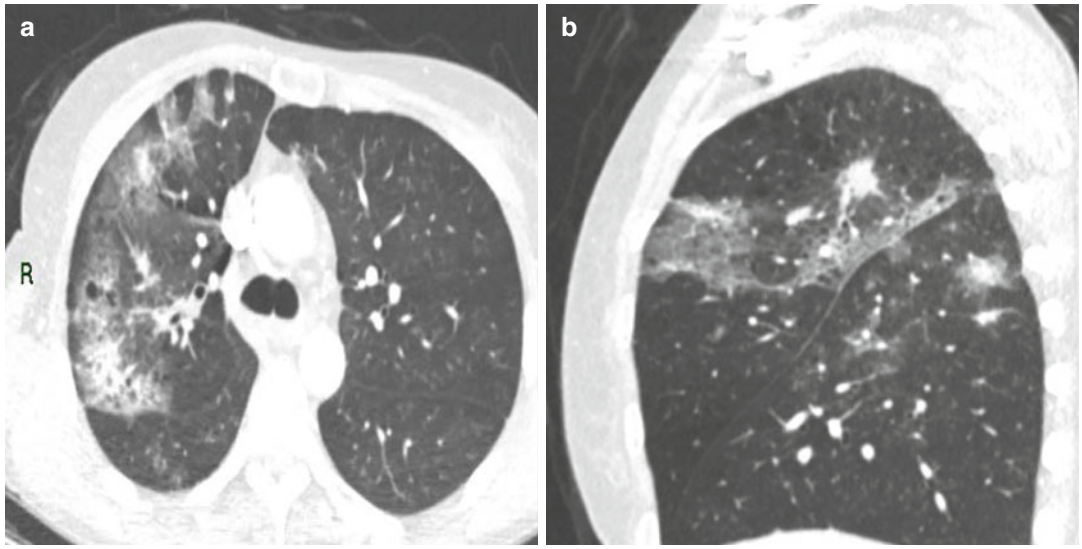


**Fig. 2** (**a**, **b**) Early radiation pneumonitis 6 weeks after the start of treatment with areas of patchy ground-glass attenuation

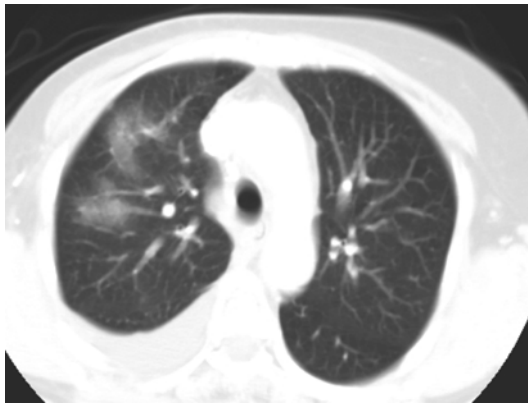

**Fig. 3** Early radiation pneumonitis changes with ground-glass attenuation in the radiation field 6 weeks after radiotherapy for a localised right side breast cancer

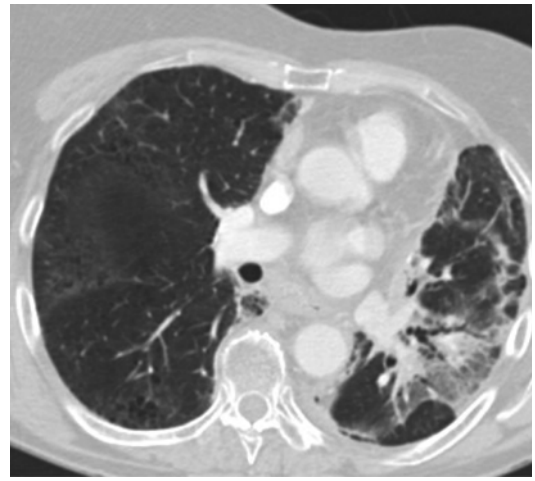

**Fig. 4** Relatively early changes of radiation pneumonitis with left-sided ground-glass attenuation 8 weeks after the start of treatment for a central lung cancer

geometric areas of involvement can be appreciated on both chest x-rays (CXR) and CT scan (Figs. 6, 7, and 8).

The earliest radiological appearances are those of hazy opacities initially ground glass not obscuring vascular margins, which may become denser and more consolidative later. These may be more ill defined and less linearly demarcated initially. Visible radiological changes have been shown to develop after about 8 weeks when treated with 40 Gy over a 4-week period. The opacities appear about 1 week earlier for each 10 Gy increment in dose (Libshitz and Shuman 1984). As might be expected, these appearances are more readily shown at CT scan than on CXR. On CT scan, they appear as scattered areas of ground-glass attenuation within the radiation field which become increasingly confluent. The

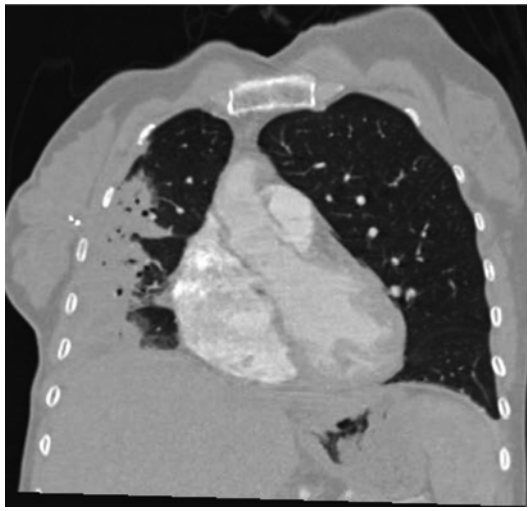

**Fig. 5** Subacute radiation pneumonitis in a patient treated with radiotherapy for breast cancer 10 weeks earlier. There is consolidation with air bronchograms which is largely limited by the radiation field and is not bounded by fissures

geometric distribution may be a particularly striking feature. They are also better shown on ventilation perfusion studies and with single-photon emission CT (SPECT) than on a standard CXR (Bell and McGivern 1988). Pleural effusions are uncommon with uncomplicated radiation pneumonitis and when present are small (Bachman and Macken 1959).

The resulting chronic fibrotic component of radiation pneumonitis develops over 6–24 months and then stabilises. The transition from the more acute inflammatory stage to the fibrotic stage is gradual. The fibrosis results in volume loss involving a well-demarcated geometric area, which becomes more apparent with time. Multiplanar reconstruction on CT scan images can show this particularly well. The shape and distribution of the radiation-induced lung disease vary with the radiation methods used and location of the different thoracic tumours (Park et al.

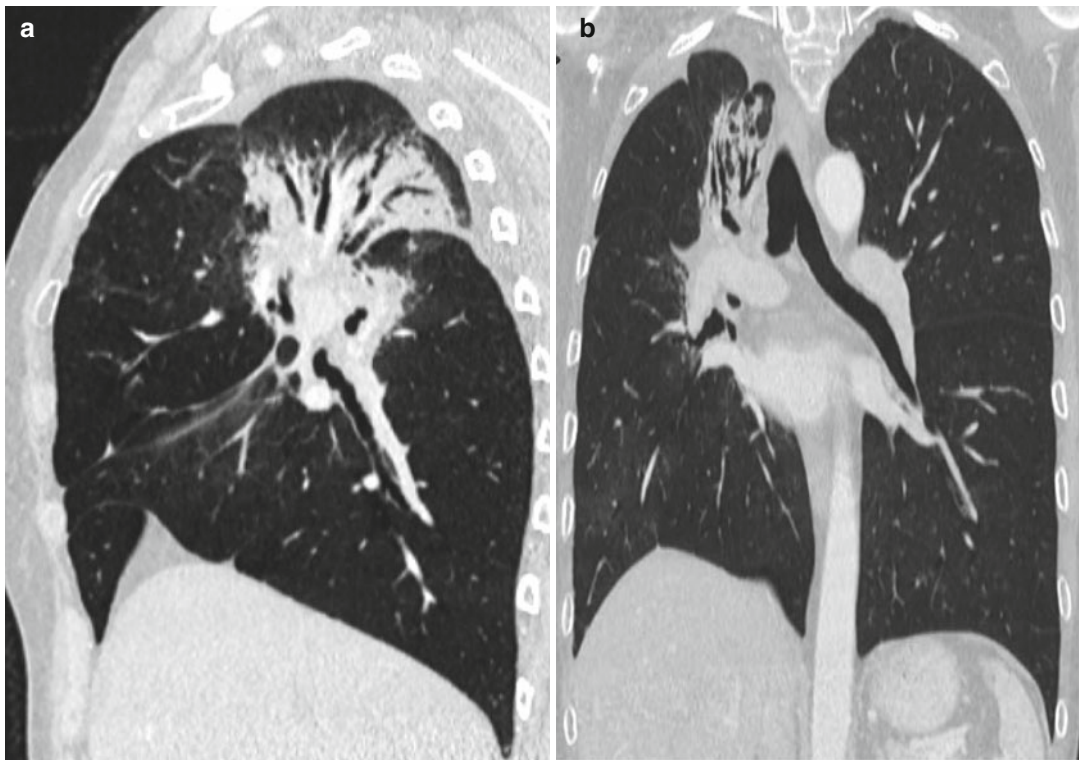


**Fig. 6** (**a**, **b**) Chronic radiation fibrosis with volume loss and bronchiectasis 12 months after radiotherapy for lung cancer

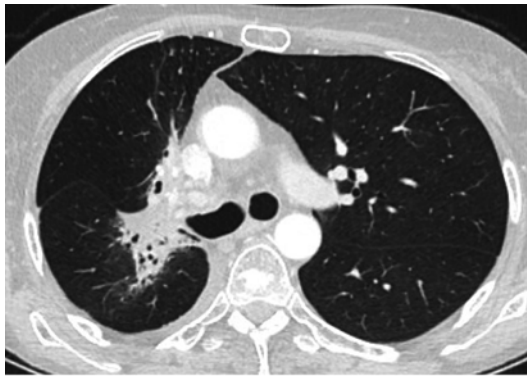

**Fig. 7** Geographical area of chronic radiation fibrosis with bronchiectasis post-lung cancer radiotherapy treatment

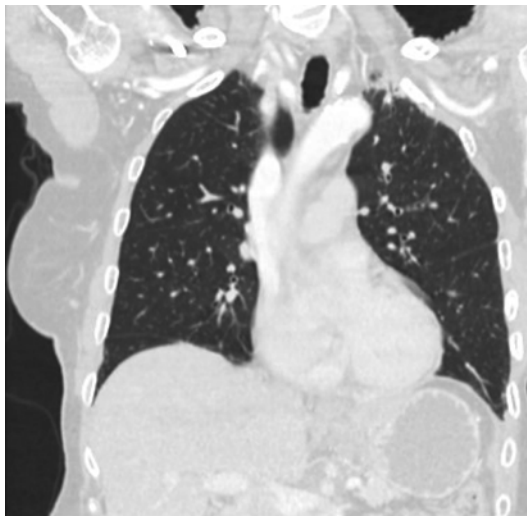

**Fig. 8** Left apical fibrosis due to previous radiotherapy for breast cancer

2000). Bronchiectasis can develop within this fibrotic component and may be a major feature (Fig. 9). It is however less common with modern dosing regimes. The bronchiectasis may be visible on CXR as parallel straight or slightly irregular lines within geometric areas of fibrosis but is much more easily appreciated on CT scan. Fibrous stranding that merges with the pleural surfaces within the radiation field may develop and be visible on CT scan (Fig. 10). The contract and volume loss may also distort adjacent structures.

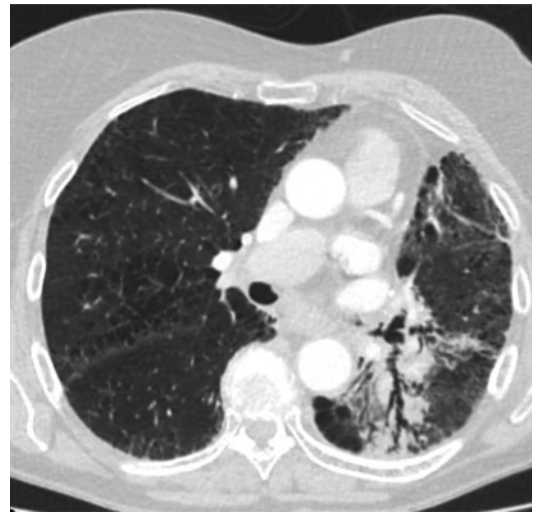

**Fig. 9** Same patient at 5 years post-radiotherapy with CT scan showing chronic post -radiotherapy fibrotic change with region of fibrosis with fairly well-defined but non-physiological borders and varicose bronchiectasis of the fibrotic region

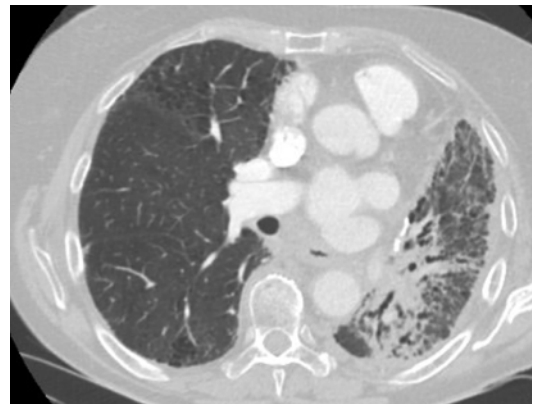

**Fig. 10** Chronic post-radiotherapy change in the left lung. The patient has undergone a previous lobectomy on the left lung and surgical clips are visible centrally. There is volume loss, fibrosis and bronchiectasis on the left lung due to chronic post-radiotherapy fibrosis. There is also subpleural stranding which merges with the pleural surface

## 3.2 Organising Pneumonia

*Organising pneumonia* with flitting areas of consolidation is another recognised complication of radiotherapy which involves the lung. It is significantly less frequent compared to radiation pneumonitis. Although it is described with radiotherapy for lung cancer, it more typically occurs with breast cancer

radiotherapy where it has a reported incidence of 1–3 %. The organising pneumonia is not strictly cryptogenic as it is related to a known cause and is best simply defined as organising pneumonia. It typically first comes to light several months after the radiotherapy treatment. It manifests itself as airspace opacification and infiltrations, which are seen throughout the lungs and keep coming and going in different lung regions for up to 2 years. The involvement of lung parenchyma outside the radiation field helps differentiate it from radiation pneumonitis (Figs. 11 and 12). A similar incidence of cryptogenic organising pneumonia was observed in patients treated with breast-conserving therapy as in post-mastectomy radiation therapy patients. It is not significantly associated with the irradiated lung volume, but is linked to an older age and smoking (Murofushi et al. 2015).

## 3.3 Prediction of Complications in the Lung

There are several methods to help predict the potential risk for developing post-radiotherapy complications particularly radiation pneumonitis. The easily identifiable risk factors are increased age and continued smoking, but other factors include the extent of the tumour, radiation field, delivery of radiation dose and lung perfusion.

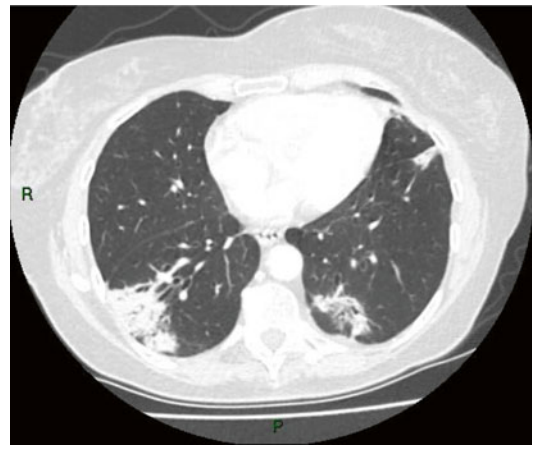


**Fig. 11** Patchy areas of bilateral consolidations with air bronchograms present outside the radiotherapy field on a CT scan performed on a lady 9 months after treatment with radiotherapy for breast cancer due to radiotherapy-related organising pneumonia

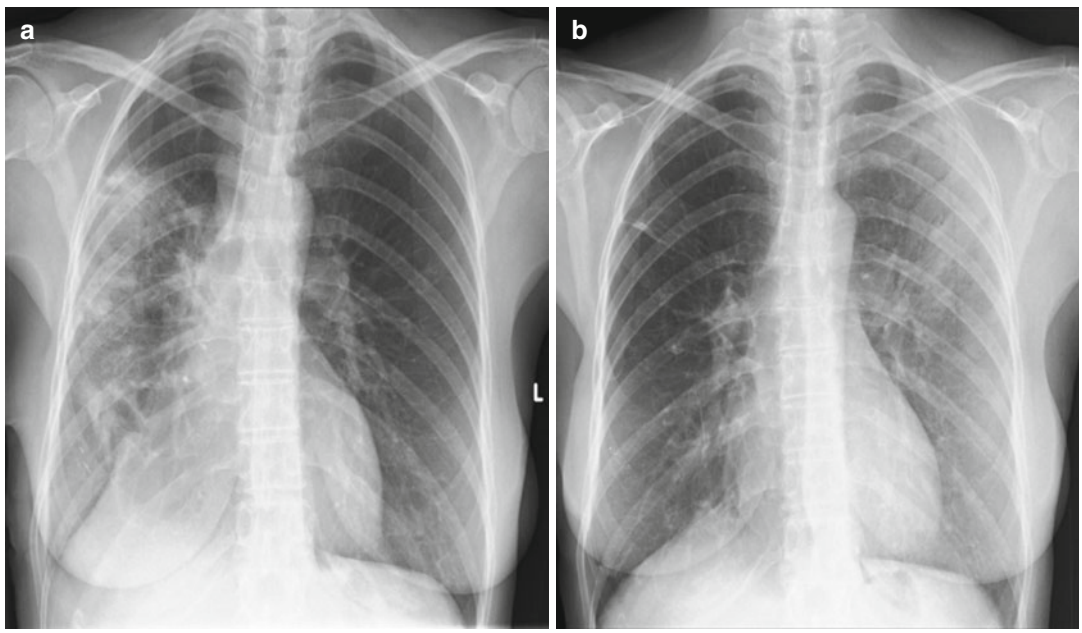


**Fig. 12** (**a**, **b**) Two chest x-rays taken on the same lady who had been treated for breast cancer with radiotherapy 6 and 9 months after the radiotherapy treatment, demonstrating flitting areas of consolidation not related to the radiation field due to radiotherapy-related organising pneumonia

Traditional perfusion scintigraphy (and more recently perfusion SPECT imaging) offers valuable insight into the regional functional perfusion activity before and after chemo- and radiotherapy for non-small lung cancer. The baseline assessment is a better measure than traditional pulmonary function tests for predicting severe radiation pneumonitis (Farr et al. 2015).

A more recent attempt using pulmonary ventilation MRI has shown that it is feasible to adapt the radiation field based on functional ventilation and that this can increase the delivered dose to the primary tumour and reduce the amount of healthy lung tissue included into the radiation field (Ireland et al. 2008; Bates et al. 2009). It is likely that MRI may offer more widely available methods in the future to incorporate the functional information into the radiation planning for lung cancer. Recent work in a rat model demonstrating the capability of performing both functional and metabolic monitoring of radiation-induced lung injury is promising to help guide radiotherapy planning and early identification of lung injury prior to the pathway to pulmonary fibrosis sets in Santyr et al. (2014).

## 4 Effects on the Heart

### 4.1 Lymphoma Radiotherapy Treatment and the Heart

Because the radiation field includes a significant portion of the heart, radiation-induced cardiac complications are a particular risk after radiotherapy for mediastinal lymphoma. Up to 5 % of patients treated with for Hodgkin's lymphoma will die from cardiac deaths within 20–25 years, while cardiac deaths account for nearly 25 % of mortality overall. The risk however has shown some reduction with more recent treatment regimes (Hoppe 1997). The risk increases over time, hence the relatively greater risk for patients who are treated at a young age (Glanzmann et al. 1998; King et al. 1996).

In a series from the Netherlands, the mean interval for developing a cardiac event is reported as around 12 years after the radiotherapy treatment. This figure is particularly significant given the young age of presentation of many lymphoma patients. The same series reported the median age for occurrence of an ischemic event was around 50 years of age. The mean total dose in the inferior part of the mediastinum in this series in the patients with an ischemic event was 36.6 Gy, and the mean fraction dose was 1.61 Gy. The actuarial cumulative risk for an ischemic event increased from 6.4 % (95 % CI 3.8 ± 10.7) at 10 years to 21.2 % (95 % CI 15 ± 30) at 20 ± 25 years (Reinders et al. 1999). Increased age, male gender and a past history of cardiac disease are all risk factors in developing significant coronary artery disease after radiotherapy. When patients do develop ischaemic heart disease after thoracic radiotherapy, coronary artery stenosis tends to occur centrally and is most likely to involve the proximal coronary arteries or the ostia (Orzan et al. 1993) (Fig. 13).

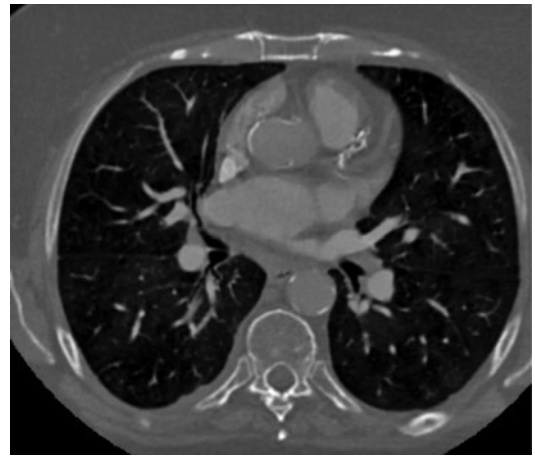

**Fig. 13** Heavy coronary artery calcification involving the proximal left anterior descending coronary artery in a patient in their late 40s previously treated with radiotherapy for Hodgkin's lymphoma

### 4.2 Breast Radiotherapy and the Heart

Treatment of left-sided breast cancer with radiotherapy results in a significant radiation dose to the heart. This particularly affects the left anterior descending coronary artery which runs down the front of the heart. (Early Breast Cancer Trialists' Collaborative Group. 2005, 2011). A significantly

increased risk of cardiac-related deaths has been observed in patients treated with radiotherapy for breast cancer. The principal cause of the excessive deaths is coronary artery disease (Darby et al. 2005; Bouillon et al. 2011; Darby et al. 2013). These deaths have been shown to be dose related with every extra Gray of radiation delivered resulting in the number of significant coronary events increasing by approximate 7.5 %. This increase in cardiac events started around 5 years after the commencement of treatment and lasted into the third decade after radiotherapy (Darby et al. 2013). Right and left internal mammary chain irradiation is also shown to be associated with an increased risk of congestive cardiac failure and increased valvular dysfunction risk with left chest wall irradiation in breast cancer patients resulting in greater risk of myocardial infarction (Hooning et al. 2007). However, modern methods of radiotherapy delivery have been changing, resulting in the delivery of a lower radiotherapy dose to the heart, and a more recent study of cardiac events in breast cancer survivors 12 years post-initial treatment did not demonstrate an increased risk for coronary artery disease as measured by the degree of coronary artery calcification present (Tjessem et al. 2015).

Premature coronary artery atherosclerosis is the cause of the majority of cardiovascular complications following thoracic radiotherapy, and the risk of such complications is closely related to the radiation dose delivered to the heart. This risk increases when other known risk factors for coronary artery disease are present such as smoking, diabetes mellitus and hypertension (King et al. 1996; Darby et al. 2013). In a series of nearly 300 patients treated for Hodgkin's lymphoma who received greater than 35 Gy, over one-fifth of the patients had abnormal perfusion studies indicating myocardial injury. In one-third of these patients, coronary artery disease with >50 % stenosis was demonstrated with the remainder suffering from primary myocardial injury (Heidenreich et al. 2007). In another series, around 40 % of 31 patients treated for Hodgkin's lymphoma were diagnosed with obstructive coronary artery disease using CT coronary angiography, after a median follow-up of 24 years (Mulrooney et al. 2014).

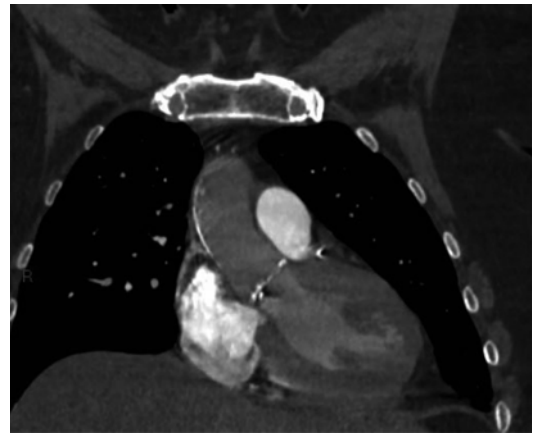

**Fig. 14** Aortic valve calcification and aortic stenosis in a 50-year-old patient treated previously with mantle radiotherapy for lymphoma

### 4.3 Valvular and Myocardial Radiotherapy Toxicity

Some patients treated with radiotherapy develop severe primary myocardial injury which can result in radiotherapy-related cardiomyopathy, mainly following lymphoma therapy. This may necessitate cardiac transplantation if long-term survival is to be achieved (Saxena et al. 2014). Other complications, such as pericardial calcification, can result in constrictive pericarditis. Heart valves' sclerosis and stenosis have also been described (Fig. 14). These are now less common as more advanced delivery methods of radiotherapy are employed (Hancock and Hoppe 1996).

## 5 Effects on the Breast

The breast is a highly sensitive organ for radiation, particularly among women. This includes the skin and the breast tissue itself. Therefore, radiotherapy fields will try to limit exposure of the breast by allowing for different portals and different beam focussing and by using hypofractionation. In spite of these precautions, radiation-induced breast damage remains of significant concern.

The skin overlying the breast is sensitive to radiation-induced damage, ranging from a

superficial radiation burn to skin cancers, with melanoma particularly feared. Subsequent to the acute radiation change, hyperpigmentation may ensue.

The development of breast cancer has a significantly longer latency period (4–25 years), and regular checks are required to ensure patients are promptly diagnosed and treated. The risk of breast cancer is particularly high in younger patients who are treated with radiotherapy to the chest. The risk of breast cancer in survivors of childhood lymphoma is estimated at between 10 and 33 % (Meadows 2001). The Childhood Cancer Survival Study estimated that survivors of childhood cancer who had been treated with radiotherapy to the chest had around 25 times the risk of developing breast cancer compared with the general US population with lymphoma survivors comprising about two-thirds of these patients (Travis et al. 2005). It has also been shown that a radiation dose of 4 Gy or more delivered to the breast was associated with a 3.2-fold increased risk compared with the risk in patients who received lower doses and no alkylating agents. The risk even increased to eightfold with doses of more than 40 Gy. The increased risk persists for at least 25 years following radiotherapy, and the risk was decreased among women who received 5 Gy or more delivered to the ovaries (Travis et al. 2003). Additional Gys of radiation was reported to increase the excess odds ratio of breast cancer by 0.27 % (Inskip et al. 2009). Another group of young patients with an increased risk of developing breast cancer is surviving patients treated with radiotherapy for childhood Wilms' tumour chest metastasis. Nearly 15 % of these patients have been shown to develop invasive breast cancer by the age of 40. Their risk of developing invasive breast cancer is around 9 times the rate of the matched general population.

## 6 Risk of Developing Secondary Cancers

Radiation gives rise to DNA damage, which induces cell death of the most vulnerable cells including tumour cells. However, mutations in DNA will also increase the possibility for cell death and malfunction or lead to the induction of malignant potential. In the latter situation, given sufficient time, tumours may develop in areas within the radiation field (Fig. 15) Interestingly, although bone marrow is often within the radiation field, the risk of leukaemia is not increased due to radiotherapy alone, but is possibly increased in combined chemoradiation therapy

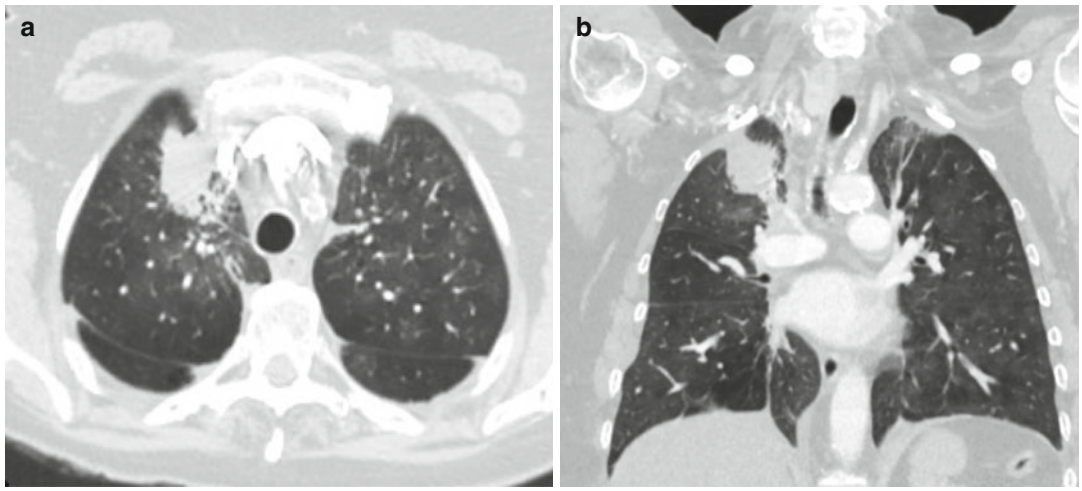


**Fig. 15** (**a**, **b**) A new lung cancer occurring in a patient in their mid 50s who had previously been treated with mantle radiotherapy for lymphoma. Note the medial fibrotic lung changes bilaterally from the previous mantle radiotherapy

(Hoppe 1997). For many of the newer chemotherapy agents, these effects are still largely unknown.

Patients treated for lymphoma most commonly develop skin cancers, particularly melanoma, within the radiation field from 10 to 15 years post-radiotherapy (van Leeuwen et al. 1994). Patients are also at perceived increased risk to develop non-Hodgkin lymphoma following combined chemotherapy and radiotherapy for primary Hodgkin lymphoma, but the overall risk seems relatively small (Swerdlow et al. 1993). Secondary solid tumours are much more common. They have a longer latent period between time of treatment and diagnosis and more often develop in patients requiring multiple therapeutic cycles (initial partial responders or those with recurrent Hodgkin's lymphoma) (Swerdlow et al. 1993; van Leeuwen et al. 1994). The risk for developing secondary solid tumours is highest in younger patients, while the relative risk decreases with age (van Leeuwen et al. 1994). Breast cancer is the most common secondary malignancy in women after radiotherapy for lymphoma and is particularly correlated with irradiated breast tissue between the ages of 10 and 30 years, with a mean latency period of approximately 15 years (Hancock et al. 1993). The risk for other secondary solid tumours is also increased, and in the chest, such tumours include pharynx, thyroid, lung and oesophageal cancers (Hancock et al. 1993).

The development of radiation-induced new *lung cancers* is a major concern, both for the treatment of primary lung cancer and for the treatment of other cancers relying on radiotherapy in the chest. In fact, the initial life expectancy improvement after chemo- and radiotherapy for Hodgkin's lymphoma starts to fall due to the mortality of other causes approximately 15–20 years after the initial diagnosis and treatment (Hoppe 1997; van Leeuwen et al. 1994). This is due to increased cardiovascular deaths and increased second malignancies. There is a 15–20 % cumulative risk for developing a secondary malignancy, which is almost fourfold the risk for the general population (Gustavsson et al. 2003; Hancock and Hoppe 1996; Swerdlow et al. 2000).

Lung cancer is the most common type of secondary solid cancer after treatment for Hodgkin's lymphoma. Compared to the general population, there is a two- to eightfold increased risk, which continues over time greater than 5 years after initial treatment (Swerdlow et al. 2000; van Leeuwen et al. 2000). Smoking history, particularly continuance of smoking after treatment for Hodgkin's lymphoma, markedly increases the risk for lung cancer development.

Radiotherapy for breast cancer particularly affects the chest wall, and sarcomas and lung cancer are most commonly seen (Fowble et al. 2001; Kirova et al. 2007; Kirova et al. 2008). Approximately nine cases of radiation-induced lung cancer can be expected to occur per year for every 10,000 women who have survived for 10 years after treatment for breast cancer with radiotherapy with an average lung dose of 10 Gy (Inskip et al. 1994). Second non-breast malignancies occur in around 8 % of patients treated with conservative surgery and radiotherapy for breast cancer. The absolute risk of developing a second non-breast cancer in this group only becomes evident after 5 years and has an absolute excess risk of about 1 % compared to the general population (Galper et al. 2002). In addition, these patients often develop contralateral breast cancer, although this may be related to genetic predisposition rather than the effects of radiotherapy. In the case of radiotherapy for lung cancer, the most common second tumours to develop are skin cancers and new lung cancers, with sarcoma of the chest wall less commonly a factor due to the beam's focus being away from the chest wall.

## 7 Oesophageal Toxicity

### 7.1 Oesophagitis

A major early complication of central thoracic radiotherapy is acute oesophagitis. It can affect patient's quality of life and interrupt treatment. The epithelial cells of the oesophagus divide rapidly and as such are susceptible to radiotherapy and chemotherapy resulting in mucositis. Acute radiation oesophagitis can develop early at

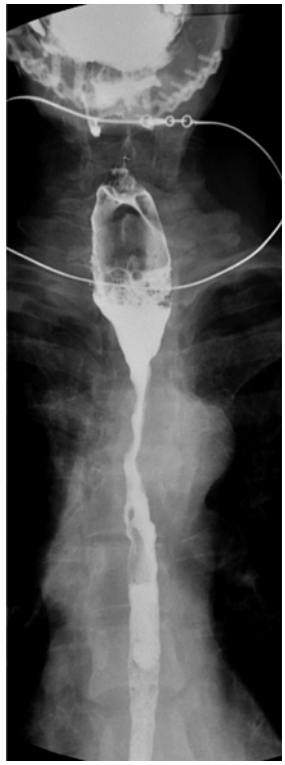

**Fig. 16** Upper oesophageal radiation stricture in a lady treated with radiotherapy for thoracic spinal metastasis

around 7–10 days and often persists for several weeks after treatment stops. Severe oesophagitis generally heals in 3–6 weeks (Fig. 16).

### 7.2 Stricture

Chronic change with stricture can also occur and may be seen 1–8 months after radiotherapy. Interruption of the primary peristalsis wave can also cause chronic dysphagia. Chronic ulceration and fistulation can also occur. The development of severe oesophagitis appears to be dose related with a trend demonstrating increased rates of acute oesophagitis for volumes receiving >40–50 Gy. It is recommended that the mean dose be kept below 34 Gy (Billiet et al. 2014).

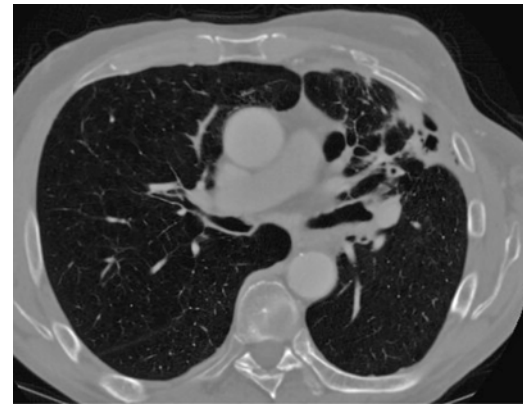

**Fig. 17** Anterior rib fracture due to osteonecrosis as a result of radiotherapy for breast cancer

## 8 Radiation Osteonecrosis

Radiation osteonecrosis or radiation osteitis is due to a severe radiation-induced injury probably due to microvascular damage resulting in altered blood supply. It results in bone necrosis and failure in healing. Any bone in the radiation field may be involved, and in the chest, this usually means the ribs. This is particularly an issue with breast radiotherapy where tumours close to the chest wall are being treated. This may result in distorted bone architecture, dystrophic soft tissue calcification and fractures (Fig. 17). These are better seen on CT scan than on plain film.

**Conclusions**

Radiotherapy of the chest can lead to a range of complications. Although many side effects are transient and the newer methods of delivery of radiotherapy have proven beneficial, serious complications and toxicities do occur. The most common acute and sometimes life-threatening event is radiation pneumonitis. The longer-term side effects include pulmonary radiation fibrosis, premature cardiovascular disease and recurrent/new cancers within the radiation field.

## References


Bachman AL, Macken K (1959) Pleural effusions following supervoltage radiation for breast carcinoma. Radiology 72:1157–1164

Bates EL, Bragg CM, Wild JM, Hatton MQ, Ireland RH (2009) Functional image-based radiotherapy planning for non-small cell lung cancer: a simulation study. Radiother Oncol 93:32–36

Bell J, McGivern D (1988) Bullimore, et al Diagnostic imaging of post-irradiation change in the chest. Clin Radiol 39:109–119

Billiet C, Peeters S, Ruysscher DD (2014) Focus on treatment complications and optimal management: radiation oncology. Transl Lung Cancer Res 3:187–191

Bouillon K, Haddy N, Delaloge S et al (2011) Long-term cardiovascular mortality after radiotherapy for breast cancer. J Am Coll Cardiol 57:445–452

Claude L, Perol D, Ginestet C, Falchero L, Arpin D, Vincent M et al (2004) A prospective study on radiation pneumonitis following conformal radiation therapy in non-small-cell lung cancer: clinical and dosimetric factors analysis. Radiother Oncol 71:175–181

Darby SC, McGale P, Taylor CW, Peto R (2005) Long-term mortality from heart disease and lung cancer after radiotherapy for early breast cancer: prospective cohort study of about 300 000 women in US SEER cancer registries. Lancet Oncol 6:557–565

Darby SC, Ewertz M, McGale P, Bennet AM, Blom-Goldman U, Bronnum D, Correa C, Cutter D, Gagliardi G, Gigante B, Jensen MB, Nisbet A, Peto R, Rahimi K, Taylor C, Hall P (2013) Risk of ischemic heart disease in women after radiotherapy for breast cancer. N Engl J Med 368:987–998

Early Breast Cancer Trialists' Collaborative Group (2005) Effects of radiotherapy and of differences in the extent of surgery for early breast cancer on local recurrence and on 15-year survival: an overview of the randomised trials. Lancet 366:2087–2106

Early Breast Cancer Trialists' Collaborative Group (2011) Effect of radiotherapy after breast-conserving surgery on 10-year recurrence and 15-year breast cancer death: meta-analysis of individual patient data for 10,801 women in 17 randomised trials. Lancet 378:1707–1716

Farr KP, Kramer S, Khalil AA, Morsing A, Grau C (2015) Role of perfusion SPECT in prediction and measurement of pulmonary complications after radiotherapy for lung cancer. Eur J Nucl Med Mol Imaging 42:1315–1324

Fowble B, Hanlon A, Freedman G, Nicolaou N, Anderson P (2001) Second cancers after conservative surgery and radiation for stages I-II breast cancer: identifying a subset of women at increased risk. Int J Radiat Oncol Biol Phys 51:679–690

Galper S, Gelman R, Recht A, Silver B, Kohli A, Wong JS, van Buren T, Baldini EH, Harris JR (2002) Second nonbreast malignancies after conservative surgery and radiation therapy for early-stage breast cancer. Int J Radiat Oncol Biol Phys 52:406–414

Glanzmann C, Kaufmann P, Jenni R, Hess OM, Huguenin P (1998) Cardiac risk after mediastinal irradiation for Hodgkin's disease. Radiother Oncol 46:51–62

Gustavsson A, Osterman B, Cavallin-Stahl E (2003) A systematic overview of radiation therapy effects in Hodgkin's Lymphoma. Acta Oncologica 42:589–604

Hancock SL, Hoppe RT (1996) Long-term complications of treatment and causes of mortality after Hodgkin's disease. Semin Radiat Oncol 6:225–242

Hancock SL, Tucker MA, Hoppe RT (1993) Breast cancer after treatment of Hodgkin's disease. J Natl Cancer Inst 85:1530–1537

Heidenreich PA, Schnittger I, Strauss HW, Vagelos RH, Lee BK, Mariscal CS, Tate DJ, Horning SJ, Hoppe RT, Hancock SL (2007) Screening for coronary artery disease after mediastinal irradiation for Hodgkin's Disease. J Clin Oncol 25:43–49

Hooning MJ, Botma A, Aleman BMP et al (2007) Long-term risk of cardiovascular disease in 10-year survivors of breast cancer. J Natl Cancer Inst 99:365–375

Hoppe RT (1997) Hodgkin's disease: complications of therapy and excess mortality. Ann Oncol 8(Suppl 1):115–118 (R1/2498)

Inoue T, Shiomi H, Oh RJ (2015) Stereotactic body radiotherapy for stage I lung cancer with chronic obstructive pulmonary disease: special reference to survival and radiation-induced pneumonitis. J Radiat Res 56:727–734

Inskip PD, Stoval M, Flannery JT (1994) Lung cancer risk and radiation dose among women treated for breast cancer. J Natl Cancer Inst 86:983–988

Inskip PD, Robison LL, Stovall M et al (2009) Radiation dose and breast cancer risk in the childhood Cancer Survivor study. J Clin Oncol 27:3901–3907

Ireland RH, Woodhouse N, Hoggard N, Swinscoe JA, Foran BH, Hatton MQ, Wild JM (2008) An image acquisition and registration strategy for the fusion of hyperpolarized helium-3 MRI and X-ray CT images of the lung. Phys Med Biol 53:6055–6063

Johansson S, Svensson H, Denekamp J (2002) Dose response and latency for radiation-induced fibrosis, edema, and neuropathy in breast cancer patients. Int J Radiat Oncol Biol Phys 52:1207–1219

King V, Constine LD, Clark D et al (1996) Symptomatic coronary artery disease after mantle irradiation for Hodgkin's disease. Int J Radiat Oncol Biol Phys 36:881–889

Kirova YM, Gambotti L, de Rycke Y, Vilcoq JR, Asselain B, Fouquet A (2007) Risk of second malignancies after adjuvant chemotherapy for breast cancer: a large-scale, single-institution review. Int J Radiat Oncol Biol Phys 68:359–363

Kirova YM, de Rycke Y, Gambotie L, Pierga JY, Asselain B, Fourquet A, Institut Curie Breast Cancer Study Group (2008) Second malignancies after breast can-

cer: the impact of different treatment modalities. Br J Cancer 98:870–874

Lamoureux K (1975) Increased clinically symptomatic pulmonary radiation reactions with adjuvant chemotherapy. Cancer Chemother Res 36:946–949 (part1)

Libshitz HI, Shuman LS (1984) Radiation-induced pulmonary change: CT findings. J Comput Assist Tomogr 8:15–19

Meadows AT (2001) Second tumours. Eur J Cancer 37: 2074–2079

Montgomery D, Campbell S, Cheng K, et al (2013) Predicting the Occurrence of Radiation Induced Pneumonitis by Texture Analysis of CT Images from Lung Cancer Patients.. Published in the Proceedings of the Fifth International Workshop on Pulmonary Image Analysis, held in conjunction with the MICCAI 2013 meeting in Nagoya, 26 Sept 2013

Mulrooney DA, Nunnery SE, Armstrong GT, Ness KK, Srivastava D, Donovan FD, Kurt BA, Metzger ML, Krasin MJ, Joshi V, Durand JB, Robison LL, Hudson MM, Flamm SD (2014) Cancer 120:3536–3544

Murofushi KN, Oguchi M, Gosho M, Kozuka T, Sakurai H (2015) Radiation Induced bronchiolitis obliterans organizing pneumonia (BOOP) syndrome in breast cancer patients is associated with age. Radiat Oncol 10:103

Nahum AE (2015) The radiobiology of hypofractionation. Clin Oncol 27:260–269

Omer H, Sulieman A, Alzimami K (2015) Risk of lung fibrosis and pneumonitis after post mastectomy electron radiotherapy. Radiat Prot Dosimetry 165:499–502

Orzan F, Brusca A, Conte MR, Prebitero P, Figliomeni MC (1993) Severe coronary artery disease after radiation therapy of the chest and mediastinum: clinical presentation and treatment. Br Heart J 69:496–500

Palma DA, Senan S, Tsujino K, Barriger RB, Rengan R, Moreno M et al (2013) Predicting radiation pneumonitis after chemoradiation therapy for lung cancer: an international individual patient data meta-analysis. Int J Radiat Oncol Biol Phys 85:444–450

Park KJ, Chung JY, Chun MS, Suh JH (2000) Radiation-induced lung disease and the impact of radiation methods on imaging features. Radiographics 20:83–98

Reinders JG, Heijmen BJM, Olofsen-can Acht MJJ et al (1999) Ischaemic heart disease after mantlefield irradiation for Hodgkin's disease in long-term follow-up. Radiother Oncol 51:35–42

Rodriques G, Lock M, D'Souza D et al (2007) Prediction of radiation pneumonitis, derived from a combined analysis of RTOG 9311 and institutional data. Int J Radiat Oncol Biol Phys 69:985–992

Santyr G, Fox M, Think K, Hegarty E, Ouriadov A, Jensen M et al (2014) Anatomical, functional and metabolic imaging of radiation-induced lung injury using hyperpolarized MRI. NMR Biomed 27:1515–1524

Saxena P, Joyce LD, Daly RC, Kushwaha SS, Schirger JA, Rosedahl J, Dearani JA, Kara T, Edwards BS (2014) Cardiac transplantation for radiation-induced cardiomyopathy: the Mayo Clinic experience. Ann Thorac Surg 98:2115–2121

Swerdlow AJ, Douglas AJ, Vaughan Hudson G et al (1993) Risk of second primary cancer in after Hodgkin's disease in patients in the British National Lymphoma Investigation: relationships to host factors, histology, and stage of Hodgkin's disease, and splenectomy. Br J Cancer 68:1006–1011

Swerdlow AJ, Barber JA, Vaughan Hudson G et al (2000) Risk of second malignancy after Hodgkin's disease in a collaborative British cohort: the relation to age at treatment. J Clin Oncol 18:498–509

Tjessem KH, Bosse G, Fossa K, Reinertsen KV, Fossa SD, Johansen S, Fossa A (2015) Coronary calcium score in 12-year breast cancer survivors after adjuvant radiotherapy with low to moderate heart exposure – relationship to cardiac radiation dose and cardiovascular risk factors. Radiother Oncol 114:328–334

Travis LB, Hill D, Dores GM et al (2003) Breast Cancer following radiotherapy and chemotherapy among young women with Hodgkin Disease. JAMA 290:465–475

Travis LB, Hill D, Dores GM et al (2005) Cumulative absolute breast cancer risk for young women treated for Hodgkin lymphoma. J Natl Cancer Inst 97: 1428–1437

van Leeuwen FE, Klokman WJ, Hagenbeek A et al (1994) Second cancer risk following Hodgkin's disease: a 20-year follow-up study. J Clin Oncol 12:312–325

van Leeuwen FE, Klokman WJ, van't Veer MB et al (2000) Long-term risk of second malignancy in survivors of Hodgkin's disease treated during adolescence or young adulthood. J Clin Oncol 18:487–497

Vogelius IR, Bentzen A (2012) Literature-based meta-analysis of clinical risk factors for development of radiation induced pneumonitis. Acta Oncol 51: 975–983

# Drug-Induced Interstitial Lung Disease in Oncology Patients

Rianne Wittenberg, Santiago Rossi, and Cornelia Schaefer-Prokop

## Contents



R. Wittenberg
Department of Radiology, Meander Medical Center, Amersfoort, The Netherlands

S. Rossi
Centro de Diagnostico Dr Enrique Rossi, Buenos Aires, Argentina

C. Schaefer-Prokop (✉)
Department of Radiology, Meander Medical Center, Amersfoort, The Netherlands

Department of Radiology, Radboud University Medical Center, Nijmegen, The Netherlands
e-mail: cornelia.schaefer-prokop@radboudumc.nl

**Abstract**

There are an ever-increasing number of drugs that can cause lung disease (Foucher and Camus 2008, Pneumotox online: the drug-induced lung diseases. See: www.pneumotox.com). Prognosis is variable from self-limiting to fast progression with potential lethal outcome. Especially for the latter, timely diagnosis and appropriate management are important. The role of imaging is eminent, given the aspecific character of clinical symptoms, the broad range of potential underlying reasons, and the potentially serious outcome. There is a broad overlap between computed tomography (CT) patterns known from interstitial lung diseases and the findings seen in drug-induced lung disease. We provide a general overview about CT patterns to be encountered in patients

Med Radiol Radiat Oncol (2015)
DOI 10.1007/174_2015_1080, © Springer International Publishing Switzerland, 2015

with drug-induced lung disease, followed by descriptions of findings related to specific drugs. A special focus lies on new molecular-targeted drugs. Aspects to consider for differential diagnosis are provided at the end of the chapter.

## Abbreviations

| | |
|---|---|
| ADR | Adverse drug reactions |
| AIP | Acute interstitial pneumonia |
| ARDS | Acute respiratory distress syndrome |
| BAL | Bronchoscopy with bronchoalveolar lavage |
| CT | Computed tomography |
| DAD | Diffuse alveolar damage |
| DIP | Desquamative interstitial pneumonia |
| EGFR | Epidermal growth factor receptor |
| EP | Eosinophilic pneumonia |
| HP | Hypersensitivity pneumonitis |
| ILD | Interstitial lung diseases |
| LIP | Lymphocytic interstitial pneumonia |
| NSIP | Nonspecific interstitial pneumonia |
| OP | Organizing pneumonia |
| PJP | *Pneumocystis jirovecii* pneumonia |
| RA | Rheumatoid arthritis |
| TNF | Tumor necrosis factor |
| UIP | Usual interstitial pneumonia |

# 1 Prevalence, Clinical Symptoms, and Diagnosis

It has been reported that adverse drug reactions (ADR) are the cause of 250.000 hospitalizations per year in the United Kingdom (Hitchen 2006). Up to 10 % of patients who receive chemotherapeutic agents develop an ADR in their lungs (Limper and Rosenow 1996), and it is very likely that this number is further increased over the last years due to new types of chemotherapeutic agents.

Clinical symptoms are often nonspecific and include shortness of breath, nonproductive cough, fever, and chest pain. Furthermore, diffusion capacity for carbon monoxide is frequently reduced. The symptoms are often acute and highly progressive but can also have a slowly progressive and more chronic course.

Not only the clinical symptoms but also the imaging findings are often nonspecific. The differential diagnosis of drug-induced lung disease can be challenging. Important for accurate diagnosis is the exclusion of other causes of lung damage. Alternative diagnoses such as (opportunistic) infection, edema due to pulmonary fluid overload, or pulmonary sequelae of the underlying lung disease have to be ruled out by clinical and radiological means. Profound knowledge of the correlations of drug effects and imaging findings is therefore essential to prevent under- or misdiagnosis of lung diseases.

## 1.1 Risk Factors

Factors such as age, coexisting hepatic and renal insufficiency, sex, ethnicity, dose, oxygen therapy, interactions with other drugs, radiation therapy, and a genetic predisposition play an important and potentially synergistic role (Rossi et al. 2000; Erasmus et al. 2002).

### 1.1.1 Age

In general childhood and old age are associated with an increased risk of drug toxicity. The elderly patient is more prone to develop severe side effects because of diminished renal and hepatic function and therefore overall reduced metabolic function. A retrospective review of bleomycin pulmonary toxicity reported that in patients older than 40 years and suffering from reduced renal function, the risk of developing a fatal toxicity could exceed 10 % (Simpson et al. 1998).

### 1.1.2 Sex

There is no evidence that gender influences the risk for drug-induced interstitial lung disease.

### 1.1.3 Ethnicity

There may be racial differences in the incidence of drug-induced interstitial lung disease: There have been reports of an increased incidence of

lung injury caused by gefitinib and bortezomib in Japan, though it is difficult to determine the relative incidences.

#### 1.1.4 Dose

For amiodarone, bleomycin, and carmustine, the dose has been found to be a significant risk factor for the development of drug-induced interstitial lung disease.

#### 1.1.5 Oxygen Therapy

The lungs are normally equipped with an extensive antioxidant network to protect against tissue damage by reactive oxygen species. This network may be insufficient, and this situation of inadequate protection is called "oxidative stress" potentially leading to acute lung injury and acute respiratory distress syndrome (ARDS).

#### 1.1.6 Drug Interaction

The role of drugs taken concomitantly is important. Drugs in the same therapeutic class can induce similar lung injury patterns. Hazardous associations have been reported for coadministration of cisplatin and bleomycin, increasing the risk for bleomycin-induced interstitial lung disease. The combination of gemcitabine and bleomycin is also very toxic.

#### 1.1.7 Radiation Therapy

Radiation therapy in combination with chemotherapy has synergistic adverse effects with respect to lung injury. Conjoint radiation therapy is associated with high rates of lung toxicity by bleomycin. Interstitial pneumonias after fractionated total body irradiation in preparation for allergenic bone marrow transplantation occurred with a significant incidence of 20 % (Oya et al. 2006).

#### 1.1.8 Underlying Lung Disease

It is controversial in the literature if preexisting lung disease is a risk factor (Schwaiblmair et al. 2012): Logistic regression analysis identified age >65 years, smoking habit, reduced lung function, and preexisting interstitial pneumonia as significant risk factor in patients with non-small cell lung cancer treated with gefitinib (Kudoh et al. 2008).

### 1.2 Diagnosis

A timely diagnosis is important, because most patients have a good prognosis when harmful drugs are withdrawn or corticosteroids are administered. CT plays a major role in making a diagnosis since it is not only the most sensitive method for detection but also the best and most accurate method to identify the extent and pattern of pulmonary parenchymal changes (Mueller et al. 2004; Silva and Mueller 2006; Walsh and Hansell 2014; Ellis et al. 2000; Myers et al. 2003).

Diagnosis of drug-induced lung disease generally depends on a temporal association between exposure to the causative agent and the development of respiratory signs and symptoms. Difficulties arise when symptoms develop after discontinuation of drug administration with variable delay rather than during treatment or when no improvement occurs despite discontinuation of the drug.

Bronchoscopy with bronchoalveolar lavage (BAL) can be helpful to exclude other causes of respiratory failure such as infection, alveolar hemorrhage, or lymphangitis carcinomatosa. Hypersensitivity pneumonitis (HP), organizing pneumonia (OP), and eosinophilic pneumonia (EP) can be excluded if the BAL is normal. Most commonly the BAL of patients with drug-induced lung disease reveals a lymphocytosis either pure or associated with signs of neutrophilic and/or eosinophilic alveolitis and an imbalanced T lymphocyte phenotype (preponderance of CD8 + cells) (Akoun et al. 1991).

History of drug exposure, clinical information, suitable radiological findings, and response to treatment (corticosteroids and discontinuation of medication) mostly provide the base for the diagnosis (Table 1). Very rarely, the diagnosis is based on biopsy and subsequent histopathology.

## 2 Mechanisms of Lung Injury and Corresponding CT Patterns

The CT patterns of drug-induced lung disease reflect the underlying histopathological changes (Rossi et al. 2000; Silva and Mueller 2006). The

**Table 1** Diagnosis of drug-induced lung disease

| | |
|---|---|
| History and medication | Patient characteristics |
| | Type, dose, and exposure time of medication |
| | Other medication |
| | Radiotherapy/oxygen therapy |
| | Preexisting lung, liver, and kidney disease |
| Clinical symptoms | Dyspnea, fever, cough, chest pain, diffusion restriction |
| Bronchoalveolar lavage (BAL) | Lymphocytosis associated with neutrophilic/eosinophilic alveolitis |
| | Imbalance of T lymphocyte phenotypes |
| CT findings | Pattern, preexisting disease, alternative diagnosis |
| Exclusion of alternative diagnosis | Infection |
| | Heart failure with edema |
| | Underlying lung disease and malignancy |
| Response to therapy | Withdrawal of medication |
| | Administration of corticosteroids |
| Histopathology | Solely in complex cases or to exclude other diseases |

histopathological patterns occurring in drug-induced lung disease are very similar to pulmonary changes known from idiopathic interstitial lung disease and parenchymal changes seen in collagen vascular diseases. The diagnosis is complicated by the fact that one drug can cause various forms of lung injuries, and on the other hand, a particular pattern can be caused by several drugs. Thus, there is no one-on-one relationship between a particular drug, imaging finding, and underlying histopathology (Cleverly et al. 2002). Preexisting lung disease, concurrent infection, or the fact that a combination of drugs is frequently given in oncologic patients further aggravates the situation.

Despite this broad overlap, for stratification purposes, it seems useful to classify CT patterns of drug-induced pulmonary disease into five subgroups according to their underlying pathomechanisms and histopathological classifications (Table 2). In association with chemotherapeutic drugs, the lung injury is by far most commonly caused by direct toxic action (mechanism I) or immune-mediated lung injury (mechanism II). Mechanisms III to V are mentioned here for completeness.

## 2.1 Lung Injury Caused by Direct Toxic Action

The balance between collagen production and destruction is disturbed by the drug itself or its metabolites. Various forms of pulmonary fibrosis are the result. Typically, the pulmonary changes occur after a certain period of time after drug administration (weeks to months, rarely years), are often dose dependent, and may be amplified by synergistic factors. Various subtypes of fibrotic lung changes can be observed:

### 2.1.1 Nonspecific Interstitial Pneumonia

By far the most common CT pattern seen in type I drug-induced lung reactions refers to nonspecific interstitial pneumonia (NSIP). However, all other forms of interstitial pneumonia such as usual interstitial pneumonia (UIP), lymphocytic interstitial pneumonia (LIP), or desquamative interstitial pneumonia (DIP) – though sometimes only in individual cases – have been described in combination with drug-induced pulmonary damage.

In NSIP a relatively homogeneous diffuse infiltration of the interstitium with mononuclear inflammatory cells, hyperplasia of pneumocytes, and fibrosis can be found. NSIP can present with a wide spectrum of CT changes. The patterns are similar to the pattern of NSIP in patients with collagen vascular disease or idiopathic NSIP. For differentiation, some authors prefer the term "interstitial pneumonia" in the context of drug-induced lung disease and use the term NSIP solely for the idiopathic form and in association with collagen vascular diseases. Patchy areas with ground glass superimposed by reticular densities are most commonly seen, frequently combined with bronchiectasis. There may be a predominance for the subpleural areas of the lung, but more often a diffuse patchy distribution is seen. The parenchymal changes can be strikingly reversible, even when it looks like

**Table 2** HRCT pattern of drug-induced lung disease

| Mechanism lung injury | CT pattern | |
|---|---|---|
| Direct toxic action | Diffuse alveolar damage (DAD) | Bilateral diffuse ground-glass opacities<br>Superimposed reticular densities (crazy paving)<br>Consolidations<br>Patchy distribution<br>Ventrodorsal and craniocaudal gradient<br>End-stage lung disease with fibrosis, honeycombing, and bronchiectasis |
| | Nonspecific interstitial pneumonia (NSIP) | Ground glass<br>Reticular densities<br>Sometimes bronchiectasien<br>Diffuse patchy or subpleural distribution |
| | Organizing pneumonia (OP) | Subpleural non-segmental or peribronchovascular consolidations<br>Slightly dilated bronchi with air bronchogram<br>Atoll (reversed halo) sign<br>Nodular pattern with tree in bud and ground glass |
| | Usual interstitial pneumonia (UIP) | Subpleural reticular changes<br>Architectural distorsion<br>Craniocaudal gradient<br>Honeycombing |
| Immune-mediated lung injuries | Hypersensitivity pneumonitis (HP) | Diffuse poorly defined centrilobular and acinar ground-glass nodules<br>Ground-glass opacities<br>Air trapping |
| | Eosinophilic pneumonia (EP) | Overlapping CT patterns<br>Peripheral non-segmental consolidation<br>Reversed halo sign<br>Ground-glass opacities<br>Nodular densities<br>Crazy-paving pattern |

irreversible "fibrosis" in the beginning. Based on the overlap of the pattern, all diseases causing an NSIP have to be considered in the differential diagnosis such as collagen vascular diseases. The most helpful finding for differential diagnosis and in favor of drug-induced lung disease is the patchy diffuse distribution and the sudden onset.

### 2.1.2 Organizing Pneumonia

Organizing pneumonia (OP) is the second most common pattern in response to drugs after NSIP, but the two patterns can also occur together. A drug-induced OP has a good prognosis and is usually reversible with treatment. OP is characterized by a proliferation of immature fibroblasts filling up the respiratory bronchioles and alveolar spaces. Drug-induced OP has the same morphological features as idiopathic OP, postinfectious OP, and OP seen in collagen vascular diseases, after lung transplantation, or in association with other immune diseases.

On CT an OP can manifest with peripheral/subpleural non-segmental consolidations and can strongly resemble eosinophilic pneumonia. Slightly dilated bronchi with air bronchograms can be seen in the consolidated areas. The lung architecture is usually preserved. The consolidations can also appear in a more linear form

following the bronchovascular bundle and marking the boundaries of the pulmonary lobule (lobular pattern). Furthermore, they can form multiple "islands" with a center of ground glass and a peripheral consolidated ring in the lung parenchyma (atoll sign with reversed halo character). At last, OP can manifest as a nodular pattern with diffuse tree-in-bud, larger nodule, and ground-glass opacities. In summary, OP can present with a variety of patterns as expression of drug-induced lung disease leading to a broad differential diagnosis. More than 35 drugs cause organizing pneumonia including minocycline and bleomycin. In bleomycin, a nodular organizing pneumonia has been described causing nodular densities typically located at the lung base and simulating metastatic nodules.

#### 2.1.3 Diffuse Alveolar Damage

Diffuse alveolar damage (DAD) corresponds clinically, radiologically, and pathologically to ARDS and represents a common form of drug-induced lung injury in oncology patients. In patients with DAD, there is necrosis of endothelial cells and alveolar pneumocytes (type II), further resulting in alveolar and interstitial edema.

Similar to ARDS, there are an acute exudative phase and a chronic proliferative or reparative phase. The former usually takes about 1 week and is characterized by edema and hyaline membrane formation; the latter typically occurs from the second week on and is characterized by bronchiectasis and destruction of lung parenchyma. Fibrotic changes can be stable but also fatally progressive under therapy. The CT pattern consists of bilateral diffuse ground-glass opacities with superimposed reticular densities (crazy paving) and/or consolidations. Similarly to ARDS, a ventrodorsal gradient may be seen. The middle and basal lung regions are most often affected. However, the distribution can also be patchy with "normal" lung areas in between. With further progression of the disease bronchiectasis, destruction of lung parenchyma and end-stage lung disease with honeycombing are seen. In the differential diagnosis, diffuse infection, massive aspiration, noxious inhalation, acute interstitial pneumonia (AIP), or exacerbation of an underlying collagen vascular disorder must be excluded.

#### 2.1.4 Usual Interstitial Pneumonia

A drug-induced pattern of usual interstitial pneumonia (UIP) is uncommon and most frequently described in combination with certain chemotherapeutics, e.g., bleomycin and methotrexate. In addition to subpleural reticular changes, bronchiectasis and signs of architectural distorsion with a craniocaudal gradient are typical findings. The dominant CT pattern includes cystic destruction of the lung parenchyma (honeycombing) comparable with the cystic parenchymal changes encountered in the idiopathic form of UIP.

### 2.2 Immune-Mediated Lung Injuries

Along with endogenous proteins, the drugs can trigger a hypersensitivity reaction (type I, immediate hypersensitivity reaction, or type III, immune complex reaction). These drug reactions occur almost immediately or within hours or days after drug exposure, are not dose dependent, and generally have a good prognosis. They may affect the airways (asthma with bronchoconstriction and hypersecretion of mucus) or the lung parenchyma in the form of a hypersensitivity reaction or eosinophilic pneumonia. Immune-mediated lung injuries are only rarely associated with chemotherapeutic agents.

#### 2.2.1 Hypersensitivity Pneumonitis

A drug-induced hypersensitivity pneumonitis (HP) is relatively rare and pathoradiologically indistinguishable from HP triggered by inhalation of antigens. The CT shows diffuse poorly defined centrilobular acinar ground-glass nodules, which may confluence to diffuse ground-glass areas. In expiration sharply demarcated hypertransparent areas may be seen reflecting air trapping in secondary lobules. HP can be caused by antitumor necrosis factor (TNF) agents such as methotrexate, BCG therapy, and cyclophosphamide.

#### 2.2.2 Eosinophilic Pneumonia

A drug-induced eosinophilic pneumonia (EP) is relatively common and may show a slow progressive course over months. It usually has a good prognosis with appropriate treatment. The alveoli

are filled with macrophages and eosinophils. Furthermore, the alveolar septa are thickened by infiltration of eosinophils, lymphocytes, and plasma cells. Most of the time, the consolidations are already visible on conventional X-ray. In accordance with OP, EP can present with different overlapping CT patterns. For example, peripheral non-segmental consolidations (also described as "negative pulmonary edema"), a "reversed halo sign," ground-glass opacities, nodular densities, and a crazy-paving pattern are described in association with EP.

### 2.3 Lung Injury Due to Neural or Humoral Mechanisms

Acute pulmonary edema and drug-induced asthma belong to this category and can be caused by numerous medications. In patients with edema, the capillary permeability is disturbed either directly or indirectly by false signals from the hypothalamus and brainstem. The systemic release of cytokines induced by chemotherapeutic agents (e.g., gemcitabine) may result in capillary leakage and pulmonary edema. Pulmonary edema induced by drugs can be more diffuse in comparison with pulmonary edema seen in heart failure, which is most often located perihilar and in the gravity-dependent lung regions. Mostly however, the drug-induced forms of edema are indistinguishable from other forms of edema.

### 2.4 Lung Injury Induced by Autoimmune Mechanisms

Drugs can induce autoimmune reactions like lupus erythematodes and vasculitis; however, this is rarely caused by cytostatic drugs. Most often they are caused by drugs such as procainamide, hydralazine, or phenytoin.

### 2.5 Drug-Induced Pulmonary Granulomatosis

Pulmonary manifestations include granulomatous vasculitis and granulomatous pneumonitis. The former is seen in drug addicts after intravenous injection of talcosis, which triggers an intrapulmonary foreign body reaction. Radiologically, you see small nodules that may coalesce later to fibrosis mainly in the perihilar area, associated with large bullae and signs of pulmonary hypertension. A number of drugs including interferon, nitrofurantoin, cocaine, methotrexate, and sirolimus can trigger a sarcoid-like granulomatosis, which have similar radiological findings as usual sarcoidosis. Small nodules are seen in a peribronchovascular distribution mostly in the upper lobes, accompanied by symmetric hilar and mediastinal lymphadenopathy.

## 3 Specific Cytotoxic Agents

In the following, we describe some of the mostly used cytotoxic agents and their potential lung-damaging effect (Foucher and Camus 2008).

### 3.1 Cyclophosphamide

Cyclophosphamide is used for treatment of malignancies (e.g., Hodgkin, follicular non-Hodgkin lymphoma, large B-cell lymphoma, lung or breast cancer) but also for immunosuppression in anti-neutrophil cytoplasmic antibody-associated granulomatous vasculitis (granulomatosis with polyangiitis), lupus erythematodes, or glomerulonephritis. The CT patterns most often seen are DAD or NSIP, rarely OP. Lung changes are not dose related and may develop more than a decade after the administration of cyclophosphamide (on average 3.5 years) (Fig. 1). A diffuse lung bleeding is a rare complication of cyclophosphamide presenting with diffuse consolidations and not necessarily hemoptysis. An underlying vasculitis needs to be excluded.

### 3.2 Bleomycin

Bleomycin is used for the treatment of squamous cell carcinoma, testicular carcinoma, or lymphomas. Bleomycin – if intratracheally applied in an animal model – leads to a rapidly progressive lung

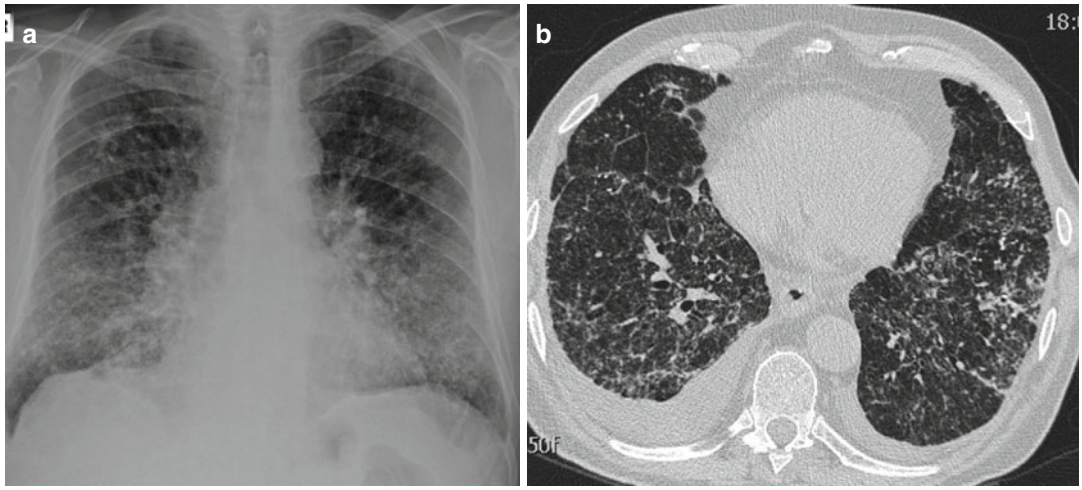


**Fig. 1** A 56-year-old patient with chronic lymphatic leukemia treated with *cyclophosphamide*, who developed widespread nodular densities and bihilar lymphadenopathy seen on a CXR (**a**). CT shows fine nodular pattern – some of them in a perilymphatic distribution – combined with reticular densities and ground glass. Additionally, there was emphysema and bilateral pleural effusion (**b**)

fibrosis. Also in humans there is a significant risk for fibrosing lung damage limiting application and dosage. Of all chemotherapeutics, bleomycin shows the strongest lung toxicity. There is dose dependency with a significantly increased risk for lung damage above a cumulative dose of 450 units. There is also a strong additive risk with increasing age, oxygen therapy, radiation therapy, or treatment for cancer recurrencies. A high intra-alveolar oxygen level, e.g., during anesthesia, strongly increases the lung toxicity of bleomycin. DAD is by far the most common pattern and the prognosis is poor. Spontaneous pneumothorax, extensive subcutaneous emphysema, and pneumomediastinum are known complications (Araujo et al. 2013) (Fig. 2). Also OP and EP are seen (Fig. 3). Rarely nodules usually <3 cm are seen, which are indistinguishable from metastases based on imaging features (Foucher and Camus 2008).

## 3.3 Methotrexate

Methotrexate is not only used for the treatment of malignancies (lung, breast, neck, nose, and throat, non-Hodgkin lymphoma) but also for immunosuppression in patients with psoriasis and rheumatoid arthritis (RA). There is no dose dependence of potential lung injury. Risk of lung damage is higher in patients treated for malignancies than for RA. Male gender, smoking, and preexisting lung fibrosis represent risk factors for a methotrexate lung in RA. Methotrexate pneumopathy is mostly reversible, and since it is associated with serum eosinophilia, it is considered a hypersensitivity reaction. The CT pattern is highly variable, but most commonly an NSIP pattern is seen. OP and DAD are much rare. Hypersensitivity pneumonitis can be seen with or without associated lymphadenopathy. In patients with rheumatoid arthritis that manifest with acute respiratory failure, the presence of a so-called methotrexate lung needs to be considered. In patients presenting with newly developed ground-glass opacity, infection (e.g., *Pneumocystis jirovecii*), edema, or an acute exacerbation of preexisting lung fibrosis should be excluded. Based on CT alone, the differentiation can be very difficult requiring other diagnostic tests such as polymerase chain reaction and BAL. Prognosis is good with appropriate treatment.

## 3.4 Fludarabine

Fludarabine is widely used for treatment of chronic lymphocytic leukemia and non-Hodgkin

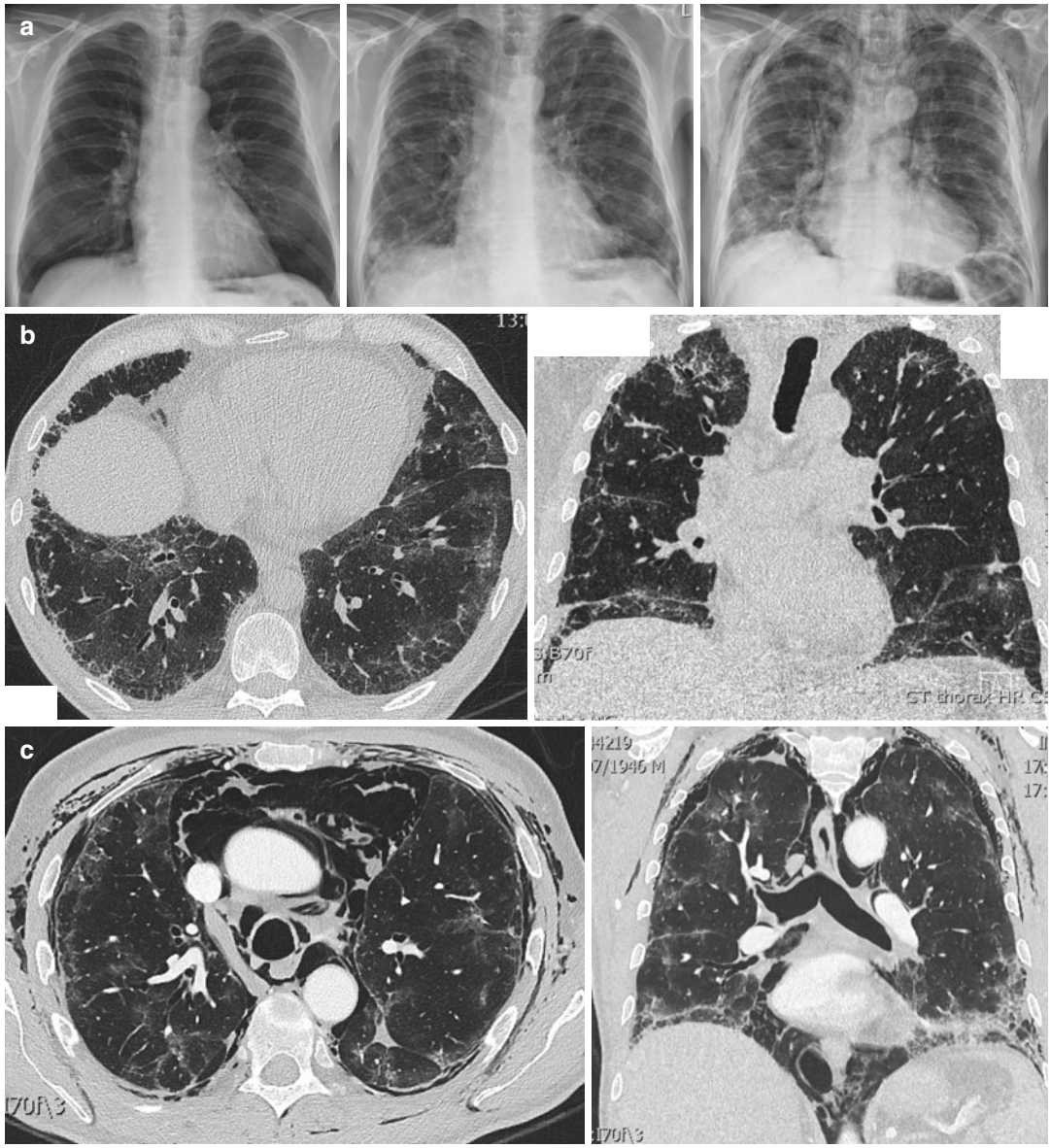


**Fig. 2** A 64-year-old patient treated with *bleomycin* for non-Hodgkin lymphoma. (**a**) Chest X-ray changed from unremarkable to sudden onset of widespread interstitial markings, further complicated by spontaneous mediastinal and subcutaneous emphysema 1 week later. The patient did not undergo mechanical ventilation. (**b**) At onset, CT shows widespread ground glass associated with reticular densities and focal consolidations. There is widening of the bronchi but no extensive architectural distorsion. (**c**) One week later the patient developed extensive mediastinal and subcutaneous emphysema. Air expanded per continuitatem in the pleural space but no collapse of the lung was seen

lymphoma. Fludarabine is frequently given together with rituximab and cyclophosphamide.

Fludarabine causes severe bone marrow suppression. The most well-described effects on the lung are therefore opportunistic pulmonary infections. Little is known about fludarabine-induced interstitial lung disease. A few case reports have been published with poorly defined interstitial or eosinophilic pneumonitis, suspected to be related to fludarabine use (Dimopoulou et al. 2006). There has been one

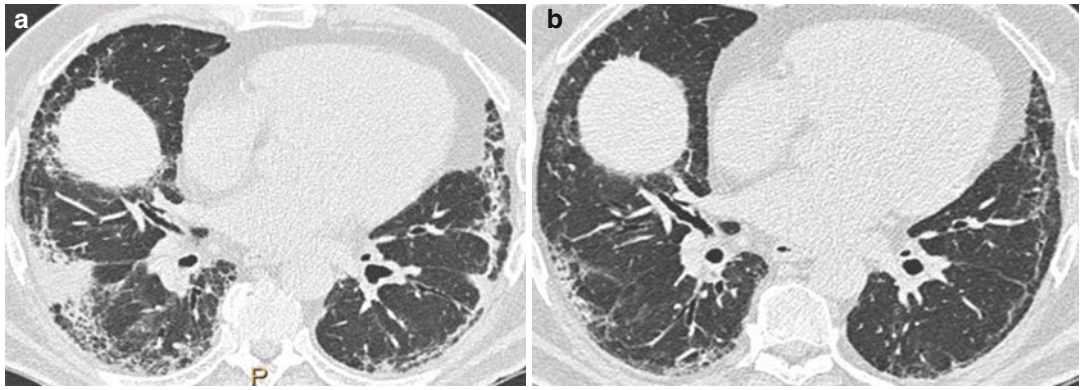


**Fig. 3** A 62-year-old woman treated with *bleomycin* for non-Hodgkin lymphoma. She developed sharply demarcated consolidations, mainly located at the lung base and following a lobular pattern typical for organizing pneumonia (**a**). Discontinuation of treatment and initiation of corticosteroid therapy resulted in fast, almost complete regression of the consolidations leaving subtle findings resembling an NSIP pattern (**b**)

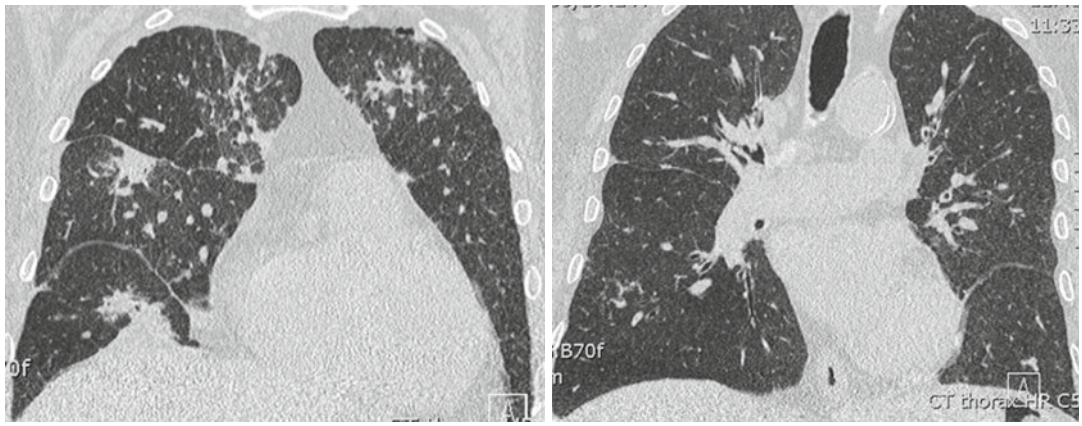

**Fig. 4** A 68-year-old woman suffering from a pancreas tumor and treated with *gemcitabine* developed bilateral sharply defined consolidations and peribronchial nodular densities representing an organizing pneumonia pattern. Additionally, there was patchy widespread ground glass and some reticular markings (**a**). Infection was excluded by bronchoalveolar lavage. CT performed 2 months later confirmed reversibility of the pulmonary findings (**b**)

case-control study published (Helman et al. 2002) showing an incidence of fludarabine-related pulmonary toxicity of 8.6 % ($n$=9/105), developed during treatment. All patients had interstitial and/or alveolar infiltrates on plain chest X-ray and/or computed tomography, while infection was excluded. Biopsy specimen revealed chronic interstitial inflammation and fibrosis, DAD, OP, or noncaseating granulomas.

## 3.5 Gemcitabine

Gemcitabine belongs to the group of antimetabolites (nucleoside analogue). It is used for treatment of pancreatic cancer, non-small cell lung cancer, breast cancer (in combination with paclitaxel), bladder cancer (in combination with cisplatin), or ovarian cancer (in combination with carboplatin). Although dyspnea is often reported within the first hours of infusion, interstitial lung diseases (ILD) are seen in <1.4 %, and there is no reported dose dependency. If an ILD is suspected, the CT findings can be highly variable ranging from NSIP, DAD, to pulmonary edema or HP (Dimopoulou et al. 2006; Tamura et al. 2013; Ioka et al. 2013; Vahid and Marik 2008) (Fig. 4). Though a rare complication, also cases with fatal veno-occlusive disease have been reported under treatment with gemcitabine.

### 3.6 Oxaliplatin

Oxaliplatin is classified as an "alkylating agent," widely used to treat metastasized colon or rectal cancer, often given in combination with other anticancer drugs. Combined chemotherapeutic regimens in conjunction with oxaliplatin are considered safe and effective treatment options and are rarely associated with pulmonary toxicity. Widespread bilateral consolidations caused by granulomatous lung disease have been reported as well as acute fibrotic complications ranging from an acute NSIP pattern with predominantly ground-glass opacities to severe fibrotic changes with traction bronchiectasis. Treatment with high-dose steroids and immunosuppressants is mostly successful, though also fatal outcome has been described in the literature and caution is recommended in patients with preexisting interstitial lung disease.

## 4 Molecular-Targeted Therapy

Traditional cytotoxic chemotherapies usually kill rapidly dividing cells in the body by interfering with cell division. Molecular-targeted therapy involves drugs designed to interfere with specific molecules necessary for tumor growth and progression. A primary goal of targeted therapies is to treat malignancies with more precision and potentially fewer side effects.

They can be classified as monoclonal antibodies (typically ending in "mab") or small molecules (typically ending in "ib") (Nicolaides et al. 2010; Abramson et al. 2013).

### 4.1 Rituximab

Rituximab is a monoclonal antibody with high affinity for CD20 surface antigens expressed by normal pre-B- and B-lymphocytes but not by stem or plasma cells. It is therefore mainly used to treat non-Hodgkin lymphoma and chronic lymphocytic leukemia without compromising humeral immunity. Although the incidence of rituximab-induced interstitial lung disease was estimated to be very rare by the manufacturer (<0.03 %), more recent studies reported an incidence of 3.5–11 % (Cha et al. 2013; Iu et al. 2008; Nieuwenhuizen et al. 2008). The CT pattern most often described is (sub)acute OP followed by NSIP (Lioté et al. 2010).

### 4.2 Cetuximab

Cetuximab is a monoclonal antibody that specifically binds to epidermal growth factor receptor (EGFR) and inhibits downstream signaling. It is approved for EGFR-positive, unresectable advanced, or recurrent colorectal cancer. Drug-induced lung injury was seen in 1.2 % with a higher incidence in elderly patients and in patients with preexisting interstitial lung disease. Patients with early onset (<90 days after starting therapy) had a higher mortality than patients with late onset (>90 days). The CT pattern ranges from ground-glass opacity or NSIP to focal organizing pneumonia or severe and widespread pattern of DAD/ARDS (Satoh et al. 2014).

### 4.3 Bevacizumab

Bevacizumab is a recombinant, humanized monoclonal antibody, which binds to and neutralizes vascular endothelial growth factor to inhibit angiogenesis. It is among others used in the treatment of metastatic breast and colon cancer, non-small cell lung cancer, and renal cell carcinoma. Bevacizumab-induced interstitial lung disease is rare (<1 % (Kang et al. 2012)). Bevacizumab is predominantly complicated by hypertension, which occurs in 22–26 % of patients. Other known adverse effects are symptomatic congestive heart failure, venous/arterial thromboembolic events, and massive life-threatening hemoptysis with a reported incidence of <5 % (Senkus and Jassem 2011; Choueiri et al. 2011). When also asymptomatic heart failure is included, incidence numbers can rise up to 19 % (Hall et al. 2013). Especially patients who have used cytostatic drugs prior or simultaneously are at risk, and evaluating patients' cardiac status before administering bevacizumab is strongly recommended.

### 4.4 Everolimus

Everolimus is an oral mammalian target of rapamycin (mTOR) inhibitor and is critical in cellular proliferation, survival, and angiogenesis (Peddi et al. 2014). It is currently used in the treatment of metastatic renal cell cancer and non-small cell lung cancer and evaluated in metastatic breast cancer, gastric cancer, hepatocellular carcinoma, neuroendocrine tumors, and non-Hodgkin lymphoma. Most reported side effects of mTOR inhibitors are dermatologic or gastrointestinal (Dy and Adjei 2013). Interstitial lung disease was reported in a meta-analysis in cancer patients with an incidence of 10.4 % (Iacovelli et al. 2012); however, outliers are reported with up to 46 % when everolimus is applied daily (Ellard et al. 2009). Similarly to gefitinib, there are suggestions for an increased risk to develop interstitial lung disease caused by everolimus in males and in the Japanese population (Nozawa et al. 2015). The CT patterns of lung injury are very variable: most often described are ground-glass opacities and parenchymal consolidations mostly seen at the lung bases (White et al. 2009) (Fig. 5). Most patients experience a low-grade pneumonitis with good prognosis, but also OP, HP, or granulomatous changes and more serious events of AIP have been described (Nieuwenhuizen et al. 2008; Peddi et al. 2014).

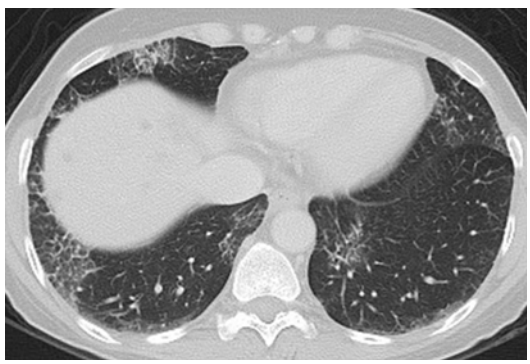

**Fig. 5** A 42-year-old patient treated with e*verolimus* for a metastatic breast tumor, showing subtle ground-glass opacities and some thickened interlobular septa mainly at the lung base in the dependent part of the lower lobes and ventrally in middle lobe and lingula

### 4.5 Erlotinib

Erlotinib is an epidermal growth factor receptor tyrosine kinase inhibitor and inhibits cell proliferation. It is mainly used in the treatment of non-small cell lung cancer, although it also has been used for treatment of metastatic pancreatic cancer. Most frequent side effects of erlotinib are skin rash and gastrointestinal complaints. Although rare but potentially fatal, a widespread interstitial lung disease can been seen with the radiological/clinical image of DAD/ARDS. The CT findings range from ground-glass opacity with or without septal thickening to multifocal consolidations with traction bronchiectasis. Both a recently published meta-analysis (Shi et al. 2014) and a review (Dy and Adjei 2013) reported an incidence of <1 % for pulmonary complications caused by erlotinib. The risk for drug-induced interstitial lung disease is higher in smokers and in patients with preexisting lung disease (Fig. 6). Drug-induced interstitial lung changes are seen more frequently with small molecules erlotinib and gefitinib than with cetuximab or panitumumab (Table 3).

### 4.6 Taxane Drug Class

Paclitaxel and docetaxel belong to the group of taxane drugs, which are used for treatment of breast, ovarium, and lung cancer. Therapy with anti-TNF-alpha or docetaxel may lead to a transudative pleural effusion, which is indistinguishable from parainfectious pleural effusion or effusion caused by the underlying disease; thus, it should not be necessarily interpreted as disease progression.

Paclitaxel is described to cause an acute pneumonitis 1 week to 2 months after therapy, which in most cases is mild and decreases under prednisone therapy. A more aggressive fibrosis is very rare. A hypersensitivity reaction as underlying pathomechanism is considered given the fact that also cases with hypotonus and bronchoconstriction have been described.

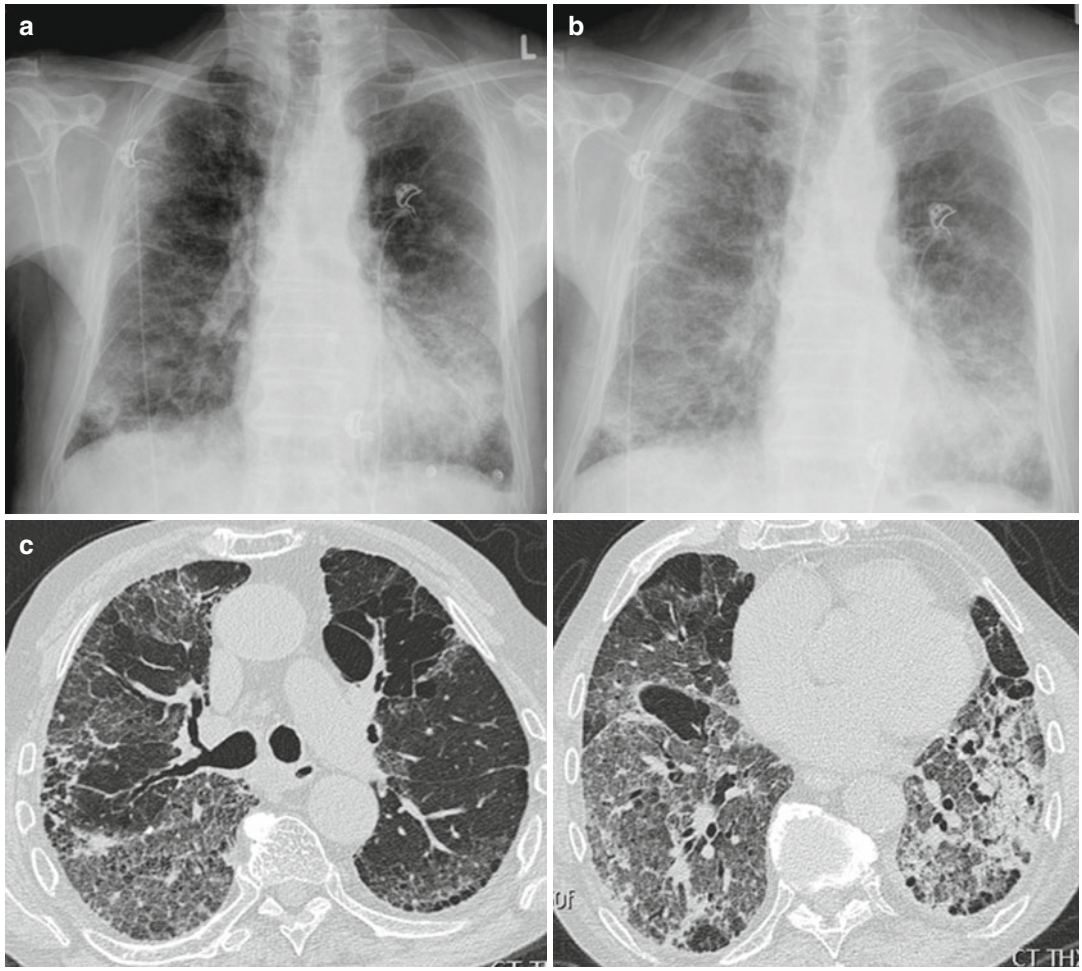


**Fig. 6** A 74-year-old patient with a non-small cell lung cancer and preexisting COPD and under treatment with *erlotinib*. Asymmetric consolidation in the left lower lobe was initially treated as pneumonia with antibiotics (**a**). Follow-up of CXR 5 days later (**b**) shows widespread bilateral opacifications. The CT at that time (**c**) demonstrates widespread diffuse increased density with crazy paving and consolidations. Findings were interpreted as diffuse alveolar damage (DAD). Patient died some days later

## 5 Secondary Lung Pathology Under Immunosuppression

A number of other lung diseases occurring during chemotherapy have to be differentiated from drug-induced lung disease. They may cause similar CT findings and represent specific diagnostic challenges.

### 5.1 Infection

Since chemotherapeutics have an immunosuppressive effect (opportunistic), infections represent a frequent complication and need to be differentiated from drug-induced lung disease.

#### 5.1.1 Aspergillus

Neutropenic patients have a considerably increased risk for an invasive aspergillus infection. The angioinvasive form presents with nodular mostly widely distributed opacities with or without surrounding halo caused by hemorrhage. The differentiation from a drug-induced lung disease is – given the different morphology – mostly not very difficult with the exception of specific types of T cell-associated lymphomas, which can also cause nodules surrounded by a halo. Since an aspergillus

**Table 3** Molecular-targeted therapy

| Targeted therapy | Malignancy | Incidence ILD (%) | CT pattern | Other side effects |
|---|---|---|---|---|
| Rituximab | Non-Hodgkin lymphoma<br>Chronic lymphocytic leukemia | 3.5–11 | (Sub)acute OP<br>NSIP | |
| Everolimus | Renal cell cancer<br>Non-small cell lung cancer<br>Breast cancer<br>Gastric cancer<br>Non-Hodgkin lymphoma<br>Hepatocellular carcinoma<br>Neuroendocrine tumors | 10.4–46 | Ground-glass opacities and consolidations at the lung base<br>OP<br>HP<br>Granulomatous changes<br>AIP | Dermatologic<br>Gastrointestinal |
| Bevacizumab | Breast cancer<br>Colon cancer<br>Non-small cell lung cancer<br>Renal cell cancer | <1 | ? | Hypertension<br>Congestive heart failure<br>Venous/arterial emboli<br>Massive hemoptysis |
| Erlotinib | Non-small cell lung cancer<br>Pancreatic cancer | <1 | DAD | |

infection can also present with consolidations or small peribronchovascular nodules, the most difficult differential diagnosis is a bacterial infection.

#### 5.1.2 *Pneumocystis jirovecii* Pneumonia

Patients with T cell immunosuppression are specifically prone for a *Pneumocystis jirovecii* pneumonia (PJP). The findings can be quite subtle, and a normal chest radiograph does not exclude an infection. In the acute phase, the typical CT pattern consists of diffuse ground-glass opacities, sometimes with subpleural/peripheral sparing and with areas of consolidations in a geographical distribution. Complete ground-glass opacification without subpleural sparing does not exclude PJP infection (Fig. 7). Later on, crazy-paving pattern may be seen. Up to 30 % of patients present with small cysts. Especially acute forms of drug-induced lung disease, e.g., acute methotrexate lung, can have a similar appearance. In opposite to an alveolar edema, the PJP infection lacks a ventrocaudal gradient and does not demonstrate interlobular thickening.

### 5.2 Edema

Patients under chemotherapy frequently get also infusion therapy to decrease the damage to kidneys and maintain adequate circulatory pressure. Pulmonary edema may be caused by increased capillary permeability (e.g., caused by gemcitabine), fluid overload, or cardiogenic functional impairment. CT shows diffuse or patchy ground glass or consolidations dependent on the amount of fluid, mostly in a symmetric more central/perihilar distribution. While alveolar edema is dependent on the position of the patient (e.g., ventrodorsal gradient in a patient lying on the back), an interstitial edema with thickened interlobular septa is not influenced by the patient's position. Edema in a patchy distribution can be difficult to differentiate from a patchy NSIP frequently seen in drug-related lung disease (Fig. 8). Sharp delineation by interlobular septa and acute onset are arguments in favor of edema. Pleural effusion or pericardiac effusion may represent associated findings caused by fluid overload.

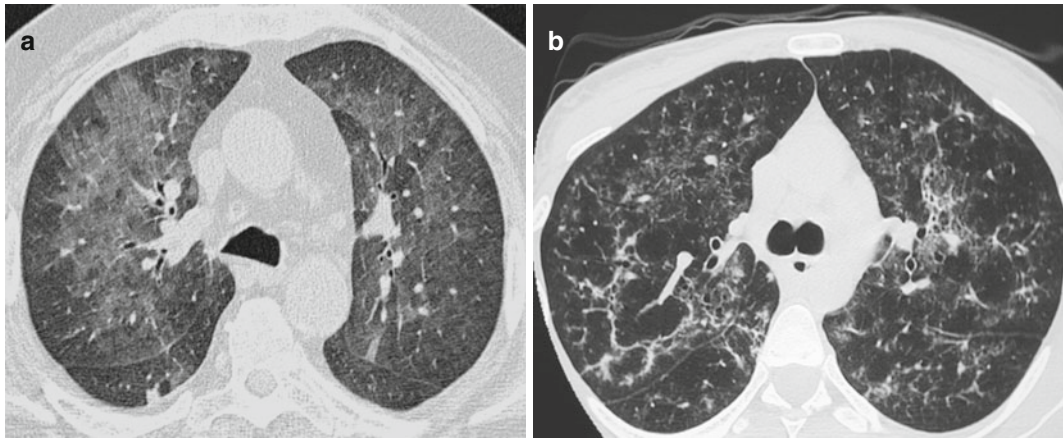


**Fig. 7** (**a**) Typical findings of an acute *Pneumocystis jirovecii* pneumonia with widespread ground-glass opacities. (**b**) In a subacute stage of infection already under treatment (different patient), the pattern changes to reticular and linear densities, which can be difficult to differentiate from an interstitial disease seen in collagen vascular diseases or drug-induced lung disease

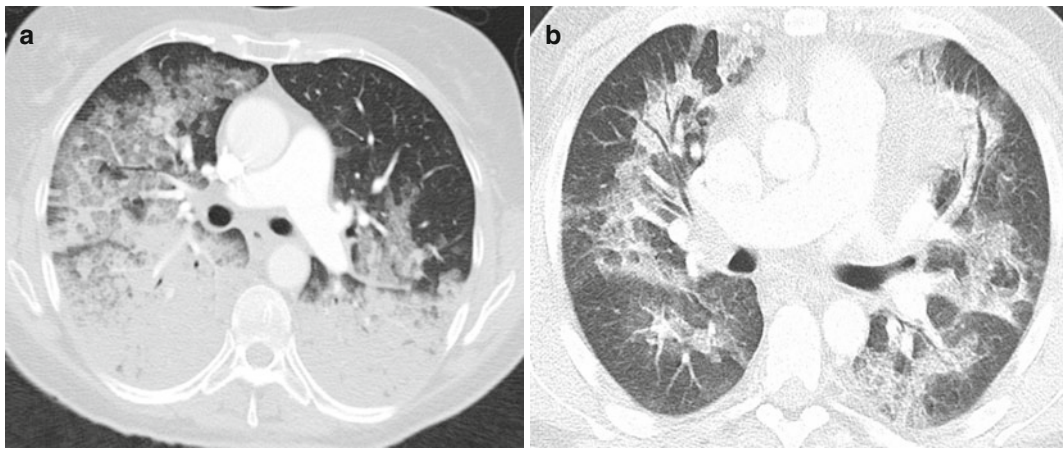


**Fig. 8** CT pattern of *pulmonary edema* is very variable and ranges from (**a**) diffuse ground-glass opacities or consolidations with a ventrodorsal gradient to (**b**) a patchy distribution of ground-glass densities. Especially the latter represents a challenging differential diagnosis: the key is mostly the more or less symmetric distribution

## 5.3 Aspiration

Dependent on the patient's status, sequelae of lung aspiration may be seen. Opacifications range from diffuse tree in bud to patchy peribronchial or confluent consolidations. In patients lying on their back, the most frequently involved parts of the lung are the upper segments of the lower lobes (right > left) and the dorsal segments of both upper lobes. Effects of aspiration (without further complication such as infection) continuously regress within few days.

## 5.4 Pulmonary Embolism

The annual incidence of venous thromboembolism in patients receiving chemotherapy is esti-

mated at 11 %. Risk can go up to 20 % or higher depending on the type of drug(s) being administered. For example, the use of bevacizumab is significantly associated with an increased risk of developing venous thromboembolism: a meta-analysis of more than 7000 patients with a variety of advanced solid tumors from 15 randomized controlled trials revealed a summary incidences of all-grade and high-grade venous thromboembolism of 11.9 % and 6.3 %, respectively (Nalluri et al. 2008).

**Conclusions**

With an increasing number of therapeutic drugs available, the list of drugs responsible for severe pulmonary disease is growing. At present there is no consensus for a definite diagnostic work-up approach. Clinical and radiological features are often difficult to distinguish from other causes of diffuse lung disease. Therefore, it is important for physicians and radiologists to be familiar with risk profiles and lung injury patterns occurring in the context of certain groups of drugs or drug combinations. The regularly updated website www.pneumotox.com provides important information and summarizes associations of drugs and lung injury patterns.

## References


Abramson RG, Abramson VH, Chan E et al (2013) Complixations of targeted drug therapies for solid malignancies: manifestations and mechanisms. AJR 200(3):475–483

Akoun GM, Cadranel JL, Rosenow EC et al (1991) Bronchoalveolar lavage cell data in drug induced pneumonitis. Allerg Immunol Paris 23(6):245–252

Araujo MS, Fernandes FL, Kay FU et al (2013) Pneumomediastinum, subcutaneous emphysema, and pneumothorax after a pulmonary function testing in a patient with bleomycin-induced interstitial pneumonitis. J Bras Pneumol 39(5):613–619

Cha SI, Choi KJ, Shin KM, Lim J, Yoo SS, Lee J, Lee SY, Kim CH, Park JY (2013) Risk factors for rituximab-induced interstitial lung diseases in patients with malignant lymphoma. Respiration 85(2):175

Choueiri TK, Mayer EL, Je Y et al (2011) Congestive heart failure risk in patients with breast cancer treated with bevacizumab. J Clin Oncol 29(6):632–638

Cleverly J, Screaton N, Hiorns M, Flint JD, Mueller NL (2002) Drug induced lung disease: high-resolution CT and histologic findings. Clin Radiol 57(4):292–299

Dimopoulou I, Bamias A, Lyberopoulos P, Dimopoulos MA (2006) Pulmonary toxicity from novel antineoplastic agents. Ann Oncol 17(3):372–379

Dy GK, Adjei AA (2013) Understanding, recognizing and managing toxicities of targeted anticancer therapies. CA Cancer J Clin 63(4):249–279

Ellard SL, Clemons M, Gelmon KA et al (2009) Randomized phase II study comparing two schedules of everolimus in patients with recurrent/metastatic breast cancer: NCIC Clinical Trials Group IND.163. J Clin Oncol 27(27):4536–4541

Ellis SJ, Cleverley JR, Mueller NL (2000) Drug induced lung disease: high resolution CT findings. AJR 175(4): 1019–1024

Erasmus JJ, McAdams HP, Rossi SE (2002) Drug induced lung injury. Semin Roentgenol 37(1):72–81

Foucher P, Camus P (2008) Pneumotox online: the drug induced lung diseases. See: www.pneumotox.com

Hall PS, Harshman LC, Srinivas S, Witteles RM (2013) The frequency and severity of cardiovascular toxicity from targeted therapy in advanced renal cell carcinoma patients. JACC Heart Fail 1(1):72–78

Helman DL Jr, Byrd JC, Ales NC, Shorr AF (2002) Fludarabine-related pulmonary toxicity: a distinct clinical entity in chronic lymphoproliferative syndromes. Chest 122(3):785–790

Hitchen L (2006) Adverse drug reactions result in 250.000 UK admissions a year. BMJ 332(7550):1109

Iacovelli R, Palazzo A, Mezi S, Morano F, Naso G, Cortesi E (2012) Incidence and risk of pulmonary toxicity in patients treated with mTOR inhibitors for malignancy. A meta-analysis of published trials. Acta Oncol 51(7): 873–879

Ioka T, Katayama K, Tanaka S, Takakura R, Ashida R, Kobayashi N, Taniai H (2013) Safety and effectiveness of gemcitabine in 855 patients with pancreatic cancer under Japanese clinical practice based on post-marketing surveillance in Japan. Jpn J Clin Oncol 43(2):139–4015

Iu X, Hong XN, Gu YJ, Wang BY, Luo ZG, Cao J (2008) Interstitial pneumonitis during rituximab-containing chemotherapy for non-Hodgkin lymphoma. Leuk Lymphoma 49(9):1778–1783

Kang HJ, Park JS, Kim DW et al (2012) Adverse pulmonary reactions associated with the use of monoclonal antibodies in cancer patients. Respir Med 106(3):443–450

Kudoh S, Kato H, Nishiwaki Y et al (2008) Japan Thoracic Radiology group interstitial lung disease in patients with lung cancer: a cohort and nested case-control study. Am J Resp Crit Care Med 177(12):1348–1357

Limper A, Rosenow E (1996) Drug induced interstitial lung disease. Curr Opin Pulm Med 2(5):396–404

Lioté H, Lioté F, Séroussi B, Mayaud C, Cadranel J (2010) Rituximab-induced lung disease: a systematic literature review. Eur Respir J 35(3):681–687

Mueller NL, White DA, Jiang H, Gemma A (2004) Diagnosis and management of drug associated interstitial lung disease. Br J Cancer 91(Suppl 2):S24–S30

Myers JL, Limper AH, Swensen SJ (2003) Drug induced lung disease: a pragmatic classification incorporating HRCT appearances. Sem Resp Crit Care Med 24(4): 445–454

Nalluri SR, Chu D, Keresztes R, Zhu X, Wu S (2008) Risk of venous thromboembolism with the angiogenesis inhibitor bevacizumab in cancer patients: a meta-analysis. JAMA 300(19):2277–2285

Nicolaides NC, Sass PM, Grasso L (2010) Advances in targeted therapeutic agents. Expert Opin Drug Discov 5(11):1123–1140

Nieuwenhuizen L, Verzijlbergen FJ, Wiltink E, Grutters JC, Biesma DH (2008) A possible role of 18F-FDG positron-emission tomography scanning in the early detection of rituximab-induced pneumonitis in patients with non-Hodgkin's lymphoma. Haematologica 93(8):1267–1269

Nozawa M, Ohzeki T, Tamada S et al (2015) Differences in adverse event profiles between everolimus and temsirolimus and the risk factors for non-infectious pneumonitis in advanced renal cell carcinoma. J Immunother 38(7):285–91. doi: 10.1097/CJI.0000000000000090

Oya N, Sasai K, Tachiiri S et al (2006) Influence of radiation dose rate and lung dose on interstitial pneumonitis after fractionated total body irradiation: acute parotitis may predict interstitial pneumonitis. Int J Hematol 83(1):86–91

Peddi PF, Shatsky RA, Hurvitz SA (2014) Noninfectious pneumonitis with the use of mTOR inhibitors in breast cancer. Cancer Treat Rev 40(2):320–326

Rossi SE, Erasmus JJ, McAdams HP, Sporn TA, Goodman PC (2000) Pulmonary drug toxicity: radiologic and pathologic manifestations. Radiographics 20:1245–1259

Satoh T, Gemma A, Kudoh S et al (2014) Incidence and clinical features of drug induced lung injury in patients with advanced colorectal cancer receiving cetuximab: results of a prospective multicenter registry. Jap J Clin Oncol 44(11):1032–3039

Schwaiblmair M, Behr W, Haeckel T et al (2012) Drug induced interstitial lung disease. Open Respir Med J 6:63–74

Senkus E, Jassem J (2011) Cardiovascular effects of systemic cancer treatment. Cancer Treat Rev 37(4): 300–311

Shi L, Tang J, Tong L, Liu Z (2014) Risk of interstitial lung disease with gefitinib and erlotinib in advanced non-small cell lung cancer: a systematic review and meta-analysis of clinical trials. Lung Cancer 83(2): 231–239

Silva CIS, Mueller NL (2006) Drug induced lung diseases: most common reaction patterns and corresponding high-resolution CT manifestations. Semin Ultrasound CT MR 27:111–116

Simpson A, Paul J, Graham J et al (1998) Fatal bleomycin pulmonary toxicity in the west of Scotland 1991-1995: a review of patients with germ cell tumors. Br J Cancer 78(8):1061–1066

Tamura M, Saraya T, Fujiwara M et al (2013) High-resolution computed tomography findings for patients with drug induced pulmonary toxicity, with special reference to hypersensitivity pneumonitis-like patterns in gemcitabine-induced cases. Oncologist 18(4):454–459

Vahid B, Marik PE (2008) Pulmonary complications of novel antineoplastic agents for solid tumors. Chest 133(2):528–538

Walsh SL, Hansell DM (2014) High-resolution CT of interstitial lung disease: a continuous evolution. Semin Respir Crit Care Med 35(1):129–144

White DA, Schwartz LH, Dimitrijevic S, Scala LD, Hayes W, Gross SH (2009) Characterization of pneumonitis in patients with advanced non-small cell lung cancer treated with everolimus (RAD001). J Thorac Oncol 4(11):1357–1363

# Part V

# Cardiovascular System

# Cardiovascular Toxicity and Monitoring Methods in Oncologic Patients

Maxim Avanesov, Andreas Block, and Gunnar K. Lund

## Contents



**Abstract**

Therapy of oncologic diseases requires a profound knowledge of the wide spectrum of available anticancer drugs and the ability of the oncologist to weigh the pros and cons of each medication in every single case individually to maintain a high standard of oncologic therapy.

Besides common side effects of anticancer drugs as headache, nausea, and diarrhea, adverse cardiovascular effects are, though less common, a crucial limitation with regard to the acceptance and continuation of the often long-standing therapy. Therefore, an appropriate choice of a single or multidrug medication, considering its special risks for cardiovascular side effects, is essential for preventing a preterm cancelation of a pivotal therapy.

This chapter offers an overview of widely used anticancer drugs, focusing on its certain cardiovascular effects, the possibility of cardioprotection, as well as important risk factors of treated patients, possibly boosting adverse cardiac effects.

Moreover, this chapter outlines commonly used monitoring methods for an appropriate surveillance, including those for high-risk oncologic patients with heart failure or arterial

M. Avanesov (✉) • G.K. Lund
Department of Diagnostic and Interventional Radiology, Center for Radiology and Endoscopy, University Medical Center Hamburg-Eppendorf, Hamburg, Germany
e-mail: m.avanesov@uke.de; g.lund@uke.de

A. Block
Department of Internal Medicine II and Clinic (Oncology Center), Center for Oncology, University Medical Center Hamburg-Eppendorf, Hamburg, Germany
e-mail: block@uke.de

Med Radiol Diagn Imaging (2015)
DOI 10.1007/174_2015_1053, © Springer International Publishing Switzerland

hypertension, and provides different treatment options in cases of manifest cardiovascular side effects.

## Abbreviations

| | |
|---|---|
| 5-FU | 5-Fluorouracil |
| ACE | Angiotensin-converting enzyme |
| BCR-ABL | Break-point cluster-Abelson |
| BMI | Body mass index |
| CHF | Congestive heart failure |
| CML | Chronic myeloid leukemia |
| CMR | Cardiac magnetic resonance imaging |
| CRCD | Chemotherapy-related cardiac dysfunction |
| ECE-1 | Endothelin-converting enzyme 1 |
| ECG | Electrocardiography |
| FDA | Food and Drug Administration |
| GIST | Gastrointestinal stromal tumor |
| HER2/erbB2 | Human epidermal growth factor receptor 2 |
| HERA | Herceptin adjuvant trial |
| LV | Left ventricle |
| LVEF | Left ventricular ejection fraction |
| NSCLC | Non-small-cell lung carcinoma |
| NYHA | New York Heart Association |
| PEG | Polyethylene glycol |
| RR | Relative risk |
| TDI | Tissue Doppler imaging |
| TKI | Tyrosine kinase inhibitor |
| VEGF | Vascular endothelial growth factor |

## 1 Introduction

Oncologic diseases are, after cardiovascular diseases, the second most common cause of death in Europe (European health report 2012). Consequently, much effort has been done to improve the number and efficacy of the available chemotherapeutics and to enhance the tolerability of these drugs. The ongoing improvement of the drug efficacy led to a continuous decrease of the mortality and morbidity of cancer patients. Additionally to the classic cytotoxic chemotherapeutics, newer anticancer drugs have successfully been introduced, i.e., several signaling inhibitors with more specific efficacy for a more individualized treatment of certain cancer types. Nevertheless, the majority of the currently used chemotherapeutics can have serious side effects, and some drugs even irreversibly impair the cardiovascular system, so that the use of this modern cancer therapy can be limited. These cardiovascular adverse effects include arrhythmias, induction of myocardial ischemia, progressive heart failure, myocardial dysfunction or arterial hypertension, vasculitis of small and large vessels, and venous or arterial thrombosis. Ewer and Lippman observed that some chemotherapeutics induced a dose-dependent, mainly irreversible cardiotoxicity, while others are dose independent and mainly cause reversible cardiac injury ((Ewer and Lippman 2005), Table 1). These authors proposed a new classification of chemotherapy-related cardiac dysfunction (CRCD) primarily based on the reversibility of the cardiotoxicity ((Ewer and Lippman 2005), Table 2). The side effects of the commonly used chemotherapeutics have to be kept in mind to perform a balancing act – to choose for each patient the drug that is mostly effective for a certain cancer type and to lower the risk of possible cardiovascular side effects to a minimum regarding several risk factors of each patient at the same time (Table 3).

The proper management of the cancer therapy is therefore crucial for an improvement in longevity and quality of life for all cancer patients. In the following we will describe in detail the cardiotoxic effects of the most commonly used chemotherapies, give an overwiev of commonly applied protection methods and possibilities of monitoring as well as treatment options in affected patients.

## 2 Cardiotoxicity of Specific Anticancer Drugs

### 2.1 Anthracyclines

Anthracyclines are highly effective drugs in the anticancer therapy of lymphoma and leukemia which have been available since the 1950s with the

**Table 1** Summary of major cardiotoxic side effects of selected chemotherapeutics

| Drug class | Drug examples | Indications | Side effects | Mechanism | Dose dependency |
|---|---|---|---|---|---|
| Anthracyclines | Doxorubicin<br>Daunorubicin<br>Epirubicin<br>Idarubicin<br>Liposomal anthracyclines | Lymphoma<br>Leukemia<br>Sarcoma<br>Breast cancer<br>Ovarian cancer | Heart failure<br>Cardiac dysfunction<br>Arrhythmias | Oxygen radical formation | Yes |
| Anti-HER2/erbB2 | Trastuzumab<br>Lapatinib | Breast cancer<br>Gastric cancer | Cardiac dysfunction | HER2 signaling | No |
| Angiogenesis inhibitors/anti-VEGF | Bevacizumab<br>Sunitinib<br>Sorafenib | Gastrointestinal cancer, NSCLC<br>Renal cell carcinoma, GIST<br>Hepatocellular carcinoma | Hypertension<br>Endovascular damage | Impaired endothelial function | Yes |
| Pyrimidine analogues | Fluorouracil (5-FU)<br>Capecitabine | Colorectal cancer<br>Breast cancer | Coronary spasms/ischemia | Vasospasm | No |
| Alkylating agents | Cyclophosphamide<br>Cisplatin | Breast cancer<br>Genitourinary cancer | Myocarditis<br>Thrombosis | Endothelial dysfunction | No |
| Antimicrotubule agents | Paclitaxel<br>Docetaxel | Breast cancer, ovarian cancer, colorectal cancer | Bradycardia | Unknown | No |
| BCR-ABL inhibitors | Imatinib<br>Dasatinib<br>Nilotinib | CML<br>GIST | Periorbital/peripheral edema<br>QT↑ | Unknown | No |

**Table 2** Chemotherapy-related cardiac dysfunction (CRCD)

| | Type I (cell injury) | Type II (cell dysfunction) |
|---|---|---|
| Drug prototype | Doxorubicin | Trastuzumab |
| Findings on biopsy | Vacuoles, necrosis, sarcomere disruption | No abnormalities |
| Mechanisms of injury | Free oxygen radical formation, oxidative stress | Inhibition of HER2 signal pathway |
| Dose effects | Dose related, cumulative | No relation to dose |
| Cardiac testing | ↓EF by echocardiography – > global wall motion dysfunction | ↓EF by echocardiography – > global wall motion dysfunction |
| Effects of recurrent application | Progressive cardiac dysfunction, > severe heart failure, > cardiac death | Apparently relatively safe for recurrent application (larger study results needed) |
| Effects of CRCD therapy | Cardiac injury is *permanent and irreversible*; recurrence (months to decades) after initial application may be linked to cardiac stress | High probability of recovery in 2–4 months, *completely reversible* |

**Table 3** Risk factors for special anticancer drugs to develop a chemotherapy-related cardiac dysfunction

| Drug | Risk factors | Common cardiac side effects |
|---|---|---|
| Anthracyclines | Cumulative dose | Heart failure |
| | Preexisting heart disease | Cardiac dysfunction |
| | Age >65 | Arrhythmias |
| | Mediastinal radiation | |
| | Female gender | |
| | Arterial hypertension | |
| | Combination chemotherapy with trastuzumab, cyclophosphamide, or paclitaxel | |
| Anti-HER2/erbB2 | Prior treatment with anthracycline, chemotherapy or antihypertensive medication | Cardiac dysfunction |
| | Lower limit of normal EF prior to therapy | |
| | Advanced age | |
| | BMI of >25 kg/m$^2$ | |
| Angiogenesis inhibitors/anti-VEGF | Preexisting hypertension | Hypertension |
| | Renal cell cancer | Endovascular damage |
| Pyrimidine analogues | Prior coronary artery disease | Coronary spasms/ischemia |
| Alkylating agents | Exposure to erythropoiesis-stimulating agents | Myocarditis |
| | Central venous catheter | Thrombosis |
| | Previous treatment with anthracyclines | |
| | Prior chest irradiation | |
| | Renal impairment | |
| Antimicrotubule agents | Prior treatment with anthracyclines | Bradycardia |

extraction of daunorubicin from the soil bacterium *Streptomyces peucetius* (Di Marco et al. 1981). Since the 1960s refined agents such as doxorubicin, epirubicin, daunorubicin, and idarubicin have shown a significant improvement in relapse and mortality and have been increasingly used in the treatment of a variety of solid organ tumors and hematologic malignancies, including leukemia, lymphoma, breast cancer, lung cancer, multiple myeloma, and sarcoma (Early Breast Cancer Trialists' Collaborative Group Ebctcg 2011). However, limitations of this highly effective drug class became soon obvious – its tendency to cause cardiac adverse effects during application, especially a cumulative dose-dependent congestive cardiomyopathy with impaired left ventricular (LV) ejection fraction (EF) (Slordal and Spigset 2006). The highest risk for cardiotoxicity was found for doxorubicin ranging from 4 to 36 % at a cumulative dose of 550 mg/m$^2$ (Bovelli et al. 2010).

This progressive cardiotoxicity tends to occur after the completion of the application of anthracyclines and may be categorized in three subtypes. The first subtype occurs acutely either with a transient decrease in myocardial contractility or electrocardiographic QT interval changes, or supraventricular and ventricular arrhythmias, immediately after infusion up to 2 weeks after termination of treatment. The second subtype has an early onset, which becomes apparent from 2 weeks up to 1 year after termination of treatment and is characterized by a chronically progressive course of systolic and/or diastolic left ventricular dysfunction. The third type occurs late >1 year after completion of therapy and is also characterized by a progressive cardiotoxicity with an ongoing decline in LV function in the 10–30 years following the initial application leading to severe congestive cardiomyopathy and to death (Bovelli et al. 2010; Yeh et al. 2004). Up to 65 % of patients with a history of a childhood malignancy treated with doxorubicin can have echocardiographic evidence of left ventricular contractile impairment (Grenier and Lipshultz 1998).

Doxorubicin is a drug prototype of type I cardiotoxicity that is characterized by dose-dependent irreversible cardiomyocyte death that is observable histologically by cell necrosis, formation of vacuoles and sarcomere disruption. Several biomolecular mechanisms of the cardiotoxicity of doxorubicin have been described in detail: (1) inhibition of DNA replication and DNA transcription, (2) free oxygen radical formation leading to DNA damage and lipid peroxidation with direct membrane damage, (3) DNA alkylation and cross-linking, and (4) inhibition of topoisomerase II (Chen et al. 2007).

Among all proposed mechanisms, free oxygen radical formation is accepted as the main cause for oxidative stress leading to activation of kinase pathways that trigger apoptotic pathways by the release of cytochrome C from mitochondria into cytoplasm, resulting in activation of caspases (Gewirtz 1999). The high metabolic activity of the myocardium is one reason for the high cardiac susceptibility to anthracycline injury. The high concentration of cardiolipin in myocytes and its high affinity for anthracyclines explain furthermore the cardiac susceptibility with a direct binding of this drug to the mitochondrial phospholipid and disruption of the association of inner mitochondrial membrane proteins with cardiolipin (Scully and Lipshultz 2007).

Clinical studies have shown that the most important factor for late cardiac toxicity is the cumulative dose of anthracyclines. It is presumed that each application of anthracyclines causes cardiomyocyte death and that these damages are balanced by compensatory mechanisms until a certain threshold is reached, above which progressive LV dysfunction occurs (Barrett-Lee et al. 2009).

In addition to the cumulative dose, other risk factors have been identified that increase the risk of anthracycline-induced cardiotoxicity, including both extremes of age, children as well as old patients >60 years; female gender; prior mediastinal radiation therapy; hypertension; concomitant treatment with cyclophosphamide, trastuzumab, or paclitaxel; and preexisting cardiac disease (Slordal and Spigset 2006; Von Hoff et al. 1979).

As a consequence, anthracycline treatment should be only performed under close monitoring of cardiac function, including ECG and echocardiography with measurements of LVEF (Bovelli et al. 2010) and respecting generally recommended maximal cumulative doses of drugs, which are defined for the following drugs: doxorubicin, 400–450 mg/m$^2$; daunorubicin, 600 mg/m$^2$; idarubicin, 100 mg/m$^2$; and epirubicin, 800–900 mg/m$^2$ (Slordal and Spigset 2006; Keefe 2002). However, the risk of cardiac dysfunction might be observed at much lower cumulative doses in patients with coexisting cardiovascular risk factors (Ryberg et al. 2008).

Additionally, cardiac biomarkers like troponin should be used for therapy monitoring because they might help to identify myocardial damage early and there is a strong relation between the prolonged troponin release after high-dose chemotherapy and poor cardiac outcome (Cardinale et al. 2000, 2006).

Cardiotoxicity is the main limitation of the treatment with anthracyclines, and this side effect was likely the greatest stimulus to improve the drug application and to find new, less-cardiotoxic alternatives.

### 2.1.1 Cardioprotection from Anthracycline-Induced Cardiotoxicity

Several approaches have been proposed to reduce anthracycline cardiotoxicity and increase tumor response:

1. Intravenous application of modified liposomal-encapsulated anthracyclines by additional molecular attachment of polyethylene glycol (PEG)-coated liposomes around the original anthracycline molecules, called pegylated anthracyclines. They decrease the circulating concentrations of free doxorubicin and increase the selective uptake of the anthracyclines in tumor cells. Consequently, it leads to a lower rate of heart failure compared to application of conventional anthracyclines (9 % vs. 25 %, $p<0.0001$) after a follow-up of >1 year (Van Dalen et al. 2010).
2. In patients with increased plasma levels of troponin I during treatment and consequently with a higher risk of development of chronic anthracycline-induced cardiotoxicity, a treatment with angiotensin-converting enzyme (ACE) inhibitors (Cardinale et al. 2006) and carvedilol (Kalay et al. 2006) in patients receiving high doses of doxorubicin (>500 mg/m$^2$) is advisable to prevent a decline in LVEF in terms of manifestation of irreversible late cardiotoxicity. The American Heart Association guidelines recommend the use of ACE inhibitors and beta-blockers in patients with asymptomatic impairment of ejection fraction and the addition of diuretics for patients with a symptomatic heart failure (Abraham et al. 2009).
3. The use of dexrazoxane, an inhibitor of topoisomerase IIβ and intracellular iron chelator, causes a reduction in incidence and severity of anthracycline-induced congestive heart failure (indicated by elevated troponin T levels up to 21% in the doxorubicin and dexrazoxane group vs. 50 % in doxorubicin group) and adverse cardiac events in children as well as in adults (Lipshultz et al. 2004; Lyu et al. 2007). After application it is converted intracellularly into an active metal ion-binding form that creates an iron complex with free iron, thereby decreasing toxic oxygen radical damage (Lipshultz et al. 2004). This effect has been proven effective in randomized trials in patients with breast cancer, soft tissue sarcoma and lymphoblastic leukemia without evidence of lower treatment efficacy or higher rate of secondary tumors (Van Dalen et al. 2011; Cvetković and Scott 2005). The cardioprotective effect of dexrazoxane was present irrespectively of preexisting cardiac risk factors and regardless of whether the drug was applied before the first dose of anthracycline or after a cumulative doxorubicin dose of >300 mg/m$^2$ (Van Dalen et al. 2011; Cvetković and Scott 2005). Therefore, the FDA approved this protective drug for clinical use in metastatic breast cancer patients who have received a cumulative doxorubicin dose of >300 mg/m$^2$.

However, potential common cardiovascular side effects include a decrease in left ventricular ejection fraction, phlebitis, and a deep vein thrombosis. Furthermore, infections, severe myelosuppression, and a threefold increase of secondary malignancies at a later stage, e.g., lymphoma and leukemia, were observed in children, so that this drug is contraindicated in patients under 18 years (Swain and Vici 2004).

## 2.2 Anti-HER2/erbB2 Cancer Drugs

Trastuzumab is one of the most commonly used recombinant, humanized monoclonal antibodies against HER2/erbB2 receptor in breast cancer cells that improves survival in breast cancer patients with overexpressed HER2 and in patients with advanced gastric cancer (Perez et al. 2011; Bang et al. 2010).

It is a prototype of type II chemotherapy-related cardiac dysfunction (CRCD) that causes a reversible myocardial contractile dysfunction rather than an irreversible myocardial injury (type I CRCD) induced by anthracyclines.

A large multicenter randomized trial involving 5.102 women with HER2-positive early breast cancer (Herceptin Adjuvant (HERA) trial) compared to the rate and outcome of trastuzumab-associated cardiac dysfunction following 1 ($n=1.703$), and 2 years ($n=1.701$) of adjuvant trastuzumab treatment given once every 3 weeks with a control group without trastuzumab therapy ($n=1.698$). The median follow-up of the HERA trial patients was 8 years. More than 94 % of patients in all three arms of HERA received an anthracycline-based chemotherapy. The median interval between anthracycline administration and the beginning of adjuvant trastuzumab was 15.3 weeks.

Primary cardiac end points were defined as cardiac death from heart failure, myocardial infarction, documented arrhythmia, and severe congestive heart failure (CHF), defined as NYHA III/IV. The study revealed an overall low incidence of cardiac death (0 % in the 1-year arm, 0.8 % in the 2-year arm vs. 0.1 % in the observation arm), severe congestive heart failure (0.8, 0.8, and 0.0 %, respectively), and significant LVEF decrease (7.2, 4.1, and 0.9 %, respectively) (de Azambuja et al. 2014). Severe congestive heart failure (CHF) was the same for 1-year and 2-year trastuzumab. Over 80 % of all patients with new onset of LVEF decrease reached acute recovery (81.2 % receiving 1-year trastuzumab and 87.5 % receiving 2-year trastuzumab, respectively) and had a favorable long-term outcome (de Azambuja et al. 2014).

Other studies showed that the incidence of cardiac dysfunction depends on the combined use of chemotherapies and implies a relationship to it. (Yeh and Bickford 2009; Martin et al. 2009). These studies report an incidence of cardiac dysfunction from 2–8 % after treatment with trastuzumab alone compared to an incidence of 2–13 % in patients with trastuzumab plus paclitaxel. The highest rate of cardiac side effects with 28 % was observed in patients with combined therapy of trastuzumab and anthracyclines (Feldman et al. 2000; Yeh and Bickford 2009; Martin et al. 2009). However, about 80 % of the patients with trastuzumab-induced cardiotoxicity had an asymptomatic impairment of LF and responded to medical treatment. Only in one trial, a minority of patients developed a clinically relevant heart failure with a NYHA stage III–IV, which was 4.1 % in patients receiving trastuzumab and 0.8 % receiving adjuvant chemotherapy of doxorubicin followed by paclitaxel without trastuzumab (Martin et al. 2009).

Although the mechanisms that trigger cardiotoxic complications are not fully understood, HER2 signaling is thought to be pivotally involved in maintaining postnatal cardiac development, function and cardioprotection (Feldmann et al. 2000; Ferrari et al. 2009). HER2/HER4 heterodimer subsequently activates various intracellular signaling pathways, which are essential for cell growth, glucose uptake and the turnover of sarcomeric proteins (Zhao et al. 1998). These HER2 pathways are thought to be downregulated by trastuzumab (Popat and Smith 2008). Moreover, experimental studies have shown that HER2-deficient mice developed dilated cardiomyopathy. Cardiomyocytes, isolated from these mice were also susceptible to anthracycline-induced toxicity (Crone et al. 2002).

Several risk factors for trastuzumab-associated cardiotoxicity were identified, including prior treatment with anthracycline chemotherapy with a cumulative dose of >300 mg/m$^2$, need for antihypertensive medication, borderline normal or reduced EF, advanced age and an increased body mass index of >25 kg/m$^2$ (Sengupta et al. 2008). Patients predisposed to general cardiovascular risk factors such as smoking, arterial hypertension, dyslipidemia, diabetes, and obesity are more likely to experience cardiac injury after trastuzumab treatment (Suter et al. 2007). However, affected patients with cardiotoxic symptoms after treatment with trastuzumab generally improve after withholding the chemotherapeutic drug for about 1.5 months (Ewer et al. 2005).

Lapatinib is a new promising anti-HER2 drug, which is an orally active, reversible dual HER1/EGFR and HER2 tyrosine kinase inhibitor (TKI). This agent is approved for patients with trastuzumab-resistant and progressive breast cancer, as it is effective against HER2p95-positive cancer. A meta-analysis revealed low rates of cardiac events in patients, previously treated either with anthracy-

clines (2.2 %) or trastuzumab (1.7 %) or without any pretreatment with 1.5 % Perez et al. 2008. An asymptomatic decrease in EF was observed in most cases, which was reversible in 88 % of the patients. No drug-related cardiac deaths occurred among patients treated with lapatinib (Popat and Smith 2008; Joensuu et al. 2006). Most potential risk factors for cardiac events include female gender, elderly age, prior myocardial ischemia, bradycardia and pretreatment with QT-prolonging medications. However, larger studies are needed though to further investigate its potential benefit over trastuzumab and the possible application of this drug in patients with high cardiac risk.

### 2.2.1 Cardioprotection from Trastuzumab-Induced Cardiotoxicity

Several studies have shown that a concomitant administration of trastuzumab and anthracyclines led to the highest incidence of cardiac side effects up to 27 % compared to 8 % after treatment with anthracyclines alone (Yeh and Bickford 2009; Martin et al. 2009). However, a sequential application of trastuzumab after chemotherapy with the anthracyclines decreased the incidence of cardiac side effects up to 5 % (Popat and Smith 2008). It is presumed that trastuzumab acts as modulator of anthracycline-induced cardiotoxicity when administered during a time range of myocyte vulnerability following anthracycline therapy.

Therefore, trastuzumab should be given after but not concurrently with anthracyclines, and a delay of 3 months might be most beneficial to reduce the trastuzumab-induced cardiotoxicity.

Some other studies, using pre-anthracycline trastuzumab regimes, scheduled short-course trastuzumab concurrently with a non-anthracycline-based chemotherapy followed by anthracyclines in a block-sequential design. In a small randomized study of 232 patients, a prior trastuzumab treatment of patients with HER2 amplification over only 9 weeks before anthracyclines led to a significant better 3-year recurrence-free survival (89 % vs. 78 %) compared to initial application of docetaxel or vinorelbine with no cases of congestive heart failure or decreased LVEF after trastuzumab therapy (Joensuu et al. 2006).

## 2.3 Angiogenesis Inhibitors/ Anti-VEGF Drugs

A variety of solid tumors, including metastatic colorectal carcinomas, renal cell carcinomas, gastrointestinal stromal tumors, and hepatocellular carcinomas, are responding to angiogenesis inhibitors that target vascular endothelial growth factor (VEGF) by use of antibodies such as bevacizumab, sunitinib, or sorafenib (Ferrara et al. 2003; Hurwitz et al. 2004). It has been shown that this drug type increases the survival rates of treated patients (Ferrara et al. 2003; Hurwitz et al. 2004).

However, it is known that every anti-VEGF drug can induce or worsen a preexisting arterial hypertension on a dose-dependent basis. Hypertension can occur at any time during treatment and might cause acute complications including heart failure, proteinuria with renal thrombotic microangiopathy, intracerebral hemorrhage, and, although infrequently, reversible posterior leukoencephalopathy (Maitland et al. 2010). A recent meta-analysis of studies with bevacizumab reported an incidence of 23.6 % for any degree of hypertension, and almost 8 % of patients developed severe hypertension requiring more intensive therapy than previously or causing a hypertensive crisis (Ranpura et al. 2010). The application of sorafenib revealed similar incidences (23.4 % all-grade hypertension vs. 5.7 % severe hypertension) (Wu et al. 2008a), while sunitinib revealed an incidence of all-grade hypertension of 21.6 and 6.8 % high-grade hypertension within the first 4 weeks of therapy, respectively (Vaklavas et al. 2010; Zhu et al. 2009).

Thromboembolic side effects, such as myocardial infarction, ischemic cerebrovascular diseases, or pulmonary arterial embolism, are rare but life-threatening side effects of bevacizumab that have been reported to occur in up to 3.8 % of patients compared to 1.7 % in the control group (Wu et al. 2008a). The risk of venous thromboembolism in cancer patients is increased with both high (≥5 mg/kg per week, RR 1.31, $p = 0.04$) and low doses of bevacizumab (RR 1.31, $p = 0.07$) and seems to vary significantly with different

types of tumors. According to a meta-analysis, the highest risk was observed in patients with colorectal cancer with an incidence of venous thromboembolism of 19.1 %. The lowest risk for venous thromboembolism was found for renal cancer with an incidence of 3.0 % (Wu et al. 2008a; Vaklavas et al. 2010; Nalluri et al. 2008). Several retrospective meta-analysis revealed an incidence of cardiac dysfunction of 1 % after sorafenib and 4.1 % after sunitinib treatment (Force et al. 2007; Di Lorenzo et al. 2009). Patients with known coronary artery disease, pre-existing LV dysfunction, or prior application of anthracyclines, have an increased risk for sunitinib-related cardiotoxicity, indicating that such cardiac high-risk patients should be monitored carefully (Force et al. 2007).

Patients who have significant impairment of EF should be monitored after they complete their sunitinib therapy, because it is still unclear whether LV dysfunction is reversible after this therapy (Force et al. 2007; Richards et al. 2011).

In a neonatal rat myocyte model, it was demonstrated that therapeutically relevant concentrations of sorafenib caused dose-dependent damage, probably due to its lack of selectivity (Hasinoff and Patel 2010). In a phase 3 trial for renal cell carcinoma, this drug caused cardiac ischemia and infarction in 3 % of patients (Yeh et al. 2004).

The pathophysiologic backgrounds of all these cardiac side effects are still poorly understood in detail, but it is probable that the inhibition of VEGF leads to an improper endothelial function and impaired nitride oxide synthesis with consequent restriction of the peripheral vasodilatation (Richards et al. 2011).

In several tumors (e.g., advanced colorectal cancer, lung cancer, renal cell cancer), VEGF plays a crucial role in the neoangiogenesis, so high "functional" VEGF levels in certain tumor types may denote dependence of tumor growth on VEGF and predict a favorable response to anti-VEGF therapy. The same subset of patients may be particularly susceptible to developing cardiovascular toxicities, because VEGF signaling inhibition may result in vasoconstriction and microvascular rarefaction.

Patients with lower VEGF levels may be less likely to develop cardiovascular toxicities and are more likely to show a lower antitumor response.

In the future, the drug-induced arterial hypertension might become a surrogate marker for efficacy of angiogenesis inhibitors, since several changes in VEGF pathways that lead to arterial hypertension are similar to those of tumor destruction (Vaklavas et al. 2010; Chu et al. 2007; Ku et al. 1993).

### 2.3.1 Cardioprotection from Anti-VEGF-Induced Cardiotoxicity

The easiest way to prevent or to treat anti-VEGF-induced hypertension is to optimally treat a pre-existing increased blood pressure by commonly used antihypertensives, including beta-blockers and ACE inhibitors.

## 2.4 Pyrimidine Analogues

Pyrimidine analogues like 5-fluorouracil (5-FU) and its oral pre-drug capecitabine are widely used for the treatment of many solid cancers, including gastrointestinal, gynecological, and head and neck cancers. Despite the association of 5-FU with arrhythmia, ECG changes, and acute heart failure, the most severe side effect is myocardial ischemia, which can become symptomatic as angina pectoris, pericarditis, dyspnea, pulmonary edema, cardiogenic shock, sudden death and acute myocardial infarction (Mir et al. 2009). The incidence of 5-FU-induced cardiotoxicity varies in the literature from 1 to 18 % (de Forni et al. 1992). Myocardial ischemia most commonly occurs after the second or third administration of these agents and lasts up to 48 h. This side effect is not related to the cumulative dose but is higher in patients with continuous infusion. Patients with a history of prior coronary artery disease have a higher incidence of 5-FU-induced ischemic cardiac side effects (de Forni et al. 1992; Becker et al. 1999). Although the exact etiology of the cardiotoxicity remains unknown, it is probable that the toxicity is related to endothelial dysfunction and vasospasm of coronary arteries (Becker et al. 1999).

Capecitabine may also induce myocardial ischemia and ventricular arrhythmias, although it seems to be less toxic than 5-FU (Collins and Weiden 1987) with a reported incidence of cardiotoxicity of 3–9 %, including myocardial infarction, ECG abnormalities, and ventricular extrasystoles (Jensen and Sorensen 2006).

### 2.4.1 Cardioprotection from Pyrimidine Analogue-Induced Cardiotoxicity

Nitroglycerin and calcium channel inhibitors are often very effective in the treatment and prevention of myocardial ischemia. Verapamil was shown to modify the arrhythmogenic side effects of 5-FU by preventing supraventricular arrhythmias (Lestuzzi et al. 2010).

## 2.5 Alkylating Agents

Cyclophosphamide and cisplatin are common and classical alkylating agents that are widely used in the treatment of solid tumors, including lung, gastrointestinal, gynecological and head and neck cancers, skin cancer, and leukemia. Besides, cyclophosphamide is also used for treatment of autoimmune diseases refractory to steroid treatments.

In generally, cyclophosphamide is well tolerated in terms of cardiotoxicity. However, high-dose rapid administration, such as application for bone marrow transplantation, might induce lethal acute pericarditis and hemorrhagic myocarditis (Eskilsson and Albertsson 1990). Pathophysiologically, direct oxidative cardiac injury has been postulated as a leading cause of all cardiac side effects. A well-known noncardiac side effect is the development of a hemorrhagic cystitis. Unlike the anthracycline-induced cardiotoxicity, the cardiac side effects associated with cyclophosphamide seem to be related to a single dose and not cumulative doses. Moreover, one of the risk factors for developing cardiac side effects is a previous treatment with anthracyclines or a prior chest irradiation (Gottdiener et al. 1981). Furthermore, exposure to erythropoiesis-stimulating agents as well as longer-lasting central venous catheter seems to increase the risk for cardiac side effects (Taniguchi 2005).

Although the exact mechanism of the therapeutic effect of cisplatin is still not fully understood, the binding to DNA leads to the formation of inter- and intrastrand cross-links, resulting in impaired DNA synthesis and replication, leading to cell apoptosis. Other severe and dose-limiting side effects include thromboembolic events, which occurred with a relatively high incidence of 18 % within 100 days of initial drug application (Taniguchi 2005). The pathogenesis of cisplatin-associated vascular side effects could include hypomagnesaemia, increased von Willebrand factor and enothelial cell damage due to an increase of procoagulant endothelial microparticles and platelet activation. Thromboembolic events can occur in the venous and arterial system in contrast to most other thrombosis risk factors that mostly involve only the venous system (Taniguchi 2005). Renal dysfunction may also play a crucial role as a risk factor, because thromboembolic events are higher in patients with renal impairment (Moore et al. 2011). Consequently, with regard to nephro- and cardiotoxic effects, a pre- and post-therapy hydration is necessary for cisplatin administration to avoid irreversible nephrotoxicity, which potentially results in heart failure due to drug-induced hypertension.

### 2.5.1 Cardioprotection from Alkylating Agent-Induced Cardiotoxicity

Thromboprophylaxis is not routinely recommended for ambulatory cancer patients. Nevertheless, prophylactic anticoagulation with warfarin or low-molecular-weight heparin is appropriate in high-risk cancer patients, which are defined as follows: (1) hospitalized patients; (2) patients who are undergoing major surgery with starting anticoagulation before surgery and continuing for at least 7–10 days, unless contraindicated, because of active bleeding or high bleeding risk; and (3) selected patients with multiple myeloma and light-chain proteins (Monreal et al. 2006; Lyman et al. 2007).

Until now it is unknown, whether cancer patients have an altered risk of coronary thrombosis after stenting. Several trials currently investigate the potential role of prophylactic low molecular heparin in patients receiving alkylating

agents. At the moment, there are no clear guidelines for the prevention of thromboembolic events in the setting of this cancer therapy and the question of prophylactic anticoagulation remains controversial in cancer patients. Therefore, the evidence-based guidelines for non-cancer patients should be applied for patients receiving alkylating agents until larger studies are completed.

## 2.6 Antimicrotubule Agents

The taxanes, e.g., paclitaxel and docetaxel, belong to an outstanding class of anticancer agents that are used in the treatment of breast cancer, ovarian cancer, and colorectal carcinoma. Furthermore, paclitaxel is also used for drug-eluting stents and has shown promising clinical outcomes regarding in-stent restenosis. Taxanes act by promoting polymerization of tubulin, resulting in dysfunctional microtubules, which disturb cell division. The most common paclitaxel-induced cardiac side effect is bradycardia with an incidence up to 30 %, although this side effect is seldom severe and intervention is rarely necessary. Other rare manifestations of cardiotoxicity include heart block with syncope, supraventricular or ventricular arrhythmias, and myocardial ischemia through unknown mechanisms (Arbuck et al. 1993).

Additionally, taxanes may potentiate anthracycline-induced cardiotoxicity by increasing the plasma levels of doxorubicin and by promoting the formation of the metabolite doxorubicinol in cardiomyocytes, which is also cardiotoxic (Salvatorelli et al. 2006). In general, docetaxel seems to cause less cardiac side effects than paclitaxel.

### 2.6.1 Cardioprotection from Antimicrotubule Agent-Induced Cardiotoxicity

It might be advisable to prolong the interval between application of anthracyclines and taxanes to reduce the risk of increased plasma levels of doxorubicin with consecutive cardiotoxic effects. Currently, there are no clear guidelines for prevention of the often asymptomatic paclitaxel-induced bradycardia.

## 2.7 BCR-ABL Inhibitors

Agents like imatinib, dasatinib, or nilotinib belong to the group of tyrosine kinase inhibitors (TKI), which are used for treatment of chronic myeloid leukemia (CML) and gastrointestinal stromal tumors. Despite the excellent clinical outcomes, especially in CML or GIST patients, recent reports revealed that imatinib may increase the risk of heart failure (Kerkela et al. 2006). Although imatinib-induced LV dysfunction is largely reversible after finishing the treatment, persistent and irreversible heart failure has also been reported in some few cases (Turrisi et al. 2010). Other common side effects of imatinib include pleural and pericardial effusion and periorbital or peripheral edema through an unknown mechanism.

Newer BCR-ABL inhibitors like nilotinib and dasatinib can prolong the QT interval, although symptomatic manifestations were recorded in only a few patients. In a recent study, only 1.4 % of patients developed tachyarrhythmia, pain in extremities, or prolonged QT interval >480 ms during a 24-month follow-up (Kantarjian et al. 2011).

### 2.7.1 Cardioprotection from BCR-ABL Inhibitor-Induced Cardiotoxicity

Currently, there are no clear guidelines for prevention of BCR-ABL inhibitor-induced cardiotoxicity. In cases of new onset of heart failure, an adequate treatment with ACE inhibitors or angiotensin II receptor blockers and β-blockers is appropriate.

# 3 Identification of Patients at Risk and Therapeutic Monitoring

A detailed patient history focused on preexisting symptoms of heart failure and potential cardiovascular risk factors such as hypertension, diabetes, cigarette smoking, and obesity is mandatory. Furthermore, a previous treatment with chemotherapy agents should be noted.

Patients who are treated with high-risk chemotherapeutics such as *anthracyclines and taxanes* should undergo a detailed cardiovascular evaluation

prior to initialization of therapy, including electrocardiography (ECG), echocardiography, and biomarkers. A baseline ECG, troponin I value and echocardiography should be obtained before the start of treatment, and these tests should be repeated every 3 months during treatment or immediately after occurrence of clinical symptoms of cardiotoxicity. After completion of treatment, follow-up should be continued for at least 3 years (Tassan-Mangina et al. 2006). However, the monitoring schedule should be individually adapted according to the type of drug, the cumulative dose received, the length of treatment and the cardiovascular risk profile of the patient. Especially for anthracyclines with a reported prevalence of cardiotoxicity of up to 25 % at 3 years of follow-up and cumulative doses above those recommended (>500 mg/m$^2$ for doxorubicin), a short-term cardiovascular surveillance from 3 months after beginning of the therapy up to 3 years is essential in order to detect the cardiotoxic effects on anticancer therapy as soon as possible (Tassan-Mangina et al. 2006). An early identification of high-risk patients is warranted, which is a fundamental challenge for oncologists to plan an individualized antineoplastic therapeutic strategy, which is most effective and at least toxic. A recent study has shown that a decreased longitudinal strain obtained by echocardiography at baseline and a detectable high-sensitivity cardiac troponin I level at 3 months of therapy were independent predictors of the development of cardiotoxicity at 6 months after anthracyclines and trastuzumab therapy in patients diagnosed with breast cancer (Sawaya et al. 2011).

### 3.1 Management of Cancer Patients with Heart Failure or Hypertension

In case of previous chemotherapy with anthracyclines for recurrent disease or a second malignancy, all drugs within the group of anthracyclines should not be used. Other potentially cardiotoxic anticancer drugs require a dose reduction, if there is no alternative with less or nondetermined heart toxicity available.

Preexisting arterial hypertension should be managed before initiating an anticancer regimen, if the progression rate of the malignancy gives such an option. Otherwise, anticancer drugs such as regorafenib or bevacizumab should be avoided in uncontrolled hypertension. Once arterial hypertension is well controlled by antihypertensive medication, this medical precondition does not compromise the anticancer drug treatment. Nevertheless, these patients require a close monitoring of their blood pressure.

Interactions of anticancer drugs with antihypertensive drugs have to be considered when treating cancer patients. Thiotepa, an ethylenimine used for the treatment of breast, ovarian and bladder cancer, interacts with diltiazem; vinca alkaloids such as vinblastine and vincristine for the treatment of malignancies such as Hodgkin and non-Hodgkin disease, testicular cancer, leukemia and rhabdomyosarcoma do interact with several calcium channel blockers including diltiazem, verapamil, felodipine and nifedipine. When using vinblastine, an increase of plasma levels should be considered. Similar interactions with calcium channel inhibitors have been described for the taxanes, paclitaxel and docetaxel, that are used for the treatment of ovarian and breast cancer, non-small-cell lung cancer, gastric cancer, head and neck cancer and pancreatic cancer.

Platinum derivatives such as cisplatin and carboplatin interact with thiazides diuretics, while oxaliplatin does not show interactions with antihypertensive drugs.

Tyrosine kinase inhibitors such as dasatinib, imatinib and sunitinib may interact with angiotensin-converting enzyme inhibitors, angiotensin II receptor antagonists, diuretics, and calcium channel blockers. In contrast, monoclonal antibodies have not been described to interfere with antihypertensive drugs (Milan et al. 2014).

## 4 Monitoring Methods Applied in Oncologic Patients

### 4.1 Echocardiography

Echocardiography is the most commonly used tool to assess LV function to identify chemotherapeutic-induced cardiotoxicity and LVEF is the most commonly used parameter in the monitoring of cardiac toxicity. A restriction

of LVEF below the normal value of 55 % or more than 10 % below a previous measurement is pathologic and requires treatment described in the following section (Altena et al. 2009). Frequent monitoring via echocardiography is recommended before, during and after potentially cardiotoxic treatment, at intervals appropriate to the severity, and progression of the disease (Todaro et al. 2013; Buck et al. 2009).

However, measurements of LVEF alone might underestimate actual cardiac toxicity because patients with a normal LVEF can have subclinical impairment in cardiac function. Moreover, it is likely that diastolic dysfunction happens before the deterioration of systolic function so that diastolic echocardiographic parameters are probably the most sensitive to early impairment of cardiac function and patients receiving chemotherapy should be screened for diastolic LV dysfunction.

Consequently, the assessment of diastolic parameters is therefore potentially useful to identify patients at risk to develop systolic dysfunction and overt heart failure (Eidem 2008).

Commonly used diastolic measurements include the E/A ratio (peak early atrial divided by peak late atrial velocities) and recent techniques include tissue velocity imaging of the early diastole, strain, and strain rate. These contemporary techniques are reliable measures of diastolic function because they are less subject to interobserver variation than the E/A ratio (Altena et al. 2009; Wang et al. 2007).

One common newly available modality to reveal signs of early cardiac dysfunction is the tissue Doppler imaging (TDI). Tassan-Mangina et al. revealed by combined use of TDI and conventional echocardiography that significant changes in diastolic LV function occurred during long-term follow-up after completion of an anthracycline therapy (Tassan-Mangina et al. 2006). Their findings highlighted the necessity of prolonged cardiac surveillance after anthracycline therapy, because in up to 25 % of patients, LVEF impairment occurred after 3 years of completion of this chemotherapy.

Another potentially useful new imaging modality is strain imaging, which measures global and regional cardiac deformation expressed as the percentage of change from the original dimension and as change per unit of time (Jurcut et al. 2008). Hare et al. observed that in patients with breast cancer undergoing therapy with trastuzumab, strain imaging could identify reductions in LV function before conventional measures (Hare et al. 2009).

However, a limitation of echocardiographic measurement of diastolic function is that this parameter significantly changes after administration of chemotherapy such as doxorubicin without any measurable changes in LV dimensions and shortening fraction (Marchandise et al. 1989). Moreover, diastolic function is load dependent, which is a limitation for follow-up investigations since hemodynamic settings can vary over time in such patients. Therefore, impaired diastolic function can be used to identify patients at risk, but these patients do not automatically develop systolic dysfunction after receiving chemotherapy.

## 4.2 Electrocardiography (ECG)

Cancer patients have to be routinely evaluated for ECG abnormalities, including ST segment and T wave changes, decreased QRS voltage, and a prolonged QT interval that are currently regarded as early markers of LV dysfunction (Horacek et al. 2009). Additionally, arrhythmias and conduction disturbances must also be carefully monitored. After baseline investigation, repeated examinations are recommendable each 12 weeks after initial start of anticancer treatment if the LVEF is >55 % and each 6 weeks when LVEF is <55 % in patients receiving trastuzumab to assess the potential QT prolongation effect of this drug, which might require a dosage adjustment or even discontinuation of a longer-lasting therapy (Todaro et al. 2013).

## 4.3 Long-Term ECG

Patients receiving certain chemotherapeutics such as dasatinib or nilotinib should be monitored by long-term ECG to screen for potentially life-threatening "torsades de pointes" ventricular tachycardia, which can occur as a result of the QT interval prolonging effect of this drugs.

### 4.4 Biomarkers

Plasma concentrations of troponin I and N-terminal pro-B-type natriuretic peptide are sensitive and specific markers for chemotherapy-induced cardiotoxicity, which are both released from myocardial cells in response to overload (Sandri et al. 2005; Cardinale et al. 2010; Koh et al. 2004). Recent publications revealed that patients receiving high-dose chemotherapy including alkylating agents, e.g., cyclophosphamide and anthracyclines, e.g., idarubicin, had a more marked reduction in LVEF that persisted through end of follow-up when the troponin level was increased after 1 month of follow-up (Cardinale et al. 2004). In contrast, it has been demonstrated that patients without troponin I elevation after treatment had good prognosis, with no significant reduction in LVEF and a very low incidence of cardiac events of about 1 % (Cardinale et al. 2004; Cardinale and Sandri 2010).

### 4.5 Cardiac Magnetic Resonance Imaging

Cardiac magnetic resonance imaging (CMR) is a very attractive alternative to echocardiography to study patients with cardiovascular toxicity because of its accuracy to quantify LV function. Currently, CMR is considered the reference standard to measure cardiac function because of its high reproducibility (Danilouchkine et al. 2005) and the well-established normal data for LV volume and function (Hudsmith et al. 2005), (Maceira et al. 2006). Furthermore, CMR is independent of the acoustic window of the individual patient, which enables imaging of the heart also in obese patients or patients with emphysema.

Another advantage of CMR is to demonstrate myocardial injury using contrast-enhanced imaging. A number of studies have shown the value of late gadolinium enhancement (LGE) CMR to identify myocardial injury in acute and chronic myocardial infarction (Kim et al. 1999), myocarditis (Friedrich et al. 2009), and hypertrophic cardiomyopathy (Harrigan et al. 2011).

Contrast-enhanced CMR was used to study the effect of potential cardiotoxic agents on myocardial injury and fibrosis. In a pilot study, Wassmuth et al. (2001) studied 22 patients receiving anthracyclines for various tumor entities. Three days after the onset of chemotherapy, patients showed an increased myocardial enhancement on CMR, which returned to normal after 28 days. At day 28, 6 of 22 patients (27 %) developed a reduced LV function with an ejection fraction of 55 % or less. Patients with a high enhancement observed at three days after therapy developed a significant decrease of LV function at 28 days indicating a relationship between early myocardial injury and development of heart failure.

Fallah-Rad et al. (2008, 2011), studied 42 patients receiving trastuzumab therapy for breast cancer using LGE CMR. Ten of the 42 patients (24 %) developed a trastuzumab-mediated cardiomyopathy within 6 months after initiation of therapy, necessitating of the drug in this group of patients. All 10 patients demonstrated a mid-myocardial delayed enhancement of the lateral LV wall, consistent with a trastuzumab-mediated cardiomyopathy (Fig. 1, (Fallah-Rad et al. 2008).

Larger-scale studies are desirable including quantitative T1 and T2 mapping to analyze the value of early CMR to predict later occurrence of chemotherapy-induced cardiomyopathy. Additionally, the presence of cardiac fibrosis detected by LGE CMR is typically associated with limited prognosis in patients after myocardial infarction (Wu et al. 2008b) and in other cardiac diseases such as hypertrophic cardiomyopathy (Bruder et al. 2010) or myocarditis (Grün et al. 2012). In patients receiving potentially cardiotoxic agents, further studies are needed to analyze the predictive value of LGE to identify patients at risk for cardiac events.

### 4.6 Myocardial Biopsy

At present, myocardial biopsy is not performed in patients with chemotherapy-induced cardiovascular toxicity because of its risks of

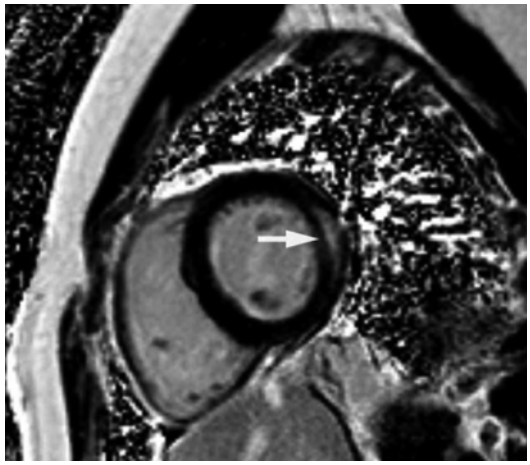

**Fig. 1** Mid-myocardial delayed enhancement of the lateral LV wall (*white arrow*) by short axis phase-sensitive reconstructed IR-TrueFISP image, consistent with a trastuzumab-mediated cardiomyopathy (Fallah-Rad et al. 2008, 2011)

complications and possible sampling error and most importantly because of the absent therapeutic consequence of the biopsy result. Myocardial biopsy can be considered in carefully selected patients, in whom an acute myocarditis has to be ruled out as a potential reason for acute heart failure.

## 5 Treatment of Chemotherapeutic-Induced Cardiotoxicity

In cases of symptomatic manifestation of chemotherapy-induced cardiotoxicity, it is crucial to consider ceasing the anticancer treatment in accordance with the severity of the complications.

In patients with asymptomatic impairment of EF, a treatment with angiotensin-converting enzyme (ACE) inhibitors, angiotensin II receptor blockers, and β-blockers is commonly recommended. In patients with clinical symptomatic heart failure, the coadministration of diuretics or aldosterone antagonists is advised (Abraham et al. 2009).

Even though anthracycline-induced LV dysfunction is frequently irreversible, a recent clinical study indicated that the ACE inhibitor enalapril and the β-blocker carvedilol resulted in a complete (42 %) or partial (13 %) recovery of EF, especially in patients in whom treatment was initiated at an early stage (Cardinale and Sandri 2010). In addition, prophylactic use of carvedilol before onset of symptoms prevents the development of late cardiotoxicity, especially in high-risk patients (Kalay et al. 2006; Cadeddu et al. 2010). A short time to HF treatment and low New York Heart Association functional class are major critical predictors of LVEF recovery, and the frequency of complete recovery from cardiac dysfunction decreases fourfold with each doubling in time to treatment (Cardinale et al. 2010).

It is conceivable that also other ACE inhibitors or β-blockers are effective in the treatment of chemotherapeutic-induced cardiotoxicity; however, at the current time, there are no larger studies to prove this assumption.

Currently, dexrazoxane is the only cardioprotective drug used in clinical practice with a proven efficacy in reducing side effects of anthracycline-based chemotherapy in cancer patients by reduction of the incidence and severity of anthracycline-induced congestive heart failure and adverse cardiac events (Lipshultz et al. 2010; Lyu et al. 2007).

Recently, erythropoietin (Hamed et al. 2006) and iloprost (Neilan et al. 2006), a stable synthetic analogue of prostacyclin, revealed promising results as cardioprotective drugs against doxorubicin-induced cardiomyocyte damage in vitro, without compromising the drug's chemotherapeutic effect. The mechanism behind the protection strategy consists of the inhibition of an endothelin-converting enzyme (ECE-1) with consecutive reduction of endothelin 1, a vasoconstrictive peptide with elevated plasmatic levels in patients treated with doxorubicin (Miyagawa et al. 2010). Nevertheless, larger studies are needed in the future to prove the benefit of these promising new agents in patients and to implement them into clinical practice.

**Conclusion**

The best treatment for chemotherapy-induced cardiotoxicity is prevention. The first step is a careful selection of patients for chemotherapy, followed by serial evaluation of clinical

condition and LV function (EF and longitudinal strain) before and during the whole course of treatment. A detailed patient history focused on cardiovascular risk factors (diabetes, obesity, hypertension, cigarette smoking) and previous treatment with chemotherapy agents is mandatory. Furthermore, the patient should undergo a complete physical examination and a comprehensive assessment of benefits from the treatment versus potential risks of cardiotoxicity should be performed. This approach is crucial to prevent the occurrence of symptomatic and life-limiting cardiotoxicity in patients who successfully have overcome cancer.

## References


Abraham WT, Jessup M, Casey DE et al (2009) 2009 focused update: ACCF/AHA Guidelines for the Diagnosis and Management of Heart Failure in Adults: a report of the American College of Cardiology Foundation/American Heart Association Task Force on Practice Guidelines: developed in collaboration with the International Society for Heart and Lung Transplantation. Circulation 119:1977–2016

Altena R, Perik PJ, van Veldhuisen DJ, de Vries EG, Gietema JA (2009) Cardiovascular toxicity caused by cancer treatment: strategies for early detection. Lancet Oncol 10(4):391–399

Arbuck SG, Strauss H, Rowinsky E, Christian M, Suffness M, Adams J, et al (1993) A reassessment of cardiac toxicity associated with Taxol. J Natl Cancer Inst Monogr (15):117–130

Bang YJ, Van Cutsem E, Feyereislova A, Chung HC, Shen L, Sawaki A, Lordick F, Ohtsu A, Omuro Y, Satoh T et al (2010) Trastuzumab in combination with chemotherapy versus chemotherapy alone for treatment of HER2-positive advanced gastric or gastro-oesophageal junction cancer (ToGA): a phase 3, open-label, randomised controlled trial. Lancet 376:687–697

Barrett-Lee PJ, Dixon JM, Farrell C et al (2009) Expert opinion on the use of anthracyclines in patients with advanced breast cancer at cardiac risk. Ann Oncol 20:816–827

Becker K, Erkenbrecher JF, Haussinger D, Frieling T (1999) Cardiotoxicity of the antiproliferative compound fluorouracil. Drugs 57:475–484

Bovelli D, Plataniotis G, Roila F, ESMO Guidelines Working Group (2010) Cardiotoxicity of chemotherapeutic agents and radio – therapy-related heart disease: ESMO Clinical Practice Guidelines. Ann Oncol 21:277–282

Bruder O, Wagner A, Jensen CJ, Schneider S, Ong P, Kispert E-M, Nassenstein K, Schlosser T, Sabin GV, Sechtem U, Mahrholdt H et al (2010) Myocardial scar visualized by cardiovascular magnetic resonance imaging predicts major adverse events in patients with hypertrophic cardiomyopathy. J Am Coll Cardiol 56(11):875–87

Buck T, Breithardt OA, Faber L et al (2009) Manual zur Indikation und Durchführung der Echokardiographie. Clin Res Cardiol Suppl 4(Suppl1):3–51

Cadeddu C, Piras A, Mantovani G et al (2010) Protective effects of the angiotensin II receptor blocker telmisartan on epirubicin-induced inflammation, oxidative stress, and early ventricular impairment. Am Heart J 160:487.e1–7

Cardinale D, Sandri MT (2010) Role of biomarkers in chemotherapy-induced cardiotoxicity. Prog Cardiovasc Dis 53:121–129

Cardinale D, Sandri MT, Martinoni A et al (2000) Left ventricular dysfunction predicted by early troponin I release after high-dose chemotherapy. J Am Coll Cardiol 36(2):517–522

Cardinale D, Sandri MT, Colombo A et al (2004) Prognostic value of troponin I in cardiac risk stratification of cancer patients undergoing high-dose chemotherapy. Circulation 109:2749–2754

Cardinale D, Colombo A, Sandri MT et al (2006) Prevention of high-dose chemotherapy-induced cardiotoxicity in high-risk patients by angiotensin-converting enzyme inhibition. Circulation 114(23):2474–2481

Cardinale D, Colombo A, Lamantia G, Colombo N, Civelli M, De Giacomi G et al (2010) Anthracycline-induced cardiomyopathy: clinical relevance and response to pharmacologic therapy. J Am Coll Cardiol 55:213–220

Chen B, Peng X, Pentassuglia L, Lim CC, Sawyer DB (2007) Molecular and cellular mechanisms of anthracycline cardiotoxicity. Cardiovasc Toxicol 7:114–121

Chu TF, Rupnick MA, Kerkela R, Dallabrida SM, Zurakowski D, Nguyen L et al (2007) Cardiotoxicity associated with tyrosine kinase inhibitor sunitinib. Lancet 370:2011–2019

Collins C, Weiden PL (1987) Cardiotoxicity of 5-fluorouracil. Cancer Treat Rep 71:733–736

Crone SA, Zhao YY, Fan L, Gu Y, Minamisawa S, Liu Y et al (2002) ErbB2 is essential in the prevention of dilated cardiomyopathy. Nat Med 8:459–465

Cvetković RS, Scott LJ (2005) Dexrazoxane: a review of its use for cardioprotection during anthracycline chemotherapy. Drugs 65:1005–1024

Danilouchkine MG, Westenberg JM, De Roos A, Reiber JC et al (2005) Operator induced variability in cardiovascular MR: left ventricular measurements and their reproducibility. J Cardiovasc Magn Reson 7(2): 447–457

de Azambuja E, Procter MJ, van Veldhuisen DJ, Agbor-Tarh D, Metzger-Filho O, Steinseifer J, Untch M, Smith IE, Gianni L, Baselga J, Jackisch C, Piccart-Gebhart MJ, Suter TM (2014) Trastuzumab-associated cardiac events at 8 years of median follow-up in the Herceptin Adjuvant trial. J Clin Oncol 32(20):2159–2165

de Forni M, Malet-Martino MC, Jaillais P, Shubinski RE, Bachaud JM, Lemaire L et al (1992) Cardiotoxicity of high-dose continuous infusion fluorouracil: a prospective clinical study. J Clin Oncol 10:1795–1801

Di Lorenzo G, Autorino R, Bruni G, Carteni G, Ricevuto E, Tudini M, Ficorella C, Romano C, Aieta M, Giordano A et al (2009) Cardiovascular toxicity following sunitinib therapy in metastatic renal cell carcinoma: a multicenter analysis. Ann Oncol 20:1535–1542

Di Marco A, Cassinelli G, Arcamone F (1981) The discovery of daunorubicin. Cancer Treat Rep 65(Suppl 4):3–8

Early Breast Cancer Trialists' Collaborative Group Ebctcg (2011) Comparisons between different polychemotherapy regimens for early breast cancer: meta-analyses of long-term outcome among 100,000 women in 123 randomised trials. Lancet 379: 432–444

Eidem BW (2008) Identification of anthracycline cardiotoxicity: left ventricular ejection fraction is not enough. J Am Soc Echocardiogr 21:1290–1292

Eskilsson J, Albertsson M (1990) Failure of preventing 5-fluorouracil cardiotoxicity by prophylactic treatment with verapamil. Acta Oncol 29:1001–1003

Ewer MS, Lippman SM (2005) Type II chemotherapy-related cardiac dysfunction: time to recognize a new entity. J Clin Oncol 23:2900–2902

Ewer MS, Vooletich MT, Durand JB et al (2005) Reversibility of trastuzumab-related cardiotoxicity: new insights based on clinical course and response to medical treatment. J Clin Oncol 23:820–7826

Fallah-Rad N, Lytwyn M, Fang T, Kirkpatrick I, Jassal DS et al (2008) Delayed contrast enhancement cardiac magnetic resonance imaging in trastuzumab induced cardiomyopathy. J Cardiovasc Magn Reson 10:5. doi:10.1186/1532-429X-10-5

Fallah-Rad N, Walker JR, Wassef A, Lytwyn M, Bohonis S, Fang T, Tian G, Kirkpatrick IDC, Singal PK et al (2011) The utility of cardiac biomarkers, tissue velocity and strain imaging, and cardiac magnetic resonance imaging in predicting early left ventricular dysfunction in patients with human epidermal growth factor receptor II-positive breast cancer treated with adjuvant trastuzumab therapy. J Am Coll Cardiol 57(22):2263–2270

Feldman AM, Lorell BH, Reis SE (2000) Trastuzumab in the treatment of metastatic breast cancer: anticancer therapy versus cardiotoxicity. Circulation 102(3):272–274

Ferrara N, Gerber HP, LeCouter J (2003) The biology of VEGF and its receptors. Nat Med 9:669–676

Ferrari R, Ceconi C, Campo G, Cangiano E, Cavazza C, Secchiero P et al (2009) Mechanisms of remodelling. Circ J 73:1973–1982

Force T, Krause DS, Van Etten RA (2007) Molecular mechanisms of cardiotoxicity of tyrosine kinase inhibition. Nat Rev Cancer 7:332–344

Friedrich MG, Sechtem U, Schulz-Menger J, Holmvang G, Alakija P, Cooper LT, White JA, Abdel-Aty H et al (2009) Cardiovascular magnetic resonance in myocarditis: a JACC white paper. J Am Coll Cardiol 53(17):1475–1487

Gewirtz DA (1999) A critical evaluation of the mechanisms of action proposed for the antitumor effects of the anthracycline antibiotics adriamycin and daunorubicin. Biochem Pharmacol 57(7):727–741

Gottdiener JS, Appelbaum FR, Ferrans VJ, Deisseroth A, Ziegler J (1981) Cardiotoxicity associated with high-dose cyclophosphamide therapy. Arch Intern Med 141:758–763

Grenier MA, Lipshultz SE (1998) Epidemiology of anthracycline cardiotoxicity in children and adults. Semin Oncol 25(4 Suppl 10):72–85

Grün S, Schumm J, Greulich S, Wagner A, Schneider S, Bruder O, Kispert E-M, Hill S, Ong P, Klingel K, Kandolf R, Sechtem U et al (2012) Long-term follow-up of biopsy-proven viral myocarditis: predictors of mortality and incomplete recovery. J Am Coll Cardiol 59(18):1604–1615

Hamed S, Barshack I, Luboshits G et al (2006) Erythropoietin improves myocardial performance in doxorubicin-induced cardiomyopathy. Eur Heart J 27:1876–1883

Hare JL, Brown JK, Leano R, Jenkins C, Woodward N, Marwick TH (2009) Use of myocardial deformation imaging to detect preclinical myocardial dysfunction before conventional measures in patients undergoing breast cancer treatment with trastuzumab. Am Heart J 158:294–301

Harrigan CJ, Peters DC, Gibson CM, Maron BJ, Manning WJ, Maron MS, Appelbaum E et al (2011) Hypertrophic cardiomyopathy: quantification of late gadolinium enhancement with contrast-enhanced cardiovascular MR imaging. Radiology 258:128–133

Hasinoff BB, Patel D (2010) Mechanisms of myocyte cytotoxicity induced by the multikinase inhibitor sorafenib. Cardiovasc Toxicol 10:1–8

Horacek JM, Jakl M, Horackova J, Pudil R, Jebavy L, Maly J (2009) Assessment of anthracycline-induced cardiotoxicity with electrocardiography. Exp Oncol 31:115–117

Hudsmith L, Petersen S, Francis JM, Robson M, Neubauer S et al (2005) Normal human left and right ventricular and left atrial dimensions using steady state free precession magnetic resonance imaging. J Cardiovasc Magn Reson 7:775–782

Hurwitz H, Fehrenbacher L, Novotny W, Cartwright T, Hainsworth J, Heim W, Berlin J, Baron A, Griffing S,

Holmgren E et al (2004) Bevacizumab plus irinotecan, fluorouracil, and leucovorin for metastatic colorectal cancer. N Engl J Med 350:2335–2342

Jensen SA, Sorensen JB (2006) Risk factors and prevention of cardiotoxicity induced by 5-fluorouracil or capecitabine. Cancer Chemother Pharmacol 58:487–493

Joensuu H et al (2006) Adjuvant docetaxel or vinorelbine with or without trastuzumab for breast cancer. N Engl J Med 354:809–820

Jurcut R, Wildiers H, Ganame J, D'hooge J, Paridaens R, Voigt JU (2008) Detection and monitoring of cardiotoxicity — what does modern cardiology offer? Support Care Cancer 16:437–445

Kalay N, Basar E, Ozdogru I et al (2006) Protective effects of carvedilol against anthracycline-induced cardiomyopathy. J Am Coll Cardiol 48:2258–2262

Kantarjian HM, Hochhaus A, Saglio G, De Souza C, Flinn IW, Stenke L, Goh Y-T, Rosti G, Nakamae H, Gallagher NJ et al (2011) Nilotinib versus imatinib for the treatment of patients with newly diagnosed chronic phase, Philadelphia chromosome positive, chronic myeloid leukaemia: 24-month minimum follow-up of the phase 3 randomised ENESTnd trial. Lancet Oncol 12:841–851

Keefe DL (2002) Trastuzumab-associated cardiotoxicity. Cancer 95:1592–1600

Kerkela R, Grazette L, Yacobi R, Iliescu C, Patten R, Beahm C et al (2006) Cardiotoxicity of the cancer therapeutic agent imatinib mesylate. Nat Med 12:908–916

Kim RJ, Fieno DS, Parrish TB, Harris K, Chen EL, Simonetti O, Bundy J, Finn JP, Klocke FJ, Judd RM et al (1999) Relationship of MRI delayed contrast enhancement to irreversible injury, infarct age, and contractile function. Circulation 100(19):1992–2002

Koh E, Nakamura T, Takahashi H (2004) Troponin-T and brain natriuretic peptide as predictors for adriamycin-induced cardiomyopathy in rats. Circ J 68:163–167

Ku DD, Zaleski JK, Liu S, Brock TA (1993) Vascular endothelial growth factor induces EDRF-dependent relaxation in coronary arteries. Am J Physiol 265(2 Pt 2): H586–H592

Lestuzzi C, Crivellari D, Rigo F, Viel E, Meneguzzo N (2010) Capecitabine cardiac toxicity presenting as effort angina: a case report. J Cardiovasc Med (Hagerstown) 11:700–703

Lipshultz SE, Rifai N, Dalton VM et al (2004) The effect of dexrazoxane on myocardial injury in doxorubicin-treated children with acute lymphoblastic leukemia. N Engl J Med 351(2):145–153

Lipshultz SE, Scully RE, Lipsitz SR et al (2010) Assessment of dexrazoxane as a cardioprotectant in doxorubicin-treated children with high-risk acute lymphoblastic leukaemia: long-term follow-up of a prospective, randomised, multicentre trial. Lancet Oncol 11:950–961

Loyola E, Sadana R, Stein C The European health report 2012: charting the way to well-being. WHO Library Cataloguing in Publication Data ISBN 978 92 890 14274

Lyman GH, Khorana AA, Falanga A, Clarke-Pearson D, Flowers C, Jahanzeb M, Kakkar A, Kuderer NM, Levine MN, Liebman H et al (2007) American Society of Clinical Oncology guideline: recommendations for venous thromboembolism prophylaxis and treatment in patients with cancer. J Clin Oncol 25:5490–5505

Lyu YL, Kerrigan JE, Lin CP, Azarva AM, Tsai YC, Ban Y et al (2007) Topoisomerase II beta mediated DNA double-strand breaks: implications in doxorubicin cardiotoxicity and prevention by dexrazoxane. Cancer Res 67(18):8839–8846

Maceira AM, Prasad SK, Khan M, Pennell DJ et al (2006) Normalized left ventricular systolic and diastolic function by Steady State Free Precession cardiovascular magnetic resonance. J Cardiovasc Magn Reson 8:417–426

Maitland ML, Bakris GL, Black HR, Chen HX, Durand JB, Elliott WJ, Ivy SP, Leier CV, Lindenfeld J, Liu G et al (2010) Initial assessment, surveillance, and management of blood pressure in patients receiving vascular endothelial growth factor signaling pathway inhibitors. J Natl Cancer Inst 102:596–604

Marchandise B, Schroeder E, Bosly A et al (1989) Early detection of doxorubicin cardiotoxicity: interest of Doppler echocardiographic analysis of left ventricular filling dynamics. Am Heart J 118:92–98

Martin M, Esteva FJ, Alba E et al (2009) Minimizing cardiotoxicity while optimizing treatment efficacy with trastuzumab: review and expert recommendations. Oncologist 14:1–11

Milan A, Puglisi E, Ferrari L, Bruno G, Losano I, Veglio F (2014) Arterial hypertension and cancer. Int J Cancer 134(10):2269–2277

Mir O, Ropert S, Alexandre J, Goldwasser F (2009) Hypertension as a surrogate marker for the activity of anti-VEGF agents. Ann Oncol 20:967–970

Miyagawa K, Emoto N, Widyantoro B et al (2010) Attenuation of doxorubicin-induced cardiomyopathy by endothelin-converting enzyme-1 ablation through prevention of mitochondrial biogenesis impairment. Hypertension 55:738–746

Monreal M, Falga' C, Valle R et al (2006) Venous thromboembolism in patients with renal insufficiency: findings from the RIETE registry. Am J Med 119:1073–1079

Moore RA, Adel N, Riedel E et al (2011) High incidence of thromboembolic events in patients treated with cisplatin-based chemotherapy: a large retrospective analysis. J Clin Oncol 29:3466–3473

Nalluri SR, Chu D, Keresztes R, Zhu X, Wu S (2008) Risk of venous thromboembolism with the angiogenesis inhibitor bevacizumab in cancer patients: a meta-analysis. JAMA 300(19):2277–2285

Neilan TG, Jassal DS, Scully MF et al (2006) Iloprost attenuates doxorubicin-induced cardiac injury in a murine model without compromising tumour suppression. Eur Heart J 27:1251–1256

Perez EA, Koehler M, Byrne J, Preston AJ, Rappold E, Ewer MS (2008) Cardiac safety of lapatinib: pooled analysis of 3689 patients enrolled in clinical trials. Mayo Clin Proc 83:679–686

Perez EA, Romond EH, Suman VJ, Jeong JH, Davidson NE, Geyer CE Jr, Martino S, Mamounas EP, Kaufman PA, Wolmark N (2011) Four-year follow-up of trastuzumab plus adjuvant chemotherapy for

operable human epidermal growth factor receptor 2-positive breast cancer: joint analysis of data from NCCTG N9831 and NSABP B-31. J Clin Oncol 29: 3366–3373

Popat S, Smith IE (2008) Therapy insight: anthracyclines and trastuzumab-the optimal management of cardiotoxic side effects. Nat Clin Pract Oncol 5(6): 324–335

Ranpura V, Pulipati B, Chu D, Zhu X, Wu S (2010) Increased risk of high-grade hypertension with bevacizumab in cancer patients: a meta-analysis. Am J Hypertens 23:460–468

Richards CJ, Je Y, Schutz FA, Heng DY, Dallabrida SM, Moslehi JJ, Choueiri TK (2011) Incidence and risk of congestive heart failure in patients with renal and nonrenal cell carcinoma treated with sunitinib. J Clin Oncol 29:3450–3456

Ryberg M, Nielsen D, Cortese G, Nielsen G, Skovsgaard T, Andersen PK (2008) New insight into epirubicin cardiac toxicity: competing risks analysis of 1097 breast cancer patients. J Natl Cancer Inst 100:1058–1067

Salvatorelli E, Menna P, Cascegna S, Liberi G, Calafiore AM, Gianni L et al (2006) Paclitaxel and docetaxel stimulation of doxorubicinol formation in the human heart: implications for cardiotoxicity of doxorubicin-taxane chemotherapies. J Pharmacol Exp Ther 318:424–433

Sandri MT, Salvatici M, Cardinale D, Zorzino L, Passerini R, Lentati P et al (2005) N-terminal pro-B-type natriuretic peptide after high-dose chemotherapy: a marker predictive of cardiac dysfunction? Clin Chem 51:1405–1410

Sawaya H, Sebag IA, Plana JC et al (2011) Early detection and prediction of cardiotoxicity in chemotherapy-treated patients. Am J Cardiol 107:1375–1380

Scully RE, Lipshultz SE (2007) Anthracycline cardiotoxicity in long-term survivors of childhood cancer. Cardiovasc Toxicol 7:122–128

Sengupta PP, Northfelt DW, Gentile F et al (2008) Trastuzumab-induced cardiotoxicity: heart failure at the crossroads. Mayo Clin Proc 83:197–203

Slordal L, Spigset O (2006) Heart failure induced by non-cardiac drugs. Drug Saf 29:567–586

Suter TM, Procter M, van Veldhuisen DJ, Muscholl M, Bergh J, Carlomagno C et al (2007) Trastuzumab-associated cardiac adverse effects in the herceptin adjuvant trial. J Clin Oncol 25:3859–3865

Swain SM, Vici P (2004) The current and future role of dexrazoxane as a cardioprotectant in anthracycline treatment: expert panel review. J Cancer Res Clin Oncol 130:1–7

Taniguchi I (2005) Clinical significance of cyclophosphamide-induced cardiotoxicity. Intern Med 44:89–90

Tassan-Mangina S, Codorean D, Metivier M et al (2006) Tissue Doppler imaging and conventional echocardiography after anthracycline treatment in adults: early and late alterations of left ventricular function during a prospective study. Eur J Echocardiogr 7:141–146

Todaro MC, Oreto L, Qamar R, Paterick TE, Carerj S, Khandheria BK (2013) Cardiooncology: state of the heart. Int J Cardiol 168:680–687

Turrisi G, Montagnani F, Grotti S, Marinozzi C, Bolognese L, Fiorentini G (2010) Congestive heart failure during imatinib mesylate treatment. Int J Cardiol 145(1):148–150

Vaklavas C, Lenihan D, Kurzrock R, Tsimberidou AM (2010) Anti-vascular endothelial growth factor therapies and cardiovascular toxicity: what are the important clinical markers to target? Oncologist 15:130–141

Van Dalen EC, Michiels EM, Caron HN, Kremer LC (2010) Different anthracycline derivates for reducing cardiotoxicity in cancer patients. Cochrane Database Syst Rev (3):CD005006

Van Dalen EC, Caron HN, Dickinson HO, Kremer LC (2011) Cardioprotective interventions for cancer patients receiving anthracyclines. Cochrane Database Syst Rev (6):CD003917

Von Hoff DD, Layard MW, Basa P et al (1979) Risk factors for doxorubicin-induced congestive heart failure. Ann Intern Med 91(5):710–717

Wang J, Khoury DS, Thohan V et al (2007) Global diastolic strain rate for the assessment of left ventricular relaxation and filling pressures. Circulation 115:1376–1383

Wassmuth R, Lentzsch S, Erdbruegger U, Schulz-Menger J, Doerken B, Dietz R, Friedrich MG et al (2001) Subclinical cardiotoxic effects of anthracyclines as assessed by magnetic resonance imaging-A pilot study. Am Heart J 141:1007–1013

Wu S, Chen JJ, Kudelka A, Lu J, Zhu X (2008a) Incidence and risk of hypertension with sorafenib in patients with cancer: a systematic review and meta-analysis. Lancet Oncol 9(2):117–123

Wu E, Ortiz JT, Tejedor P, Lee DC, Bucciarelli-Ducci C, Kansal P, Carr JC, Holly TA, Lloyd-Jones D, Klocke FJ et al (2008b) Infarct size by contrast enhanced cardiac magnetic resonance is a stronger predictor of outcomes than left ventricular ejection fraction or end-systolic volume index: prospective cohort study. Heart 94(6):730–736

Yeh ET, Bickford CL (2009) Cardiovascular complications of cancer therapy: incidence, pathogenesis, diagnosis, and management. J Am Coll Cardiol 53:2231–2247

Yeh ET, Tong AT, Lenihan DJ et al (2004) Cardiovascular complications of cancer therapy: diagnosis, pathogenesis, and management. Circulation 109:3122–3131

Zhao YY, Sawyer DR, Baliga RR, Opel DJ, Han X, Marchionni MA et al (1998) Neuregulins promote survival and growth of cardiac myocytes: persistence of ErbB2 and ErbB4 expression in neonatal and adult ventricular myocytes. J Biol Chem 273: 10261–10269

Zhu X, Stergiopoulos K, Wu S (2009) Risk of hypertension and renal dysfunction with an angiogenesis inhibitor sunitinib: systematic review and meta-analysis. Acta Oncol 48:9–17

# Part VI

# Pediatrics

# Pediatric Brain Tumors: Imaging of Late Effects in Pediatric Brain Tumor Survivors

G. Tallen, M. Warmuth-Metz, P. Hernáiz Driever, and Stefan M. Pfister

## Contents




**Abstract**

Primary tumors of the central nervous system (CNS) are the most frequent solid tumors in childhood and adolescence. In Germany, about 400 patients are newly diagnosed with a CNS tumor each year. Thanks to continuously optimized diagnostics, supportive care regimens, and multicentric, multimodal treatment concepts, their overall survival (OS) has increased from below 50 % up to 70 % over the last decades. Both tumor and treatment, and still developing CNS structures, make survivors prone to a risk of acquiring brain function deficits that are much higher than in adulthood or other childhood cancer survivors. Hence, this specifically vulnerable group of childhood cancer survivors must deal with chronic health conditions that may have serious impact on their physical, mental, emotional, and psychosocial development as well as their activity and participation as members of the society.



G. Tallen
Department of Pediatric Oncology/Hematology, Charité-Universitätsmedizin Berlin, Campus Virchow-Klinikum, Augustenburger Platz 1, Berlin 13353, Germany

Department of Pediatrics, Faculty of Medicine, University of Calgary, 2888 Shaganappi Trail N.W., Calgary, AL T3B 6A8, Canada

M. Warmuth-Metz
Department of Neuroradiology, Universität Würzburg, Josef-Schneider-Straße 11, Würzburg 97080, Germany

P. Hernáiz Driever
Department of Pediatric Oncology/Hematology, Charité-Universitätsmedizin Berlin, Campus Virchow-Klinikum, Augustenburger Platz 1, Berlin 13353, Germany

S.M. Pfister (✉)
Division of Pediatric Neurooncology (B062), Deutsches Krebsforschungszentrum (DKFZ), Im Neuenheimer Feld 280, Heidelberg 69120, Germany

Department of Pediatric Hematology and Oncology, Heidelberg University Hospital Im Neuenheimer Feld 430, Heidelberg 69120, Germany
e-mail: s.pfister@dkfz.de


Med Radiol Radiat Oncol (2015)
DOI 10.1007/174_2015_1084, © Springer International Publishing Switzerland

Due to the heterogeneity of pediatric brain tumors and corresponding treatment concepts, not all survivors share the same risk of developing such sequelae. Neuroimaging in surveillance plays a critical role in differentiating underlying neuroanatomical processes that are responsible for the brain function deficits observed. It helps improving current treatment strategies and interventional concepts for management of late effects as well as identifying risk factors.

Based on the international literature, the following chapter reviews and discusses the current understanding, options, and limitations of pediatric neuroimaging regarding common tumor- and treatment-related late effects in pediatric brain tumor survivors.

## Abbreviations

| | |
|---|---|
| CNS | Central nervous system |
| CNS-PNET | Primitive neuroectodermal tumor of the CNS |
| CSF | Cerebrospinal fluid |
| CSI | Craniospinal irradiation |
| CRT | Cranial radiotherapy |
| CT | Computed tomography |
| DSA | Digital subtractive angiography |
| DTI | Diffusion tensor |
| MR | Imaging |
| FDG | Fluorodeoxyglucose |
| FLAIR | Fluid-attenuated inversion recovery |
| MR | Magnetic resonance |
| MRI | Magnetic resonance imaging |
| OS | Overall survival |
| PET | Positron emission tomography |
| RT | Radiotherapy |
| SMN | Secondary malignant neoplasm |
| WBRT | Whole brain RT |

## 1 Introduction

*Necessity of Imaging Surveillance for Improving Survival Quality of Pediatric Brain Tumor Survivors Who Are Still Growing Up*

Primary tumors of the central nervous system (CNS) are the most frequent solid tumors and, following leukemias, the second most frequent malignancies in childhood and adolescence. They account for about 20 % of the pediatric oncology population in Germany (Kaatsch and Grabow 2012).

About 400 children and adolescents are newly diagnosed with a CNS tumor in Germany each year (Kaatsch and Grabow 2012; Registry 2014). About 95 % of them are treated as per prospective, multicenter therapy optimization studies or non-interventional registries, respectively. As a result, overall survival (OS) for children and teenagers with CNS tumors in Germany has increased from below 50 % up to 70 % over the last decades (Kaatsch and Grabow 2012). For many patients with medulloblastoma or low-grade glioma, the most frequent childhood CNS tumors, survival rates even reach 80 % or 90 %, respectively (Friedrich et al. 2013; von Bueren et al. 2011; Gnekow et al. 2012; von Hornstein et al. 2011). OS varies depending on patient's age, type and site of the tumor, its response to therapy, as well as late effects, which can be caused by the tumor itself and by the intensive treatments, such as neurosurgery, radiotherapy (RT), and chemotherapy. Overall, 2 of every 3 pediatric patients with brain tumors may be long-term survivors entering their next phase of life including adulthood.

However, pediatric brain tumor survivors and their stakeholders, such as families and communities, health-care professionals, and scientists as well as the educational and health-care systems, are facing a double-edged sword: increasing quantity of survival and promising new treatments vs. multifactorial late effects and a lack of understanding about how these may impact the quality of survival. In particular, tumor growth and surgery close to eloquent and still developing CNS structures and cranial RT (CRT) with or without intrathecal chemotherapy make survivors prone to a risk of developing neuropsychological deficits that is much higher than in other childhood cancer survivors (Oeffinger et al. 2006). As a result, this specifically vulnerable group of childhood cancer

survivors must deal with chronic health conditions, such as neurological and neurocognitive impairments as well as emotional changes and problems in psychosocial functioning. These can have serious impact on their physical and mental development, participation, and activity (Schultz et al. 2007; Ness et al. 2005; Zeltzer et al. 2008, 2009).

However, due to the heterogeneity of pediatric brain tumors and associated treatment concepts, not all of the survivors may develop these problems or at least may experience them to different degrees. Therefore, imaging for analysis, surveillance, and differentiation of potentially underlying neuroanatomical processes is crucial in order to identify new risk factors, thereby helping to improve both current treatment strategies and interventional concepts for management of late effects. Hence, surveillance imaging should not only include the long-term follow-up but also the acute period, i.e., the time immediately after diagnosis and before and during treatment. The corresponding radiological results require refined interpretation that carefully takes into consideration the multifactorial emergence of late effects as outlined below.

Acute and long-term functional outcome after neurosurgery largely depends on the anatomical site of the tumor, neurosurgical technique, expertise of the surgeon, as well as the patient's age and clinical condition prior to surgery (Müller 2013; Pillai et al. 2012; Benesch et al. 2006; Wendt et al. 2014). Postoperative deficits such as neurovascular events (stroke), seizures, palsies, oculomotor, visual and coordination impairments, as well as diencephalic damage with endocrinopathies and reduced neurocognitive function are not rare, and both adjuvant RT and chemotherapy may be covariates (Sterkenburg et al. 2014; Hoffmann et al. 2014; Özyurt et al. 2014). Also, drainage-requiring hydrocephalus often negatively influences outcome, in particular cognitive performance (Aarsen et al. 2009; Merchant et al. 2009; Pietilä et al. 2012; Di Rocco et al. 2013; Thomale et al. 2013; Abhaya et al. 2013). Potentially enhancing factors like the degree and duration of ventricular dilatation, shunting technique, and adjuvant therapy, as well as the underlying structural damage and associated radiological sequelae, still need evaluation. Another example representing "surgical neurotoxicity" is cerebellar mutism or posterior fossa syndrome (CMS/PFS). It affects up to a quarter of patients shortly after resection of a large posterior fossa tumor and can lead to a variety of long-term neuropsychological deficits, potentially due to a disrupted fronto-cerebellar circuit, imaging options of which will be discussed later in this chapter (Sect. 2.2.3).

Like neurosurgery, CRT and craniospinal irradiation (CSI) are effective mainstays of local tumor control. Current standard treatment strategies in pediatric neuro-oncology are based on CRT and/or CSI either as single local or adjuvant treatment. However, the developing brain of children and adolescents, especially young children, is vulnerable to radiation damage. RT-induced late effects are multifactorial, thus influenced by the radiation field, applied techniques, and single and total doses. Some of them may be enhanced by neurosurgery and/or chemotherapy and put the young patients at risk of exhibiting serious changes in CNS structure and biochemistry. The result is a broad spectrum of neuropsychological impairments, which may include cerebrovascular complications, compromised neurocognitive function, as well as an increased risk of developing secondary malignant neoplasms (SMN), to name a few (Rueckriegel et al. 2012a; Morris et al. 2009a; Muelle et al. 2013; Anderson et al. 1999; Reddick et al. 2014; Lawrence et al. 2010; Fouladi et al. 2004; Rueckriegel et al. 2015; Shalitin et al. 2011; Palmer et al. 2013; Willard et al. 2014; Musial-Bright et al. 2011; Packer et al. 2003; Whelan et al. 2010; Effinger et al. 2014; Sabin et al. 2014; Garcia-Puig et al. 2012; Ball et al. 1992). Therefore, early radiological detection of RT-induced CNS injury is crucial for prevention of late effects or their successful management, respectively.

Neuronal injury following RT has been primarily classified based on the time after radiation exposure, in which symptoms develop (Valk and Dillon 1991; Duffner 2004). "*Acute damage*" usually occurs within the first weeks after

RT as a result of transient vasogenic edema and presents as a temporary worsening of symptoms. "*Early delayed injury"* is defined as transitional, deep gray and white matter changes occurring during 1–6 months following radiation, while "*late injury"* starts much later (months to years) after RT and is progressive and often permanent (Hoppe-Hirsch et al. 1990; Anderson 2003). Late radiation injury involves leukencephalopathy, brain atrophy, necrosis, endocrine dysfunction, and cognitive decline (Valk and Dillon 1991; Duffner 2004; Hoppe-Hirsch et al. 1990; Anderson 2003; Monje and Palmer 2003). Damaged endothelial cells or demyelination, respectively, attend all stages of radiation injury. Therefore, they should be monitored by imaging, in particular since they may lead to additional neuronal damage by enhancing capillary permeability and replacing hydrophobic myelin by water, thereby increasing vasogenic edema or initiate demyelination, respectively (Valk and Dillon 1991).

During the last decades, continuous optimization of radiological techniques significantly contributed to a better understanding of the anatomical and biochemical underpinnings caused by pediatric brain tumors and associated treatments (Vézina 2008). The magnetic resonance imaging (MRI) characteristics of most tumor entities are well described in the international literature and beyond the scope of this chapter. Many features have been specifically associated with medulloblastoma, dysembryoplastic neuroepithelial tumor, pilocytic astrocytoma, and pleomorphic xanthoastrocytoma, partially by diffusion and fluid-attenuated inversion recovery (FLAIR) techniques (Koeller and Henry 2001; Erdem et al. 2001). Also, conventional MRI is the gold standard imaging method for treatment planning and providing prognostic information for pediatric patients with certain brainstem gliomas (Fischbein et al. 1996). For some pediatric patients, for example, with infiltrative brainstem, optic pathway gliomas (with coexisting neurofibromatosis type 1), or certain tectal tumors, respectively, specific MRI features even help determining the tumor diagnosis, thereby obviating the need for histological confirmation, thus neurosurgical intervention. Following neurosurgery as well as RT and chemotherapy, recurrent disease can be identified by basic MRI prior to symptoms as outlined later in this chapter (Sect. 2.5). The impact of such surveillance scanning on prognosis has been discussed, in particular regarding medulloblastoma patients. But since neurosurgical techniques and treatment strategies for the salvage of relapses have been continuously optimized, the benefits of detecting small recurrences early – even before clinical symptoms occur – have been recognized by now (Shaw et al. 1997; Saunders et al. 2003).

However, basic MRI is unable to differentiate between tumor and other enhancing structures, such as the various radiation injury or neurotoxic damage caused by progressive or recurrent disease (Vézina 2008). Also, subarachnoid tumor dissemination may not always be easy to detect. However, various MRI-based functional imaging techniques have proven efficient in differentiating these changes, particularly those associated with radiation injury: A recent study introduced delayed contrast MRI for calculating high-resolution treatment response assessment maps (TRAMs) as a promising approach for distinguishing between different tissues with enhancement in patients with CNS tumors (Zach et al. 2015). Other techniques include proton magnetic resonance spectroscopic imaging (MRSI) and diffusion tensor imaging (DTI), which are not only useful for staging and treatment planning of CBT [reviewed in (Lemort et al. 2007)] but also for differentiation between tumor tissue and radiation necrosis as well as for surveillance and characterization of changes in white matter integrity and CNS metabolism (Vézina 2008). Late-delayed effects were detected by DTI also in pediatric brain tumor survivors after RT of medulloblastoma, particularly in the frontal lobe (Qiu et al. 2007) – structures of which play a key role in working memory and therefore may contribute to socio-emotional functions via maintaining neural overlaps in neural networks (Robinson et al. 2014). Additional reports have shown associations between abnormal imaging results in pediatric brain tumor survivors with

compromised neurocognitive function (Khong et al. 2003; Mabbott et al. 2006).

Various long-term late effects in pediatric brain tumor survivors may be correlated with radiological findings. For example, certain imaging studies highlight the negative effects of CRT and/or chemotherapy with methotrexate on white matter development (Khong et al. 2006; Reddick et al. 2003), implying that the cognitive decline associated with radiation may be a result of dysfunctional white matter structures (Fouladi et al. 2004; Rueckriegel et al. 2015; Garcia-Puig et al. 2012; Ball et al. 1992; Reddick et al. 2003). However, most reports on RT-related late effects are based on dated treatment protocols, while the current concepts of CRT or CSI particularly focus on the fine-tuning of target volume as well as on dose reductions, beam orientation, and optimization of fractionation regimens. They will therefore most likely result in positive changes of late effect patterns both clinically and radiologically. Hence, multicenter prospective analyses are now required, which correlate late effects with imaging findings after whole brain RT (WBRT) alone (–/+ chemotherapy), WBRT + boost to tumor site/posterior fossa (–/+ chemotherapy), or partial CRT/CSI alone ("local field") (–/+ chemotherapy), respectively, and evaluate the dose-effect dependency with respect to dose distribution within the CNS. Also, the numerous functional MRI techniques, which appear to be valuable for early and long-term evaluation of late effects, have been mostly validated for adult CNS tumor patients or survivors. These promising observations require confirmation by studying large, population-based pediatric cohorts, since routine use of functional imaging parameters will contribute to reduced toxicity in pediatric brain tumor survivors. Last but not least, imaging in children can be challenging, primarily due to issues of a patient's age, size, sedation, and artifacts.

The following paragraphs will provide the current understanding, options, and limitations of pediatric imaging regarding common tumor- and treatment-related late effects in pediatric brain tumor survivors.

## 2 Neuroradiological Evaluation of Late Effects in Pediatric Brain Tumor Survivors

### 2.1 Neurovascular Disease

#### 2.1.1 Cerebrovascular Disease After Brain Tumor Therapy in Childhood and Adolescence

Cerebrovascular disease is an emerging risk factor for childhood cancer survivorship, especially after CRT. The overall relative risk for a cerebrovascular event in this group is estimated to be tenfold compared to healthy siblings (Oeffinger et al. 2006). Survivors of primary CNS tumors are among the groups with highest incidences (Morris et al. 2009a; Bowers et al. 2006). The risk of stroke is increased for all brain tumor survivors in comparison to the healthy population. It is further increased in former patients who underwent irradiation (Bowers et al. 2006). Brain tumor survivors after CRT have a 40-fold risk of cerebrovascular events when compared to the general population. The cumulative incidence is 6.9 % over a 25-year period after diagnosis (Bowers et al. 2006). A well-recognized risk factor is the total irradiation dose. In this context, any of the following steps in the cascade of pathophysiological events may differentially contribute to cerebrovascular disease and individually determine the degree of the resulting health conditions ranging from transient and treatable to persistent, chronic, and progressive.

Irradiation leads to vascular injury, thereby weakening the blood-brain barrier on the microvasculature level and increasing vessel permeability. As a result, the initiation of inflammatory processes, thus release of a myriad of proinflammatory substances (such as prostaglandins, leukotrienes, TNF-alpha), is enhanced in all sizes of vessels (Yuan et al. 2006). Eventually, activated von Willebrand factor concerts with tissue factors to foster the thrombotic cascade, which will subsequently compromise vascular integrity and function, including endothelial cell detachment, thereby allowing microthrombi formation on the subendothelium of all types of CNS vasculature.

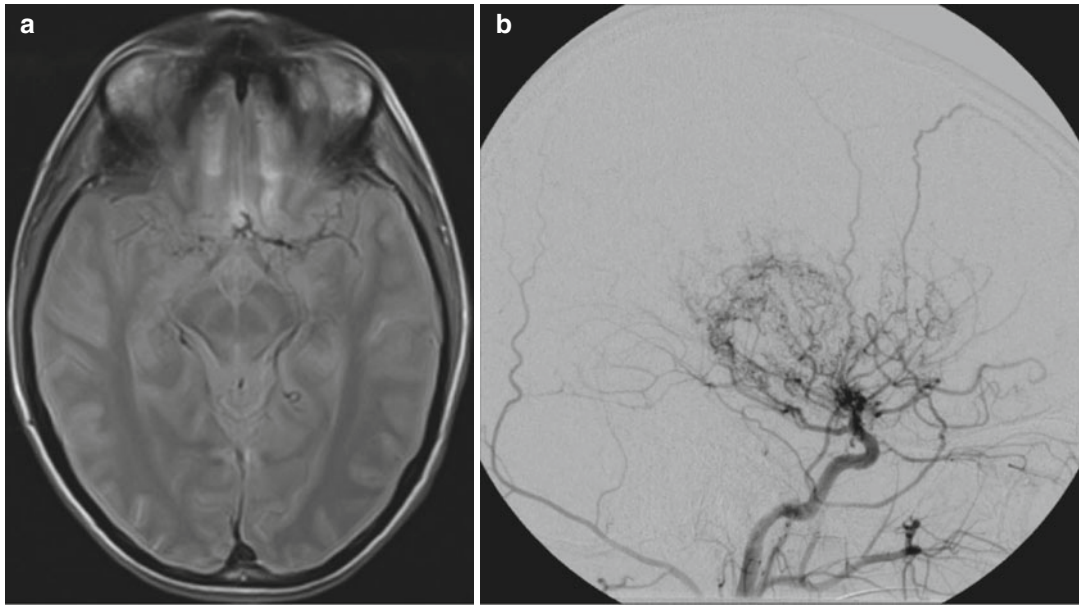


**Fig. 1** Imaging of Moyamoya syndrome. (**a**) MRI: Proton density-weighted MRI showing a loss of normal flow void in the middle and anterior cerebral artery on the right, and marked stenoses on the left side. (**b**) DSA: The injection into the right common carotid artery shows a supraclinoid closure of the vessel and multiple corkscrew-like small collateral vessels

Subsequent monocyte infiltration of the intima induces premature atherosclerosis (Gaber et al. 2003; Stewart et al. 2010; Wilson et al. 2009). This intimal fibrosis and macrophage activation induces fatty streaks in vessels that further promote stenosis and thrombosis (Stewart et al. 2010). The affected vessel walls are prone to dilatation and tortuosity, which in the individual pediatric brain tumor survivor may lead to either vascular malformations, microangiopathy, or Moyamoya syndrome, to name a few (Sects. 2.1.2, 2.1.3, 2.1.4, and 2.1.5) (Fajardo 2005).

Individual host-related risk factors are known as covariates of the pathophysiological mechanisms mentioned above. They may trigger certain cerebrovascular events and/or disease. For example, neurofibromatosis type 1 germline mutation is a well-recognized risk factor for cerebrovascular events, particularly after treatment with CRT (Desai et al. 2006; Hersh and American 2008; Rosser et al. 2005; Ullrich et al. 2007). Other risk factors include metabolic syndrome (e.g., low high-density lipoproteins, insulin resistance), a common late effect of tumors and RT of the hypothalamic-pituitary axis, as well as sedentary life style (de Haas et al. 2010; Green et al. 2012; Meacham et al. 2010; Oudin et al. 2011; Talvensaari et al. 1996).

### 2.1.2 Moyamoya Syndrome

Moyamoya syndrome is characterized by constriction of the distal internal carotid artery or the major (middle and anterior) arteries of the Circle of Willis. In cases of complete stenosis of the internal carotid artery, thus obliteration of the corresponding collateralization, patients often survive on the collateral circulation from the basilar artery. The term "Moyamoya" is Japanese for the appearance of "smoke" on relevant angiographs resultant from the collateral tangles formed by tiny vessels in response to stenosis. Also, changes in flow patterns, signal voids due to the development of collaterals, the "ivy sign" on post-contrast T1-weighted images, FLAIR imaging indicating slow flow in leptomeningeal vessels, as well as parenchymal infarction are supportive of the diagnosis. For establishing the definite diagnosis, Moyamoya syndrome needs to be confirmed by conventional angiography (Fig. 1). Common clinical symptoms are strokes,

recurrent transient ischemic attacks (TIAs), focal sensorimotor deficits, seizures, and/or migraine-like headaches. Strokes may be followed by secondary hemorrhages, for example, due to rupture of the weak neovascular vessel walls.

Moyamoya syndrome has been reported as the most common vascular abnormality in 345 pediatric patients and followed by serial imaging surveillance and clinical evaluation. Twelve patients (3.5 %) developed Moya-moya syndrome, 11 of whom presented with a combination of acute neurologic symptoms, while one patient was diagnosed based on routine follow-up imaging, which also revealed previous infarction in a silent region. Major risk factors for developing Moyamoya syndrome in this study were young age, tumor and radiation to the optic chiasm, and neurofibromatosis type 1 germline mutation. Most patients developed progressive multi-vessel steno-occlusive vascular disease. The risk of infarction was higher after cranial irradiation (75 %) compared to that of patients with Moyamoya syndrome alone (39 %). Development of Moyamoya syndrome following irradiation is a dose- and time-dependent process. In the past 35 years, 60 cases of Moyamoya syndrome after CRT have been reported, 52 of which were children (Ullrich et al. 2007). At high risk are particularly pediatric patients who receive CRT for treatment of craniopharyngioma (Liu et al. 2009). Major MRI characteristics are vascular wall thickening, ring enhancement, and internal carotid narrowing. However, these features may also suggest irradiation arteriitis, thereby requiring thorough differentiation (Aoki et al. 2002). In cases of insufficient collateralization, surgical cerebrovascular intervention is indicated (Fung et al. 2005).

### 2.1.3 Siderosis

Superficial siderosis of the CNS is thought to be caused by chronic subarachnoid hemorrhage that leads to deposition of ferritin and hemosiderin in subpial tissues, thus proliferation of microglia and astrocytes in the cerebellum, brainstem, vestibulocochlear nerves, and other sites (Anderson 2003). Tumors in the brain and, more frequently, in the spine, especially ependymomas, but also cerebellar astrocytomas and medulloblastoma can be associated with chronic subarachnoid hemorrhage, even many years after successful treatment (Anderson et al. 1999; McCarron et al. 2003). Resultant cardinal clinical features include slowly progressive bilateral sensorineural hearing loss, ataxia, and corticospinal tract dysfunction (Anderson et al. 1999). Bleeding sources may be multiple, small, and residual lesions in the dural left after tumor resection and RT (Anderson 2003). Cerebrospinal fluid (CSF) findings are rather unspecific but often contain erythrocytes and protein. Specific MRI signs include a hypointense rim surrounding the brainstem, cerebellar fissures, and cranial nerves. Treatment may only be successful, if the source of bleeding is identified and obliterated surgically. The prognosis of patients depends on the identification and ligation of the bleeding source(s) by the neurosurgeon. Imaging is crucial to establish the diagnosis but might fail to identify the bleeding source.

### 2.1.4 Mineralizing Microangiopathy and Smart Syndrome

#### Mineralizing Microangiopathy

Mineralizing non-inflammatory microangiopathy is seen mostly after irradiation (even with relatively low doses, such as 15 Gy) or intrathecal methotrexate application. It mainly affects the small cerebral vessels, especially the Aa. perforantes, which subsequently obliterate. After a mean lag time of about 10 months, calcifications appear in the basal ganglia and white matter. Histological examination exhibits calcifications as well as mucopolysaccharide and necrotic deposits in and around the small cerebral vessels (Price 1979; Price and Birdwell 1978). This vasculopathy may be clinically asymptomatic, if not accompanied by other late effects or only by leukencephalopathy (Sect. 2.2.2). Symptoms may vary based on localization and extent of vasculopathy. In a series of autopsies of pediatric leukemia patients, up to 17 % were found to have mineralizing microangiopathy after RT (Price and Birdwell 1978).

#### Smart Syndrome

The term SMART syndrome summarizes *s*troke-like *m*igraine *a*ttacks after RT – a rare condition

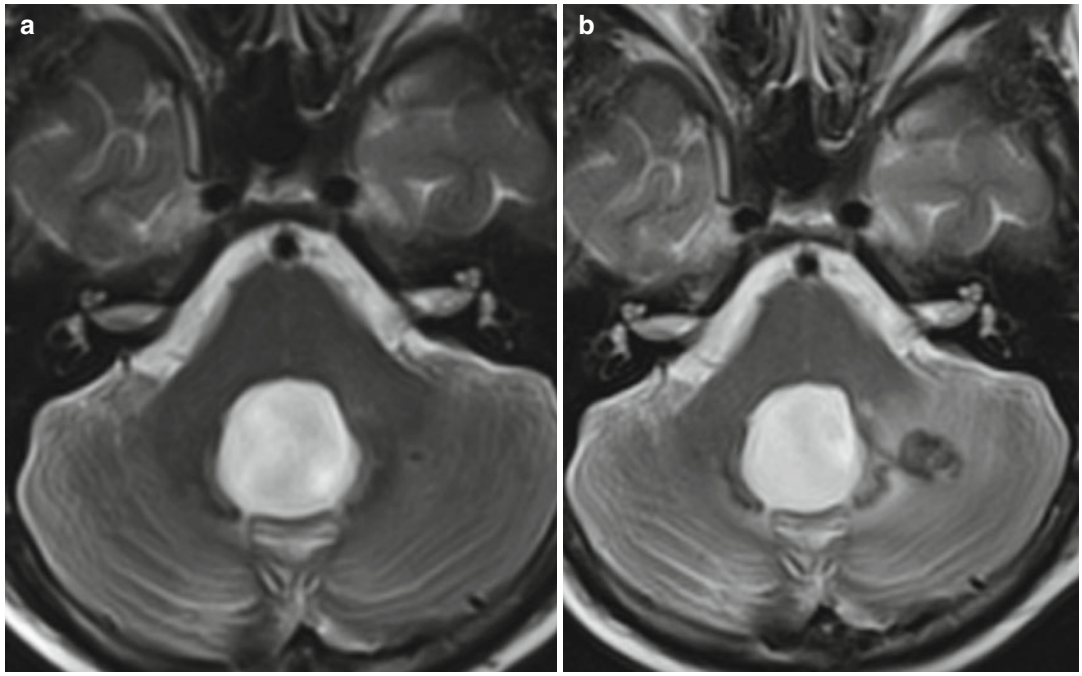


**Fig. 2** Cavernoma. Sudden increase in size (**b**) of a small possible cavernous hemangioma (**a**) in the left cerebellar hemisphere 18 months after combined treatment of a primarily disseminated MB. The increase was accompanied by acute cerebellar symptoms

after RT for posterior fossa tumors (typically with doses higher than 50 Gy), which can occur up to 35 years after therapy. It was first described in 1995 by Shuper et al. (Shuper et al. 1995). Patients present with complex migraines with transient and recurrent neurologic impairments such as hemiparesis, aphasia, and sensory disturbances. SMART syndrome mostly affects male survivors and those without a family history of migraine (incidence twice as high as in females). Diagnostic criteria include reversible headaches associated with stroke-like symptoms and a history of CRT. As potential covariates, mitochondrial encephalopathy, lactic acidosis and stroke (MELAS syndrome), and genetic hemiplegic migraine are currently being discussed. The pathomechanism is supposed to include direct RT-induced neuronal/endothelial damage, thus dysfunction, vascular instability, and vasospasm that may eventually lead to hypoxia and ischemia and mainly affect the posterior CNS circulation. MRI may reveal temporal and occipital gadolinium enhancement as well as gyral swelling. Many patients with SMART syndrome have been treated with cytostatic agents as well. However, the role of chemotherapy as a risk factor for developing this late effect still needs to be elucidated. Therapy is mainly symptomatic with no specific modality being identified as most effective (Armstrong et al. 2014; Partap 2012).

### 2.1.5 Vascular Malformations (Telangiectasia, Cavernoma, Aneurysm)

Vascular damage after RT of pediatric brain tumors predisposes vessels to dilate and form tortuosities (Fajardo 2005). In some survivors, these may form into cavernous, venous-based malformations, aneurysms, or, on a smaller vessel size level, telangiectasias resembling ectatic capillaries within normal brain tissues. In follow-up series of routine surveillance, up to 20 % of survivors presented with incidental telangiectasias independent of the radiation dose applied (Koike et al. 2004) and with clinical symptoms ranging from seizures and headache to neurological deficits due to hemorrhage. Instead, cavernous malformations present as dilated vein-like "caverns" (Fig. 2) with low blood flow.

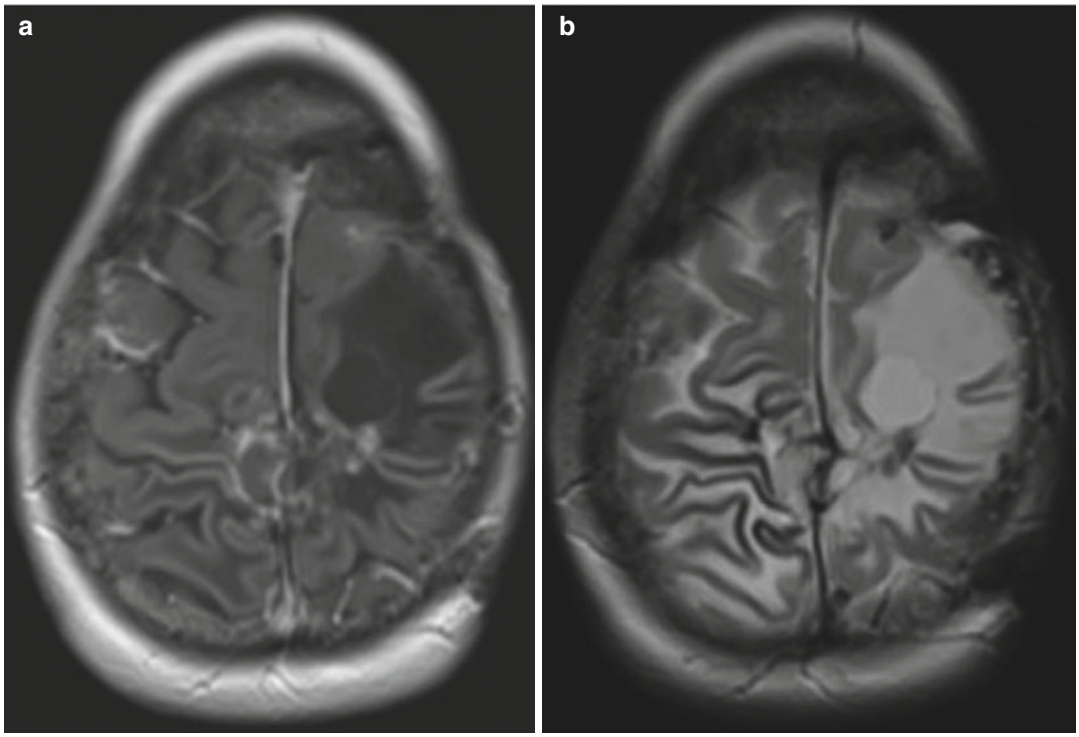


**Fig. 3** Radionecrosis. Chronic and constant curvilinear contrast enhancement (**a**) after reirradiation of a recurrent CNS-PNET involving the superior sagittal sinus in a girl with paraparesis. The T2-weighted hemosiderin deposition in the thinned cortex indicates bleeding (**b**)

Manifestation of symptoms varies individually and is dependent on the site of the lesion and on its propensity to bleed. Cavernomas may cause seizures or other neurological deficits, but mainly remain asymptomatic (Burn et al. 2007).

## 2.2 Gray and White Matter Disease

### 2.2.1 Radionecrosis

Although potentially of significant impact on quality of survival, the frequency and clinical consequences of radionecrosis in children and adolescents after RT for brain tumors have only been reported on by a few groups so far. Radionecrosis is defined as (normal) tissue death caused by irradiation. One of the few studies (Strenger et al. 2013) describes a series of 107 children, 5 of whom (4.7 %) showed radiological evidence of radionecrosis up to 10 years after RT. These data are well in line with analyses of larger, adult brain tumor cohorts (Ruben et al. 2006). Total RT dose, fractionation size, and concomitant or subsequent chemotherapy appear to be the major covariates for the risk of developing radionecrosis (Ruben et al. 2006). Consequently, the risk is even higher for patients receiving irradiation for treatment of tumor progression or relapse (Fig. 3). The major clinical challenge is to distinguish between radionecrosis, pseudoprogression, and progressive or recurrent disease (Sect. 2.5) or SMN in the radiation field (Sect. 2.6). Whereas some morphological MRI features are described as relatively specific for radionecrosis rather than tumor relapse including a "soap bubble-like interior" and a "Swiss cheese-like interior," only re-biopsy of the suspected region brings an unambiguous answer for a significant proportion of patients (Kumar et al. 2000; Rabin et al. 1996). Other methods to confirm a basic MRI diagnosis include FDG-PET or MR spectroscopy (Tan et al. 2011).

### 2.2.2 Leukencephalopathy

First reports on leukencephalopathy after cerebral irradiation with or without concomitant chemotherapy were described in the 1970s in pediatric patients treated for hematologic malignancies. Imaging and pathoanatomical findings primarily define leukencephalopathy (see below and Figs. 4 and 5). They may appear immediately or weeks and up to months after initiation of therapy and can be associated with a plethora of both focal and general neurologic symptoms (such as seizures, dysphagia, dysarthria, tremor, ataxia, spastic hemi- and tetraplegia, amnesia, apathy, and dementia) (Dietrich et al. 2001; Kellie et al. 2005; Lovblad et al. 1998).

The following three degrees of severity are distinguished by MRI: grade 1, mild increase in subarachnoid space, mild ventriculomegaly, small (+/− multiple) focal T2 hyperintensities, involving less than 33 % of susceptible areas; grade 2, moderate increase in subarachnoid space, moderate ventriculomegaly, focal T2 hyperintensities extending toward the centrum semiovale or 33 – 66 % of susceptible areas; and

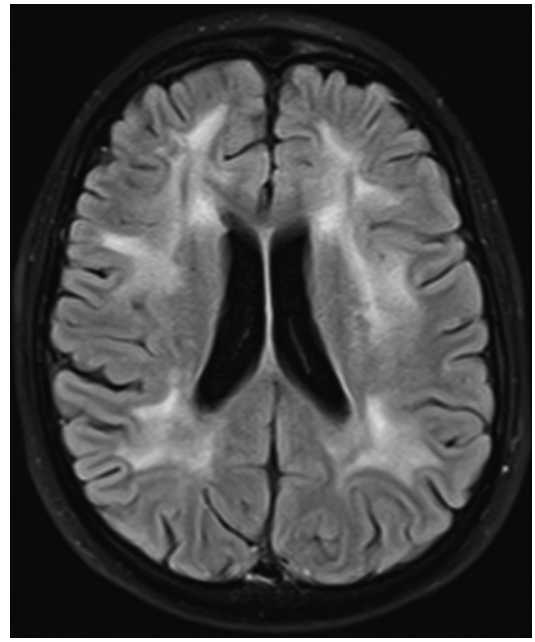

**Fig. 4** Leukencephalopathy. Confluating FLAIR hyperintensities in the white matter at the level of the centrum semiovale (LEP grade III) after combined treatment of a disseminated medulloblastoma. Note also a moderate atrophy with mildly enlarged ventricles and sulci

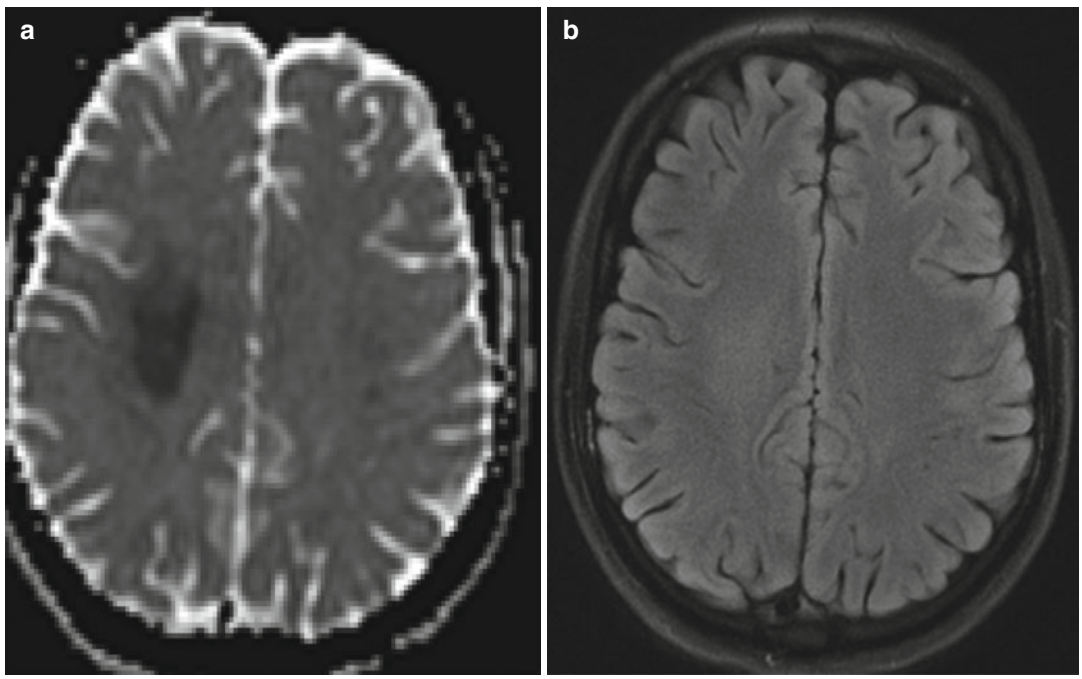


**Fig. 5** Acute methotrexate-induced leukencephalopathy. Apparent diffusion coefficient (ADC) images (**a**) provide improved visibility of an area of restricted diffusion in comparison to the corresponding FLAIR image (**b**) at sudden onset of hemiparesis – a characteristic of acute methotrexate encephalopathy

grade 3, severe increase in subarachnoid space, severe ventriculomegaly, T2 hyperintensities involving nearly all white matter or diffuse low attenuation (Green et al. 2012). Findings may additionally include lacunes and focal white matter lesions of up to 15 mm in diameter (Kellie et al. 2005).

The mechanisms responsible for the development of leukencephalopathy are still incompletely understood. Biopsy and autopsy revealed scattered focal white matter lesions, as well as diffuse cerebral atrophy, vasculopathy, demyelination, axonal swelling and fragmentation, coagulative necrosis, and focal mineralization. Vasculopathy is most certainly due to endothelial cell damage, whereas demyelination is mainly caused by glial cell damage. Modulating factors may be immune responses mediated by damaged glial cells. Irradiation dose and fractionation size as well as the routes of chemotherapy administration (especially of methotrexate) are known to play a role in the development of clinical symptoms. For example, larger total irradiation doses and lower fractionation sizes, intrathecal chemotherapy, and whole brain irradiation vs. focal RT enhance the probability of leukencephalopathy development and resulting chronic health conditions (see below) (Price 1979; Kellie et al. 2005). Furthermore, the dynamics of CSF flow and renal clearance of chemotherapeutics also regulate the severity and process of leukencephalopathy, since higher area-under-the-curve values are associated with an increased risk of leukencephalopathy. Last but not least, methotrexate and/or irradiation, respectively, may increase the sensitivity of neuronal tissue to subsequent treatment with additional chemotherapy (Flament-Durand et al. 1975).

The prognosis depends on the extent of leukencephalopathy and ranges from restitutio ad integrum, subacute process, and slow progression to cognitive decline and other neuropsychological deficits that may result in compromised academic achievement and reduced activity and participation (Mulhern et al. 2001; Steen et al. 2001). Subacute forms may resolve in up to 2/3 of patients within a median time of 6 months after onset. Although its clinical consequences may significantly compromise a pediatric brain tumor survivor's quality of survival, specific treatment of leukencephalopathy remains a challenge (Kellie et al. 2005). Therefore, imaging surveillance studies of leukencephalopathy should be performed to generate data and identify additional risk factors in order to optimize current treatment protocols.

### 2.2.3 Posterior Fossa Syndrome/ Cerebellocerebral Diaschisis

Posterior fossa syndrome or cerebellar mutism syndrome (CMS) is a frequently described complication following posterior fossa tumor removal. It was first described by Rekate et al. (Rekate et al. 1985) and is characterized by a disturbance of neuropsychological function that leads to akinetic mutism. It can extend to posterior fossa syndrome (PFS), which includes ataxia, muscular hypotonia, hemi- or tetraparesis, and cranial nerve deficits. The incidence of postoperative CMS ranges from 8 to 29 %. It manifests either immediately or with a delay of 1–2 days after surgery. The duration of CMS is largely variable and believed to be reversible in most patients (Rekate et al. 1985; Pollack 1997). Nevertheless, a relevant number of children may develop a lasting cerebellar cognitive affective syndrome (Levisohn et al. 2000). Intraoperative damage as well as postoperative disturbances, such as vasospasm or cerebral edema, may play a causative role (Levisohn et al. 2000; Wells et al. 2008). The anatomical structures most prone to injury associated with CMS are cerebellar midline structures, dentate nucleus, and the dentatothalamo-cortical outflow tracts (Pollack 1997; Pollack et al. 1995). Risk factors for CMS are midline tumors or brainstem involvement, large tumor size, and histology, as it occurs relatively more often in medulloblastoma patients. Risk factors that have been described inconsistently include gross radiological tumor removal and vermal incision (Pollack 1997; Levisohn et al. 2000; Pollack et al. 1995).

Earlier studies applied different imaging techniques in order to elucidate the pathophysiological understanding of the development of CMS. Single photon emission computed tomography (SPECT) revealed inconsistent findings of local hypoperfusion in mute patients after

posterior fossa surgery. Various MRI findings were suggestive of ischemia, edema, and structural damage of midline structures as contributing factors (Pollack et al. 1995; Ersahin et al. 2002). Since younger children are far more prone to develop CMS after posterior fossa surgery than older children and younger age is also associated with less favorable outcome, developmental factors – such as neuronal lesion due to incompletely myelinated pathways – have been hypothesized to play a role as well (Ronning et al. 2005). As an anatomical substrate for white matter lesions, efferent dentatothalamo-cortical (DTC) outflow tracts have been supposedly affected in cases of CMS (Morris et al. 2009b). Also, DTI has been used to identify white matter lesions in patients suffering from PFS. Significantly reduced fractional anisotropy (FA) values were identified in DTC pathways. Similarly, generation of FA maps using tract-based spatial statistics showed damage to supratentorial white matter microstructures in pediatric cerebellar tumor survivors after adjuvant therapy and without (Fig. 6). Tractography of white matter tracts connecting the cerebellum and the frontal lobes, i.e., frontocerebellar association fibers (FCF), revealed significant diminished values in pediatric patients with symptoms of CMS when compared to patients without symptoms of CMS or with healthy peers, respectively. Using a semiquantitative analysis of anatomical structures, significant differences of the fiber tract signals were observed in the superior cerebellar peduncles and midline cerebellar structures in patients with symptoms of CMS compared to neurologically unaffected children or healthy controls ($p < 0.01$). Statistically significant differences in FA values also were found in the frontal lobe and in the superior cerebellar peduncles (Rueckriegel et al. 2015; Rueckriegel et al. 2010; Rueckriegel et al. 2012b; Soelva et al. 2013). Avulam et al. identified hypertrophic olivary degeneration as a late imaging marker of CMS, depicting the ruptured Guillain-Mollaret triangle as a critical structure underpinning CMS (Avula et al. 2015).

## 3 Infections

Infections of the CNS in pediatric brain tumor patients are usually a result of treatment-induced immunosuppression. They represent a common cause of neuropsychological deficits in this cohort. The clinical symptoms may be subtle or even absent. Supportive care regimens including the use of glucocorticoids and nonsteroidal anti-inflammatory drugs (NSAID) typically suppress fever as one of the cardinal warning symptoms. Thus, patients, particularly when neutropenic, require routine clinical monitoring followed by promptly initiated blood and CSF tests as well as adequate imaging upon any suspicious sign of (CNS) infection. Clinical, laboratory, and imaging results and eventually the clinical course help differentiating between meningitis, meningoencephalitis, brain abscess, and shunt infection (Pfister 2012).

The most common type of infection is meningitis (Pruitt 2003). In case of neurological abnormalities, an infectious cause is often difficult to exclude, thereby prompting empiric broad antibiotic treatment, especially in patients with granulocytopenia, who have a higher morbidity and mortality in comparison to oncologic patients with normal white blood cell count (Sommers and Hawkins 1999). Both viruses and other pathogens can damage glial cells, neurons, and/or endothelial and stromal cells of the CNS. This leads to vascular leakage and glial proliferation – in case of meningitis even into the subarachnoidal space. The inflammation may spread pursuant to pial vascular architecture into cortical structures, thereby causing meningoencephalitis. Serous leptomeningitis is exclusively associated with hyperemia and enhanced CSF production. In contrast, encephalitis is defined as inflammation of the brain parenchyma. Apart from continuous spread, it may also arise via hematogenic distribution. Depending on the type of primarily affected structures, i.e. white or gray matter, CNS infections are further subdivided into leukoencephalitis or polioencephalitis. A brain abscess is a circumscribed infection of the parenchyma. A shunt infection may be restricted to a ventriculitis or develop into meningoencephalitis.

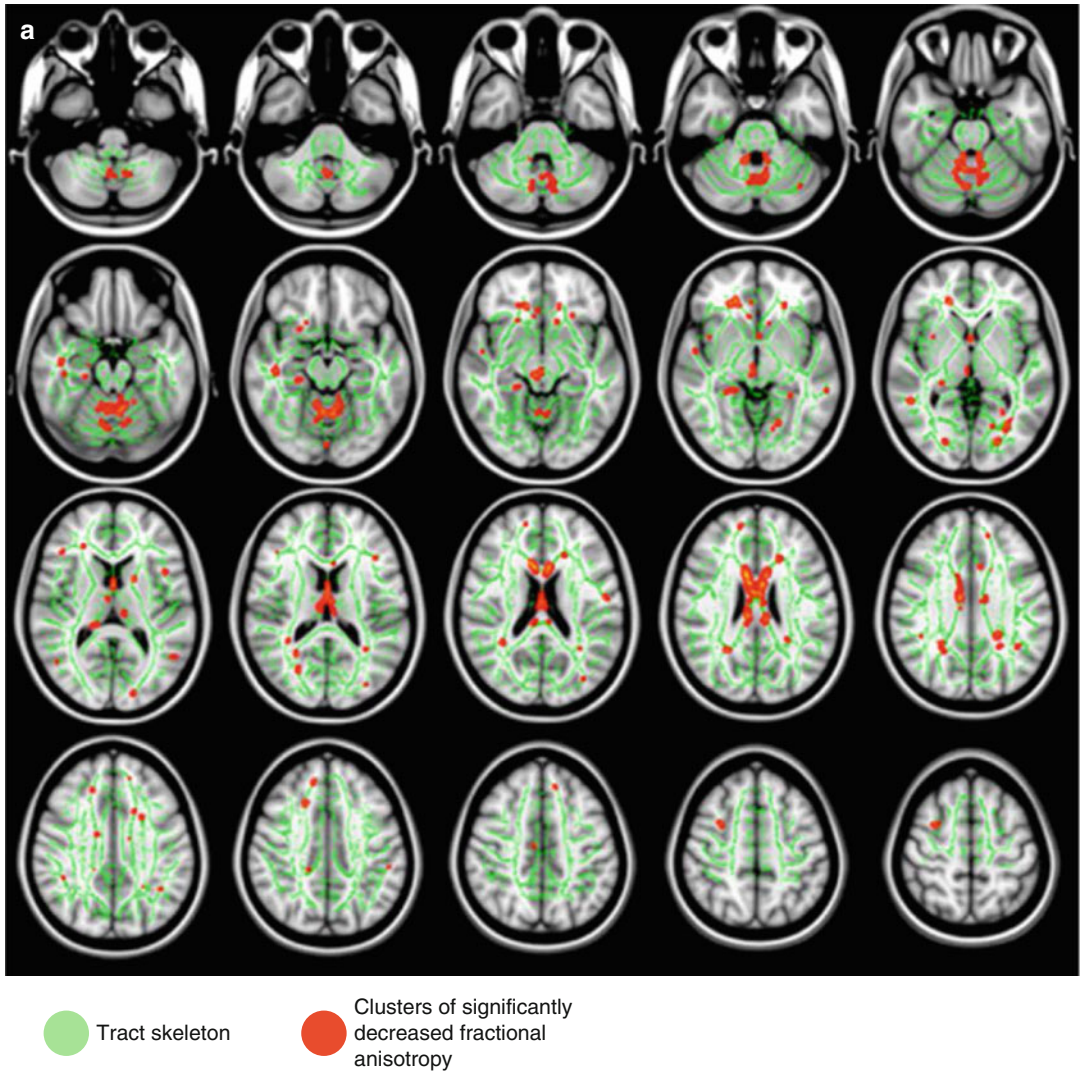


**Fig. 6** Cerebellar mutism syndrome. (**a**) Clusters of decreased fractional anisotropy (FA) in medulloblastoma patients. Tract skeleton (thresholded at FA > 0.2) and clusters of significantly decreased fractional anisotropy ($p < 0.05$) were derived from averaged fractional anisotropy images of the patient group and the concordant control group. These structures were superimposed on the Montreal Neurological Institute 152 (MNI152) standard brain. Axial slices (5 mm). Clusters were thickened to visualize that the skeleton represents the whole tract. (**b**) Clusters of decreased fractional anisotropy (FA) in pilocytic astrocytoma patients. Tract skeleton (thresholded at FA > 0.2) and clusters of significantly decreased fractional anisotropy ($p < 0.05$) were derived from averaged fractional anisotropy images of the pilocytic astrocytoma patient group and the concordant control group. These structures were superimposed on the MNI152 standard brain. Axial slices (5 mm). Clusters were thickened to visualize that the skeleton represents the whole tract. (**c**) Decrease of fractional anisotropy (FA) in superior cerebellar peduncles. Tract skeleton (thresholded at FA > 0.2) and clusters of significantly decreased fractional anisotropy ($p < 0.05$) were derived from averaged fractional anisotropy images of the patient groups and their concordant control group. These structures were superimposed on the MNI152 standard brain. Superior cerebellar peduncles of medulloblastoma patients were bilaterally affected by decrease of fractional anisotropy, while the superior cerebellar peduncles of pilocytic astrocytoma patients were not. (**d**) Decrease of fractional anisotropy (FA) in medial cerebellar peduncles. Tract skeleton (thresholded at fractional anisotropy > 0.2) and clusters of significantly decreased fractional anisotropy ($p < 0.05$) were derived from averaged fractional anisotropy images of the patient groups and their concordant control group. These structures were superimposed on the MNI152 standard brain. Fractional anisotropy of middle cerebellar peduncles was neither affected in medulloblastoma nor in pilocytic astrocytoma patients

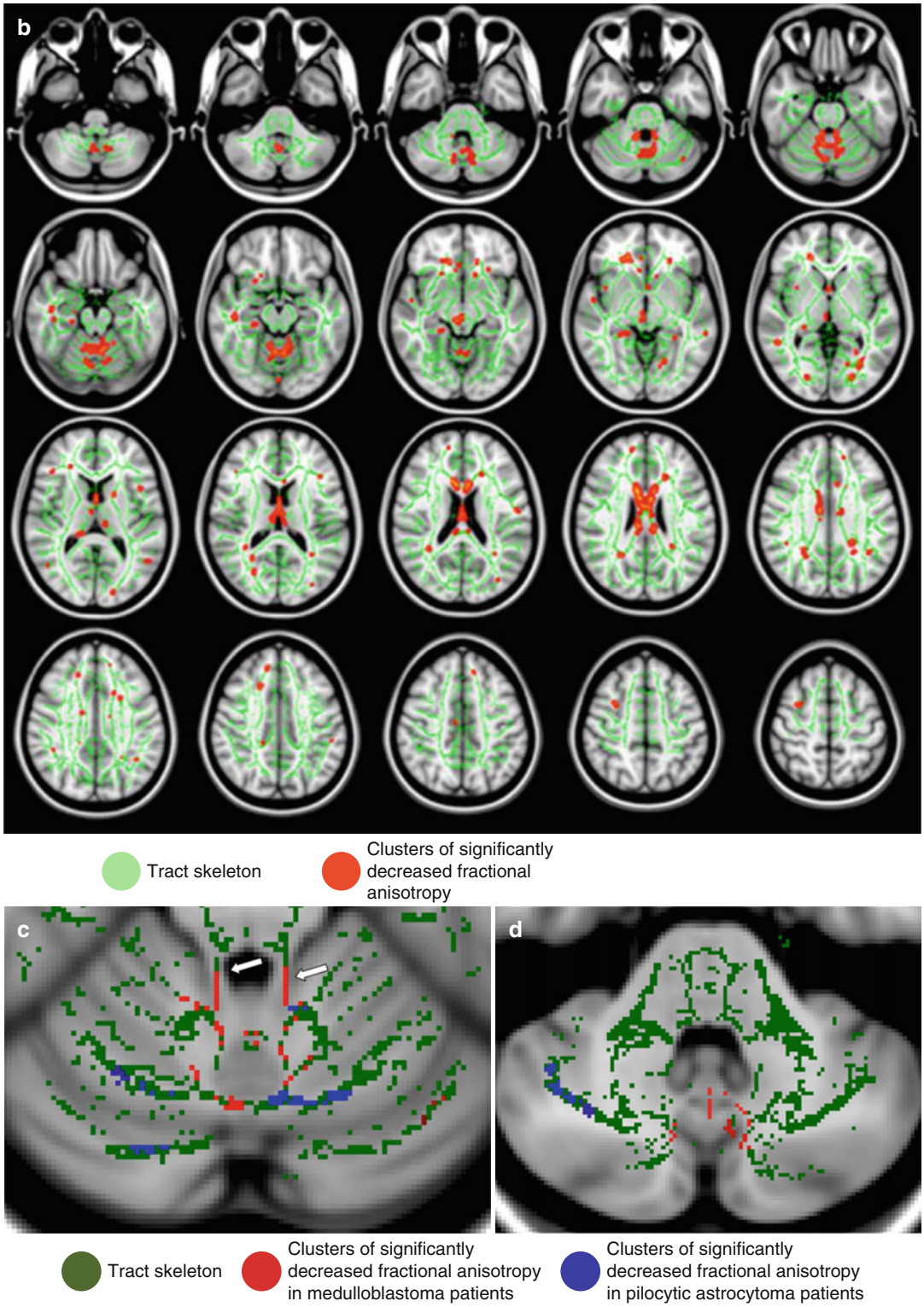


**Fig. 6** (continued)

Primary risk factors of CNS infections in pediatric oncology are (*a*) antitumoral therapy (Sommers and Hawkins 1999), (*b*) neurosurgery (Sommers and Hawkins 1999), (*c*) intraventricular chemotherapy (infections due to intracerebral catheters occur to 2–23 % of patients (Sommers and Hawkins 1999; Mechleb et al. 2003; Chamberlain et al. 1997) with the frequency of catheter replacement not being associated with the incidence of infection (Mechleb et al. 2003; Pfisterer et al. 2003)), and (*d*) age (in a prospective study of fungemias, pediatric oncologic patients showed a tenfold higher incidence of fungal meningitis than adults (11.4 % *vs*. 0.8 %)) (Krupova et al. 2000).

Imaging allows detection of inflammatory changes of the brain parenchyma and evaluation of response to anti-infectious and anti-inflammatory treatment. It aims at excluding brain edema, hydrocephalus, hemorrhage, infarctions, cerebritis, brain abscess, subdural empyema, parameningeal foci of infection (sinusitis, mastoiditis), intracranial air due to dural fistula, meningeal and ventricular ependymal involvement, as well as sequelae of infection such as sinus vein thrombosis and calcifications. MRI is usually superior to computed tomography (CT), except for diagnosis of hemorrhage. CT is more useful in detecting calcifications (such as in toxoplasmosis) and evaluating bony structures, while MRI is superior regarding the evaluation of gray vs. white matter infection. Contrast enhancement series and T1- and T2-weighted studies are mandatory, while diffusion-weighted imaging and MR angiography have proven helpful. Overall, the use of glucocorticoids in combination with granulocytopenia and anemia may compromise the specificity and sensitivity of imaging techniques (Pruitt 2003; Hedlund and Boyer 1999; Ashwal 1995).

## 4 Posterior Reversible Encephalopathy Syndrome (PRES)

A rare condition potentially compromising treatment outcome in pediatric neuro-oncology is the *p*osterior *r*eversible *e*ncephalopathy *s*yndrome (PRES). It is diagnosed based on both clinical and imaging findings. Patients frequently present with headaches, seizures, speech difficulties, mental disturbancies, and visual impairment. The latter are specific for PRES and allow to differentiate this complication from methotrexate leukencephalopathy (Baytan et al. 2010; Hinchey et al. 1996; Lee et al. 2008; Won et al. 2009). The visual deficits range from hemianopsia, visual field loss, blurred vision, and hallucinations to complete cortical blindness. The underlying mechanism seems to be sudden onset of hypertension superseding autoregulation of the blood-brain barrier, thereby leading to capillary leakage and vasogenic edema. The predilection of the posterior cerebral region seems to be due to a reduced sympathetic innervation of the vertebrobasilar system (Baytan et al. 2010; Hinchey et al. 1996; Lee et al. 2008; Won et al. 2009). Risk factors include renal dysfunction, immune suppression and administration of certain chemotherapeutic agents (vincristine, high-dose methotrexate, cytarabine, cisplatin, gemcitabine, asparaginase, cyclosporine) (Marinella and Markert 2009), and hypomagnesemia, which suppresses cortical function by causing calcium-magnesium imbalances (Al-Tweigeri et al. 1999). Besides, chemotherapy may have a direct toxic effect on endothelial cells.

Imaging reveals characteristic abnormalities on T2-weighted images of the bilateral occipitoparietal region. Diffusion-weighted imaging is isointense due to vasogenic edema (Baytan et al. 2010). Fluid attenuation may reveal lesions due to cerebral fluid suppression. Current therapeutic concepts are mainly symptomatic and include long-term anticonvulsive treatment. PRES usually resolves within days to weeks but may recur as chronic epilepsy after 8–24 months (Lucchini et al. 2008).

## 5 (Pseudo)Progression and Recurrent Disease

Depending on the type, histological grade, initial response of the tumor to therapy, and other individual prognostic factors, every pediatric brain tumor survivor is facing the risk of progressive or recurrent disease, particularly during the first 10 years after

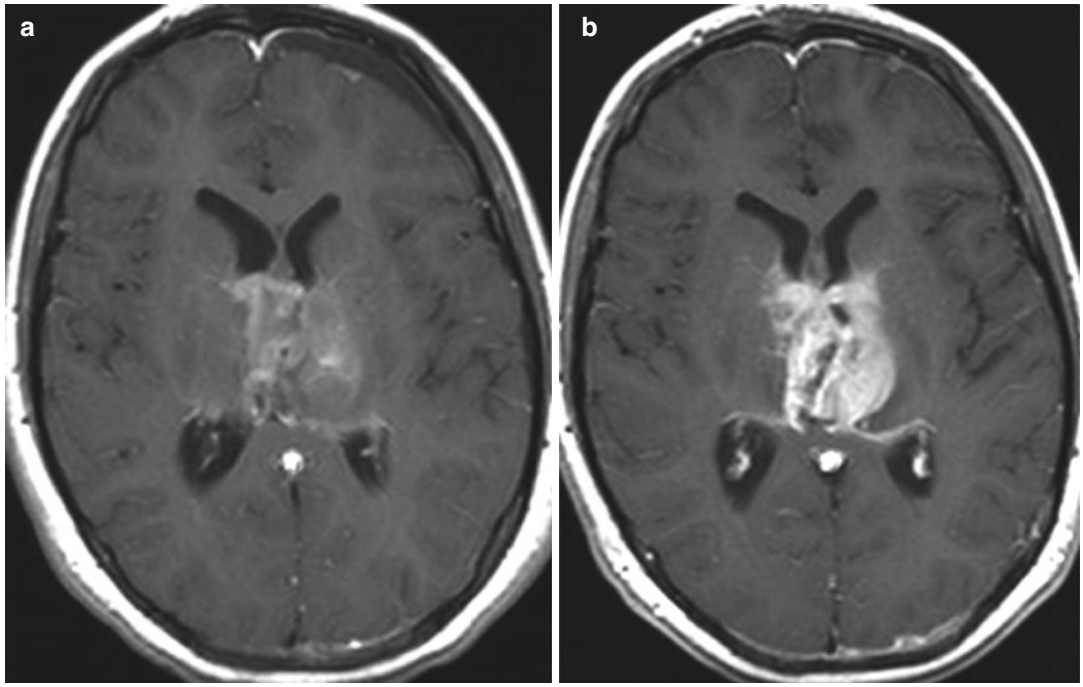


**Fig. 7** Pseudoprogression: Temporarily increasing and intensified enhancement after chemoradiation of an anaplastic astrocytoma of the thalami (**b**). (**a**: MRI prior to RT)

therapy. Like treatment of the primary tumor, second-line therapy is mostly based on multicenter, multidisciplinary approaches, which are continuously being optimized (Bode et al. 2014; Müller et al. 2014). However, considering that in general, relapse is still one of the most frequent causes of death in childhood cancer survivors and that coping with the fear of recurrent disease can severely impact quality of survival, surveillance imaging plays a major role in the management of both progressive and recurrent disease as well as distinguishing these from post-radiation treatment effects.

Post-radiation treatment effects can be divided into pseudoprogression or, as outlined earlier (Sect. 2.2.1), radiation necrosis. Pseudoprogression is caused by temporary interruption of myelin synthesis secondary to RT-induced damage to glial cells. According to various reports, the T1 gadolinium enhancement at the tumor site seen on MRI (Fig. 7) is only of transient nature and usually recovers spontaneously without treatment (Rider 1963; Wilson et al. 1977). In contrast, radiation necrosis (Sect. 2.2.1) usually presents with a space-occupying necrotic lesion with mass effect.

Both progressive and recurrent disease can develop at any anatomical site of the CNS including the initial tumor localization and the leptomeninges. In fact, the leptomeninges are a frequent site of dissemination in children and adolescents with CNS tumors, affecting up to 20 % of patients at the time of diagnosis or progression (Chamberlain 1997; Packer et al. 1985). Leptomeningeal disease occurs more often in pediatric patients with CNS-PNET than with ependymoma, germ cell tumors, or high-grade gliomas. CSF and dissemination to the leptomeninges at the time of disease progression are often associated with an unfavorable prognosis. Administration of intrathecal chemotherapy is a common treatment modality of current protocols to prevent or treat leptomeningeal disease. Like parenchymatous relapse or progression, leptomeningeal tumor dissemination needs to be considered as a disease affecting the entire CNS, thereby, in addition to clinical and CSF monitoring, requiring radiological evaluation of both the brain and spinal cord.

Survivors may show radiological findings suggestive of post-radiation treatment effects or

progressive or recurrent disease, respectively. However, differentiating post-radiation treatment effects from tumor tissue by MRI alone remains a challenge. Therefore, understanding both the clinical and imaging sequelae that promote a reliable differential diagnosis between these conditions is crucial in order to develop and establish rational surveillance schedules.

In cases of pseudoprogression, edema and contrast enhancement may be resulting from the radiation-induced, temporarily dysfunctional blood-brain barrier. To our knowledge, there have been no studies of biopsies obtained from patients with pseudoprogression to confirm the idea of vascular alterations as typically observed in radionecrosis (Sect. 2.2.1). However, a correlation between *O*(6)-methylguanine-DNA methyltransferase (MGMT) methylation status and the risk of pseudoprogression has been reported for malignant gliomas (Brandes et al. 2008) and may apply to other CNS tumor entities as well.

While progressive and recurrent (including leptomeningeal) disease may be either asymptomatic or present with focal neurologic deficits at any time depending on the size and site of the process, the major difference in clinical presentation between pseudoprogression and radionecrosis necrosis is timing. Compared to radionecrosis, which typically occurs 3 months to 3 years after treatment, pseudoprogression usually appears earlier (i.e., within the first 3 months after RT) (Brandsma et al. 2008) and is frequently presenting as an enhancing lesion on routine follow-up MRI in asymptomatic patients. In fact, most survivors with pseudoprogression do not develop any clinical symptoms. Only a few suffer complications resultant from temporary demyelination. These may present as deterioration of preexisting impairments, temporary neurocognitive decline, somnolence syndrome, or subacute rhombencephalitis (Fink et al. 2012) .

Although histological confirmation of the diagnosis is still safest, significant improvements have been made for a noninvasive approach to distinguish between radiation necrosis, pseudoprogression, and progressive or recurrent tumor, respectively. While contrast-enhanced MRI has its benefits, a multi-modality approach of surveillance imaging, i.e., the combined use of basic MRI and functional imaging techniques such as MR spectroscopy and FDG-PET, has proven efficient for differentiating between tumor tissue and post-radiation treatment effects. It is also capable of detecting a proportion of asymptomatic, particularly late relapses, thereby providing lead time for early treatment initiation. In this context, prospective studies will help to further define the pathophysiological, molecular, clinical, and radiological differences between pseudoprogression, radionecrosis, and progressive or recurrent disease as a basis for the development and establishment of guided schedules for surveillance imaging in pediatric brain tumor survivors.

## 6 Secondary Malignancies

A serious late effect of treatment for pediatric brain tumors is the development of a secondary malignancy. Overall, childhood cancer survivors have an approximately fivefold increased risk to develop a second tumor when compared to the age-matched normal population (Cai et al. 2012). The risk seems to be associated with high-field RT, high-dose chemotherapy, and young age at primary treatment (You et al. 2013). The most frequent histological diagnoses include primary CNS tumors (40 %, mostly high-grade gliomas, medulloblastoma, and meningioma), sarcomas, thyroid cancer, leukemia, and head and neck cancer (Cai et al. 2012; Ning et al. 2015). However, the proportion of secondary malignancies might be underestimated, since the practice of re-biopsying (late) relapses is only changing slowly, and it is evident by now that a significant proportion of clinically and radiologically appearing relapses of the primary tumor are in fact biologically completely unrelated secondary malignancies. As a consequence, a medulloblastoma expert group recently recommended to re-biopsy every suspected relapse, which occurs 3 years or later after initial diagnosis, to exclude a secondary malignancy (personal communication). Furthermore, there is growing evidence that pediatric brain tumor survivors with a secondary malignancy have a much higher likelihood of an underlying (often previously undiagnosed)

hereditary cancer predisposition syndrome such as Li-Fraumeni syndrome, Mismatch repair deficiency, Gorlin's syndrome, familial adenomatous polyposis, or Fanconi anemia. Both the fact that a significant proportion of relapses are probably secondary tumors and the prevalence of underlying hereditary predisposition should be carefully considered, when evaluating radiological findings in these patients.

## Conclusion

Imaging technologies for pediatric brain tumor survivors are continuously improving. However, most of the multiple MRI functional parameters have been validated only for adult CNS tumor cohorts so far and require multicentric validation in the pediatric population. While central analysis of conventional MRI follow-up studies is fairly straightforward, interpretation of functional imaging studies remains more of a challenge, since various functional techniques are operator dependent (such as single voxel spectroscopy, susceptibility perfusion). Last but not least, regular upgrades by MRI vendors may render the previous study data invalid, thereby compromising the options of historical comparison.

Future prospective studies analyzing tumor- and treatment-related late effects in large cohorts of pediatric brain tumor survivors by combining standardized and unified functional imaging and clinical assessment methods will help expanding our current knowledge and would help to better understand how certain radiological findings correlate with cognitive and other neuropsychological functions. Finally, considering the broad spectrum of changes in CNS maturation during childhood and adolescence, longer-term surveillance imaging, possibly even longer than recommended in current treatment protocols, may be helpful to determine the impact of tumor- and treatment-related late effects on this dynamic process. These types of studies will not only help to shape less pernicious RT protocols but can also contribute to our understanding of the process of healthy vs. compromised neuropsychological development by further evaluating how the developing CNS deals with insults that pose a substantial risk on the quality of survivorship.

## References

Aarsen FK et al (2009) Cognitive deficits and predictors 3 years after diagnosis of a pilocytic astrocytoma in childhood. J Clin Oncol 27:3526 (July 20, 2009)

Abhaya AV, Piscione J, Bouffet E (2013) Long-term quality of life in children treated for posterior fossa brain tumors. J Neurosurg Pediatr 12:235

Al-Tweigeri T, Magliocco AM, DeCoteau JF (1999) Cortical blindness as a manifestation of hypomagnesemia secondary to cisplatin therapy: case report and review of literature. Gynecol Oncol 72:120

Anderson NE (2003) Late complications in childhood central nervous system tumour survivors. Curr Opin Neurol 16:677

Anderson N, Sheffield S, Hope J (1999) Superficial siderosis of the central nervous system: a late complication of cerebellar tumors. Neurology 52:163

Aoki S et al (2002) Radiation-induced arteritis: thickened wall with prominent enhancement on cranial MR images report of five cases and comparison with 18 cases of Moyamoya disease. Radiology 223:683

Armstrong AE, Gillan E, DiMario FJ Jr (2014) SMART syndrome (stroke-like migraine attacks after radiation therapy) in adult and pediatric patients. J Child Neurol 29:336

Ashwal S (1995) Neurologic evaluation of the patient with acute bacterial meningitis. Neurol Clin 13:549

Avula S et al (2015) Diffusion abnormalities on intraoperative magnetic resonance imaging as an early predictor for the risk of posterior fossa syndrome. Neuro Oncol 17:614

Ball W, Prenger E, Ballard E (1992) Neurotoxicity of radio/chemotherapy in children: pathologic and MR correlation. AJNR Am J Neuroradiol 13:761

Baytan B, Ozdemir O, Demirkaya M, Evim MS, Gunes AM (2010) Reversible posterior leukoencephalopathy induced by cancer chemotherapy. Pediatr Neurol 43:197

Benesch M et al (2006) Late sequela after treatment of childhood low-grade gliomas: a retrospective analysis of 69 long-term survivors treated between 1983 and 2003. J Neurooncol 78:199 (2006/06/01, 2006)

Bode U et al (2014) Treatment of recurrent primitive neuroectodermal tumors (PNET) in children and adolescents with high-dose chemotherapy (HDC) and stem cell support: results of the HITREZ 97 multicentre trial. J Neurooncol 120:635 (2014/12/01, 2014)

Bowers DC et al (2006) Late-occurring stroke among long-term survivors of childhood leukemia and brain tumors: a report from the Childhood Cancer Survivor Study. J Clin Oncol: Off J Am Soc Clin Oncol 24:5277

Brandes AA et al (2008) MGMT promoter methylation status can predict the incidence and outcome of

pseudoprogression after concomitant radiochemotherapy in newly diagnosed glioblastoma patients. J Clin Oncol 26:2192 (May 1, 2008)

Brandsma D, Stalpers L, Taal W, Sminia P, van den Bent MJ (2008) Clinical features, mechanisms, and management of pseudoprogression in malignant gliomas. Lancet Oncol 9:453

Burn S, Gunny R, Phipps K, Gaze M, Hayward R (2007) Incidence of cavernoma development in children after radiotherapy for brain tumors. J Neurosurg 106:379

Cai Y, Cao L, Bao X, Xie L (2012) Second malignant neoplasms in childhood malignant brain tumour: a long-term population-based study. J Paediatr Child Health 48:990

Chamberlain MC (1997) Pediatric leptomeningeal metastases: outcome following combined therapy. J Child Neurol 12(53) (January 1, 1997)

Chamberlain MC, Kormanik PA, Barba D (1997) Complications associated with intraventricular chemotherapy in patients with leptomeningeal metastases. J Neurosurg 87:694

de Haas EC et al (2010) The metabolic syndrome in cancer survivors. Lancet Oncol 11:193

Desai SS, Paulino AC, Mai WY, Teh BS (2006) Radiation-induced moyamoya syndrome. Int J Radiat Oncol Biol Phys 65(1222)

Di Rocco F, Jucá CE, Zerah M, Sainte-Rose C (2013) Endoscopic third ventriculostomy and posterior fossa tumors. World Neurosurg 79:S18.e15

Dietrich U et al (2001) White matter disease in children treated for malignant brain tumors. Childs Nerv Syst: ChNS 17:731

Duffner PK (2004) Long-term effects of radiation therapy on cognitive and endocrine function in children with leukemia and brain tumors. Neurologist 10:293

Effinger K et al (2014) Oral and dental late effects in survivors of childhood cancer: a Children's Oncology Group report. Support Care Cancer 22:2009 (2014/07/01, 2014)

Erdem E, Zimmerman R, Haselgrove J, Bilaniuk L, Hunter J (2001) Diffusion-weighted imaging and fluid attenuated inversion recovery imaging in the evaluation of primitive neuroectodermal tumors. Neuroradiology 43:927

Ersahin Y, Yararbas U, Duman Y, Mutluer S (2002) Single photon emission tomography following posterior fossa surgery in patients with and without mutism. Childs Nerv Syst: ChNS 18:318

Fajardo LF (2005) The pathology of ionizing radiation as defined by morphologic patterns. Acta Oncol 44:13

Fink J, Born D, Chamberlain M (2012) Radiation necrosis: relevance with respect to treatment of primary and secondary brain tumors. Curr Neurol Neurosci Rep 12:276 (2012/06/01, 2012)

Fischbein N et al (1996) Radiologic classification of brain stem tumors: correlation of magnetic resonance imaging appearance with clinical outcome. Pediatr Neurosurg 24:9

Flament-Durand J, Ketelbant-Balasse P, Maurus R, Regnier R, Spehl M (1975) Intracerebral calcifications appearing during the course of acute lymphocytic leukemia treated with methotrexate and X-rays. Cancer 35:319

Fouladi M et al (2004) White matter lesions detected by magnetic resonance imaging after radiotherapy and high-dose chemotherapy in children with medulloblastoma or primitive neuroectodermal tumor. J Clin Oncol 22:4551 (November 15, 2004)

Friedrich C et al (2013) Treatment of young children with CNS-primitive neuroectodermal tumors/pineoblastomas in the prospective multicenter trial HIT 2000 using different chemotherapy regimens and radiotherapy. Neuro Oncol 15:224 (February 1, 2013)

Fung LW, Thompson D, Ganesan V (2005) Revascularisation surgery for paediatric moyamoya: a review of the literature. Childs Nerv Syst: ChNS 21:358

Gaber MW et al (2003) Differences in ICAM-1 and TNF-alpha expression between large single fraction and fractionated irradiation in mouse brain. Int J Radiat Biol 79:359

Garcia-Puig M et al (2012) Neurotoxicity due to methotrexate in paediatric patients. Description of the clinical symptoms and imaging findings. Rev Neurol 54:712

Gnekow AK et al (2012) Long-term follow-up of the multicenter, multidisciplinary treatment study HIT-LGG-1996 for low-grade glioma in children and adolescents of the German Speaking Society of Pediatric Oncology and Hematology. Neuro Oncol 14:1265 (October 1, 2012)

Green DM et al (2012) Risk factors for obesity in adult survivors of childhood cancer: a report from the Childhood Cancer Survivor Study. J Clin Oncol: Off J Am Soc Clin Oncol 30:246

Hedlund GL, Boyer RS (1999) Neuroimaging of postnatal pediatric central nervous system infections. Semin Pediatr Neurol 6:299

Hersh JH, American G (2008) Academy of Pediatrics Committee on Health supervision for children with neurofibromatosis. Pediatrics 121(633)

Hinchey J et al (1996) A reversible posterior leukoencephalopathy syndrome. N Engl J Med 334:494

Hoffmann A, Gebhardt U, Sterkenburg AS, Warmuth-Metz M, Müller HL (2014) Diencephalic syndrome in childhood craniopharyngioma—results of German multicenter studies on 485 long-term survivors of childhood craniopharyngioma. J Clin Endocrinol Metab 99:3972

Hoppe-Hirsch E et al (1990) Medulloblastoma in childhood: progressive intellectual deterioration. Childs Nerv Syst 6:60

Kaatsch P, Grabow D (2012) The German cohort of long-term survivors of childhood cancer. A population-based cohort in the German Childhood Cancer Registry. Bundesgesundheitsblatt Gesundheitsforschung Gesundheitsschutz 55:843

Kaatsch P, Spix C, German Childhood Cancer Registry - Report 2013/14 (1980–2013). Institute of Medical Biostatistics, Epidemiology and Informatics (IMBEI)

at the University Medical Center of the Johannes Gutenberg University Mainz, 2014
Kellie SJ et al (2005) Late magnetic resonance imaging features of leukoencephalopathy in children with central nervous system tumours following high-dose methotrexate and neuraxis radiation therapy. Eur J Cancer 41:1588
Khong P-L et al (2003) Diffusion-tensor imaging for the detection and quantification of treatment-induced white matter injury in children with medulloblastoma: a pilot study. Am J Neuroradiol 24:734 (April 1, 2003)
Khong P-L et al (2006) White matter anisotropy in post-treatment childhood cancer survivors: preliminary evidence of association with neurocognitive function. J Clin Oncol 24:884 (February 20, 2006)
Koeller KK, Henry JM (2001) From the archives of the AFIP. RadioGraphics 21:1533
Koike S et al (2004) Asymptomatic radiation-induced telangiectasia in children after cranial irradiation: frequency, latency, and dose relation. Radiology 230:93
Krupova Y et al (2000) Prospective study on fungemia in children with cancer: analysis of 35 cases and comparison with 130 fungemias in adults. Support Care Cancer 8:427
Kumar AJ et al (2000) Malignant gliomas: MR imaging spectrum of radiation therapy- and chemotherapy-induced necrosis of the brain after treatment. Radiology 217:377
Lawrence YR et al (2010) Radiation dose–volume effects in the brain. Int J Radiat Oncol Biol Phys 76:S20
Lee VH, Wijdicks EF, Manno EM, Rabinstein AA (2008) Clinical spectrum of reversible posterior leukoencephalopathy syndrome. Arch Neurol 65:205
Lemort M, Canizares-Perez AC, Van der Stappen A, Kampouridis S (2007) Progress in magnetic resonance imaging of brain tumours. Curr Opin Oncol 19:616
Levisohn L, Cronin-Golomb A, Schmahmann JD (2000) Neuropsychological consequences of cerebellar tumour resection in children: cerebellar cognitive affective syndrome in a paediatric population. Brain: J Neurol 123(Pt 5):1041
Liu AK et al (2009) Vascular abnormalities in pediatric craniopharyngioma patients treated with radiation therapy. Pediatr Blood Cancer 52:227
Lovblad K et al (1998) Pure methotrexate encephalopathy presenting with seizures: CT and MRI features. Pediatr Radiol 28:86
Lucchini G et al (2008) Encephalopathy syndrome in children with hemato-oncological disorders is not always posterior and reversible. Pediatr Blood Cancer 51:629
Mabbott DJ, Noseworthy MD, Bouffet E, Rockel C, Laughlin S (2006) Diffusion tensor imaging of white matter after cranial radiation in children for medulloblastoma: Correlation with IQ. Neuro Oncol 8:244 (July 1, 2006)
Marinella MA, Markert RJ (2009) Reversible posterior leucoencephalopathy syndrome associated with anticancer drugs. Intern Med J 39:826
McCarron MO et al (2003) Superficial siderosis of the central nervous system many years after neurosurgical procedures. J Neurol Neurosurg Psychiatry 74:1326 (September 1, 2003)
Meacham LR et al (2010) Cardiovascular risk factors in adult survivors of pediatric cancer – a report from the childhood cancer survivor study. Cancer Epidemiol Biomark Prevent: Publ Am Assoc Cancer Res Cosponsored by the American Society of Preventive Oncology 19(170)
Mechleb B, Khater F, Eid A, David G, Moorman JP (2003) Late onset Ommaya reservoir infection due to Staphylococcus aureus: case report and review of Ommaya Infections. J Infect 46:196
Merchant TE, Conklin HM, Wu S, Lustig RH, Xiong X (2009) Late effects of conformal radiation therapy for pediatric patients with low-grade glioma: prospective evaluation of cognitive, endocrine, and hearing deficits. J Clin Oncol 27:3691 (August 1, 2009)
Monje M, Palmer T (2003) Radiation injury and neurogenesis. Curr Opin Neurol 16:129
Morris B et al (2009a) Cerebrovascular disease in childhood cancer survivors: A Children's Oncology Group Report. Neurology 73:1906
Morris EB et al (2009b) Proximal dentatothalamocortical tract involvement in posterior fossa syndrome. Brain: J Neurol 132:3087
Muelle S et al (2013) Radiation, atherosclerotic risk factors, and stroke risk in survivors of pediatric cancer: a report from the Childhood Cancer Survivor Study. Int J Radiat Oncol Biol Phys 86:649
Mulhern RK et al (2001) Risks of young age for selected neurocognitive deficits in medulloblastoma are associated with white matter loss. J Clin Oncol: Off J Am Soc Clin Oncol 19:472
Müller H (2013) Childhood craniopharyngioma. Pituitary 16:56 (2013/03/01, 2013)
Müller K et al (2014) Postponed is not canceled: role of craniospinal radiation therapy in the management of recurrent infant medulloblastoma—an experience from the HIT-REZ 1997 and 2005 studies. Int J Radiat Oncol Biol Phys 88:1019
Musial-Bright L, Fengler R, Henze G, Hernáiz Driever P (2011) Carboplatin and ototoxicity: hearing loss rates among survivors of childhood medulloblastoma. Childs Nerv Syst 27:407 (2011/03/01, 2011)
Ness KK et al (2005) Limitations on physical performance and daily activities among long-term survivors of childhood cancer. Ann Intern Med 143:639
Ning M, Perkins S, Dewees T, Shinohara E (2015) Evidence of high mortality in long term survivors of childhood medulloblastoma. J Neurooncol 122:321 (2015/04/01, 2015)
Oeffinger KC et al (2006) Chronic health conditions in adult survivors of childhood cancer. N Engl J Med 355:1572
Oudin C et al (2011) Prevalence and risk factors of the metabolic syndrome in adult survivors of childhood leukemia. Blood 117:4442
Özyurt J et al (2014) Remote effects of hypothalamic lesions in the prefrontal cortex of craniopharygioma patients. Neurobiol Learn Mem 111:71

Packer R et al (1985) Leptomeningeal dissemination of primary central nervous system tumors of childhood. Ann Neurol 18:217

Packer RJ et al (2003) Long-term neurologic and neurosensory sequelae in adult survivors of a childhood brain tumor: Childhood Cancer Survivor Study. J Clin Oncol 21:3255 (September 1, 2003)

Palmer SL et al (2013) Processing speed, attention, and working memory after treatment for medulloblastoma: an international, prospective, and longitudinal study. J Clin Oncol 31:3494 (October 1, 2013)

Partap S (2012) Stroke and cerebrovascular complications in childhood cancer survivors. Semin Pediatr Neurol 19:18

Pfister HW (2012) Leitlinien für. In: Diener HC, Weimar C (eds) Diagnostik und Therapie in der Neurologie. Thieme Verlag, Stuttgart, pp 1–12

Pfisterer W, Muhlbauer M, Czech T, Reinprecht A (2003) Early diagnosis of external ventricular drainage infection: results of a prospective study. J Neurol Neurosurg Psychiatry 74:929

Pietilä S et al (2012) Neurological outcome of childhood brain tumor survivors. J Neurooncol 153 (2012/05/01, 2012)

Pillai S et al (2012) Intracranial tumors in infants: long-term functional outcome, survival, and its predictors. Childs Nerv Syst 28:547 (2012/04/01, 2012)

Pollack IF (1997) Posterior fossa syndrome. Int Rev Neurobiol 41:411

Pollack IF, Polinko P, Albright AL, Towbin R, Fitz C (1995) Mutism and pseudobulbar symptoms after resection of posterior fossa tumors in children: incidence and pathophysiology. Neurosurgery 37:885

Price RA (1979) Histopathology of CNS leukemia and complications of therapy. Am J Pediatr Hematol Oncol 1:21

Price RA, Birdwell DA (1978) The central nervous system in childhood leukemia. III. Mineralizing microangiopathy and dystrophic calcification. Cancer 42:717

Pruitt AA (2003) Nervous system infections in patients with cancer. Neurol Clin 21:193

Qiu D, Kwong DLW, Chan GCF, Leung LHT, Khong P-L (2007) Diffusion tensor magnetic resonance imaging finding of discrepant fractional anisotropy between the frontal and parietal lobes after whole-brain irradiation in childhood medulloblastoma survivors: reflection of regional white matter radiosensitivity? Int J Radiat Oncol Biol Phys 69:846

Rabin BM et al (1996) Radiation-induced changes in the central nervous system and head and neck. RadioGraphics 16:1055

Reddick WE et al (2003) Developmental model relating white matter volume to neurocognitive deficits in pediatric brain tumor survivors. Cancer 97:2512

Reddick WE et al (2014) Prognostic factors that increase the risk for reduced white matter volumes and deficits in attention and learning for survivors of childhood cancers. Pediatr Blood Cancer 61:1074

Rekate HL, Grubb RL, Aram DM, Hahn JF, Ratcheson RA (1985) Muteness of cerebellar origin. Arch Neurol 42:697

Rider W (1963) Radiation damage to the brain – a new syndrome. J Can Assoc Radiol 14:67

Robinson KE et al (2014) Functional neuroimaging of working memory in survivors of childhood brain tumors and healthy children: Associations with coping and psychosocial outcomes. Child Neuropsychol 5:1–24

Ronning C, Sundet K, Due-Tonnessen B, Lundar T, Helseth E (2005) Persistent cognitive dysfunction secondary to cerebellar injury in patients treated for posterior fossa tumors in childhood. Pediatr Neurosurg 41:15

Rosser TL, Vezina G, Packer RJ (2005) Cerebrovascular abnormalities in a population of children with neurofibromatosis type 1. Neurology 64:553

Ruben JD et al (2006) Cerebral radiation necrosis: Incidence, outcomes, and risk factors with emphasis on radiation parameters and chemotherapy. Int J Radiat Oncol Biol Phys 65:499

Rueckriegel SM et al (2010) Differences in supratentorial damage of white matter in pediatric survivors of posterior fossa tumors with and without adjuvant treatment as detected by magnetic resonance diffusion tensor imaging. Int J Radiat Oncol Biol Phys 76(859)

Rueckriegel SM, Driever PH, Bruhn H (2012a) Supratentorial neurometabolic alterations in pediatric survivors of posterior fossa tumors. Int J Radiat Oncol Biol Phys 82:1135

Rueckriegel SM, Driever PH, Bruhn H (2012b) Supratentorial neurometabolic alterations in pediatric survivors of posterior fossa tumors. Int J Radiat Oncol Biol Phys 82(1135)

Rueckriegel SM, Bruhn H, Thomale UW, Hernáiz Driever P (2015) Cerebral white matter fractional anisotropy and tract volume as measured by MR imaging are associated with impaired cognitive and motor function in pediatric posterior fossa tumor survivors. Pediatr Blood Cancer 62:1252

Sabin N et al (2014) Incidental detection of late subsequent intracranial neoplasms with magnetic resonance imaging among adult survivors of childhood cancer. J Cancer Surviv 8:329 (2014/09/01, 2014)

Saunders DE, Hayward RD, Phipps KP, Khean Chong W, Wade AM (2003) Surveillance imaging of intracranial medulloblastoma in children: how effective, how often, and for how long? J Neurosurg 99(280)

Schultz KAP et al (2007) Behavioral and social outcomes in adolescent survivors of childhood cancer: a report from the Childhood Cancer Survivor Study. J Clin Oncol 25:3649 (August 20, 2007)

Shalitin S et al (2011) Endocrine outcome in long-term survivors of childhood brain tumors. Horm Res Paediatr 76:113

Shaw DW, Geyer JR, Berger MS, Milstein J, Lindsley KL (1997) Asymptomatic recurrence detection with surveillance scanning in children with medulloblastoma. J Clin Oncol 15:1811 (May 1, 1997)

Shuper A, Packer RJ, Vezina LG, Nicholson HS, Lafond D (1995) 'Complicated migraine-like episodes' in children following cranial irradiation and chemotherapy. Neurology 45:1837

Soelva V et al (2013) Fronto-cerebellar fiber tractography in pediatric patients following posterior fossa tumor surgery. Childs Nerv Syst: ChNS 29:597

Sommers LM, Hawkins DS (1999) Meningitis in pediatric cancer patients: a review of forty cases from a single institution. Pediatr Infect Dis J 18:902

Steen RG et al (2001) Effect of ionizing radiation on the human brain: white matter and gray matter T1 in pediatric brain tumor patients treated with conformal radiation therapy. Int J Radiat Oncol Biol Phys 49(79)

Sterkenburg AS et al (2014) Kraniopharyngeom mit hypothalamischer Adipositas – Stationäre Rehabilitation ohne Einfluss auf die Gewichtszunahme bei Kindern und Jugendlichen. Klin Padiatr 226:344 (28.11.2014)

Stewart FA, Hoving S, Russell NS (2010) Vascular damage as an underlying mechanism of cardiac and cerebral toxicity in irradiated cancer patients. Radiat Res 174:865

Strenger V et al (2013) Incidence and clinical course of radionecrosis in children with brain tumors. Strahlenther Onkol 189:759 (2013/09/01, 2013)

Talvensaari KK, Lanning M, Tapanainen P, Knip M (1996) Long-term survivors of childhood cancer have an increased risk of manifesting the metabolic syndrome. J Clin Endocrinol Metab 81:3051

Tan H, Chen L, Guan Y, Lin X (2011) Comparison of MRI, F-18 FDG, and 11C-Choline PET/CT for their potentials in differentiating brain tumor recurrence from brain tumor necrosis following radiotherapy. Clin Nucl Med 36:978

Thomale U-W, Gebert A, Haberl H, Schulz M (2013) Shunt survival rates by using the adjustable differential pressure valve combined with a gravitational unit (proGAV) in pediatric neurosurgery. Childs Nerv Syst 29:425

Ullrich NJ et al (2007) Moyamoya following cranial irradiation for primary brain tumors in children. Neurology 68:932

Valk P, Dillon W (1991) Radiation injury of the brain. AJNR Am J Neuroradiol 12:45

Vézina L-G (2008) Imaging of central nervous system tumors in children: advances and limitations. J Child Neurol 23:1128 (October 1, 2008)

von Bueren AO et al (2011) Treatment of young children with localized medulloblastoma by chemotherapy alone: Results of the prospective, multicenter trial HIT 2000 confirming the prognostic impact of histology. Neuro Oncol 13:669 (June 1, 2011)

von Hornstein S et al (2011) Impact of chemotherapy on disseminated low-grade glioma in children and adolescents: Report from the HIT-LGG 1996 trial. Pediatr Blood Cancer 56:1046

Wells EM, Walsh KS, Khademian ZP, Keating RF, Packer RJ (2008) The cerebellar mutism syndrome and its relation to cerebellar cognitive function and the cerebellar cognitive affective disorder. Dev Disabil Res Rev 14:221

Wendt S, Shelso J, Wright K, Furman W (2014) Neoplastic causes of abnormal puberty. Pediatr Blood Cancer 61:664

Whelan KF et al (2010) Ocular late effects in childhood and adolescent cancer survivors: a report from the childhood cancer survivor study. Pediatr Blood Cancer 54:103

Willard VW, Conklin HM, Boop FA, Wu S, Merchant TE (2014) Emotional and behavioral functioning after conformal radiation therapy for pediatric ependymoma. Int J Radiat Oncol Biol Phys 88:814

Wilson C, Crafts D, Levin V (1977) Brain tumors: criteria of response and definition of recurrence. Natl Cancer Inst Monogr 46:197

Wilson CM, Gaber MW, Sabek OM, Zawaski JA, Merchant TE (2009) Radiation-induced astrogliosis and blood-brain barrier damage can be abrogated using anti-TNF treatment. Int J Radiat Oncol Biol Phys 74(934)

Won SC, Kwon SY, Han JW, Choi SY, Lyu CJ (2009) Posterior reversible encephalopathy syndrome in childhood with hematologic/oncologic diseases. J Pediatr Hematol Oncol 31:505

You S, Lyu C, Kim D-S, Suh C-O (2013) Second primary brain tumors following cranial irradiation for pediatric solid brain tumors. Childs Nerv Syst 29:1865 (2013/10/01, 2013)

Yuan H et al (2006) Effects of fractionated radiation on the brain vasculature in a murine model: blood-brain barrier permeability, astrocyte proliferation, and ultrastructural changes. Int J Radiat Oncol Biol Phys 66(860)

Zach L et al (2015) Delayed contrast extravasation MRI: a new paradigm in neuro-oncology. Neuro Oncol 17:457 (March 1, 2015)

Zeltzer LK et al (2008) Psychosocial outcomes and health-related quality of life in adult childhood cancer survivors: s report from the Childhood Cancer Survivor Study. Cancer Epidemiol Biomarkers Prev 17:435 (February 1, 2008)

Zeltzer LK et al (2009) Psychological status in childhood cancer survivors: a report from the childhood cancer survivor study. J Clin Oncol 27:2396 (May 10, 2009)

# Part VII

# Pelvis and Genitourinary

# Imaging of Complications and Toxicity Following Tumour Therapy: Pelvis and Genitourinary (Male)

A. Shah, S.A. Sohaib, and D-M. Koh

## Contents



A. Shah, FRCR • D-M. Koh, MD, MRCP, FRCR
Department of Diagnostic Radiology, Royal Marsden Hospital, Sutton, Surrey, UK

S.A. Sohaib, MRCP, FRCR (✉)
Department of Diagnostic Radiology, Royal Marsden Hospital, Sutton, Surrey, UK

Department of Diagnostic Radiology,
Royal Marsden NHS Foundation Trust,
Down Road, Sutton, Surrey SM2 5PT, England, UK
e-mail: aslam.sohaib@rmh.nhs.uk

**Abstract**

This chapter discusses the imaging of the complications and toxicity associated with treatment of the male genitourinary tract with particular focus on the imaging features which should alert the radiologist to the unwanted consequences of treatments, as well as imaging characteristics that may mimic or obscure any underlying disease.

## 1 Prostate Cancer

Prostate cancer is the second most common cancer worldwide in males. Patients with disease confined to the prostate gland now face an array of management options. These include watchful waiting, active surveillance or active treatment with radiotherapy (brachytherapy, external beam irradiation therapy, stereotactic body radiotherapy, CyberKnife), hormonal therapy, minimally invasive therapy (cryotherapy, high-intensity focused ultrasound) and radical prostatectomy.

### 1.1 Surgery

#### 1.1.1 Primary Tumour

Surgery for localised prostate cancer remains the most definitive treatment. Excellent results can be achieved by open radical prostatectomy in the

Med Radiol Radiat Oncol (2015),
DOI 10.1007/174_2015_1081, © Springer International Publishing Switzerland

hands of an experienced surgeon. However, the results by laparoscopic or robot-assisted radical prostatectomy can be comparable to those of open radical prostatectomy. The da Vinci Robotic system, which is the most frequently employed robot-assisted surgical platform, has three to four robotic arms controlled by the surgeon at the console. The arms have sophisticated rotational capabilities, which mimic movements of the human wrist. Using laparoscopic or robot-assisted laparoscopic radical prostatectomy can reduce blood loss compared with conventional open prostatectomy (Finkelstein et al. 2010). Robot-assisted laparoscopic radical prostatectomy can also result in faster and better return to continence, decrease in operation time and reduction in hospital stay.

### 1.1.2 Nodal Disease

Nodal disease is an independent prognostic factor in patients with prostate cancer. However, controversy remains as to when to perform nodal surgery or the extent of nodal dissection. Patient selection for nodal dissection is based on risk versus benefit, for which there is no current consensus. However, published literature suggests that pelvic lymph node dissection could be omitted in patients with low-risk disease without significant impact on disease recurrence at follow-up (Weight et al. 2008).

As the lymphatic drainage of the prostate is not limited to the obturator and external iliac lymph nodes, conventional pelvic lymph node dissection confined to these nodal regions may miss involved nodes as demonstrated by one study (Heidenreich et al. 2002) that compared extended template pelvic lymph node dissection in 103 consecutive patients with 100 patients who underwent conventional nodal dissection. As part of an extended nodal dissection, lymph nodes were removed from the external iliac, internal iliac, obturator, common iliac and presacral nodes. Interestingly, the incidence of nodal involvement was higher (26 %) in the group who underwent extended nodal dissection compared with conventional surgery (12 %). This suggests that extended pelvic nodal dissection may be more appropriate in high-risk patients, although this carries a greater potential for complications.

### 1.1.3 Imaging Following Surgery

After radical prostatectomy, the prostate gland is notably absent (Fig. 1). On MRI a non-enhancing ring of low signal is frequently seen at the vesicourethral anastomosis in keeping with fibrosis (Allen et al. 2008).

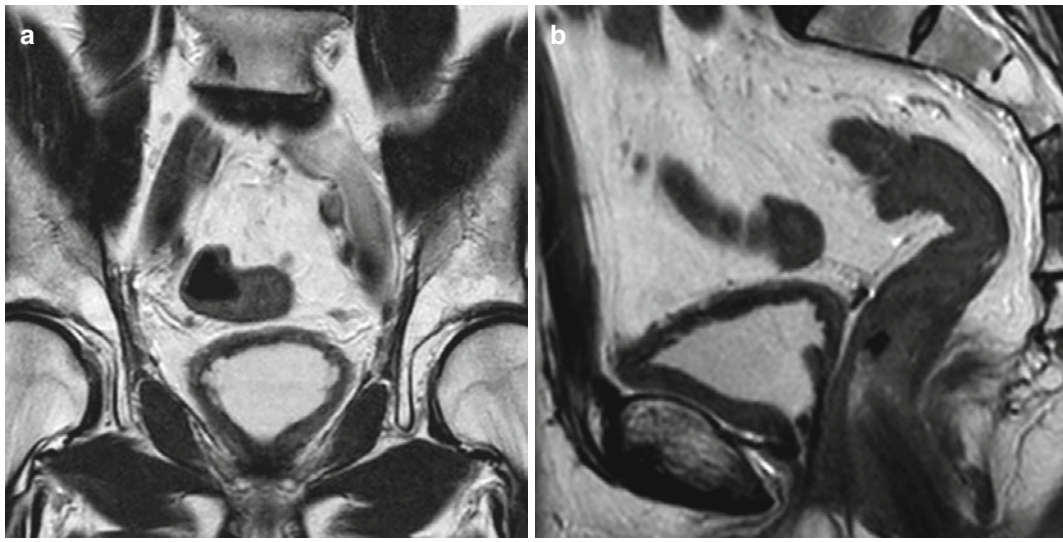


**Fig. 1** Appearances following radical retropubic prostatectomy. (**a**) Coronal and (**b**) sagittal T2-weighted images through the prostate bed show the caudal decent of the bladder. The bladder neck and urethral anastomosis display the low signal intensity changes. The reduced amount of retropubic fat is in keeping with a retropubic prostatectomy

Seminal vesicle remnants are variable in appearance but are usually present to some extent and also usually contain fibrosis. Appearances following the different surgical accesses do not differ tremendously, although the retropubic fat pad and dorsal venous complex are much reduced following a retropubic approach (Fig. 1). Anterior rectal wall scarring may be present following a transperineal approach. Other benign postoperative appearances, such as the visualisation of residual gland or a bulking agent, should be recognised so that the radiologist can distinguish these findings from active recurrent disease (Allen et al. 2008).

On imaging, postsurgical soft tissue stranding will be visible in the anterior abdominal wall and along port sites used for laparoscopic or robot-assisted prostatectomy. Due to loss of the prostate gland, the bladder base and pelvic floor will be caudally displaced (Fig. 1). On CT, radiodense surgical sutures or clips are usually visible at the bladder neck. Typically, the distal seminal vesicles are spared. Small amounts of reactive free fluid may be seen in the adjacent peritoneal compartment above, together with intraperitoneal air, in keeping with the recent surgery. Acutely following surgery, there may also be fluid-filled dilated loops of small and/or large bowel reflecting postsurgical ileus. A urinary catheter is usually left traversing the vesico-urethral anastomosis, and the balloon of the catheter can be identified within the urinary bladder. If pelvic lymph node dissection is undertaken, radiodense surgical clips are usually visible along the pelvic sidewalls, and often, the location of these clips reveals the extent of nodal dissection.

The surgical field should be scrutinised for abnormal and asymmetrical high-density collection that suggests haematoma formation. This may be more apparent by its high T1 signal intensity on MRI. Asymmetrical low-density collection raises the likelihood for postsurgical seroma or urinoma. Gas densities, when present within collections, are suspicious for abscess formation, especially when accompanied by signs and symptoms of infection. However, cellulose patches used in surgery may return inhomogeneous CT densities, which should not be misinterpreted as enteric perforation or infection

### 1.1.4 Complications Following Surgery

Urinary leaks can occur around the vesico-urethral anastomosis at the bladder base (Fig. 2). This is recognised as contrast extravasation on radiographic or CT cystography, associated with

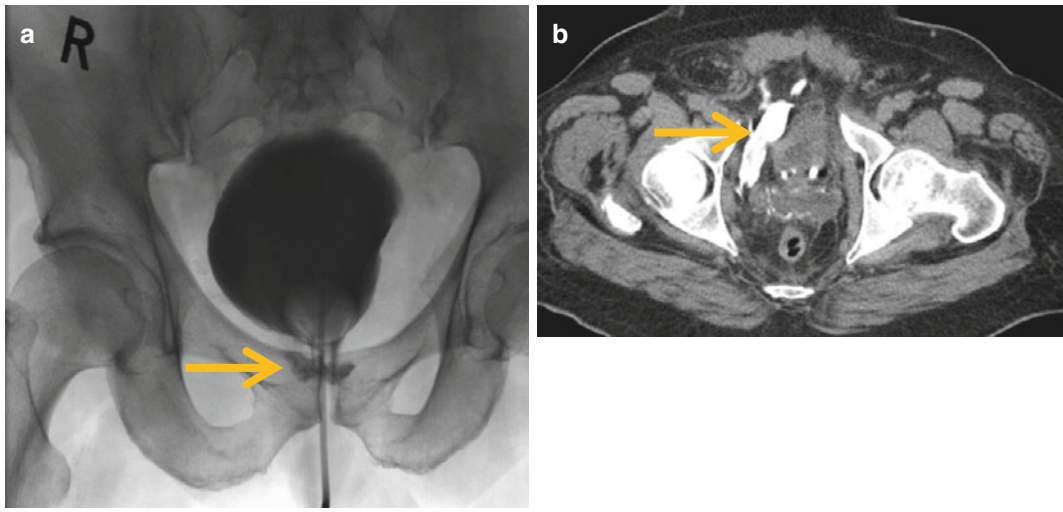


**Fig. 2** Anastomotic leak following a radical prostatectomy. (**a**) Fluoroscopic cystogram demonstrates an extraperitoneal urine leak (*arrow*) at the level of the anastomosis. (**b**) Axial images from the CT cystogram 15 min after intravenous contrast media injection show extravasation of contrast media (*arrow*) anteriorly into the paravesical space confirming the presence of a urine leak

extraperitoneal extension below the pelvic floor. Following robot-assisted laparoscopic radical prostatectomy, intraperitoneal urinary leak can occur, although this is relatively rare. CT cystography is useful to demonstrate contrast extravasation into the peritoneal cavity, and the presence of significant ascites in the absence of other causes should also raise suspicion. Even more unusual are intraperitoneal fluid collections from ureteral damage, which may rarely occur after laparoscopic surgery. These low-density fluid collections become opacified in the excretory phase of a CT urogram.

Fistula formation between the urethra and the anal or rectal canal may occur following surgery. Although CT may demonstrate the abnormal communication, MRI may be superior in demonstrating the site of abnormality.

Following pelvic sidewall nodal dissection, lymphoceles (Fig. 3) are common although their incidence is reportedly lower following robot-assisted or laparoscopic surgery compared with open surgery (Solberg et al. 2003). The majority of these are asymptomatic, found adjacent to surgical clips along the nodal dissection chain and will resolve spontaneously. On CT, lymphoceles are thin walled containing uniform low-density fluid (typically < 10 HU) but may be large (>5 cm in size) and bilateral. Large symptomatic lymphoceles causing local pressure effects may require drainage.

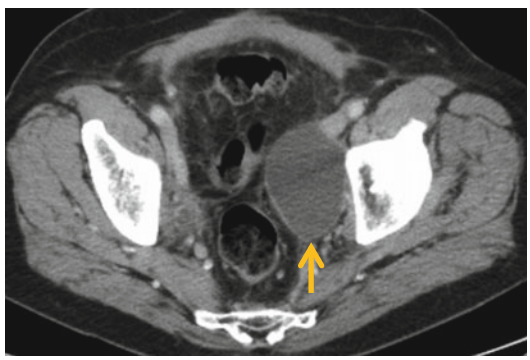

**Fig. 3** Lymphocele. CT shows as well-defined fluid density *(arrow)* behind the left external iliac vessels in keeping with a pelvic side wall lymphocele

## 1.2 Radiotherapy

The delivery of radiotherapy in prostate cancer is becoming increasingly sophisticated. Radiotherapy can be delivered in a variety of ways. Whilst the common side effects of radiotherapy are usually not associated with imaging findings, it is worthwhile understanding the range of side effects and toxicity that can be encountered.

### 1.2.1 External Beam Radiation Therapy (EBRT)

EBRT is one of the primary treatments for patients with localised or locally advanced prostate cancer. Conventional EBRT is delivered using a 4-field (AP, PA, left lateral and right lateral) technique. There is data to support the use of whole-pelvis radiotherapy in patients with increased risk of non-organ-confined cancer, to include pelvic lymph nodes if their risk of involvement exceeds 15 % (Roach et al. 2003).

There are no large, multicentre, randomised control trials evaluating EBRT against other therapies. Data from nonrandomised studies comparing radical prostatectomy (RP) and EBRT shows, in general, urinary dysfunction (especially incontinence) was more common after RP and bowel dysfunction after EBRT (Wilt et al. 2008).

With advances in computer-based treatment planning, there have been several improvements to conventional EBRT allowing more accurate targeting of radiation to allow increased tumour dose whilst reducing toxicity to surrounding structures. These include 3-dimensional conformal radiotherapy (3D-CRT), intensity-modulated radiation therapy (IMRT) and proton beam radiation therapy (PBRT).

It has been established that a significant reduction in rectal toxicity can be achieved using conformal compared with conventional radiotherapy (Dearnaley et al. 1999). These findings form the basis of dose-escalation protocols to improve the treatment efficacy, and there is little doubt that dose escalation improves both metastasis-free and cancer-specific survival (Hanks et al. 2002; Jacob et al. 2004) However, the use of 3D-CRT

for dose escalation is limited by side effects (Michalski et al. 2010). Whilst there is no randomised control trial evidence to support superiority of one type of therapy over another, meta-analysis of randomised dose-escalation trials suggests lower late gastrointestinal toxicity with IMRT or PBRT than 3D-CRT (Ohri et al. 2012).

### 1.2.2 Brachytherapy

There are two main forms of brachytherapy. Low-dose brachytherapy involves permanent placement of small radioactive 'seeds' into the prostate under transrectal ultrasound guidance (Figs. 4 and 5). The seeds contain a pre-planned prescription dose of radioisotope and are placed transperineally into the prostate to allow uniform coverage of the prostate and a margin around it. It is commonly used as a monotherapy for patients with low or intermediate-risk prostate cancer or in combination with EBRT for high-risk patients. High-dose-rate (HDR) brachytherapy involves administration of treatment through temporary catheters that contain the radioactive source. This type of brachytherapy is mostly used in combination with EBRT for intermediate to high-risk disease.

A recent review demonstrates that brachytherapy provides excellent outcomes in patients with low-risk disease (Grimm et al. 2012). For intermediate-risk disease, the combination of EBRT and brachytherapy appears to be equivalent to brachytherapy alone (Grimm et al. 2012). For high-risk patients, the combination of EBRT and brachytherapy plus or minus hormonal therapy appears more superior to localised therapy alone (Grimm et al. 2012).

The best candidates for brachytherapy are low-risk prostate cancer patients with a prostate volume of <50 ml. Large prostate size complicates needle placement and requires more seeds to achieve the prescribed dose thus increasing the risk of urinary side effects. Brachytherapy is usually contraindicated in patients with a history of transurethral resection of the prostate, moderate to severe storage symptoms and in those with a history of abdomino-perineal resection.

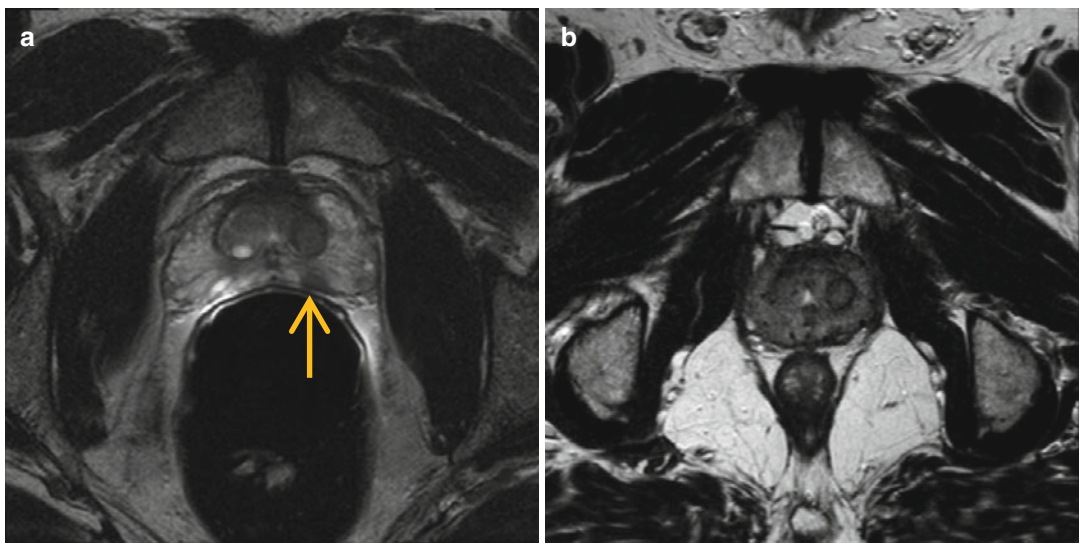


**Fig. 4** Effects of brachytherapy treatment on the prostate. (**a**) Axial T2-weighted images with endorectal coil through the prostate shows a small tumour (*arrow*) in the left peripheral zone mid-gland. (**b**) Axial T2-weighted images through the prostate following insertion of radioactive seed and treatment with brachytherapy show that the prostate has become smaller and generally of lower signal. Furthermore there is less differentiation between the central gland and peripheral zone

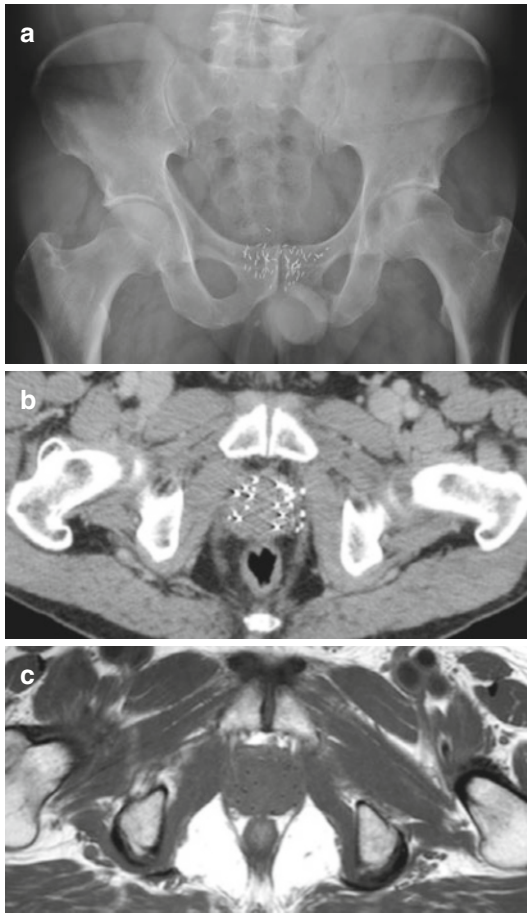


**Fig. 5** Brachytherapy seed position on imaging. (**a**) Pelvic radiograph showing the position and orientation of the brachytherapy seeds. (**b**) Axial CT and (**c**) axial T1-weighted images through the prostate show the position of the radioactive seeds. The seeds are seen as dense material on the CT and as signal voids on MR imaging

In general, there is a lower morbidity with brachytherapy compared with surgery or EBRT. Early side effects include urinary retention usually due to bladder outlet obstruction, haematuria, urethritis and infection. About 90 % of patients experience grade 1–2 lower urinary tract symptoms during the first 12 months after the procedure (Grimm et al. 1996). Acute retention requiring catheterisation has a reported incidence of 5.5–42 % (Crook et al. 2002; Locke et al. 2002). Later effects include worsening of storage symptoms, rectal symptoms such as proctitis or faecal urgency, fistulae, radiation osteitis and urethral strictures.

Rectal toxicity develops approximately a year after the procedure and persists for up to 2 years with grade 2 and 3 rectal toxicity occurring in 2–12 % and grade 4 rectal toxicity occurring in 0.4–2 % of patients (Emara et al. 2012). Urethral strictures develop in 9–10 % of patients (Zelefsky et al. 2000).

Erectile function is maintained in 50–80 % of patients with variations dependent on several factors including pre-treatment erectile function, age and pharmacologic assistance (Stone and Stock 2007). An American study comparing outcomes in 1913 patients reported rates of erectile function of 35 %, 58 % and 37 % for radical prostatectomy, brachytherapy and EBRT, respectively (Alemozaffar et al. 2011).

In addition, implanted seeds can be misplaced into the surrounding structures (Fig. 5) such as bladder or rectum, or they can migrate, for example, to the lung. A small, randomised study has shown that using stranded rather than loose seeds is associated with better seed retention and less seed migration (Reed et al. 2007).

### 1.2.3 Proton Beam Radiation Therapy (PBRT)

There is interest in the use of PBRT because unlike EBRT, which uses photons that deposit radiation along their path, almost all the radiation dose from protons is deposited at the end of the particle's path in tissue (Bragg peak) with a very sharp fall-off for proton beams beyond deposition depth. This means that theoretically, normal, surrounding tissues could be spared.

There are no randomised trials comparing IMRT with PBRT. Two planning studies comparing conformal proton therapy with IMRT have reported conflicting results; one study suggested that whilst IMRT is superior in terms of bladder sparing, there is no difference in terms of rectal dose sparing (Trofimov et al. 2007); the other suggested that PBRT is better at reducing dose to normal structures (Vargas et al. 2008).

### 1.2.4 Complications and Imaging Post-radiotherapy

The morbidity from radiation therapy relates to the volume of tissue irradiated, the dose delivered and the inherent radiosensitivity of the organ. Whilst discussion of radiotherapy planning techniques is beyond the scope of this chapter, it must be stated that the single most important factor in reduction of radiation-related toxicity is dose minimisation through careful design of radiotherapy treatment.

A few fiducial markers usually gold grains/seeds are sometimes inserted into the prostate to help localise the prostate and its variation in position during the course of treatment with external beam radiotherapy (Fig. 6). These markers, as well as brachytherapy seeds, are visible on imaging. On CT, streak artefacts are seen arising from the implants. Gradient-echo MR sequences accentuate these seeds and may obscure underlying disease but help to identity the fiducial markers as part of radiotherapy planning (Fig. 6). Diffusion-weighted MRI using echo-planar technique is usually unhelpful after brachytherapy because of the susceptibility artefacts.

Following external beam radiotherapy and brachytherapy, the prostate gland typically shrinks in volume with reduction in the T2 signal intensity of the peripheral zone, thus diminishing the contrast between tumour and the normal gland (Fig. 4).

It is helpful to categorise the commonly encountered morbidities according to the following organ systems: skin, bowel, bladder, pelvic bones and nerves, although many of the associated complications may not be visible on imaging.

### 1.2.5 Skin

Radiation causes perturbation of the epidermis and dermis, sometimes resulting in reddening and commonly hair loss. This is uncommon with improved techniques for targeting dose.

### 1.2.6 Bowel

The distal colon and rectum are most commonly affected by pelvic radiotherapy as they lie within the radiation field. The fixed portions of colon such as the rectum are most vulnerable. Patients with a history of previous radiation or abdominal surgery are at an increased risk as a result of adhesion formation since the bowel is less able to move from the radiation field. Segments of diverticular disease may be susceptible to develop diverticulitis and fistulation after treatment. Such issues need to be identified on the pre-treatment imaging. Acute toxicity usually manifests as diarrhoea, tenesmus, mucoid discharge and rectal bleeding if there is ulceration.

Small bowel involvement leads to abdominal pain, nausea and watery diarrhoea. Late symptoms are more insidious and can develop months to years after therapy and not infrequently

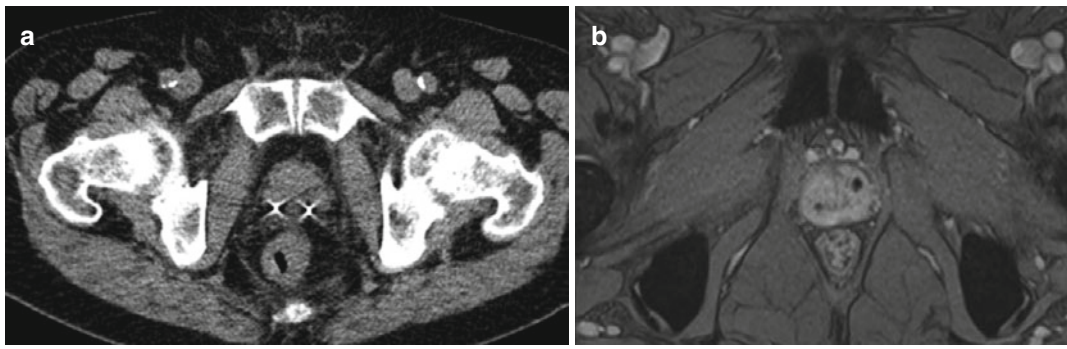


**Fig. 6** Fiducial (gold grains) marking the position of the prostate for radiotherapy planning. (**a**) Axial CT shows two gold grains with the prostate. (**b**) Gradient-echo (T2*-weighted) images show the fiducial markers as signal voids

without a history of symptoms of acute toxicity. If the small bowel has been affected in particular the terminal ileum, then malabsorption may occur (Harris et al. 2012).

Imaging findings of small bowel-related toxicity are uncommon with modern radiotherapy. CT and MRI have largely superseded barium studies in evaluating these features. With pelvic radiotherapy, the terminal ileum is particularly vulnerable because of proximity to the field as well as its relatively fixed position. Multifocal involvement does occur and conventional CT or MR enteroclysis may be of value to demonstrate which bowel segments are involved in order to plan surgery and avoid 'short bowel' syndrome. In practice, CT or MR enterography has largely replaced conventional enteroclysis, which requires nasojejunal intubation, whereas CT or MR enterographic images are acquired following oral contrast administration without the need for nasojejunal intubation. Both CT and MR enterographic techniques have the benefit of depicting the entire bowel wall and extra-intestinal pathologies

The findings of radiation enteritis include bowel wall oedema (Fig. 8), thickening, ulceration, contrast enhancement in a long segment of bowel, stricturing particularly at sites of previous anastomosis and fistulation. Often the appearances are non-specific and need clinical correlation, but the abnormality conforms to the radiotherapy field (Horton et al. 2000). Features that suggest malignancy include mass-like thickening, infiltration of adjacent tissues and nodal enlargement (Stoker 2010).

There is no clear evidence to support the use of MRI over CT, although MRI offers better soft tissue contrast in patients with lack of fat and anorexia due to small bowel disease. MRI also has the advantage of multiphasic imaging (arterial, portal and delayed venous) without radiation exposure, as well as the ability to image the jejunum in the early phase (15 min) and colonic loops in the later phase (1st hour or later) after oral contrast agent administration (Cronin et al. 2010; Kayhan et al. 2010). The main disadvantages of MRI are long acquisition times and motion artefacts.

### 1.2.7 Bladder

Radiation-induced injury to the urinary tract or the genital system has been reported to cause symptoms affecting quality of life in up to 30 % of prostate cancer patients (Turini et al. 2003; Bloch et al. 2007). The bladder wall thickening observed at CT and MR imaging is often worse than the clinical symptoms. On MRI, high T2 signal intensity is seen in the outer layer of the bladder (Fig. 7) with enhancement of the mucosal layer on T1-weighted images (Addley et al. 2010).

The likelihood for long-term complications depends on the volume of bladder irradiated and the total dose with toxicity increasing when the total dose exceeds 60 Gy. On MRI, in the chronic phase, the bladder is small volume and poorly distensible and often has a thin low T2 signal intensity mural band in keeping with fibrosis.

Fistula formation is a rare but serious complication with a frequency of 1 in 250 to 1 in 1000 in patients undergoing brachytherapy. On CT, important indirect signs of bladder fistulation include intravesical air (90 %), focal bladder wall thickening (90 %), thickening of adjacent bowel wall (85 %) and extraluminal mass containing air (75 %) (Goldman et al. 1985). Where possible, the CT should be performed with rectal contrast administration, delayed excretory phase imaging and multi-planar reconstruction to enhance visualisation. The actual fistulous tract is only occasionally identified on CT.

The role of MRI is well established in the delineation of perianal and intestinal fistulae in inflammatory bowel disease but less so for enterovesical fistula. Small series, however, show a high sensitivity for diagnosing the presence of a vesical fistula and also its aetiology (Ravichandran et al. 2008). MRI findings overlap with CT, but the morphology and anatomical location are easier to appreciate on MR with the characteristic finding of focal disruption in the bladder muscularis on T2-weighted sequences, representing fistula penetration of the bladder wall (Outwater and Schiebler 1993). Post-contrast MR imaging is not usually needed to achieve the high diagnostic sensitivity (Tang et al. 2012).

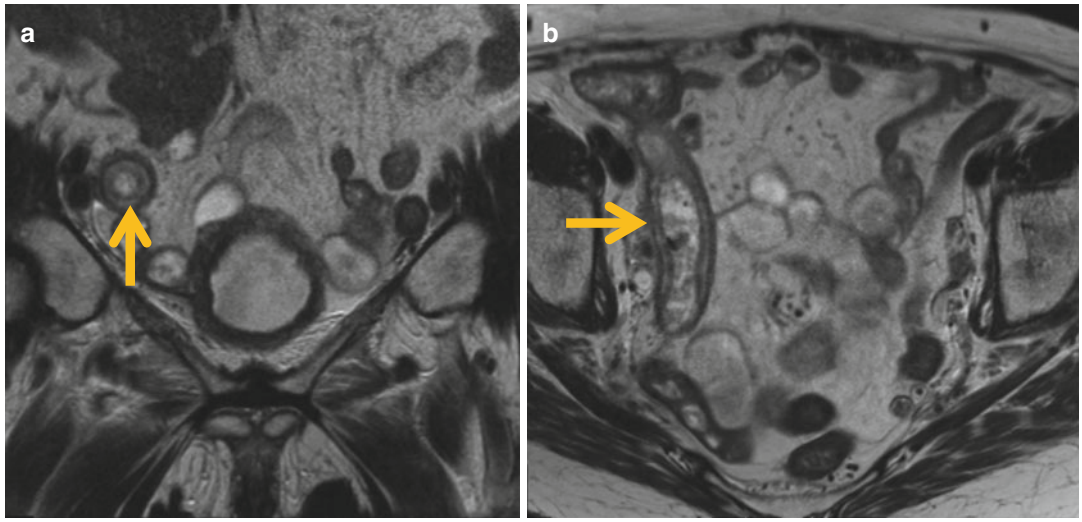


**Fig. 7** Radiation-related changes to bladder and small bowel loop. (**a**) Axial and (**b**) coronal T2-weighted images through the pelvis in a patient who received pelvic radiotherapy for bladder cancer. The bladder is small volume with thickened wall with some intermediate signal intensity changes in bladder wall muscles. The small bowel loop on the right side shows some oedematous (*arrow*) changes within its wall

### 1.2.8 Nerves

Pelvic irradiation exposes both sympathetic and parasympathetic nerves resulting in erectile and ejaculatory dysfunction, which is beyond the sensitivity of current imaging methods to reliably detect. Erectile dysfunction is dependent upon several factors mainly pre-treatment erectile function and age.

### 1.2.9 Bones

A number of pelvic bones can receive radiation dose during radiotherapy of cancers within the pelvis. Insufficiency fractures are a type of stress fracture resulting from normal stress applied to abnormal bone that has lost its normal architecture, which should not be mistaken for metastatic disease.

Pelvic irradiation is an established risk factor for insufficiency fracture (Fig. 8), and whilst the association is well documented in gynaecological and colorectal studies with a 5-year incidence of 8.2–19.7 %, there is a paucity of data in prostate cancer (Oh et al. 2008). The data available for prostate cancer suggests that insufficiency fractures are rare in this group with a 5-year incidence of 6.8 % (Igdem et al. 2010). Sacral fractures are most common followed by pubic rami and femoral neck. Less commonly, acetabular protrusion and avascular necrosis of the femoral neck can occur.

Plain films are relatively insensitive for detecting insufficiency fractures. When they are seen, they appear as sclerotic bands, cortical disruptions or even visible fracture lines usually in the sacral ala (Blake and Connors 2004). Occasionally, they can have an aggressive appearance, with areas of sclerosis and periosteal reaction, mimicking malignancy and leading to unnecessary workup (Blake and Connors 2004). The appearance may even mimic metastatic disease on CT.

Bone scan is a very sensitive method for detecting pelvic insufficiency fractures (Fig. 8), seen as increased radionuclide uptake, sometimes bilaterally and symmetrically in a characteristic H appearance (Schneider et al. 1985). However, a meta-analysis showed that the typical H appearance was documented in just 40 % (Finiels et al. 1997), and unilateral involvement may be misdiagnosed as metastatic disease.

MRI is highly sensitive for demonstrating the bone marrow oedema that results from fractures (Fig. 8), returning low signal intensity on T1-weighted and high signal intensity on

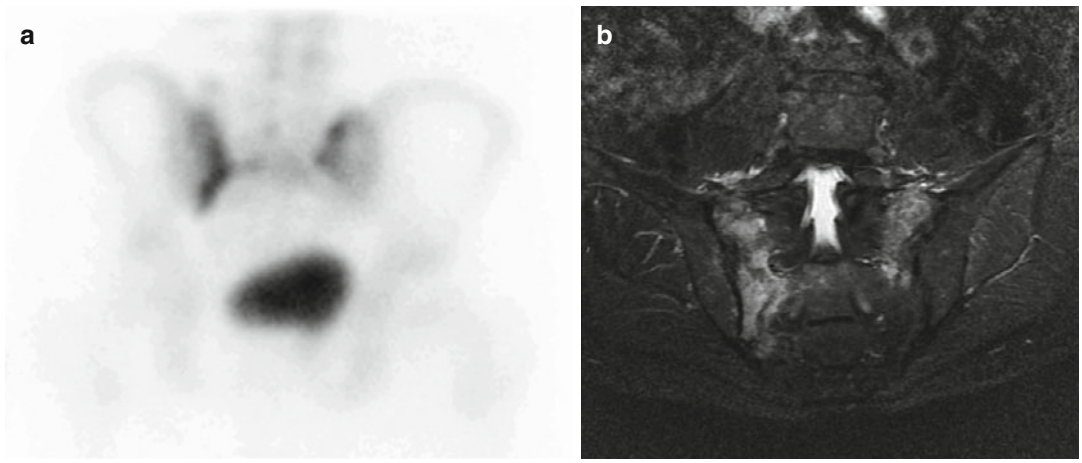


**Fig. 8** Bilateral sacral insufficiency fractures. (**a**) Planar coronal projection images of the pelvis from a Tc-MDP bone scan and (**b**) coronal STIR images through the sacrum show bilateral insufficiency fractures

T2-weighted and short tau inversion recovery (STIR) images (Blomlie et al. 1996; Grangier et al. 1997). The presence of fracture lines (linear low signal intensity on T1-weighted and STIR images) and no focal or discrete mass lesion help establish the diagnosis (Blake and Connors 2004). It can sometimes be difficult to detect the fracture line on unenhanced T1-weighted images because reactive bone marrow changes associated with the fracture are also of low signal intensity and contrast administration can help to differentiate.

### 1.2.10 Secondary Malignancy

Patients may be at a higher risk of developing secondary malignancies, such as bladder or rectal cancers (Baxter et al. 2005; Chrouser et al. 2005). One study reports increased relative risks of 15 % and 34 %, at 5 and 10 years after external beam radiotherapy (EBRT), respectively, relative to treatment with surgery (Brenner et al. 2000). However, it is unclear how applicable these rates are for more sophisticated conformal radiotherapy or brachytherapy, where much lower radiation dose levels are delivered to the bladder and rectal tissue. Indeed, a large cohort study showed that the incidence of secondary malignancy after EBRT or brachytherapy is lower than previously reported and not significantly different following radical prostatectomy when adjusted for patient age and smoking history. Among patients who developed a secondary malignancy, the likelihood of mortality was not significantly different among the cohorts (Zelefsky et al. 2012).

## 1.3 Chemotherapy and Hormonal Treatment

Prostate cancer cells undergo apoptosis when deprived of androgenic stimulation; any treatments that ultimately result in the suppression of androgen activity are referred to as androgen deprivation therapy (ADT). The main categories include luteinising hormone-releasing hormone (LHRH) agonists and anti-androgens. Eventually all metastatic prostate cancer becomes resistant to ADT – the so-called castrate-resistant prostate cancer (CRPC). New therapies such as abiraterone have recently been approved for the treatment of metastatic CRPC.

The adverse effects of ADT include osteoporosis, greater incidence of clinical fractures, obesity, insulin resistance and greater risk for diabetes and cardiovascular disease. ADT is associated with a 21–54 % relative increase in fracture risk (Shahinian et al. 2005; Smith et al. 2006). In addition, ADT increases bone turnover and decreases bone mineral density, which is a surrogate for fracture risk (Daniell et al. 2000).

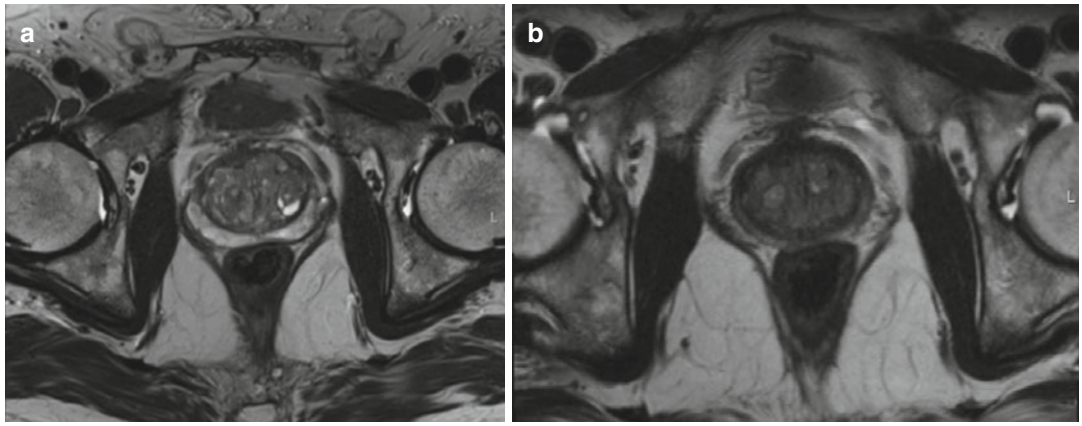


**Fig. 9** Effect of hormonal treatment on the prostate. Axial T2-weighted images (**a**) before and (**b**) after treatment with hormone shows the less clarity between the zonal anatomical regions within the prostate

To prevent osteoporosis in men on ADT, patients should be screened for osteoporosis prior to the initiation of ADT with dual X-ray absorptiometry (DXA) scans (Diamond et al. 2004) and treatment (alendronate, risedronate, zoledronic acid, denosumab and teriparatide) prescribed if necessary.

Treatment with ADT also induces changes within the prostate gland, resulting in glandular involution and loss of the normal high T2 signal intensity on MRI (Fig. 9). This can also diminish the T2-weighted contrast between the tumour and the normal glandular tissues. As such, functional imaging techniques (e.g. dynamic contrast-enhanced MRI and diffusion-weighted MRI) are increasingly used to assess the prostate in the post-therapy setting (Barchetti and Panebianco 2014).

## 1.4 Focal Therapy

Until recently, prostate cancer treatment focussed on whole gland therapy; however with better imaging localisation of cancer within the gland, there is growing interest in focal treatment. Preliminary results have shown that these techniques can limit genitourinary complications arising from whole gland therapy.

Focal therapies have taken different approaches. First, a hemi-ablative method treating the half of the gland associated with cancer. This has been applied using high-intensity focused ultrasound (HIFU), the main limitations being that prostate cancer is rarely unilateral and there are risks of overtreatment as low-volume, low-grade lesions are treated in the same way as high-volume, high-grade cancers (Ahmed et al. 2011). Second, focal therapy can be targeted to the cancer itself or the 'index lesion'.

### 1.4.1 High-Intensity Focused Ultrasound (HIFU)

This technique focuses and deposits a large pulse of high-energy ultrasonic waves to a single area, thereby raising the temperature of the targeted tissue to between 65 and 80° C in 2–3 s and results in coagulative necrosis to tissue typically measuring approximately $3 \times 3 \times 10$ mm. The beam is then moved to the adjacent site and so on to treat the area of interest. There is minimal or no damage to the tissue in the path of the ultrasound beam (Huber et al. 1996). HIFU offers the opportunity to repeat treatment safely as necessary (Fig. 10).

One study evaluated the imaging appearances of the prostate gland post-HIFU. Initial post-HIFU images showed central non-enhancement, surrounded by an enhancing rim (Fig. 10). At 6 months, the prostate was reduced in volume and appeared predominantly low signal intensity on T2-weighted images (Fig. 10). The volume of prostate enhancing on the initial post-treatment

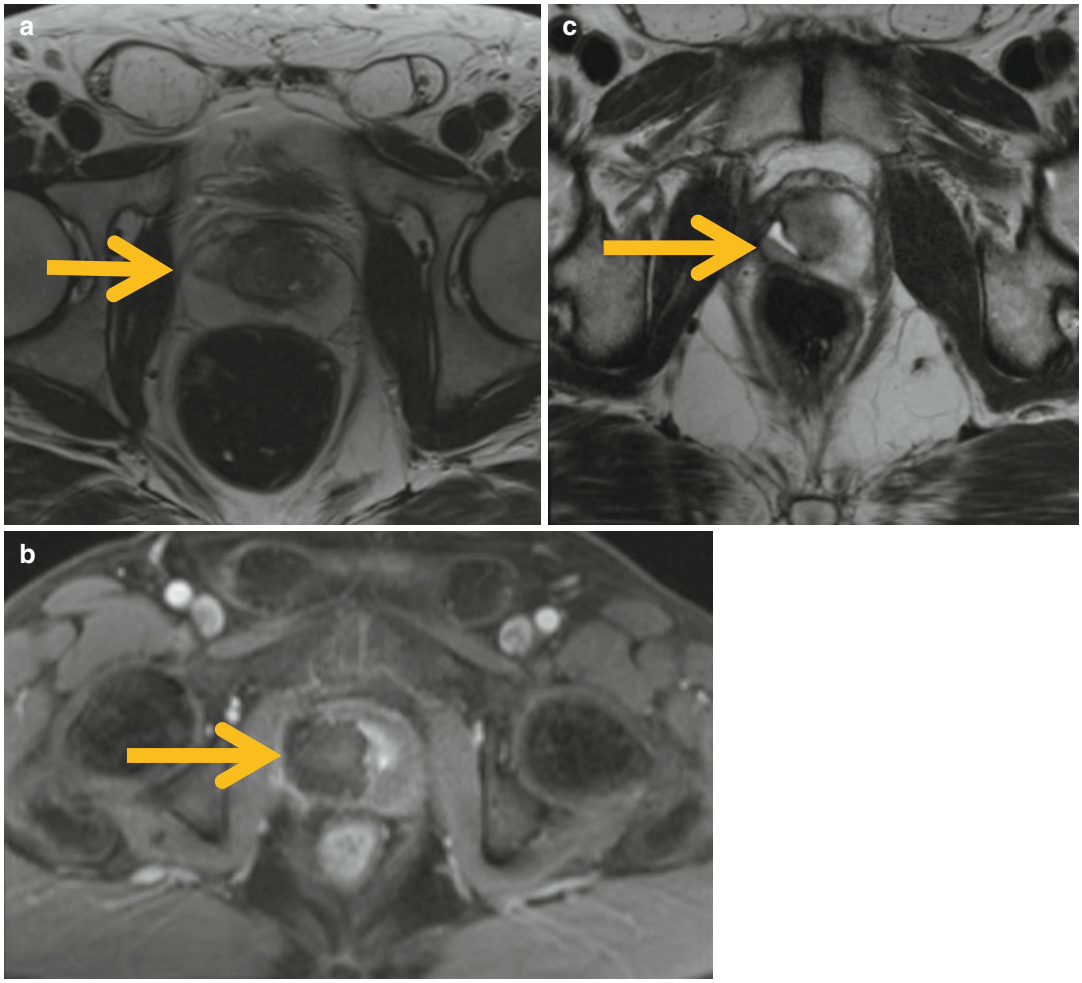


**Fig. 10** Effect of high-intensity focus ultrasound (HIFU) treatment on the prostate gland. (**a**) Axial T2-weighted images through the prostate show a small tumour (*arrow*) confined to the prostate in the right peripheral zone mid-gland. (**b**) Axial fat-suppressed T1-weighted images through the prostate 1 week following HIFU treatment show necrosis (*arrow*) to the right hemi-prostate. (**c**) Axial T2-weighted images through the prostate 9 months after the HIFU treatment show scarring and atrophy (*arrow*) in the right hemi-prostate

image correlated well with serum PSA level nadir and with volume at 6 months (Kirkham et al. 2008).

A large, multicentre trial is underway to evaluate disease control and long-term follow-up (Dickinson et al. 2013). Complications of modern series with HIFU may be summarised as stress incontinence, 5–10 %; fistula, 0–0.7 %; stricture, 9–12 %; UTI, 5–13 % and impotence, 55–70 % (Aus 2006) (Fig. 11). Performing a combination of HIFU and TURP decreases the risk of post-treatment urinary retention (Vallancien et al. 2004).

### 1.4.2 Cryotherapy

Cryotherapy involves initial freezing and subsequent thawing of tissue to cause cell injury and also induce an inflammatory response, which results in cell death (Nomura and Mimata 2012).

Whole gland cryotherapy has been used to treat low-intermediate-risk disease, but there is no long-term data to support its use over radical prostatectomy. In one study, ice ball formation was clearly and sharply visualised as an area of signal-void using a BLADE T2 sequence (Gangi et al. 2012). The technique has also been applied

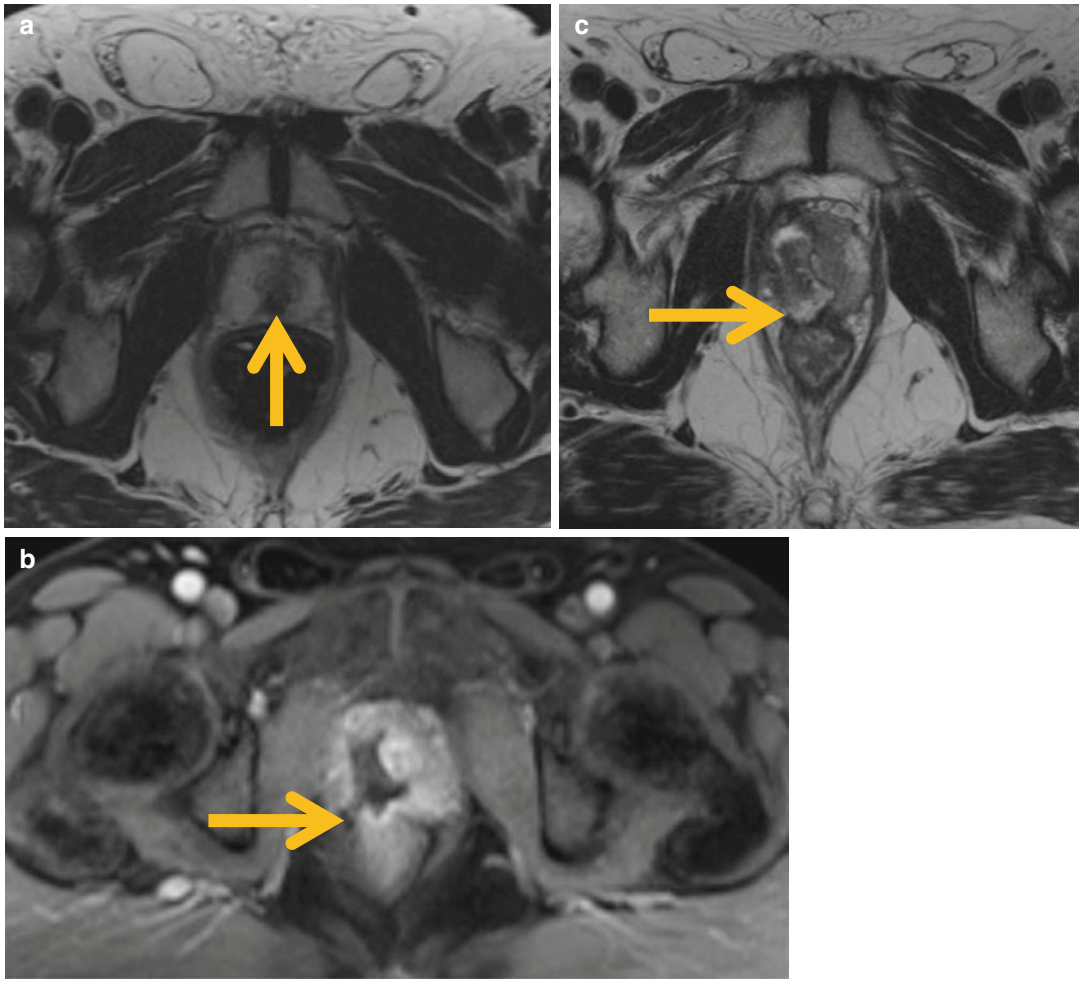


**Fig. 11** Rectal injury following high-intensity focus ultrasound (HIFU) treatment to the prostate gland. (**a**) Axial T2-weighted images through the prostate show a small tumour (*arrow*) in the peripheral zone near the apex of the prostate. (**b**) Axial fat-suppressed T1-weighted and (**c**) axial T2-weighted images through the prostate 1 month after the HIFU treatment show necrosis to the right side of the prostate including the apical lesion. There has been injury to the anterior rectal wall (*arrow*)

to treat local disease recurrence following radical prostatectomy (Woodrum et al. 2013).

Erectile dysfunction is a significant complication of this procedure, but there is now renewed interest to apply cryotherapy focally with the potential for nerve sparing. In addition to erectile dysfunction, other main complications include incontinence and voiding problems.

One of the largest studies to report on focal cryoablation of the prostate is from the national Cryo On-line Database (COLD) registry, in which 1160 patients were followed for a median time of 1.8 years. Biochemical disease-free survival was found to be 75.7 % and although not all patients were biopsied after cryotherapy. There was a 3.7 % local failure rate. Urinary continence was high, at 98.4 %; however, maintenance of sexual function was not as high as might have been expected with spontaneous erections maintained in 58.1 % of patients (Ward and Jones 2012).

Overall, as a relatively new modality of therapy, focal cryotherapy needs further evaluation in longer-term studies before recommendations can be made regarding its efficacy.

## 2 Bladder

The majority of bladder cancers are transitional cell carcinomas. 70 % of patients present with superficial tumours, which have a propensity to recur but have a good prognosis whilst 30 % present with muscle-invasive disease, which carries a poorer outlook. Intravesical treatment is used for carcinoma in situ and non-muscle-invasive tumours. For muscle-invasive disease, total cystectomy offers the best chance of cure but carries significant morbidity. Thus, bladder-preserving approaches including transurethral tumour resection combined with radiation and chemotherapy are also used in clinical practice.

### 2.1 Surgery

Surgical treatment depends on the local tumour stage. Non-muscle-invasive tumours are usually treated by transurethral endoscopic resection, whereas muscle-invasive tumours often necessitate cystectomy and pelvic nodal lymphadenectomy. The acute complications of radical surgery are similar to those of prostatectomy, which includes haemorrhage, infection, urinary leakage and lymphoceles.

Following cystectomy, a neo-bladder may be fashioned to preserve continence or an ileal conduit constructed as urinary diversion. This often results in normal dilatation of the pelvicalyceal system, and interpretation of hydronephrosis in this context may be difficult. The neo-bladder should not be mistaken as a fluid collection.

### 2.2 Radiotherapy

In the acute phase, radiation-induced cystitis can present as haematuria. Chronic changes of fibrosis can lead to frequency and incontinence due to a small-volume, non-distensible bladder.

MRI is optimal for demonstrating sequential changes within the bladder wall. In the acute phase, there is high T2-weighted signal intensity mucosal thickening with loss of the normal low signal intensity of the bladder muscularis. Mucosal haemorrhage is recognised as a high T1 signal intensity rind along the inner bladder wall. It may initially be limited to the posterior wall or trigone with relative sparing anteriorly, but over time, the entire bladder may become involved (Sugimura et al. 1990).

In the long term, there is chronic bladder wall thickening, poor distensibility and patchy enhancement of the bladder mucosa or outer wall following contrast administration. The relative rate of contrast enhancement can sometimes help distinguish between radiation-related changes and residual tumour. The former enhances gradually and persistently whilst the latter rapidly and intensely. A variety of studies have looked at the use of dynamic contrast-enhanced MRI to differentiate between tumour, oedema and fibrosis. One such study found that using a single-slice technique, with slices every 8 s, that an enhancement ratio of 1.54 greater than baseline at 80s was discriminatory for tumour (Dobson et al. 2001).

Radiation-induced ureteric injury is less common and comprises two main types: stricture formation, most often in the distal ureter just above the vesico-ureteric junction, and vesico-ureteric reflux.

### 2.3 Chemotherapy

Chemotherapy is often used in a neoadjuvant setting. Cisplatin-based regimens are used for invasive disease whilst mitomycin and bacillus Calmette-Guerin (BCG) are used intravesically for non-invasive cancers. Intravesical treatment can cause bladder fibrosis. Cyclophosphamide and ifosphamide can also induced haemorrhagic cystitis.

## 3 Kidneys

Renal cell carcinoma (RCC) is the commonest primary renal malignancy accounting for approximately 90 % of renal tumours. The tumour stage determines the treatment options, which are weighed up against the patient's co-morbidities

especially the renal function. Treatment options include surgery, radiation therapy, thermoablation (includes cryoablation (CA) and radiofrequency ablation (RFA)), chemotherapy and immunotherapy.

### 3.1 Surgery

Due to the increase of incidentally discovered renal masses, the detection of stage 1 disease (<7 cm) is now a common clinical scenario. Traditionally, radical nephrectomy was the standard surgical approach, but increasingly guidelines advocate the use of nephron-sparing techniques to avoid predisposing patient to chronic kidney failure and its complications (Thompson et al. 2008; Campbell et al. 2009). In selected patients with significant co-morbidities, active surveillance is well supported as an appropriate strategy to monitor small renal masses and treat if there is progression (Abou Youssif et al. 2007).

Following nephron-sparing surgery CT is mainly used to assess for potential complications, with MRI used for patients with impaired renal function. Fluid collections, such as seroma, can accumulate rapidly, and these show the typical imaging features of fluid. The clinical status determines the management of these patients, and aspiration may be required to exclude or treat an abscess. Sometimes oxidised cellulose (Surgicel) used at the site of renorrhaphy can be mistaken for an abscess on imaging. The lack of signs and symptoms of infection and awareness that oxidised cellulose was used should lead to a conservative management (Sarwani et al. 2007). Damage to the collecting system with an urinoma formation can also result in fluid around the kidney. Urinoma can be distinguished from other collections by the accumulation of excreted contrast material on CT urogram or following aspiration of fluid subsequently found to have a high creatinine level. Haematomas have the typical appearance on imaging. They are generally managed conservatively but may rarely active bleeding may require angiographic embolisation.

Cancer patients are regularly followed up, and it is often on follow-up examinations that post-surgical changes can be differentiated from recurrent or residual disease, based on a change in appearance. Normal involuting appearances such as post-operative granuloma, fatty involution at the excision site and linear parenchymal defects should not be misinterpreted as disease. Mass-like changes may also occur within the retroperitoneal space, which may simulate disease. A mass-like lesion is defined as a lesion that shows increased attenuation in the neighbouring fat but with no significant enhancement or mass effect and is seen to resolve with time (Lee et al. 2007). Tumours enhance more in the vascular phase and show decreased enhancement during the parenchymal/excretory phase, whereas fibrosis demonstrated sustained enhancement (Lang et al. 2004; Sarwani et al. 2007). Tumours presented as speculate masses, whereas scars have long, spidery projections. Furthermore tumours increase in volume over time, whereas scars decrease.

### 3.2 Chemotherapy

Chemotherapy is used in metastatic renal cancer. Targeted therapies with anti-angiogenic agents such as sunitinib are effective in metastatic disease. Responders to these targeted therapies have improved survival compared with non-responders. The majority of complications associated with treatment have no radiological manifestations. However, an increased risk of bleeding has been reported in patients receiving tyrosine kinase treatment.

### 3.3 Focal Therapy

The most commonly used focal therapies are radiofrequency ablation (RFA) and cryoablation. Microwave ablation and high-intensity focused ultrasound have also been trialled but are less widely available. Data regarding these emerging modalities is difficult to interpret because of lack of pre-procedural biopsy confirming a malignant lesion, wide variability in the definition of

oncological outcomes and lack of long-term follow-up (Kapoor et al. 2013).

Both RFA and cryoablation can be performed percutaneously under imaging guidance or laparoscopically. Following treatment, imaging surveillance is essential to detect residual or recurrent malignancy as renal tumours remains in situ. It also provides assessment of the overall treatment success and procedural complications. Most recommend obtaining unenhanced and contrast-enhanced CT or MR images after ablation; however, controversies exist regarding how often and for how long imaging should be performed (Venkatesan et al. 2011). Typically imaging is obtained at 3 and 6 months after ablation. Subsequent imaging depends on the clinical condition of the patient but usually thereafter at 6- to 12-month intervals.

Retrospective series report that minimally invasive ablation procedures are generally well tolerated with a low risk of major complication. A post-RFA syndrome characterised by flu-like symptoms and fever has been described in up to one third of patients (Wah et al. 2005). Haemorrhage, urinary leaks and damage to surrounding structures are the potential risks. Rare complications include retroperitoneal haemorrhage requiring angiography, obstructive haematuria requiring stent placement, pulmonary embolus and delayed urosepsis. In addition, there was a biopsy-proven occurrence of metastasis along a cryoprobe tract (Atwell et al. 2010). As with post-operative complication (see above), imaging with CT is usually performed to assess and manage these problems.

Following ablation, successfully treated tumours appear as focal masses that demonstrate no enhancement and frequently decrease in size over time. They appear as low attenuation areas on CT and on MR imaging as hypointense on T2-weighted and iso- to hyperintense on T1-weighted images (Kawamoto et al. 2007). Ablated tumours often have internal areas of increased attenuation on CT and increased signal intensity on MR images due to proteinaceous debris and/or haemorrhagic products (Zagoria 2004). Areas of contrast enhancement at initial follow-up usually indicate residual viable RCC and primary treatment failure. The pattern of residual or recurrent tumours often manifests as a focus of nodular or crescentic enhancement on post ablation images (Zagoria 2004; Venkatesan et al. 2011). Of note, attenuation of 10–20 HU can sometimes be seen following successful ablation, and, in cases of cryoablation, a thin peripheral rim of enhancement often persists for several months following therapy (Wile et al. 2007). Enhancement or enlargement at subsequent imaging after initial negative imaging findings is considered indicative of local tumour recurrence (Venkatesan et al. 2011).

### 3.4 Radiotherapy

Radiotherapy is reserved for treatment of the primary tumour in patients whose poor medical condition precludes a surgical or targeted approach. More commonly it is used for the symptomatic treatment of painful osseous metastases, and several modalities have been shown to provide good relief of bone pain (Hunter et al. 2012; Zelefsky et al. 2012).

## 4 Testes

Testicular cancer is the commonest cancer in males aged 15–35 and has an excellent prognosis with >95 % of patients diagnosed surviving the disease (Sohaib et al. 2011). The most common type is a germ cell tumour (approximately 95 % of all testicular tumours). These can be further subdivided into seminomas and non-seminomatous germ cell tumour (NSGCT); about 40 % of germ cell tumours are seminomas and the rest NSGCT.

### 4.1 Surgery

Surgery in the form of radical inguinal orchidectomy is usually the primary treatment for testicular tumours. Following surgery, patients may be

managed with surveillance, radiation therapy or chemotherapy depending on the type and stage of tumour. Retroperitoneal lymph node dissection (RPLND) is usually performed for residual masses following chemotherapy.

### 4.2 Chemotherapy

Germ cell tumours are very chemo-sensitive solid tumours, and conventional regimes can cure over 90 % of patients with disseminated disease. Therefore, patients with testicular cancer become long-term survivors, and recognising as well as reducing the toxicities from therapy is important.

#### 4.2.1 Secondary Malignancy

The most common cancer in patients following the initial diagnosis is a second testicular cancer with a risk of 2–5 %, and in fact, the risk remains high for patients treated with surgery alone implying this is not a radiotherapy or chemotherapy treatment effect.

The risk of solid tumours is also elevated with survivors twice as likely to develop a cancer outside the testicle as the general population. In the largest study to date, cancers of the lung, bladder, colon, pancreas and stomach accounted for almost 60 % of the total excess number of solid tumours. Men who undergo chemotherapy are also at increased risk of developing myeloid leukaemia with high doses of etoposide being the main risk factor (Travis et al. 2005).

#### 4.2.2 Other Effects

Other adverse effects of the commonly used chemotherapeutic agents used in the treatment of GCTs include nephrotoxicity commonly due to cisplatin as well as impaired gonadal function with reduced spermatogenesis and lowered testosterone. Neurotoxicity is common especially sensory neuropathy with cisplatin, and cardiovascular toxicity (dyslipidaemia, hypertension, early atherosclerosis and coronary artery disease) is one of the main late complications.

## 5 Penis

Penile cancer has an incidence of less than 1 per 100,000 in the UK and USA (Barnholtz-Sloan et al. 2007). Over 95 % of penile cancers are squamous cell carcinomas, with rare instances of sarcomas, melanomas or small cell carcinomas. Penile cancers are staged using a TNM classification with inguinal nodal involvement being the biggest predictor for poor disease-free survival. There are no randomised control trials on the treatment of penile cancer due to the small numbers of patients. Therapeutic options depend upon the histologic type, location and size of the tumour and assessment of inguinal lymphadenopathy.

For men with a low risk of recurrence, organ-preserving treatments are an option. These include topical creams (e.g. 5-fluorouracil), laser ablation (e.g. carbon-dioxide and argon), Mohs micrographic surgery (involving layer-by-layer excision of the penile lesion) and partial penectomy. A more radical surgical approach (total penectomy) is reserved for cases that are unsuitable for conservative treatment or relapses. Inguinal lymphadenectomy may be performed at the time of the penile surgery or later. Inguinal lymphadenectomy is associated with significant morbidity in 30–50 % of cases with lymphoedema and skin flap necrosis (Singh et al. 2005).

Radiation therapy is used for localised disease as well as to treat more advanced disease in patients who would not be surgical candidates. External beam radiotherapy (EBRT) or brachytherapy is used. The rate of tumour control appears to be inferior to surgical treatment (Crook et al. 2009). The main complications include urethral mucositis, oedema and secondary infection in the early phase and dyschromia, superficial necrosis, urethral stricture, fistula formation and meatal stenosis in the late phase (Delannes et al. 1992; Pizzocaro et al. 1997). Circumcision is necessary prior to radiotherapy to prevent oedema and allow full exposure for treatment.

Chemotherapy is used for inoperable tumours in a neoadjuvant setting as well as for metastatic disease.

Imaging complements clinical examination and is used to assess the primary lesion, and nodal and distant disease (Singh et al. 2005). MR imaging provides the best assessment of the primary lesion before and after treatment. In general T2-weighted and gadolinium-enhanced T1-weighted images can evaluate the depth invasion of the tumour, recurrent disease and effects of treatment on the primary site of disease.

## Conclusions

In summary, imaging plays a central role in the assessment of treatment toxicity in patients with genitourinary cancers. The myriad of different therapies for these cancers leads to differing patterns of complication. The application and interpretation of imaging in these situations require that the radiologist understands the malignancy, the treatment administered and the potential problems that may arise.

**Acknowledgement** The authors gratefully acknowledge the support of the NIHR Biomedical Research Centre for Cancer at The Royal Marsden NHS Foundation Trust and The Institute of Cancer Research, London, UK.

## References

Abou Youssif T, Kassouf W et al (2007) Active surveillance for selected patients with renal masses: updated results with long-term follow-up. Cancer 110(5):1010–1014

Addley HC, Vargas HA et al (2010) Pelvic imaging following chemotherapy and radiation therapy for gynecologic malignancies. Radiographics Rev Publ Radiol Soc North Am Inc 30(7):1843–1856

Ahmed HU, Freeman A et al (2011) Focal therapy for localized prostate cancer: a phase I/II trial. J Urol 185(4):1246–1254

Alemozaffar M, Regan MM et al (2011) Prediction of erectile function following treatment for prostate cancer. JAMA 306(11):1205–1214

Allen SD, Thompson A et al (2008) The normal post-surgical anatomy of the male pelvis following radical prostatectomy as assessed by magnetic resonance imaging. Eur Radiol 18(6):1281–1291

Atwell TD, Callstrom MR et al (2010) Percutaneous renal cryoablation: local control at mean 26 months of followup. J Urol 184(4):1291–1295

Aus G (2006) Current status of HIFU and cryotherapy in prostate cancer – a review. Eur Urol 50(5):927–934; discussion 934

Barchetti F, Panebianco V (2014) Multiparametric MRI for recurrent prostate cancer post radical prostatectomy and postradiation therapy. BioMed Res Int 2014:316272

Barnholtz-Sloan JS, Maldonado JL et al (2007) Incidence trends in primary malignant penile cancer. Urol Oncol 25(5):361–367

Baxter NN, Tepper JE et al (2005) Increased risk of rectal cancer after prostate radiation: a population-based study. Gastroenterology 128(4):819–824

Blake SP, Connors AM (2004) Sacral insufficiency fracture. Br J Radiol 77(922):891–896

Bloch S, Love A et al (2007) Psychological adjustment of men with prostate cancer: a review of the literature. BioPsychoSocial Med 1:2

Blomlie V, Rofstad EK et al (1996) Incidence of radiation-induced insufficiency fractures of the female pelvis: evaluation with MR imaging. AJR Am J Roentgenol 167(5):1205–1210

Brenner DJ, Curtis RE et al (2000) Second malignancies in prostate carcinoma patients after radiotherapy compared with surgery. Cancer 88(2):398–406

Campbell SC, Novick AC et al (2009) Guideline for management of the clinical T1 renal mass. J Urol 182(4): 1271–1279

Chrouser K, Leibovich B et al (2005) Bladder cancer risk following primary and adjuvant external beam radiation for prostate cancer. J Urol 174(1):107–110; discussion 110–101

Cronin CG, Lohan DG et al (2010) Does MRI with oral contrast medium allow single-study depiction of inflammatory bowel disease enteritis and colitis? Eur Radiol 20(7):1667–1674

Crook J, McLean M et al (2002) Factors influencing risk of acute urinary retention after TRUS-guided permanent prostate seed implantation. Int J Radiat Oncol Biol Phys 52(2):453–460

Crook J, Ma C et al (2009) Radiation therapy in the management of the primary penile tumor: an update. World J Urol 27(2):189–196

Daniell HW, Dunn SR et al (2000) Progressive osteoporosis during androgen deprivation therapy for prostate cancer. J Urol 163(1):181–186

Dearnaley DP, Khoo VS et al (1999) Comparison of radiation side-effects of conformal and conventional radiotherapy in prostate cancer: a randomised trial. Lancet 353(9149):267–272

Delannes M, Malavaud B et al (1992) Iridium-192 interstitial therapy for squamous cell carcinoma of the penis. Int J Radiat Oncol Biol Phys 24(3):479–483

Diamond TH, Higano CS et al (2004) Osteoporosis in men with prostate carcinoma receiving androgen-deprivation therapy: recommendations for diagnosis and therapies. Cancer 100(5):892–899

Dickinson L, Ahmed HU et al (2013) A multi-centre prospective development study evaluating focal therapy using high intensity focused ultrasound for localised prostate cancer: The INDEX study. Contemp Clin Trials 36(1):68–80

Dobson MJ, Carrington BM et al (2001) The assessment of irradiated bladder carcinoma using dynamic contrast-enhanced MR imaging. Clin Radiol 56(2):94–98

Emara AM, Chadwick E et al (2012) Long-term toxicity and quality of life up to 10 years after low-dose rate brachytherapy for prostate cancer. BJU Int 109(7):994–1000

Finiels H, Finiels PJ et al (1997) Fractures of the sacrum caused by bone insufficiency. Meta-analysis of 508 cases. Presse Med 26(33):1568–1573

Finkelstein J, Eckersberger E et al (2010) Open versus laparoscopic versus robot-assisted laparoscopic prostatectomy: the European and US Experience. Rev Urol 12(1):35–43

Gangi A, Tsoumakidou G et al (2012) Percutaneous MR-guided cryoablation of prostate cancer: initial experience. Eur Radiol 22(8):1829–1835

Goldman SM, Fishman EK et al (1985) CT in the diagnosis of enterovesical fistulae. AJR Am J Roentgenol 144(6):1229–1233

Grangier C, Garcia J et al (1997) Role of MRI in the diagnosis of insufficiency fractures of the sacrum and acetabular roof. Skeletal Radiol 26(9):517–524

Grimm PD, Blasko JC et al (1996) Does brachytherapy have a role in the treatment of prostate cancer? Hematol Oncol Clin North Am 10(3):653–673

Grimm P, Billiet I et al (2012) Comparative analysis of prostate-specific antigen free survival outcomes for patients with low, intermediate and high risk prostate cancer treatment by radical therapy. Results from the Prostate Cancer Results Study Group. BJU Int 109(Suppl 1):22–29

Hanks GE, Hanlon AL et al (2002) Dose response in prostate cancer with 8-12 years' follow-up. Int J Radiat Oncol Biol Phys 54(2):427–435

Harris V, Benton B et al (2012) Bile acid malabsorption after pelvic and prostate intensity modulated radiation therapy: an uncommon but treatable condition. Int J Radiat Oncol Biol Phys 84(5):e601–e606

Heidenreich A, Varga Z et al (2002) Extended pelvic lymphadenectomy in patients undergoing radical prostatectomy: high incidence of lymph node metastasis. J Urol 167(4):1681–1686

Horton KM, Corl FM et al (2000) CT evaluation of the colon: inflammatory disease. Radiographics Rev Publ Radiol Soc North Am Inc 20(2):399–418

Huber P, Debus J et al (1996) Therapeutic ultrasound in tumor therapy. Principles, applications and new developments. Radiologe 36(1):64–71

Hunter GK, Balagamwala EH et al (2012) The efficacy of external beam radiotherapy and stereotactic body radiotherapy for painful spinal metastases from renal cell carcinoma. Pract Radiat Oncol 2(4):e95–e100

Igdem S, Alco G et al (2010) Insufficiency fractures after pelvic radiotherapy in patients with prostate cancer. Int J Radiat Oncol Biol Phys 77(3):818–823

Jacob R, Hanlon AL et al (2004) The relationship of increasing radiotherapy dose to reduced distant metastases and mortality in men with prostate cancer. Cancer 100(3):538–543

Kapoor A, Touma NJ et al (2013) Review of the efficacy and safety of cryoablation for the treatment of small renal masses. Canad Urol Assoc J=Journal de l'Association des urologues du Canada 7(1-2):E38–E44

Kawamoto S, Permpongkosol S et al (2007) Sequential changes after radiofrequency ablation and cryoablation of renal neoplasms: role of CT and MR imaging. Radiographics Rev Publ Radiol Soc North Am Inc 27(2):343–355

Kayhan A, Oommen J et al (2010) Magnetic resonance enterography in Crohn's disease: standard and advanced techniques. World J Radiol 2(4):113–121

Kirkham AP, Emberton M et al (2008) MR imaging of prostate after treatment with high-intensity focused ultrasound. Radiology 246(3):833–844

Lang EK, Thomas R et al (2004) Multiphasic helical CT criteria for differentiation of recurrent neoplasm and desmoplastic reaction after laparoscopic resection of renal mass lesions. J Endourol/Endourol Soc 18(2):167–171

Lee MS, Oh YT et al (2007) CT findings after nephron-sparing surgery of renal tumors. AJR Am J Roentgenol 189(5):W264–W271

Locke J, Ellis W et al (2002) Risk factors for acute urinary retention requiring temporary intermittent catheterization after prostate brachytherapy: a prospective study. Int J Radiat Oncol Biol Phys 52(3):712–719

Michalski JM, Bae K et al (2010) Long-term toxicity following 3D conformal radiation therapy for prostate cancer from the RTOG 9406 phase I/II dose escalation study. Int J Radiat Oncol Biol Phys 76(1):14–22

Nomura T, Mimata H (2012) Focal therapy in the management of prostate cancer: an emerging approach for localized prostate cancer. Advance Urol 2012:391437

Oh D, Huh SJ et al (2008) Pelvic insufficiency fracture after pelvic radiotherapy for cervical cancer: analysis of risk factors. Int J Radiat Oncol Biol Phys 70(4):1183–1188

Ohri N, Dicker AP et al (2012) Late toxicity rates following definitive radiotherapy for prostate cancer. Can J Urol 19(4):6373–6380

Outwater E, Schiebler ML (1993) Pelvic fistulas: findings on MR images. AJR Am J Roentgenol 160(2): 327–330

Pizzocaro G, Piva L et al (1997) Up-to-date management of carcinoma of the penis. Eur Urol 32(1):5–15

Ravichandran S, Ahmed HU et al (2008) Is there a role for magnetic resonance imaging in diagnosing colovesical fistulas? Urology 72(4):832–837

Reed DR, Wallner KE et al (2007) A prospective randomized comparison of stranded vs. loose 125I seeds for prostate brachytherapy. Brachytherapy 6(2):129–134

Roach M 3rd, DeSilvio M et al (2003) Phase III trial comparing whole-pelvic versus prostate-only radiotherapy and neoadjuvant versus adjuvant combined androgen suppression: Radiation Therapy Oncology Group 9413. J Clin Oncol: Off J Am Soc Clin Oncol 21(10):1904–1911

Sarwani NI, Motta Ramirez GA et al (2007) Imaging findings after minimally invasive nephron-sparing renal therapies. Clin Radiol 62(4):333–339

Schneider R, Yacovone J et al (1985) Unsuspected sacral fractures: detection by radionuclide bone scanning. AJR Am J Roentgenol 144(2):337–341

Shahinian VB, Kuo YF et al (2005) Risk of fracture after androgen deprivation for prostate cancer. N Engl J Med 352(2):154–164

Singh AK, Saokar A et al (2005) Imaging of penile neoplasms. Radiographics Rev Publ Radiol Soc North Am Inc 25(6):1629–1638

Smith MR, Boyce SP et al (2006) Risk of clinical fractures after gonadotropin-releasing hormone agonist therapy for prostate cancer. J Urol 175(1):136–139; discussion 139

Sohaib SA, Cook G et al (2011) Imaging studies for germ cell tumors. Hematol Oncol Clin North Am 25(3): 487–502, vii

Solberg A, Angelsen A et al (2003) Frequency of lymphoceles after open and laparoscopic pelvic lymph node dissection in patients with prostate cancer. Scand J Urol Nephrol 37(3):218–221

Stoker J (2010) MRI of the gastrointestinal tract. Springer, Berlin/Heidelberg

Stone NN, Stock RG (2007) Long-term urinary, sexual, and rectal morbidity in patients treated with iodine-125 prostate brachytherapy followed up for a minimum of 5 years. Urology 69(2):338–342

Sugimura K, Carrington BM et al (1990) Postirradiation changes in the pelvis: assessment with MR imaging. Radiology 175(3):805–813

Tang YZ, Booth TC et al (2012) Imaging features of colovesical fistulae on MRI. Br J Radiol 85(1018): 1371–1375

Thompson RH, Boorjian SA et al (2008) Radical nephrectomy for pT1a renal masses may be associated with decreased overall survival compared with partial nephrectomy. J Urol 179(2):468–471; discussion 472–63

Travis LB, Fossa SD et al (2005) Second cancers among 40,576 testicular cancer patients: focus on long-term survivors. J Natl Cancer Inst 97(18):1354–1365

Trofimov A, Nguyen PL et al (2007) Radiotherapy treatment of early-stage prostate cancer with IMRT and protons: a treatment planning comparison. Int J Radiat Oncol Biol Phys 69(2):444–453

Turini M, Redaelli A et al (2003) Quality of life and economic considerations in the management of prostate cancer. Pharmacoeconomics 21(8):527–541

Vallancien G, Prapotnich D et al (2004) Transrectal focused ultrasound combined with transurethral resection of the prostate for the treatment of localized prostate cancer: feasibility study. J Urol 171(6 Pt 1): 2265–2267

Vargas C, Fryer A et al (2008) Dose-volume comparison of proton therapy and intensity-modulated radiotherapy for prostate cancer. Int J Radiat Oncol Biol Phys 70(3):744–751

Venkatesan AM, Wood BJ et al (2011) Percutaneous ablation in the kidney. Radiology 261(2):375–391

Wah TM, Arellano RS et al (2005) Image-guided percutaneous radiofrequency ablation and incidence of post-radiofrequency ablation syndrome: prospective survey. Radiology 237(3):1097–1102

Ward JF, Jones JS (2012) Focal cryotherapy for localized prostate cancer: a report from the national Cryo On-Line Database (COLD) Registry. BJU Int 109(11):1648–1654

Weight CJ, Reuther AM et al (2008) Limited pelvic lymph node dissection does not improve biochemical relapse-free survival at 10 years after radical prostatectomy in patients with low-risk prostate cancer. Urology 71(1):141–145

Wile GE, Leyendecker JR et al (2007) CT and MR imaging after imaging-guided thermal ablation of renal neoplasms. Radiographics Rev Publ Radiol Soc North Am Inc 27(2):325–339; discussion 339–40

Wilt TJ, MacDonald R et al (2008) Systematic review: comparative effectiveness and harms of treatments for clinically localized prostate cancer. Ann Intern Med 148(6):435–448

Woodrum DA, Kawashima A et al (2013) Magnetic resonance imaging-guided cryoablation of recurrent prostate cancer after radical prostatectomy: initial single institution experience. Urology 82(4):870–875

Zagoria RJ (2004) Imaging-guided radiofrequency ablation of renal masses. Radiographics Rev Publ Radiol Soc Am Inc 24(Suppl 1):S59–S71

Zelefsky MJ, Hollister T et al (2000) Five-year biochemical outcome and toxicity with transperineal CT-planned permanent I-125 prostate implantation for patients with localized prostate cancer. Int J Radiat Oncol Biol Phys 47(5):1261–1266

Zelefsky MJ, Greco C et al (2012) Tumor control outcomes after hypofractionated and single-dose stereotactic image-guided intensity-modulated radiotherapy for extracranial metastases from renal cell carcinoma. Int J Radiat Oncol Biol Phys 82(5): 1744–1748

# Female Pelvis: Genital Organs

Rosemarie Forstner and Teresa Margarida Cunha

## Contents



**Abstract**

Gynecologic cancers account for 10–15 % of female malignancies, but the genital organs may also be affected in pelvic irradiation of other organs and in systemic treatment.

Depending on cancer type and stage, surgery, radiotherapy, and chemotherapy are treatment options. Advances in therapy result in markedly improved survival rates in pelvic malignancies. In these patients treatment-related side effects are more common than recurrence, but their differentiation may be challenging. This is why it is pivotal that the radiologist is aware of the type of treatment and the spectrum of normal posttreatment findings, pitfalls, and complications. Postirradiation sequelae may complicate the early phase but may also occur with a latency of many years. Side effects of targeted agents differ from those of classical cytotoxic agents, and particularly in the latter ovarian function may be impaired.

## Definitions

| | |
|---|---|
| CT | computed tomography |
| MRI | magnetic resonance imaging |
| RT | radiotherapy |
| WI | weighted imaging |

R. Forstner (✉)
Department of Radiology, Landeskliniken Salzburg, Paracelsus Medical University,
Müllner Hauptstr. 48, Salzburg 5020, Austria
e-mail: R.Forstner@salk.at

T.M. Cunha
Department of Radiology, Instituto Português de Oncologia de Lisboa Francisco Gentil,
Rua Prof. Lima Basto, Lisbon 1099-023, Portugal
e-mail: tmargarida@gmail.com

Med Radiol Diagn Imaging (2015)
DOI 10.1007/174_2015_1054, © Springer International Publishing Switzerland

## 1 Introduction

Advances in treatment result in continuously increasing rates of long time cancer survivors after gynecological and other pelvic cancers. Thus, the clinical interest focuses also on radiotherapy or other treatment-related side effects affecting quality of life issues, e.g., integrity of pelvic organ function and pertaining to fertility. Apart from radiotherapy, a broad spectrum of chemotherapy agents may cause genital organ dysfunction both during and after treatment. However, although in symptomatic patients the likelihood of treatment-induced injury is higher than pelvic recurrence for uterine cancers, their differentiation remains challenging (Addley et al. 2010). Correlation of post- and pretreatment imaging and integration of clinical information including radiation therapy technique, radiation field, dose, and time frame since therapy will allow differentiation of therapy-induced complications from tumor recurrence in the majority of cases (Bluemke et al. 1991; Maturen et al. 2013).

Serial follow-up in CT and MRI, advanced MRI using DWI and perfusion studies, and/or PET/CT will assist in problem solving in equivocal cases (Sala et al. 2010; Meads et al. 2014).

## 2 Treatment of Gynecologic Cancer

Therapy options in gynecologic cancers depend on various factors, e.g., organ of origin, histology, imaging findings, stage, and patient age and medical condition. Optimally treatment follows stage-dependent regimen according to the different tumor types and is based on multidisciplinary consensus (ESMO clinical practice guidelines; cancer topics). In the majority of female cancers, surgery remains the mainstay of treatment. Radiation and chemotherapy are performed as adjuncts to surgery in advanced or in high-risk endometrial cancer. Concomitant chemoradiation is the therapy of choice in advanced or in large-size cervical cancer.

Adjuvant chemotherapy has been widely used in the postoperative treatment of ovarian cancer. Alternatively, neoadjuvant chemotherapy has been introduced in advanced ovarian cancer (Raja et al. 2012). Currently, novel targeted chemo- and immunotherapeutic agents are used in combination with classical chemotherapy, often in clinical trials, in advanced or recurrent disease (Raja et al. 2012).

Pelvic cancer is treated with irradiation at doses of 30–70 Gy, often in conjunction with other therapies (McConnell Greven and Paunesku 2005). Main treatment of pelvic irradiation remains external beam RT and brachytherapy for uterine cancers. New 3D conformal external radiation therapy techniques (e.g., stereotactic intensity-modulated radiotherapy) and proton therapy focus dose delivery on the target tumor volume, and thus significantly reduce radiation exposure to adjacent tissues and organs (*Maturen et al*. 2013; Bluemke et al. 1991).

Embryo and oocyte cryoconservation now present established methods for children and females desiring fertility preservation before undergoing chemotherapy (Loren et al. 2013). Ovarian transposition is widely used in the same age group before radiotherapy or before receiving chemoradiation with minimally gonadotoxic agents (Irtan et al. 2014; Wo and Viswanathan 2009).

## 3 Treatment-Related Imaging Findings

### 3.1 Gynecologic Cancers Treated with Surgery

#### 3.1.1 Normal Postoperative Imaging Findings and Complications

Several months after radical hysterectomy, the normal vaginal cuff is symmetrical and displays very low SI on T2WI (Antunes and Cunha 2013). During intracavitary radiotherapy small pockets of air surrounding the vaginal cylinder applicators present a normal finding (Hassouna et al.

2014). Vaginal edema and thickening of the vaginal stump exhibiting high SI on T2WI is typically seen in the early postoperative period (Paspulati and Dalal 2010). Vaginal vault hematoma or hemorrhage occurs most commonly within the first week after surgery (Paspulati and Dalal 2010) (Fig. 1). Relevant complications include secondary infection and abscess formation due to bowel injury. Large amounts of intraperitoneal air are highly indicative of bowel injury. Open surgery is associated with increased risk of rectal injury, while small bowel is more often injured during laparoscopic surgery (Maturen et al. 2013; Bluemke et al. 1991).

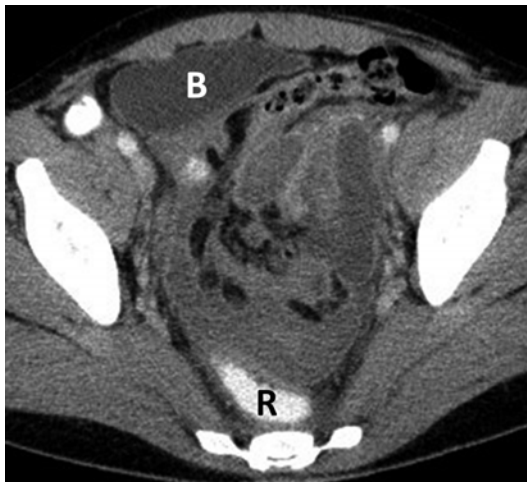


**Fig. 1** Diffuse pelvic hematoma 10 days after hysterectomy. Transaxial CT demonstrates encapsulated lesions with thin peripheral enhancement throughout the pelvis. They are surrounding the bowel and follow the tissue planes along the pelvic sidewalls. HU ranging from 20 to 50 HU and lack of air support the diagnosis of subacute hematomas. Bladder (*B*), rectum (*R*)

Bladder and ureteral iatrogenic trauma is most commonly found after radical hysterectomy, with adhesions, prior radiation therapy, and pelvic inflammatory disease (PID) as predisposing factors (Ostrzenski et al. 2003).

Ureteral injury may also be caused by ligation or ischemia from stripping of the periureteral fascia and is found in 0.4–2 % after laparoscopic hysterectomies (Maturen et al. 2013). Ureteral injury, typically at 2–3 cm from the lateral edge of the cervix, may resolve or become clinically evident by complications, e.g., urinoma (Fig. 2), stricture, or fistula formations. Bowel obstruction is rather found as delayed complication secondary to adhesions than in the early postoperative period (Paspulati and Dalal 2010).

Lymphoceles are commonly found following radical hysteroscopy and lymph node dissection

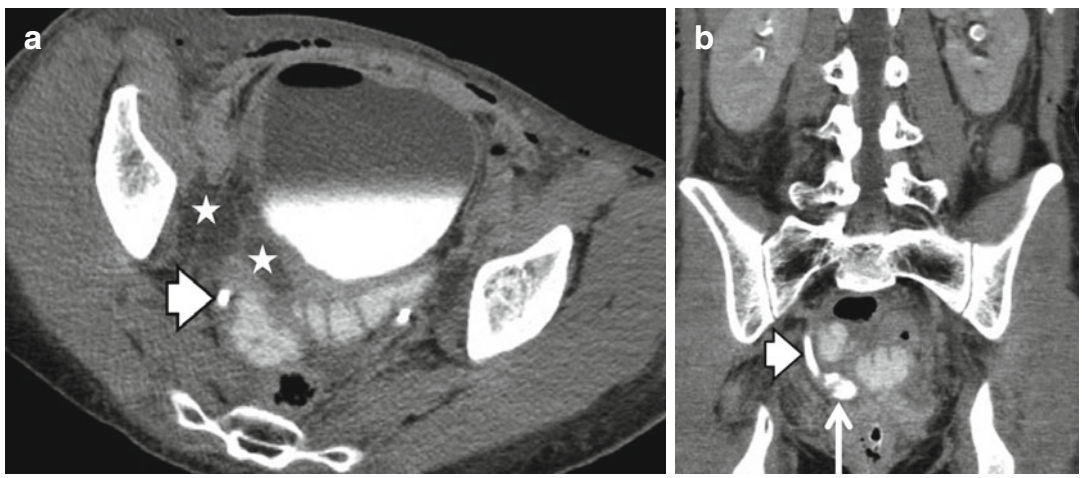


**Fig. 2** Ureteral injury after radical hysterectomy. Transaxial (**a**) and coronal (**b**) CT urography scans 5 days after surgery show loculated pelvic fluid collections (*) and contrast extravasation (*arrow*) along the right ureter (*arrowhead*). The distal 3 cm of the ureter are prone to surgical injury

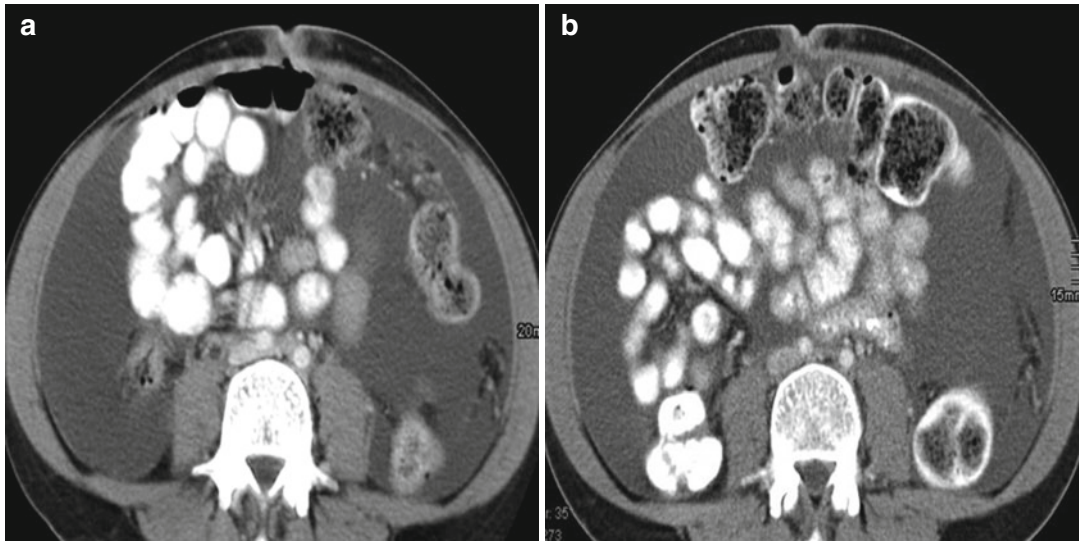


**Fig. 3** Chylous ascites following laparoscopic lymphadenectomy. CT at the umbilical level in a 27-year-old female with cervical cancer. Large amounts of ascites measuring 10–20 HU are identified 1 month after surgery (**a**) and in the follow-up of 3 months (**b**)

for genital cancers. They present ovoid sharply delineated cystic structures along the pelvic sidewall developing at approximately 2 weeks after surgery and may be noted for one year or longer. Complications are rare and include pain, thrombophlebitis, or superinfection (Tam et al. 2008).

Chylous ascites is seen extremely rarely following radiation therapy and after extensive retroperitoneal lymphadenectomy in gynecologic malignancies (Boran et al. 2004) (Fig. 3). Inguinal seromas and lymphoceles present typical postoperative findings following vulvar cancer surgery.

#### 3.1.1.1 Ovarian Transposition (Oophoropexy): Normal Imaging Findings and Complications

Ovarian transposition is performed in children and in women of reproductive age before pelvic radiotherapy for pelvic sarcomas, cervical cancer, anorectal cancer, and Hodgkin's lymphoma to preserve ovarian function. Reported data evaluating its efficacy vary, as this treatment approach may be limited by radiation scatter, ovarian remigration, vascular injury, and gonadotoxic effect of chemotherapy agents (Morgan et al. 2012; Sella et al. 2005). In one study endocrine function of the ovaries was maintained in 90 % of patients treated with vaginal brachytherapy and in 60 % treated by postoperative external radiotherapy and brachytherapy for cervical cancer (Morice et al. 2000; Irtan et al. 2014). In ovarian transposition the ovaries are fixed outside the radiation field, most commonly above the pelvic brim to the paracolic gutters anterior of the psoas muscles (Wo and Viswanathan 2009). Pelvic pain and increased incidence of functional ovarian cysts (24 %) and of peritoneal inclusion cysts are reported following this procedure (Sella et al. 2005; Wo and Viswanathan 2009) (Fig. 4). Transposed ovaries should not be misdiagnosed as peritoneal implants in postoperative imaging. Metallic surgical clip markings in CT will facilitate differentiation (Fig. 4), as well as meticulous analysis of ovarian morphology including ovarian follicles on T2WI (Sella et al. 2005).

## 3.2 Gynecologic Cancers Treated with Irradiation and/or Chemotherapy

### 3.2.1 General Aspects in Treatment-Related Side Effects

The majority of patients undergoing treatment for gynecologic cancers will remain asymptomatic, but morbidity varies considerably among

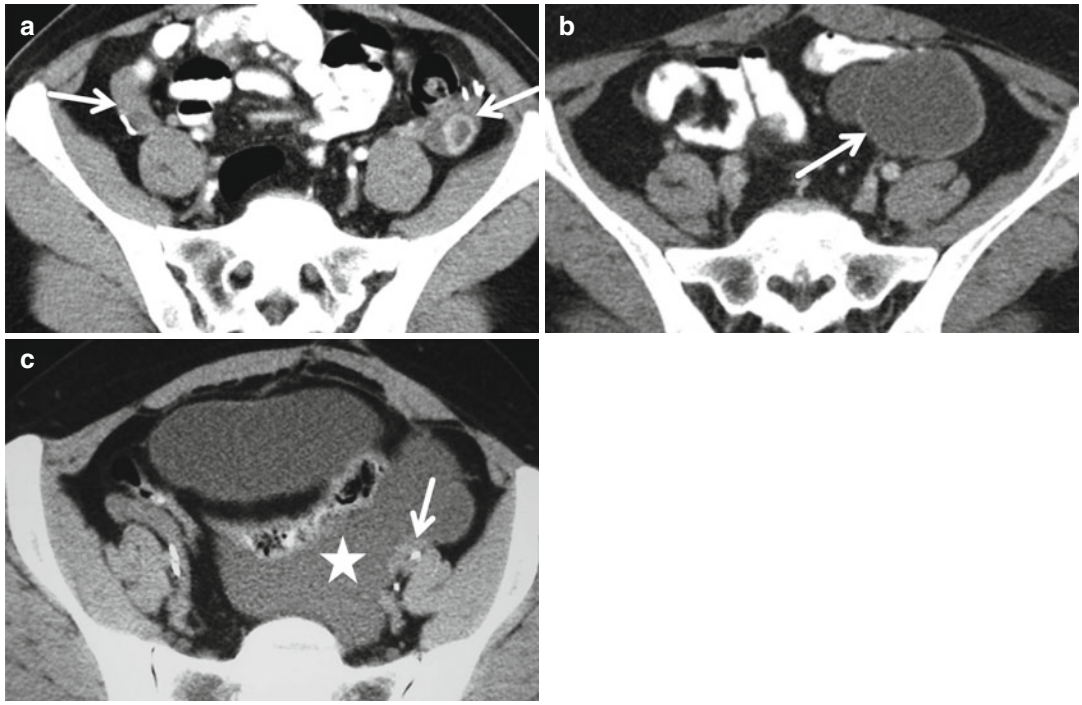


**Fig. 4** Spectrum of CT findings in ovarian transposition. Both transposed ovaries (*arrows*) can be identified due to surgical clips (**a**). In the left ovary, a normal corpus luteum can be identified (**a**). Cyst formation (*arrow*) in a left transposed ovary (**b**). A multiloculated cystic lesion (*) surrounding the left ovary (*arrow*) presents a peritoneal pseudocyst, a finding only seen in functioning ovaries (**c**)

different individuals (West and Barnett 2011). Radiotherapy-induced injury also varies among the different tissue types and is directly determined by dose and radiation technique. Concomitant chemotherapy and radiosensitizers may act synergistically to inducing damage to the female pelvis (Kwek et al. 2006). The side effects of novel molecularly targeted therapies may differ from those of classical cytotoxic chemotherapy, and new complications may arise (Torrisi et al. 2011).

Radiation injury is recognized as a dynamic and progressive process with immediate and delayed side effects to the female genital organs (Jeraj et al. 2010). Most sensitive to radiation injury are organs with a rapid cellular turnover. This explains why small bowel mucosa and the anus are more vulnerable than the uterus during radiotherapy. Connective tissues respond in a delayed pattern with edema, inflammation, and microvascular damage, resulting in increased tissue vulnerability, ulcerations, and delayed healing (McConnell Greven and Paunesku 2005). Delayed tissue injury starts at about 6 months after treatment and may deteriorate gradually (McConnell Greven and Paunesku 2005) within a time range of up to 10 years or longer. The 5-year actuarial risk of severe complications of irradiation in gynecologic cancer ranges from 2 to 5 %, typically affecting bladder and bowel, and extremely rarely the female genital organs (Jereczek-Fossa et al. 2002; Weiss et al. 1999).

### 3.2.2 Normal Posttreatment Imaging Findings and Complications in the Female Pelvis

#### 3.2.2.1 Vulva and Skin

Gross vulvar edema, a typical early finding during radiation, is visualized as high SI on T2WI and diffuse enhancement after gadolinium T1WI (McConnell Greven and Paunesku 2005). Reticular pattern and abundance of the subcutaneous fat present chronic radiation changes and are most prominent along the anterior abdominal

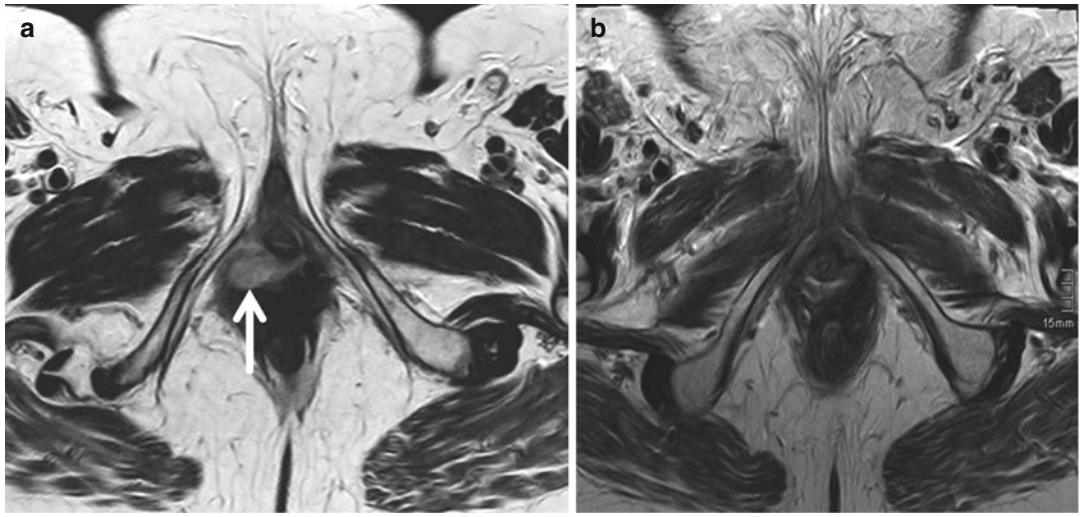


**Fig. 5** Radiotherapy-associated changes of mons pubis. 84-year-old female before (**a**) and after irradiation (**b**) of perineal metastasis (*arrow*) of endometrial cancer. Three years after radiotherapy (**b**), diffuse haziness of the fat of the mons pubis and inguinal region and increased reticular pattern due to edema and fibrosis can be identified

wall including the mons pubis (Fig. 5). Subcutaneous fibrotic bands may also demarcate the radiation ports (Fig. 6).

#### 3.2.2.2 Cervix and Vagina

Cervical cancer responds to chemoradiation with tumor shrinkage and low SI replacing the intermediate SI of cervical cancer on T2WI (Antunes and Cunha 2013). This is seen immediately (within 3–6 months) following radiotherapy (Fig. 7). A delayed response (6–9 months) has been described for large cervical cancers (Engin 2006; Flueckinger et al. 1992). Parametrial fibrosis displaying low SI on T2WI is most evident in areas of previous tumor invasion (Engin 2006). Complete reconstitution of the normal cervical anatomy and low SI of cervical stroma indicate tumor-free status (97 % PPV for exclusion tumor recurrence) (Hricak et al. 1993). However, particularly, within the first 3 months of treatment, differentiation between residual tumor and post-irradiation changes is not possible (Engin 2006). Pretreatment hypervascularity, intratumoral increase of DWI in the first 2 weeks after RT, and immediate response during RT have been associated with a better prognosis in women with cervical cancer (Harry et al. 2008; Mayr et al. 1996).

Local complications after RT include cervical and vaginal stenosis (Fig. 8) and necrosis. The latter exhibits intermediate to high SI and often areas of air within the irradiated tumor on T2WI. In the early phase after RT, intratumoral necrosis including fistula formation may be better visualized with contrast-enhanced T1WI.

Sagittal T2WI, optimally with contrast gel filling, is best suited to show the level of obstruction

**Fig. 6** Spectrum of delayed radiation-induced injuries after cervical cancer. In a 76-year-old female CT and MRI was performed in a secondary left vulva cancer (*arrow* in **a**) developing 16 years following radiotherapy. Both transaxial CT (**b**, **c**) and MRI using T1WI and STIR (**d**, **e**) show extensive fibrosis and edema in the anterior and posterior subcutaneous tissues along the radiation field. In these sections radiotherapy-related inhomogeneous osseous structure is seen in both SIG joints. Coronal CT (**f**) demonstrates hydronephrosis and mild dilation of the right ureter due to distal ureteral stenosis (*arrow* in **f**), consistent with chronic radiation injury

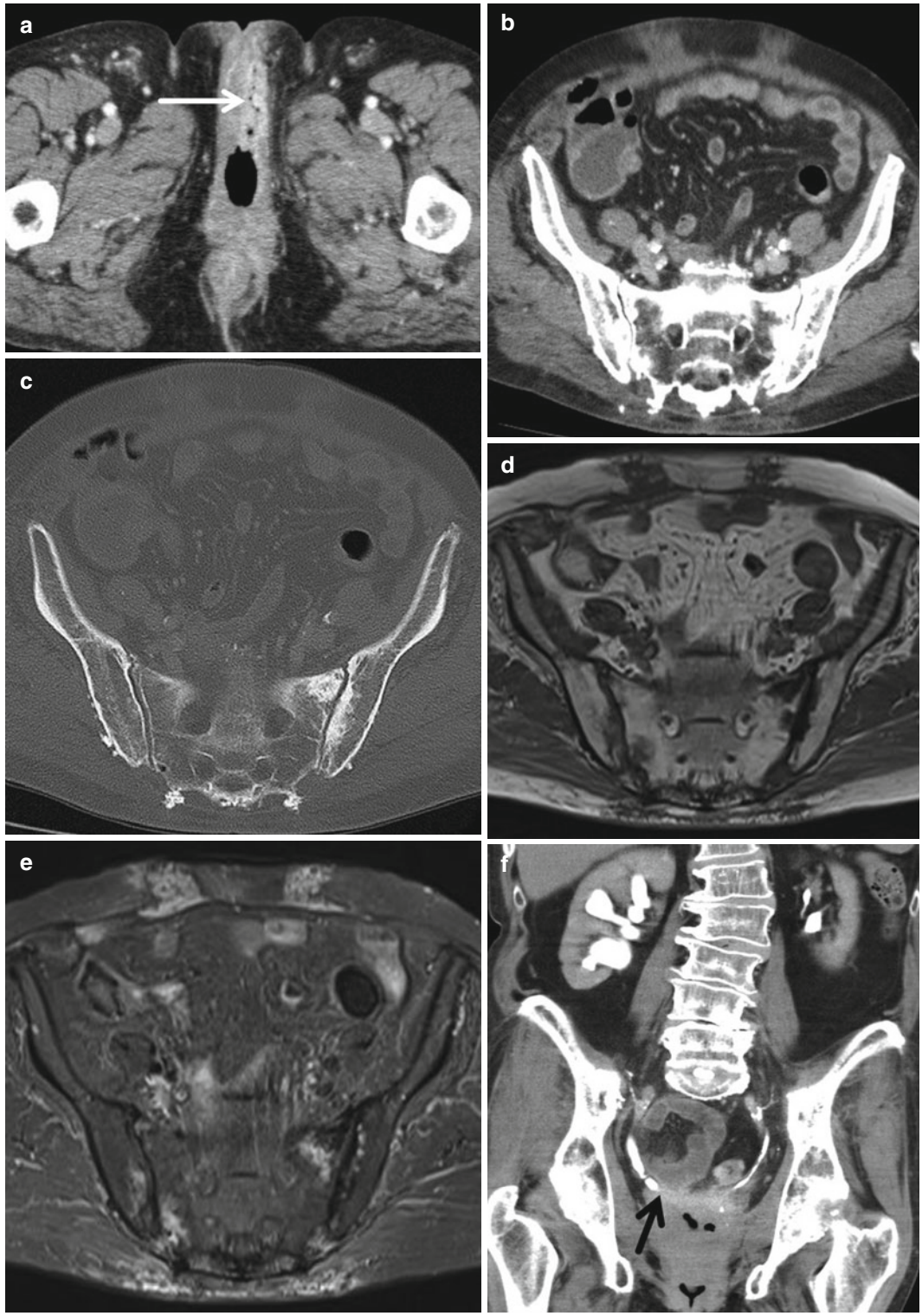

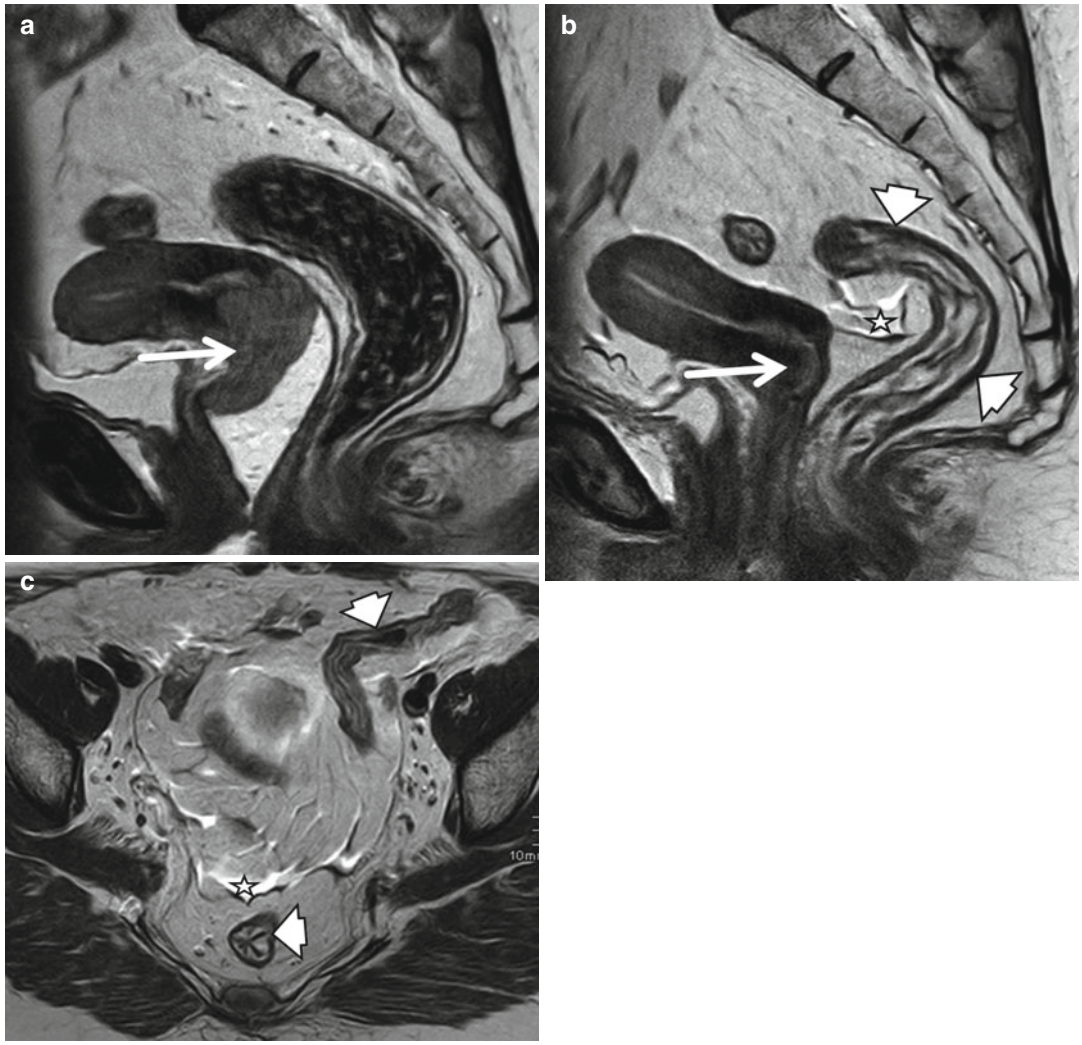


**Fig. 7** Immediate response following radiochemotherapy. Sagittal T2WI before (**a**) and sagittal (**b**) and transaxial T2WI MRI (**c**) at 3 months following treatment in a 54-year-old female with cervical cancer stage 2a (*arrow*). Reconstitution of the normal cervical signal (*arrow* in **b**) with some irregularities at the anterior cervix is visualized. Note the development of circular wall thickening of the rectum and sigmoid colon (*arrowheads*) and abundance of pelvic fat. Small pockets of ascites (*) can be identified as well as thickening of peritoneal fascias due to pelvic irradiation (**b**, **c**)

in cervical or vaginal stenosis (Brown et al. 2005). It also allows differentiation of fibrous adhesions after radiotherapy from residual or recurrent tumor (Brown et al. 2005; Schieda et al. 2014). MRI is also superior to CT to assess complications of uterine obstruction (Fig. 8), including hydrometrium, mucometrium, hematometrium, or pyometrium (Schieda et al. 2014). Vaginal atrophy, vaginal shortening of 1.5 cm, and vaginal stenosis present delayed complications (median of 9 months), particularly following combined external radiotherapy and brachytherapy (McConnell Greven and Paunesku 2005). Vaginal stenosis was identified in one study in 35 % of patients undergoing radiotherapy for cervical cancer in a 6-month follow-up (Brand et al. 2006).

#### 3.2.2.3 Uterus

Radiation injury results in endometrial damage, microvascular trauma, and fibrosis of the

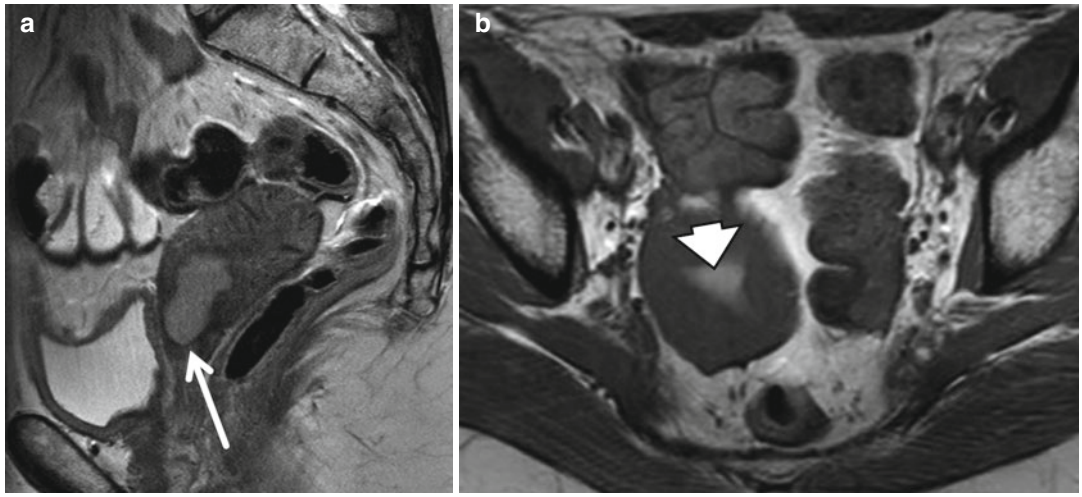


**Fig. 8** Mucometra due to cervical stenosis. In a 43-year-old female treated with radiochemotherapy for cervical cancer 5 years ago, distension of the uterine cavity and the endocervical canal to the level of the exocervix (*arrow*) is demonstrated on sagittal T2WI (**a**). Transaxial T1WI (**b**) shows high signal of the endometrial cavity (*arrowhead*) in the retroflexed uterus, indicating mucinous contents

myometrium (Kwek et al. 2006). Endometrial atrophy is found at about 6–8 weeks after intracavitary irradiation. Radiotherapy in fractionated doses has been reported to cause severe complications in less than 5 % of patients during a 5-year follow-up (McConnell Greven and Paunesku 2005). At imaging, irradiation of the postmenopausal uterus will not change uterine morphology. In contrast, the irradiated uterus of a premenopausal female resembles that of postmenopausal age. This includes indistinct junctional zone and outer myometrium and thinning and low SI of the endometrium and myometrium after 6 months following radiotherapy (Addley et al. 2010; Antunes and Cunha 2013) (Fig. 9).

Uterine perforation has been reported in 8 % of brachytherapy procedures. Imaging, particularly MRI, will render crucial anatomical information before this procedure including uterine retroflexion or cervical stenosis. Ultrasound guidance for device placement is recommended to avoid this complication (Small et al. 2011).

#### 3.2.2.4 Ovaries

Ovarian granulosa cells are more radiosensitive than oocytes and maturing follicles (Wo and Viswanathan 2009). Besides dose the patient age at the time of pelvic irradiation will determine the degree of ovarian injury. Women older than 40 years are under a high risk of permanent ovarian failure, even with low doses of irradiation. Late radiation injury comprises ovarian atrophy and fibrosis and thick-walled hyaline vessels (McConnell Greven and Paunesku 2005). In imaging, these ovaries in premenopausal women exhibit smaller volumes than normal ovaries and reduced number and size of follicles (Fig. 9), but cyclic changes of folliculogenesis may resume. Hydrosalpinx caused by tubal obstruction may be seen after hysterectomy and uterine radiation therapy, both in pre- and postmenopausal age (Hricak et al. 1993).

#### 3.2.2.5 Urologic Complications

Due to their vicinity, the bladder, urethra, and ureters are also affected in radiotherapy of uterine cancers. Among these, the bladder is the most radiosensitive, with radiation cystopathy reported in 3–12 % (Schieda et al. 2014). Acute radiation cystitis exhibits mucosal enhancement and in more severe cases uniform wall thickening with high SI on T2WI due to edema respectively inflammation (Hricak et al. 1993) (Fig. 7). It is usually found within the first 3–6 months after radiotherapy and is self-limiting (Sugimura et al. 1990; Iyer and Jhingran 2006; Addley et al.

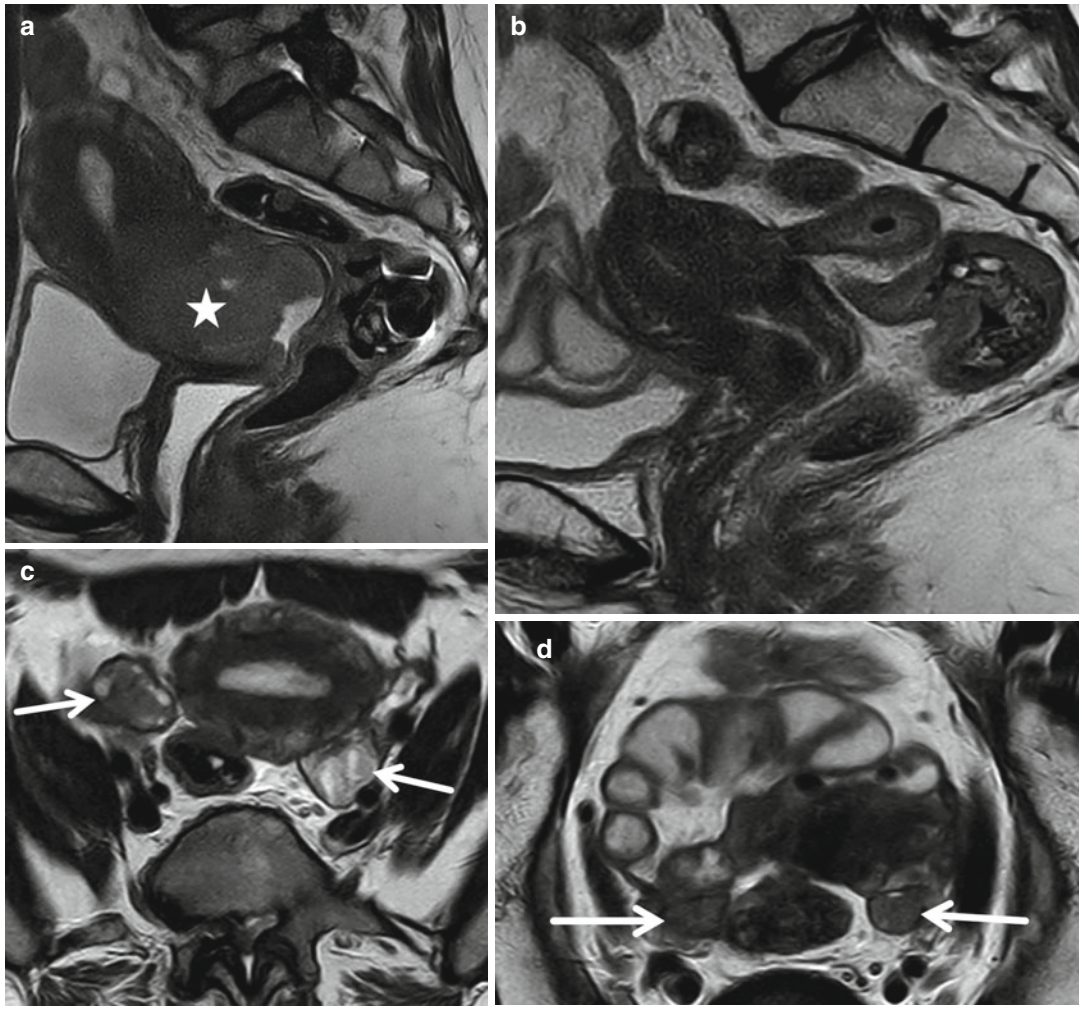


**Fig. 9** Radiotherapy-induced uterine and ovarian atrophy in premenopausal age. Sag T2WI of cervical cancer (*) stage 1b2 (**a**). No evidence of residual cervical tumor is seen in a 7-month follow-up (**b**). Transaxial oblique T2WI before radiotherapy demonstrates normal ovaries (*arrows* in **c**). Shrinkage of the ovaries (*arrows*) and reduction of number and size of follicles are noted after 7 months (**d**)

2010). Chronic changes include circumferential thickening exhibiting low SI on T2WI due to fibrosis, and rarely, a small fibrotic bladder may result. Ureteral strictures occur in only 1–3 % of patients treated with brachytherapy and external beam RT for pelvic malignancies. Typical imaging findings include hydronephrosis and involvement of the distal ureter with smooth tapering (Fig. 6). It may develop with a delay ranging between 6 months and 10 years following radiation therapy. MRI using DWI or PET/CT best assist in differentiation of central pelvic recurrence from radiotherapy-related ureteric strictures (Engin 2006).

#### 3.2.2.6 Radiotherapy Effects on Soft Tissues and Other Pelvic Structures

Edematous changes of pelvic fat and muscles within the radiation field peak at around 3 to 6 months after radiotherapy and then subside (McConnell Greven and Paunesku 2005; Blomlie et al. 1996). Widening of the presacral space, abundance and increased attenuation of perirectal

fat, and thickening of mesorectal fascia include typical findings related to pelvic irradiation (Capps et al. 1997) (Fig. 7). Chronic fibrotic changes including thickening of the pelvic sidewalls, pelvic fascia, and ligaments and tapering and strictures are seen later during radiation therapy (Capps et al. 1997). Concentric wall thickening and narrowing of the rectum and sigmoid colon present long-term sequelae after RT. Small amounts of ascites in the cul-de-sac or within peritoneal pockets are found in the acute and chronic phase after radiotherapy (Capps et al. 1997; Blomlie et al. 1996; Iyer and Jhingran 2006) (Fig. 7).

Fatty bone marrow conversion, typically sharply limited by the radiation field, begins as early as 2 weeks and is completed by approximately 8 weeks in 90 % of patients undergoing radiotherapy. These findings are permanent in adults, but seem reversible in children (Yankelevitz et al. 1991; Stevens et al. 1990). The spectrum of late bony abnormalities ranges from radiation-induced osteitis to patchy areas of lysis and sclerosis (Fig. 6) to insufficiency fractures and avascular necrosis, typically involving the sacral ala and pubic bones (Iyer and Jhingran 2006).

Chemotherapy-related osteoporosis and chronic use of corticosteroids also increase the risk of sacral insufficiency fractures. MRI is highly sensitive in the detection of these often occult insufficiency fractures. They are most commonly noted by one year after treatment. An incidence of 34 % of symptomatic women with insufficiency fractures was reported in endometrial cancer treated with adjuvant radiotherapy and surgery (Iyer and Jhingran 2006).

Other treatment-related side effects include myositis and synovitis (Kwek et al. 2006). Premature arteriosclerosis, aneurysm, stenosis, and arteritis may rarely arise as delayed complications caused by pelvic radiotherapy respectively chemotherapy related (Viswanathan et al. 2014).

Perioperative period, lymphoceles, anti-angiogenic targeted agents, and some classical chemotherapeutic agents, e.g., gemcitabine and cisplatin, are associated with increased risk of pelvic vein thrombosis (Torrisi et al. 2011). In patients presenting with peripheral edema, imaging will assist in differentiation of pelvic or retroperitoneal recurrence causing lymphatic obstruction from edema of the lower extremities as a side effect of some chemotherapy regimen (Torrisi et al. 2011).

## 3.3 Effects of Tamoxifen Treatment on the Female Genital Organs: Imaging Findings and Complications

Tamoxifen has been widely used as effective hormonal therapy in breast cancer. It is a selective estrogen receptor modulator binding with estrogen receptors in the breast (Conzen 2014). However, due to its additional antagonistic activity tamoxifen has an estrogen-like effect on the postmenopausal uterus. Up to 50 % of women using tamoxifen will develop endometrial abnormalities within 6–36 months. These comprise a spectrum of endometrial changes, including cystic atrophy, endometrial hyperplasia, and polyps. Additional findings are subendometrial cysts, adenomyosis, uterine leiomyomas, and small amounts of pelvic ascites (Ascher et al. 1996).

Postmenopausal women under tamoxifen therapy typically have endometrial widening of 9–13 mm and sonographically hyperechoic endometrium with multiple small cystic spaces (Conzen 2014). Tamoxifen increases the risk of endometrial polyps, both in pre-and in postmenopausal age (American College of Obstetricians and Gynecologists 2014). Their reported incidence ranges between 8 and 36 %; they tend to be larger (>5 cm) and are associated with a higher risk of malignancy compared to polyps in untreated women (Polin and Ascher 2008). Saline sonohysterography allows the differentiation of polyps from endometrial thickening. Ascher et al. described two different patterns on MRI under tamoxifen exposure. In patients with atrophy or proliferative changes, the T2WI SI of the endometrium was diffusely hyperintense. In patients with polyps, the endometrial signal was heterogeneous and a lattice-like pattern was seen in the endometrial

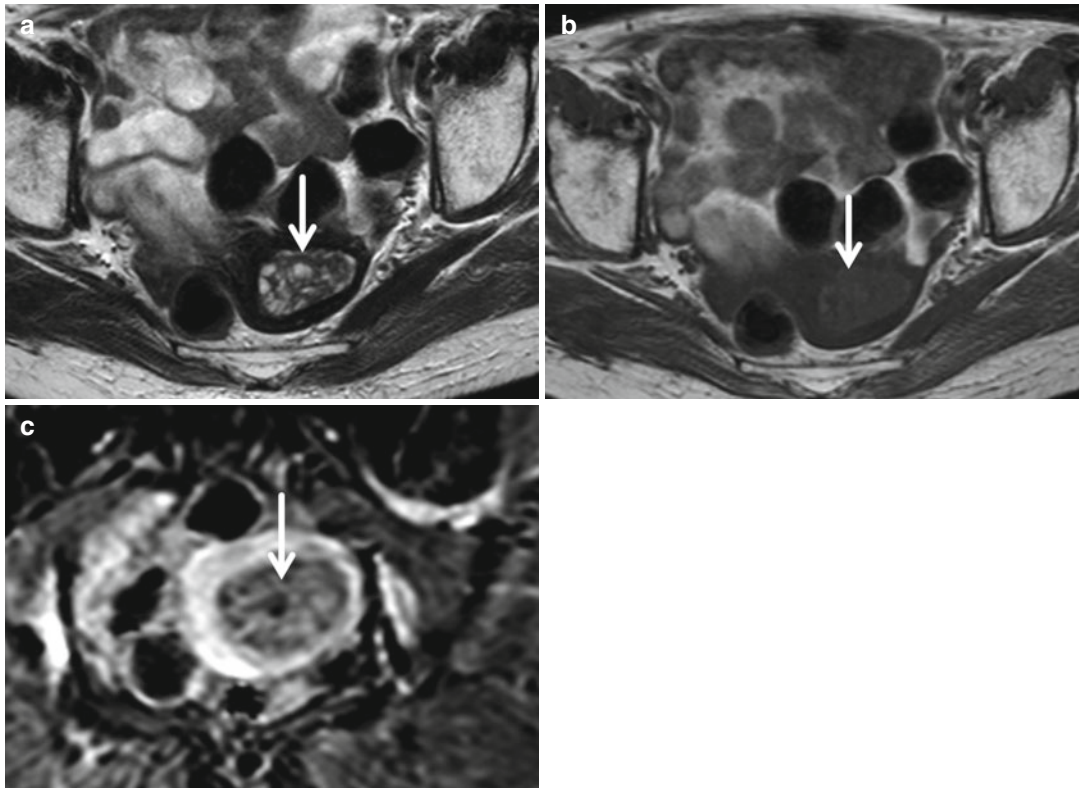


**Fig. 10** Typical polyp under tamoxifen treatment in postmenopausal age. Transaxial (**a**) T2WI demonstrates endometrial widening by a lesion with lattice-like morphology (*arrow*). It exhibits higher SI than myometrium on T1WI (**b**) and inhomogeneous morphology on T1WI and on T1FS with contrast (**c**)

cavity (Ascher et al. 1996) (Fig. 10). In the uterus, tamoxifen has also been associated with an increased risk (1.3–7.5x) of endometrial cancer and with a minimally increased rate of uterine sarcomas (Wysowski et al. 2002; Conzen 2014). In these patients endometrial cancer is almost exclusively found in ages 50 years or more and is related to the duration of treatment (Conzen 2014). Premenopausal women under tamoxifen therapy seem not at an increased risk to develop endometrial cancer (Conzen 2014). However, in premenopausal age, multiple ovarian cysts similar to ovarian hyperstimulation syndrome may be rarely seen (Maddedu et al. 2014) (Fig. 11).

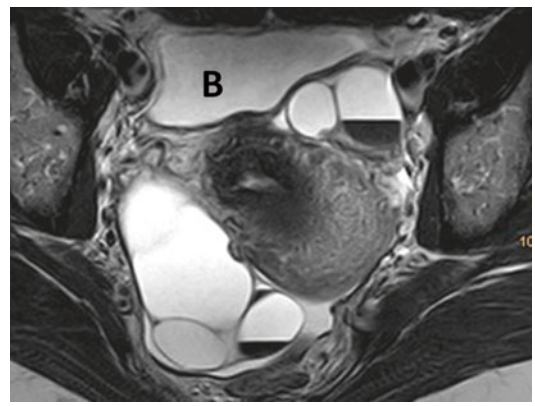


**Fig. 11** Tamoxifen effect on the ovaries in premenopausal age. Bilateral ovarian enlargement with multiple thin-walled hemorrhagic cysts is demonstrated on transaxial T2WI. Minimal ascites is seen in both ovarian fossas. Bladder (*B*)

## 3.4 Special Aspects in Females Treated for Gynecologic Cancers

### 3.4.1 Fistulas

Pelvic radiotherapy in general, pelvic surgery following radiotherapy, advanced tumor stage, high dose delivered to rectum and bladder, and biopsies include risk factors for fistula formation (Feddock et al. 2014). Fistulas may develop early during therapy or with a delay of up to three decades after pelvic irradiation (Addley et al 2010). Their incidence ranges from 1 to 4 % but can be as high as 22–48 % for advanced tumor stages (Feddock et al. 2014). In a retrospective study of 325 patients treated with external RT and brachytherapy, 8.2 % developed fistulas. 22 % resulted from primary disease, 25 % from recurrent disease, and more than 50 % of fistulas were toxicity related. In this study stage IV disease and postradiation biopsy were the most significant predictors of fistula formation (Feddock et al. 2014). Main types are rectovaginal or vesicovaginal fistulas. Cloaca formation has become rare with advances in radiotherapy. In CT a fistula may be diagnosed by indirect signs, e.g., presence of air and/or abnormal contrast media in the bladder or vagina. Rectal opacification and multiplanar delayed contrast-enhanced series may improve visualization of the fistula. MRI is the modality of choice for fistula assessment which exhibits central hyperintense SI and peripheral hypointense SI due to chronic inflammation and fibrosis (Golabebek et al. 2013; Semelka et al. 1997). Sagittal T2WI usually allows best visualization of the fistula and its communications (Fig. 12); alternatively contrast-enhanced 3D T1W series may also be helpful (Golabebek et al. 2013).

Differentiation of recurrent disease with fistula formation due to necrosis may be challenging. Serial follow- up and imaging findings in CT or MRI, such as the presence of a focal enhancing mass or low ADC on DWI and FDG avidity in PET/CT, are typical features of recurrence (Sala et al. 2010; Meads et al. 2014).

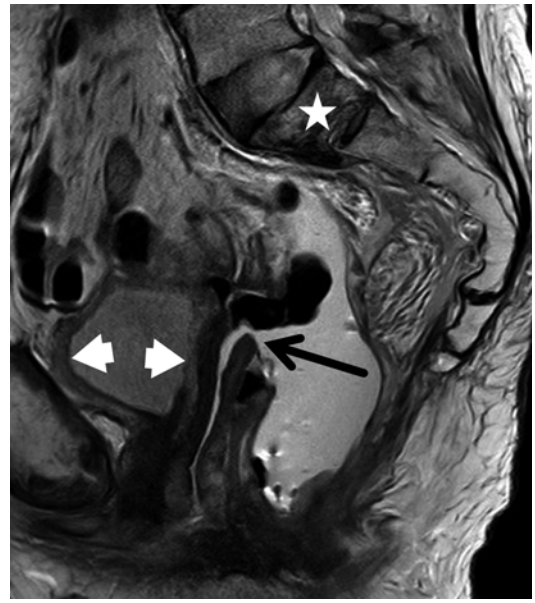

**Fig. 12** Rectovaginal fistula. Rectal gel opacification facilitates visualization of the fistula (*arrow*) between the vaginal vault and rectum on sagittal T2WI. Circumferential bladder wall thickening (*arrowheads*), edema, and abundance of presacral fat and sacral fracture (*) present other sequelae of pelvic irradiation 2 years before

### 3.4.2 Secondary Malignancies Related to Pelvic Irradiation

Radiation exposure is linked to an increased incidence (3–5 %) of secondary neoplasm. Typical feature is the long latency of 10 years or more after irradiation and a histology differing from the treated cancer (Fig. 6). The risk is strongly associated with the dose delivered, the area of radiation and age, with highest risk for secondary cancers of the genital organs in ages younger than 60 years (Onsrud et al. 2013). Radiation-induced sarcomas in the pelvis are extremely rare but also share some common features. Histologically, they encompass aggressive histologies and poorer prognoses than usual soft tissue sarcomas (Lagrange et al. 2000). In a multi-institutional study analyzing 80 patients with sarcoma after radiotherapy, 12 patients had previous treatment for uterine and ovarian cancer.

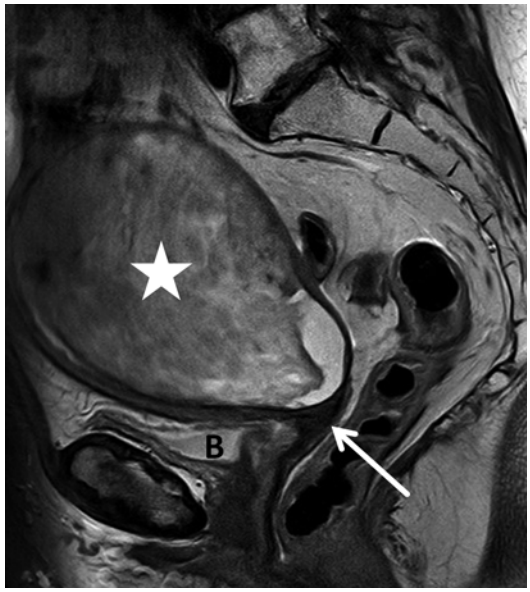


**Fig. 13** Radiotherapy-associated uterine carcinosarcoma. 12 years after radiotherapy of cervical cancer, the uterus is enlarged and exhibits an inhomogeneous mass (*) arising from the endometrial cavity. Postirradiation the cervix is small and displays a normal low-intensity signal (*arrow*). Bladder (*B*)

In accordance with other irradiated sites, malignant fibrous histiocytoma (MFH) (5), now classified as pleomorphic undifferentiated sarcoma, was the most common tumor type. Other histologies included malignant schwannoma (2), sarcoma with fusiform cells (2), leiomyosarcoma (1), fibrosarcoma (1), and osteosarcoma (1) (Lagrange et al. 2000).

Among uterine cancers carcinosarcoma is estimated to be radiation induced in 5–30 % of cases (Kanthan and Senger 2011) (Fig. 13). In one series 13 out of 114 uterine sarcomas were linked to radiotherapy and had a latency period of 11–30 (median 17) years (Mark et al. 1996).

### 3.4.3 Impact of Cancer Treatment on Female Reproduction

Fertility and ovarian dysfunction have become an important clinical issue in long-term survivors of cancers in childhood and in cancer patients in fertile age (Loren et al 2013). Adverse effects on the female reproductive organs occur in all ages in women undergoing cancer treatment, but degree and persistence of damage depend predominantly on patient age and on duration and the type of treatment (Meirow and Nugent 2001). Radiation injury to the uterus in young age leads to reduced uterine volume and impaired blood flow, resulting in infertility, high risk of early pregnancy loss, and premature labor (Critchley et al. 1992). Children are less sensitive to radiation-induced ovarian toxicity as compared to more advanced age, owing to their larger ovarian follicular reserve (Meirow and Nugent 2001). However, premature ovarian failure, defined as amenorrhea in women <40 years of age, is a treatment-related side effect of childhood cancer. Estimated dose for radiation-induced permanent ovarian damage is 20 Gy in women <40years and only 6 Gy in older age (Meirow and Nugent 2001).

The effects of chemotherapy on ovarian function are not yet fully understood. Furthermore, different chemotherapy drugs act through a spectrum of mechanism and effect different ovarian cell types (Torrisi et al. 2011). Chemotherapy may affect ovarian function immediately or delayed. The classical immediate chemotherapy-induced effect is amenorrhea that may become permanent (Morgan et al. 2012). In contrast to radiotherapy-related injury, advanced age is the central risk factor for ovarian failure during or immediately after chemotherapy. Chemotherapy agents may be classified according to their gonadotoxic effect into different risk groups (Wo et al. 2009). High-risk substances are alkylating agents, e.g., cyclophosphamide, busulfan, melphalan, etc. Cisplatin is estimated as intermediate risk, and other agents, e.g., adriamycin, 5-fluorouracil, vincristin, and methotrexate, are associated with a low risk of ovarian failure (Wo et al. 2009; Morgan et al. 2012).

**Conclusion**

Treatment options in cancer of the female reproductive system include surgery, radiotherapy, and chemotherapy or depending on tumor type and stage their combination.

In the female pelvis, treatment-related side effects most commonly occur in the first weeks after surgery and within the first months of radiotherapy. In this period, imaging plays

also a central role in the assessment of treatment response and in visualization of early radiotherapy-associated complications, particularly affecting bowel and pelvic soft tissues. However, due to the ever-increasing rate of cancer survivors, treatment-related side effects and complications have to be taken in consideration in the spectrum of differential diagnosis. Some of these, e.g., hydronephrosis due to distal ureteral stenosis or fistulae to vagina and bladder, and irradiation-associated secondary cancers, may occur with a latency of several years to decades after treatment. Impaired fertility and ovarian dysfunction have become an important issue in patients treated for pelvic cancers in childhood and in fertile age. In combination with appropriate clinical information, imaging, including correlation with previous findings and integration of functional imaging techniques, will allow for differentiation between therapy-induced complications and tumor recurrence in the majority of cases. Thus, radiology plays a central role in the multidisciplinary management of these patients.

## References


Addley HC, Vargas HA, Moyle PL, Crawford R, Sala E (2010) Pelvic imaging following chemotherapy and radiation therapy for gynecologic malignancies. Radiographics 3:1843–1856

American College of Obstetricians and Gynecologists (2014) Committee opinion. Number 601

Antunes D, Cunha TM (2013) Recurrent cervical cancer: how can radiology be helpful. OMICS J Radiol 2013(2):138. doi:10.4172/2167-7964 1000138

Ascher S, Johnson JC, Barnes WA, Bae CJ et al (1996) MR imaging appearance of the uterus in postmenopausal women receiving tamoxifen therapy for breast cancer: histopathologic correlation. Radiology 200: 105–110

Blomlie V, Rofstad EK, Tvera K, Lien HH (1996) Noncritical soft tissues of the female pelvis: serial MR Imaging before, during, and after radiation therapy. Radiology 199:461–468

Bluemke DA, Fishman EK, Kuhlman JE, Zunreich ES (1991) Complications of radiation therapy: CT evaluation. Radiographics 11:581–600

Boran N, Cil AP, Tulunay G et al (2004) Chylous ascites following para-aortic lymphadenectomy: a case report. Gynecol Oncol 93:711–714

Brand AH, Bull CA, Cakir B (2006) Vaginal stenosis in patients treated with radiotherapy for carcinoma of the cervix. Int J Gynecol Cancer 16:288–293

Brown MA, Mattrey R, Stamato S, Sirlin CB (2005) MRI of the female pelvis using vaginal gel. Am J Roentgenol 185:1221–1227 www.cancer.gov/cancertopics/…/treatment

Capps GW, Fulcher AS, Szucs RA, Turner MA (1997) Imaging features of radiation induced changes in the abdomen. Radiographics 17:1455–1473

Conzen SD (2014) Managing the side effects of tamoxiphen. www.update.com 2014

Critchley H, Wallace W, Shalet SM et al (1992) Abdominal irradiation in childhood: the potential for pregnancy. Br J Obstet Gynecol 99:392–394

Engin G (2006) Cervical cancer: MR imaging findings before, during and after radiation therapy. Eur Radiol 16:313–324

ESMO clinical practice guidelines. Gynecologic cancers www.esmo.org/Guidelines/Gynaecological-Cancers

Feddock J, Randall M, Kudrimoti M et al (2014) Impact of post-radiation biopsies on development of fistulae in patients with cervical cancer. Gynecol Oncol 133:263–267

Flueckinger F, Ebner F, Poschauko H et al (1992) Cervical cancer before and after primary radiation therapy – a 2 year follow-up study. Radiology 184:89–93

Golabebek T, Szymanska A, Szopinski T, et al. (2013) Enterovesical fistula: aetiology, imaging, and management. Gastroenterol Res Pract 2013(617967):8 www.hindawi.com/journals/grp/2013/617967

Harry VN, Semple SI, Gilbert FJ, Parkin DE (2008) Diffusion weighted MRI in the early detection of response to chemoradiation in cervical cancer. Gynecol Oncol 111:213–220

Hassouna A, Bahadur YA, Constantinescu C (2014) Assessment of air pockets in high-dose rate vaginal cuff brachytherapy using cylindrical applicators. J Contemp Brachytherapy 6:271–275

Hricak H, Swift PS, Campos Z et al (1993) Irradiation of the cervix uteri: value of unenhanced and contrast-enhanced MR imaging. Radiology 189:381–388

Irtan S, Orbach D, Helfre S, Sarnacki S (2014) Ovarian transposition in prepubescent and adolescent girls with cancer. Lancet Oncol 14:601–608

Iyer R, Jhingran A (2006) Radiation injury: imaging findings in the chest, abdomen and pelvis after therapeutic radiation. Cancer Imaging 6:S131–S139

Jeraj R, Cao J, Ten Haken RK, Hahn C, Marks L (2010) Imaging for assessment of radiation-induced normal tissue effects. Int J Radiat Oncol Biol Phys 76(3 Suppl):S140–S144

Jereczek-Fossa BA, Jassem J, Badzio A (2002) Relationship between acute and late normal tissue injury after postoperative radiotherapy in endometrial cancer. Int J Radiat Oncol Biol Phys 52:476–482

Kanthan R, Senger JL (2011) Uterine carcinosarcomas (malignant mixed Müllerian tumours): a review with special emphasis on controversies in management. Obstetr Gynecol Int. Article ID:470795

Kwek JW, Iyer RB, Dunnington J, Faria S, Silverman PM (2006) Spectrum of imaging findings in the abdomen after radiotherapy. AJR Am J Roentgenol 187: 1204–1211

Lagrange JL, Ramaioli A, Chateau MC et al (2000) Sarcoma after radiation therapy: retrospective multiinstitutional study of 80 histologically confirmed cases. Radiology 216:197–205

Loren AW, Mangu PB, Beck LN et al (2013) Fertility preservation for patients with cancer: American society of clinical oncology clinical practice guideline update. J Clin Oncol 31:2500–2510

Maddedu C, Gramignano G, Kotsonis P et al (2014) Ovarian hyperstimulation in premenopausal women during adjuvant tamoxifen treatment for endocrine-dependent breast cancer. Oncol Lett 8:1279–1282

Mark RJ, Poen J, Tran LM et al (1996) Postirradiation sarcoma of the gynecologic tract. A report of 13 cases and a discussion of the risk of radiation-induced gynecologic malignancies. Am J Clin Oncol 19: 59–64

Maturen KE, Feng MU, Wasnik AP et al (2013) Imaging effects of radiation therapy in the abdomen and pelvis: evaluating "innocent bystanders" tissues. Radiographics 33:599–619

Mayr NA, Yuh WTC, Magnotta VA et al (1996) Tumor perfusion studies using fast magnetic resonance imaging technique in advanced cervical cancer: a new non invasive predictive assay. Int J Radiat Oncol 36:623–633

McConnell Greven K, Paunesku T (2005) Radiation complications of the pelvis. In: Small W Jr, Woloschak G (eds) Radiation toxicity: a practical guide. Chapter 6. Springer, pp 125–153. ISBN: 978-1-4020-8053-1 (Print) 978-0-387-25354-1 (Online)

Meads C, Davenport C, Malysiak S et al (2014) Evaluating PET-CT in the detection and management of recurrent cervical cancer: systematic reviews of the diagnostic accuracy and subjective elicitation. BJOG 121:398–407

Meirow D, Nugent D (2001) The effects of radiotherapy and chemotherapy on female reproduction. Hum Reprod Update 7:535–543

Morgan S, Anderson RA, Gourley C et al (2012) How do chemotherapeutic agents damage the ovary. Hum Reprod Update 18:525–535

Morice P, Juncker L, Rey A et al (2000) Ovarian transposition for patients with cervical carcinoma treated by radiosurgical combination. Fertil Steril 74:743–748

Onsrud M, Cvancarova M, Hellebust TB et al (2013) Long- term outcomes after pelvic radiation for early-stage endometrial cancer. J Clin Oncol 31:3951–3965

Ostrzenski A, Radolinski B, Ostrzenska KM (2003) A review of laparoscopic ureteral injury in pelvic surgery. Obstet Gynecol Surv 58:794–799

Paspulati RM, Dalal TA (2010) Imaging of complications following gynecologic surgery. Radiographics 2010(30): 625–642

Polin SA, Ascher SM (2008) The effect of tamoxifen on the genital tract. Cancer Imaging 8:135–145

Raja FA, Chopra N, Ledermann JA (2012) Optimal first-line treatment in ovarian cancer. Ann Oncol 23(Suppl 10):x118–x127

Sala E, Rockall A, Rangarajan D, Kubick–Huch RA (2010) The role of dynamic contrast-enhanced and diffusion-weighted magnetic resonance imaging in the female pelvis. Eur J Radiol 76:367–385

Schieda N, Malone SC, Al Danadan O et al (2014) Multimodality organ-based approach to expected imaging findings, complications and recurrent tumour in the genitourinary tract after radiotherapy. Insights Imaging 5:25–40

Sella T, Mironov S, Hricak H (2005) Imaging of transposed ovaries in patients with cervical carcinoma. AJR Am J Roentgenol 184:1602–1610

Semelka RC, Hricak H, Kim B et al (1997) Pelvic fistulas: appearance on MR images. Abdom Imaging 22:91–95, 1997

Small W Jr, Strauss JB, Hwang CS, Cohen L, Lurain J (2011) Should uterine tandem applicators ever be placed without ultrasound guidance? No: a brief report and review of the literature. Int J Gynecol Cancer 21:941–944

Stevens SK, Moore SG, Kaplan ID (1990) Early and late bone marrow changes after irradiation: MR evaluation. AJR Am J Roentgenol 154:745–750

Sugimura K, Carrington BM, Quivey JM, Hricak H (1990) Postirradiation changes in the pelvis. Assessment with MRI. Radiology 175:805–813

Tam KF, Lam KW, Chan K, Ngan HY (2008) Natural history of pelvic lymphocytes observed by ultrasound after bilateral lymphadenectomy. Ultrasound Obstet Gynecol 32:87–90

Torrisi JM, Schwartz LH, Gollub MJ et al (2011) CT findings of chemotherapy-induced toxicity: what the radiologist need to know about the clinical and radiologic manifestations of chemotherapy toxicity. Radiology 258:41–56

Viswanathan C, Truong MT, Sagebiel TL, Bronstein J et al (2014) Abdominal and pelvic complications of non-operative oncologic therapy. Radiographics 34:941–961

Weiss E, Hirnle P, Arnold Bofinger H, Hess CF, Bamberg M (1999) Therapeutic outcome and relation of acute and late side effects in the adjuvant radiotherapy of endometrial carcinoma stage I and II. Radiother Oncol 53:37–44

West CM, Barnett GC (2011) Genetics and genomics of radiotherapy toxicity: towards prediction. Genome Med 3:52

Wo JY, Viswanathan AN (2009) Impact of radiotherapy on fertility, pregnancy, and neonatal outcomes in female cancer patients. Int J Radiat Biol Phys 73:1304–1312

Wysowski DK, Honig SF, Beits J (2002) Uterine sarcoma associated with tamoxifen use. N Engl J Med 346:1832–1833

Yankelevitz DF, Henschke KI, Knapp PH, Nisce L et al (1991) Effect of radiation therapy on thoracic and lumbar bone marrow: evaluation with MR imaging. AJR Am J Roentgenol 1991(157):87–92

# Part VIII

# Bone Marrow and Spine

# Radiotherapy Induced Changes in Spine and Spinal Contents

Joana Ramalho and Mauricio Castillo

## Contents




**Abstract**

Radiotherapy is a well-established therapeutic modality in oncology that results in survival benefits in several different cancer types, including breast, prostate, rectum, brain, lung, and head and neck cancers. It is generally used to control or eliminate malignant cells as a definitive treatment or a part of adjuvant therapy and to prevent tumor recurrence after surgery. It may also be used as palliative treatment for local disease control or symptomatic pain relief.

Side effects from radiation are usually limited to the area confined to the treatment field, and most of them are predictable and expected. The main effects on the bone include bone marrow fatty conversion, disruption of normal growth and bone maturation, scoliosis, osteonecrosis, insufficiency fractures, and secondary neoplasm formation. To evaluate radiation-induced effects on the bone marrow, it is essential to understand the normal composition and distribution of bone marrow and the normal age-related pattern of bone marrow maturation. Magnetic resonance imaging (MRI) is the only imaging technique that allows direct visualization of bone marrow with high spatial resolution.

In this chapter, the bone marrow composition and distribution will be covered, routine MRI sequences for bone marrow evaluation will be explained, and the radiation-induced changes and radiation-induced complications will be discussed.



J. Ramalho, MD (✉) • M. Castillo, MD, FACR
Division of Neuroradiology,
University of North Carolina,
Chapel Hill, NC 27599, USA
e-mail: joana-ramahlo@netcabo.pt;
mauricio_castillo@med.unc.edu


Med Radiol Diagn Imaging (2014)
DOI 10.1007/174_2014_1039, © Springer International Publishing Switzerland

## 1 Introduction

The exact mechanism of cell death due to radiation is still an area of investigation. Evidence supports double-stranded breaks of nuclear DNA as the most important cellular effect of radiation. This breakage leads to irreversible loss of the reproductive integrity of the cell, apoptosis, and eventual cell death.

Radiation effects are caused by one of two types of energy, photon or charged particles. In photon therapy or standard X-ray radiation therapy, most of the radiation effects result from indirect ionization of water forming free radicals, particularly hydroxyl radicals that then damage the DNA. Charged particles, such as protons and boron, carbon, and neon ions, cause direct damage to DNA through direct energy transfer resulting in double-stranded breaks. Opposite to standard X-ray radiation, protons and other charged particles have relatively large mass and little lateral side scatter into tissue and thus focused on the tumor.

Radiation can also affect the processes of the cell cycle necessary for growth, senescence, and apoptosis. Many of these processes are only now beginning to be elucidated and manipulated in order to make radiation therapy more effective.

There are two main reasons for spinal exposure to radiation: (1) an intentional delivery to treat primary or secondary bone lesions or (2) its inevitable inclusion into a radiation field which intends to treat an adjacent neoplasm. In either case, the nature, severity, and longevity of side effects depend mainly on patient age; treatment characteristics including type of radiation, dose, fractionation, and concurrent chemotherapy; and existence of trauma or infection in the irradiated bone.

The quantitative assessment of a particular bone marrow cell type is only possible with histopathological examination; however, MRI can determine the relative proportion of active and non-active cellular components, which makes it the imaging method of choice to evaluate postradiation changes in the bone marrow.

## 2 Bone Marrow Composition and Distribution

Bone marrow can be basically dived into three components: red marrow, yellow marrow, and supporting structures such as trabecular bone and fibrous tissue reticulum, perfused by a rich sinusoidal network of capillaries.

The terms red and yellow marrow come from the macroscopic bone marrow appearance: red marrow is more cellular containing the hematopoietic stem cells and blood cells progenitors, while yellow marrow contains more fat and is less cellular.

Red and yellow marrows are not homogenous tissues; their contents and distribution change substantially with age and homeostatic requirements and also differ by gender.

The red marrow (hematopoietic marrow) composition is approximately 40–60 % lipids, 30–40 % water, and 10–20 % proteins. In young children, red marrow is approximately 40 % water, 40 % fat, and 20 % proteins, while by 70 years of age, that proportion has changed to 60 % fat and 10 % proteins. Red marrow consists of 60 % hematopoietic cells and 40 % adipocytes in the young but only about 30 % hematopoietic cells in the elderly (Poe 2010; Burdiles and Babyn 2009; Hwang and Panicek 2007; Steiner et al. 1993; Snyder et al. 1975). In contrast, yellow marrow (fatty marrow) is nearly entirely composed of adipocytes (95 %) and its chemical composition is 80 % fat, 15 % water, and 5 % proteins (Hwang and Panicek 2007; Steiner et al. 1993; Snyder et al. 1975). These differences are important to understand the normal and abnormal appearance of marrow on different MR sequences.

At birth, the majority of the bone marrow is hematopoietically active (red marrow). Soon thereafter, it undergoes a predictable pattern of conversion to yellow marrow. The transition occurs over two decades, beginning in the appendicular skeleton and extending in a symmetric and centripetal manner into the central skeleton. In the late third decade of life, the bone marrow distribution achieves its mature state with red marrow throughout the axial skeleton, including skull, spine, sternum, clavicles, scapulae, pelvis, and in the humeral and femoral proximal metaphyses.

Normal bone marrow conversion is rarely uniform, and there is great variability among patients and some differences in the patterns seen in the cervical, thoracic, and lumbar segments. Ricci et al. described four patterns of spine marrow conversion: (1) central fat along the upper and lower margins of the basivertebral veins that begins in younger patients and may persist for many years; (2) band-like and triangular-like foci of fat along the vertebral endplates and vertebral body corners that is usually associated with adjacent disk degeneration; (3) tiny foci of scattered red and yellow marrow, known as speckled pattern; and (4) large round areas of yellow marrow and poorly defined areas of red marrow. Except for the transition from the infantile homogenous red marrow to pattern 1, the patterns do not progress in a predictable or clinically useful fashion (Poe 2010; Ricci et al. 1990).

Under specific conditions, red marrow proliferation or hyperplasia occurs in areas where yellow marrow had become the dominant component, a process known as reconversion. Reconversion follows the reverse order of marrow conversion, in an overall centripetal fashion, from the axial to the appendicular skeleton.

## 3 Magnetic Resonance Imaging of the Bone Marrow

The MRI appearance of the bone marrow is determined by the amount of protein, water, fat, and cells and depends on the MR pulse sequences used.

Routine MRI sequences include T1-weighted spin-echo (SE) images, T2-weighted SE or fast spin-echo images (FSE), fat saturation T2-weighted or STIR (short tau inversion recovery) images, and post-contrast T1-weighted images (Fig. 1).

On T1-WI (T1-weighted images), yellow marrow has high signal intensity, similar to the signal of the subcutaneous fat, while red marrow has intermediate signal, lower than subcutaneous fat but higher than disk or muscle. However, the exact signal is dependent of the proportion of red and yellow marrow.

Bone trabeculae decrease signal intensity in the vertebral body by creating local field inhomogeneities and may contribute to the high T1-WI bone marrow signal seen in elderly women. These are generally thin trabeculae due to osteoporosis (Poe 2010).

On T2-WI yellow marrow shows intermediate and high signal intensity on SE and FSE sequences, respectively. Fatty marrow has higher signal than muscle and equal or slightly lower than subcutaneous fat. Because water and fat are closer in signal intensity, there is decreased contrast on T2 sequences. Red marrow has a slightly lower signal than yellow marrow.

Bone marrow contrast can be accentuated by using fat-suppressed sequences, either chemically selective fat saturation technique (fat-sat T2-WI) or inversion recovery fat saturation technique (STIR).

On fat-sat T2-WI, a selective radiofrequency saturation pulse and dephasing gradient is applied based on the 210-Hz chemical shift which suppresses the lipid signal but only minimally affects the signal from non-lipid tissues such as water. This narrow saturation band usually provides higher signal-to-noise ratio than STIR sequences but requires a very homogenous magnetic field. To achieve reliable fat saturation, the frequency-selective saturation pulse must be equal to the resonance frequency of lipid. Inhomogeneities of the magnetic field will shift the resonance frequencies of both water and lipid; this discrepancy results in poor fat suppression or, even worse, in saturation of the water signal instead of the lipid signal. Additionally, substantial inhomogeneities can be caused by local magnetic susceptibility differences such as those found on air-bone interfaces or around orthopedic implants (Daldrup-Link et al. 2007).

On STIR sequence, the optimal inversion time is the point in which no signal is generated by fat, which results in suppression of the fat signal with preservation of water signal. This sequence is insensitive to magnetic field inhomogeneities and tends to produce a more homogenous fat suppression with high tissue contrast; however, it has limited signal-to-noise ratio. Another limitation is that the signal from tissue or fluid with a T1 signal similar to that of fat will be suppressed (e.g., hemorrhage or gadolinium) limiting its applications after contrast administration (Shah and Hanrahan 2011; Daldrup-Link et al. 2007). On either fat saturation T2-W sequences, the fatty marrow shows signal intensity lower than

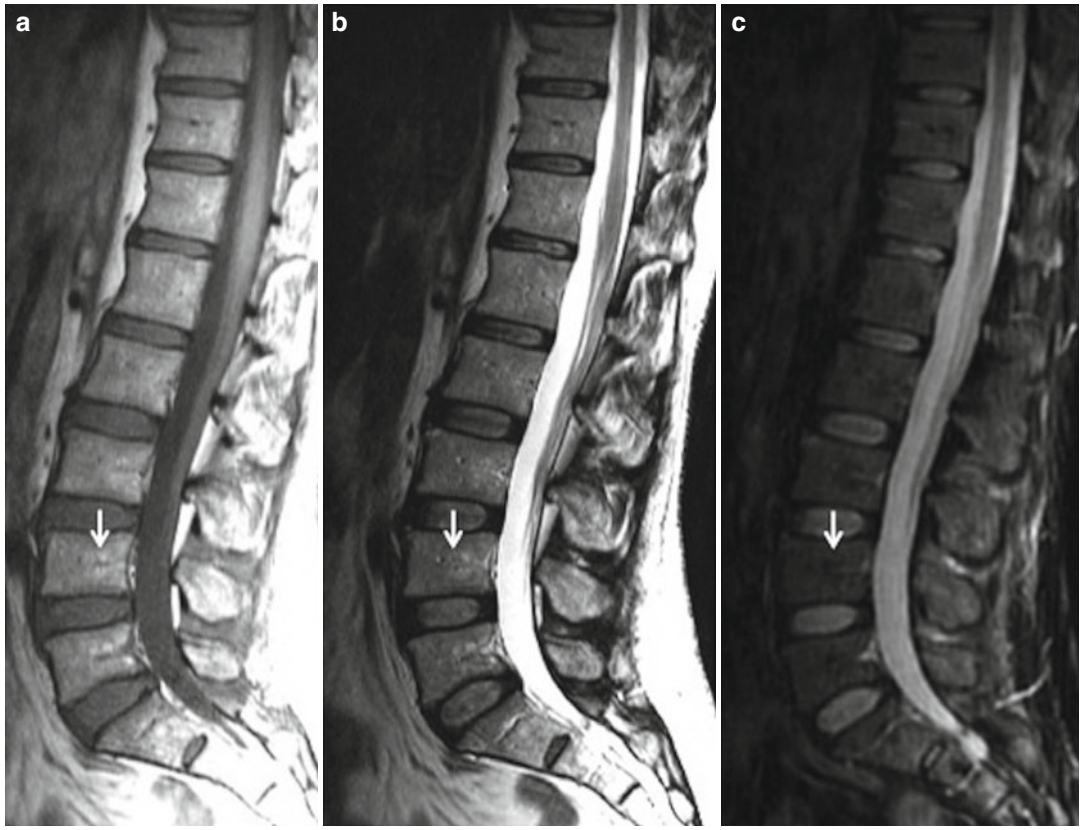


**Fig. 1** MRI of normal bone marrow. Midline sagittal T1-WI (**a**), T2-WI (**b**), and STIR (**c**) images show the normal appearance of the bone marrow in a young adult. On T1- and T2-WI, yellow marrow is seen as areas of high signal intensity. Note the typical speckled pattern seen as tiny foci of yellow marrow scattered in the vertebral body as well as the central fat along the upper and lower margins of the basivertebral veins (*arrows*). On STIR image (**c**), these fatty areas are suppressed and show low signal intensity

muscle whereas hematopoietic marrow shows intermediate signal similar to that of muscle (Shah and Hanrahan 2011).

Gadolinium-enhanced T1-WI may be helpful in detecting marrow lesions. However, bone marrow-enhancing lesions may be difficult to distinguish if they become isointense to normal bone marrow. Fat saturation T1-WI that suppresses the signal of normal fat allows better identification of enhancing lesions (Shah and Hanrahan 2011).

Bone marrow enhancement decreases markedly with increasing age and conversion to fatty marrow. Although there is significant variability among subjects (Shah and Hanrahan 2011; Montazel et al. 2003), adult normal bone marrow does not significantly enhance after contrast administration, while neonate and young child normal marrow substantially enhances (Poe 2010).

Several non-routine MRI sequences may be used to obtain additional information about spinal bone marrow including diffusion-weighted imaging (DWI), in- and out-of-phase MRI, MR spectroscopy (MRS), and dynamic contrast-enhanced MRI (DCE-MRI).

The utility of DWI on differentiating benign from metastatic spinal lesions is controversial. However, it may be helpful in treatment follow-up, by evaluating the progressive changes in bone marrow, tending to show decreased signal in successful treatment compared with increased signal associated with tumor progression or recurrence.

Chemical shift or in- and out-of-phase imaging takes advantage of the difference in resonance frequencies between fat and water protons, which are abundant in the bone marrow. Water and fat protons are in phase with one another at a TE of

4.6 ms and are 180° opposed at a TE of 2.4 ms at 1.5 T. When a given voxel contains both fat and water, there will be some signal loss on images that are obtained when the protons are in their opposed phase. Since normal red marrow has both water-based elements (cells) and some degree of fat, hematopoietic marrow will show signal loss when comparing out-of-phase to in-phase images. Radiation therapy may alter the expected bone marrow signal loss in the opposed-phase images (Shah and Hanrahan 2011).

In spine spectroscopy, the global MR signal from the bone is divided into the two major peaks separated by 3.1 ppm: water and lipids. The water peak is originating mostly from red marrow, while the lipid peak arises mainly from yellow marrow (Shah and Hanrahan 2011). MRS has been used to illustrate the increase bone marrow fat content with age (Shah and Hanrahan 2011; Chellinger et al. 2000).

DCE-MRI has also been used to characterize bone marrow. It has shown higher perfusion in hematopoietic marrow compared with yellow marrow because red marrow contains numerous fenestrated vessels, large vascular pools and channels, and small amounts of poorly vascularized fat (Shah and Hanrahan 2011).

All these methods have been used to measure the fat content or the water/fat fractions; however, these techniques need further clinical validation and have so far not been used for routine imaging.

New macromolecular contrast media (MMCM) may provide more specific information on bone marrow blood volume and permeability. Small molecular Gd chelates can only estimate the blood volume (immediate post-contrast scans) and extracellular space (later post-contrast scans) of the normal or abnormal bone marrow because these small molecules permeate readily and nonselectively across normal and abnormal capillaries in the bone marrow. These new macromolecular contrast agents are so large so that their diffusion across microvessels is affected by their permeability. This may be helpful for the treatment monitoring of antiangiogenic drugs which specifically and readily decrease microvascular permeability, but which have no immediate effect on the blood volume. At this time, none of the MMCMs are FDA approved (Daldrup-Link et al. 2007).

Another class of contrast agents that may be useful in bone marrow imaging is ultrasmall superparamagnetic iron oxide particles (USPIO). These particulate iron oxide contrast agents are phagocytized by macrophages in normal bone marrow where they induce a T2-shortening effect (Daldrup-Link et al. 2007).

Combined PET and MR imaging, either by retrospective spatial registration of individual data from PET and MR images or by simultaneous data acquisition on combined PET-MR systems, may also be useful for the evaluation of the bone marrow (Somer et al. 2003; Pichler et al. 2006). PET-MR imaging has been described as superior, at least for some applications, compared to PET- CT because of its improved intrinsic soft tissue contrast and potential direct bone marrow depiction (Daldrup-Link et al. 2007).

## 4 Radiation-Induced Changes on Normal Bone Marrow

For many decades, radiation therapy has been established as a treatment method for primary or secondary bone tumors as well as for abdominal and pelvic tumors.

The effects of radiation on bone marrow have been well described by histological and gross anatomic studies. These studies have shown that irradiated bone marrow becomes hypocellular with destruction of the sinusoidal vasculature followed by fatty marrow replacement of the normal hematopoietic marrow.

Irradiated bone marrow undergoes characteristic time-dependent changes. In the acute phase (1–3 days), the bone marrow develops edema, which appears hypointense on T1-WI and hyperintense on fat-sat T2-W and STIR images. Contrast-enhanced T1-WI may show transiently increased enhancement of the bone marrow during this phase. During the first week, focal T1-WI hyperintense and T2-WI/STIR hypointense areas of hemorrhage may be seen. The red marrow ultimately undergoes conversion to fatty marrow, which appears very bright on T1-WI and dark on fat-suppressed images confined to the expected area of the radiation port and demarcated by a sharp line (Daldrup-Link et al. 2007; Wang 2012) (Figs. 2 and 3). Two patterns of

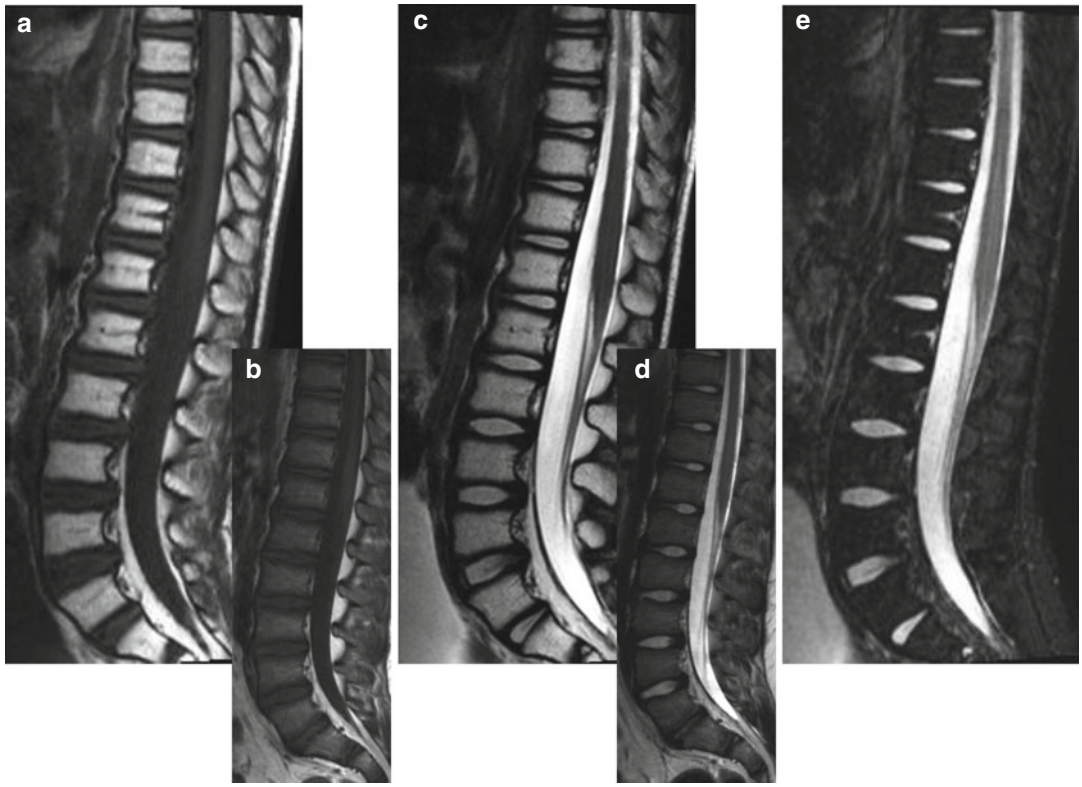


**Fig. 2** Diffuse fatty marrow radiation-induced conversion. Mid-sagittal T1-WI (**a**), T2-WI (**c**) and STIR (**e**) of a children who underwent whole spine radiation therapy (photon therapy or standard X-ray radiation therapy) showing diffuse high T1 and T2-WI signal intensity with diffuse low signal intensity on STIR image, suggesting fatty marrow conversion. Compare the T1-WI (**b**) and T2-WI (**d**) of a healthy patient about the same age

marrow conversion have been described on T1-W sequences: (1) homogenous diffuse increased signal and (2) a band-like pattern with a peripheral region of intermediate signal intensity bordering a central zone of hyperintense signal. This fatty conversion may last up to 2 years (Seneterre et al. 1991; Wang et al. 2004). Contrast-enhanced scans show decreased enhancement of the fatty converted bone marrow, which may be related to a reduction in cellularity and vascularity (Daldrup-Link et al. 2007).

Some studies (Romanos et al. 2013; Blomlie et al. 1995) have reported that radiation-induced changes with small but measurable fatty conversion may occur outside the irradiation field but the etiology and significance of such changes remain unclear. The bone marrow outside the irradiation field may show similar MRI signal changes compared to bone marrow within the irradiation field but to a much lower degree. Otake et al. found markedly decreased contrast enhancement of bone marrow both inside and outside the radiation portal (Hwang and Panicek 2007; Otake et al. 2002). Interpretation of these findings differs, the most attractive explanation being fatty conversion due to scatter irradiation (Otake et al. 2002; Blomlie et al. 1995).

The differential diagnosis of diffusely increased T1 hyperintensity includes normal variations, irradiated marrow, osteoporosis, heterogeneous fatty marrow, and multiple hemangiomas. Rare diagnoses are anorexia and aplastic anemia (Hanrahan and Shah 2011).

There has been controversy over the exact time when edema, hemorrhage, and fatty degeneration appear and disappear (Stevens et al. 1990; Yankelevitz et al. 1991; Blomlie et al. 1995). Dependent on the radiation dose, the fatty conversion may be detected with MRI as early as

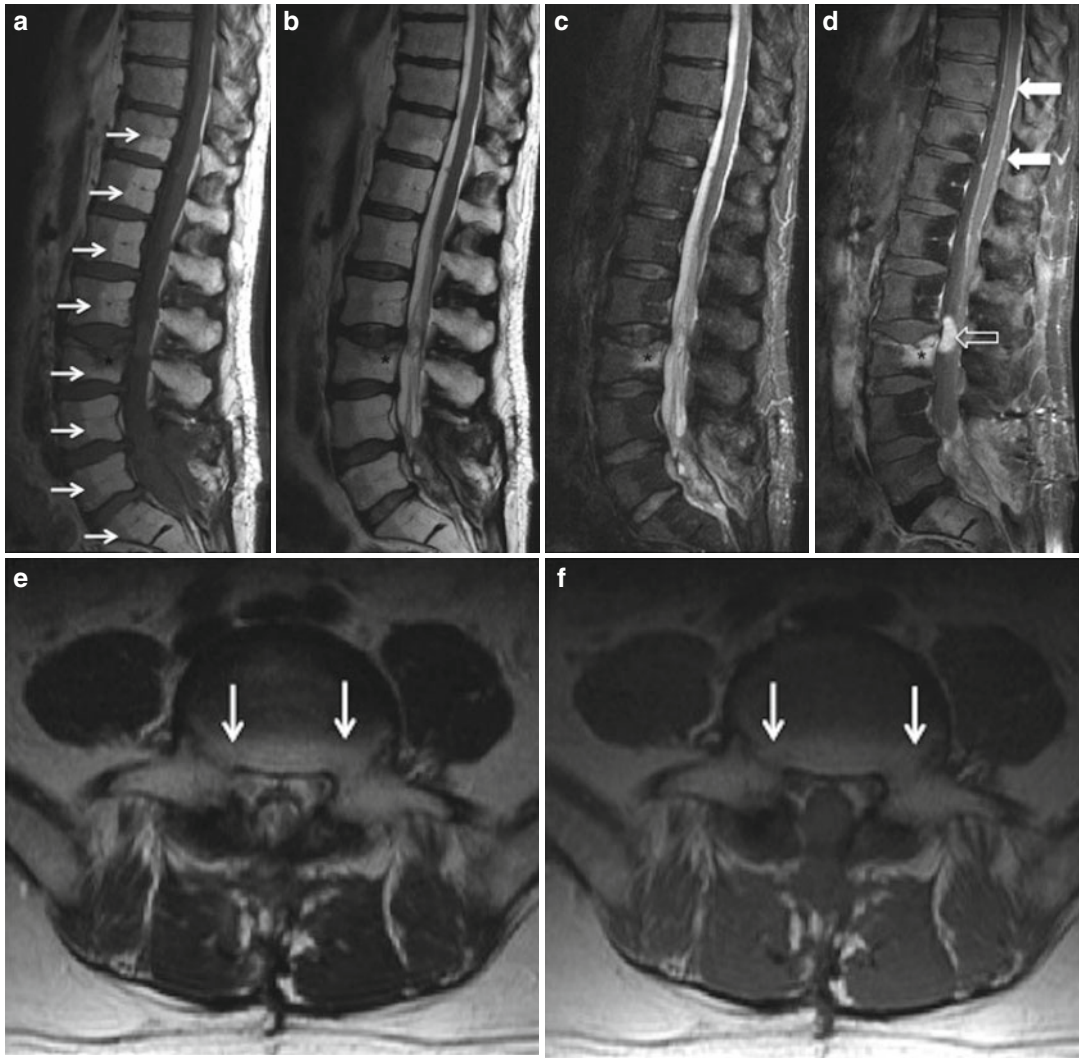


**Fig. 3** Focal fatty marrow radiation-induced conversion. Midline sagittal T1-WI (**a**), T2-WI (**b**), STIR (**c**) and post-contrast fat-saturated T1-WI (**d**), and axial T1-WI (**e**) and T2-WI (**f**) at the level of L5 of a patient with melanocytosis who underwent proton therapy. Note the well-defined fatty marrow conversion involving the posterior aspect of the vertebral bodies seen as areas of high signal intensity on T1- and T2-WI and low signal intensity on fat-saturated sequences (STIR and post-contrast T1-WI) demarcated by a sharp line (*arrows*). Note also the partially collapsed vertebra (L3) (*) with an area of low T1, high T2, and FLAIR signal intensity with enhancement after gadolinium administration in the posterior and superior aspect of the vertebral body, the adjacent epidural soft tissue mass with homogenous enhancement (*open arrow*), and the thick and nodular meningeal enhancement due to tumor recurrence (*block arrow*)

10–14 days after therapeutic radiation (Yankelevitz et al. 1991). In some cases, edema may persist for weeks and fatty transformation may only become apparent months after the irradiation. It has been accepted that this fatty conversion is reversible after an irradiation dose lower than 30–40 Gy and irreversible after an irradiation dose greater than 40 Gy.

Sacks et al. found that the two most important factors affecting the ability of marrow to regenerate were patient age and radiation dose. In their study, 48 patients under 18 years of age who

underwent radiation therapy had full marrow regeneration independent of radiation dose (Sacks et al. 1978).

The time frame of reconversion after low-dose irradiation has also not been determined so far and is variable and influenced by additional chemotherapy or other treatment regimens, location and extent of the affected area, and age of the patient. The red marrow depletion resulting from fatty conversion may induce a compensatory hypercellularity in peripheral skeleton.

## 5 Radiation-Induced Complications

### 5.1 Bone Growth Disturbances

In children radiation therapy may cause impairment of skeletal maturation. The severity of the impairment in bone growth depends on the age of the patient and the radiation dose. Irradiation of the spine may cause scoliosis, which is characteristically concave towards the irradiation field if only one side of the spine was irradiated. There is usually an associated impairment of the paraspinal muscle growth and an impairment of the vertical growth of the irradiated vertebrae.

### 5.2 Irradiation Osteitis

The most common effect of radiation therapy in the bone is an inflammatory reaction, named "radiation osteitis." It was initially described by Ewing and it is now considered a nonspecific pathological process that mainly affects adult patients.

Radiation causes damage to osteoblasts with resorption of bone matrix and subsequent bone atrophy. Bone atrophy is followed by repair with bone deposition on persistent trabeculae. Imaging studies may demonstrate mottled areas of osteopenia and sclerosis and areas of coarse trabeculation, a pattern referred to as "radiation osteitis." Osteitis may be associated with insufficiency fractures, and some investigators believe that radiation osteitis predisposes to osteoradionecrosis.

MRI may show T1 hypointense and T2/STIR hyperintense inhomogeneous signal in areas of edema in the radiation field with a narrow zone of transition between it and the adjacent nonirradiated bone marrow without associated extraosseous soft tissue mass (Daldrup-Link et al 2007). Slight to mild contrast enhancement may be seen after gadolinium administration.

### 5.3 Osteoradionecrosis/Avascular Necrosis

Osteoradionecrosis is a serious complication of radiation therapy that commonly occurs in patients treated for head and neck malignancies. It affects mainly the mandible and maxilla, and it is more frequently associated with corticosteroid administration. However, osteoradionecrosis may involve any bone within the irradiation field, and despite being extremely rare in the spine, cases have been reported in the literature particularly affecting the cervical spine (Rolton et al. 2011; Store and Boysen 2000).

Osteoradionecrosis or avascular necrosis is thought to be caused by alterations in bone blood supply from radiation-induced microvascular damage, fibrosis and endothelial proliferation, blocked arterial inflow and venous outflow, compromised perfusion, and finally anoxia and death of bone marrow cells. Radiation necrosis seems to be dose dependent and is associated with doses of 50 Gy or higher.

Early forms of osteoradionecrosis have a nonspecific MRI appearance, characterized by extensive and diffuse marrow edema seen as new areas of heterogeneous signal within the marrow of an irradiated area (intermediate or low T1-WI signal and intermediate or high T2-WI signal). Adjacent muscles may also appear edematous and show intense contrast enhancement. General differential diagnosis includes tumor recurrence, metastases, radiation-induced secondary tumor such as sarcoma, or osteomyelitis that also occurs in

association with osteoradionecrosis, especially in severe cases.

The classic MRI appearance of advanced bone marrow infarction is a segmental area of low signal intensity in the subchondral bone on T1-WI outlining a central area of marrow, which may have variable signal intensity. This crescentic, ringlike, well-defined band of low signal intensity on T1-WI is thought to represent the reactive interface between the necrotic and reparative zones and typically extends to the subchondral plate. On T2-WI, this peripheral band classically appears hypointense with an adjacent hyperintense line, known as the "double line sign." The hyperintense inner zone represents hyperemic granulation tissue, and the hypointense outer zone represents adjacent sclerotic bone (Daldrup-Link et al 2007).

Osteoradionecrosis of the spine may involve a single vertebra seen on MRI as a wedge-shaped lesion with a collection of fluid (fluid sign) or air (vacuum cleft) in the central area or adjacent to the endplate of a collapsed vertebral body (Yu et al. 2007). Reduction of the intervertebral space and sclerosis of the vertebral endplates may also be seen (Rolton et al. 2011; Wyk et al. 2009). The fluid collection appears as a well-circumscribed area of low signal intensity on T1 and high signal on T2-WI, while the air collection is generally seen with low signal intensity in all sequences and a signal void on gradient-echo images caused by magnetic susceptibility effects.

In the upper cervical spine, osteonecrosis may involve two adjacent vertebral bodies (atlantoaxial or atlantooccipital regions) and the intervening joint spaces with collapse of subchondral bone, reactive soft tissue swelling, and ulceration of the posterior pharyngeal mucosa (Wu et al. 2012) (Fig. 4).

Despite the variable MRI appearance of osteoradionecrosis, this entity must be differentiated from recurrent tumor or metastatic disease since treatment differs completely. While additional antibiotic administration, sequestrectomy or surgical fusion, or hyperbaric oxygen therapy may be required in patients with osteoradionecrosis, further chemotherapy or radiation therapy is mandatory for recurrent disease.

## 5.4 Insufficiency Fractures/Stress Fractures

As stated before, exposure of bone to radiation primarily damages osteoblasts, resulting in reduced production of bone matrix. Unopposed osteoclastic bone resorption leads to progressive osteopenia and atrophy in the affected area which becomes prone to insufficiency-type fractures after minor trauma (Rolton et al. 2011).

Fractures of irradiated bones, such as sacral insufficiency fractures or collapsed vertebrae, may occur within a few months after radiotherapy and may present a diagnostic challenge by mimicking osseous metastases. The correct diagnosis is crucial to avoid unnecessary biopsies and to guide appropriate treatment approach.

Fracture incidence after radiation therapy substantially increases in patients with additional risk factors, such as osteoporosis. The incidence of radiation-induced sacral insufficiency fractures seen on MRI is 20–80 % (Blomlie et al. 1995; Mammone and Schweitzer 1995), most commonly affecting postmenopausal women.

Recently collapsed vertebral bodies show low T1- and high T2-WI signal intensities and may enhance after contrast material administration and therefore may be difficult to differentiate from malignant infiltration. The most reliable MRI sign suggesting benign etiology is visualizing the fracture line, as a T2- or post-contrast T1-WI linear hypointensity in the compressed vertebral body or adjacent to a compressed endplate. This finding represents compacted bone, which is absent in pathological compression fractures.

MRI may depict sacral fractures earlier than CT by revealing the surrounding edema, before the fracture line become visible. Marrow edema is seen as an area of increased signal intensity on T2-W and STIR images and low signal intensity

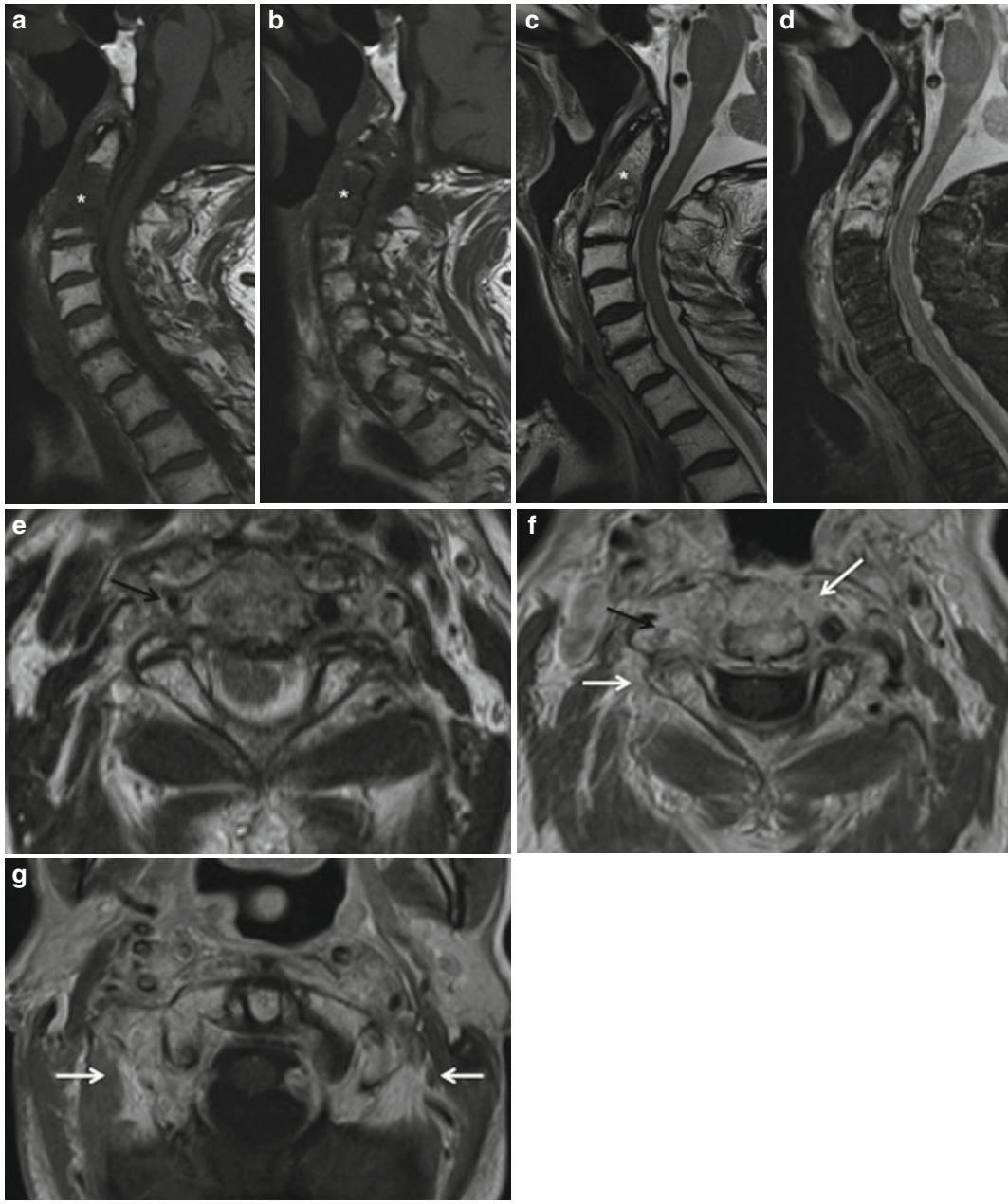


**Fig. 4** Osteoradionecrosis C2–C3. Sagittal T1-WI at the midline (**a**) and off-midline (**b**), midsagittal T2-WI (**c**) and STIR (**d**), axial T2-WI (**e**) and post-contrast T1-WI (**f**) at the C2–C3 level and post-contrast T1-WI (**g**) at C1–C2 level of a patient who underwent radiation therapy for head and neck cancer. The images show abnormal bone marrow signal involving C2 and C3, with low T1-WI, heterogeneous T2, and high FLAIR signal intensity (*), with avid contrast enhancement after gadolinium administration, collapse of the intervertebral space, involvement of the joint spaces, and reactive soft tissue swelling with post-contrast T1 enhancement (*white arrows*). Note the diffuse replacement of the bone marrow that indicates previous radiation therapy. There is also asymmetry of the vertebral arteries (*black arrow*)

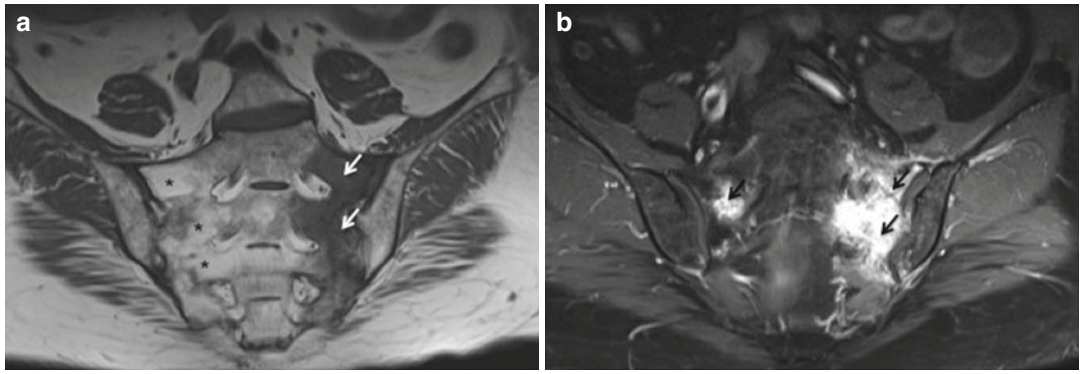


**Fig. 5** Sacral insufficiency fractures. Coronal T1-WI (**a**) and STIR (**b**) of a patient with bilateral sacral fractures after radiation therapy. On T1-WI, areas of fatty marrow replacement are seen (*) due to radiation therapy. The fractures are seen as areas of edema (*arrows*) with low T1-WI and high FAIR intensity involving both sacral alae more prominent on the left side

on T1-WI. A hypointense ill-defined fracture line is usually evident within the area of edema. Enhancement can be prominent on post-contrast T1-WI. Sacral fractures usually show a vertical fracture line through the sacral alae parallel to the sacroiliac joint often associated with a transverse component known as "H pattern" or "Honda sign" (Figs. 5, 6, and 7).

## 5.5 Radiation-Induced Neoplasms

Radiation-induced tumors in patients who receive radiotherapy before 2 years of age are usually benign. The most commonly reported tumor in this group of patients is osteochondroma.

In patients who received radiotherapy during adulthood, induced tumors are more likely to be malignant. Osteosarcoma and fibrosarcoma are generally considered to be the most common radiation-induced tumors in this population.

### 5.5.1 Benign Tumors

Osteochondroma is thought to be induced with radiation doses ranging from 16 to 64 Gy. The development of osteochondromas is inversely related to the age of the patient at the time of radiation therapy. The latency for the development of these tumors is highly variable, but usually they appear within 5 years of therapy. Any bone within the radiation portal may be affected.

Radiation-induced osteochondromas are histologically and radiologically identical to osteochondromas that arise spontaneously, but sarcomatous degeneration of an irradiation-induced osteochondroma is extremely rare, although incidental cases have been reported (Daldrup-Link et al 2007).

Osteochondromas are composed of cortical and medullary bone with an overlying hyaline cartilage cap that demonstrates continuity with the underlying parent bone cortex and medullary canal. The cartilage cap is variable in appearance: it may be thin and difficult to identify or be thick with ringlike calcification and irregular subchondral bone. A cartilage cap of over 1.5 cm in thickness is suspicious for malignant degeneration. When located in the spinal canal, they may cause nerve root or spinal cord compression.

MRI is the best imaging technique to assess cartilage cap thickness. Cartilage cap appears as does cartilage elsewhere with intermediate to low signal on T1- and high signal on T2-WI. After gadolinium administration, enhancement is usually seen in the tissue that covers the cartilaginous cap, which is fibrovascular; however, the cartilaginous cap itself should not enhance.

Other benign radiation-induced tumors are fibrous dysplasia and aneurysmal bone cysts.

### 5.5.2 Malignant Tumors

Sarcoma is a rare complication of radiation therapy, representing 1.5–3 % of all bone sarcomas.

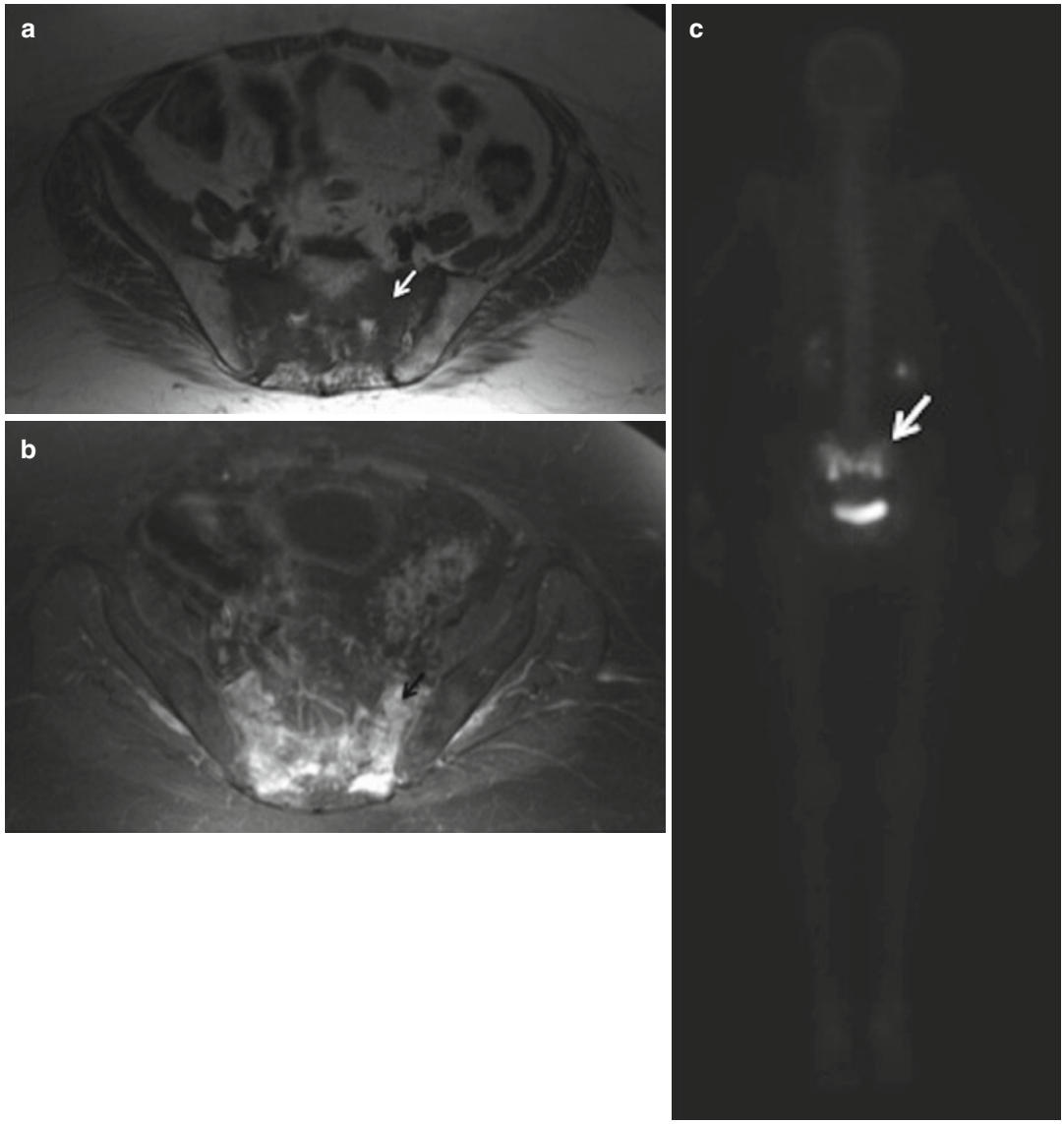


**Fig. 6** Sacral insufficiency fractures. T1-WI (**a**) and STIR (**b**) MR images show the characteristic "H pattern" of insufficiency sacral fractures with low T1 and high STIR signal intensity (*arrows*). Positron emission tomography (PET) study (**c**) shows radionuclide uptake in the same area (*arrow*)

The definition criteria of radiation-induced sarcomas were proposed by Cahan et al. and modified by Arlen et al. and include (1) treatment with therapeutic irradiation at least 3 years prior to the development of sarcoma, (2) a sarcoma arising within the field of previous therapeutic irradiation, and (3) differing histology between the sarcoma and the primary tumor that required radiotherapy (Cahan et al. 1948; Arlen et al. 1971). The latency period between radiation exposure and sarcoma formation is the major controversial criterion and has been modified by several investigators. It was recently suggested by the sarcoma team at Memorial Sloan Kettering Cancer Center (MSKCC) (Gladdy et al. 2010) that a latency of 6 months is sufficient to diagnose a secondary

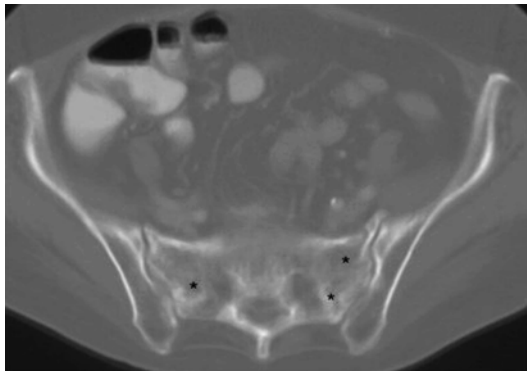

**Fig. 7** Sacral insufficiency fractures. Coronal CT bone window shows bilateral insufficiency ill-defined fractures (*) difficult to characterize with this imaging technique

sarcoma, which contrasts with the generally accepted time frame of several years.

The pathophysiology of radiation-induced bone sarcomas is not fully understood. Identifiable risk factors are young age at treatment and treatment-related factors, including high radiation dose and simultaneous chemotherapy with alkylating agents (Virtanen et al. 2006; Menu-Branthomme et al. 2004; Hawkins et al. 1996). However, there is no consensus regarding the lowest dose required to induce these tumors. The minimum threshold of radiation dose varies across different studies and appears to be between 20 and 50 Gy (Kalra et al. 2007; Rowland et al. 1983; Tabone et al. 1999).

Additionally, secondary sarcomas occur more commonly in patients with hereditary retinoblastoma suggesting a genetic susceptibility. The "p53 gene" is involved in the maintenance of genomic integrity in its role as a tumor suppressor that either allows DNA repair to take place or induces apoptosis when the damage is beyond repair. In a study by Nakanishi et al., 14 mutations of the p53 gene were found in every case of radiation-induced soft tissue sarcoma, while the mutation rate in sporadic soft tissue sarcomas was 20 %. Radiation-induced sarcomas are also characterized by complex karyotypes with frequent loss of material from chromosome arm 3p.15 (Kalra et al. 2007).

The incidence of secondary sarcomas is increasing, probably related with the increase survival of irradiated patients as a result of adjuvant systemic chemotherapy and other treatments as well as the increased use of therapeutic irradiation, particularly in the treatment of breast cancer (Labidi-Galy et al. 2011).

Most of these tumors are high-grade radioresistant tumors, and the prognosis is thought to be worse than for primary bone sarcomas. However, overall survival has improved in the last years, and recent studies (Shaheen et al. 2006; Inoue et al. 2000; Otake et al. 2002) show that aggressive treatment with surgical resection with negative margins and chemotherapy improves the prognosis. The most common histological subtypes are osteosarcoma and malignant fibrous histiocytoma, although other histologies (e.g., angiosarcoma, rhabdomyosarcoma) can occur. It is estimated that the risk of developing osteosarcoma in irradiated bone is 0.03–0.8 % (Kalra et al. 2007; Huvos et al. 1985; Koshurnikova et al. 2000; Arlen et al. 1971; Mark et al. 1994; Enneking et al. 1980; Kaplan and Meier 1958; Nakanishi et al. 1998; Mertens et al. 2000).

## 5.6 Radiation-Induced Myelopathy and Radiculopathy

Radiation therapy can cause toxicity to either the central or peripheral nervous system when these structures are included in the treatment field.

### 5.6.1 Radiation-Induced Myelopathy

Radiation-induced myelopathy is a relatively rare but serious complication of radiation therapy. Several syndromes of radiation injury to the spinal cord have been described; the most prominent are acute transient radiation myelopathy and chronic progressive radiation myelopathy also known as delayed radiation myelopathy. Other less common manifestations of radiation injury include acute paralysis secondary to ischemia and hemorrhage within the spinal cord and a lower motor neuron syndrome secondary to loss of motor neuron cell bodies from the conus medullaris or alternatively from radiation damage to motor fibers in the nerve roots of the cauda equina (Kadir et al. 2012; Bowen et al. 1996).

Radiation dose, time between radiotherapy applications, affected spinal cord level, and associated chemotherapy affect the incidence and severity of myelopathy (Kadir et al. 2012). However, there is no uniformly accepted definition of the term "spinal cord tolerance," and no precise threshold dose for spinal cord tolerance has been determined (Gocheva 2000).

Acute transient radiation myelopathy is a self-limiting early delayed reaction, usually treated with corticosteroids. The pathogenesis remains unknown but transient demyelination of the posterior columns of the spinal cord is accepted as an underlying mechanism. It occurs after a latent period of 2–4 months and is characterized by paresthesia in the back and extremities upon neck flexion or extension, which is known as Lhermitte syndrome. This syndrome typically lasts for a few months followed by complete clinical recovery. There is no correlation of Lhermitte syndrome with chronic progressive radiation myelopathy.

Conversely, chronic progressive radiation myelopathy, also known as delayed radiation myelopathy, is progressive and permanent and is one of the most devastating complications of radiotherapy. It generally occurs after a latent time of approximately 1 year but has been reported up to 3–4 years after radiation. Clinical symptoms and signs can manifest in various combinations of motor and sensory deficits depending on the anatomic level of cord injury and can be fatal if the damage occurs at the upper cervical level.

The pathogenesis of chronic progressive radiation myelopathy is still controversial. Glial and vascular damage hypothesis have been proposed. According to the "glial theory," radiation induces DNA damage in oligodendrocytes and their progenitor cells resulting in myelin breakdown and destruction of white matter. According to the "vascular hypothesis," vascular injury secondary to irradiation causes circulation disturbances and induces white matter lesions (Kadir et al. 2012). Histopathological findings demonstrate white matter necrosis, demyelination, venous wall thickening, and hyalinization and are now accepted that both of these mechanisms play a role in the pathogenesis of delayed radiation myelopathy.

Chronic progressive radiation myelopathy diagnostic criteria include the following: (1) the affected spinal cord segment must be in the irradiated field, (2) symptomatology must correspond to the involved spinal cord segment, and (3) the latency period should be more than 6 months. In addition, absence of spinal cord metastases or primary spinal cord lesions is required for the diagnosis (Kadir et al. 2012; Maranzano et al. 2001; Yasui et al. 1992). Several therapies such as corticosteroids, anticoagulation, and hyperbaric oxygen have been tried with limited benefits.

MRI shows initially cord swelling and usually a long intramedullary lesion with increased signal on T2-WI and enhancement after gadolinium administration (Fig. 8). These findings correlate with neurological symptoms. In the chronic stage, MRI may demonstrates cord atrophy.

### 5.6.2 Radiation-Induced Peripheral Neuropathy

Involvement of the peripheral nervous system is rare but has a considerable impact on quality of life of patients considered cured of their primary malignancies. Radiation-induced peripheral neuropathy is better understood through recognition of various clinical presentations corresponding to injuries to nerve roots and nerve plexus or nerve trunks affecting upper and lower extremities.

The pathophysiological mechanisms are not yet fully understood. However, microvascular injury and radiation-induced fibrosis with axonal degeneration and demyelination occurring in mature nerve tissues play a central role. As described for other radiation-induced changes, the effects of radiation correlate with dose, technique, and concomitant use of chemotherapy.

The main upper limb injury called *chronic brachial plexopathy,* also known as *delayed progressive radiation-induced brachial plexopathy,* is a progressive process with a period of latency that varies from several months to decades. Clinically, it begins with subjective paresthesias or dysesthesias, which decrease with the development of hypoesthesias and then anesthesia. Motor weakness is progressive, often delayed by several months, and later associated with fascicu-

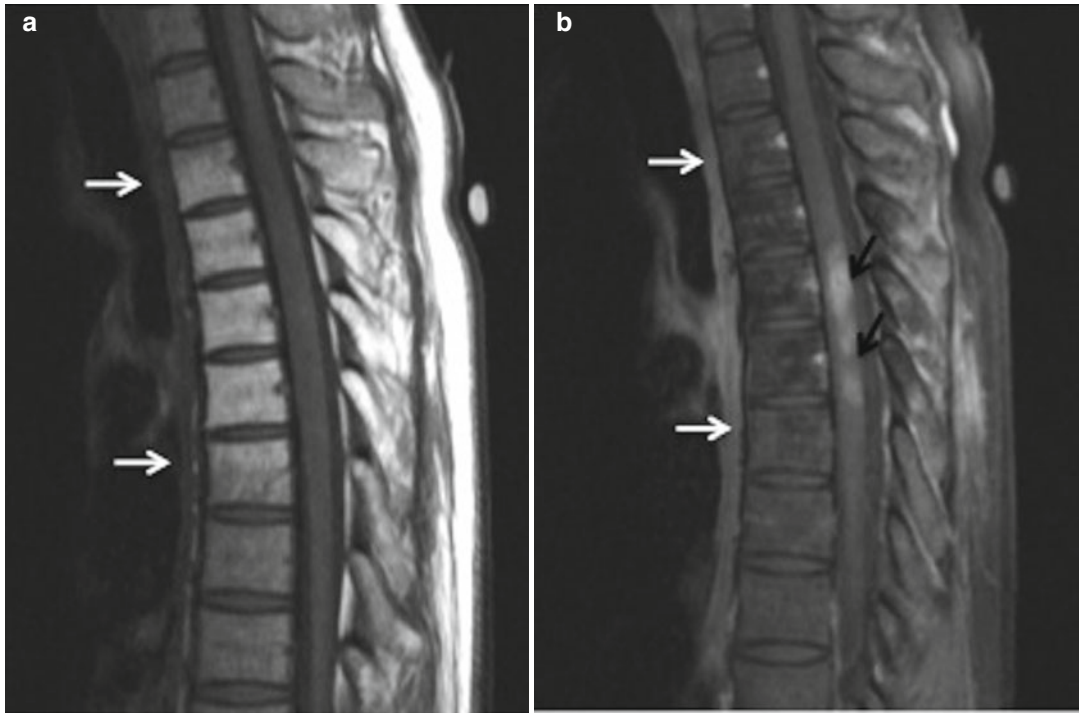


**Fig. 8** Radiation induced myelopathy. Mid-sagittal T1-WI (**a**) and post-contrast fat sat T1-WI (**b**) of a patient who underwent conventional radiation therapy. The characteristic radiation-induced fatty marrow conversion is well seen as an area of high T1-WI and low fat sat T1-WI signal intensity, with perfect delineated borders that correspond to the radiation port (*white arrows*). On post-contrast image (**b**) an enhanced intramedullary lesion with the length of two vertebral bodies is depicted suggestive of radiation-induced myelitis (*black arrows*)

lations and amyotrophy. Symptoms vary with the level of plexus damage (Delanian et al. 2012).

A rare upper limb injury is *early transient radiation-induced peripheral neuropathy*, which has been described mainly after breast cancer irradiation occurring within 1 year after treatment. Initial symptoms include distal paresthesias with proximal pain. Moderate motor deficits occur immediately or after months. After 3–6 months of stability, neurological signs usually regress. Direct and transient effects on Schwann cells, which cause reversible demyelination, may be the result of compression from reversible radiation-induced edema (Delanian et al. 2012).

Lower limb radiation-induced peripheral neuropathy is rare and includes delayed progressive lumbosacral radiculoplexopathy and acute transient lumbosacral plexopathy.

*Delayed progressive lumbosacral radiculoplexopathy* affects the lumbosacral spinal cord, nerve roots, the lumbosacral plexus, and large nerve trunks. Unlike chronic brachial plexopathy, sensory symptoms and paresthesias are absent or noted very late in contrast to signs of peripheral neurogenic motor involvement, such as amyotrophy and fasciculations. Central signs are lacking, apart from those due to cord damage. Subcutaneous paraspinal muscle atrophy is seen and corresponds to the radiotherapy port. Disease progression generally proceeds in a stepwise fashion with periods of stabilization and recurrences. Biopsy of nerve roots of the cauda equina shows fibrotic lesions and vascular dilation corresponding to cavernomas. The evolution of this condition is difficult to predict, but in some patients, spontaneous stabilization has been noticed (Delanian et al. 2012).

*Acute transient lumbosacral plexopathy* was recently reported after pelvic radiation therapy. As described for transient brachial-induced

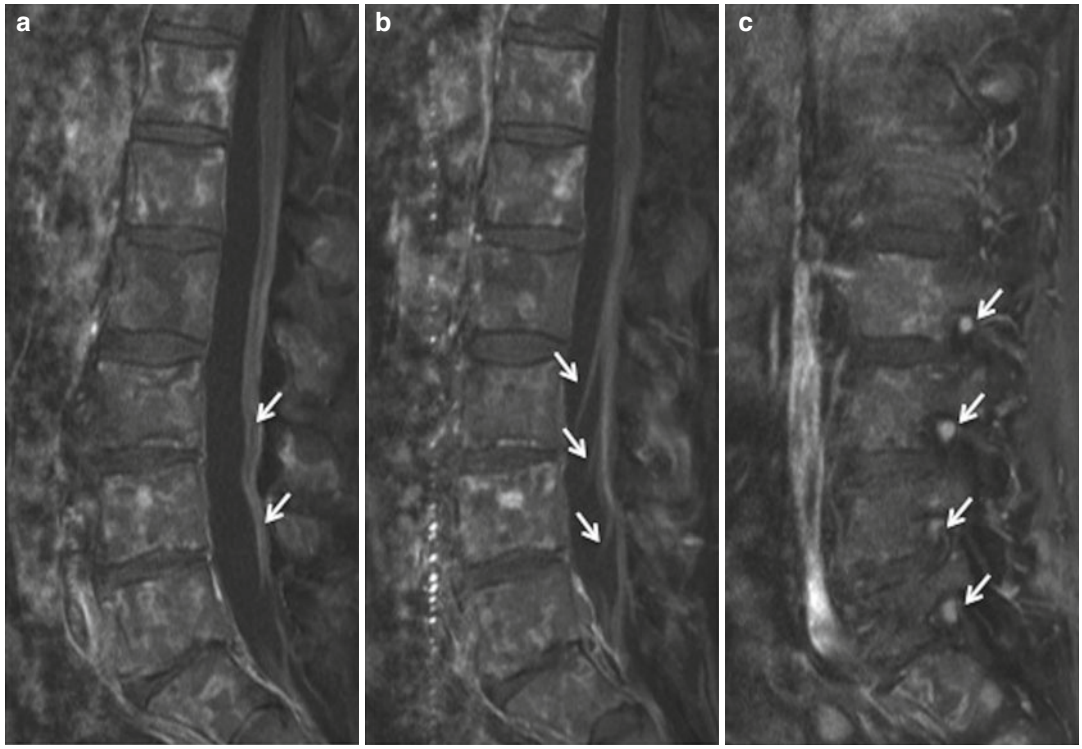


**Fig. 9** Radiation-induced neuropathy. Post-contrast fat sat sagittal T1-WI at midline (**a**), off-midline (**b**) and at the level of the neural foramina (**c**) show lumbar-sacral nerve roots thickening with diffuse enhancement (*arrows*) suggestive of radiation-induced neuropathy

plexopathy, symptoms worsen over months then stabilize before regressing, often completely.

In general, electrophysiological studies reveal findings of peripheral neuropathy. It is often difficult to distinguish radiation-induced neuropathy from peripheral nerve tumor invasion. Radiation-induced disorders are usually painless which distinguishes them from tumor-related plexopathies, which are typically painful (Delanian et al. 2012).

MRI may be useful to differentiate radiation-induced neuropathy from tumor recurrence, but this is often difficult. MRI of radiation-induced neuropathy may show nerve root thickening with diffuse and/or nodular enhancement after gadolinium administration (Fig. 9). Unlike tumor recurrence, this enhancement is usually faint and the abnormalities are restricted to the field of prior radiation therapy. Associated bone marrow changes may also be seen supporting the diagnosis. Radiation can also produce a marked fibrotic reaction seen as soft tissue masses undistinguished from tumor recurrence. In such cases, surgical exploration may be necessary to establish the correct diagnosis. Radiation-induced lumbosacral radiculopathy with multiple spinal root cavernomas is a rare entity recently described that may mimic carcinomatous meningitis on MRI (Ducray et al. 2008). Correct diagnosis of these syndromes is important in order to avoid inappropriate treatment and spinal root/nerve biopsies. Treatment for radiation-induced peripheral neuropathy is symptomatic. A curative treatment is not currently available.

## Conclusion

Radiation therapy changes in normal spinal bone marrow include red marrow depletion that is characterized histologically by hypocellular or acellular marrow on a background of diffuse fatty replacement. Radiation therapy complications include (1) bone growth

disturbances, such as scoliosis and impairment of the vertical bone growth; (2) radiation osteitis which is a nonspecific pathological process; (3) osteoradionecrosis, caused by a hypoxic, hypocellular, and hypovascular environment in which the basic metabolic demands for cellular survival cannot be met; (4) insufficiency fractures caused by normal stress on an abnormal bone with decreased elastic resistance; (5) radiation-induced bone tumors; and (6) central and peripheral nervous system toxicity with myelopathy and radiculopathy resulting from compressive radiation-induced fibrosis, ischemia, or both.

The mechanisms by which all these changes occur are not totally understood; however, side radiation therapy effects depend mainly on patient age, treatment itself, genetic susceptibility, and existence of previous pathology in the irradiated bones.

The radiologist must recognize radiation-induced changes in bone marrow on MRI and differentiate them from progressive or recurrent disease, to assure the appropriate clinical management of these patients.

## References


Arlen M, Higinbotham NL, Huvos AG et al (1971) Radiation-induced sarcoma of bone. Cancer 28:1087–1099

Blomlie V, Rofstad EK, Skonsberg A et al (1995) Female pelvic bone marrow: serial MR imaging before, during and after radiation therapy. Radiology 194:537–543

Bowen J, Gregory R, Squier M et al (1996) The post-irradiation lower motor neuron syndrome neuronopathy or radiculopathy? Brain 119:1429–1439

Burdiles A, Babyn PS (2009) Pediatric bone marrow MR imaging. Magn Reson Imaging Clin N Am 17(3): 391–409

Cahan WG, Woodard HQ et al (1948) Sarcoma arising in irradiated bone; report of 11 cases. Cancer 1:3–29

Chellinger D, Lin CS, Fertikh D et al (2000) Normal lumbar vertebrae: anatomic, age, and sex variance in subjects at proton MR spectroscopy: initial experience. Radiology 215:910–916

Daldrup-Link HE, Henning T, Link TM (2007) MR imaging of therapy-induced changes of bone marrow. Eur Radiol 17:743–761

Delanian S, Lefaix JL, Pradat PF (2012) Radiation-induced neuropathy in cancer survivors. Radiother Oncol 105:273–282

Ducray F, Guillevin R, Psimaras D et al (2008) Postradiation lumbosacral radiculopathy with spinal root cavernomas mimicking carcinomatous meningitis. Neuro Oncol 10:1035–1039

Enneking WF, Spanier SS, Goodman MA (1980) A system for the surgical staging of musculoskeletal sarcoma. Clin Orthop 153:106–120

Gladdy RA, Qin LX, Moraco N et al (2010) Do radiation-associated soft tissue sarcomas have the same prognosis as sporadic soft tissue sarcomas? J Clin Oncol 28:2064–2069

Gocheva L (2000) Radiation tolerance of the spinal cord: doctrine, dogmas, data. Arch Oncol 8(3):131–134

Hanrahan CJ, Shah LM (2011) MRI of spinal bone marrow: part 2, T1-weighted imaging-based differential diagnosis. Am J Roentgenol 197:1309–1321

Hawkins MM, Wilson LM, Burton HS et al (1996) Radiotherapy, alkylating agents, and risk of bone cancer after childhood cancer. J Natl Cancer Inst 88:270–278

Huvos AG, Woodward HQ, Cahan WG et al (1985) Postirradiation osteogenic sarcoma of bone and soft tissues: a clinicopathologic study of 66 patients. Cancer 55:1244–1255

Hwang S, Panicek DM (2007) Magnetic resonance imaging of bone marrow in oncology, part 1. Skeletal Radiol 36:913–920

Inoue YZ, Frassica FJ, Sim FH et al (2000) Clinicopathologic features and treatment of postirradiation sarcoma of bone and soft tissue. J Surg Oncol 75:42–50

Kadir T, Sarica FB, Ozgur K et al (2012) Delayed radiation myelopathy: differential diagnosis with positron emission tomography/computed tomography examination. Asian J Neurosurg 7(4):206–209

Kalra S, Grimer RJ, Spooner D et al (2007) Radiation-induced sarcomas of bone. J Bone Joint Surg Br 89-B:808–813

Kaplan EL, Meier P (1958) Nonparametric estimation from incomplete observations. J Am Stat Assoc 53:457–481

Koshurnikova NA, Gilbert ES, Sokolnikov M et al (2000) Bone cancers in Mayak workers. Radiat Res 154:237–245

Labidi-Galy SI, Tassy L, Blay JY (2011) Radiation-induced soft tissue sarcoma. http://sarcomahelp.org/radiation-induced-sarcoma.html

Wu LA, Liu HM, Wang CW et al (2012) Osteoradionecrosis of the upper cervical spine after radiation therapy for head and neck cancer: differentiation from recurrent or metastatic disease with MR imaging. Radiology 264–1: 136–145

Maranzano E, Bellavita R, Floridi P et al (2001) Radiation–induced myelopathy in long–term surviving metastatic spinal cord compression patients after hypofractionated radiotherapy: a clinical and magnetic resonance imaging analysis. Radiother Oncol 60: 281–288

Mammone J and Schweitzer ME (1995) MRI of occult sacral insufficiency fractures following radiotherapy. Skeletal Radiol 24(2):101–104

Mark RJ, Poen J, Tran LM et al (1994) Postirradiation sarcomas: a single-institution study and review of the literature. Cancer 73:2653–2662

Menu-Branthomme A, Rubino C, Shamsaldin A et al (2004) Radiation dose, chemotherapy and risk of soft tissue sarcoma after solid tumours during childhood. Int J Cancer 110:87–93

Mertens F, Larramendy M, Gustavsson D et al (2000) Radiation-associated sarcomas are characterized by complex karotypes with frequent rearrangements of chromo- some arm 3p. Cancer Genet Cytogenet 116: 89–96

Montazel JL, Divine M, Lepage E et al (2003) Normal spinal bone marrow in adults: dynamic gadolinium-enhanced MR imaging. Radiology 229:703–709

Nakanishi H, Tamita Y, Myoui A et al (1998) Mutation of the p53 gene in postirradiation sarcoma. Lab Invest 78:727–733

Otake S, Mayr NA, Ueda T, Magnotta VA, Yuh WTC (2002) Radiation-induced changes in MR signal intensity and contrast enhancement of lumbosacral vertebrae: do changes occur only inside the radiation therapy field? Radiology 222:179–183

Pichler BJ, Judenhofer MS, Catana C et al (2006) Performance test of an LSO- APD detector in a 7-T MRI scanner for simultaneous PET/MRI. J Nucl Med 47:639–647

Poe LB (2010) Evaluating the varied appearances of normal and abnormal marrow. MRI Web Clinic – December 2010. http://radsource.us/appearances-of-normal-and-abnormal-marrow

Ricci C, Cova M, Kang YS et al (1990) Normal age-related patterns of cellular and fatty bone marrow distribution in the axial skeleton: MR imaging study. Radiology 177:83–88

Rolton DJ, Blagg SE, Hughes RJ (2011) Osteoradionecrosis of the lumbar spine 25 years after radiotherapy. J Bone Joint Surg Br 93-B:1279–1281

Romanos O, Solomou E, Georgiadis P et al (2013) Magnetic resonance imaging and image analysis of post – radiation changes of bone marrow in patients with skeletal metastases. J BUON 18(3):789

Rowland RE, Stehney AF, Lucas HF (1983) Dose-response relationships for radium-induced bone sarcomas. Health Phys 44:15–31

Sacks EL, Goris ML, Glatstein E et al (1978) Bone marrow regeneration following large field radiation: influence of volume, age, dose, and time. Cancer 42:1057–1065

Seneterre E, Weissleder R, Jaramillo D et al (1991) Bone marrow: ultrasmall superparamagnetic iron oxide for MR imaging. Radiology 179:529–533

Shah LM, Hanrahan CJ (2011) MRI of spinal bone marrow: part 1, techniques and normal age-related appearances. Am J Roentgenol 197:1298–1308

Shaheen M, Deheshi BM, Riad S et al (2006) Prognosis of radiation- induced bone sarcoma is similar to primary osteosarcoma. Clin Orthop Relat Res 450:76–81

Snyder WS, Cook MJ, Nasset ES, et al International Commission on Radiological Protection (1975) Report of the task group on reference man. Oxford: Pergamon; pp. 79–98

Somer EJ, Marsden PK, Benatar NA et al (2003) PET-MR image fusion in soft tissue sarcoma: accuracy, reliability and practicality of interactive point-based and automated mutual information techniques. Eur J Nucl Med Mol Imaging 30:54–62

Steiner RM, Mitchell DG, Rao VM, Schweitzer ME (1993) Magnetic resonance imaging of diffuse bone marrow disease. Radiol Clin North Am 31:383–409

Stevens SK, Moore SG, Kaplan ID (1990) Early and late bone marrow changes after irradiation: MR evaluation. Am J Roentgenol 154:745–750

Store G, Boysen M (2000) Mandibular osteoradionecrosis: clinical behaviour and diagnostic aspects. Clin Otolaryngol Allied Sci 25:378–384

Tabone MD, Terrier P, Pacquement H et al (1999) Outcome of radiation-related osteosarcoma after treatment of childhood and adolescent cancer: a study of 23 cases. J Clin Oncol 17:2789–2795

Virtanen A, Pukkala E, Auvinen A (2006) Incidence of bone and soft tissue sarcoma after radiotherapy: a cohort study of 295,712 Finnish cancer patients. Int J Cancer 118:1017–1021

Wang DT (2012) Magnetic resonance imaging of bone marrow: a review – part I. J Am Osteopath Coll Radiol 1(2):2–12

Wang CK, Li CW, Hsieh TJ et al (2004) Characterization of bone and soft-tissue tumors with in vivo 1H MR spectroscopy: initial results. Radiology 232:599–605

Wyk FC, Sharma MP, Tranter R (2009) Osteoradionecrosis of the cervical spine presenting with quadriplegia in a patient previously treated with radiotherapy for laryngeal cancer: a case report. J Med Case Reports 3:7262

Yankelevitz DF, Henshke CI, Knapp PH et al (1991) Effect of radiation therapy on thoracic and lumbar bone marrow: evaluation with MR imaging. Am J Roentgenol 157:87–92

Yasui T, Yagura H, Komiyama M et al (1992) Significance of gadolinium- enhanced magnetic resonance imaging in differentiating spinal cord radiation myelopathy from tumor: case report. J Neurosurg 77:628–631

Yu CW, Hsu CY, Shih TT et al (2007) Vertebral osteonecrosis: MR imaging findings and related changes on adjacent levels. AJNR Am J Neuroradiol 28:42–47

# Bone Marrow: Chemotherapy

Björn Jobke and Hans Bloem

## Contents




B. Jobke (✉)
Department of Radiology,
Deutsches Krebsforschungszentrum (DKFZ),
German Cancer Research Center,
Im Neuenheimer Feld 280, Heidelberg 69120, Germany
e-mail: b.jobke@dkfz-heidelberg.de

H. Bloem
Department of Radiology,
Leiden University Medical Center,
PO Box 9600, Leiden 2300 RC, The Netherlands



**Abstract**

Most systemic diseases affecting the bone marrow (BM) will have a major impact on disease progression and life expectancy. Toxic effects on bone marrow caused by exogenic agents such as chemotherapy or other medications that are non-cell specific significantly influence treatment outcome and survival. The bone marrow with its active hematopoietic components, vital microenvironment, and complex cellular interactions among each other and with adjacent support tissue such as bone is vulnerable to a vast number of toxic stresses. We are just


Med Radiol Radiat Oncol (2015)
DOI: 10.1007/174_2015_1051, 

beginning to understand the role of normal and yet disease-unaffected bone marrow in patients treated for various illnesses. Morphological and compositional changes, as imaged with MRI, reflect a static picture of dynamic and ongoing biochemical cellular process. Newer techniques, for example, diffusion-weighted MR imaging brings us now closer to the cellular level. This is particularly important for the correct interpretation of bone marrow signal changes in cancer patients receiving chemotherapy. Bone marrow edema, hypo- or aplasia, reconversion, and necrosis are the most frequent changes associated with a broad spectrum of chemotherapeutic agents and their additives. The knowledge of chemotherapeutic regimes and the timeline of administration are essential for the interpretation of bone marrow.

## Definitions

| | |
|---|---|
| Wb | Whole-body |
| SI | Signal intensity |
| -w | -Weighted image(s) |
| fs | Fat-saturated |
| Gd | Gadolinium |

## 1 Introduction

Bone marrow imaging is the domain of magnetic resonance (MR) imaging with its excellent soft tissue contrast and high spatial resolution. MR imaging of bone marrow, with a whole-body approach in particular, presents a sensitive and more general view of the entire medullary space, whereas a bone marrow biopsy or aspiration gives information of the cellular composition on a local level with representative information depending greatly on the harvest site.

The number of studies investigating pathological conditions of bone marrow such as multiple myeloma or lymphoma is impressive but due to the increasing variety of available techniques on the verge of confusion to the clinical investigator. Studies investigating age-related changes of normal bone marrow with more recent available MR techniques are increasing, but the number of prospective studies that focus on specific chemotherapy-induced changes in normal bone marrow is significantly smaller. Nowadays, rapidly changing chemotherapy treatment protocols and second- or third-line therapies make interpretation harder for the radiologist. This chapter will give an overview of the appearance of normal bone marrow, applicable MR sequences and present examples of chemotherapy – or related substances in cancer patients – induced changes in the disease-unaffected bone marrow.

## 2 Normal Bone Marrow

Bone marrow is one of the largest organs of the human body, weighting approximately 3 kg, distributed within a mesh network of trabecular bone and protected by cortical bone (Bartl 2012) (Fig. 1). Trabecular bone provides structural support for bone marrow with an ongoing exchange of signaling between osteocytes within the mineralized bone and bone surface cells as well as with the adjacent bone marrow cells. It has to be remembered that MR signal changes in the skeleton may arise either from the medullary space or from the trabecular bone. Thus, CT can provide additional information with respect to mineralized matrix.

MRI is especially suited to monitor bone marrow in a whole-body approach, non-invasively and without radiation. Bone marrow imaging has a high sensitivity to signal changes but a low specificity since a wide variety of hematopoietic and osseous changes result in similar signal pattern. Basic knowledge of normal bone marrow composition (see Chap. 8 and Table 1), normal variants, and differences in red and yellow marrow over time is necessary to understand MR signal intensities (Vahlensieck and Schmidt 2000; Vande Berg et al. 2009; Van Berg et al. 2012).

### 2.1 Bone Marrow Conversion and Reconversion

The composition of bone marrow changes with age and is a dynamic process influenced by internal and external factors. The composition

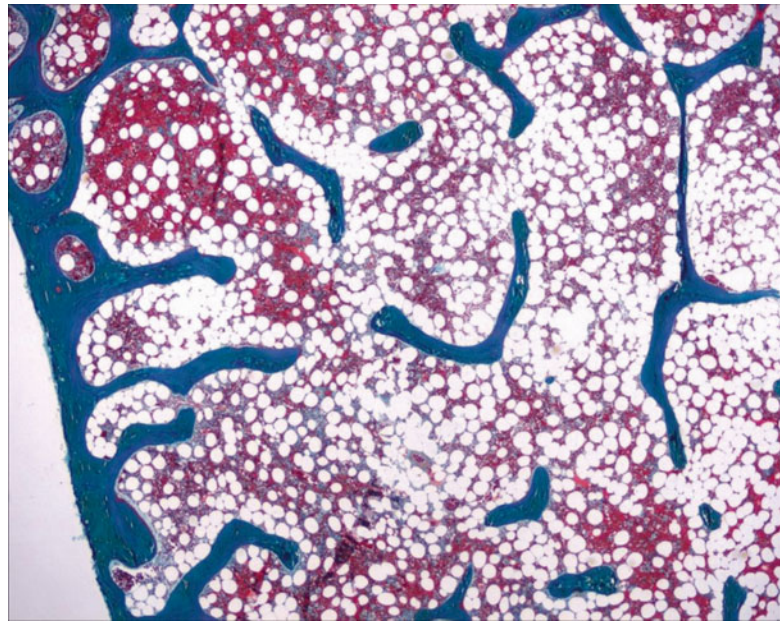

**Fig. 1** Normal BM. Histology section (Goldner stain) with trabeculae in *blue-green* and marrow in *red*. Fat cells (vacuoles in *white*) are distributed evenly (Courtesy: Dr. B. Jobke for Springer publication)

**Table 1** Bone marrow cellularity

| Age | Site | Cellularity (red/yellow) |
|---|---|---|
| Neonate | All bones | 100/0 |
| Child | Most bones | 70/30 |
| Adult | Axial skeleton | 50/50 |
| Old age | Axial skeleton | 30/70 |

gradually changes from birth to adulthood with the conversion from red to yellow marrow and reaches a static stage between 25 and 30 years of age. The speed of conversion is gender dependent, faster in males than in females (Hwang and Panicek 2007a; Shapiro 2006).

Bone marrow fatty conversion progressively starts distally in the extremities and migrates proximally within the extremities towards the axial skeleton in terms of the whole body and from the diaphysis to the metaphysis on the level of the long bones. In the vertebral bodies, conversion begins around the basilar veins, close to the endplates or in a diffuse distribution (Vahlensieck and Schmidt 2000). The epiphysis shows fatty conversion very early in childhood. Later in life, red marrow is reduced to flat bones, the spine and pelvis and becomes gradually more fatty, particularly in para-articular regions (Vahlensieck and Schmidt 2000). MR evaluation of marrow changes in children treated for cancer is especially challenging due to age-related changes in the distribution of normal hematopoietic marrow.

With age and increasing bone degeneration, red marrow is replaced by fatty marrow. Bone marrow fat can be quantified non-invasively using proton MR spectroscopy (MRS) and is anticipated to be a valuable surrogate marker for the assessment of osteoporosis and fracture risk (Bredella 2010; Patsch 2013).

Marrow reconversion is the reverse process of yellow marrow replacement by red marrow in a reverse order from spine and pelvis to the periphery, diaphysis following metaphysis. This process may appear in a heterogeneous pattern with a diffuse recolonization of hematopoietic cells.

## 2.2 Benign Hematopoietic Marrow Hyperplasia

Relative bone marrow hypercellularity is observed in children and adolescents due to different states of chronic hypoxia as, for example, in smokers or due to anemia as seen in marathon runners, during menstruation, or in pregnancy. Marrow hyperplasia is also associated with cardiac insufficiency and with obesity (Shellock

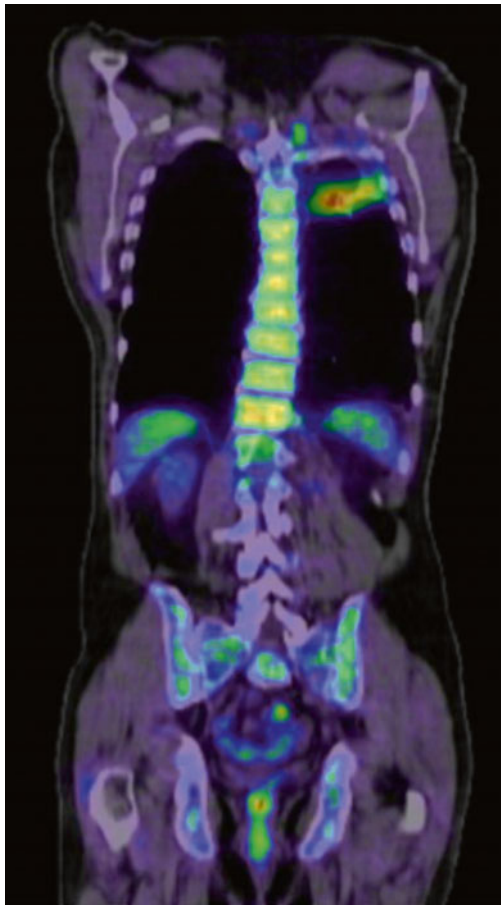

**Fig. 2** Fused PET/CT. A 76-year-old patient with bronchial carcinoma in the upper left lobe and following G-CSF with marked hypermetabolic BM in the axial skeleton (Courtesy: Dr. B. Jobke for Springer publication)

et al. 1992). Other stressors may involve systemic illness and cancer. Under treatment situations, it is most frequently seen in patients treated with hematopoietic growth factors such as granulocyte colony-stimulating factors (G-CSF) (Ollivier et al. 2006) (Fig. 2).

Low to intermediate signal on T1-weighted images in the dorsal part of metaphysis, bilaterally around the knee in young patients is indicative of benign hematopoietic marrow hyperplasia (Lang et al. 1992). The epiphysis, as a very particular anatomic region, is generally not involved during this process and remains with a homogenous fatty marrow signal (Vande Berg et al. 2009).

On whole-body (wb) diffusion-weighted imaging (DWI), bone marrow hypocellularity demonstrates decreased signal intensity on high *b*-value images (Fig. 3).

Marrow hypercellularity presents as diffuse increases in signal intensity on high *b*-values (Padhani et al. 2011, 2013). Changes in background bone marrow cellularity can affect the visibility of bone marrow metastases. Bony metastases can become less conspicuous against increasing background signal intensities when granulocyte colony-stimulating factor (G-CSF) is used to prevent chemotherapy-induced neutropenia.

Benign hematopoietic marrow hyperplasia is most likely a form of marrow reconversion but may be seen in individuals without an underlying condition.

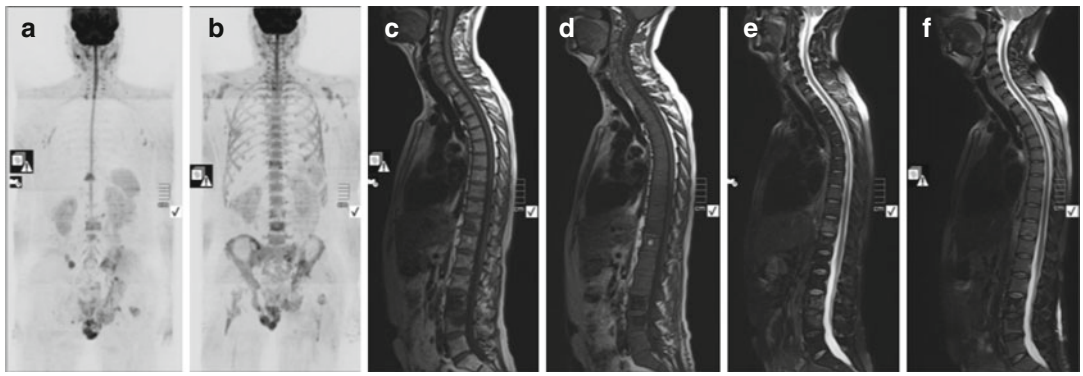


**Fig. 3** BM stimulation after C-GSF. A 53-year-old male with PSA oligosecretory metastatic castrate-resistant prostate cancer, failed abiraterone therapy. (**a**, **c**) DWI: b900 MIP projections (inverted scale) show overall low BM cellularity reflected by reduced signal intensity of the skeletal outline. T1w image shows age-related fatty BM in the spine and hypointense lesions correlation with areas of diffusion restriction, related to metastatic disease. (**b**, **d**) After four cycles of docetaxel chemotherapy with G-CSF support, DWI background BM hyperplasia in the axial skeleton. T1w images of the spine showing the replacement of BM fat consistent with BM hyperplasia. (**e**, **f**) T2w fs images before and after G-CSF show mild increase in normal marrow background signal consistent with BM hyperplasia (Courtesy of Prof. Anwar Padhani, Mount Vernon Cancer Centre, London, UK)

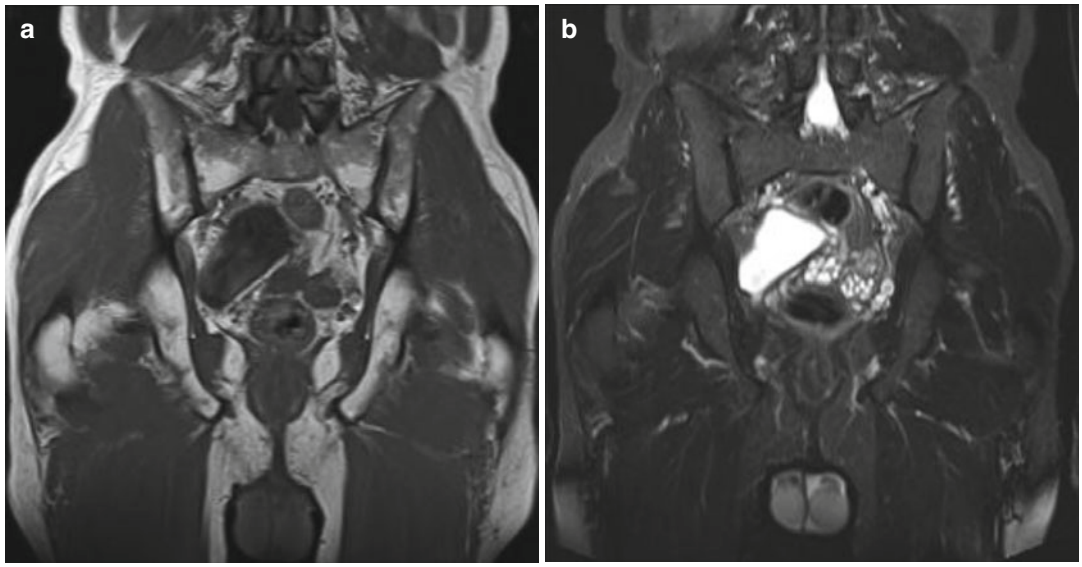


**Fig. 4** BM heterogeneity in the pelvis. (**a**) Coronal T1w shows relatively symmetrical BM heterogeneities in the sacrum and dorsal ilium. (**b**) The TIRM sequence nicely demonstrates fat suppression in yellow as well as red marrow areas (Courtesy: Dr. B. Jobke for Springer publication)

### 2.3 Bone Marrow Heterogeneity

Bone marrow signal heterogeneities without any clinical relevance are frequently observed in healthy individuals as well as in cancer patients (Fig. 4).

Following repetitive cycles of chemotherapy, bone marrow regeneration does not appear in a homogeneous but rather in a heterogeneous pattern and with focal patches of red marrow hyperplasia (van Kaick and Delorme 2008). The age-related changes in composition of bone marrow can be often observed in the pelvis with a heterogeneous pattern of yellow marrow and red marrow with high fat content in an asymmetrical distribution. T1-weighed spin-echo (SE) images, chemical shift imaging (CSI), and DWI are helpful tools to exclude the suspicion of malignancy.

## 3 MR Sequences for Bone Marrow Imaging

Bone marrow, to some extent, is imaged in almost every MRI performed. Higher field strength brings advantages in terms of signal-to-noise ratio and anatomic details, but clear prognostic advantages in patients have yet to be proven. Some important aspects of routine and non-routine MR sequences are pointed out.

### 3.1 Field Strength

Advantages with 3 T over 1.5 T MR have been stated with improved visualization of anatomic structures at the spine (Shapiro 2006; Zhao et al. 2009).

Field strength also affects the imaging of bone marrow because of increased susceptibility effects (increased T2*) originating from the trabeculae at higher field strengths that result in lower signal of overall bone marrow in non-fat-saturated sequences. T1 values increase, depending on tissue type by 10–20 %, while T2 decreases with approximately 10 % in solid tissues. Compared to 1.5 T protocols, TR should be increased by approximately 20 %, while TE can be slightly shortened. Diffusion increases with field strength, making diffusion imaging more sensitive at higher field strength (Gold et al. 2004).

Proton-density weighted images may underestimate or mask signal abnormalities.

### 3.2 Spin-Echo Imaging

In clinical practice, fast (F) or turbo (T)SE sequences have replaced conventional SE sequences. Theoretical disadvantages such as blurring secondary to prolonged echo trains have been solved by pulse sequence design. The main advantage is the short acquisition time. The most important change relative to conventional SE sequences, to take into account, is the relatively high signal intensity of fat in bone marrow on T2-weighted FSE sequences. This is secondary to J-coupling. Therefore, frequency-selective fat suppression or STIR is needed in combination with TSE or FSE to produce high contrast between lesions and normal marrow.

Despite many new sequence developments, T1-weighted images with a high fat to water contrast are still considered essential for bone marrow evaluation. T2-weighted images without fat suppression are generally not useful for bone marrow interpretation due to less contrast between red and yellow marrow and similar signal loss in neoplastic infiltrations (Vahlensieck and Schmidt 2000).

### 3.3 Dynamic Contrast-Enhanced Imaging

Dynamic contrast-enhanced (DCE)-MR imaging can evaluate the vascularization of bone marrow. Major interindividual variations of contrast enhancement in normal individuals (3–59 % increase in SI) have been demonstrated with significantly higher contrast enhancement in younger individuals (Baur et al. 1997). As a rule of thumb, the authors found an increase >40 % SI, a sign of pathologic bone marrow involvement.

Contrast enhancement in normal bone marrow is not only age dependent but is also influenced by anatomical location. SI decreases from cranial to caudal in the lumbar spine (Hillengass et al. 2011a, b) in accordance with decreasing bone mineral density and increasing marrow fat (Liney et al. 2007).

### 3.4 Pulse Sequences

On T1-weighted images (with 1.5 T), bone marrow signal intensities which are equal to or lower than skeletal muscle and/or intervertebral disk in the spine are generally pathological (Carroll et al. 1997). False positives in that series included increased marrow iron stores from hemosiderosis or primary/secondary hemochromatosis and profound anemia with markedly hypercellular hematopoietic marrow. Degenerated disks with signal loss may be a source of error.

Similar results have been shown for 3 T MR although with higher accuracy when using skeletal muscle as a reference (Zhao et al. 2009).

### 3.5 Gradient Echo

Gradient-echo (GE) sequences are especially suitable to describe fat containing marrow demonstrating signal loss in opposed-phase images (Lang et al. 1992). The signal intensity from either red marrow or fatty marrow is decreased on opposed-phase imaging because both types of marrow contain fat and water. Susceptibility artifacts from the trabecular bone in gradient-echo T2w images reduce both red and yellow marrow signals. This is particularly true for anatomical regions with high bone density, for example, epiphysis and apophysis (Vahlensieck and Schmidt 2000) (Fig. 5).

### 3.6 Diffusion-Weighted Imaging

The cellular content of bone marrow can be assessed using DIXON and diffusion MR techniques. WB-DWI is an emerging imaging technique because it is sensitive to bone marrow cellular density, the relative proportion of fat and marrow cells, water content, and bone marrow perfusion (Padhani et al. 2011, 2013; Dietrich et al. 2009).

Reduced water content, the hydrophobic nature of fat and poorer perfusion, and larger-sized fat cells, all contribute to lower signal intensities and ADC values of the yellow bone marrow while with increasing cellularity, water content and

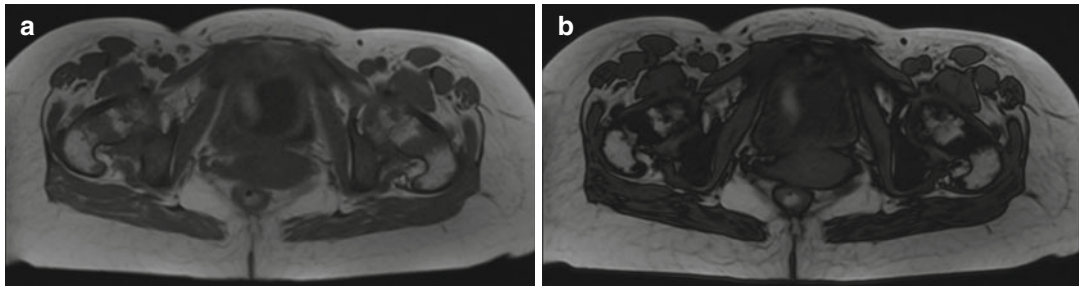


**Fig. 5** Normal BM. (**a**) In-phase GRE of the proximal femora demonstrating heterogeneous signal from red and yellow BM. (**b**) Signal drop in opposed-phase images in red marrow containing fat cells and no signal drop in fat marrow in the femoral head and greater trochanter (Courtesy: Dr. B. Jobke for Springer publication)

greater perfusion, mixed yellow-red bone marrow returns higher signal intensities and paradoxically higher ADC values (Hillengass et al. 2011a; Padhani et al. 2013) (Fig. 3, see above).

False-positive findings on DWI may be due to infection, bone marrow edema, bone infarcts, vertebral hemangiomas, bone marrow islands, and bone marrow hyperplasia due to G-CSF.

This can be overcome by correlating high *b*-value DW images with ADC maps and anatomical sequences. In contrast, causes for false-negative findings are low levels of bone marrow infiltration such as in smoldering multiple myeloma or when background bone marrow hyperplasia obscures the presence of metastases. Diffusion-weighted echo-planar imaging technique is limited by poor spatial resolution and by susceptibility and chemical shift effects.

### 3.7 Chemical Shift Imaging

Chemical shift-based fat suppression can help evaluate bone marrow infiltration. Neoplastic tissue will not show signal loss in opposed-phase images, in contrast to normal fatty or hematopoietic red marrow, both containing adipocytes (see also Chap. 8).

## 4 Chemotherapy: Short- and Long-Term Toxicity Effects

Early chemotherapeutic effects can start within hours and days after administration of chemotherapy and express cytotoxic effects with cell edema and cell death.

In contrast to radiotherapy alone, late effects of chemotherapy are thought to result predominantly from parenchymal cellular depletion with sparing of the microcirculation and fibro-connective tissue stroma (Dreyer et al. 2005).

Radiologists and clinicians need to be aware of late-effects syndromes secondary to chemotherapy to distinguish from recurrent or metastatic disease. These late effects from all types of therapeutic interventions (chemo, radiation, surgery) are predictable events that occur in a different time frame from those of tumor progression and are summarized in the LENT-criteria ("*L*ate *E*ffects of *N*ormal *T*issue") (Hall 2011).

Secondary malignant neoplasms (SMNs) comprise one of the most potentially life-threatening sequelae, representing about one in six of all cancers reported to the National Cancer Institute's Surveillance, Epidemiology, and End Results (SEER) Program (Travis et al. 2013; Wood et al. 2012).

Despite the fact that today more than 75 % of children with cancer can be cured of their disease, long-term adverse events can have a major impact on life quality (Rosoff 2006). The overall survival rate for all cancers is about 66 % (Wood et al. 2012). Children have higher thresholds for acute toxicity enabling them to receive higher dosage of chemotherapy agents than adults, but growing children are more vulnerable to the delayed adverse musculoskeletal sequelae of chemotherapy. Since most chemotherapeutics agents are cell cycle dependent, the severity of acute toxicities varies according to the proliferation kinetics of individual cell populations. Tissues

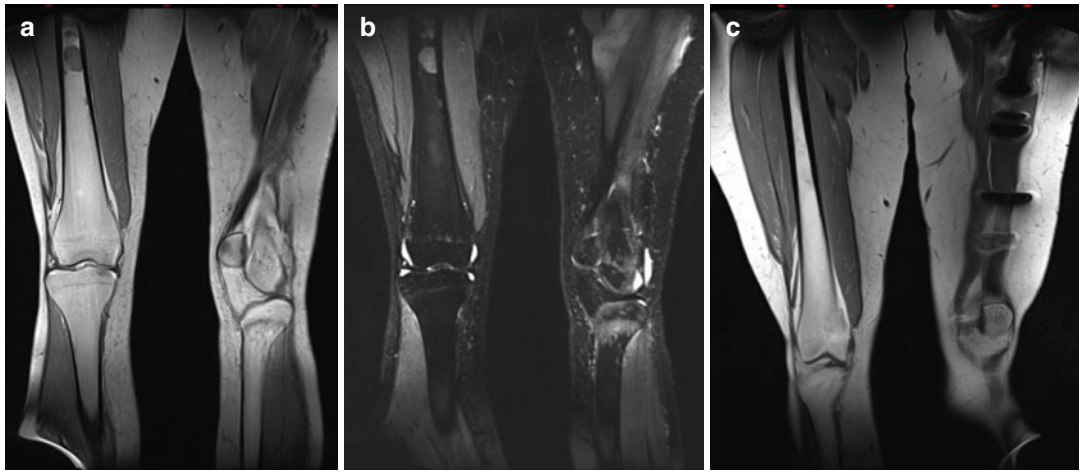


**Fig. 6** Sarcoma patient treated with chemotherapy from 2009 to 2010. Tumor endoprosthesis on the left and sequelae of marrow changes from 2010 (**a**, **b**) with focal red BM hyperplasia in the mid-shaft of the right femur and heterogeneous in the proximal left tibia. (**a**) T1w and (**b**) STIR, which had resolved completely in 2014 (**c**) T1w (With permission from Prof. Dr. H.U. Kauczor, University Hospital Heidelberg, Germany)

like bone marrow with high cell turnover rates are most susceptible. Tissues with slow replication rate, such as muscle cells and connective tissue, are least susceptible.

The combination of radio- and chemotherapy potentiate the risk of developing late effects and the incidence of secondary cancers rises significantly. The most frequent secondary cancer following chemotherapy is acute myeloid leukemia (AML). The risk to develop AML increases already 2 years following therapy with a peak risk incidence between 5 and 10 years following chemotherapy (Travis et al. 2013). The incidence of solid bone or soft tissue tumors following chemotherapy is relatively rare compared to radiation-induced bone tumors.

## 5 Chemotherapy-Induced Changes in Normal Bone Marrow

During the first days after initiation of chemotherapy, a decrease in the signal intensity of hematopoietic marrow is observed on T1w MR images (bone marrow aplasia, see below). Simultaneous increases in water-sensitive sequences such as STIR are most likely due to edema secondary to an increase in vascular permeability and cell death (Daldrup-Link et al. 2007). Very few prospective studies investigated post-chemo MR signal changes. Altehoefer et al. found a significant 33 % increase in signal intensity on STIR images at the first scan, 26 days following induction chemotherapy, reflecting temporary bone marrow edema, normalizing shortly after peripheral stem cell transplantation and G-CSF (Altehoefer et al. 1997, 2001).

Within 1–2 weeks, chemotherapy causes a myeloid depletion with a decrease in marrow cellularity and fatty marrow replacement with an increase in signal intensity on T1-weighted images and a low signal intensity on fat-suppressed sequences. After 3–4 weeks, hematopoietic recovery occurs with a reconversion of yellow to red marrow in the opposite way to marrow conversion, that is, from the axial to the appendicular skeleton (Hwang and Panicek 2007a, b).

On out-of-phase GE images, one can see a drop in signal intensity from normal hematopoietic marrow and no change in signal from malignant cells (van Kaick and Delorme 2008; Ollivier et al. 2006). Posttreatment changes occur frequently, and knowledge of signal patterns is essential to avoid misinterpretation. Without the clinical information and timeline of chemotherapy, image interpretation is often impossible and prone to misinterpretation (Fig. 6).

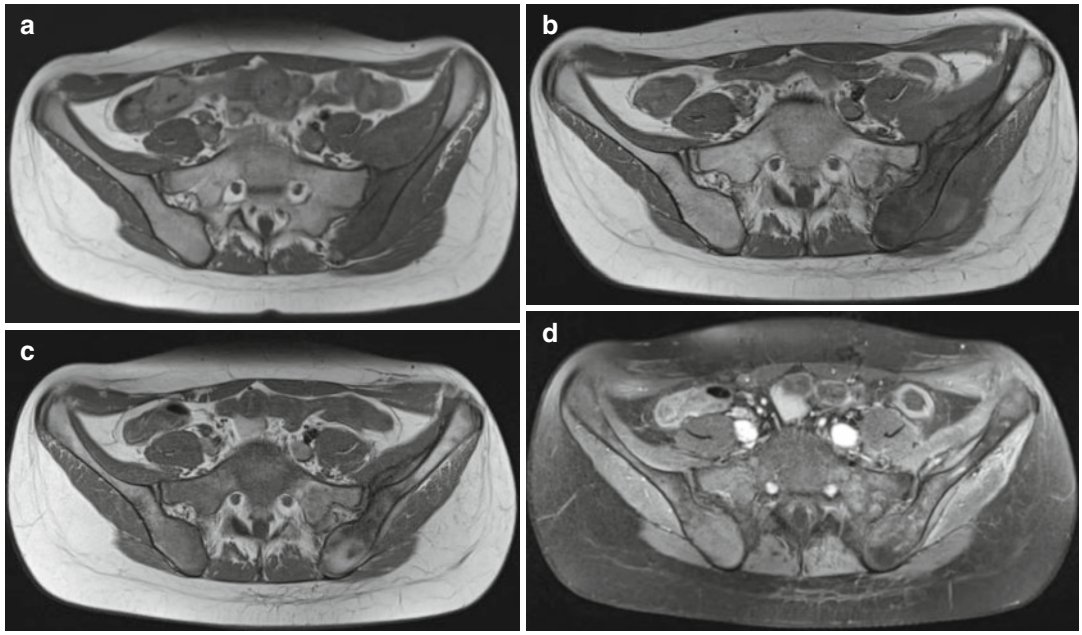


**Fig. 7** BM changes following chemotherapy in a 16-year-old patient with Ewing sarcoma in the left ilium. (**a**) The images show consecutive native T1w images before chemotherapy, (**b**) 2 months into chemotherapy with a slight increase in T1w signal (BM hypoplasia), and (**c**, **d**) BM reconversion 1 year after cessation of chemotherapy with BM rebound on the healthy right side expressed by marked signal increase in the post gadolinium fs image (Courtesy: Dr. B. Jobke for Springer publication)

### 5.1 Cytotoxic Chemotherapy and Bone Marrow Hypo-/Aplasia

Early cytotoxic damage leads to hypo- or aplastic bone marrow within hours and days of treatment start, much earlier than alterations in peripheral blood parameters become apparent. Pereira et al. found a T1w signal increase in 87 %, after 6–8 days as a result of bone marrow aplasia along with increased STIR signal with a slow and variable normalization following blood stem cell transplantation between 3 weeks and 4 months. An important diagnostic difficulty is that water-sensitive STIR sequences detect intra- and extracellular water molecules, reflecting cellularity as well as edema, hemorrhages, and necrosis, respectively (Pereira et al. 1999). A similar phenomenon has to be accounted for when results from MRS are investigated. Thus, STIR sequences show early bone marrow edema during aplasia and marrow cellularity. Together with T1w images, a characterization of aplasia and reconstitution of bone marrow after blood stem cell transplantation is feasible (Fig. 7).

### 5.2 Cachexia and Serous Atrophy

Serous atrophy of the bone marrow is a condition observed in cachectic cancer patients, in anorexia nervosa, and in patients with HIV. Histology shows fat atrophy and a marked increase in extracellular gelatinous material consisting of hyaluronic acid (Fig. 8). MR depicts a signal from the bone marrow equivalent to water, with unspecific low signal intensity on T1w images, and high signal intensity on fluid-sensitive sequences (STIR, frequency-selective fat saturation). No contrast enhancement of the bone marrow is depicted in serous atrophy, thus discriminating it from malignant disease. Serous atrophy is reversible, depending on the overall body status of the subject (Noebauer-Huhmann and Uffmann 2012).

### 5.3 Imatinib (Gleevec) and Bone Marrow Edema

A small study on children under Gleevec for neurofibromatosis showed bone marrow signal

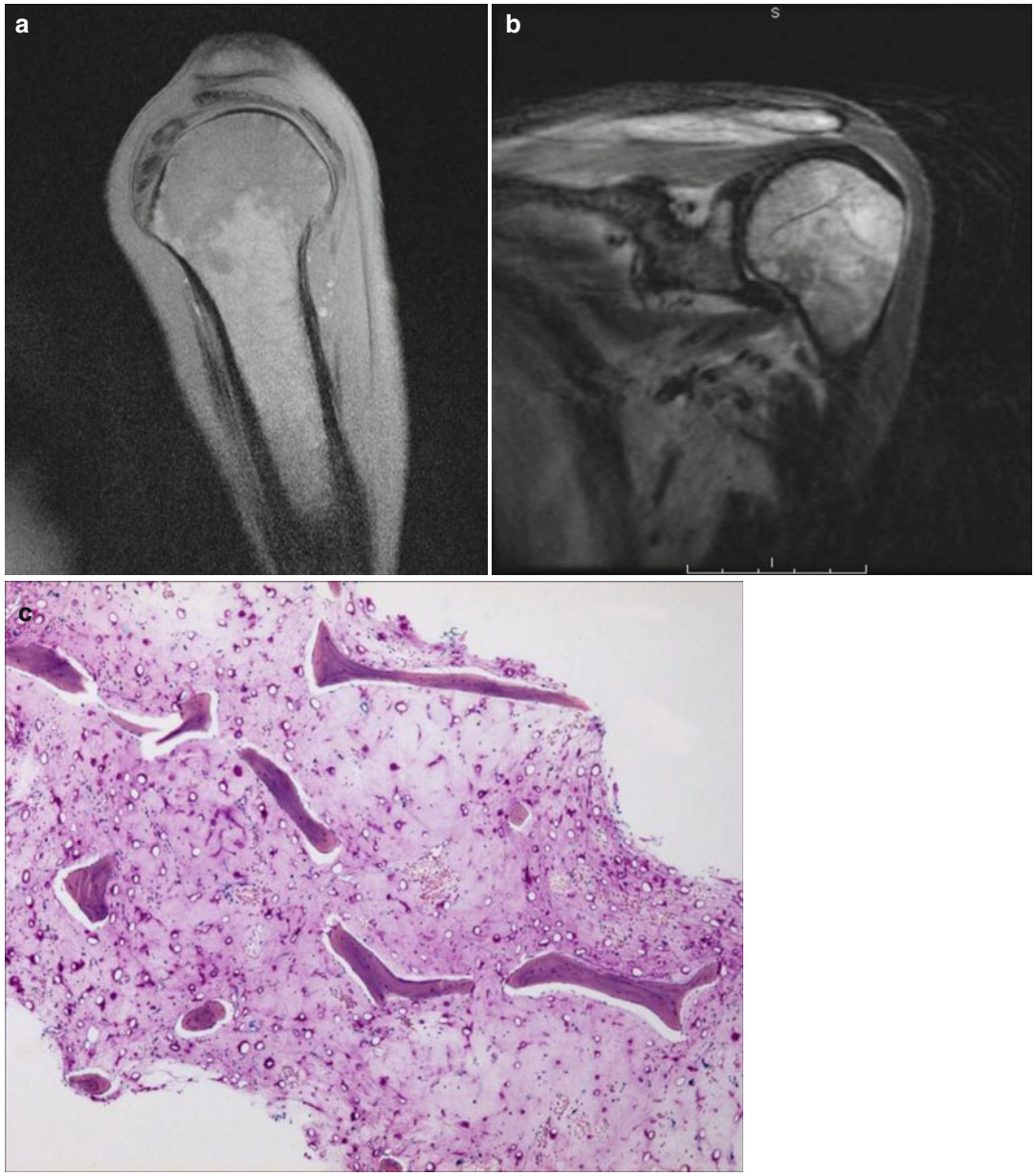


**Fig. 8** Serous atrophy. (**a**, **b**) Proximal humerus from a cachectic cancer patient showing low T1w signal in the humeral head with corresponding high signal in the STIR image (With permission from Dr. Miriam Bredella, MGH, Harvard, Boston, USA). (**c**) Young adult with anorexia nervosa, progressive bone loss, and gelatinous extracellular matrix with aplastic BM (HE stain)

changes on STIR images in 14 of 16 patients. The signal change was asymmetrical in 64 %. The appendicular skeleton was involved in all patients and the axial skeleton in 3 patients. Decreased signal was seen in 69 % after a mean duration of 1.3 years of treatment. The authors believe that the signal changes reflect bone marrow edema (Karmazyn et al. 2012). They change over time and may completely regress after termination of medication. Few case reports demonstrate bone marrow necrosis under Gleevec. It has to be pointed out that the majority of patients present

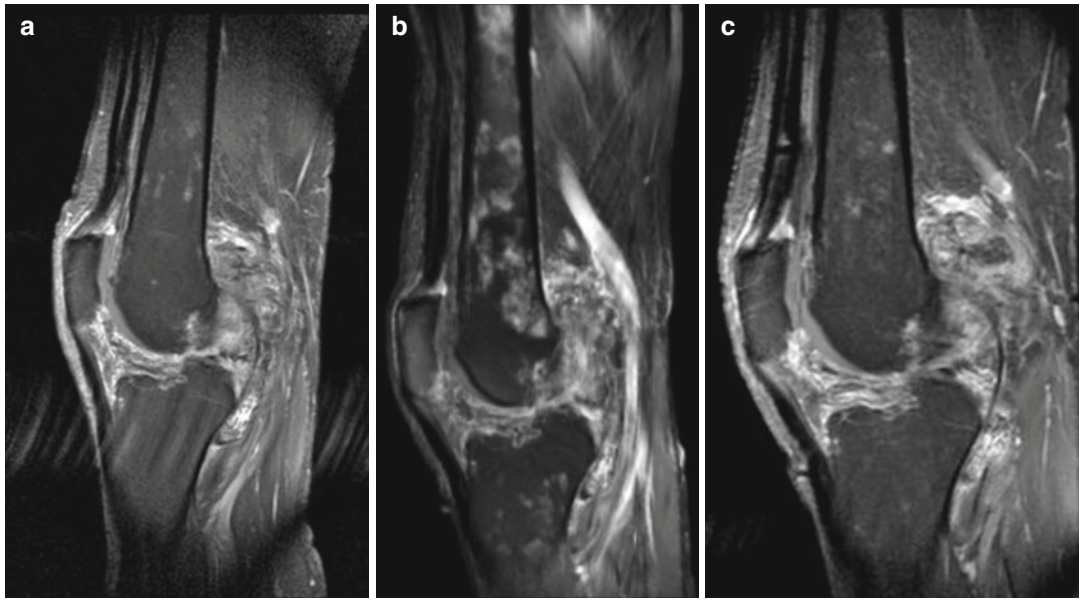


**Fig. 9** A patient with tenosynovial giant cell tumor (PVNS) in the knee joint seen as a large soft tissue mass. The patient was treated with a tyrosinase inhibitor (Gleevec°). At the start of systemic therapy, normal BM with some red marrow nests is seen on (**a**) T1w fs Gd-enhanced images. (**b**) Five months later, marked nodular changes are seen as high signal intensity areas. (**c**) Two years later after cessation of treatment, the marrow changes had disappeared (Courtesy: Dr. B. Jobke and Dr. H. Bloem for Springer publication)

with systemic disease and a treatment response mechanism on occult neoplastic tissue may be possible (Vanel et al. 2007; Burton et al. 2002; Campiotti et al. 2007; Matsue et al. 2006; Tamura et al. 2004). The incidence of bone marrow edema-like signal change under Gleevec is yet unknown. Gleevec has also been shown to alter bone metabolism (Berman et al. 2006) (Fig. 9).

## 5.4 G-CSF and Bone Marrow Reconversion

Granulocyte colony-stimulating factor (G-CSF) is used to stimulate myeloid cell production in order to reduce leukopenia in patients undergoing aggressive chemotherapy and before stem cell transplantation. It gives rise to a recolonization of the fatty marrow by red marrow (marrow rebound). A low signal intensity on T1-weighted images and a mildly increased signal on T2-weighted and STIR images are MR findings consistent with reconversion of yellow to red marrow (Fig. 10). A study on 19 tumor patients receiving G-CSF demonstrated higher water content in the femoral and vertebral bone marrow 5–10 days after administration measured by MRS (Layer et al. 2000). Altehoefer et al. described the same phenomenon with a maximum MR signal change in T1w images 2 weeks after administration and normalization after 6–8 weeks later (Altehoefer et al. 2001). STIR images may present a persistent signal reduction, up to 8–9 weeks compared to pre-chemo images, probably caused by mild fibrosis. The T1w signal changes may be homogeneously diffuse, simulating a marrow-infiltrative tumor, or focal and patchy. It generally shows a symmetric appearance but asymmetric distribution may appear (Vande Berg et al. 2009) (Fig. 11). The recolonized red marrow enhances on post-contrast T1w fat-saturated images but in a limited way (<40 %) compared to diffuse neoplastic infiltration (Baur et al. 1997; Hillengass et al. 2011a). In a research setting, the lack of ultrasmall-particle superparamagnetic iron ore (USPIO) uptake may indicate a tumor progression or recurrence (Daldrup-Link et al. 2009).

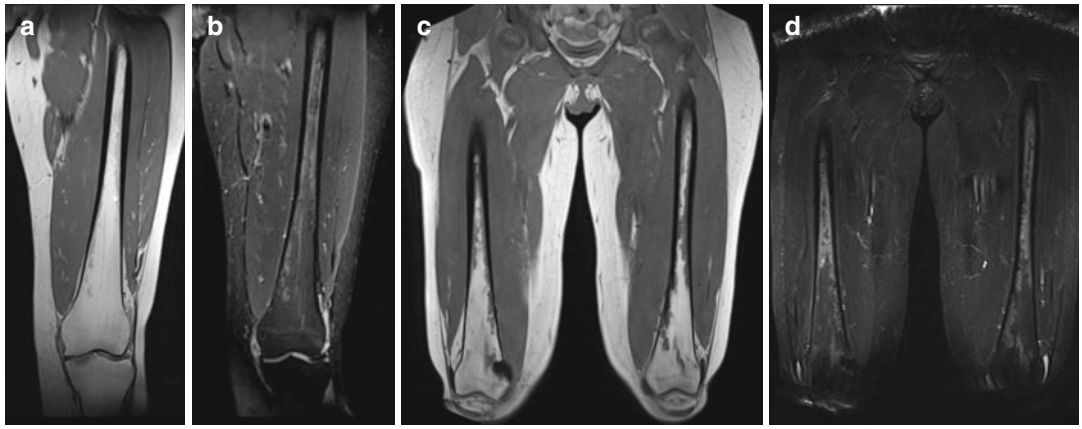


**Fig. 10** A patient treated with chemotherapy. (**a**, **b**) Before and (**c**, **d**) 2 months into chemotherapy showing marked symmetrical BM rebound proximally with extension into the diaphysis and distal metaphysis in a subcortical distribution. (**c**) T1w signal drop is equal to muscle (**d**) intermediate to hyperintense on STIR (Courtesy: Dr. B. Jobke for Springer publication)

Difficulties in interpretation may be encountered when chemotherapy and G-CSF are administered simultaneously, which often is the case, and without knowledge of pre-medication images.

## 5.5 Antiangiogenic Drugs and Microcirculation

Angiogenesis-inhibiting drugs, increasingly used in oncology, may induce bone marrow alterations. So far, studies on imaging effects of normal bone marrow are still lacking. New drugs with antiangiogenic activity, such as bevacizumab that binds and inactivates vascular endothelial growth factor (VEGF) or VEGF-tyrosine kinase inhibitors seem promising. New macromolecular contrast medium (MMCM) agents can most likely monitor this treatment response in patients (Berger et al. 2009), although larger patients cohorts have yet to be investigated. Thalidomide has been shown to possess antiangiogenic potential among other antitumoral effects and is being studied for the treatment of multiple myeloma in particular. A study by Wasser et al. showed that DCE-MRI can quantify significant changes of bone marrow microcirculation solely during treatment with thalidomide combined with chemotherapy, not with thalidomide alone (Wasser et al. 2004).

## 5.6 Corticosteroids and Bone Marrow Infarcts

Prolonged corticosteroid therapy induces osteoporosis and leads to fat conversion (Fig. 12) and/or bone marrow infarcts (histopathologically equal to avascular necrosis (AVN) or osteonecrosis depending on the location within a bone). The magnitude of fat conversion correlates with steroid intake and is higher in patients with ischemic bone lesions (Vande Berg et al. 1999). AVN is caused by vascular insufficiency, compromised bone marrow perfusion, and finally anoxia and death of bone marrow cells. AVN is a well-known complication in 10 % of long-term survivors of bone marrow transplantation receiving high doses of steroids and is seen in 1–10 % of patients in the initial treatment phase of leukemias or lymphomas (Daldrup-Link et al. 2007) but may also appear independently without treatment in cases of disseminated bone marrow involvement. Cases of secondary malignant transformation of bone marrow infarcts of the long bones into

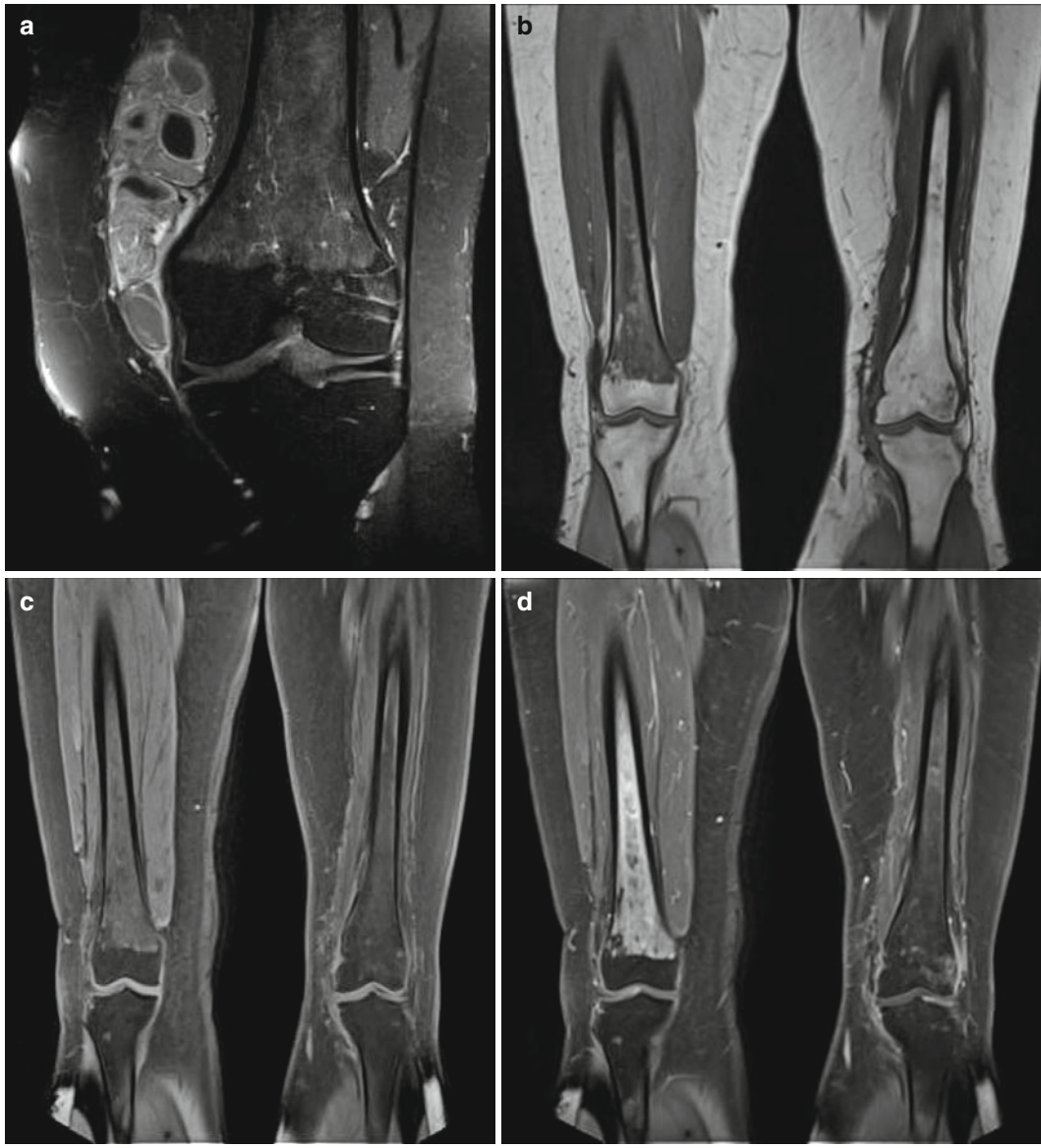


**Fig. 11** A patient with synovial sarcoma under chemotherapy and G-CSF. (**a**) T1w fs images after Gd administration show homogeneous red BM rebound in the left femur with sparing of the epiphysis. Synovial sarcoma in parosseal medial location. (**b–d**) T1w-, T1w fs-, T1w fs Gd images of both legs 1 year later show a similar presentation in the right leg. Note the lack of BM rebound in the tibia. The left leg (primary tumor location) now shows a marked reduction in tumor size following additional radiation to the tumor and femur. Hence, the former BM rebound returned to fatty transformation (Courtesy: Dr. B. Jobke for Springer publication)

sarcoma, for example, pleomorphic undifferentiated sarcoma/malignant fibrous histiocytoma, have been reported (Duong et al. 2004).

AVN may appear under treatment, but a latency period of months and years following treatment is frequently observed (Hanna and Fletcher 2004). As opposed to bone marrow necrosis in hematological disorders such as sickle-cell disease, steroid-induced bone marrow necrosis is generally clinically asymptomatic,

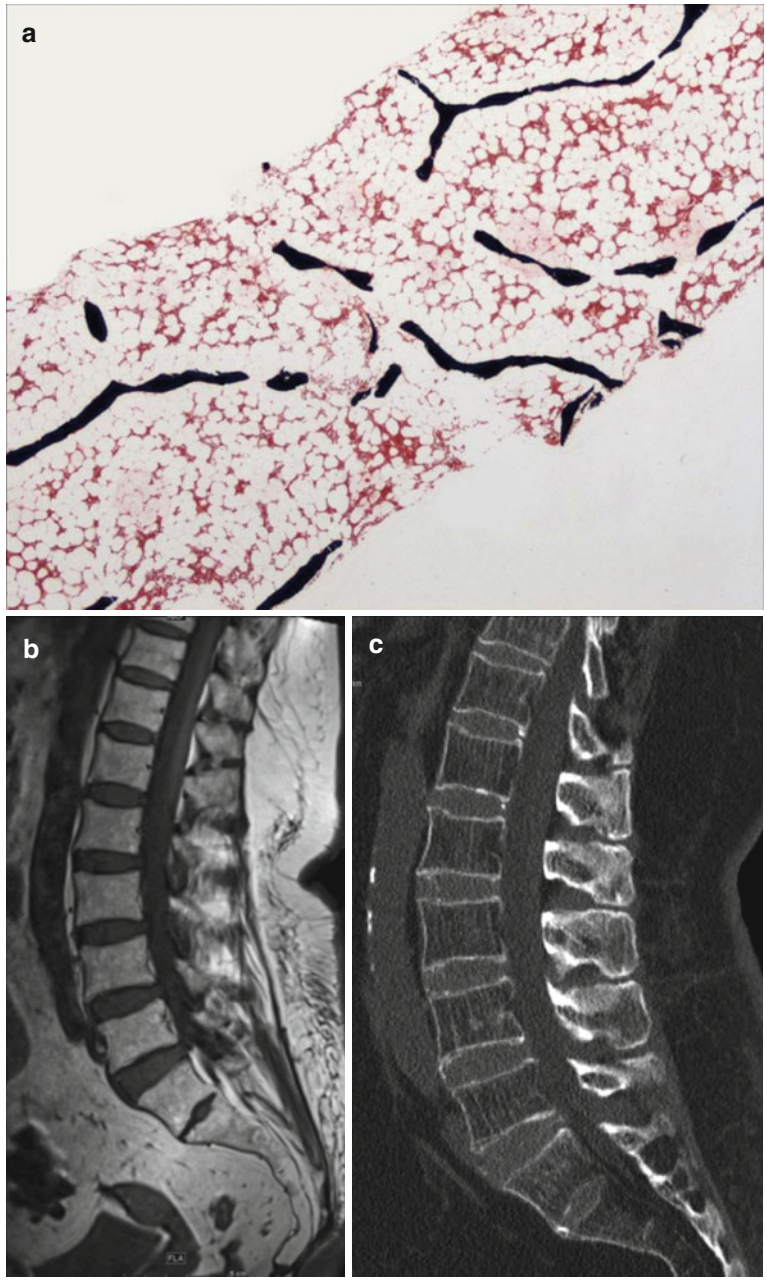


**Fig. 12** Steroid osteoporosis (**a**–**c**). (**a**) Iliac crest biopsy from a 44-year-old male patient following 5 years of steroid medication and bisphosphonate treatment. Thinning of trabeculae maintaining some network architecture (*black*) with peritrabecular fatty marrow accumulation without bone cells on the bone surface characterizing a low turnover steroid–induced osteoporosis. (**b**) T1w image shows fatty marrow transformation and (**c**) bone loss with trabecular rarefaction in CT (Courtesy: Dr. B. Jobke for Springer publication)

unless subchondral collapse occurs (Umans et al. 2000). Bone marrow infarcts may appear in cancer patients with disseminated metastatic disease following chemotherapy.

The risk to develop AVN increases in combination with radiotherapy. Bones with end-arterial supply and poor collaterals are especially prone to AVN, such as the subchondral epiphyseal joint

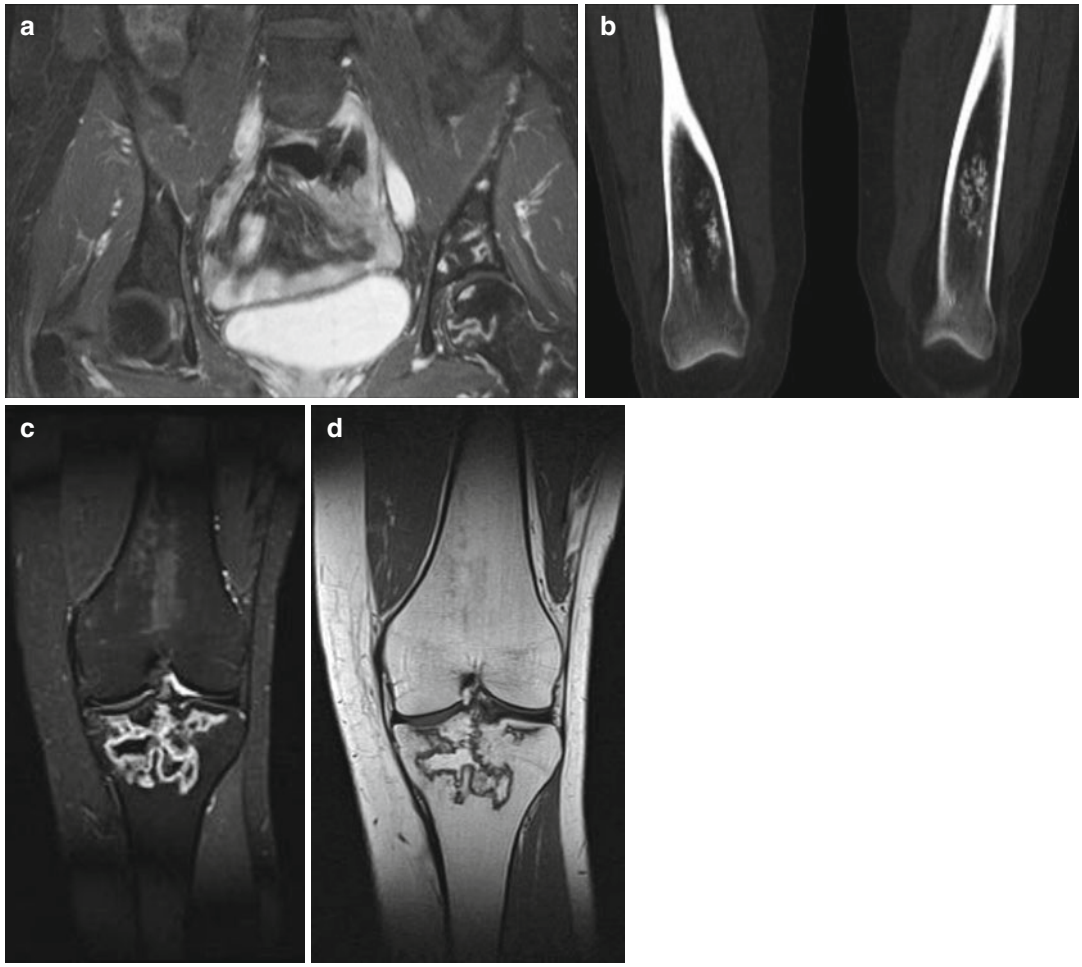


**Fig. 13** BM infarction. (**a**) Curvilinear signal intensity in the pelvis and femoral head following a patient with disseminated metastatic disease and chemotherapy. (**b**) CT, calcified demarcation of old marrow infarcts. (**c**, **d**) MR of tibial head infarcts demonstrates peripheral enhancement of necrotic tissue with central T1w hyperintense fat signal (Courtesy: Dr. B. Jobke for Springer publication)

regions of hips, shoulders, and knees, as well as the metaphysis of long bones (Ollivier et al. 2006) (Figs. 13 and 14).

Early forms of AVN are characterized by diffuse marrow edema. T2-hyperintense areas of edema may be extensive and are nonspecific in their MR appearance. Steroid-related causes for edema-like signal changes can be occult insufficiency fractures or osteomyelitis; therefore, patients need to be kept under surveillance.

The appearance in mature stages of AVN is equal to idiopathic avascular necrosis, for detailed description we refer to the specialty literature. Bone marrow infarcts in the spine under steroids and/or chemotherapy are rare and frequently associated with underlying systemic lymphoproliferative (e.g., lymphomas) (Tang et al. 2007) or hematological disorders such as leukemia, sickle-cell anemia, or thalassemia. This makes their primary cause difficult to identify. Their appearance in the spine is very variable, often multisegmental in the central part of the vertebral body with an oval morphology. Peripheral rim enhancement can be seen on T1-weighted fat-saturated post Gd-enhanced images.

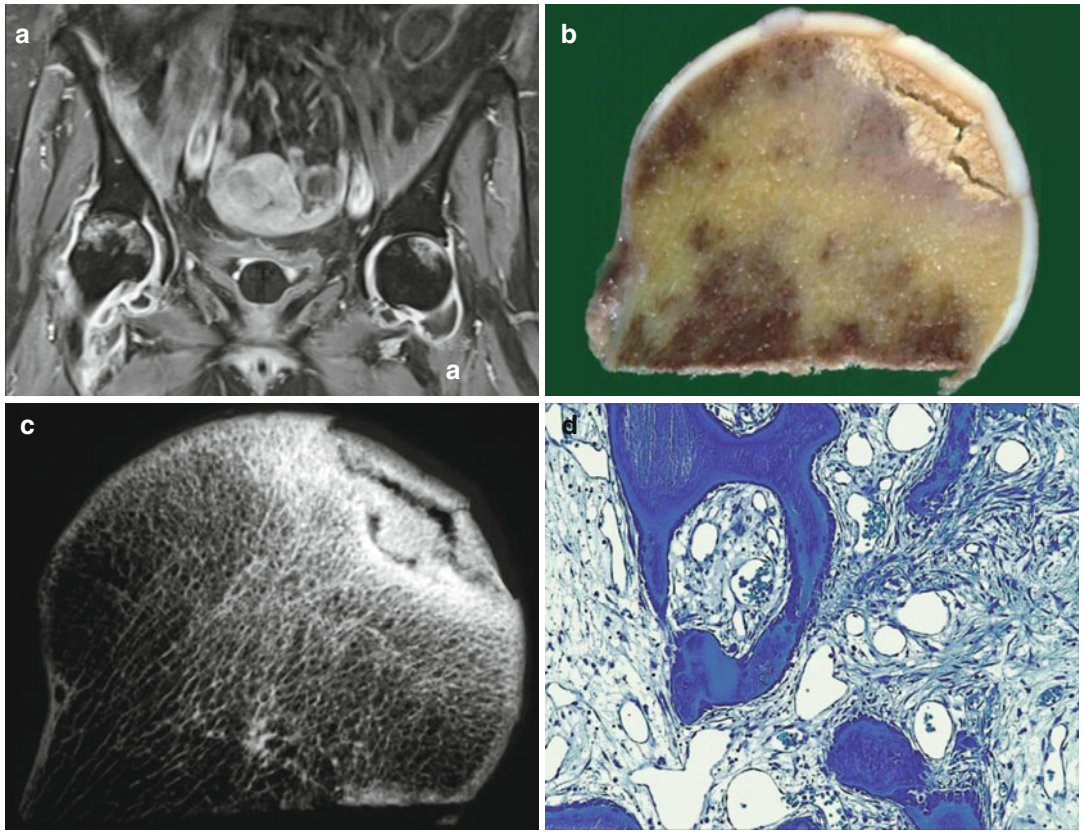


**Fig. 14** MR of bilateral femoral head osteonecrosis. (**a**) Bilateral subchondral signal increase in T1w fat-saturated Gd-enhanced images. (**b**–**d**) Specimen/section radiography/ histology: (**b**) subchondral necrotic zone (*yellow*) with fracture line (**c**) with sclerotic borders and (**d**) reactive fibrosis and bone remodeling from peripheral zone (Courtesy: Dr. B. Jobke for Springer publication)

## 5.7 Immunosuppressive Drugs and Infection

Chemotherapy and immunosuppressive drugs compromise the immune system and increase the risk for secondary infections.

Following intensive chemotherapy, granulocytopenic patients can develop multifocal osteomyelitis. In cancer patients with good surveillance, this is rarely observed. In particular, however, elderly, immunocompromised patients, diabetics, and intravenous drug users are at increased risk of developing hematogenous spondylodiscitis (Calderone and Larsen 1996; Kourbeti et al. 2014). Also, the sites of avascular necrosis are at risk of hosting osteomyelitis. This is not uncommonly seen in patients with extensive AVN irrespective of the cause.

Patients on disease-modifying antirheumatic drugs (DMARDs) have an overall elevated risk of 1.5× to acquire an infection anywhere in the body (Zink et al. 2014). A number of new agents to track target cells are under investigation, among them leukocytes labeled cells to specifically track inflammation (Daldrup-Link et al. 2009). Proof for clinical benefit has yet to been performed. Thus, conventional MR sequences, including gadolinium-enhanced T1-weighted fat-suppressed images, scintigraphy, and PET are the mainstay to verify or rule out an infectious process of the bone marrow (Fig. 15).

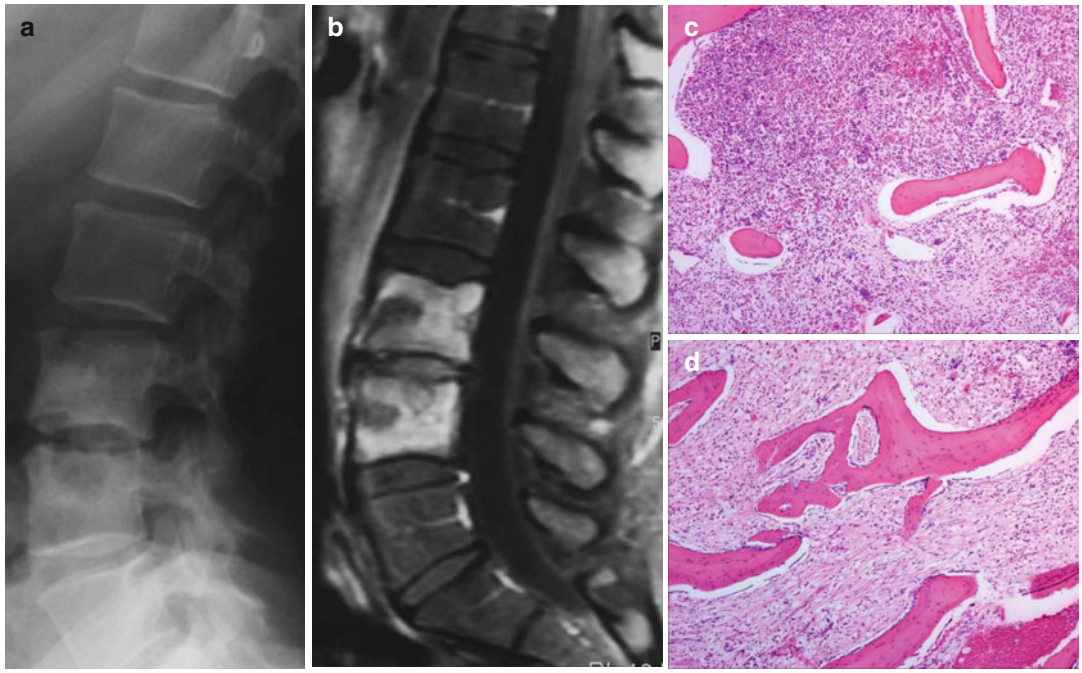


**Fig. 15** A 13-year-old girl with chronic sclerosing spondylodiscitis of L3/4. (**a**) Lateral spine radiograph shows endplate sclerosis L4/5 with (**b**) pronounced Gd enhancement throughout the intervertebral disk and vertebrae. (**c**) Histology shows some leukocytes and massive lympho- and plasmocyte infiltrates with (**d**) sclerosis and fibrosis (HE stain) (Courtesy: Dr. B. Jobke for Springer publication)

## 6 Skeletal Effects of Chemotherapeutic Agents and Related Substances

### 6.1 Methotrexate Osteopathy

In children, methotrexate can cause osteopenia, severe bone pain, and metaphyseal insufficiency fractures (Schwartz and Leonidas 1984).

### 6.2 Aromatase Inhibitors

In breast cancer treatment, both hormonal therapy with aromatase inhibitors in postmenopausal women and chemotherapy-induced ovarian failure in premenopausal women can cause significant loss of bone mass, increasing the risk of fractures (Hirbe et al. 2006).

A number of other drugs interfere and damage other organ functions that are related to bone homeostasis. Vincristine, an antimetabolite, has a neurotoxic potential that may result in neuropathic arthropathy (Charcot-type). Isofosfamid has a known nephrotoxicity leading to a diminished phosphate reabsorption that results in hypophosphatemic rickets.

## 7 Osteonecrosis of the Jaw and Biphosphonates

Bisphosphonates (BP) are potent inhibitors of tumor-induced osteoclast-mediated bone resorption. BP are used as adjuvant therapy for the treatment of tumor-induced hypercalcemia and metastatic bone pain and their complications. With widespread use and long-term administration of BP, cases of osteonecrosis of the jaw (ONJ) are increasingly reported (Solomon et al. 2013). Oversuppression of bone turnover and antiangiogenic effects of BP are considered to be contributing factors. Concomitant chemotherapy and corticosteroid treatment, in particular, may

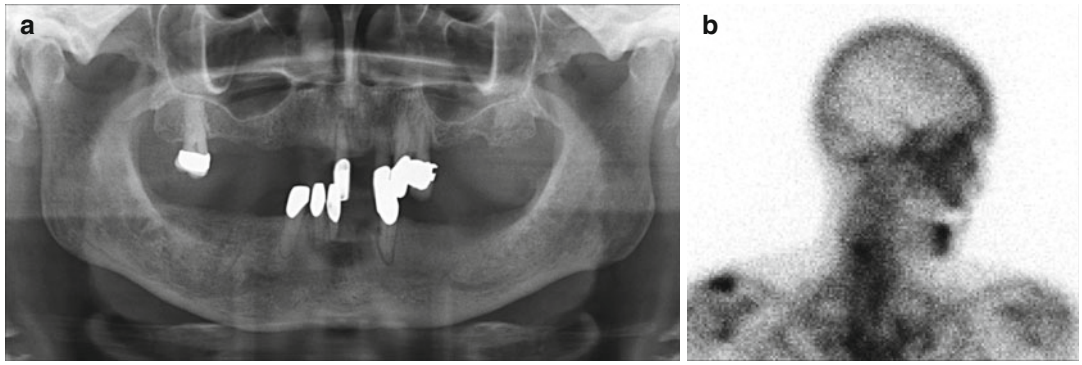


**Fig. 16** ONJ. A 60-year-old patient following BP and denosumab therapy with (**a**) radiographic lucency in toothless region 14 and 13 with correlating (**b**) scintigraphic uptake in the anterior mandibular due to focal reactive bone remodeling (Courtesy: Dr. B. Jobke for Springer publication)

result in immunosuppression and thereby predispose to ongoing local sepsis following dental procedures (Khosla et al. 2008). MRI features are unspecific with T1w signal decrease. CT provides better delineation of bony reactions, and scintigraphy has the highest sensitivity in detecting osseous inflammatory changes (Fig. 16).

Another complication of bisphosphonate therapy nowadays more frequently observed is the subtrochanteric transverse femur fracture, secondary to loss of elasticity of bone treated with bisphosphonates.

## 8 Bone Marrow/Stem Cell Transplantation and Increased Hematopoiesis

Immediately after transplantation, bone marrow edema is seen as low T1 signal and increased T2 signal. Usually it presents in bilateral and symmetric distribution, T1-weighted signal intensity higher than that of muscle. Persisting focal red bone marrow accumulations initially or long after bone marrow transplantation have been described.

Within 3 months and up to 14 months after bone marrow transplantation, a characteristic band pattern in the vertebral body with an intermediate signal intensity adjacent to the endplates and a central zone bright on T1-weighted images can be seen (Stevens et al. 1990). Others could not confirm this finding of "band pattern" (Pereira et al. 1999) and describe a more "mottled" appearance. Kauczor et al. found even 2 years after autologous blood stem cell transplantation, including total body irradiation and myeloablative chemotherapy, a persistent signal increase on T1-weighted images in 10 patients compared to baseline (Kauczor et al. 1993) (Fig. 17).

Marked hematopoiesis increases the amount of red marrow, resembling recurrent tumoral disease. USPIO-enhanced MRI can differentiate these from tumor deposits as cells of the reticuloendothelial system are present in the reconverted marrow but not present/substantially reduced in tumor deposits (Daldrup-Link et al. 2009).

## 9 Chronic Blood Transfusions/ Epo and Iron Deposits

In the absence of iron-chelation treatment, chronically transfused patients are predisposed to accumulation of hemoglobin degradation products, especially iron, in bone marrow and other organs, due to increased hemolysis. The same phenomenon is observed in 38.5 % of children receiving bone marrow transplantation (Kornreich et al. 1997). At the joint level, this is a factor predisposing to degenerative osteoarthritis. In addition, these patients are at risk of developing osteonecrosis, growth disturbances, infection, and crystal deposition diseases.

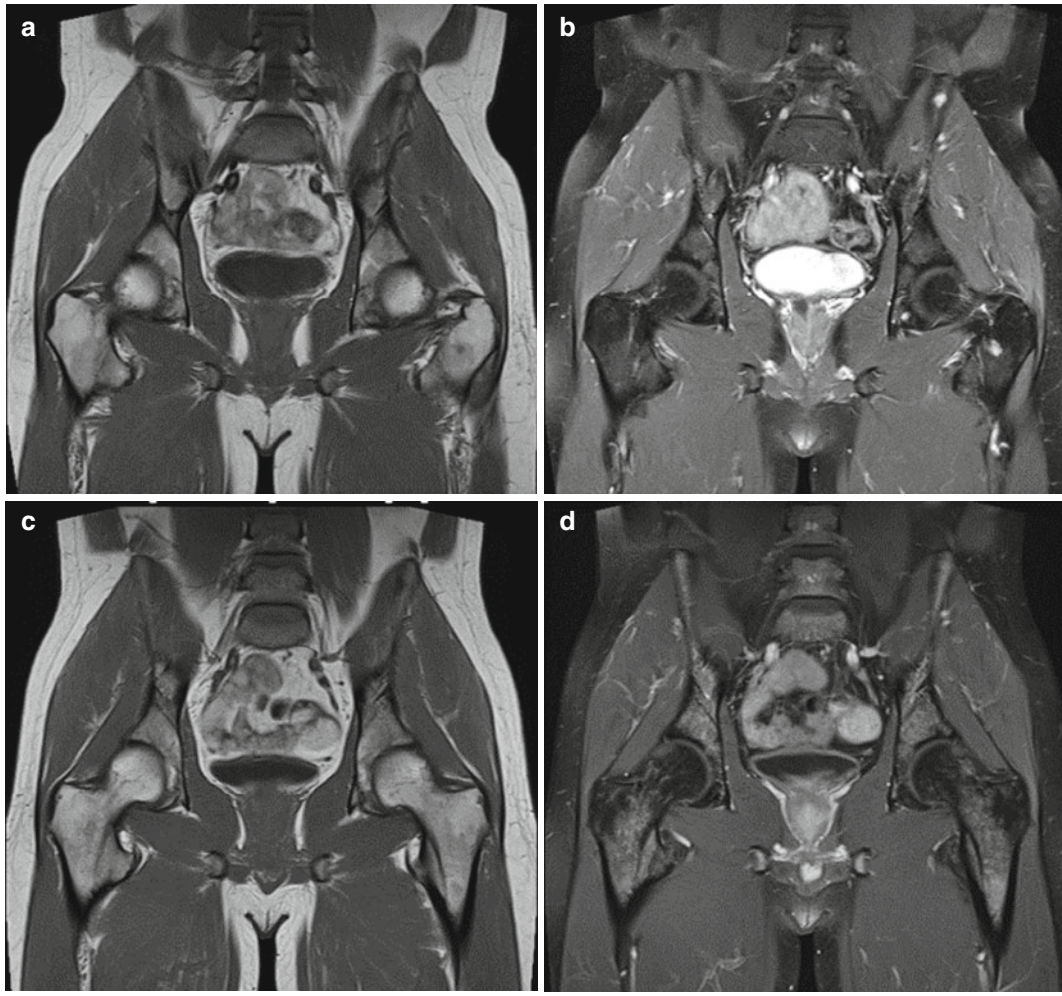


**Fig. 17** BM transplant in a 28-year-old patient with Ewing sarcoma (**a**–**d**). The images show consecutive native T1w- and T1w fat-saturated images post gadolinium from (**a+b**) following 10/2013 and (**c+d**) following 1/2014 a 6th cycle of VIDE (EWING 2008 protocol) plus treosulfan, melphalan, and a BM transplant 1/2014 with marked BM contrast enhancement in the pelvis and femora, less obvious in the native T1w image and signal loss (Courtesy: Dr. B. Jobke for Springer publication)

Iron deposits cause a reduction in signal intensity related to a decrease in T1 and T2 relaxation time in the central and peripheral skeleton, involving areas of high red marrow concentration (Fig. 18). Magnetic field heterogeneities induced by iron atoms make gradient-echo sequences more sensitive to identify iron deposits than spin-echo sequences.

Erythropoietin (Epo) stimulates and modulates the terminal survival, growth, and proliferation of erythrocytes precursor. It is used to treat severe anemia caused, for example, by end-stage kidney failure, tumor, or chemotherapy-induced anemia. The target organ of erythropoietin is the bone marrow (Ghanem et al. 2007). A study on 16 patients treated with Epo vs. 16 patients receiving placebo showed, relative to the pretreatment MR, significant signal changes at the spine in a "scattered or homogeneous pattern" after a mean of 6 weeks using T1-weighted SE-(decreased signal), Turbo-STIR-, and opposed-phase images (increased signal), reflecting stimulated erythropoiesis. After 12 weeks, the vertebral bone marrow signal return to pre-Epo baseline values (Ghanem et al. 2007).

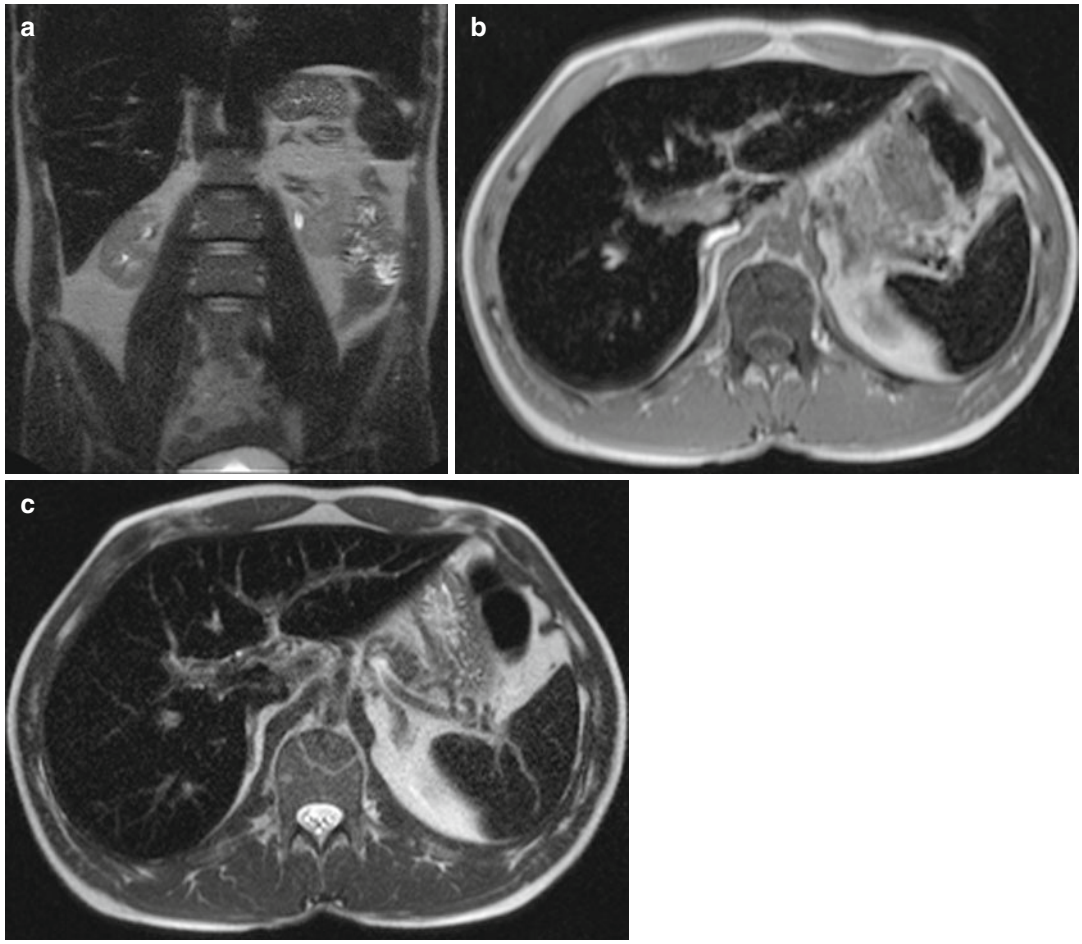


**Fig. 18** BM siderosis. A 40-year-old patient with evident siderosis of BM, liver, and spleen with marked signal drop in T1-(*b*) and T2w images (**a+c**), following multiple blood transfusions (Courtesy: Dr. B. Jobke for Springer publication)

Anemia itself has a wide range of bone marrow changes including increased hematopoiesis, resulting in reconversion or delayed conversion, and, in severe cases, bone marrow expansion and extramedullary hematopoiesis. As a consequence of widening of the medullary spaces and thinning of the cortical bone, the incidence of insufficiency fractures is also increased (Noebauer-Huhmann and Uffmann 2012).

## 9.1 Iron-Chelation Therapy

Prevention of iron overload can be performed by iron chelation with desferrioxamine (DFX) and deferiprone. However, these drugs may also cause toxic skeletal changes.

Dysplastic changes have been described in approximately one-third of these patients. Diffuse vertebral flattening (platyspondyly) in the thoracic and lumbar spine can be observed and about one-third of the children, in whom desferrioxamine therapy was initiated in early childhood, show growth retardation (Noebauer-Huhmann and Uffmann 2012). Bone marrow infarcts and epiphyseal osteonecrosis are observed less frequently.

**Conclusion**

A general understanding of the normal bone marrow composition and dynamic,

age-dependent changes are essential in order to appreciate often subtle changes in cellular composition under the influence of cancer treatment.

Awareness of short and potential long-term secondary chemotherapeutic effects on normal bone marrow is key for the correct interpretation of bone marrow signal changes in cancer patients. Bone marrow edema, hypo- or aplasia, reconversion, and necrosis are the most frequent signs associated with a broad spectrum of chemotherapeutic agents and their additives such as cortisone or G-CSF. Without the knowledge of clinical information about the timeline of chemotherapy and add-ons, the interpretation of suspicious bone marrow signal changes remains a tenuous task.

Aside from conventional spin-echo sequences, several newer MR techniques (e.g., GE, CSI, DWI, DCE, and MRS) support the interpretation of benign and malignant bone marrow changes.

Still, the detection of chemotherapy specific bone marrow changes is challenging and oftentimes unspecific. This demonstrates the need for more studies using latest imaging protocols in the enlarging field of oncological radiology.

## References


Altehoefer C, Laubenberger J, Lange W, Kraus A, Allmann KH, Uhrmeister P, Langer M (1997) Prospective evaluation of bone marrow signal changes on magnetic resonance tomography during high-dose chemotherapy and peripheral blood stem cell transplantation in patients with breast cancer. Invest Radiol 32:613–620

Altehoefer C, Bertz H, Ghanem NA, Langer M (2001) Extent and time course of morphological changes of bone marrow induced by granulocyte-colony stimulating factor as assessed by magnetic resonance imaging of healthy blood stem cell donors. J Magn Reson Imaging 14:141–146

Bartl R (2012) Histology of normal bone and bone marrow and their main disorders. In: Baur-Melnyk A (ed) Medical radiology. Springer, Berlin/Heidelberg, pp 3–20

Baur A, Stabler A, Bartl R, Lamerz R, Scheidler J, Reiser M (1997) MRI gadolinium enhancement of bone marrow: age-related changes in normals and in diffuse neoplastic infiltration. Skeletal Radiol 26:414–418

Berger FH, van Dijke CF, Maas M (2009) Diffuse marrow changes. Semin Musculoskelet Radiol 13:104–110

Berman E, Nicolaides M, Maki RG, Fleisher M, Chanel S, Scheu K, Wilson BA, Heller G, Sauter NP (2006) Altered bone and mineral metabolism in patients receiving imatinib mesylate. N Engl J Med 354: 2006–2013

Bredella MA (2010) Perspective: the bone-fat connection. Skeletal Radiol 39:729–731

Burton C, Azzi A, Kerridge I (2002) Adverse events after imatinib mesylate therapy. N Engl J Med 346: 712–713

Calderone RR, Larsen JM (1996) Overview and classification of spinal infections. Orthop Clin North Am 27:1–8

Campiotti L, Codari R, Appio L, Ultori C, Solbiati F, Maria GA, Venco A (2007) Bone marrow necrosis related to imatinib mesylate therapy for cml bilineal blast crisis. Leuk Res 31:1768–1770

Carroll KW, Feller JF, Tirman PF (1997) Useful internal standards for distinguishing infiltrative marrow pathology from hematopoietic marrow at MRI. J Magn Reson Imaging 7:394–398

Daldrup-Link HE, Henning T, Link TM (2007) MR imaging of therapy-induced changes of bone marrow. Eur Radiol 17:743–761

Daldrup-Link HE, Mohanty A, Cuenod C, Pichler B, Link T (2009) New perspectives on bone marrow contrast agents and molecular imaging. Semin Musculoskelet Radiol 13:145–156

Dietrich O, Biffar A, Reiser MF, Baur-Melnyk A (2009) Diffusion-weighted imaging of bone marrow. Semin Musculoskelet Radiol 13:134–144

Dreyer Z, Blah J, Bleyer A (2005) Late effects of childhood cancers and its treatment. In: Principles and practice of pediatric oncology. Lippincott Williams & Wilkins, Philadelphia, pp 1431–1461

Duong S, Sallis JG, Zee SY (2004) Malignant fibrous histiocytoma arising within a bone infarct in a patient with sickle cell trait. Int J Surg Pathol 12:67–73

Ghanem N, Lerche A, Lohrmann C, Altehoefer C, Henke M, Langer M (2007) Quantitative and semiquantitative evaluation of erythropoietin-induced bone marrow signal changes in lumbar spine MRI in patients with tumor anemia. Onkologie 30:303–308

Gold GE, Han E, Stainsby J, Wright G, Brittain J, Beaulieu C (2004) Musculoskeletal MRI at 3.0 T: relaxation times and image contrast. AJR Am J Roentgenol 183:343–351

Hall E (2011) Radiobiology for the radiologist. Lippincott Williams & Wilkins, Philadelphia

Hanna SL, Fletcher BD (2004) Musculoskeletal effects of therapy in patients treated for hematological malignancies. In: Guermazi A (ed) Radiological imaging in hematological malignancies, Medical radiology. Springer, Berlin/Heidelberg, pp 485–509

Hillengass J, Bauerle T, Bartl R, Andrulis M, McClanahan F, Laun FB, Zechmann CM, Shah R, Wagner-Gund B, Simon D, Heiss C, Neben K, Ho AD, Schlemmer HP, Goldschmidt H, Delorme S, Stieltjes B (2011a) Diffusion-weighted imaging for non-invasive and

quantitative monitoring of bone marrow infiltration in patients with monoclonal plasma cell disease: a comparative study with histology. Br J Haematol 153: 721–728

Hillengass J, Stieltjes B, Bauerle T, McClanahan F, Heiss C, Hielscher T, Wagner-Gund B, Habetler V, Goldschmidt H, Schlemmer HP, Delorme S, Zechmann CM (2011b) Dynamic contrast-enhanced magnetic resonance imaging (DCE-MRI) and diffusion-weighted imaging of bone marrow in healthy individuals. Acta Radiol 52:324–330

Hirbe A, Morgan EA, Uluckan O, Weilbaecher K (2006) Skeletal complications of breast cancer therapies. Clin Cancer Res 12:6309s–6314s

Hwang S, Panicek DM (2007a) Magnetic resonance imaging of bone marrow in oncology, part 1. Skeletal Radiol 36:913–920

Hwang S, Panicek DM (2007b) Magnetic resonance imaging of bone marrow in oncology, part 2. Skeletal Radiol 36:1017–1027

Karmazyn B, Cohen MD, Jennings SG, Robertson KA (2012) Marrow signal changes observed in follow-up whole-body MRI studies in children and young adults with neurofibromatosis type 1 treated with imatinib mesylate (Gleevec) for plexiform neurofibromas. Pediatr Radiol 42:1218–1222

Kauczor HU, Brix G, Dietl B, Jarosch K, Knopp MV, van Kaick G (1993) Bone marrow after autologous blood stem cell transplantation and total body irradiation: magnetic resonance and chemical shift imaging. Magn Reson Imaging 11:965–975

Khosla S, Burr D, Cauley J, Dempster DW, Ebeling PR, Felsenberg D, Gagel RF, Gilsanz V, Guise T, Koka S, McCauley LK, McGowan J, McKee MD, Mohla S, Pendrys DG, Raisz LG, Ruggiero SL, Shafer DM, Shum L, Silverman SL, Van Poznak CH, Watts N, Woo SB, Shane E (2008) Oral bisphosphonate-induced osteonecrosis: risk factors, prediction of risk using serum CTX testing, prevention, and treatment. J Oral Maxillofac Surg 66:1320–1321

Kornreich L, Horev G, Yaniv I, Stein J, Grunebaum M, Zaizov R (1997) Iron overload following bone marrow transplantation in children: MR findings. Pediatr Radiol 27:869–872

Kourbeti IS, Ziakas PD, Mylonakis E (2014) Biologic therapies in rheumatoid arthritis and the risk of opportunistic infections: a meta-analysis. Clin Infect Dis 58:1649–1657

Lang P, Fritz R, Vahlensieck M, Majumdar S, Berthezene Y, Grampp S, Genant HK (1992) Residual and reconverted hematopoietic bone marrow in the distal femur. Spin-echo and opposed-phase gradient-echo MRT. Rofo 156:89–95

Layer G, Sander W, Traber F, Block W, Ko Y, Ziske CG, Konig R, Vahlensieck M, Schild HH (2000) The diagnostic problems in magnetic resonance tomography of the bone marrow in patients with malignomas under G-CSF therapy. Radiologe 40:710–715

Liney GP, Bernard CP, Manton DJ, Turnbull LW, Langton CM (2007) Age, gender, and skeletal variation in bone marrow composition: a preliminary study at 3.0 Tesla. J Magn Reson Imaging 26:787–793

Matsue K, Takeuchi M, Koseki M, Uryu H (2006) Bone marrow necrosis associated with the use of imatinib mesylate in a patient with Philadelphia chromosome-positive acute lymphoblastic leukemia. Ann Hematol 85:542–544

Noebauer-Huhmann I-M, Uffmann M (2012) Anemias and bone marrow insufficiency. In: Baur-Melnyk A (ed) Medical radiology. Springer, Berlin/Heidelberg, pp 193–220

Ollivier L, Gerber S, Vanel D, Brisse H, Leclere J (2006) Improving the interpretation of bone marrow imaging in cancer patients. Cancer Imaging 6:194–198

Padhani AR, Koh DM, Collins DJ (2011) Whole-body diffusion-weighted MR imaging in cancer: current status and research directions. Radiology 261:700–718

Padhani AR, van Ree K, Collins DJ, D'Sa S, Makris A (2013) Assessing the relation between bone marrow signal intensity and apparent diffusion coefficient in diffusion-weighted MRI. AJR Am J Roentgenol 200:163–170

Patsch JM, Li X, Baum T, Yap SP, Karampinos DC, Schwartz AV, Link TM (2013) Bone marrow fat composition as a novel imaging biomarker in postmenopausal women with prevalent fragility fractures. J Bone Miner Res Aug;28(8):1721–1728. doi: 10.1002/jbmr.1950

Pereira PL, Schick F, Einsele H, Farnsworth CT, Kollmansberger C, Mattke A, Duda SH, Claussen CD (1999) MR tomography of the bone marrow changes after high-dosage chemotherapy and autologous peripheral stem-cell transplantation. Rofo 170: 251–257

Rosoff PM (2006) The two-edged sword of curing childhood cancer. N Engl J Med 355:1522–1523

Schwartz AM, Leonidas JC (1984) Methotrexate osteopathy. Skeletal Radiol 11:13–16

Shapiro MD (2006) MR imaging of the spine at 3 T. Magn Reson Imaging Clin N Am 14:97–108

Shellock FG, Morris E, Deutsch AL, Mink JH, Kerr R, Boden SD (1992) Hematopoietic bone marrow hyperplasia: high prevalence on MR images of the knee in asymptomatic marathon runners. AJR Am J Roentgenol 158:335–338

Solomon DH, Mercer E, Woo SB, Avorn J, Schneeweiss S, Treister N (2013) Defining the epidemiology of bisphosphonate-associated osteonecrosis of the jaw: prior work and current challenges. Osteoporos Int 24:237–244

Stevens SK, Moore SG, Amylon MD (1990) Repopulation of marrow after transplantation: MR imaging with pathologic correlation. Radiology 175:213–218

Tamura T, Tasaka T, Fujimoto M, Matsuhashi Y, Fukumot T, Mano S, Kuwajima M, Nagai M (2004) Massive bone marrow necrosis in a patient with chronic myelocytic leukemia following imatinib mesylate therapy. Haematologica 89:ECR32

Tang YM, Jeavons S, Stuckey S, Middleton H, Gill D (2007) MRI features of bone marrow necrosis. AJR Am J Roentgenol 188:509–514

Travis LB, Demark WW, Allan JM, Wood ME, Ng AK (2013) Aetiology, genetics and prevention of secondary neoplasms in adult cancer survivors. Nat Rev Clin Oncol 10:289–301

Umans H, Haramati N, Flusser G (2000) The diagnostic role of gadolinium enhanced MRI in distinguishing between acute medullary bone infarct and osteomyelitis. Magn Reson Imaging 18:255–262

Vahlensieck M, Schmidt HM (2000) The normal bone marrow and its variations in MRT. Radiologe 40:688–693

Van Berg BC, Omnoumi P, Galant C, Michoux N, Lecouvet FE (2012) MR imaging of the normal bone marrow and normal variants. In: Baur-Melnyk A (ed) Medical radiology. Springer, Berlin/Heidelberg, pp 21–48

van Kaick G, Delorme S (2008) Therapy-induced effects in normal tissue. Radiologe 48:871–880

Vande Berg BC, Malghem J, Lecouvet FE, Devogelaer JP, Maldague B, Houssiau FA (1999) Fat conversion of femoral marrow in glucocorticoid-treated patients: a cross-sectional and longitudinal study with magnetic resonance imaging. Arthritis Rheum 42:1405–1411

Vande Berg BC, Lecouvet FE, Galant C, Simoni P, Malghem J (2009) Normal variants of the bone marrow at MR imaging of the spine. Semin Musculoskelet Radiol 13:87–96

Vanel D, Bonvalot S, Pechoux CL, Cioffi A, Domont J, Cesne AL (2007) Imatimid-induced bone marrow necrosis detected on MRI examination and mimicking bone metastases. Skeletal Radiol 36:895–898

Wasser K, Moehler T, Neben K, Nosas S, Heiss J, Goldschmidt H, Hillengass J, Duber C, Kauczor HU, Delorme S (2004) Dynamic MRI of the bone marrow for monitoring multiple myeloma during treatment with thalidomide as monotherapy or in combination with CED chemotherapy. Rofo 176:1285–1295

Wood ME, Vogel V, Ng A, Foxhall L, Goodwin P, Travis LB (2012) Second malignant neoplasms: assessment and strategies for risk reduction. J Clin Oncol 30:3734–3745

Zhao J, Krug R, Xu D, Lu Y, Link TM (2009) MRI of the spine: image quality and normal-neoplastic bone marrow contrast at 3 T versus 1.5 T. AJR Am J Roentgenol 192:873–880

Zink A, Manger B, Kaufmann J, Eisterhues C, Krause A, Listing J, Strangfeld A (2014) Evaluation of the RABBIT Risk Score for serious infections. Ann Rheum Dis 73:1673–1676

# Part IX

# Liver and Gastrointestinal

# Imaging of Gastrointestinal Complications and Toxicity Following Tumor Therapy

Chitra Viswanathan

## Contents



C. Viswanathan, MD
Division of Diagnostic Imaging, Department of Diagnostic Radiology, University of Texas MD Anderson Cancer Center, Houston, TX, USA
e-mail: chitra.viswanathan@mdanderson.org

**Abstract**

With the recent advances in drug therapy, it is more important than ever to understand the possible gastrointestinal complications of the different chemotherapeutic agents and their imaging manifestations. The targeted agent bevacizumab causes delayed wound healing, perforation, and fistulae. Enterocolitis due to immune-modulating agents such as ipilimumab requires rapid diagnosis and treatment in order to prevent bowel damage. Splenic side effects such as splenomegaly and rupture can occur with chemotherapy. Pancreatitis can occur with the targeted agents sunitinib and sorafenib. Changes to the liver due to oxaliplatin may have adverse effects on plans for surgical resection and should be conveyed to the clinician. Complications in the bowel due to radiation include stricture, enteritis, and proctitis. Radiation-induced liver disease can be seen after radiation for tumors of the esophagus, pancreas, and stomach. Radiation-induced malignancies can occur any time from a few years to many years after the initial radiation therapy. Many of these treatment-related complications may be clinically occult until late stages. It is imperative that the radiologist be able to recognize the abdominal toxicities of cancer therapy to make a rapid and correct diagnosis and to convey these findings to the clinician to impact management and prevent misdiagnosis.

Med Radiol Diagn Imaging (2014)
DOI: 10.1007/174_2014_1049, © Springer International Publishing Switzerland

## Abbreviations

| | |
|---|---|
| 5-FU | 5-Fluorouracil |
| ATE | Arterial thromboembolism |
| CT | Computed tomography |
| CTLA-4 | Cytotoxic T-lymphocyte-associated protein 4 |
| G-CSF | Granulocyte colony-stimulating factor |
| GI | Gastrointestinal |
| GIST | Gastrointestinal stromal tumor |
| MRI | Magnetic resonance imaging |
| PET-CT | Positron emission tomography/computer tomography |
| PI | Pneumatosis intestinalis |
| TKI | Tyrosine kinase inhibitor |
| VEGF | Vascular endothelial growth factor |
| VEGFR | Vascular endothelial growth factor receptor |
| VTE | Venous thromboembolism |

## 1 Introduction

There continues to be significant scientific advancement in the field of oncology with regard to chemotherapy and radiation, which impacts patient survival. For example, chemotherapy has evolved from the use of conventional agents and single drug therapy to the use of targeted agents and multidrug therapies. However, there are side effects to these therapies that impact patient morbidity and mortality. Imaging, particularly computed tomography (CT), magnetic resonance imaging (MRI), and positron emission tomography/computer tomography (PET-CT), plays a critical role in the management of the oncologic patients. It is imperative that the radiologist be familiar with the mechanism of these therapies and the potential toxicities from chemotherapy and radiation that can be seen on imaging. This chapter will discuss the imaging appearance of the effects and complications of chemotherapy and radiation on the gastrointestinal organs.

## 2 Gastrointestinal (GI) Tract

### 2.1 Chemotherapy

#### 2.1.1 GI Fistula, Perforation, and Delayed Leak

Fistulization, perforation, and delayed anastomotic leak are complications seen with the use of targeted agents such as bevacizumab. The mechanism of action is thought to relate to the inhibition of vascular endothelial growth factor (VEGF) signaling, causing inhibition of angiogenesis, leading to abnormalities of the blood vessels resulting in poor wound healing and fistula formation (Tirumani et al. 2014). Bevacizumab also causes ischemic necrosis through this pathway, leading to perforation (Badgwell et al. 2008). Risk factors include tumors involving the colon, serosal implants, and concurrent or prior chemotherapy and radiation. It can occur at sites of malignancy involved in the gastrointestinal tract, but can also occur in patients treated for malignancy outside the GI tract (Armstrong et al. 2012). Symptoms may include nausea, vomiting, and abdominal pain. CT signs include free air, pneumatosis intestinalis (PI), free fluid, bowel obstruction, and abscess formation (Fig. 1). Clinicians should be alerted as to findings, so they can stop the agent.

#### 2.1.2 Enterocolitis

Cytotoxic, targeted, and immune-modulating drugs can cause diarrhea and inflammation of the colon and small bowel (Parithivel et al. 2011; Teraishi et al. 2008). The mechanism of action is thought to be due to the action of the drug and the target. For example, in ipilimumab, the colitis results from disruption of the GI mucosal immunity due to blockage of the cytotoxic T-lymphocyte-associated protein 4 (CTLA-4). There is a correlation between the development of colitis and response to treatment (Weber et al. 2012).

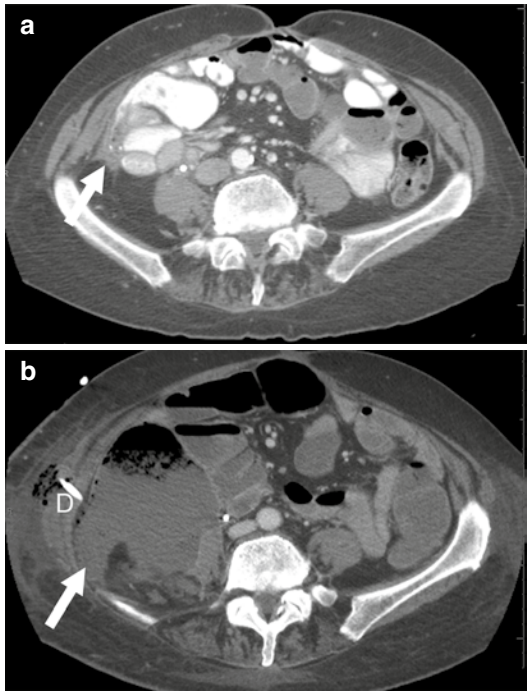


**Fig. 1** Perforation due to bevacizumab. A 60-year-old female with metastatic appendiceal carcinoma developed right lower quadrant abdominal pain, nausea, and vomiting 24 h after the administration of bevacizumab. (**a**) CT prior to therapy shows metastatic serosal implant (*white arrow*) adjacent to the small bowel in the right lower quadrant. (**b**) CT after the administration of bevacizumab shows interval development of perforation and abscess formation (*white arrow*) in the right lower quadrant. The patient underwent percutaneous drainage (*D*); there is air and stranding near the drain. The presence of serosal implants is a risk factor for perforation while on treatment with bevacizumab

Signs of enterocolitis on CT include small bowel submucosal edema, mesenteric engorgement, bowel wall thickening, fluid-fluid levels, and bowel distention (Fig. 2). Enterocolitis can quickly progress to obstruction and perforation, and rapid diagnosis is critical. Ipilimumab-related colitis is potentially fatal, and the clinician must be immediately notified to start treatment early and discontinue the drug (Kim et al. 2013; Gangadhar and Vonderheide 2014).

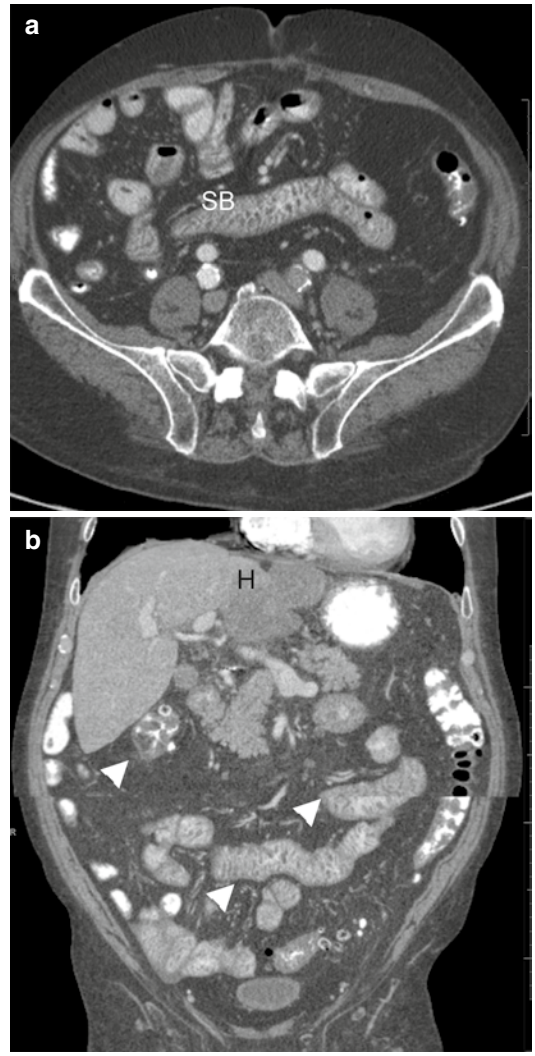


**Fig. 2** Enteritis due to bevacizumab and erlotinib. An 82-year-old male with hepatocellular carcinoma. The patient had failed sorafenib therapy and was treated with 10 cycles of bevacizumab and erlotinib. (**a**) Axial CT shows submucosal edema of the small bowel (*SB*). (**b**) Coronal CT better shows the extent of enteritis and colitis (*arrowheads*). *H* Hepatocellular carcinoma

### 2.1.3 Pneumatosis Intestinalis (PI)

Agents that target VEGF, such as bevacizumab (inhibitor of VEGF-A) and the multitarget/tyrosine kinase inhibitors (TKI) sunitinib and sorafenib (inhibitors of the VEGF-receptor),

have been shown to cause pneumatosis (Jarkowski et al. 2011; Coriat et al. 2011). The inhibition of the VEGF by these drugs leads to decreased vascularity, which causes ischemia of the gastrointestinal cells and leads to PI (Jarkowski et al. 2011; Coriat et al. 2011). PI has also been seen with conventional agents, such as 5-fluorouracil (5-FU) and multidrug induction chemotherapy for leukemia (Shin et al. 2012), and newer drugs such as cetuximab (Yoon et al. 2011). Patients are usually asymptomatic; however, acute symptoms of diarrhea and pain and chronic symptoms of weight loss, bloody stools, and constipation can be seen.

Findings of PI on CT include bowel subserosal and submucosal air cysts, which may also be associated with portal venous air or pneumoperitoneum (Fig. 3) (Ho et al. 2007). Treatment depends on the clinical status of the patient and the extent of the pneumatosis. Cessation of the causative agent usually results in resolution of the PI on subsequent imaging. Awareness of this potential side effect prevents misdiagnosis.

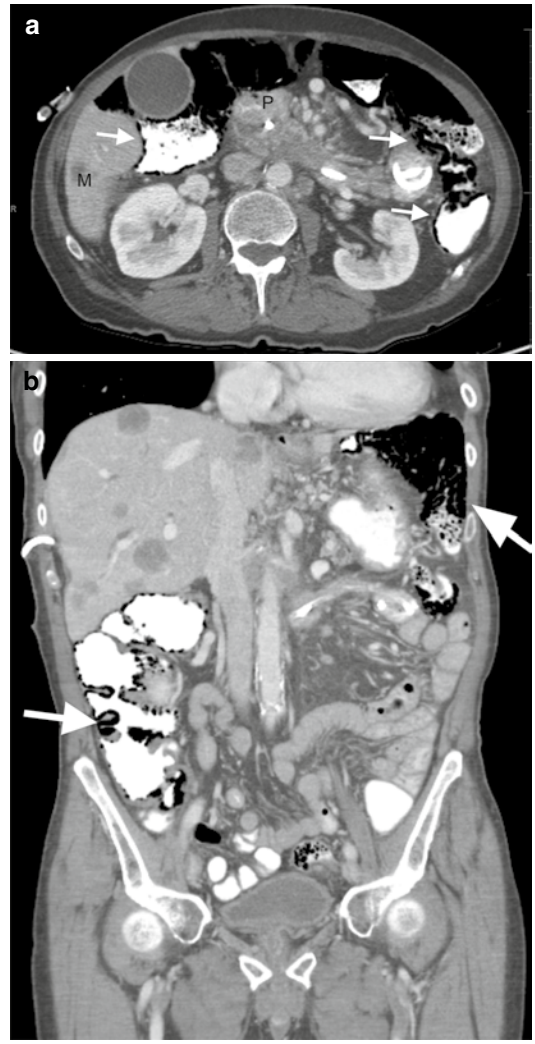


**Fig. 3** Pneumatosis intestinalis due to folinic acid, 5-FU, and oxaliplatin (FOLFOX). A 74-year-old male with pancreatic cancer with liver metastases treated with FOLFOX presented for follow-up imaging. Axial (**a**) and coronal (**b**) CT shows the pancreatic malignancy (*P*) with stent in place and liver metastatic disease (*M*). There is interval development of air cysts within the colonic wall (*arrows*). This can be an incidental finding on restaging imaging, but the clinician should be notified of this finding to ascertain the patient is asymptomatic

## 2.2 Radiation

### 2.2.1 Stomach and Duodenum

The relative immobility of the stomach and duodenum contributes to the susceptibility to radiation, which can cause effects at doses of 50 Gy. Radiation effects include inflammatory change, non-healing ulcers, strictures, and contour deformity (Iyer and Jhingran 2006). On CT, there may be inflammatory change, wall thickening, or surrounding fluid, which may mimic metastatic disease.

### 2.2.2 Bowel

The most common site for radiation injury to the small bowel is the terminal ileum. The small bowel is very radiosensitive, with concurrent chemotherapy increasing the risk for radiation injury. Changes due to radiation include submucosal edema, fistula formation, ulceration, adhesions, and fibrosis. On imaging, there is submucosal edema, wall thickening, and separation of bowel loops in the acute phase; dilation of small bowel loops, fixation of the loops, adhesions, and increase in peritoneal soft tissue can be seen in the chronic phase (Fig. 4) (Libshitz et al. 1996).

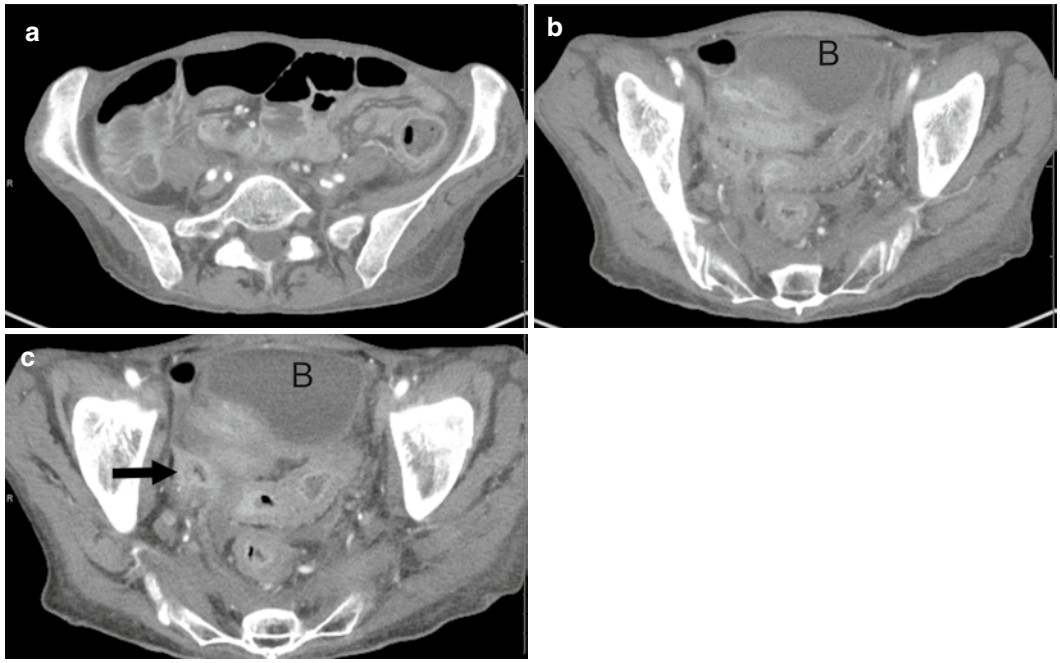


**Fig. 4** Late radiation change in small bowel. A 55-year-old female with cervical cancer treated with radiation and chemotherapy. Two years after the completion of therapy, the patient developed abdominal pain and weight loss. (**a**) Axial CTs **a** and **b** show small dilation and wall thickening of the small bowel along with rectosigmoid wall thickening. There is also increased pelvic soft tissue. *B* bladder. (**b**) Axial CT images **a** and **b** show small bowel dilation and wall thickening, along with rectosigmoid wall thickening. There is also increased pelvic soft tissue. *B* bladder. (**c**) Axial CT scan obtained 2 weeks after **a** and **b** shows interval development of a small walled off collection with air consistent with contained perforation (*arrow*)

The rectum and the sigmoid receive nearly the entire dose of radiation used to treat gynecologic and other malignancies. Radiation proctitis can be acute or chronic and manifest with rectal bleeding (Viswanathan et al. 2014). Imaging findings in early radiation change include wall thickening and adjacent stranding (Fig. 5). Imaging findings of late radiation complication include strictures, fistula, obstruction, and widening of the presacral space (Coia et al. 1995; Maturen et al. 2013).

## 3 Spleen

### 3.1 Chemotherapy

#### 3.1.1 Splenomegaly and Thrombocytopenia

Splenomegaly and thrombocytopenia can occur as a result of the oxaliplatin portion of the FOLFOX treatment for metastatic colorectal cancer. Damage to the liver leads to portal hypertension and subsequent splenomegaly (Slade et al. 2009). The size of the spleen may also be a useful marker for the progression of the hepatic injury (Overman et al. 2010).

Imaging shows an enlarged spleen, without or with other changes of portal hypertension (Fig. 6). Comparison to films over time may help in this diagnosis. This side effect can be insidious and may only be realized when the patient has thrombocytopenia.

#### 3.1.2 Splenic Infarct

Splenic infarct has been reported with bevacizumab, sorafenib, and sunitinib. The mechanism of chemotherapy-related infarct is thought to be multifocal, with the disruption of vascular endothelial cell proliferation, inhibition of smooth

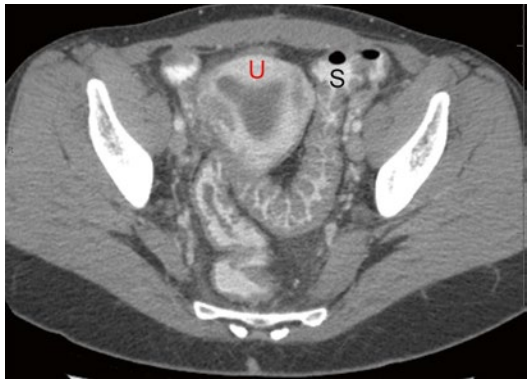


**Fig. 5** Early radiation change in rectosigmoid. A 41-year-old female with stage IB2 poorly differentiated squamous cell carcinoma of the cervix was treated with chemotherapy and radiation. Five months after the completion of radiation, the patient complained of abdominal pain and rapid transit diarrhea. Axial CT scan showed diffuse bowel wall thickening of the rectosigmoid (*S*) compatible with radiation change. *U* uterus with hydrocolpos due to cervical tumor (not shown)

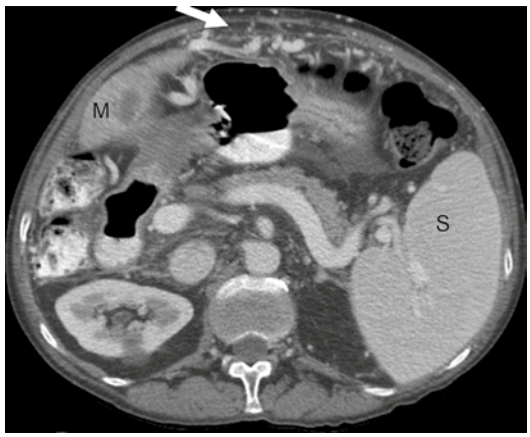


**Fig. 6** Splenomegaly due to FOLFOX. A 59-year-old male with colorectal cancer metastatic to the liver diagnosed 2 years prior and treated with 23 cycles of FOLFOX. CT scan shows enlargement of the spleen (*S*) and splenic vein with formation of collateral vessels (*arrow*). *M* metastatic disease. Treatment with oxaliplatin causes sinusoidal injury to the liver, leading to portal hypertension, ascites, splenomegaly, and collateral vessels. Small-volume ascites is also seen on both images

muscle cell proliferation, and increase in erythropoietin (Kim et al. 2011).

On imaging, new linear or wedge-shaped hypodense areas may be present in the spleen. The patients may or may not be symptomatic.

#### 3.1.3 Splenic Rupture

There are case reports of spontaneous splenic rupture that have been seen in patients treated with induction chemotherapy for leukemia, granulocyte colony-stimulating factor (G-CSF) for neutropenia, and imatinib for gastrointestinal stromal tumor (GIST). Patients will present with symptoms of diffuse abdominal pain and hypotension. Rapid diagnosis and treatment is crucial (Zeidan et al. 2014).

CT imaging findings include hemoperitoneum, high-density fluid or extravasation indicating acute bleeding, low density within the spleen, and perisplenic stranding.

### 3.2 Radiation

The spleen is very radiation sensitive, and alteration in splenic function and atrophy can occur at doses as low as 4–8 Gy. Fibrosis can occur at higher doses.

## 4 Pancreas

### 4.1 Chemotherapy

#### 4.1.1 Pancreatitis/Pancreatic Inflammation

Pancreatitis can occur as a result of treatment with the conventional agents such as vincristine and tamoxifen and is now seen with the newer TKI, such as pazopanib, sunitinib, and sorafenib. Drug-associated pancreatitis is usually mild to moderate and improves with cessation of the drug (Howard et al. 2012).

CT findings may include peripancreatic stranding, peripancreatic fluid +/− ascites, enlargement of the pancreas, and decrease in pancreatic density due to edema (Fig. 7).

Late pancreatic atrophy has been reported with sorafenib. In a case report, two patients treated with sorafenib for more than 2 years developed pancreatic insufficiency. The damage to the pancreas leads to pancreatic exocrine insufficiency, resulting in diarrhea. Volumetric CT showed atrophy with decrease in the size of the pancreas from the time of initiation of the drug (Hescot et al. 2013).

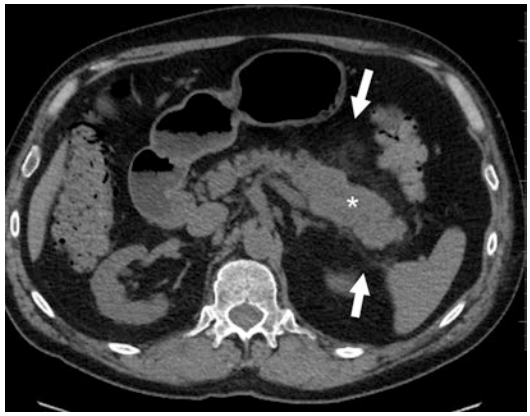

**Fig. 7** Drug-related pancreatitis due to pazopanib. A 56-year-old male with synovial sarcoma of the thigh with lung metastases. The patient had received ifosfamide and adriamycin in the past and recently initiated pazopanib daily for 4 months since the diagnosis of lung metastases. Axial CT after 4 months of pazopanib shows enlargement of the distal portion of the pancreas (*star*) with adjacent peripancreatic stranding (*arrows*), findings suspicious for drug-related pancreatitis

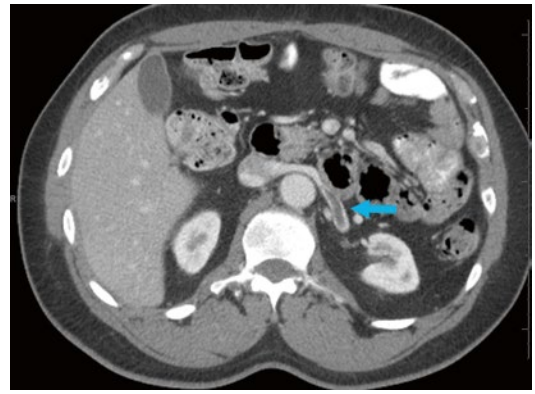

**Fig. 8** Renal vein thrombosis due to regorafenib. A 61-year-old male with metastatic gastrointestinal stromal tumor (GIST) had progression of tumor on imatinib and sunitinib and was switched to regorafenib. Axial CT after 2 months of daily regorafenib shows interval development of filling defect in the left renal vein (*blue arrow*) compatible with thrombus. Regorafenib is a multi-kinase inhibitor with antiangiogenic activity. The timing of therapy and onset of thrombus are helpful in diagnosing chemotherapy-related VTE. The patient was placed on anticoagulation and chemotherapy continued

### 4.2 Radiation

The pancreas is relatively radioresistant. Damage to the acinar cells at higher doses can result in pancreatitis. In the late stage, fibrosis may be present.

## 5 Vessels

### 5.1 Chemotherapy

#### 5.1.1 Hemorrhage/Bleeding

Chemotherapy-related hemorrhage has been seen in patients treated with imatinib for GIST, with an incidence of 5 % (Hecker et al. 2010). The mechanism is thought to be due to tumor-related necrosis. Gastrointestinal and vaginal bleeding has also been associated with the use of the VEGF/VEGFR agents bevacizumab, sorafenib, and sunitinib due to their action on the endothelial cell and disruption of blood vessels. Symptoms may occur as early as 1 day after the administration of the inciting agent and include sudden onset of abdominal pain and hypotension. This is accompanied with a sudden decrease in the hemoglobin and hematocrit.

CT signs of hemorrhage include hemoperitoneum, increase in size of tumor or metastases, and new high- or low-density fluid within or adjacent to the tumor and metastases. The increase in size should not be construed as progression of disease.

#### 5.1.2 Thromboembolism

Chemotherapy can lead to both arterial thromboembolism (ATE) and venous thromboembolism (VTE). ATE has been seen in patients treated with VEGF/VEGFR agents and is mostly seen in the cerebrovascular and cardiac vessels but also can involve the aorta and the vessels of the mesentery and extremities. The incidence of VTE is approximately 1–14 % in patients treated with VEGF/VEGFR inhibitors and TKI, and there is a slightly higher risk in combination therapy (Fig. 8) (Abramson et al. 2013).

### 5.2 Radiation

Radiation vasculopathy may occur at doses of 20 Gy. Acute changes of radiation affect the vessel intima, and chronic changes affect the entire

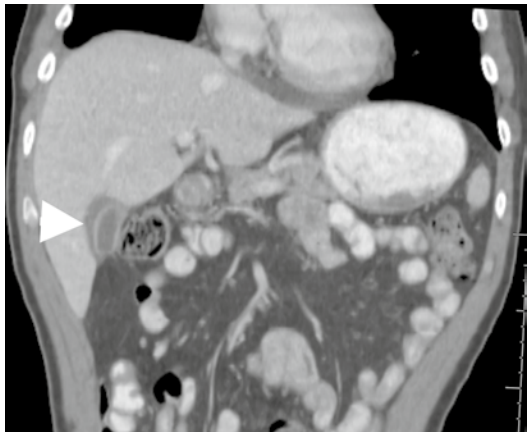

**Fig. 9** Pericholecystic fluid due to everolimus. A 45-year-old male with advanced metastatic renal cell carcinoma treated with daily everolimus ×6 weeks. Restaging coronal CT shows interval development of pericholecystic fluid (*arrowhead*). The development of pericholecystic fluid and ascites can occur as a result of chemotherapy and is not necessarily diagnostic of inflammation or progression of disease

vessel wall. Occlusion of the blood vessels can occur after radiation treatment and may require vascular graft (Maturen et al. 2013).

## 6 Mesentery/Peritoneum

### 6.1 Chemotherapy

#### 6.1.1 Fluid Retention

Fluid retention can be seen as a result of chemotherapy, such as with docetaxel or TKI, due to capillary leak syndrome. It may also be seen because of the side effect of congestive heart failure with drugs such as sunitinib. Patients may present with weight gain, edema, ascites, pleural effusion, pericholecystic fluid, and pericardial effusion (Fig. 9). The development of ascites on follow-up CT is therefore not definitely representative of metastatic disease when patients are on agents such as imatinib (Torrisi et al. 2011).

#### 6.1.2 Increased Retroperitoneal and Mesenteric Opacity

Increase in the opacity of the retroperitoneal and mesenteric fat due to lymphocyte infiltration in patients treated with ipilimumab can occur during any time in the administration of this agent.

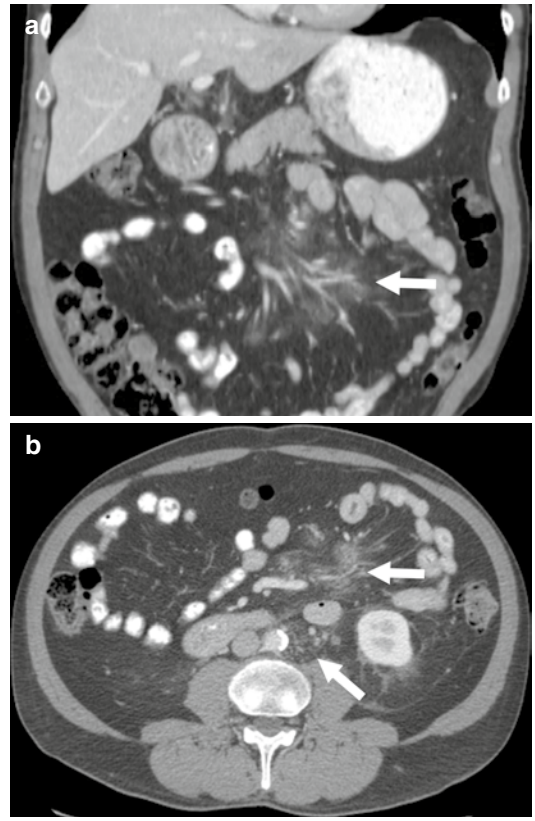


**Fig. 10** Mesenteric and retroperitoneal stranding due to ipilimumab. A 67-year-old male with metastatic melanoma received a total of 11 cycles of ipilimumab and temozolomide. (**a**) Coronal CT after 4 months of chemotherapy shows increased hazy density of the mesenteric fat (*arrow*). (**b**) Axial CT shows increased opacity of the retroperitoneal and mesenteric fat (*arrows*). The patient had skin rash, fatigue, and dyspnea due to therapy, and he was taken off the study 6 months after this scan

This finding is clinically silent, appearing as a new increased retroperitoneal fat opacity finding on CT, and usually resolves spontaneously or after cessation of therapy (Bronstein et al. 2011). CT findings of increased retroperitoneal fat opacity due to therapy may mimic metastatic disease, lymphoma, Castleman's disease, and retroperitoneal fibrosis (Fig. 10).

**Conclusion**

Knowledge of the imaging appearances of the gastrointestinal side effects of chemotherapy and radiation is essential for the radiologist in the assessment of the patient with cancer. Newer chemotherapeutic agents are being

developed to enhance patient survival but come with specific associated toxicities, such as perforation, pancreatitis, and colitis. Complications from radiation can have acute and chronic presentations. By detecting these toxicities early at imaging and even before they are clinically apparent, and then conveying them to the clinician, the radiologist can highly impact patient management and help guide treatment.

## References


Abramson RG, Abramson VG, Chan E et al (2013) Complications of targeted drug therapies for solid malignancies: manifestations and mechanisms. AJR Am J Roentgenol 200:475–483

Armstrong TS, Wen PY, Gilbert MR, Schiff D (2012) Management of treatment-associated toxicites of anti-angiogenic therapy in patients with brain tumors. Neuro Oncol 14:1203–1214

Badgwell BD, Camp ER, Feig B et al (2008) Management of bevacizumab-associated bowel perforation: a case series and review of the literature. Ann Oncol 19: 577–582

Bronstein Y, Ng CS, Hwu P, Hwu W-J (2011) Radiologic manifestations of immune-related adverse events in patients with metastatic melanoma undergoing anti–CTLA-4 antibody therapy. Am J Roentgenol 197: W992–W1000

Coia LR, Myerson RJ, Tepper JE (1995) Late effects of radiation therapy on the gastrointestinal tract. Int J Radiat Oncol Biol Phys 31:1213–1236

Coriat R, Ropert S, Mir O et al (2011) Pneumatosis intestinalis associated with treatment of cancer patients with the vascular growth factor receptor tyrosine kinase inhibitors sorafenib and sunitinib. Invest New Drugs 29:1090–1093

Gangadhar TC, Vonderheide RH (2014) Mitigating the toxic effects of anticancer immunotherapy. Nat Rev Clin Oncol 11:91–99

Hecker A, Hecker B, Bassaly B et al (2010) Dramatic regression and bleeding of a duodenal GIST during preoperative imatinib therapy: case report and review. World J Surg Oncol 8:47

Hescot S, Vignaux O, Goldwasser F (2013) Pancreatic atrophy–a new late toxic effect of sorafenib. N Engl J Med 369:1475–1476

Ho LM, Paulson EK, Thompson WM (2007) Pneumatosis intestinalis in the adult: benign to life-threatening causes. AJR Am J Roentgenol 188:1604–1613

Howard SA, Krajewski KM, Thornton E et al (2012) Decade of molecular targeted therapy: abdominal manifestations of drug toxicities–what radiologists should know. AJR Am J Roentgenol 199:58–64

Iyer R, Jhingran A (2006) Radiation injury: imaging findings in the chest, abdomen and pelvis after therapeutic radiation. Cancer Imaging 6:S131–S139

Jarkowski A 3rd, Hare R, Francescutti V, Wilkinson N, Khushalani N (2011) Case report of pneumatosis intestinalis secondary to sunitinib treatment for refractory gastrointestinal stromal tumor. Anticancer Res 31:3429–3432

Kim SOHS, Baek YH, Lee SW, Han JS, Kim BG, Cho JH, Nam KJ (2011) Splenic infarction associated with sorafenib use in a hepatocellular carcinoma patient. World J Gastroenterol 17:267–270

Kim KW, Ramaiya NH, Krajewski KM et al (2013) Ipilimumab-associated colitis: CT findings. AJR Am J Roentgenol 200:W468–W474

Libshitz HI, DuBrow RA, Loyer EM, Charnsangavej C (1996) Radiation change in normal organs: an overview of body imaging. Eur Radiol 6:786–795

Maturen KE, Feng MU, Wasnik AP et al (2013) Imaging effects of radiation therapy in the abdomen and pelvis: evaluating "innocent bystander" tissues. RadioGraphics 33:599–619

Overman MJ, Maru DM, Charnsangavej C et al (2010) Oxaliplatin-mediated increase in spleen size as a biomarker for the development of hepatic sinusoidal injury. J Clin Oncol 28:2549–2555

Parithivel K, Ramaiya N, Jagannathan JP et al (2011) Everolimus- and temsirolimus-associated enteritis: report of three cases. J Clin Oncol 29:e404–e406

Shin DK, Oh J, Yoon H, Kim JE, Chong SY, Oh D (2012) Asymptomatic pneumatosis intestinalis following chemotherapy for B lymphoblastic leukemia with recurrent genetic abnormalities in an adolescent patient. Korean J Hematol 47:74–76

Slade JH, Alattar ML, Fogelman DR et al (2009) Portal hypertension associated with oxaliplatin administration: clinical manifestations of hepatic sinusoidal injury. Clin Colorectal Cancer 8:225–230

Teraishi F, Shimamura H, Suzuki T et al (2008) Cytomegalovirus colitis after systemic chemotherapy in a patient with recurrent colon cancer: a case report. J Med Case Reports 2:289

Tirumani SH, Shinagare AB, Jagannathan JP, Krajewski KM, Ramaiya NH (2014) Multidetector-row CT of tumour-bowel fistula: experience at a tertiary cancer centre. Clin Radiol 69:e100–e107

Torrisi JM, Schwartz LH, Gollub MJ, Ginsberg MS, Bosl GJ, Hricak H (2011) CT findings of chemotherapy-induced toxicity: what radiologists need to know about the clinical and radiologic manifestations of chemotherapy toxicity. Radiology 258:41–56

Viswanathan AN, Lee LJ, Eswara JR et al (2014) Complications of pelvic radiation in patients treated for gynecologic malignancies. Cancer 120:3870–3883

Weber JS, Kahler KC, Hauschild A (2012) Management of immune-related adverse events and kinetics of response with ipilimumab. J Clin Oncol 30:2691–2697

Yoon S, Hong YS, Park SH, Lee JL, Kim TW (2011) Pneumatosis intestinalis after cetuximab-containing chemotherapy for colorectal cancer. Jpn J Clin Oncol 41:1225–1228

Zeidan AM, Mitchell M, Khatri R et al (2014) Spontaneous splenic rupture during induction chemotherapy for acute myeloid leukemia. Leuk Lymphoma 55:209–212

# Imaging Liver Complications of Cancer Therapy

Sharon Z. Adam, Michal Mauda-Havakuk, Ravit Geva, and Arye Blachar

## Contents




### Abstract

The liver is often affected by the different therapies used to treat malignancies. Hepatic complications can result from systemic chemotherapeutic therapy, external beam irradiation of the liver, transarterial therapies using chemotherapeutic agents or radiation-emitting particles, and ablative techniques.

Systemic chemotherapeutic agents often cause steatosis and steatohepatitis and less frequently cirrhosis, pseudocirrhosis, hepatic veno-occlusive disease, and focal benign lesions such as nodular regenerative hyperplasia, focal



S.Z. Adam
Department of Radiology,
Tel Aviv Sourasky Medical Center,
Tel Aviv 64239, Israel

Department of Diagnostic Radiology,
Northwestern University Feinberg School of Medicine,
Chicago, IL, USA

M. Mauda-Havakuk
Department of Radiology,
Tel Aviv Sourasky Medical Center,
Tel Aviv 64239, Israel

R. Geva
Department of Oncology,
Tel Aviv Sourasky Medical Center,
Tel Aviv 64239, Israel

A. Blachar, MD (✉)
Computed Tomography and Magnetic Resonance Imaging Division, The Tel Aviv University Sackler School of Medicine,
Tel Aviv 64239, Israel

Department of Radiology, Tel Aviv Sourasky Medical Center, Tel Aviv 64239, Israel
e-mail: ablachar@gmail.com


Med Radiol Radiat Oncol (2014)
DOI: 10.1007/174_2014_1042, 

nodular hyperplasia, and peliosis hepatis. When administered transarterially, there can be accidental embolization of other organs, tumor rupture, periportal edema, biliary damage, abscess formation, and hepatic infarction.

Radiation therapy can cause radiation-induced liver disease when administered externally or transarterially. When it is administered transarterially, inadvertent embolization of the cystic artery can occur, resulting in gallbladder ischemia.

Percutaneous ablative techniques (radiofrequency ablation, microwave ablation, ethanol injection, cryoablation, and laser interstitial thermotherapy), due to their invasive nature, may cause similar complications. These include abscess formation, biliary and vascular injury, hepatic infarction, and hepatic insufficiency. When noninvasive high-intensity focused ultrasound is used, complications are less common, mainly thermal damage to adjacent tissues and possibly thermal biliary damage.

## 1 Introduction

The liver is the second most common site for metastatic malignant disease as well as a site of primary malignancy (mostly in cirrhotic patients). Given the livers' role in metabolizing pharmaceutical agents, it is often affected by systemic pharmaceutical therapies used for treatment of malignant hepatic neoplasms leading to systemic and liver-specific complications.

Pharmaceutical agents used in oncology are divided to conventional chemotherapeutic agents and biological agents. Chemotherapeutic agents have been suggested to induce hepatic parenchymal injuries including steatosis, chemotherapy-associated steatohepatitis (CASH), cirrhosis and pseudocirrhosis, and hepatic veno-occlusive disease (HVOD)/sinusoidal obstruction syndrome (SOS). The different agents used to treat primary and secondary hepatic malignancies, such as irinotecan, oxaliplatin, and tamoxifen to name but a few, have different effects on the liver, as will be discussed. The resulting hepatic changes are associated with an increase in postoperative morbidity and mortality, thus demonstrating the importance of close follow-up and evaluation of the extent of the liver damage (Parikh et al. 2003; Zorzi et al. 2007).

Radiation has long been used for treatment of cancer, using nonselective external irradiation of tissues. In recent years, radiation treatments have improved and better irradiation equipment is utilized, now using computed tomography to plan and guide the irradiation treatment. In addition, various types of targeted semi-invasive treatments have been developed for the selective treatment of primary and secondary hepatic lesions, when a surgical approach has been deemed inappropriate.

In recent years, multiple local regional interventional techniques have been employed for the treatment of cancer. These include transarterial chemoembolization and various ablation techniques.

In this chapter, we review the imaging findings of oncological treatment-induced hepatic complications. We will first discuss systemic chemotherapy- and chemoembolization-induced complications. We then discuss the effects of external beam hepatic irradiation and selective radioembolization on the hepatic parenchyma. Finally, we will discuss the imaging findings of targeted hepatic ablation therapy complications.

## 2 Hepatic Complications Due to Systemic Chemotherapy Treatment

### 2.1 Hepatic Steatosis and Steatohepatitis

Nonalcoholic fatty liver disease (NAFLD) is the most common cause of abnormal liver function in adults in the United States. Hepatic steatosis (Fig. 1) may represent the hepatic manifestation of the metabolic syndrome and can lead to steatohepatitis and cirrhosis. The histological definition of hepatic steatosis is infiltration of the hepatocytes by fat droplets. Steatosis severity can be assessed by a reproducible pathological grading system, the nonalcoholic fatty liver dis-

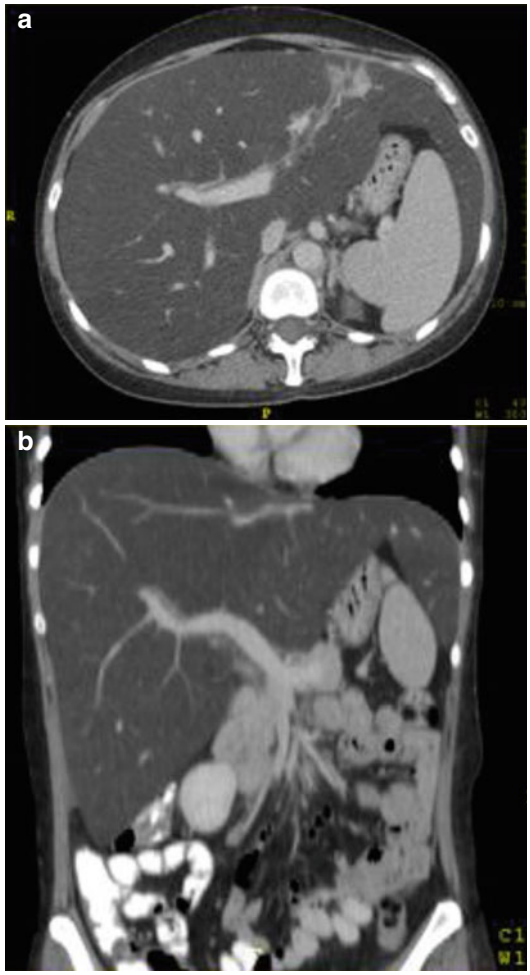


**Fig. 1** (**a**, **b**) *Hepatic steatosis post-chemotherapy*, axial (**a**) and coronal (**b**) post-contrast CT images showing marked hypodensity of the liver parenchyma evident even after contrast injection

ease activity score (NAS) (Robinson et al.). Steatosis is the most common side effect of chemotherapy. Several chemotherapeutic agents such as tamoxifen, irinotecan, 5-fluorouracil, and leucovorin that are used for treating breast and colorectal cancer may cause steatosis (Torrisi et al. 2011; Khan et al. 2009). A study conducted by Jean-Nicolas et al. reported that 8.9 % of 406 patients that underwent hepatic resection for colorectal metastasis between 1992 and 2005 had steatosis on pathological analysis (Vauthey et al. 2006). Miyake et al. reported, using CT criteria, that 15 of 43 patients (34.9 %) with colon cancer treated with 5-fluorouracil developed hepatic steatosis (Miyake et al. 2005). Diagnosing steatosis is especially important in patient with colorectal metastases who are being considered for metastesectomy, because it increases the risk of hepatic failure, especially after hepatic resection. The gold standard for diagnosis is liver biopsy despite its invasiveness and sampling error.

At ultrasound, the normal liver parenchyma has a homogeneous echotexture with echogenicity equal to or slightly greater than that of the renal cortex and spleen. Fatty infiltration increases the liver echogenicity which becomes higher than renal cortical and splenic echogenicities. Sonoelastography is a technique used for measuring hepatic stiffness reflecting hepatic fatty infiltration extent. In transient elastography, a pulse-echo acquisition is performed to follow the propagation of a shear wave and measure its velocity, which is directly related to the tissue stiffness (or elastic modulus). The results are expressed in kilopascals (kPa). The stiffer the tissue, the faster the propagation of the shear wave. Fatty liver has lower values than normal liver tissue.

At CT, the liver attenuation is decreased by fatty infiltration (Fig. 1). Hepatic fatty infiltration is defined by a few methods. It can be represented quantitatively by comparing liver and splenic attenuations on unenhanced exams. A liver-to-spleen attenuation ratio of <0.8 has a high specificity (100 %) for diagnosis of moderate to severe steatosis (Singh et al. 2013). A liver and spleen attenuation difference of at least 10 HU on unenhanced CT, or a liver attenuation of less than 40 HU, is also considered diagnostic (Yajima et al. 1982). Lawrence et al. suggest that diffuse hepatic steatosis can be diagnosed on post-contrast-enhanced scans when hyper-attenuating areas can be seen in locations typical for focal fatty sparing, such as in segment four (Lawrence et al. 2012).

MRI is excellent for detection of hepatic fat even in microscopic quantity. Various techniques like chemical shift imaging (CSI), proton spectroscopy, and MR elastography can be utilized for this purpose. MR elastography is a method

for quantitatively imaging tissue stiffness that requires specific hardware and software. Shear wave motion is produced within the liver and a gradient-echo MR elastography sequence is used to acquire images, showing the shear wave propagation within the liver by encoding tissue motion into the phase of the measured MR signal. The shear wave images are processed to produce quantitative images of hepatic stiffness (elastograms). Chen et al. demonstrated that using MR elastography, differentiating steatosis, steatohepatitis, and fibrosis is possible. Patients with inflammation but without fibrosis have greater liver stiffness than those with simple steatosis but lower stiffness than those with fibrosis (Chen et al. 2011).

Steatohepatitis. Individuals with hepatic steatosis alone are thought to have a benign long-term prognosis. However, up to 25 % of these patients may develop nonalcoholic steatohepatitis (NASH), which may then progress to cirrhosis. The histological features of steatohepatitis include various degrees of steatosis, lobular inflammation, and ballooning of hepatocytes. When these changes are found in association with chemotherapeutic treatment, they are termed CASH (chemotherapy-associated steatohepatitis). Currently, differentiating steatosis and steatohepatitis requires a liver biopsy. New noninvasive techniques are being developed including serologic biomarkers, ultrasound-based transient elastography, and MR elastography.

Reissfelder et al. (2014) reported that inflammatory cells within the liver were significantly more often present in the liver parenchyma and portal fields in patients that received neoadjuvant chemotherapy compared with patients that did not (12.2 % vs 0 %; $P = .008$). Furthermore, moderate to severe steatosis (23.3 % versus 0 %; $P = .01$) and steatohepatitis (15.5 % vs. 0 %; $P = .05$) exclusively existed in chemotherapeutically treated livers. In operated patients steatosis was not associated with postoperative complications, whereas steatohepatitis correlated with morbidity. Another study showed an increased 90-day mortality in cancer patients who had steatohepatitis compared with patients who did not have steatohepatitis (Vauthey et al. 2006). Behrns et al. (1998) and Kooby et al. (2003) reported increased morbidity and mortality rates according to steatosis severity. Unfortunately, these authors did not distinguish between patients with steatosis and those with steatohepatitis.

## 2.2 Liver Parenchymal Injury

Advanced stages of hepatocellular injury may rarely progress to cirrhosis (Fig. 2) or pseudocirrhosis.

Cirrhosis is the final result of chronic damage to the liver from various etiologies, characterized by parenchymal injury leading to extensive fibrosis and nodular regeneration. Usual clinical manifestations result from portal hypertension, portosystemic shunting, and hepatic insufficiency. Common complications are ascites, gastrointestinal bleeding, encephalopathy, and coagulopathy.

At ultrasound, morphological changes associated with cirrhosis can be seen including liver surface irregularity, heterogeneity of liver echotexture, splenomegaly, and left-to-right liver volume redistribution. Color and power Doppler ultrasound are accurate in assessing liver macrovascular anatomy and changes secondary to portal hypertension. Contrast-enhanced ultrasound allows the study of the microvascular component of the hepatic circulation. The interval between the appearance of contrast microbubbles (purely intravascular) in the portal vein (or hepatic artery) and hepatic veins, known as hepatic transit time, shortens progressively as liver fibrosis progresses, due to intrahepatic arteriovenous shunting and arterialization of the liver vasculature. Transient elastography can be used to assess liver stiffness. The normal value is around 5 kPa, whereas in cirrhotic patients, liver stiffness measurements range from 12.5 to 75.5 kPa (Berzigotti and Castera 2013).

CT and MR (Fig. 2) initially show heterogeneity of the hepatic parenchyma and surface nodularity. Morphological changes of cirrhosis include caudate lobe hypertrophy, segmental hypertrophy of the lateral segments (II, III) of the left lobe,

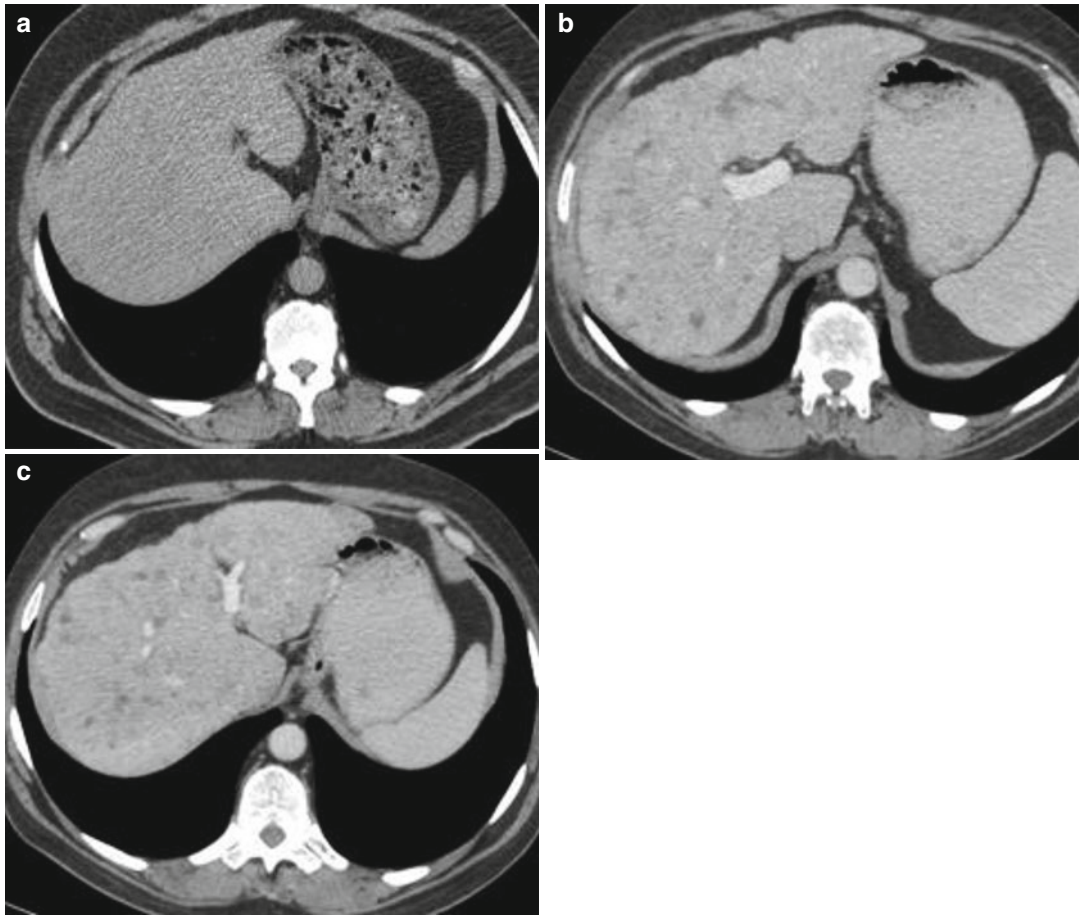


**Fig. 2** (**a**, **b**) *Chemotherapy-induced cirrhosis*: axial CT images, (**a**) non-contrast CT of the normal liver prior to treatment, (**b**) and (**c**) contrast-enhanced images during the portal venous phase, posttreatment, showing nodularity of the liver and caudate lobe enlargement

and segmental atrophy of the posterior segments (VI, VII) of the right lobe and medial segment (IV) of the left lobes. The enlargement of the hilar periportal space, the notch sign, an expanded gallbladder fossa, and generalized widening of the interlobar fissures are also considered typical of cirrhosis. Progressive hepatic fibrosis leads to increased vascular resistance at the level of the hepatic sinusoids resulting in portal hypertension, ascites, and development of portosystemic shunts and collaterals in various areas such as at the lower end of the esophagus, gastric fundus, splenorenal system, and in the abdominal wall. The paraumbilical veins and the left gastric vein, both draining into the portal vein, can recanalize.

In MR, MR elastography is used to evaluate liver stiffness in cirrhotic patients (Brancatelli et al. 2007).

Methotrexate (MTX) is used to treat osteosarcoma and central nervous system lymphoma. MTX in high doses usually causes an increase in transaminase levels in 60–80 % of patients. However, in those undergoing treatment for chronic diseases, such as rheumatoid arthritis, it has been reported to cause fibrosis and cirrhosis. Patients treated with daily oral MTX, fibrosis, or cirrhosis are reported to develop more than twice as frequently as in those taking the drug intermittently by parenteral route (Thatishetty et al. 2013). Gemcitabine used to treat pancreatic, lung, breast, urothelial, and ovarian cancer has a

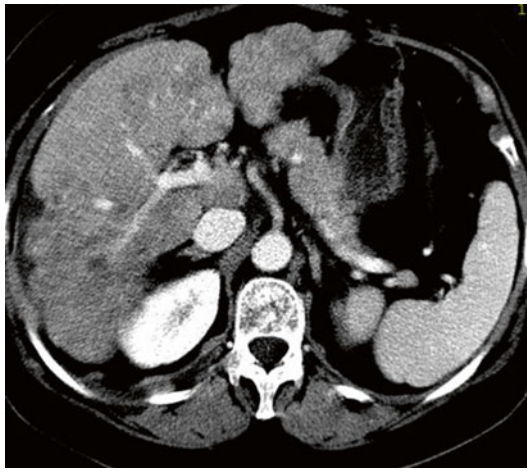

**Fig. 3** Axial post-contrast CT image of a 57-year-old female with metastatic breast carcinoma, showing multiple hepatic ill-defined metastases, hepatic nodularity, heterogeneity, and capsular retraction consistent with pseudocirrhosis

relatively safe profile. Wasif Saif et al. (2007) published a case of early and active fibrosis developing after 8 weeks of treatment for pancreatic adenocarcinoma as seen at MRI. There are a few additional case reports in the literature.

Pseudocirrhosis (Fig. 3) is a condition in which progressive shrinkage and distortion of the liver lead to an appearance that is macroscopically indistinguishable from late-stage cirrhosis. It is usually found in patients with treated metastatic breast cancer or lymphoma, most often after prolonged chemotherapy treatment. Histology typically shows dense fibrosis associated with residual tumor, and the absence of bridging fibrosis distinguishes this condition from true cirrhosis (Robinson 2009). The imaging features of pseudocirrhosis are similar to those of true cirrhosis (Fig. 3) (Young et al. 1994; Schreiner et al. 1998). Ascites, splenomegaly, and varices are often present due to associated portal hypertension. At MRI nodules of relatively normal tissue are separated by bands of dense fibrosis that are hypointense on T1-weighted images and hyperintense on T2-weighted images and show delayed gadolinium enhancement. No correlation has been found between specific chemotherapy regimens and hepatic contour changes (Young et al. 1994; Qayyum et al. 2007).

## 2.3 Hepatic Veno-Occlusive Disease (HVOD)

HVOD, also known as sinusoidal obstruction syndrome (SOS), is a rare but serious complication of systemic chemotherapy treatment. It is reported more commonly with myeloablative chemotherapy and total body irradiation prior to allogeneic bone marrow transplantation (Cefalo et al. 2010).

HVOD is characterized by necrosis of the hepatocytes, sinusoidal fibrosis, and occlusion of the hepatic venules with subsequent hepatic congestion (Robinson et al. 2011). The clinical presentation includes jaundice, tender hepatomegaly, and unexplained weight gain with or without ascites. Liver enzymes may be abnormal and thrombocytopenia may develop (Cefalo et al. 2010; Richardson and Guinan 1999).

At ultrasound there is a decrease in hepatic vein diameter to less than 3 mm. At Doppler ultrasound there is a high hepatic arterial resistive index (RI) of 0.75 or more, decreased velocity, or even flow reversal in the portal vein. Visualization of the paraumbilical vein is also suggestive of HVOD (Mahgerefteh et al. 2011).

CT findings of HVOD include hepatomegaly, splenomegaly, gallbladder wall thickening, decreased hepatic attenuation, ascites, and periportal cuffing, as well as signs of blood flow abnormalities in the hepatic arterial or portal venous systems (Mahgerefteh et al. 2011). In liver transplant patients, periportal edema, ascites, and right hepatic vein narrowing can distinguish between HVOD and GVHD (graft versus host disease) that can be similar clinically but requires a different treatment (Mahgerefteh et al. 2011; Erturk et al. 2006).

Vauthey et al. examined 406 patients that underwent hepatic resection of colorectal metastases. Pathologic review showed grade 2–3 sinusoidal dilation in 18.9 % of patients treated with oxaliplatin compared with 1.9 % of patients that were not treated with chemotherapy. There was no increase in perioperative morbidity or mortality in patients with sinusoidal obstruction (Vauthey et al. 2006). It is not well understood how oxaliplatin initiates sinusoidal obstruction.

Furthermore, it is unclear how oxaliplatin-induced sinusoidal obstruction affects subsequent liver regeneration after resection (Robinson et al. 2011). HVOD is a relatively serious complication with high morbidity and mortality and with no specific treatment.

DeLeve et al. propose a common mechanism for HVOD, nodular regenerative hyperplasia (NRH), peliosis hepatis, and sinusoidal dilatation. All are manifestations of vascular injury that have been recently associated with drug toxicity in patients treated for metastatic colorectal cancer; damage to sinusoidal endothelial cells and sometimes to hepatic venular endothelial cells seems to be the common link in these four types of liver injury (DeLeve et al. 2002).

## 2.4 Focal Benign Lesions Associated with Chemotherapy: Nodular Regenerative Hyperplasia (NRH), Focal Nodular Hyperplasia (FNH), and Peliosis Hepatis

### 2.4.1 NRH

NRH is defined histologically as nodules of regenerative hepatocytes, without fibrous septa, distributed diffusely across the hepatic parenchyma. It is often associated with non-cirrhotic portal hypertension. Although its pathogenesis remains unclear, it is thought to result from liver regeneration after ischemic injury due to intrahepatic microvascular occlusion. Hillaire et al. reported prothrombotic disorders in half of the cases presenting with non-cirrhotic portal hypertension (Hillaire et al. 2002). Among 274 patients treated with oxaliplatin, NRH was found at histopathology in 24.5 % of patients (Rubbia-Brandt et al. 2010).

Diagnosing NRH is challenging. At ultrasound, NRH nodules are usually not visible due to small size and isoechogenicity. When visualized, NRH lesions are usually represented by one or more well-delineated hypoechoic or isoechoic tiny nodules with a sonolucent rim, an appearance which is indistinguishable from metastases (Clouet et al. 1999). At CT, NRH nodules remain isodense or hypodense on both arterial and portal venous phases, distinguishing NRH from the other common benign hepatic lesions: focal nodular hyperplasia and hepatic adenomas (Mahamid et al. 2005). The significance of magnetic resonance imaging in the diagnosis of NRH is still controversial; NRH lesions appear hyperintense on T1-weighted images and are iso- or hypointense on T2-weighted images (Horita et al. 2002). After gadolinium contrast injection, the sensitivity and specificity of NRH diagnosis are 70–80 % (Zech et al. 2007).

### 2.4.2 FNH

FNH (Fig. 4) is a common benign hepatic neoplasm that is usually detected incidentally and is seen mostly in women. It is thought to be a hyperplastic response of the liver to local vascular abnormality. Nonneoplastic disorganized hepatocytes surrounding a central scar are evident at histology.

At ultrasound typical FNH will demonstrate a central scar with prominent centrifugal arterial flow on Doppler examination. However, this is only seen in 20 % of cases. The echogenicity of both the mass and its scar is variable.

At non-contrast CT scanning, the lesion is usually hypo- or isodense, but may appear hyperdense if the rest of the liver is fatty. A hypodense central scar can be seen in up to 60 % of lesions over 3 cm in size. FNH demonstrates bright arterial contrast enhancement except for the central scar, which remains hypodense (Fig. 4). Enlarged central arteries may be seen. In the portal venous phase, the lesion mostly becomes isodense to the liver. The scar demonstrates enhancement on delayed scans in up to 80 % of cases. At MRI, FNH will appear at T1-weighted images as iso- to hypointense and at T2-weighted images as iso- to hyperintense. On post-contrast injection T1-weighted images, FNH will enhance homogeneously, early in the arterial phase, and will be isointense in the portal phase. The central scar retains contrast on delayed scans.

Donadon et al. reported two patients with colorectal cancer and no liver lesions at CT staging prior to resection. After treatment with FOLFOX (oxaliplatin, leucovorin, and fluorouracil) and

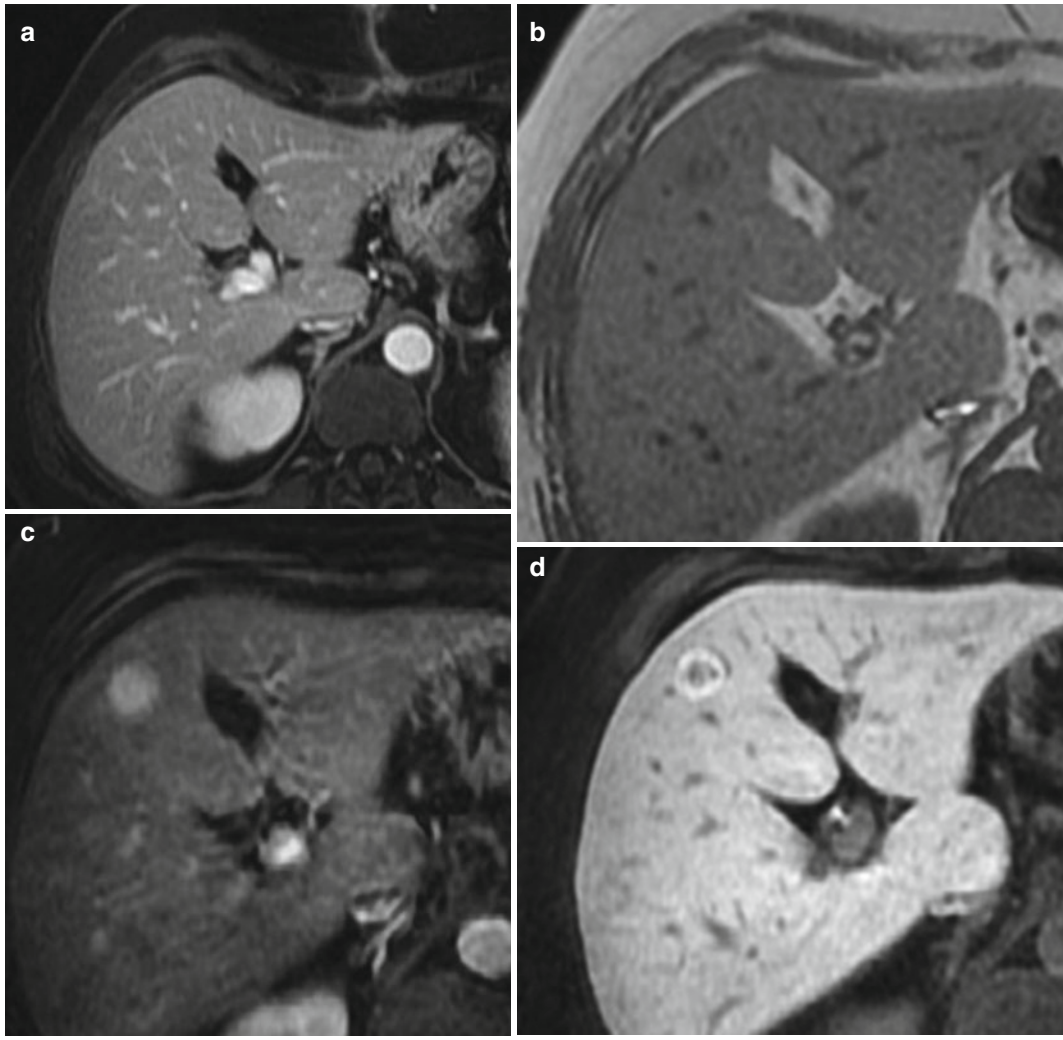


**Fig. 4** (**a**–**d**) *FNH*. MR images pre- and posttreatment with a hepatobiliary contrast agent (Gd-EOB-DTPA). Pretreatment T1-weighted MR image post-gadolinium injection showing no lesion (**a**) and 6 years later a lesion that is slightly hypointense on posttreatment T1-weighted MR image (**b**), posttreatment T1-weighted MR image post-gadolinium during the hepatic arterial phase showing a hypervascular lesion with intense homogeneous enhancement (**c**), posttreatment T1-weighted MR image post-gadolinium during the hepatobiliary phase showing peripheral ring enhancement of the lesion with a central isointense area. Notice the enhancement of the significant hepatic parenchyma typical during this phase (**d**) (Courtesy of Giuseppe Brancatelli, University of Palermo)

surgery, a follow-up CT of both patients showed multiple bilateral focal liver lesions which did not show increased FDG uptake at FDG-PET/CT. Both patients also had normal CEA and CA19-9 levels. In both cases the lesions were nonetheless misdiagnosed as colorectal liver metastases and treated with hepatic resection. The histology review showed typical findings consistent with the diagnosis of multiple FNHs (Donadon et al. 2013).

### 2.4.3 Peliosis Hepatis

Peliosis hepatis (Fig. 5) is a rare benign disorder causing sinusoidal dilatation resulting in multiple blood-filled lacunar spaces within the liver parenchyma. It is often asymptomatic, but may be associated with hepatomegaly, ascites, portal hypertension, cholestasis, and hepatic failure. In rare cases, hepatic rupture and intraperitoneal hemorrhage have been reported. At ultrasound,

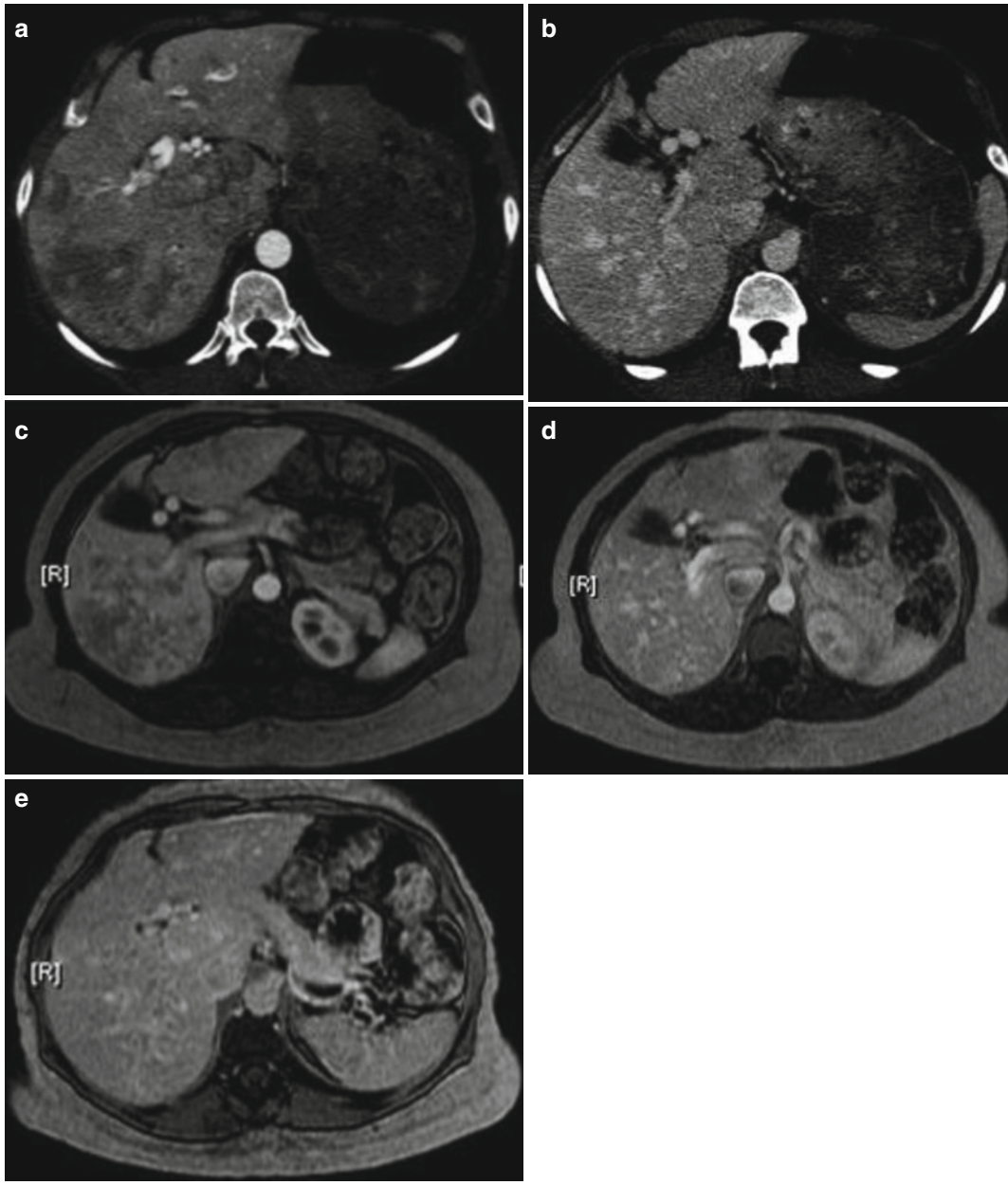


**Fig. 5** *Peliosis hepatis*. Axial CT images during the hepatic arterial phase and portal venous phase showing hypodense lesions with central early enhancement in the hepatic arterial phase (**a**), filling with contrast during the portal venous phase (**b**). Axial T1-weighted MR images in the hepatic arterial phase (**c**), portal venous phase (**d**), and delayed phase (**e**) showing the same type of enhancement as seen at CT images and the isointensity of the lesions in the delayed phase (**e**)

peliosis will appear as a homogeneous hypoechoic lesion in patients with hepatic steatosis and as a hyperechoic lesion in patients with a normal liver. When complicated by hemorrhage, the lesions will be heterogeneously hypoechoic. At CT, findings vary with lesion size and presence of hemorrhage or thrombosis within the cavities (Fig. 5). At unenhanced CT, peliotic lesions

usually appear as multiple areas of low attenuation. After contrast material injection, during the arterial phase, peliotic lesions typically show early globular enhancement and multiple small central accumulations of contrast material (the so-called target sign). During the portal venous phase, a centrifugal progression of enhancement without a mass effect on hepatic vessels is usually observed. The lesions will become progressively isoattenuating on the delayed phase. The signal intensities of the lesions on.

MR examinations largely depend on the age and status of the blood component. At T2-weighted sequences, peliotic lesions are usually hyperintense to the liver parenchyma with multiple foci of high signal, most likely attributable to hemorrhagic necrosis. At T1-weighted sequences, the lesions are hypointense because of the presence of subacute blood, although isointense and hyperintense foci are also described in the literature. At T1-weighted images after contrast material injection, peliotic lesions usually show enhancement. Similar to CT, the enhancement is typically centrifugal; however, a recent report described an unusual centripetal enhancement pattern that may be confused with that of a hemangioma (Iannaccone et al. 2006).

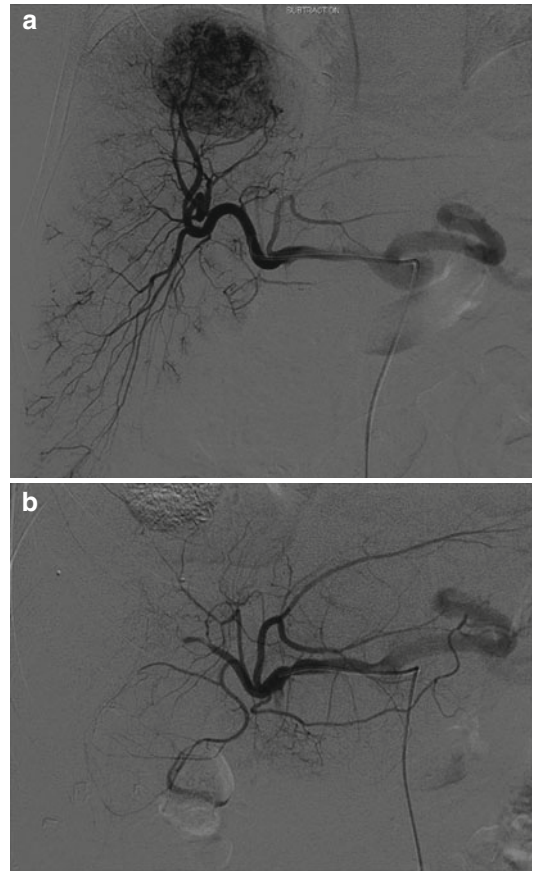


**Fig. 6** *Chemoembolization of a patient with HCC.* Angiography before (**a**) and after (**b**) transarterial chemoembolization in a patient with HCV and HCC showing right hepatic artery occlusion due to the treatment (These images are courtesy of Issac Kori, Tel Aviv Medical Center, Israel)

## 3 Hepatic Complications Due to Transarterial Chemoembolization

Transarterial chemoembolization is an angiographic technique for the selective targeting of hepatic lesions. In this procedure the arterial blood supply of the lesion is embolized in order to induce necrosis and a chemotherapeutic agent is administered selectively to the lesion (Qian 2011). In the conventional procedure a mixture of a cytotoxic drug emulsified with ethiodized oil (known as Lipiodol or Ethiodol), which is radiopaque, is injected into the arterial branch supplying the lesion. This is then followed by bland embolization using gelatin of particulate agents. In a newer approach, drug-eluting beads, which are not radiopaque (polyvinyl alcohol microspheres), are used, mixed with a contrast agent (Fig. 6). These beads slowly release the chemotherapeutic agent, providing a more sustained treatment, with fewer systemic side effects (Nawawi et al. 2010). Assessment on posttreatment CT is problematic since these beads are not radiopaque. However, since the contrast material is injected with the beads, there have been reports of a slightly increased density on post-procedure non-contrast CT performed within 12 h of the procedure that may allow assessment of the injection accuracy in relation to the lesion (Golowa et al. 2012). After the procedure, most patients (90 %) suffer from a post-embolization syndrome, which is diagnosed clinically (Clark 2006). It is a combination of fatigue, abdominal pain, nausea, vomiting, anorexia, fever, and cachexia. This is an early transient complication that is not evident radiologically (Qian 2011).

The most common radiologically evident complication is nontargeted accidental embolization. This can occur in many organs. In the hepaticobiliary system, it can be seen in the gallbladder, when Lipiodol is inadvertently injected into the cystic artery and is deposited in the gallbladder wall. In some cases (Clark 2006; Wagnetz et al. 2010), acute ischemic or chemical cholecystitis may develop due to obstruction of the cystic artery by the embolization material. Clinically there is right upper quadrant pain, and radiologically, the findings are similar to those of acalculous cholecystitis (Barie and Eachempati 2010), with gallbladder wall edema evident at imaging as wall thickening with a lucent layer in the gallbladder wall, pericholecystic fluid, pericholecystic fat stranding on CT, and infrequently gallbladder distension. At scintigraphy the gallbladder is not visible or is questionably visible. However, as this condition is usually self-limiting and rarely requires intervention, the appearance of signs of wall gangrene (sloughed mucosa, intramural gas) and progression to perforation are rare (Wagnetz et al. 2010). The risk for gallbladder gangrene is highest when the procedure is a nontargeted right hepatic lobe embolization, with an incidence ranging from 0.3 to 10 % (Brennan and Ahmed 2013), and is obviously reduced in selective injections distal to the origin of the cystic artery. When the non-radiopaque drug-eluting beads are injected, the embolized particles are not seen, but the findings are similar.

Periportal edema is another complication that may infrequently be seen after transarterial chemoembolization. At CT it appears as a hypodense area encircling the portal veins. At MRI it is seen as a hyperintense periportal rim on T2-weighted images (Karcaaltincaba et al. 2007), and at ultrasound, it appears as a collar of low periportal reflectivity (Worthy et al. 1994) surrounding the portal veins.

Rupture of the targeted tumor may infrequently occur after transarterial chemoembolization and is more commonly seen in peripheral tumors. It is manifested as acute bleeding from the tumor, with hypotension, blood in the abdominal cavity, and active extravasation visible at imaging (Jia et al. 2013).

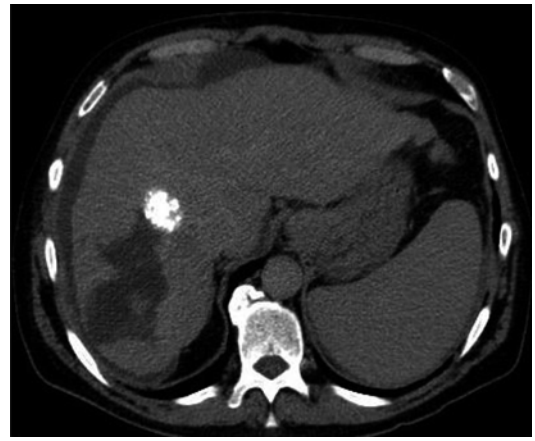

**Fig. 7** *Post-transarterial chemoembolization hepatic abscess* in a patient with HCV and HCC. Non-contrast-enhanced CT showing Lipiodol within the lesion and an irregular hypodense area consistent with a fluid collection proved to be an abscess (These images are courtesy of Issac Kori, Tel Aviv Medical Center, Israel)

Bilomas and biliary ischemia are also potential complications, with a higher incidence when using drug-eluting beads (compared to Lipiodol) and when treating metastases rather than HCC (due to the protective nature of the hypertrophied peribiliary plexus seen in cirrhosis). Biliary ischemia causes disruption of the biliary ductal integrity, with formation of bilomas. Bilomas are seen at cross-sectional imaging as well-defined or only slightly irregular intrahepatic fluid collections. Its pseudocapsule is usually unidentifiable (Mortele and Ros 2001). At ultrasound, they are well-marginated anechoic loculations, with thin, mildly echogenic walls, and without septations (Zegel et al. 1981). Biliary ischemia can also lead to the formation of biliary strictures, leading to upstream segmental biliary dilatation evident in all imaging modalities, but best visualized at MRCP.

Hepatic infarction is rare, even in cases of reduced portal flow (as in portal vein thrombosis or in the presence of transjugular intrahepatic portosystemic shunts). It is seen as a wedge-shaped hypoechoic, hypodense, or T1 hypointense and T2 hyperintense region. Arterial occlusion can occur as well, in angiography, the hepatic arteries will not be filled after contrast injection due to thrombosis (Fig. 6).

Liver abscess formation (Fig. 7) is another possible complication, occurring in approximately 1–14 % (Nawawi et al. 2010), and is

more likely to occur in the presence of a biliary stent or a bilioenteric anastomosis. It can form either due to superimposed infection of a prior biloma or due to infection of the necrotic center of the treated tumor. At ultrasound, liver abscess appears as a hypoechoic loculation, manifesting internal echoes, with a thick wall (Zegel et al. 1981). At CT, a liver abscess appears as a thick-walled hypodense loculation. At MRI, the abscess is usually T2 hyperintense and T1 hypointense at MR, with a strong rim enhancement, often (50 %) with perilesional edema (Mortele and Ros 2001).

## 4 Hepatic Complications Due to External Beam Radiation: Radiation-Induced Liver Disease

Before targeted radioembolization of hepatic lesion emerged as a viable and successful method, external beam irradiation was the only option. It has been in use for many years, and its toxicity is well known and extensively described.

The classic injury caused by radiation is the clinical entity known as "radiation-induced liver disease" (RILD), formerly referred to as radiation hepatitis. This is a subacute phenomenon, occurring 1 week to 3 months following treatment (even as late as 7 months) (Lawrence et al. 1995). It is manifested clinically by fatigue, weight gain and increased abdominal girth due to ascites, right upper quadrant discomfort, a varying degree of jaundice (usually minimal or absent), moderately elevated hepatocellular liver enzymes, and a substantially elevated alkaline phosphatase. The pathophysiology behind this entity is veno-occlusive disease (VOD), or more accurately termed sinusoidal obstructive syndrome (SOS) (Mahgerefteh et al.) – severe sinusoidal congestion surrounding central veins occluded by fibrotic tissue (Lawrence et al. 1995) (Maor and Malnick 2013). This injury is dose and volume related, and as such, stereotactic delivery methods allow for higher radiation doses to be delivered without causing hepatic injury.

There is hepatomegaly at all imaging modalities. Hepatic radiological changes are seen in all patients, even in asymptomatic patients, and after doses lower than needed for clinically evident RILD (Maturen et al. 2013). Therefore, the diagnosis is clinically based, and the radiological changes themselves are not considered diagnostic of RILD. The imaging appearance in all modalities reflects the reduced portal flow, increased arterial flow, and venous congestion. Multiphase CT at the early stages of injury may show a region of reduced density on all phases, typical of liver congestion and edema. Later, as the disease progresses, the appearance is variable with a hallmark appearance of a hyperdense area during the portal phase in the later severe cases, corresponding to veno-occlusive disease. At MRI the irradiated region appears hypointense on T1-weighted images and hyperintense on T2-weighted images, and following gadolinium injection, a hyperintensity appears during the arterial phase and is sustained well into the portal and late phases (as opposed to HCC). RILD causes dysfunction and damage to both Kupffer cells and hepatocytes; therefore, at MRI, utilizing liver-specific contrast agents, the irradiated zone appears hypointense on T1 when using both reticuloendothelial specific agents and hepatocyte-specific agents (Okamoto et al. 2014). PET/CT shows a region of increased uptake corresponding to the irradiated region. These imaging changes have a sharp demarcated border, so called "geographic" changes, caused by the sharp border of the irradiated field.

In some rare cases, veno-occlusive hepatocyte injury may appear as a focal mass (pseudolesion) on hepatobiliary phase MRI obtained after injection of hepatocyte-specific contrast agent. This pseudolesion is hypointense on T1 (Maturen et al. 2013). A ring-enhancing lesion was also reported at CT, appearing several weeks after radiation treatment and resolving spontaneously (Iwasa et al. 2013).

With time the irradiation treatment may result in fibrosis of the affected area, evident at imaging as focal atrophy, sometimes with capsular retraction and with compensatory hypertrophy of other unaffected liver segments.

## 5 Hepatic Complications Due to Radioembolization

Radioembolization is an angiographic procedure, in which pure beta-emitting $^{90}$Ytrium microspheres, made of either glass or resin, are selectively injected into the hepatic vasculature (Dubel and Soares 2008). The aim of this treatment is to achieve a localized high irradiation dose of hepatic lesions, with relatively low doses affecting the normal liver parenchyma (Lam et al. 2013). Complications of radioembolization are mostly clinical (Peterson et al. 2013). The post-radioembolization syndrome is a transient acute complication similar to the post-chemoembolization syndrome described earlier.

It is important to be aware of the typical expected appearance of treated radioembolization lesions. Initially the lesion usually enlarges and undergoes cavitation, with a ring-like peripheral enhancement, and associated periportal edema (Maturen et al. 2013). Differentiating treated lesions from viable tumor is challenging. Diffusion-weighted MR has been reported to be useful for this purpose with viable tumor demonstrating restricted diffusion (Maturen et al. 2013).

At a later stage radioembolization-induced liver disease (REILD), formerly known as radiation hepatitis, may develop. This is a clinical diagnosis, based on the presence of ascites, variable degree of jaundice, and elevated bilirubin and alkaline phosphatase levels, and is indistinguishable from RILD caused by external beam radiation. The occurrence rate is unclear, with some series reporting an incidence rate of up to 5 % after a single procedure (Lam et al. 2013). The radiological manifestations are similar to RILD manifestations caused by external beam radiation, but affecting only the radioembolization perfusion zone. At CT, hypodense regions appear after radioembolization, appearing heterogeneous when using a low dose regimen (under 100 Gy) (Murthy et al. 2005). The typical appearance is different in cirrhotic and non-cirrhotic livers. Arteriovenous shunts that usually form in cirrhotic livers alter the perfusion pattern of the injected microspheres that sometimes form clusters, thus creating an irregular and unpredictable affected area with a heterogeneous appearance. That is the reason for the more common and severe appearance of REILD in cirrhotic livers (Maor and Malnick 2013). The hepatic changes seen after the treatment may be transient and usually diminish over time.

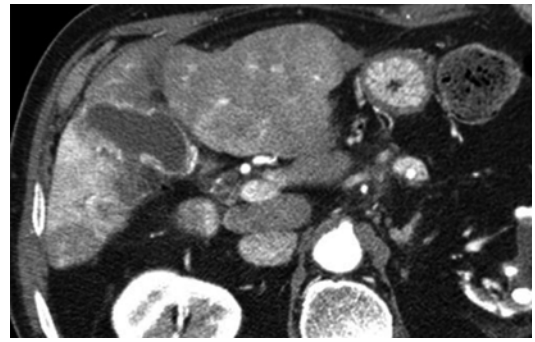

**Fig. 8** *Post-radioembolization*. Axial contrast-enhanced CT image during the arterial phase of a case of post-radioembolization cholecystitis, showing gallbladder wall thickening and irregularity, disruption of the gallbladder wall, and pericholecystic fat infiltration (Image courtesy of Frank H. Miller, Northwestern University Feinberg School of Medicine, Chicago, USA)

Acalculous ischemic cholecystitis due to obstruction of the cystic artery by the embolization material may also occur with typical radiological findings of cholecystitis similar to those caused by TACE, as described under "Sect. 3" (Fig. 8).

## 6 Hepatic Complications Due to Ablative Techniques

Ablation of hepatic tumor lesions can be achieved by several techniques using various imaging modalities and different ablative measures. Thermal ablation techniques include (Qian 2011; Vogl et al. 2013):

1. Radiofrequency (RF) ablation as the most widely used technique and is usually performed with CT or ultrasound guidance.
2. Laser interstitial thermotherapy (LITT), performed with MRI guidance.
3. Microwave (MW) ablation that may be performed percutaneously, with CT, ultrasound, or MRI guidance, or via laparotomy.
4. High-intensity focused ultrasound (HIFU), performed with ultrasound or MRI guidance,

is a noninvasive technique, opposed to the other thermal ablation techniques.
5. Cryoablation may be performed percutaneously with CT or ultrasound guidance, or more frequently at surgery (cryosurgical ablation) (Qian 2011).
6. Ethanol injection, and much less frequently acetic acid injection, can also be used to achieve lesion necrosis and may be performed with ultrasound, CT, or MRI guidance.

## 6.1 Percutaneous Ablative Techniques

All percutaneous ablative techniques are aimed at achieving lesion necrosis and have similar complications related to the percutaneous procedure itself. Complications are infrequent, with the total reported complication rate ranging from 7.7 to 8.9 %. Most of these are minor complications (Qian 2011; Vogl et al. 2013). Insufficient attention has been given to the actual hepatic complication rate which is unclear. The most available information regarding complications is from reports of RF ablation, MW ablation, and ethanol injection techniques. LITT is much less frequently used and is mostly experimental (Qian 2011; Eichler et al. 2012). The preferred modality for imaging after ablation is either contrast-enhanced CT or MR.

Abscess formation after ablative treatments is rare with a reported incidence of less than 1 % and in some studies as low as 0.3 %. An abscess can either be intralesional, perilesional, or perihepatic. It is important to remember that it is common to see gas bubbles at the ablation area and in the portal vein immediately after thermal ablation. These gas bubbles are not indicative of infection. The hepatic parenchymal gas bubbles are usually absorbed within 6 h after the procedure, and the portal venous gas bubbles are absorbed within 24 h (Brennan and Ahmed 2013). This is the reason why CT, rather than ultrasound, is the preferred modality for the evaluation of post-ablation complications. A rim of enhancement surrounding the ablated area is very commonly seen after the ablation, with a reported incidence of up to 80 % following RF ablation. This finding is indicative of inflammation and usually resolves within 4–6 weeks. An abscess should be suspected only if peri-procedural fever persists for more than 10 days and the amount of gas fails to diminish or even increases over time. In the early post-ablative period, up to 4 weeks, the area of ablation has a variable appearance. At CT, it is often heterogeneous and appears hypodense or hyperdense, sometimes with an associated linear hyperdensity representing the needle tract. At MRI, it is heterogeneously hyperintense on T1-weighted images, sometimes with a central hypointensity, and heterogeneously hypointense on T2-weighted images due to coagulative necrosis, mostly containing some blood products. Over time the ablated area becomes increasingly homogeneous and should decrease in size due to fibrosis. When the ablation area remains hypodense and increases in size, fluid collection, biloma, or abscess should be suspected. An abscess usually has a characteristic thick rim of enhancement, surrounding a hypodense or T1 hypointense and T2 hyperintense core, in the appropriate clinical setting.

Bile duct injury is another complication, reported to occur in less than 1 % in most studies (Livraghi et al. 2012; Cha et al. 2013; Curley et al. 2004). Some degree of upstream biliary dilatation is described in up to 18 % of RF ablation procedures (Brennan and Ahmed 2013). However, it usually improves over time and does not represent a true stricture. True strictures are usually evident 3–6 months after treatment and are seen in 0.4 % of MW ablations, for example (Liang et al. 2009). Small duct strictures adjacent to the ablated lesion are more common and may cause atrophy of the segment they drain. Larger ducts are involved less frequently, because they are more centrally located, and relatively protected from thermal damage due to the heat-sink effect created by adjacent large vessels. Strictures are best imaged with MRCP, but CT or ultrasound can also show the segmental biliary dilatation resulting from strictures. Bile duct injury that may lead to biliary leaks, bilomas, and fistulas is exceedingly rare, occurring in less than 0.1 % of cases (Curley et al. 2004; Bertot et al. 2011). Bilomas can form along

the needle tract or adjacent to the ablation zone. They are usually well-defined thin-walled fluid collections. Cholangitis has also been rarely reported. Biliary complications are more frequent with ethanol injection than with other ablation techniques. It has been suggested that ethanol injection results in inflammation of adjacent bile ducts and that in some cases ethanol may enter the bile duct lumen damaging the walls (Cha et al. 2013). Gallbladder wall thickening is usually seen when the ablation zone is in proximity to the gallbladder and has been described in thermal ablation techniques as well as ethanol injection, in as many as 2.8 % in microwave ablation and 8.3 % in ethanol injection (Brennan and Ahmed 2013; Cha et al. 2013; Liang et al. 2009; Kim et al. 2009). Gallbladder wall thickening should not be confused with acute cholecystitis when the appropriate clinical setting is lacking. It is usually self-limiting and is unimportant.

Vascular complications have been reported after ablations, mostly hemorrhage, but also arterioportal fistulas/shunts and pseudoaneurysms. Thermal injury to large vessels is uncommon due to the heat-sink effect, and vascular injury is usually the result of the invasiveness of the procedure itself. Hemorrhage is usually mild and may result in subcapsular or intrahepatic hematomas. These are usually seen along the needle tract, inside the treated lesion. In some cases intraperitoneal hemorrhage may also be seen. Severe intractable hemorrhage, requiring intervention, is very rare, occurring in less than 0.1 % of cases (Liang et al. 2009), and hemorrhage requiring blood transfusions is reported in less than 0.3 % of cases (Livraghi et al. 2012). CT and MRI can detect hemorrhage and hematomas, but due to availability and cost, CT is most commonly used to image suspected acute bleeding. Ultrasound is also often used to evaluate the amount of free fluid, as a sign of acute bleeding. Small arterioportal fistulas can be seen in the immediate post-ablation period but are usually transient (Brennan and Ahmed 2013) and occur in up to 0.3 % of cases (Liang et al. 2009). At cross-sectional imaging, arteriography arterioportal fistulas appear as wedge-shaped areas of increased arterial phase enhancement with early filling of the adjacent portal vein branches. Larger, hemodynamically significant fistulas that might require endovascular therapy occur less frequently.

Arterial damage can lead to pseudoaneurysm formation. CT will demonstrate an irregular strongly enhancing lesion in the arterial phase, and Doppler ultrasound will demonstrate flow inside the lesion. Pseudoaneurysms usually thrombose spontaneously. Doppler ultrasound is a useful, cheap, and available method for follow-up. When thrombosed, ultrasound will show a focus of hyperechogenicity consistent with a hematoma at the pseudoaneurysm site, with no evident flow on Doppler ultrasound. In case spontaneous thrombosis fails to occur, coil embolization should be performed. Venous thrombosis has also been rarely reported after ablations, usually involving the portal veins and less frequently the hepatic veins (Kim et al. 2011). It occurs in approximately 1.1 % of cases after RF ablation, 0.3 % of cases after microwave ablation, and as low as 0.001 % of cases after ethanol injection (Livraghi et al. 2012; Cha et al. 2013). Hepatic infarction is extremely rare, due to the liver's dual blood supply. However, it may occur in approximately 0.1 % of patients. An infarct appears as a wedge-shaped region that is hypoechoic on ultrasound, hypodense on CT, and T1 hypointense and T2 hyperintense on MRI. Hepatic insufficiency, usually due to hepatic decompensation in cirrhotic patients, can also occur, reported in less than 0.1 %. This is usually seen in advanced-stage cirrhotic livers and is difficult to diagnose radiologically. In normal livers acute hepatic insufficiency usually manifests as a diffusely hypodense liver on non-contrast CT, with a variable degree of hepatic size alteration, either reduction or increase in size (Shakil et al. 2000).

## 6.2 High-Intensity Focused Ultrasound (HIFU)

This is a noninvasive technique that uses focused ultrasound beams to achieve coagulative necrosis (Jung et al. 2011; Zhou 2011). A post-ablation syndrome similar to post-embolization syndrome can occur in 11.4 %, but is a clinical diagnosis with no

radiological manifestations. Despite the noninvasive nature of the procedure, it is based on causing thermal damage using the ultrasound beam. The damage may affect tissues adjacent to the treated lesion. Biliary injury leading to biliary obstruction has been described as a complication of this procedure.

In conclusion, the liver is a common site for complications resulting from both systemic chemotherapy and liver-specific therapies such as irradiation, transarterial therapies, and ablation procedures. These complications range from mild, self-limiting conditions to severe, life-threatening illnesses, most of them evident on imaging, so radiologists should be aware of these conditions to be able to correctly diagnose them.

## References


Barie PS, Eachempati SR (2010) Acute acalculous cholecystitis. Gastroenterol Clin North Am 39(2):343–357, x. doi:10.1016/j.gtc.2010.02.012

Behrns KE, Tsiotos GG, DeSouza NF, Krishna MK, Ludwig J, Nagorney DM (1998) Hepatic steatosis as a potential risk factor for major hepatic resection. J Gastrointest Surg 2(3):292–298

Bertot LC, Sato M, Tateishi R, Yoshida H, Koike K (2011) Mortality and complication rates of percutaneous ablative techniques for the treatment of liver tumors: a systematic review. Eur Radiol 21(12):2584–2596. doi:10.1007/s00330-011-2222-3

Berzigotti A, Castera L (2013) Update on ultrasound imaging of liver fibrosis. J Hepatol 59(1):180–182. doi:10.1016/j.jhep.2012.12.028

Brancatelli G, Federle MP, Ambrosini R, Lagalla R, Carriero A, Midiri M, Vilgrain V (2007) Cirrhosis: CT and MR imaging evaluation. Eur J Radiol 61(1):57–69. doi:10.1016/j.ejrad.2006.11.003

Brennan IM, Ahmed M (2013) Imaging features following transarterial chemoembolization and radiofrequency ablation of hepatocellular carcinoma. Semin Ultrasound CT MR 34(4):336–351. doi:10.1053/j.sult.2013.04.004

Cefalo MG, Maurizi P, Arlotta A, Scalzone M, Attina G, Ruggiero A, Riccardi R (2010) Hepatic veno-occlusive disease: a chemotherapy-related toxicity in children with malignancies. Paediatr Drugs 12(5):277–284. doi:10.2165/11531840-000000000-00000

Cha DI, Lee MW, Rhim H, Choi D, Kim YS, Lim HK (2013) Therapeutic efficacy and safety of percutaneous ethanol injection with or without combined radiofrequency ablation for hepatocellular carcinomas in high risk locations. Korean J Radiol 14(2):240–247. doi:10.3348/kjr.2013.14.2.240

Chen J, Talwalkar JA, Yin M, Glaser KJ, Sanderson SO, Ehman RL (2011) Early detection of nonalcoholic steatohepatitis in patients with nonalcoholic fatty liver disease by using MR elastography. Radiology 259(3):749–756. doi:10.1148/radiol.11101942

Clark TW (2006) Complications of hepatic chemoembolization. Semin Interv Radiol 23(2):119–125. doi:10.1055/s-2006-941442

Clouet M, Boulay I, Boudiaf M, Soyer P, Nemeth J, Kiselman R, Rymer R (1999) Imaging features of nodular regenerative hyperplasia of the liver mimicking hepatic metastases. Abdom Imaging 24(3):258–261

Curley SA, Marra P, Beaty K, Ellis LM, Vauthey JN, Abdalla EK, Scaife C, Raut C, Wolff R, Choi H, Loyer E, Vallone P, Fiore F, Scordino F, De Rosa V, Orlando R, Pignata S, Daniele B, Izzo F (2004) Early and late complications after radiofrequency ablation of malignant liver tumors in 608 patients. Ann Surg 239(4):450–458

DeLeve LD, Shulman HM, McDonald GB (2002) Toxic injury to hepatic sinusoids: sinusoidal obstruction syndrome (veno-occlusive disease). Semin Liver Dis 22(1):27–42. doi:10.1055/s-2002-23204

Donadon M, Di Tommaso L, Roncalli M, Torzilli G (2013) Multiple focal nodular hyperplasias induced by oxaliplatin-based chemotherapy. World J Hepatol 5(6):340–344. doi:10.4254/wjh.v5.i6.340

Dubel GJ, Soares GM (2008) Regional infusion-radioembolization. Surg Oncol Clin N Am 17(4):957–985, xii. doi:10.1016/j.soc.2008.04.008

Eichler K, Zangos S, Gruber-Rouh T, Vogl TJ, Mack MG (2012) Magnetic resonance-guided laser-induced thermotherapy in patients with oligonodular hepatocellular carcinoma: long-term results over a 15-year period. J Clin Gastroenterol 46(9):796–801. doi:10.1097/MCG.0b013e3182641806

Erturk SM, Mortele KJ, Binkert CA, Glickman JN, Oliva MR, Ros PR, Silverman SG (2006) CT features of hepatic venoocclusive disease and hepatic graft-versus-host disease in patients after hematopoietic stem cell transplantation. AJR Am J Roentgenol 186(6):1497–1501. doi:10.2214/ajr.05.0539

Golowa YS, Cynamon J, Reinus JF, Kinkhabwala M, Abrams M, Jagust M, Chernyak V, Kaubisch A (2012) Value of noncontrast CT immediately after transarterial chemoembolization of hepatocellular carcinoma with drug-eluting beads. J Vasc Interv Radiol 23(8):1031–1035. doi:10.1016/j.jvir.2012.04.020

Hillaire S, Bonte E, Denninger MH, Casadevall N, Cadranel JF, Lebrec D, Valla D, Degott C (2002) Idiopathic non-cirrhotic intrahepatic portal hypertension in the West: a re-evaluation in 28 patients. Gut 51(2):275–280

Horita T, Tsutsumi A, Takeda T, Yasuda S, Takeuchi R, Amasaki Y, Ichikawa K, Atsumi T, Koike T (2002) Significance of magnetic resonance imaging in the diagnosis of nodular regenerative hyperplasia of the liver complicated with systemic lupus erythematosus: a case report and review of the literature. Lupus 11(3):193–196

Iannaccone R, Federle MP, Brancatelli G, Matsui O, Fishman EK, Narra VR, Grazioli L, McCarthy SM, Piacentini F, Maruzzelli L, Passariello R, Vilgrain V

(2006) Peliosis hepatis: spectrum of imaging findings. AJR Am J Roentgenol 187(1):W43–W52. doi:10.2214/ajr.05.0167

Iwasa S, Mayahara H, Tanaka T, Ito Y (2013) Ring-enhancing lesion associated with radiation-induced liver disease. J Clin Oncol 31(14):e243–e244. doi:10.1200/jco.2012.46.7217

Jia Z, Tian F, Jiang G (2013) Ruptured hepatic carcinoma after transcatheter arterial chemoembolization. Curr Ther Res Clin Exp 74:41–43. doi:10.1016/j.curtheres.2012.12.006

Jung SE, Cho SH, Jang JH, Han JY (2011) High-intensity focused ultrasound ablation in hepatic and pancreatic cancer: complications. Abdom Imaging 36(2):185–195. doi:10.1007/s00261-010-9628-2

Karcaaltincaba M, Haliloglu M, Akpinar E, Akata D, Ozmen M, Ariyurek M, Akhan O (2007) Multidetector CT and MRI findings in periportal space pathologies. Eur J Radiol 61(1):3–10. doi:10.1016/j.ejrad.2006.11.009

Khan AZ, Morris-Stiff G, Makuuchi M (2009) Patterns of chemotherapy-induced hepatic injury and their implications for patients undergoing liver resection for colorectal liver metastases. J Hepatobiliary Pancreat Surg 16(2):137–144. doi:10.1007/s00534-008-0016-z

Kim SW, Rhim H, Park M, Kim H, Kim YS, Choi D, Lim HK (2009) Percutaneous radiofrequency ablation of hepatocellular carcinomas adjacent to the gallbladder with internally cooled electrodes: assessment of safety and therapeutic efficacy. Korean J Radiol 10(4):366–376. doi:10.3348/kjr.2009.10.4.366

Kim AY, Rhim H, Park M, Lee MW, Kim YS, Choi D, Lim HK (2011) Venous thrombosis after radiofrequency ablation for hepatocellular carcinoma. AJR Am J Roentgenol 197(6):1474–1480. doi:10.2214/ajr.11.6495

Kooby DA, Fong Y, Suriawinata A, Gonen M, Allen PJ, Klimstra DS, DeMatteo RP, D'Angelica M, Blumgart LH, Jarnagin WR (2003) Impact of steatosis on perioperative outcome following hepatic resection. J Gastrointest Surg 7(8):1034–1044

Lam MG, Louie JD, Iagaru AH, Goris ML, Sze DY (2013) Safety of repeated yttrium-90 radioembolization. Cardiovasc Intervent Radiol 36(5):1320–1328. doi:10.1007/s00270-013-0547-9

Lawrence TS, Robertson JM, Anscher MS, Jirtle RL, Ensminger WD, Fajardo LF (1995) Hepatic toxicity resulting from cancer treatment. Int J Radiat Oncol Biol Phys 31(5):1237–1248. doi:10.1016/0360-3016(94)00418-k

Lawrence DA, Oliva IB, Israel GM (2012) Detection of hepatic steatosis on contrast-enhanced CT images: diagnostic accuracy of identification of areas of presumed focal fatty sparing. AJR Am J Roentgenol 199(1):44–47. doi:10.2214/ajr.11.7838

Liang P, Wang Y, Yu X, Dong B (2009) Malignant liver tumors: treatment with percutaneous microwave ablation–complications among cohort of 1136 patients. Radiology 251(3):933–940. doi:10.1148/radiol.2513081740

Livraghi T, Meloni F, Solbiati L, Zanus G (2012) Complications of microwave ablation for liver tumors: results of a multicenter study. Cardiovasc Intervent Radiol 35(4):868–874. doi:10.1007/s00270-011-0241-8

Mahamid J, Miselevich I, Attias D, Laor R, Zuckerman E, Shaoul R (2005) Nodular regenerative hyperplasia associated with idiopathic thrombocytopenic purpura in a young girl: a case report and review of the literature. J Pediatr Gastroenterol Nutr 41(2):251–255

Mahgerefteh SY, Sosna J, Bogot N, Shapira MY, Pappo O, Bloom AI (2011) Radiologic imaging and intervention for gastrointestinal and hepatic complications of hematopoietic stem cell transplantation. Radiology 258(3):660–671. doi:10.1148/radiol.10100025

Maor Y, Malnick S (2013) Liver injury induced by anticancer chemotherapy and radiation therapy. Int J Hepatol 2013:815105. doi:10.1155/2013/815105

Maturen KE, Feng MU, Wasnik AP, Azar SF, Appelman HD, Francis IR, Platt JF (2013) Imaging effects of radiation therapy in the abdomen and pelvis: evaluating "innocent bystander" tissues. Radiographics 33(2):599–619. doi:10.1148/rg.332125119

Miyake K, Hayakawa K, Nishino M, Morimoto T, Mukaihara S (2005) Effects of oral 5-fluorouracil drugs on hepatic fat content in patients with colon cancer. Acad Radiol 12(6):722–727. doi:10.1016/j.acra.2005.02.010

Mortele KJ, Ros PR (2001) Cystic focal liver lesions in the adult: differential CT and MR imaging features. Radiographics 21(4):895–910. doi:10.1148/radiographics.21.4.g01jl16895

Murthy R, Nunez R, Szklaruk J, Erwin W, Madoff DC, Gupta S, Ahrar K, Wallace MJ, Cohen A, Coldwell DM, Kennedy AS, Hicks ME (2005) Yttrium-90 microsphere therapy for hepatic malignancy: devices, indications, technical considerations, and potential complications. Radiographics 25(Suppl 1):S41–S55. doi:10.1148/rg.25si055515

Nawawi O, Hazman M, Abdullah B, Vijayananthan A, Manikam J, Mahadeva S, Goh K (2010) Transarterial embolisation of hepatocellular carcinoma with doxorubicin-eluting beads: single centre early experience. Biomed Imaging Interv J 6(1):e7. doi:10.2349/biij.6.1.e7

Okamoto D, Nishie A, Asayama Y, Tajima T, Ishigami K, Kakihara D, Nakayama T, Ohga S, Yoshitake T, Shioyama Y, Honda H (2014) Gadolinium ethoxybenzyl diethylenetriamine pentaacetic acid-enhanced MR finding of radiation-induced hepatic injury: relationship to absorbed dose and time course after irradiation. Magn Reson Imaging. doi:10.1016/j.mri.2014.02.019

Parikh AA, Gentner B, Wu TT, Curley SA, Ellis LM, Vauthey JN (2003) Perioperative complications in patients undergoing major liver resection with or without neoadjuvant chemotherapy. J Gastrointest Surg 7(8):1082–1088

Peterson JL, Vallow LA, Johnson DW, Heckman MG, Diehl NN, Smith AA, Tzou KS, Paz-Fumagalli R, Kim S, Ko SJ, Daugherty LC, Kim GP, Brown N, Mori KW, Buskirk SJ (2013) Complications after 90Y microsphere radioembolization for unresectable hepatic tumors: an evaluation of 112 patients. Brachytherapy 12(6):573–579. doi:10.1016/j.brachy.2013.05.008

Qayyum A, Lee GK, Yeh BM, Allen JN, Venook AP, Coakley FV (2007) Frequency of hepatic contour abnormalities and signs of portal hypertension at CT

in patients receiving chemotherapy for breast cancer metastatic to the liver. Clin Imaging 31(1):6–10. doi:10.1016/j.clinimag.2006.09.028

Qian J (2011) Interventional therapies of unresectable liver metastases. J Cancer Res Clin Oncol 137(12): 1763–1772. doi:10.1007/s00432-011-1026-9

Reissfelder C, Brand K, Sobiegalla J, Rahbari NN, Bork U, Schirmacher P, Buchler MW, Weitz J, Koch M (2014) Chemotherapy-associated liver injury and its influence on outcome after resection of colorectal liver metastases. Surgery 155(2):245–254. doi:10.1016/j.surg.2013.07.022

Richardson P, Guinan E (1999) The pathology, diagnosis, and treatment of hepatic veno-occlusive disease: current status and novel approaches. Br J Haematol 107(3):485–493

Robinson PJ (2009) The effects of cancer chemotherapy on liver imaging. Eur Radiol 19(7):1752–1762. doi:10.1007/s00330-009-1333-6

Robinson S, Manas DM, Pedley I, Mann D, White SA (2011) Systemic chemotherapy and its implications for resection of colorectal liver metastasis. Surg Oncol 20(2):57–72. doi:10.1016/j.suronc.2009.10.002

Rubbia-Brandt L, Lauwers GY, Wang H, Majno PE, Tanabe K, Zhu AX, Brezault C, Soubrane O, Abdalla EK, Vauthey JN, Mentha G, Terris B (2010) Sinusoidal obstruction syndrome and nodular regenerative hyperplasia are frequent oxaliplatin-associated liver lesions and partially prevented by bevacizumab in patients with hepatic colorectal metastasis. Histopathology 56(4):430–439. doi:10.1111/j.1365-2559.2010.03511.x

Saif MW, Shahrokni A, Cornfeld D (2007) Gemcitabine-induced liver fibrosis in a patient with pancreatic cancer. JOP 8(4):460–467

Schreiner SA, Gorman B, Stephens DH (1998) Chemotherapy-related hepatotoxicity causing imaging findings resembling cirrhosis. Mayo Clin Proc 73(8):780–783. doi:10.4065/73.8.780

Shakil AO, Jones BC, Lee RG, Federle MP, Fung JJ, Rakela J (2000) Prognostic value of abdominal CT scanning and hepatic histopathology in patients with acute liver failure. Dig Dis Sci 45(2):334–339

Singh D, Das CJ, Baruah MP (2013) Imaging of non alcoholic fatty liver disease: a road less travelled. Indian J Endocrinol Metab 17(6):990–995. doi:10.4103/2230-8210.122606

Thatishetty AV, Agresti N, O'Brien CB (2013) Chemotherapy-induced hepatotoxicity. Clin Liver Dis 17(4):671–686, ix–x. doi:10.1016/j.cld.2013.07.010

Torrisi JM, Schwartz LH, Gollub MJ, Ginsberg MS, Bosl GJ, Hricak H (2011) CT findings of chemotherapy-induced toxicity: what radiologists need to know about the clinical and radiologic manifestations of chemotherapy toxicity. Radiology 258(1):41–56. doi:10.1148/radiol.10092129

Vauthey JN, Pawlik TM, Ribero D, Wu TT, Zorzi D, Hoff PM, Xiong HQ, Eng C, Lauwers GY, Mino-Kenudson M, Risio M, Muratore A, Capussotti L, Curley SA, Abdalla EK (2006) Chemotherapy regimen predicts steatohepatitis and an increase in 90-day mortality after surgery for hepatic colorectal metastases. J Cin Oncol 24(13):2065–2072. doi:10.1200/jco.2005.05.3074

Vogl TJ, Farshid P, Naguib NN, Zangos S (2013) Thermal ablation therapies in patients with breast cancer liver metastases: a review. Eur Radiol 23(3):797–804. doi:10.1007/s00330-012-2662-4

Wagnetz U, Jaskolka J, Yang P, Jhaveri KS (2010) Acute ischemic cholecystitis after transarterial chemoembolization of hepatocellular carcinoma: incidence and clinical outcome. J Comput Assist Tomogr 34(3):348–353. doi:10.1097/RCT.0b013e3181caaea3

Worthy SA, Elliott ST, Bennett MK (1994) Low-reflectivity periportal collar on hepatic ultrasound. Br J Radiol 67(803):1050–1051

Yajima Y, Narui T, Ishii M, Abe R, Ohtsuki M, Goto Y, Endo S, Yamada K, Ito M (1982) Computed tomography in the diagnosis of fatty liver: total lipid content and computed tomography number. Tohoku J Exp Med 136(3):337–342

Young ST, Paulson EK, Washington K, Gulliver DJ, Vredenburgh JJ, Baker ME (1994) CT of the liver in patients with metastatic breast carcinoma treated by chemotherapy: findings simulating cirrhosis. AJR Am J Roentgenol 163(6):1385–1388. doi:10.2214/ajr.163.6.7992734

Zech CJ, Seiderer J, Reinisch W, Ochsenkuhn T, Schima W, Diebold J, Wrba F, Reiser MF, Schoenberg SO (2007) Thioguanin-induced nodular regenerative hyperplasia of the liver-ROC analysis of different MR techniques. Eur Radiol 17(7):1898–1905. doi:10.1007/s00330-006-0544-3

Zegel HG, Kurtz AB, Perlmutter GS, Goldberg BB (1981) Ultrasonic characteristics of bilomas. J Clin Ultrasound 9(1):21–24

Zhou YF (2011) High intensity focused ultrasound in clinical tumor ablation. World J Clin Oncol 2(1):8–27. doi:10.5306/wjco.v2.i1.8

Zorzi D, Laurent A, Pawlik TM, Lauwers GY, Vauthey JN, Abdalla EK (2007) Chemotherapy-associated hepatotoxicity and surgery for colorectal liver metastases. Br J Surg 94(3):274–286. doi:10.1002/bjs.5719

# Index





H. Kauczor, T. Bäuerle (eds.), *Imaging of Complications and Toxicity following Tumor Therapy*, Medical Radiology, DOI 10.1007/978-3-319-12841-2